A study of high output two-stroke diesel engines - scavenging, supercharging and compounding

Chen, Changyou

Award date:
1986

Awarding institution:
University of Bath

A STUDY
OF HIGH OUTPUT
TWO-STROKE DIESEL ENGINES
- SCAVENGING, SUPERCHARGING AND COMPOUNDING

submitted by:
Chen Changyou
for the Degree of Ph. D.
of the University of Bath
1986

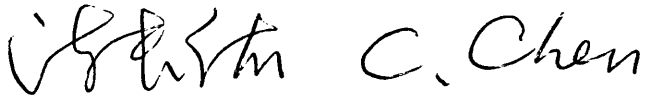

ProQuest LLC
789 East Eisenhower Parkway
P.O. Box 1346
Ann Arbor, MI 48106-1346

ACKNOWLEDGEMENTS

The author would like to express sincere thanks to Professor F.J. Wallace, for his supervision, continueous encouragement and advice throughout the duration of this work.

He wishes to thanks Dr. M. Tarabad for his suggestions in making and running the engine cycle simulation program.

He wishes to thanks Dr. S.J. Charlton for his suggestions in designing the model rig.

The author is indebted to Mr. D. Rushton for his work in making the model rig.

Many Thanks are due to Mrs. Hazel Ford, Dr. C.L. White, Dr. M. Wilson, Mr. D. Howard, Mr. S.M. Manton, Mr. A.J. Sutton and Mr. D.S. Moore for their help in my studying in U.K.

The author wishes to record his thanks to the Academic Institution for providing the ORS Award and to the Ford Co. for the sponsorship.

Finally, acknowledgement is given to the financial support by the Chinese Commission of Education.

SUMMARY

This thesis has investigated the three main aspects of two-stroke diesel engines: scavenging, supercharging and compounding.

(1). scavenging

As a non-predictive model of the scavenging process, the generalized thermodynamic model has been introduced. This model can give a thermodynamic description for any possible scavenging process. As predictive models, the phenomenological fluid dynamic models: the steady jet model and the unsteady jet model, have been suggested. Based on jet mixing and propagation, these models can give an approximate description of velocity and concentration fields for the uniflow scavenging process, thus obviating the uncertainty of the thermodynamic models. A group of model laws for scale modelling the scavenging process has been established. The experimental work on a simple water rig has been done.

(2). supercharging and compounding

Three engine models have been built into programs CSPS, CSP3Z and CSPMZ for modelling the two-stroke engine. Based on engine model CSP3Z, program CSP3ZTC has been made for simulating the turbocharged engines. Using program CSPMZ, the author has predicted the performance of the Ford ceramic two-stroke opposed-piston diesel engine, and optimized the port design of the Ford engine. The optimization procedure is suitable for any uniflow scavenged engine. Using program CSP3ZTC, the author has predicted the performance for the turbocharged Ford caramic engine without and with a blower. Using program CSPS, the author has estimated the operating characteristics for the differential compound two-stroke engine for a 30-48 ton truck. Furthermore, the author has suggested a new compound engine system with three continueously variable transmissions between the engine and compressor, the engine and output shaft, the power turbine and output shaft respectively.

CONTENTS

TABLES AND FIGURES

NOTATION

Units are S. I. unless stated.

Chapter 1

r_{ch}	Relative charge.
r_{pu}	Purity.
η_{ch}	Charging efficiency.
η_{sc}	Scavenging efficiency.
η_{tr}	Trapping efficiency.
λ	Delivery ratio.
λ_{sc}	Scavenging ratio.

Chapter 2

C_a^a	Mass concentration of air within the air zone.
C_g^a	Mass concentration of residual gas within the air zone.
C_a^g	Mass concentration of air within the residual gas zone.
C_g^g	Mass concentration of residual gas within the residual gas zone.
C_a^m	Mass concentration of air within the mixing zone.
C_g^m	Mass concentration of residual gas within the mixing zone.
C_a^i	Mass concentration of air within the genaral zone.
C_g^i	Mass concentration of residual gas within the genaral zone.
D^a	Discharge proportion coefficient of the air zone.
D^g	Discharge proportion coefficient of the residual zone.
D^m	Discharge proportion coefficient of the mixing zone.
h	Specific absolute enthalpy
h^a	Specific absolute enthalpy of the air zone.
h^g	Specific absolute enthalpy of the residual gas zone.
h^m	Specific absolute enthalpy of the mixing zone.
h^i	Specific absolute enthalpy of the general zone.
h_{in}^i	Specific absolute enthalpy flowing into the general zone.
h_{out}^i	Specific absolute enthalpy flowing out of the general

zone.

i^a Intake proportion coefficient of the air zone.

i^m Intake proportion coefficient of the mixing zone.

M Reference mass.

m_{in} Mass flowing into the cylinder.

$m_{in,A}$ Mass flowing into the cylinder at the end of phase A.

m_{out} Mass flowing out of the cylinder.

m^a Mass within the air zone.

m^a_A Mass within the air zone at the end of phase A.

m^a_{in} Mass flowing into the air zone.

m^a_{out} Mass flowing out of the air zone.

m^g Mass within the residual gas zone.

m^g_A Mass within the residual gas zone at the end of phase A.

m^g_o Mass within the residual gas zone at the beginning of the scavenging process.

m^g_{out} Mass flowing out of the residual gas zone.

m^l Mass within the general zone.

m^l_a Mass of air within the general zone.

m^l_g Mass of residual within the general zone.

m^l_{in} Mass flowing into the general zone.

m^l_{out} Mass flowing out of the general zone.

m^m Mass within the mixing zone.

m^m_a Mass of air within the mixing zone.

$m^m_{a,A}$ Mass of air within the mixing zone at the end of phase A.

m^m_g Mass of residual gas within the mixing zone.

m^m_{in} Mass flowing into the mixing zone.

m^m_{out} Mass flowing out of the mixing zone.

P Cylinder pressure.

Q^a Heat transfer from the air zone.

Q^g Heat transfer from the residual gas zone.

Q^m Heat transfer from the mixing zone.

Q^l Heat transfer from the general zone.

R Specific gas constant.

T Cylinder temperature.

T_a Temperature of the air zone.

T_g Temperature of the residual zone.

T_m	Temperature of the mixing zone.
U	Specific internal energy.
U^a	Specific internal energy of the air zone.
U^g	Specific internal energy of the residual zone.
U^i	Specific internal energy of the general zone.
U^m	Specific internal energy of the mixing zone.
V^a	Volume of the air zone.
V^g	Volume of the residual zone.
V^i	Volume of the general zone.
V^m	Volume of the mixing zone.
V_{cyl}	Cylinder volume.
γ	Ratio of specific heats.
Δ	Variation.
η_A	Volumetric ratio of the residual gas zone at the end of phase A.
$\eta_{ch.A}$	Charging efficiency at the end of phase A.
$\eta_{ch.B}$	Charging efficiency at the end of phase B.
η_o	Volumetric ratio of the mixing zone at the beginning of the scavenging process.
λ_A	Delivery ratio at the end of phase A.
λ_B	Delivery ratio at the end of phase B.

Chapter 3

A	Area.
A_w	Wall area.
C	Constant.
C_1	Constant.
C_2	Constant.
C_d	Discharge coefficient.
D	Cylinder bore.
F^i	Equivalence ratio of the general zone i.
f_s	Stoichoimetric fuel-air ratio.
m_f^i	Mass of burnt fuel within the general zone i.
$m_{f.in}^i$	Mass of burnt fuel flowing into the general zone i.
$m_{f.o}^i$	Mass of burnt fuel within the general zone i at the beginning of the scavenging process.
$m_{f.out}^i$	Mass of burnt fuel flownig out of the general zone i.

m_s	Sum of air mass and the air mass consumed in the combustion.
m_s^i	Sum of air mass and the air mass consumed in the combustion within the general zone i.
$m_{s.in}^i$	Sum of air mass and the air mass consumed in the combustion flowing into the general zone i.
$m_{s.o}^i$	Sum of air mass and the air mass consumed in the combustion within the general zone i at the beginning of the general zone i.
$m_{s.out}^i$	Sum of air mass and the air mass consumed in the combustion flowing out of the general zone i.
P	Pressure.
$(P-P_o)$	The difference between cylinder pressure with combustion and cylinder pressure at the same point in the same conditions except for the absence of any combustion.
P_d	Pressure at the downstream volume.
P_{tr}	Trapped pressure.
P_u	Pressure at the upstream volume.
Q_h	Heat transfer through the head.
Q_l	Heat transfer through the liner.
Q_p	Heat transfer through the piston.
Q_w	Heat transfer through the wall.
R_u	Specific gas constant of the upstream volume.
t	Time.
T_{cyl}	Cylinder temperature.
T_l	Temperature of the general zone i.
T_{tr}	Trapped temperature.
T_u	Temperature within the upstream volume.
T_w	Wall temperature.
V_m	Mean piston speed.
V_s	Cylinder swept volume.
V_{tr}	Trapped volume.
α	Heat transfer coefficient.
Π	Pressure ratio.
Π_{cr}	Critical pressure ratio.
Ψ_m	Compressible flow function.

Chapter 4

Section 4.2

A_e	Exhaust port area.
A_{in}	Mean inlet port area.
A_o	Initial effective flow area.
A_r	Reduced area.
A_s	Inlet port area.
a_{cyl}	Sonic velocity in the cylinder.
a_e	Sonic velocity in the exhast manifold.
a_r	Sonic velocity at the exhaust port opening.
b	Parameter.
c_i	Air mass concentration within zone i.
D	Delay array
e	Parameter.
N	Engine speed.
P_{cyl}	Cylinder pressure.
P'_{cyl}	Cylinder pressure at which choked flow ceases.
P_e	Exhaust manifold pressure.
P_r	Cylinder pressure at the exhaust port opening.
P_s	Inlet manifold pressure.
R	Cylinder radius.
r	Jet radius.
T	Time ratio.
V_i	Volume of zone i.
w_c	Connective velocity.
w_m	Mean velocity.
w_i	Axial velocity.
w_r	Recirculating velocity.
X	Sonic velocity ratio of exhaust to cylinder.
X'	Sonic velocity ratio of exhaust to choked condition.
X_r	Sonic velocity ratio of exhaust to release.
z	Axial length.
α	Crank angle.
θ	Intermediate variable.
φ	Intake angle.
ρ	Density.

τ_b	Blowdown period.
τ_s	Scavenge period.

Section 4.3

b	Jet width.
e	Specific total internal energy.
$e^{m.l}$	Specific total internal energy in the l-th zone within region m.
F_o	Initial injected momentum flux.
$F_o^{m.l}$	Initial injected momentum flux for the l-th zone within region m.
G_z	Axial flux of linear momentum.
G_θ	Axial flux of angular momentum.
$h_{in}^{m.l}$	Specific absolute enthalpy flowing into the l-th zone with region m.
$h_{out}^{m.l}$	Specific absolute enthalpy flowing out of the l-th zone with region m.
$m^{m.l}$	Mass for the l-th zone within region m.
$m_a^{m.l}$	Air mass for the l-th zone within region m.
$m_g^{m.l}$	Residual gas mass for the l-th zone within region m.
$m_{in}^{m.l}$	Mass flowing into the l-th zone within region m.
$m_{out}^{m.l}$	Mass flowing out of the l-th zone within region m.
$m_f^{m.l}$	Mass of burnt fuel in the l-th zone within region m.
$m_{f.in}^{m.l}$	Mass of burnt fuel flowing into the l-th zone within region m.
$m_{f.o}^{m.l}$	Mass of burnt fuel in the l-th zone within region m at the beginning of the scavenging process.
$m_{f.out}^{m.l}$	Mass of burnt fuel flowing out of the l-th zone within region m.
$m_s^{m.l}$	Mass of the air mass trapped and the air mass cosumed in combustion of the burnt fuel in the l-th zone within region m.
$m_{s.in}^{m.l}$	Mass of the air mass trapped and the air mass cosumed in combustion of the burnt fuel flowing into the l-th zone within region m.
$m_{s.o}^{m.l}$	Mass of the air mass trapped and the air mass cosumed in combustion of the burnt fuel in the l-th zone within

region m at the beginning of the scavenging process.

$m^{m.l}_{s.out}$ Mass of the air mass trapped and the air mass cosumed in combustion of the burnt fuel flowing out of the l-th zone within region m.

$\dot{m}_c$ Effective convection mass flow rate.

n Normal to the main flow.

$Q^{m.l}$ Heat transfer from the l-th zone within region m.

S_z Initial swirl rate.

r Radius.

U Radial velocity, velocity of the main flow.

U_o Initial velocity at the input ports.

V Tangential velocity.

$V^{m.l}$ Volume of the l-th zone within region m.

$v^{m.l}$ Tangential velocity of the l-th zone within region m.

$v^{m.l}_{in}$ Tangential velocity flowing into the l-th zone within region m.

$v^{m.l}_{out}$ Tangential velocity flowing out of the l-th zone within region m.

W Axial velocity.

$w^{m.l}$ Axial velocity of the l-th zone within region m.

$w^{m.l}_{in}$ Axial velocity flowing into the l-th zone within region m.

$w^{m.l}_{out}$ Axial velocity flowing out of the l-th zone within region m.

ϵ Eddy diffusivity.

ϵ_{rz} rz- eddy diffusivity.

$\epsilon_{r\theta}$ rθ- eddy diffusivity.

θ Tangential direction.

ρ_o Initial density at the inlet ports.

ρ_s Density of the surrounding fluid.

Chapter 5

c Constant.

l_m Mixing length.

U Mean velocity.

ϵ Turbulence dissipation rate.

κ Turbulence kinetic energy.

C_{in}	OH concentration of the mass retained in the tank.
C_j	OH concentration of the mass injected.
C_{ja}	Air mass fraction concentration in the residual gas region in the jetting region.
C_{out}	OH concentration of the mass discharged from the tank.
C_r	OH concentration of the residual mass.
C_{ra}	Air mass fraction concentration in the residual gas region in the residual gas region.
D	Mass diffusivity.
e	Specific total internal energy.
Ec	Eckert number.
Eu	Euler number.
Fr	Froude number.
h	Specific absolute enthalpy.
j_n	Material diffusion flux.
L	Length.
L_c	Engine characteristic length.
L_m	Model characteristic length.
m_{in}	Mass retained in the tank.
m_j	Injected mass.
$m_{j.in}$	Injected mass retained in the tank.
$m_{j.out}$	Injected mass discharged from the tank.
m_{out}	Mass discharged from the tank.
m_r	Initial residual mass.
$m_{r.in}$	Residual mass retained in the tank.
$m_{r.out}$	Residual mass discharged from the tank.
PH	PH value.
POH	POH value.
Pr	Prandtl number.
q_n	Heat diffusion flux.
Re	Reynolds number.
R_l	Length scaling factor.
R_t	Time scaling factor.
R_u	Velocity scaling factor.
S	Control surface area.
Sc	Schmidt number.

Sr	Strouhal number.
t	Process time.
T_e	Engine characteristic time.
T_m	Model characteristic time.
U	Convective velocity.
u	Specific internal energy.
U_e	Engine characteristic velocity.
U_m	Model characteristic velocity.
V	Volume.
v	Moving velocity of the control surface.
W	Model width.
α	Thermal diffusivity.
δ	Model thickness.
δ_n	Normally directed vector.
κ	Thermal conductivity.
μ	Dynamic viscosity.
ν	Kinematic viscosity.
τ_n	Momentum diffusion flux.

Chapter 7

A	Constant.
a_1	Constant.
a_2	Constant.
a_3	Constant.
B	Constant.
C	Constant.
C_{d1}	Shape parameter of diffusion burning.
C_{d2}	Shape parameter of diffusion burning.
C_{p1}	Shape parameter of premix burning.
C_{p2}	Shape parameter of premix burning.
K	Constant.
m_a	Accumulated fuel mass.
M_d	Non-dimensionalized fuel mass in the diffusion burning.
m_d	Fuel mass in the diffusion burning.
M_f	Fuel mass supplied to engine per minute.
M_p	Non-dimensionalized fuel mass in the premix burning.
m_p	Fuel mass in the premix burning.

M_t	Non-dimensionalized total injected fuel mass.
m_t	Total injected fuel mass.
n	Polytropic exponent.
N_o	Reference engine speed.
P_m	Mean cylinder pressure.
P_{max}	Maximum cylinder pressure.
Q_{12}	Heat release.
r_c	Boost pressure ratio.
V_p	Mean piston velocity.
W_{12}	Work.
β	Ratio of premixed burnt fuel mass to total.
Δ	Burning duration.
δ	Ignition delay.
ΔU_{12}	Difference of internal energy.
θ_i	Ignition time.
τ	Non-dimensionalized time.

Chapter 8

DHI	Degree of heat insulation.
fmep	Friction mean effective pressure.
$h_{ad\ c}$	Compressor isentropic enthalpy rise.
N	Rotational speed.
W_c	Compressor power.
η_c	Compressor efficiency.

Chapter 9

D	Compressor tip diameter.
f_a	Sectional area scaling factor.
f_d	Diameter scaling factor.
f_m	Mass flow scaling factor.
W_c	Compressor power.
W_e	Engine power.
$W_{gear\ loss}$	Power loss to gear train.
$W_{o/s}$	Output shaft power.
W_t	Turbine power.
θ_o	Dynamic loss ratio.

τ_f	Friction torque.
τ_{in}	Input torque.
τ_{out}	Output torque.
ω_{in}	Angular velocity of the input shaft.
ω_{out}	Angular velocity of the output shaft.

Part 1 GENERAL

Chapter 1 INTRODUCTION

1.1 CENTRAL TOPICS OF THIS THESIS

For a power system with an internal combustion engine as motive power, increasing power at the output shaft implies an increase of air-taking capacity and improvement of output shaft brake thermal efficiency.

Without increasing engine size, three ways are open materially to increase air-taking capacity:

(1). increasing engine speed.
(2). supercharging and intercooling.
(3). using the two-stroke cycle principle.

Improving output shaft brake thermal efficiency implies

(4). improving the combustion process.
(5). reducing the friction and accesories' loss.
(6). suppressing the cooling loss.
(7). regenerating the lost energy.
(8). matching the engine and transmission.

It is notable that in item (6), when the engine is thermally insulated, the heat prevented from being transferred to the coolant will appear mainly in the exhaust gases.

This thesis focuses attention on the characteristics of the high output two-stroke diesel engines, i.e. the following topics:

(1). scavenging,
(2). supercharging
and
(3). compounding a two-stroke engine power system.

1.2 SCAVENGING

1.2.1 TWO-STROKE CYCLE

The two-stroke cycle requires one revolution of the crankshaft for each power stroke. From the standpoint of thermodynamics, compared with the four-stroke cycle, it allows doubling the output from the same size of engine by doubling the number of power strokes. The two-stroke cycle is applicable to both compression-ignition operation and spark-ignition operation. However, the scope of this thesis is limited within the former. From the standpoint of mechanical design, it makes some simplification of valve mechanism possible. The largest reciprocating-piston engines (up to 43000 bhp) and the smallest engines (down to 0.02 bhp) follow the two-stroke cycle. Many medium sized engines where weight or space is at a premium, use the two-stroke cycle principle.

In a four-stroke cycle engine the charge is drawn into the cylinder by the piston. In a two-stroke engine there is no suction stroke and the charge must be pressed into the cylinder by a pump or blower. The operation of clearing the cylinder of exhaust gases and filling it more or less completely with fresh charge is called **scavenging**. [1.1]

1.2.2 SCAVENGING PROCESS

The scavenging process may be subdivided into three periods:

(1). the **blowdown period** in which the exhaust ports or valve are opened, the products of combustion pass to the exhaust manifold, and the cylinder pressure falls rapidly. The **blowdown angle** is defined as the crank angle from exhaust port opening to the point at which the cylinder pressure equals the pressure in the inlet manifold, that is, to the beginning of inflow of air into the cylinder. In an ideal design when the cylinder pressure equals the air supply pressure, the inlet ports open. Actually, the inlet ports open probably earlier or later than the ideal point.

(2). the **scavenge period** in which both the exhaust and inlet ports or valve(s) are open, fresh air charge flows into the cylinder and residual gas is discharged from the cylinder. The scavenge period continues as long as the inlet ports are open, and the total pressure in the inlet manifold exceeds the pressure in the cylinder, and the cylinder pressure is greater than the total pressure in the exhaust manifold.

(3). the **charging period** in which the exhaust ports close before or after the inlet ports are closed. If the exhaust ports close first, there is a better chance for the cylinder pressure to build up to a value higher than the exhaust pressure during the subsequent period before the inlet ports close. If the inlet ports close first, there may be some escape of fresh air charge to the exhaust system.

1.2.3 FUNDAMENTAL REQUIREMENTS OF SCAVENGING SYSTEM

(1) **economy**: The power taken from the the engine and used for compressing the scavenging air must not be excessive, that is, the pressure drop between the inlet and exhaust ports and the air flow rate must not be excessive.
(2) **reliability**: The operation must repeat stably even under unfavourable running conditions caused by fouling of the inlet and exhaust ports, deteriorating sealing of the inlet and exhaust ports, or accidental reduction of the air supply. The scavenging system must be resistant to fouling especially when the engine operates on poor quality fuel.

1.2.4 METHODS OF SCAVENGING

1.2.4.1 Cross scavenging

The air enters the cylinder through the inlet ports directed off centre, this produces an upward movement of the air which forces the exhaust gases to travel in a U-shaped path, i.e. to form a cross flow. In the cross-scavenging engine the inlet ports and the exhaust ports are on opposite sides of the cylinder liner, as shown in Fig. 1.1a.

1.2.4.2 Loop scavenging

In this case the air stream is directed on to the unported wall and the gas stream follows an O-shaped, i.e. a loop path. This system can be divided into two groups:

(1) with exhaust ports located above the inlet ports as in the MAN system, as shown in Fig. 1.1b;
(2) with exhaust ports located between two groups of inlet ports as in the

Schnuerle system, as shown in Fig. 1.1c.

1.2.4.3 Uniflow scavenging

The air enters the cylinder from one end and leaves it from the opposite end, normally with intake swirl to improve the scavenging quality. This system also can be subdivided into two groups:

(1) with inlet or exhaust valve(s) fitted in the cylinder head, as shown in Figs. 1.1d and e;
(2) with opposed pistons to control respectively the inlet and exhaust ports, as shown in Fig. 1.1f.

1.2.5 COMPARISON OF DIFFERENT SCAVENGING SYSTEMS

1.2.5.1 Cross scavenging

This may give higher output per unit weight and bulk because the cross scavenged engine without valve-camshaft mechanism can run at higher piston speeds. But its scavenging efficiency is comparatively low because too early short-circuiting of fresh mixture is difficult to avoid completely. Although much work remains to be done in this field, the following general relations seem to be established.

With cross scavenging system, it is necessary to direct the incoming air so that it follows an axial path close to the inlet side of the cylinder wall on its way toward the cylinder head. This objective can be accomplished either by a properly designed deflector on the piston or by inlet ports designed to direct the air toward the side of the cylinder away from the exhaust ports.

With supercharging, and at high piston speeds this system can obtain high specific output.

1.2.5.2 Loop scavenging

The scavenging efficiency of such system is good. One obvious disadvantage of this system is the limitation on port area. However, for long-stroke engines operating at low piston speeds, this arrangement has

proved satisfactory.

The addition of auxiliary valves gives the advantages of unsymmetrical timing to loop-scavenging cylinders. At present, the commercial use of these devices is confined to large cylinder running at low piston speeds.

1.2.5.3 Uniflow scavenging

Uniflow scavenging with opposed pistons

Both excellent scavenging efficiency and high flow capacity cause engines of this type to obtain high mean effective pressures. Here, the problem is to decide whether the increased specific output outweighs the disadvantage of the required complicated mechanical arrangement. When high specific output is important, this system is very attractive and quite widely used in locomotive and submarine engines. Incidentally, the only successful diesel aircraft engine holds the world's record for specific output of diesel engines.

Uniflow scavenging with poppet-valve

This system shows excellent performance. Hence, again, the gain in specific output may not mean a gain in output per unit of bulk and weight, especially if speed is limited by the poppet valve gear.

1.2.6 BASIC DEFINITIONS IN THE SCAVENGING PROCESS

Trapped volume: it is the cylinder volume at the commencement of the compression stroke.

Delivery ratio:

$$\lambda = \frac{\text{Mass of delivered air}}{\text{Trapped volume} \cdot \text{density in inlet manifold}} \qquad (1.1)$$

Scavenging ratio:

$$\lambda_{sc} = \frac{\text{Mass of delivered air}}{\text{Mass of trapped cylinder charge}} \qquad (1.2)$$

Trapping efficiency:

$$\eta_{tr} = \frac{\text{Mass of delivered air retained}}{\text{Mass of delivered air}} \qquad (1.3)$$

Charging efficiency:

$$\eta_{ch} = \frac{\text{Mass of delivered air retained}}{\text{Trapped volume} \cdot \text{density in inlet manifold}} \qquad (1.4)$$

Scavenging efficiency:

$$\eta_{sc} = \frac{\text{Mass of delivered air retained}}{\text{Mass of trapped cylinder charge}} \qquad (1.5)$$

Relative charge:

$$r_{ch} = \frac{\text{Mass of trapped cylinder charge}}{\text{Trapped volume} \cdot \text{density in inlet manifold}} \qquad (1.6)$$

Purity:

$$r_{pu} = \frac{\text{Mass of air in trapped cylinder charge}}{\text{Mass of trapped cylinder charge}} \qquad (1.7)$$

It is obvious that the following equations are valid.

$$\eta_{ch} = \lambda \cdot \eta_{tr} \qquad (1.8)$$

$$\eta_{sc} = \lambda_{sc} \cdot \eta_{tr} \qquad (1.9)$$

$$r_{ch} = \frac{\lambda}{\lambda_{sc}} = \frac{\eta_{ch}}{\eta_{sc}} \qquad (1.10)$$

From the previous equations, it is evident that the two groups of parameters:

(1) delivery ratio and charging efficiency,
(2) scavenging ratio and scavenging efficiency

are distinguished by the different reference conditions. The former is related to the inlet manifold conditions, the latter is related to the trapped conditions in the cylinder. The relative charge gives a connection of these two groups of parameters.

The purity indicates the total air content trapped in the cylinder including the fresh air trapped in the cylinder and the remaining air in the cylinder from the residual gas in the previous cycle.

1.3 SUPERCHARGING

1.3.1 NECESSITY OF SUPERCHARGING

In a certain sense, practically all two-stroke engines are supercharged. Instead of aspirating ambient air, it is forced into the cylinder by a pump or blower. However, the amount of air so forced into the cylinder does not exceed the amount which the same cylinder receives under the air density at the temperature in the inlet manifold and the trapped pressure in the cylinder. It is evident that the trapped pressure is between the pressures in the inlet and exhaust manifolds. If the pressure in the exhaust manifold is atmospheric, even if the amount of air so delivered exceeds the cylinder displacement by 30 to 50 per cent, nevertheless, most of that extra air is short-circuited between the inlet and exhaust ports. The power required to scavenge, and hence the fuel consumption, increases rapidly with increasing delivery ratio. An optimum point may be reached at which net power output reaches a peak. Therefore, the only feasible way to achieve

large gains in output is by increasing the exhaust pressure and the inlet pressure together. [1.2], [1.3]

The necessity for increasing exhaust pressure immediately suggests the use of an restriction in the exhaust system. The restriction may be either passive or active, or their combination.

Passive exhaust restriction is purely a restriction which produces a pressure drop between the exhaust ports and the surroundings and extracts no exhaust energy.

Active exhaust restriction is a device which not only constitutes a flow resistance in the exhaust system but also recovers the useful energy of exhaust gas.

1.3.2 PASSIVE EXHAUST RESTRICTION AND PURELY ENGINE-DRIVEN SUPERCHARGER

Passive exhaust restrictions are further classified into several types:

(1). port-scavenging with short exhaust ports, see Fig. 1.2a.
(2). port-scavenging with a rotating sleeve valve in the exhaust ports, see Fig. 1.2b.
(3). port-scavenging with opposed-piston, see Fig. 1.2c.
(4). U-cylinder with one piston controlling the inlet ports and the other controlling the exhaust ports, see Fig. 1.2d.
(5). with exhaust valves, see Fig. 1.2e.
(6). with sleeve valve, see Fig. 1.2f.

Passive exhaust restrictions are used only for building up a proper back pressure to improve the trapping effectiveness of the scavenging air, and hence to increase output power, not for recovering the useful work from exhaust of the base engine. Therefore, the engine is the only source of motive power in the power system with such a passive exhaust restriction, and the compressor must be driven by the engine.

The following two types of compressor can be used as a supercharger.

(1). positive displacement compressors such as multi-vaned compressor. Roots compressor. Lysholm compressor. screw compressor. VW scroll compressor. [1.4] KKK wankel system rotary compressor. [1.5] see Fig. 1.3a to f.
(2). turbodynamic compressor such as centrifugal compressor. see Fig. 1.3g.

The positive displacement compressors have steep constant speed lines. The pressure ratio is largely independent of speed. The flow rate is directly proportional to speed and quite independent of pressure ratio. The displacement compressors have no choke. no surge. can run over a wide range. and obtain a large pressure ratio with small flow rate. They have a good efficiency.

The turbocompressors have constant speed lines with a variable slope: for centrifugal compressor they are practically level at the surge line. but drop off rapidly. The pressure ratio is dependent of speed. The flow rate is proportional to speed. In the performance maps. there exist a surge region in the left. Therefore. they cannot run stably with small flow and high pressure ratio. They can obtain an excellent efficiency at high speed. The difficulty in using a centrifugal supercharger arises from the very high shaft speed at which it must operate. A gear train with a large step-up ratio is necessary. and this makes the simple and cheap centrifugal supercharger expensive.

1.4 TURBOCHARGED. SUPERCHARGED AND COMPOUNDED SYSTEMS

1.4.1 ACTIVE EXHAUST RESTRICTION AND ENGINE COMPOUNDING SYSTEM

Active exhaust-restrictions may further be classified into two groups:

(1). **direct recovery**

The exhaust gases of the base engine are expanded in a device.

(a) exhaust-driven turbine
The exhaust turbine extracts the useful work of exhaust gases to drive a compressor or to feed to the output shaft of the power system.

(b) exhaust-driven Comprex pressure-wave supercharger
The exhaust gases expand in the Comprex supercharger to boost the inflowing air charge. [1.6]

(2). **Indirect recovery**

The exhaust energy of the base engine is used as a heat source for a separate closed system of a continuous heat engine, for instance, a Rankine bottoming cycle heat engine to return the useful work as mechanical power to the output shaft of the power plant.

The introduction of an active exhaust restriction device gives the power system another source of motive power. The crucial task is to organise the mechanical, pneumatic and thermal connections and to improve performance.

1.4.2 BASIC REQUIREMENTS FOR AUTOMOTIVE ENGINE SYSTEMS

(1). **efficiency**: better fuel economy throughout the complete range of engine speed.
(2). **driveability**: wide operating range of speed and load and sufficient torque backup, hence better acceleration and fast responsiveness to an increase in power demand without noticeable delay.
(3). **compactness**: small space requirements and low weight.

1.4.3 PROBLEMS IN TWO-STROKE ENGINE COMPOUNDING SYSTEM

1.4.3.1 Reliability and durability

High output means considerably higher mechanical and thermal loadings, which often give rise to reliability and durability concerns. Especially thermally insulated engines further aggravate the problem of thermal loading on the elements of the combustion chamber and turbocharger. Port-scavenging systems provide greater freedom in the combustion chamber. The combustion chamber may be easily placed in the cylinder head. This relieves the thermal loading on the piston.

1.4.3.2 Matching

Compared with four-stroke engines, the matching problem of a two-stroke engine system is aggravated by its special characteristics. Two-stroke engines require more scavenging air. But more scavenging air implies lower exhaust temperature because of dilution of exhaust gases with short-circuited air, which causes a decrease in the exhaust energy available to drive the turbine.

In the two-stroke engine the charging of the cylinder requires a positive pressure drop between the inlet and exhaust ports throughout a wide speed range.

Hence, substantial difficulties have been encountered in matching the thermodynamic and fluid dynamic characteristics of the supercharger with those of the two-stroke engine. Low speed torque and transient response have therefore tended to be poor, the inadequacies becoming more pronounced with power-rating increase, and incidentally setting severe limitation on transmission optimization.

1.4.4 TURBOCHARGING SCHEMES

The turbocharged engine is the simplest engine system for improving the thermal efficiency and increasing the power output. However, the engine-turbocharger aggregate comprises a relatively slow speed reciprocating engine and an ultra high speed turbomachine. The former operates cyclically, thus resulting in pulsating flows in the inlet and exhaust manifolds, and the latter ideally requires the flow conditions to be steady. Matching the two machines to satisfy the performance requirements over a wide range is difficult, especially such problems as the turbocharger inefficiency at low engine speeds and the inadequate flow range continue to arouse concern.

For improving the low speed torque, the following measures have been proposed.

(1). supplementing the exhaust gas energy by external means, e.g. pelton wheel drive suggested by Timoney [1.7] or air injection proposed by Ledger et al. [1.8], see Fig. 1.4a, b.
(2). efficient use of exhaust energy, e.g. with the divided entry

turbines [1.9] or a pulse converter. [1.10], see Fig. 1.4c, d, e.
(3). the use of a waste gate to limit turbocharger speed and boost pressure at high engine speeds and to achieve an increase boost pressure at low engine speeds, see Fig. 1.4f.

For tailoring the turbocharger performance characteristics to suit a wide range of flow rate, the following methods have been suggested.

(1). variable geometry compressor with a continuously variable vaned diffuser [1.11] or inlet guide vanes [1.12], see Fig. 1.5a, b. By rotating the vanes, the variable vaned diffuser can accommodate the change of flow angle due to variation of flow rate, thus decreasing the incidence loss and improving the diffusion process. By increasing the inlet vane angle in the direction from negative to positive pre-whirl, the mass flow rate and pressure ratio at constant compressor speed are reduced. The surge line shifts quite significantly to the left. The efficiency contours have the same tilting tendency as that of varying flow rate. Thus, it seems possible that the optimum compressor efficiency can be maintained over a wide flow range.

(2). variable geometry turbine with a pivoting vane system [1.13] or a variable area volute [1.14], see Fig. 1.5c, d. By varying blade angle with speed or mass flow rate, both the effective turbine area and rotor inlet gas angle may be controlled. In particular, the effect of turbine area control improves utilization of the exhaust gas energy by the turbine at low engine speed, without over-speeding the turbocharger or over-boosting the engine at high engine speed, by increasing effective turbine area under these conditions.

(3). sequential turbocharging. By fitting two or three turbochargers in parallel on a common exhaust manifold, the system can be considered as a variable geometry turbocharger in discrete steps, [1.15] see Fig. 1.5e. At rated conditions all are in operation, but with decrease of speed one and then two turbochargers are cut-out by closing appropriate valves. In effect this reduces the total turbine area, hence raises the turbine (and therefore compressor) pressure ratio at low engine speed.

1.4.5 ENGINE SYSTEM SCHEMES

The inherent difficulties in matching and sizing make simple addition of a supercharger to an engine impossible if the best performance throughout the speed and load range is to be obtained. Hence numerous compound engine systems have been developed. To further improve the performance, some compound engine systems introduce extra external energy sources, for example, a combustor in the Hyperbar supercharging system [1.16] and a battery electric motor in the engine-electric hybrid vehicles by JPL [1.17]. Some compound engine systems are listed as follows.

(1). conventional turbocharged engine with a conventional turbocharger, and with or without auxiliary blower, see Fig. 1.6a.
(2). conventional supercharged engine with a Comprex supercharger, see Fig. 1.6b.
(3). Cummins positive displacement compound system with a positive displacement expander and a compressor, see Fig. 1.6c, [1.18]
(4). Cummins turbocompound engine with an exhaust power turbine, see Fig. 1.6d, [1.19]
(5). BBC integrated power system with a power turbine operating in parallel with a turbocharger, see Fig. 1.6e, [1.20]
(6). conventional turbocharged engine with a hydrostatic shunt transmission, see Fig. 1.6f, [1.21]
(7). Hyperbar supercharging system with an auxiliary combustor, see Fig. 1.6g,
(8). JPL engine-electric hybrid system, see Fig. 1.6h,
(9). Rankine cycle compound engine system, see Fig. 1.6i, [1.22]
(10). Perkins differentially supercharged engine with a 3 speed transmission, see Fig. 1.6j, [1.23]
(11). Wallace's differential compound engine without transmission gear box, see Fig. 1.6k. [1.24]

Thus while the main attention in recent years has focussed on four-stroke engines, Wallace earlier built a differential compound two-stroke engine. [1.25]

1.4.6 WALLACE'S DIFFERENTIAL COMPOUND ENGINE (DCE)

The Wallace DCE mechanical arrangement is shown in Fig. 1.7. The engine is connected with the fully floating epicyclic gear train providing the

differential link between output shaft and compressor, such that any decrease in output shaft speed, at fixed engine speed, is accompanied by a corresponding increase in compressor speed and hence compressor mass flow delivery. This in turn leads to extremely favourable air margins for both low speed torque and good transient response under low output shaft speed conditions. The geared power turbine provides additional torque backup, further amplified greatly by the use of the turbine continuously variable transmission (CVT) which allows the turbine to operate at optimum speed. The turbine variable nozzles are a means of both limiting boost pressure under low output shaft speed conditions and ensuring optimum efficiency under all conditions.

A microprocessor control is implemented to ensure operation within safe limits of all parameters and for rapid transient conditions.

The unique feature of the DCE is its ability to feed power to, rather than absorb power from, the engine due to the compound mode of operation, with resultant efficiency benefits, particularly when coupled with adiabatic or semi-adiabatic operation.

The DCE can legitimately be regarded as the logical embodiment in a single powertrain, of the advances made in the separate fields of engine, transmission, turbomachinery and microprocessor control technology. The DCE combines the thermodynamic advantage of compounding, so far at the expense of considerably higher complication and capital cost, with the smooth torque rise and good transient response associated with the best CVT, and through continuous optimization using a microprocessor control system, with outstanding overall economy. [1.26]

It is obvious that the substitution of a two-stroke engine will add the advantage of compactness to the DCE.

1.5 SUMMARY

The task of the author is to work for the investigation and development of high output two-stroke diesel engines. Hence the central topics of this thesis are scavenging, supercharging and compounding in two-stroke diesel engines with special reference to the differential compound engine.

REFERENCES

[1.1] P.H. Schweitzer
"Scavenging of Two-Stroke Cycle Diesel Engines"
The Macmillan Press, 1949

[1.2] K. Zinner
"Supercharging of Internal Combustion Engines"
Springer-Verlag, 1978

[1.3] N. Watson and M.S. Janota
"Turbocharging the Internal Combustion Engine"
The Macmillan Press, 1982

[1.4] K.D. Emmenthal, C. Muller and O. Schafer
"Verdrangerlader fur Volkswagen-Motoren"
MTZ, Vol. 46, No. 9, 1985

[1.5] A. Bahr
"Der KKK-Ro-Lader"
MTZ, Vol. 47, No7/8, 1986

[1.6] A. Wunsch
"Aufladung von Fahrzeug-Dieselmotoren mit Abgasturbolader und mit der Druckwellenmaschine Comprex"
MTZ 31 pp 17-23, 1970

[1.7] S.G. Timoney
"A New Concept in Traction Power Plants"
Proc. Instn. Mech. Engrs., Vol. 180, Pt 2A, No. 3, pp.69-82, 1965-66

[1.8] J.D. Ledger, R.S. Benson and N. Furukawa
"Performance Characteristics of a Centrifugal Compressor with Air Injection"
Proc. Instn. Mech. Engrs., Vol. 187, 1973

[1.9] F. Pischinger and A. Wunsch

"The Characteristic Behaviour of Radial Turbines and its Influence on the Turbocharging Process"
Proc. CIMAC, 1977

[1.10] E. Meier
"The Application of Pulse Converters to Four-Stroke Engines with Exhaust gas Turbocharging"
Brown Boveri Rev., vol 55, no. 8, 1968

[1.11] A. Whitfield, F.J. Wallace and R.C. Atkey
"The Effect of Variable Geometry on the Operating Range and Surge Margin of a Centrifugal Compressor"
ASME, 76-GT-98, 1976

[1.12] C. Rodgers
"The Performance of Centrifugal Compressor Channel Diffusers"
ASME, 82-GT-10, 1982

[1.13] J.R. Arvin and N.L. Osborn
"Design features and Operating Experiences of the Aerodyne Dallas VATN Turbocharger"
SAE 830013, 1983

[1.14] R.M. Chapple, P.F. Flynn and J.M. Mulloy
"Aerodynamic Design of Fixed and Variable Geometry Nozzle Turbine Casings"
ASME, Jl. Eng. Power, Vol. 102, Jan. 1980

[1.15] P. Tholen and I. Kilimann
"Investigations on Highly Turbocharged Air-Cooled Diesel Engine"
ASME, 77-DGP-11, 1977

[1.16] J. Melchior and T. Andre-Talamon
"Hyperbar System of High Super-Charging"
SAE 740723, 1974

[1.17] J.J. Sandberg
"Hybrid Vehicles - Costs and Potential"

SAE 8100271, 1981

[1.18] R. Kamo, L. Tozzi and R.Sekar
"Light Duty Vehicle Diesel Engine Assessment Program - Passenger Car Diesel Engine of the Future"
SAE Publication 120, 1983

[1.19] M.C. Brands, J.R. Werner, J.L. Hoehne and S. Kramer
"Vehicle Testing of Cummins Turbocompound Diesel Engine"
SAE 810073, 1981

[1.20] R. Chellini
"Power Turbine on Large Diesel Save 3 % Fuel Consumption"
Diesel and Gas Turbine Worldwide, May, 1986

[1.21] D.E. Bowns and K.E. Edge
"The Optimization of Four-Stroke Diesel Engine Hydrostatic Systems"
<Land Transport Engines - Economics versus Environment>
IMechE Conference , paper 21/77, 1977

[1.22] I. Williamson
"Truck Engines - the Future ?"
Leyland Technology Seminar, 1982

[1.23] J.G. Dawson, W.J. Hayward and P.W. Glamann
"Some Experiences with a Differentially Supercharged Diesel Engine"
Proc. Instn. Mech. Engrs. Vol. 178 part 2A No.6, 1963-64

[1.24] F.J. Wallace
"The Differential Compound Engine"
SAE 670110, 1967

[1.25] F.J. Wallace
"Operating Characteristics of Compound Engine Schemes for Traction Purposes Based on Opposed Piston Two Stroke Engines and Differential Gearing"
Proc. Instn. Mech. Engrs. P2(b)/63, 1963

[1.26] F.J. Wallace and R.M. Kimber

"Optimization of the Differential Compound Engine Using Microprocessor Control"

SAE 810256, 1981

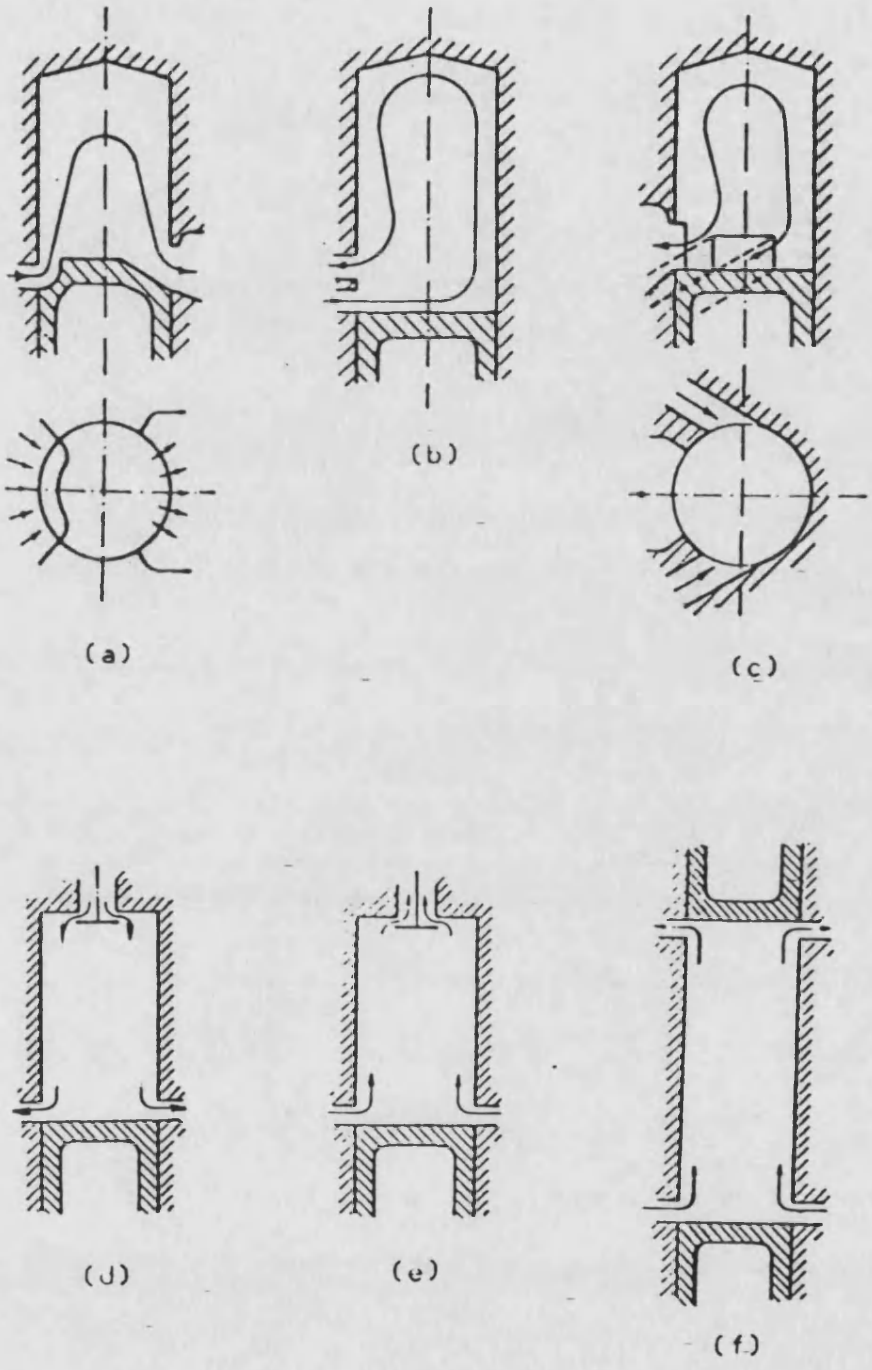

(a). cross scavenging;
(b). loop scavenging, MAN type;
(c). loop scavenging, Schnuerle type;
(d). uniflow scavenging, poppet inlet valve;
(e). uniflow scavenging, poppet exhaust valve;
(f). uniflow scavenging, opposed piston.

Fig. 1.1 Methods of Scavenging

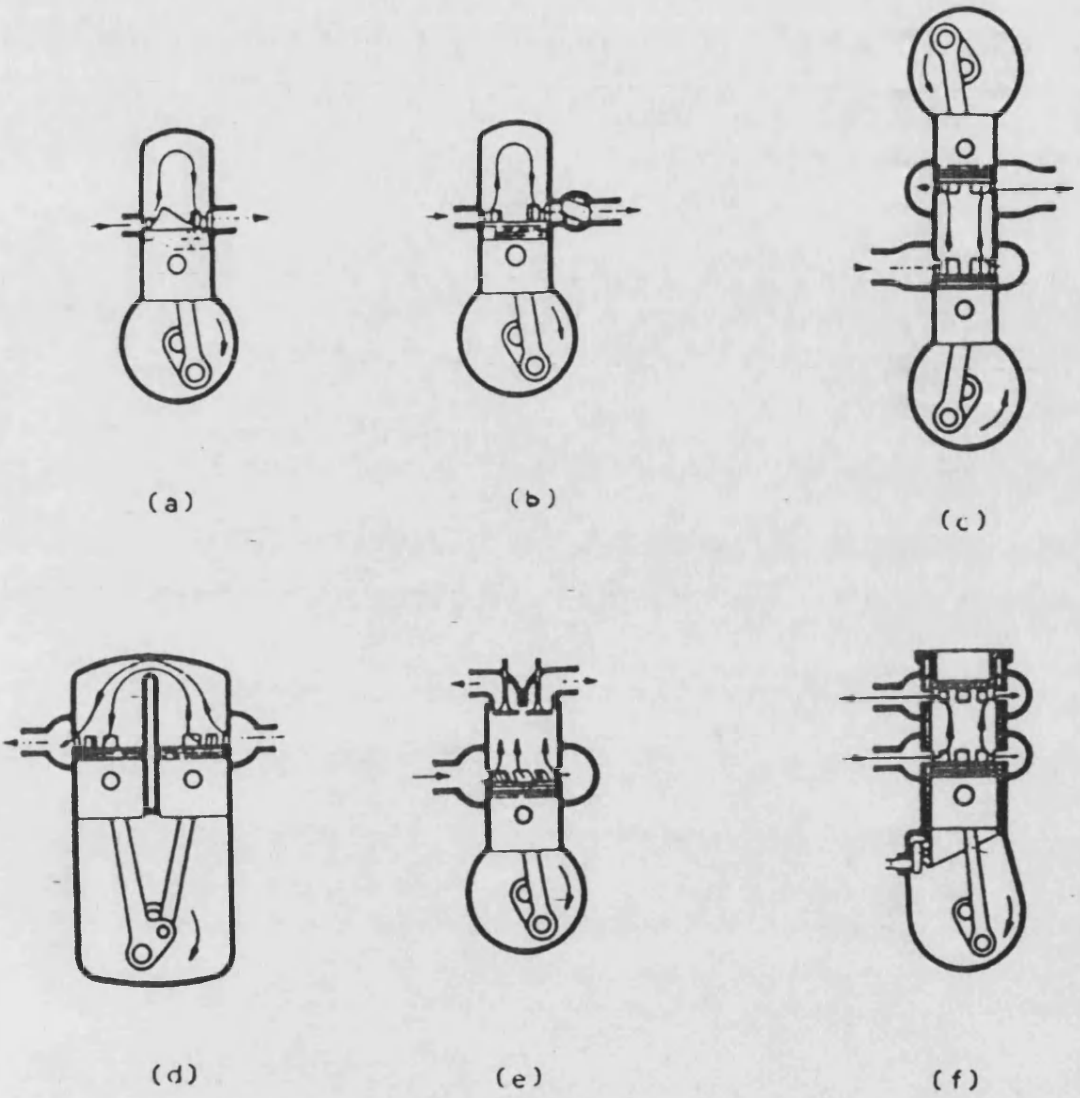

(a). port-scavenging with short exhaust ports,
(b). port-scavenging with a rotating sleeve valve
in the exhaust ports,
(c). port-scavenging with opposed-piston,
(d). U-cylinder with one piston controlling the inlet ports
and the other controlling the exhaust ports,
(e). with exhaust valves,
(f). with sleeve valve.

Fig. 1.2 Passive Exhaust Restrictions

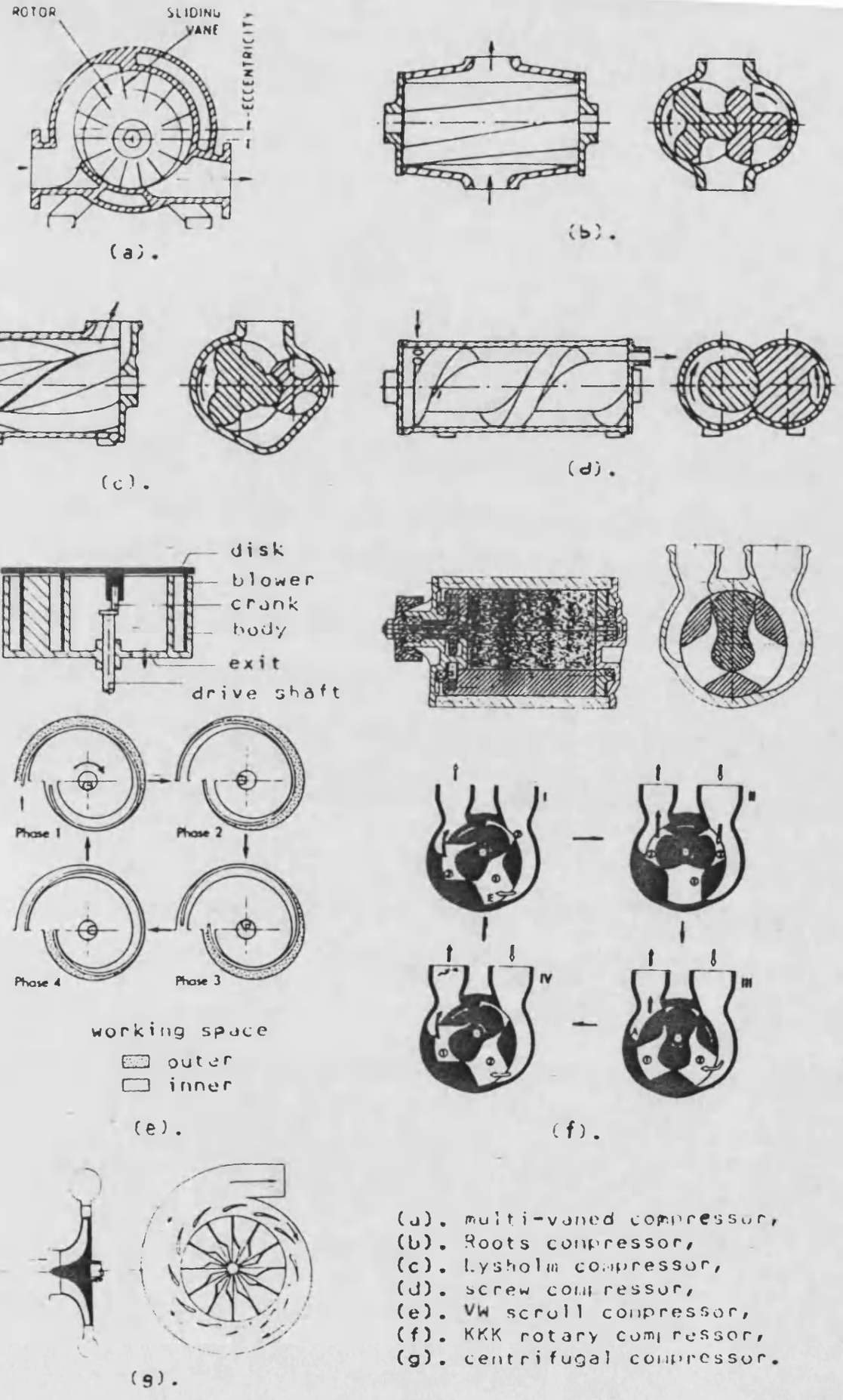

Fig. 1.3 Supercharging Compressors

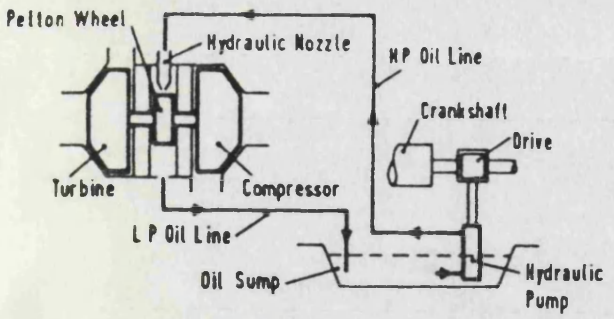

(a).

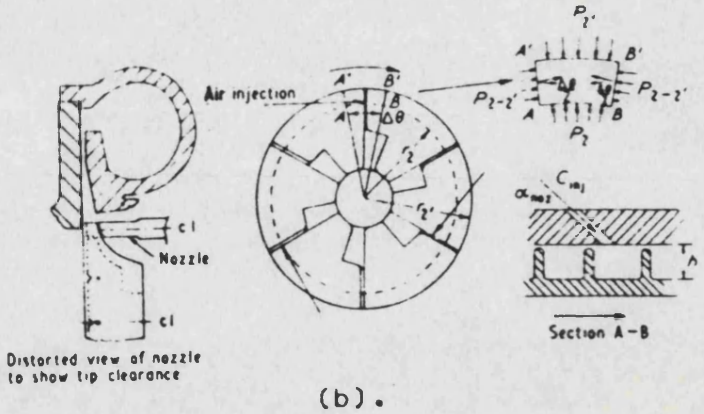

(b).

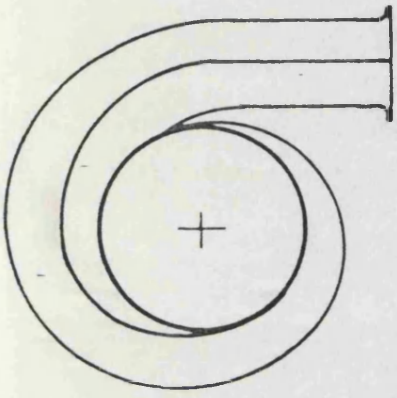

(c).

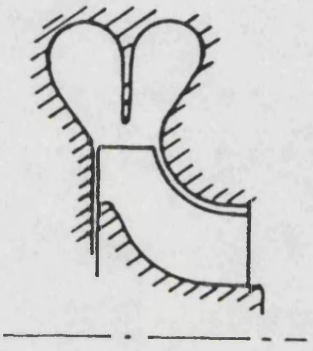

(d).

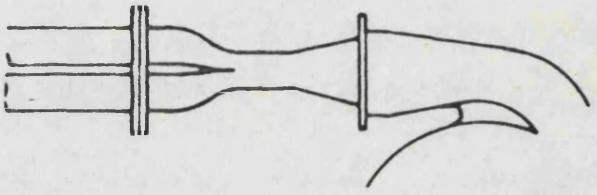

(e).

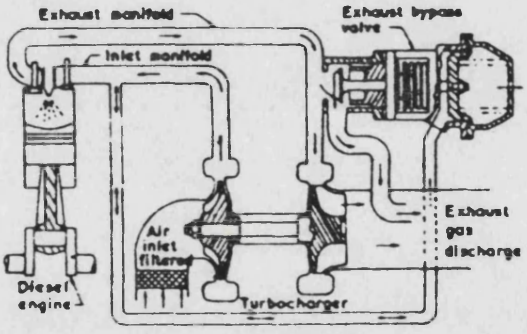

(f).

(a). pelton wheel drive,
(b). air injection,
(c). circumferentially divided entry turbine,
(d). meridionally divided entry turbine,
(e). pulse converter,
(f). waste gate.

Fig. 1.4 Various Moassures for Improving Low Speed Torque

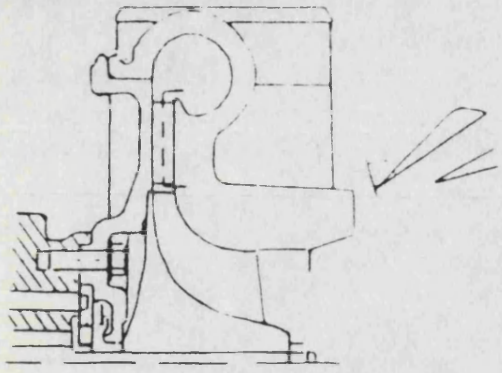

(a).

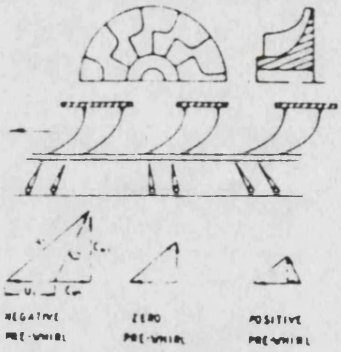

(b).

(c).

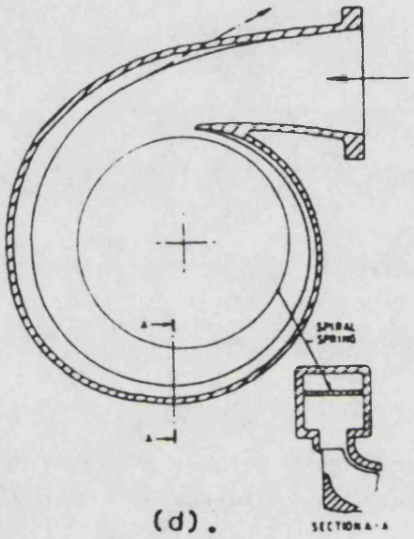

(d).

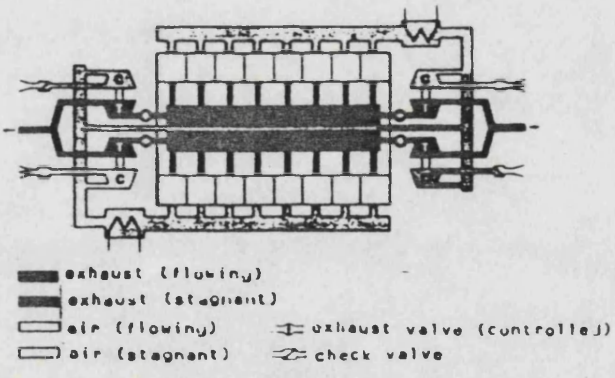

(e).

(a). compressor with variable vaned diffuser,
(b). compressor with variable inlet guide vanes,
(c). turbine with a pivoting vane system,
(d). turbine with a variable area volute,
(e). sequential turbocharging.

Fig. 1.5 Variable Geometry Turbochargers

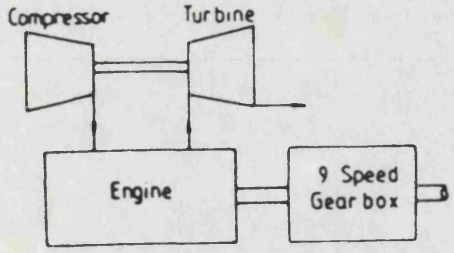

(a)

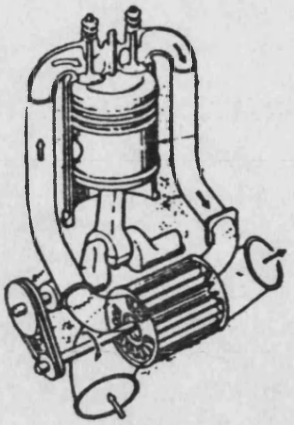

(b)

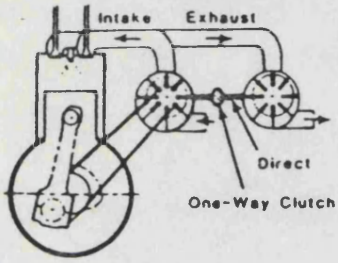

(c)

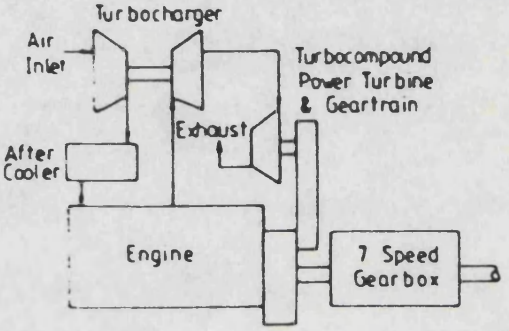

(d)

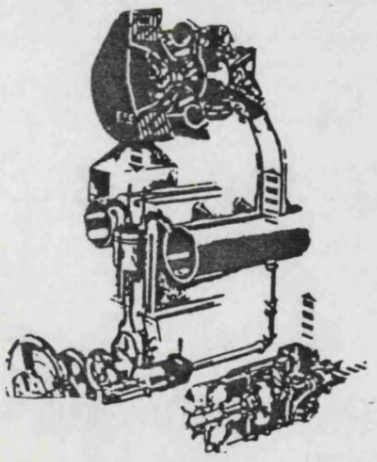

(e)

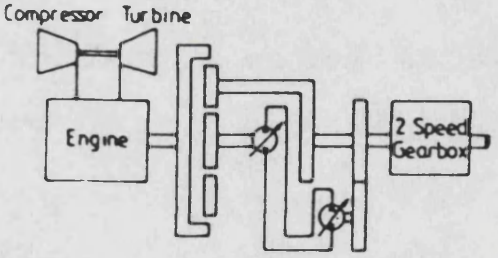

(f)

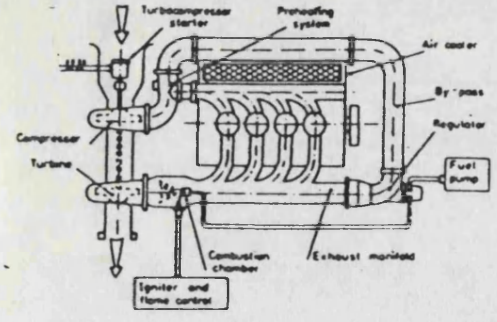

(g)

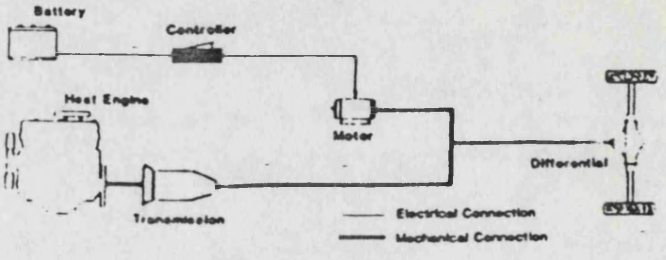

(h)

Fig. 1.6 Engine Systems

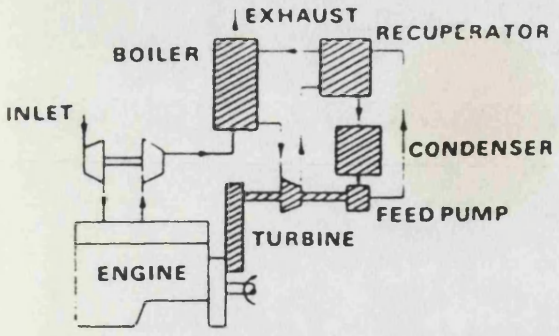

(i)

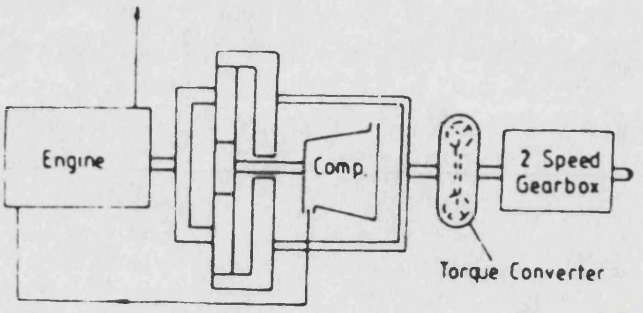

(j)

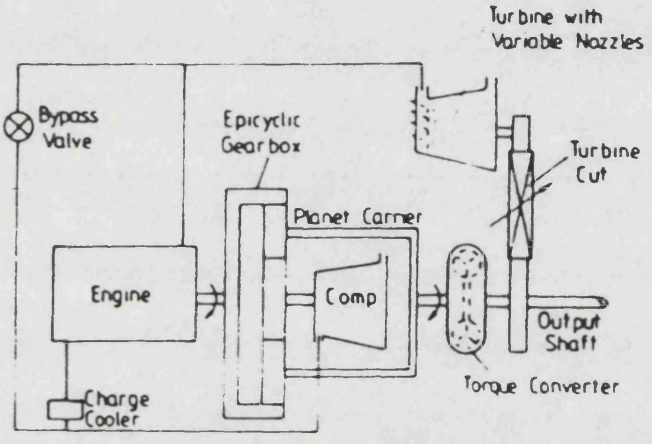

(k)

(a). conventional turbocharged engine with a conventional turbocharger,
(b). conventional supercharged engine with a Comprex supercharger,
(c). Cummins positive displacement compound system with a positive displacement expander and a compressor,
(d). Cummins turbocompound engine with an exhaust powor turbind,
(e). BBC integrated power system with a power turbine operating in parallel with a turbocharger,
(f). conventional turbocharged engine with a hydrostatic shunt transmission,
(g). Hyperbar supercharging system with an auxiliary combustor,
(h). JPL engine-electric hybrid system,
(i). Rankine cycle compound engine system.
(j). Perkins differentially supercharged engine with a 3 speed transmission,
(k). Wallace's differential compound engine without transmission gear box.

Fig. 1.6 (cont.)

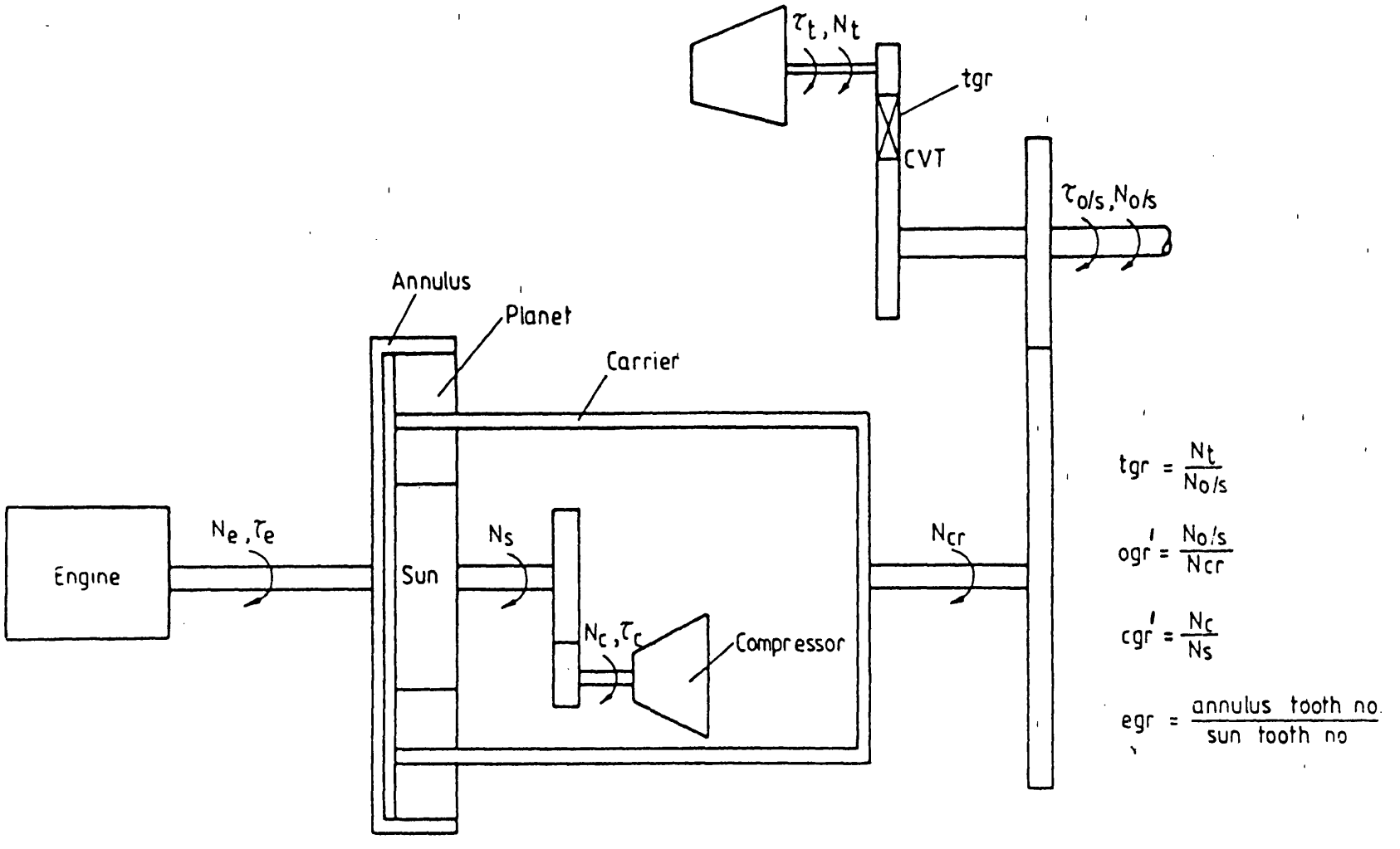

Fig. 1.7 DCE Mechanical Arrangement

Part 2 SCAVENGING

Chapter 2 ISOBARIC AND ISOCHORIC THERMODYNAMIC SCAVENGING MODEL

2.1 INTRODUCTION

During the scavenge period the cylinder is open to both the inlet and exhaust systems at the same time. The flow processes are extremly complex and simplifying assumptions must be made. A number of models of increasing complexity have been developed to describe the scavenging process. Basically these models can be grouped into two classes:

(1). Thermodynamic models which omit the investigation of the fluid dynamic behaviour, and give only a description of the thermodynamic properties, based on the presupposition of an artificial history of the flow and concentration fields.
(2). Fluid dynamic models which involve the study of the flow processes, hence provide full information of the flow, concentration and thermodynamic property fields, obviating the need for the artificial history.

Furthermore, the thermodynamic model may be subdivided into two types:

(a). Isobaric and isochoric models which assume that both the cylinder pressure and volume are constant during the scavenging process.
(b). varying pressure and volume models in which both the pressure and volume are temporal variables.

The former gives a simple description of the thermodynamic properties which is suitable to quantitatively assess the scavenging process for the ideal cycle. The latter provides an appropriate description of the thermodynamic properties which is applicable to calculate the scavenging process in the step-by-step simulations.

This chapter will focus on the isobaric and isochoric model and derive a generalized conclusion from which all the present isobaric and isochoric models, from the Hopkinson model [2.1] in 1914 up to the Baudequin and Rochelle model [2.2] in 1980, can be deduced.

2.2 PHYSICAL DESCRIPTION

In essence, the flow in the cylinder during the scavenging process belongs to the category of unsteady jets. The fresh air in the form of a jet is injected into the cylinder. The cylinder head and walls and the top surface of the cylinder enclose the jet. As a consequence of momentum transfer between the jet and surroundings, residual gas is entrained from the surroundings across the boundaries of the jet. Hence the jet is divided into two regions: a mixing zone M and an air zone A, as shown in Fig. 2.1. The entrainment induces secondary flow within the surrondings, called recirculating flow. The recirculation causes the zone to change into two zones: a mixing zone M and a residual gas zone G. Therefore, the cylinder is virtually divided into three zones: a mixing zone, an air zone and a residual gas zone. The compositions within the air zone and the gas zone maintain their initial values in the inlet manifold and in the cylinder at the beginning of the scavenging process, respectively. However, the composition within the mixing zone is temporally and spatially variable.

After the beginning of the scavenging process, the jet flowing through the inlet ports propagates in the cylinder and eventually arrives at the exhaust ports. Before its arrival, the jet pushes residual gas out through the exhaust ports. The first phase, in which solely the residual gas discharges into the exhaust manifold, is called the displacement scavenging phase, as shown in Fig. 2.2a.

Subsequently a combined flow possibly including air, residual gas and an air-gas mixture passes through the exhaust ports. The discharge proportions of air, gas and mixture depend on running condition, port geometry and layout, piston geometry and position. The functions describing these discharge proportions are temporal variables. This second phase, called mixing scavenging, continues until the mixing zone disappears, as shown in Fig. 2.2b.

After the mixing scavenging phase, some "dead space" of residual gas may be left. Only pure air passes through the exhaust ports. This third phase is called the short-circuiting phase. The residual gas within the "dead space" cannot escape and its amount depends on the scavenging system, as shown in Fig. 2.2c.

The thermodynamic method neglects the fluid dynamic behaviour of the scavenging process. Hence, the thermodynamic method needs an artificial description of flow and concentration fields. In this simplified model, the assumptions are as follows:

(1). constant cylinder pressure during the scavenging process
(2). constant cylinder volume, hence no external work to be done
(3). dividing the cylinder into three zones: air zone, residual gas zone and mixing zone
(4). homogeneous temperature and concentration within each zone
(5). neglect of heat transfer between the zone and walls
(6). ideal gases, with the same constant specific heat
(7). zero-valued formation heats at 0 K, i.e.

$h = u = 0$. at $T = 0$.

whence

$$h = \frac{\gamma}{\gamma - 1} RT$$

$$u = \frac{1}{\gamma - 1} RT$$

where γ is the ratio of specific heats.

(8). specifying an artificial history of intake proportion within the air and mixing zones, and of discharge proportion within the air, mixing and residual gas zones.
(9). neglect of mass, momentum and heat transfer between the zones.

It is notable that actually the air flowing through the inlet ports first exclusively enters the air zone, and then entrainment and recirculation form the mixing zone. However, instead of the mixing history in the cylinder, the discharge history is important for predicting the scavenging process. For convenience, the idealized model considers that a part of the air injected directly mixes with a given amount of residual gas and forms the mixing zone and another part mingles with the air zone, also shown in Fig. 2.2. Incorporated with variable coefficients of intake and exhaust proportions, this treatment can describe any discharge history. By means of a proper choice of parameter, in principle, this model can infinitely approximate any real scavenging process.

2.3 MATHEMATICAL TREATMENT

2.3.1 GOVERNING EQUATIONS (IDEALIZED TREATMENT)

2.3.1.1 Conservation of mass

For the general zone i,

$$\Delta m^{i} = \Delta m^{i}_{in} - \Delta m^{i}_{out} \qquad (2.1)$$

change of mass in the zone = mass flowing into the zone − mass flowing out of the zone

For the air zone,

$$\Delta m^{a} = \Delta m^{a}_{in} - \Delta m^{a}_{out} \qquad (2.2)$$

where Δm^{a}_{in} is the air mass entering the the air zone through inlet ports.

Δm^{a}_{out} is the air mass discharged from the air zone through exhaust ports.

For the residual gas zone,

$$\Delta m^{g} = -\Delta m^{g}_{out} \qquad (2.3)$$

where Δm^{g}_{out} is the residual gas mass discharged from the gas zone through exhaust ports.

For the mixing zone,

$$\Delta m^{m} = \Delta m^{m}_{in} - \Delta m^{m}_{out} \qquad (2.4)$$

where Δm^{m}_{in} is the air mass entering the mixing zone through inlet ports.

Δm^{m}_{out} is the mixture mass discharged from the mixing zone through exhaust ports.

2.3.1.2 Composition equation

The mass concentrations of air and residual gas within the general zone i are respectively.

$$c_a^i = \frac{m_a^i}{m_a^i + m_g^i} \qquad (2.5)$$

$$c_g^i = \frac{m_g^i}{m_a^i + m_g^i} \qquad (2.6)$$

where m_a^i is the air mass within the zone

m_g^i is the residual gas mass within the zone

It is obvious that.

for the air zone.

$$c_a^a = 1 \qquad (2.7)$$

$$c_g^a = 0 \qquad (2.8)$$

for the residual gas zone.

$$c_a^g = 0 \qquad (2.9)$$

$$c_g^g = 1 \qquad (2.10)$$

and for the mixing zone.

$$c_a^m = \frac{m_a^m}{m_a^m + m_g^m} \qquad (2.11)$$

$$c_g^m = \frac{m_g^m}{m_a^m + m_g^m} \qquad (2.12)$$

2.3.1.3 Conservation of energy

For the general zone i,

$$\Delta(m^i u^i) = \sum(\Delta m^i_{in} h^i_{in}) - \sum(\Delta m^i_{out} h^i_{out}) - \Delta Q^i - P\Delta V^i \qquad (2.13)$$

change of internal energy in the zone = enthalpy flowing into the zone − enthalpy flowing out of the zone − heat transfer from the zone − external work done by the zone

where h^i_{in} is the specific absolute enthalpy within the upstream zone

For the air zone,

$$\Delta(m^a u^a) = \Delta m^a_{in} h^a_{in} - \Delta m^a_{out} h^a_{out} - \Delta Q^a - P\Delta V^a \qquad (2.14)$$

For the gas zone,

$$\Delta(m^g u^g) = -\Delta m^g_{out} h^g_{out} - \Delta Q^g - P\Delta V^g \qquad (2.15)$$

For the mixing zone,

$$\Delta(m^m u^m) = \Delta m^m_{in} h^a_{in} - \Delta m^m_{out} h^m_{out} - \Delta Q^m - P\Delta V^m \qquad (2.16)$$

2.3.1.4 Equation of state

Using local properties, the equation of state is used for each zone

$$PV^i = m^i_i RT \qquad (2.17)$$

2.3.1.5 Volume constraint

The volumes of the air, gas and mixing zones add up to the total volume of cylinder.

$$V^a + V^g + V^m = V_{cyl} \qquad (2.18)$$

2.3.2 BOUNDARY CONDITION

For the inlet ports, the sum of air mass injected into the air and mixing zones equates to the total air mass flowing into the cylinder

$$\Delta m_{in}^{a} + \Delta m_{in}^{m} = \Delta m_{in} \qquad (2.19)$$

The coefficients of intake proportion are defined as,

for the air zone,

$$I^{a} = \frac{\Delta m_{in}^{a}}{\Delta m_{in}} \qquad (2.20)$$

for the mixing zone,

$$I^{m} = \frac{\Delta m_{in}^{m}}{\Delta m_{in}} \qquad (2.21)$$

and evidently,

$$I^{a} + I^{m} = 1 \qquad (2.22)$$

Here, it is notable that in this model fresh air never enters the gas zone.

For the exhaust ports, the sum of mass discharged from the air, gas and mixing zones should be added up to form the total mass flowing out of the cylinder

$$\Delta m_{out}^{a} + \Delta m_{out}^{g} + \Delta m_{out}^{m} = \Delta m_{out} \qquad (2.23)$$

The coefficients of discharge proportion are,

for the air zone,

$$D^{a} = \frac{\Delta m_{out}^{a}}{\Delta m_{out}} \qquad (2.24)$$

for the gas zone,

$$D^{g} = \frac{\Delta m_{out}^{g}}{\Delta m_{out}} \qquad (2.25)$$

for the mixing zone.

$$D^m = \frac{\Delta m^m_{out}}{\Delta m_{out}} \qquad (2.26)$$

and evidently.

$$D^a + D^g + D^m = 1 \qquad (2.27)$$

From the equation of volume constraint (2.18), the energy equations of all the three zones (2.14), (2.15) and (2.16) may be added to give the overall energy balance equation.

$$\Delta(m^a u^a + m^g u^g + m^m u^m) = \Delta m_{in} h^a - \Delta m_{out}(D^a h^a + D^g h^g + D^m h^m) - \Delta Q_{cyl} - P\Delta V_{cyl} \qquad (2.28)$$

From the assumptions of constant volume, ideal gas and zero-valued formation heat at 0 K, the left-hand side of equation (2.28) becomes

$$\Delta\left(\frac{m^a RT_a}{\gamma-1} + \frac{m^g RT_g}{\gamma-1} + \frac{m^m RT_m}{\gamma-1}\right)$$

$$= \frac{P}{\gamma-1}\Delta(V^a + V^g + V^m) = 0 \qquad (2.29)$$

where T_a is the air temperature injected which is constant

T^a is the residual gas temperature which is constant

T^g_m is the mixture temperature which is variable with mixture composition.

Due to the assumptions of isochoric and adiabatic processes, from equation (2.28),

$$\frac{\Delta m_{out}}{\Delta m_{in}} = \frac{h^a}{D^a h^a + D^g h^g + D^m h^m} = \frac{T_a}{D^a T_a + D^g T_g + D^m T_m} \qquad (2.30)$$

Because of the assumptions of ideal gas and constant specific heat, the following relationship can be obtained

$$T_m = \frac{m^m_a T_a + m^m_g T_g}{m^m} \qquad (2.31)$$

hence,

$$\frac{\Delta m_{out}}{\Delta m_{in}} = \frac{T_a}{D^a T_a + D^g T_g + D^m (m^m_a T_a + m^m_g T_g)/m^m} \qquad (2.32)$$

which gives the relation between the mass flowing into the cylinder and the mass flowing out of the cylinder.

From the equation of mass conservation for the air zone,

$$\Delta m^a = \Delta m^a_{in} - \Delta m^a_{out}$$

$$= I^a \Delta m_{in} - D^a \Delta m_{out} \qquad (2.33)$$

both sides being divided by Δm_{in}.

$$\frac{\Delta m^a}{\Delta m_{in}} = I^a - D^a \frac{\Delta m_{out}}{\Delta m_{in}} \qquad (2.34)$$

where $\Delta m^a = \Delta m^a_a$ because there exists only pure air within the air zone

Similarly, for the gas zone,

$$\frac{\Delta m^g}{\Delta m_{in}} = - D^g \frac{\Delta m_{out}}{\Delta m_{in}} \qquad (2.35)$$

where $\Delta m^g = \Delta m^g_g$ because there exists only pure residual gas within the gas zone. It is noted that air never enters the gas zone, and only residual gas discharges from the gas zone.

The composition within the mixing zone varies. From the conservation of air mass within the mixing zone,

$$\Delta m_a^m = \Delta m_{in}^m - c_a^m \Delta m_{out}^m \tag{2.36}$$

the following equation can be obtained

$$\frac{\Delta m_a^m}{\Delta m_{in}} = I^m - \frac{m_a^m}{m^m} D^m \frac{\Delta m_{out}}{\Delta m_{in}} \tag{2.37}$$

Again, from the conservation of residual gas within the mixing zone

$$\Delta m_g^m = -c_g^m \Delta m_{out}^m \tag{2.38}$$

hence

$$\frac{\Delta m_g^m}{\Delta m_{in}} = - \frac{m_g^m}{m^m} D^m \frac{\Delta m_{out}}{\Delta m_{in}} \tag{2.39}$$

The five first-order ordinary differential equations (2.32), (2.34), (2.35), (2.37) and (2.39) constitute a simultaneous system. Provided the coefficients of intake and discharge proportions, I and D, are specified, the system can be solved.

2.4 COMPUTATIONAL PROCEDURE AND RESULTS

The system of five simultaneous ordinary differential equations (2.32), (2.34), (2.35), (2.37) and (2.39) is solved by the fourth-order Runge-Kutta method. The coefficients of intake and exhaust proportions may be set arbitrarily.

The step length for the input variables, i.e. delivery ratio, is taken as 0.02. The curve of charging efficiency in the perfect mixing scavenging process is applied to the estimation of accuracy. Compared with the theoretical solution the errors of the computational results are maintained within 1.0%.

In addition, a comparison between experimental and computational results is made for the three scavenging systems: uniflow, loop and cross scavenging systems. The experimental work using model tests was conducted by List [2.3]. In principle, the coefficients of intake and discharge proportions are variable with the delivery ratio. In reality, in the

following computations the coefficients of intake and discharge proportion are assumed to be maintained constant during each phase, and adjusted to obtain the computational results with an accuracy of 2 %. In these calculations, the temperatures of fresh air and residual gas are equal to 300 and 800 K respectively. Fig. 2.3 shows the comparison. Table 2.1 lists the characteristic parameters and coefficients of intake and exhaust proportions in these computations.

As for the scavenging efficiency of the three scavenging systems, the uniflow scavenging system is superior, and the cross scavenging system is inferior. The reason is that cross scavenging causes too early short-circuiting and too large a "dead space" of remaining residual gas, and the uniflow scavenging system, especially with swirl, intensifies the entrainment and postpones the advent of short-circuiting and diminishes the "dead space". The analysis of parameters in the computations coincides with the analysis of experimental work. This confirms the versatility of the generalized model.

2.5 DERIVATION OF FORMULAE OF A SIMPLIFIED ANALYTICAL MODEL

In the previous section, those computations with the constant coefficients of intake and discharge proportions have obtained the satisfactory results. Actually, once the coefficients are constant, an analytical form of this model can be derived. As previously mentioned, this model considers the scavenging process as a process composed of the following three phases: (see Fig. 2.2)

Phase A: the displacement scavenging phase during which only residual gas is discharged from the cylinder, and at the end of which an amount of pure residual gas remains until the end of the process.
Phase B: the mixing scavenging phase in which a combined flow is discharged from the mixing zone and the air zone until the disappearance of the mixing zone.
Phase C: the short-circuiting phase during which a flow of fresh air passes straight through the exhaust ports.

2.5.1 PHASE A: DISPLACEMENT SCAVENGING

At the beginning of the scavenging process, the total mass of residual gas is

$$m_o^g = \frac{P_a V_{cyl}}{RT_g} \qquad (2.40)$$

The air from the inlet manifold flows into the cylinder through the inlet port. A portion of the air mixes with a specified initial volume of residual gas, its volumetric ratio to the cylinder volume being η_o, and forms the mixing zone. This means that at the beginning of the scavenging process the mixing zone is composed of the residual gas of $\eta_o m_o^g$, and the residual gas zone is of $(1-\eta_o)m_o^g$, as shown in Fig. 2.4. Another portion of the air injected produces the air zone. The coefficients of intake proportion are I^m for the mixing zone, and I^a for the air zone. It is noted that the air from inlet manifold never enters the residual gas zone, hence the following equation is valid.

$$I^m + I^a = 1 \qquad (2.41)$$

On the exhaust side, only the flow from the residual gas zone passes through the exhaust ports. Therefore, the coefficient of discharge proportion in the residual gas zone equates to one, and the other two coefficients in the mixing zone and the air zone equate to zero, i.e.

$$D^g = 1 \qquad (2.42)$$

$$D^a = 0 \qquad (2.43)$$

$$D^m = 0 \qquad (2.44)$$

Phase A continues until the volume of remaining residual gas reaches a specified value, its volumetric ratio to the cylinder volume being η_A. This means that throughout phase A the residual gas mass of $\eta_o m_o^g$ is intactly contained in the mixing zone, while the residual gas mass in the gas zone reduces from $(1-\eta_o)m_o^g$ to $\eta_A m_o^g$, as shown in Fig. 2.4.

The system of equations (2.32), (2.34), (2.35), (2.37) and (2.39) respectively becomes as follows

$$\frac{\Delta m_{out}}{\Delta m_{in}} = \frac{T_a}{T_g} \tag{2.45}$$

$$\frac{\Delta m^a}{\Delta m_{in}} = I^a \tag{2.46}$$

$$\frac{\Delta m^g}{\Delta m_{in}} = -\frac{T_a}{T_g} \tag{2.47}$$

$$\frac{\Delta m^m_a}{\Delta m_{in}} = I^m \tag{2.48}$$

$$\frac{\Delta m^m_g}{\Delta m_{in}} = 0 \tag{2.49}$$

It is easy to find their integral solutions for phase A.

$$m_{out} = \frac{T_a}{T_g} m_{in} \tag{2.50}$$

$$m^a = I^a m_{in} \tag{2.51}$$

$$m^g = m^g_o - \frac{T_a}{T_g} m_{in} \tag{2.52}$$

$$m^m_a = I^m m_{in} \tag{2.53}$$

$$m^m_g = m^m_{g,o} = \eta_o \frac{P_a V_{cyl}}{RT_g} \tag{2.54}$$

From equations (2.51) and (2.53), the following equation can be obtained:

$$m^a + m^m_a = m_{in} \tag{2.55}$$

The reference mass M is defined by,

$$\frac{P_a V_{cyl}}{R T_a}$$

With both sides being divided by M, from the definitions of the delivery ratio and charging efficiency, equation (2.55) becomes,

$$\eta_{ch} = \lambda \qquad (2.56)$$

When phase A ends, it is noted that the following relationships are valid

$$m^m_{a,A} + m^a_A = m_{in,A} = \lambda_A M \qquad (2.57)$$

$$m^m_{a,A} = l^m \lambda_A M \qquad (2.58)$$

$$m^m_{g,A} = \eta_o \frac{P_a V_{cyl}}{R T_g} = \eta_o \frac{T_a}{T_g} M \qquad (2.59)$$

where the additional subscript A means the end of phase A.

From equation (2.52), the specified volumetric ratios are substituted

$$m^g_A = m^g_o - \frac{T_a}{T_g} m_{in,A} \qquad (2.60)$$

$$\eta_A \frac{P_a V_{cyl}}{R T_g} = (1-\eta_o) \frac{P_a V_{cyl}}{R T_g} - \frac{T_a}{T_g} m_{in,A} \qquad (2.61)$$

$$\text{i.e.} \quad \lambda_A = 1 - \eta_o - \eta_A \qquad (2.62)$$

The physical meaning of equation (2.62) is obvious, because the volumetric ratio of the residual gas zone at the end of phase A is reduced from the initial ratio $(1-\eta_o)$ to the final ratio η_A, that is, the gas zone makes the room of the volumetric ratio $1-\eta_o-\eta_A$ for fresh air, as shown in Fig. 2.4. That indicates that when the delivery ratio reaches λ_A, phase A ends and one obtains the charging efficiency $\eta_{ch,A} = \lambda_A$.

2.5.2 PHASE B: MIXING SCAVENGING

The boundary condition at the inlet ports is the same as that for phase A. However, the condition at the exhaust ports is different. The residual gas no longer passes through the exhaust ports, but the air-gas mixture and the air do. The corresponding coefficients of exhaust proportion satisfy the following equation

$$D^g = 0 \quad \text{(assumption)} \tag{2.63}$$

$$D^m + D^a = 1 \tag{2.64}$$

This phase continues until the air-gas mixture in the mixing zone ceases to discharge, following a certain level of air supplied.

The original full system of equations (2.32), (2.34), (2.35), (2.37) and (2.39) respectively takes the following simplified forms

$$\frac{\Delta m_{out}}{\Delta m_{in}} = \frac{1}{D^a + D^m T_m / T_a} \tag{2.65}$$

$$\frac{\Delta m^a}{\Delta m_{in}} = l^a - D^a \frac{1}{D^a + D^m T_m / T_a} \tag{2.66}$$

$$\frac{\Delta m^g}{\Delta m_{in}} = 0 \quad \text{(assumption)} \tag{2.67}$$

$$\frac{\Delta m^m_a}{\Delta m_{in}} = l^m - D^m c^m_a \frac{1}{D^a + D^m T_m / T_a} \tag{2.68}$$

$$\frac{\Delta m^m_g}{\Delta m_{in}} = - D^m c^m_g \frac{1}{D^a + D^m T_m / T_a} \tag{2.69}$$

where

$$c^m_a = \frac{m^m_a}{m^m_a + m^m_g}$$

$$c^m_g = \frac{m^m_g}{m^m_a + m^m_g}$$

and

$$T_m = \frac{m^m_a T_a + m^m_g T_g}{m^m_a + m^m_g}$$

hence

$$\frac{T_m}{T_a} = \frac{m^m_a + m^m_g T_g/T_a}{m^m_a + m^m_g}$$

From equations (2.68) and (2.69), the following equations can be derived

$$\frac{\Delta m^m_a}{\Delta m^m_g} = \frac{(D^m - I^m)}{D^m} \frac{m^m_a}{m^m_g} - \frac{I^m}{D^m}(D^a + D^m \frac{T_g}{T_a}) \qquad (2.70)$$

From equations (2.66) and (2.69)

$$\frac{\Delta m^a}{\Delta m^m_g} = \frac{(D^a - I^a)}{D^m} \frac{m^m_a}{m^m_g} + \frac{(D^a - I^a(D^a + D^m T_g/T_a))}{D^m} \qquad (2.71)$$

And from equation (2.69)

$$\frac{\Delta m_{in}}{\Delta m^m_g} = -\frac{((D^a + D^m T_g/T_a) + m^m_a/m^m_g)}{D^m} \qquad (2.72)$$

It is necessary for the system (2.70), (2.71) and (2.72) to distinguish between two different cases.

2.5.2.1 Case I: $I^m \neq D^m$

Using the method of integrating factors, the solution of equation (2.70) can be achieved

$$m^m_a = \left(\frac{m^m_{a,A}}{m^m_{g,A}} + (D^a + D^m T_g/T_a)\right) m^m_{g,A} \left(\frac{m^m_g}{m^m_{g,A}}\right)^{\frac{(D^m - I^m)}{D^m}} - (D^a + D^m T_g/T_a) m^m_g \qquad (2.73)$$

After the substitution of the previous equation (2.73) into equation (2.71), its solution can be obtained

$$m^a = m^a_A + D^a\left(1-\frac{T_g}{T_a}\right)\left(m^m_g - m^m_{g.A}\right)$$

$$-\left(\frac{m^m_{a.A}}{m^m_{g.A}} + \left(D^a + D^m\frac{T_g}{T_a}\right)\right) m^m_{g.A}\left(\left(\frac{m^m_g}{m^m_{g.A}}\right)^{\frac{(D^m-I^m)}{D^m}} - 1\right)$$

(2.74)

Similarly, from equation (2.72)

$$m_{in} = m_{in.A}$$

$$+\frac{1}{(D^m-I^m)}\left(\frac{m^m_{a.A}}{m^m_{g.A}} + \left(D^a + D^m\frac{T_g}{T_a}\right)\right) m^m_{g.A}\left(1-\left(\frac{m^m_g}{m^m_{g.A}}\right)^{\frac{(D^m-I^m)}{D^m}}\right)$$

(2.75)

Equations (2.73) and (2.74) may be substituted by equation (2.75) and added up to give

$$m^m_a + m^a = m^m_{a.A} + m^a_A$$

$$+\frac{T_g}{T_a} m^m_{g.A}\left(1-\left(1-\frac{(D^m-I^m)(m_{in}-m_{in.A})}{m^m_{a.A}+m^m_{g.A}(D^a+D^m T_g/T_a)}\right)^{\frac{D^m}{(D^m-I^m)}}\right)$$

(2.76)

With both sides divided by M and substituted by equations (1.4), (2.57), (2.58), (2.59) and (2.62), the previous equation (2.76) changes into the following equation

$$\eta_{ch} = (1-\eta_A) - \eta_o\left(1 - \frac{(D^m-I^m)(\lambda-(1-\eta_o-\eta_A))}{I^m(1-\eta_o-\eta_A)+\eta_o(D^m+D^a T_a/T_g)}\right)^{\frac{D^m}{(D^m-I^m)}}$$

(2.77)

It is now necessary that case I should be subdivided into two different situations to investigate

2.5.2.1.1 Situation 1: $D^m > I^m$, i.e. $D^a < I^a$

From the requirement that the fractional exponent function in equation (2.77) must give a positive real solution, the following inequality can be obtained.

$$\lambda < \frac{1}{(D^m - I^m)} \left(I^m (1-\eta_o-\eta_A) + \eta_o \left(D^m + D^a \frac{T_a}{T_g}\right)\right) + (1-\eta_o-\eta_A) \tag{2.78}$$

and the maximum of delivery ratio is called λ_B. Phase B continues until the delivery ratio achieves λ_B, and then the mixing zone vanishes, and the charging efficiency reaches the maximum.

$$\eta_{ch,B} = 1-\eta_A \tag{2.79}$$

where the additional subscript B means the end of phase B. The physical meaning of this equation is that when phase B ends, fresh air occupies all the cylinder space except the residual gas "dead space" of $\eta_A V_{cyl}$, as shown in Fig. 2.4.

2.5.2.1.2 Situation 2: $D^m < I^m$, i.e. $D^a > I^a$

Equation (2.77) can be changed into the following form

$$\eta_{ch} = (1-\eta_A) - \eta_o \left(\frac{I^m (1-\eta_o-\eta_A) + \eta_o (D^m + D^a T_a/T_g)}{(I^m - D^m)\lambda + D^m (1-\eta_o-\eta_A) + \eta_o (D^m + D^a T_a/T_g)} \right) \frac{D^m}{(I^m - D^m)} \tag{2.80}$$

Phase B can continue without limitation of delivery ratio. With increase of air supply, the charging efficiency approximates to the same maximum.

$$\eta_{ch,B} = 1-\eta_A$$

2.5.2.2 Case II: $I^m = D^m$

It is noted that if $I^m = D^m$, then $I^a = D^a$

Similarly, the following solutions of equations (2.70), (2.71) and (2.72) can be obtained

$$m^m_a = m^m_{a.A} - (D^a + D^m\frac{T_g}{T_a})(m^m_g - m^m_{g.A}) \qquad (2.81)$$

$$m^a = m^a_A + \frac{D^a}{D^m}(1 - (D^a + D^m\frac{T_g}{T_a}))(m^m_g - m^m_{g.A}) \qquad (2.82)$$

$$m_{in} = m_{in.A} - \frac{1}{D^m}((D^a + D^m\frac{T_g}{T_a})m^m_{g.A} + m^m_{a.A})\,Ln(\frac{m^m_g}{m^m_{g.A}}) \qquad (2.83)$$

By transformation, the formula of charging efficiency can be derived as follows

$$\eta_{ch} = (1-\eta_A) - \eta_o \exp(-\frac{D^m(\lambda-(1-\eta_o-\eta_A))}{D^m(1-\eta_o-\eta_A)+\eta_o(D^m+D^aT_a/T_g)}) \qquad (2.84)$$

Phase B could carry on infinitely. With increase of delivery ratio, the charging efficiency approaches the limit

$$\eta_{ch.B} = 1 - \eta_A$$

which is the same as that in case I.

2.5.3 PHASE C: SHORT-CIRCUITING

Actually, only under the situation 1: $D^m > I^m$, the scavenging model includes phase C. In phase C, the mixing zone disappears. Only the air zone connects with both inlet and exhaust ports. The coefficients of proportion become as follows

$$D^g = 0 \qquad (2.85)$$

$$D^m = 0 \qquad (2.86)$$

$$D^a = 1 \tag{2.87}$$

and

$$l^g = 0 \tag{2.88}$$

$$l^m = 0 \tag{2.89}$$

$$l^a = 1 \tag{2.90}$$

Hence, the system (2.32), (2.34), (2.35), (2.37) and (2.39) respectively becomes

$$\frac{\Delta m_{out}}{\Delta m_{in}} = 1 \tag{2.91}$$

$$\frac{\Delta m^a}{\Delta m_{in}} = 0 \tag{2.92}$$

$$\frac{\Delta m^g}{\Delta m_{in}} = 0 \tag{2.93}$$

$$\frac{\Delta m^m_a}{\Delta m_{in}} = 0 \tag{2.94}$$

$$\frac{\Delta m^m_g}{\Delta m_{in}} = 0 \tag{2.95}$$

It is easy to get the formula of charging efficiency

$$\eta_{ch} = \eta_{ch,B} = 1-\eta_A \tag{2.96}$$

The physical meaning of this equation is that during phase C the charging efficiency maintains a constant because due to short-circuiting all the fresh air flowing into the cylinder, at the same time, is discharged from the cylinder, as shown in Fig. 2.4.

2.5.4 SUMMARY

In summary, the formulae of the scavenging model are

Phase A:

$$\eta_{ch}=\lambda \qquad (2.56)$$

Phase B:

(1). $D^m > l^m$

$$\eta_{ch} = (1 - \eta_A) - \eta_o\left(1 - \frac{(D^m-l^m)(\lambda-(1-\eta_o-\eta_A))}{l^m(1-\eta_o-\eta_A)+\eta_o(D^m+D^a T_a/T_g)}\right)\frac{D^m}{(D^m-l^m)}$$

$$\lambda \leq \frac{1}{(D^m-l^m)}\left(l^m(1-\eta_o-\eta_A) + \eta_o\left(D^m+D^a\frac{T_a}{T_g}\right)\right) + (1-\eta_o-\eta_A)$$

(2.77)

(2). $D^m = l^m$

$$\eta_{ch} = (1-\eta_A) - \eta_o \exp\left(-\frac{D^m(\lambda-(1-\eta_o-\eta_A))}{D^m(1-\eta_o-\eta_A)+\eta_o(D^m+D^a T_a/T_g)}\right)$$

(2.84)

(3). $D^m < l^m$

$$\eta_{ch}= (1-\eta_A) - \eta_o\left(\frac{l^m(1-\eta_o-\eta_A)+\eta_o(D^m+D^a T_a/T_g)}{(l^m-D^m)\lambda+D^m(1-\eta_o-\eta_A)+\eta_o(D^m+D^a T_a/T_g)}\right)\frac{D^m}{(l^m-D^m)}$$

(2.80)

Phase C:

$$\eta_{ch} = 1-\eta_A \qquad (2.96)$$

2.6 DERIVATION OF EXISTING MODELS FROM THE GENERALIZED MODEL

In this section, the equations of the previous pages are used to derive the scavenging formulations of a number of well known workers.

2.6.1 HOPKINSON'S MODEL[2.1]

Main hypothesis: Only the mixing zone
Only phase B

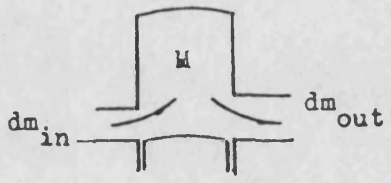

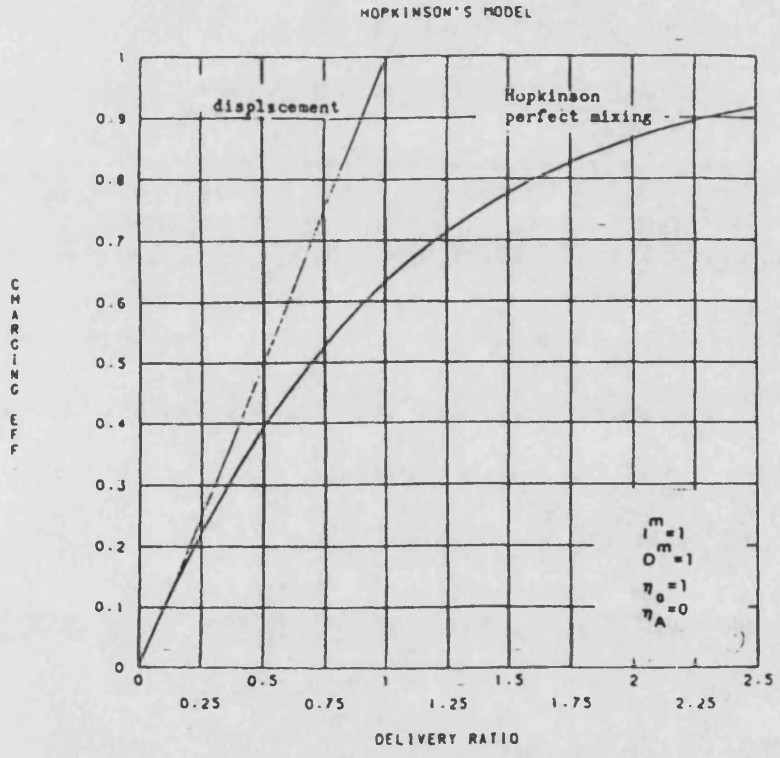

Formula of charging efficiency: from equations (2.84)

$$\eta_{ch} = 1 - e^{-\lambda}$$

Remarks: Only one scavenging curve
No initial displacement scavenging phase

2.6.2 BENSON'S MODEL[2.4]

Main hypothesis: Two zones: the residual gas zone and the mixing zone
No air zone
Two phases-phase A and phase B
No remaining residual gas after the end of phase A

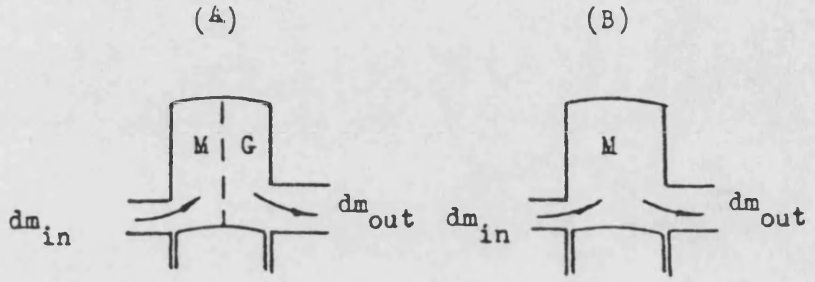

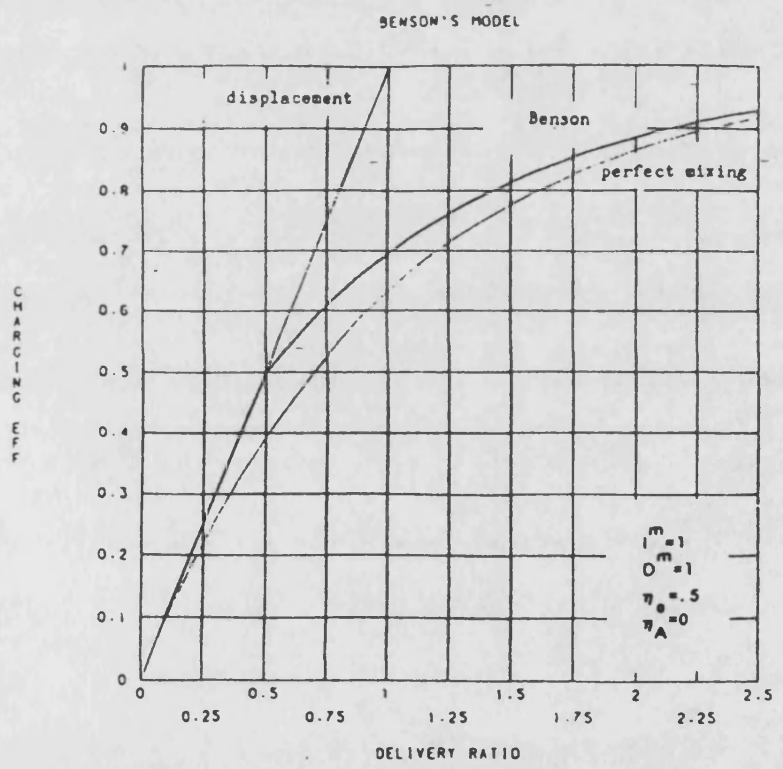

Formula of charging efficiency: from equations (2.56) and (2.84)

$$\eta_{ch} = \lambda \qquad (\lambda \leq \lambda_A = 1 - \eta_o)$$

$$\eta_{ch} = 1 - \eta_o e^{-(\lambda-(1-\eta_o))} \qquad (\lambda > \lambda_A)$$

Remarks: No short-circuiting of fresh air
No "dead space" of residual gas
No curves under $\eta_{ch} = 1 - e^{-\lambda}$

2.6.3 MAEKAWA'S MODEL[2.5]

Main hypothesis: Two zones
No phase A
No remaining residual gas
Isothermal process
$D^m > I^m$

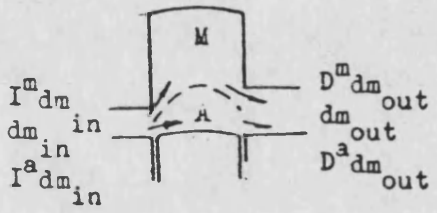

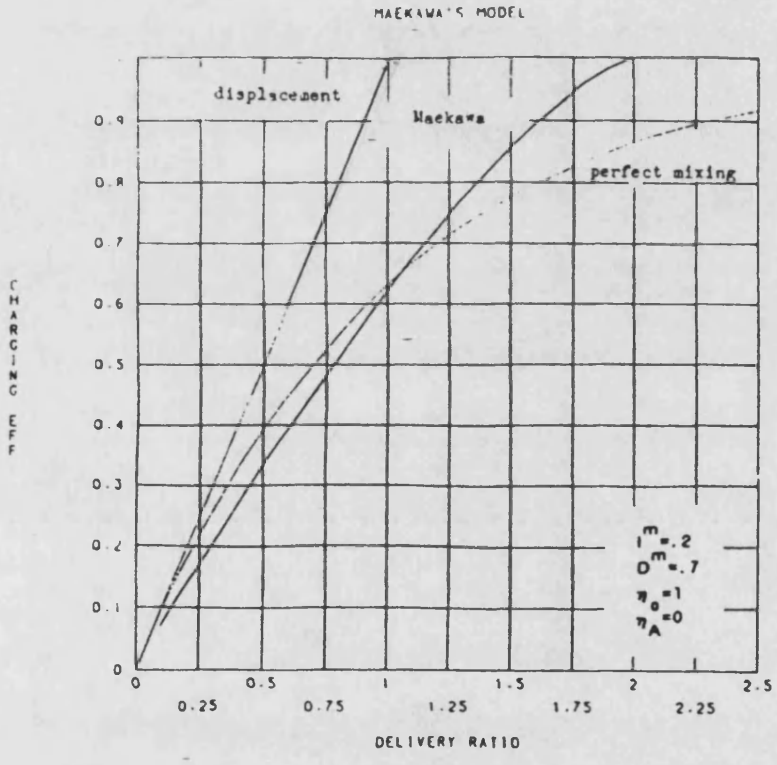

Formula of charging efficiency: from equations (2.77) and (2.92)

$$\eta_{ch} = 1 - (1 - (D^m - I^m)\lambda)\frac{D^m}{(D^m - I^m)} \qquad (D^m > I^m \text{ and } \lambda \leq \lambda_B = \frac{1}{(D^m - I^m)})$$

$$\eta_{ch} = 1 \qquad (\lambda > \lambda_A)$$

Remarks: No initial displacement phase
No "dead space" of residual gas
Isothermal idealization

2.6.4 SYNTHESIS OF BENSON AND MAEKAWA'S MODELS[2.2]

Main hypothesis: Three zones
No remaining residual gas
Isothermal process

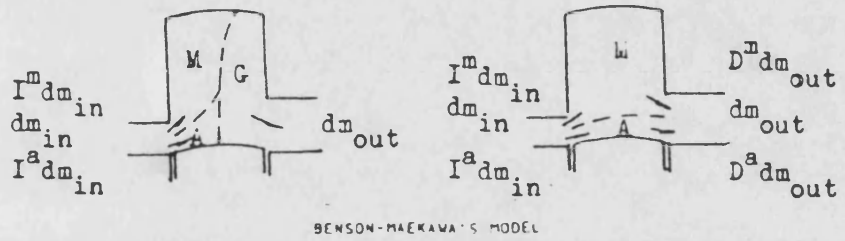

BENSON-MAEKAWA'S MODEL

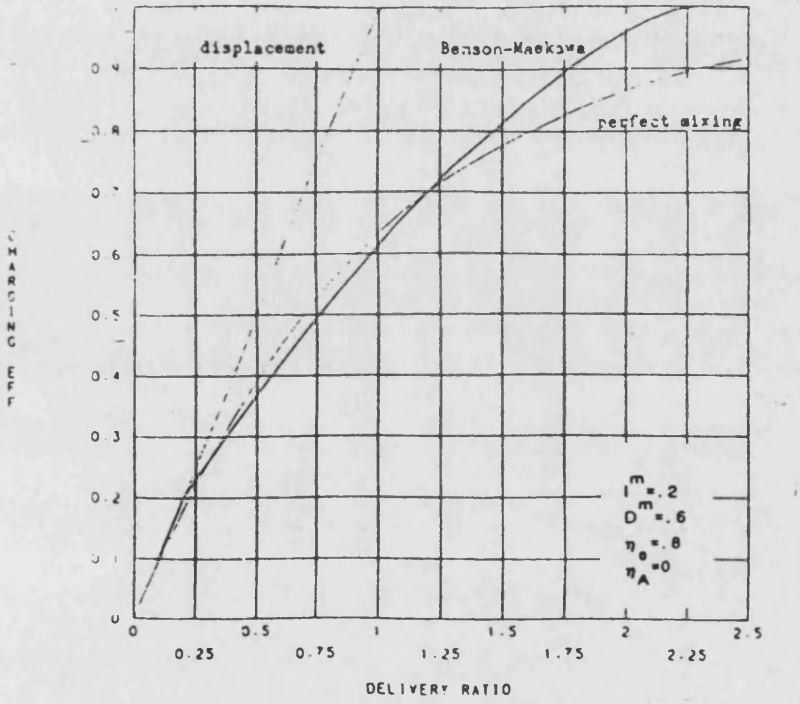

Formula of charging efficiency: from equations (2.56), (2.77) and (2.92)

$$\eta_{ch} = \lambda \qquad (\lambda < \lambda_A = 1-\eta_o)$$

$$\eta_{ch} = 1 - \eta_o\left(1 - \frac{(D^m - I^m)(\lambda-(1-\eta_o))}{I^m(1-\eta_o)+\eta_o}\,\frac{D^m}{(D^m-I^m)}\right)$$

$$(D^m > I^m \text{ and } \lambda \leq \lambda_B = \frac{I^m(1-\eta_o)+\eta_o}{(D^m-I^m)} + (1-\eta_o))$$

$$\eta_{ch} = 1 \qquad (\lambda > \lambda_B)$$

Remarks: No "dead space" of residual gas
Isothermal idealization

2.6.5 THE MODIFIED BENSON MODEL[2.2]

Main hypothesis: Two zones: the residual gas zone and the mixing zone
No air zone
Two phases: phase A and phase B
Remaining residual gas at the end of the scavenging process

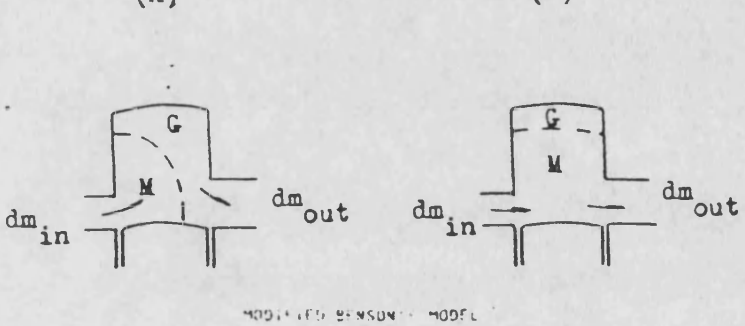

MODIFIED BENSON MODEL

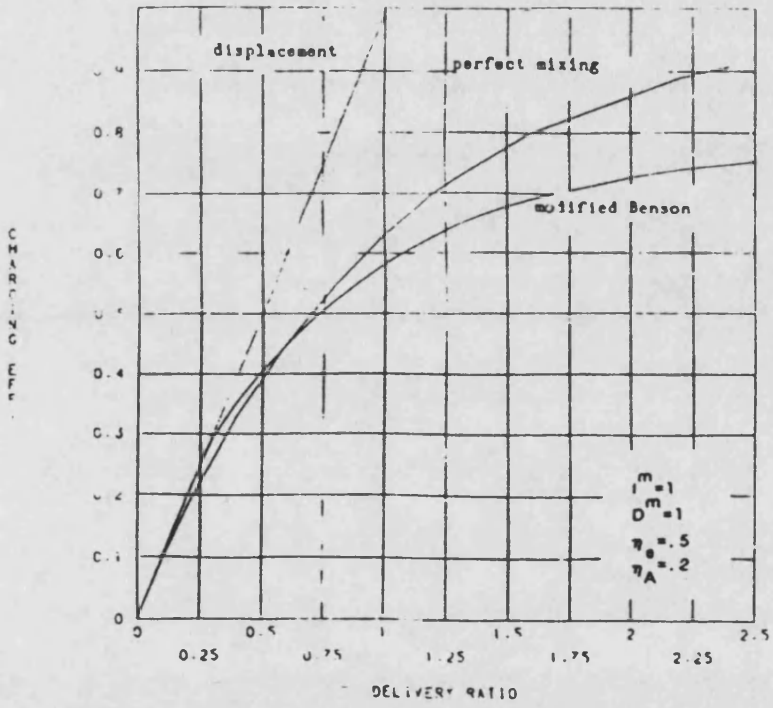

Formula of charging efficiency: from equations (2.56) and (2.84)

$$\eta_{ch} = \lambda \qquad (\lambda < \lambda_A = 1-\eta_o-\eta_A)$$

$$\eta_{ch} = (1-\eta_A)-\eta_o \exp\left(-\frac{\lambda-(1-\eta_o-\eta_A)}{(1-\eta_A)}\right) \qquad (\lambda > \lambda_A)$$

Remark: No short-circuiting of fresh air

2.6.6 THE MODIFIED MAEKAWA MODEL[2.2]

Main hypothesis: Three zones

Two phases: phase A and phase B

No remaining residual gas after the end of the process

Isothermal process

$D^m > I^m$

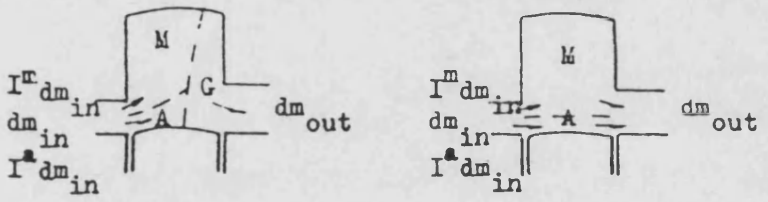

MODIFIED MAEKAWA'S MODEL

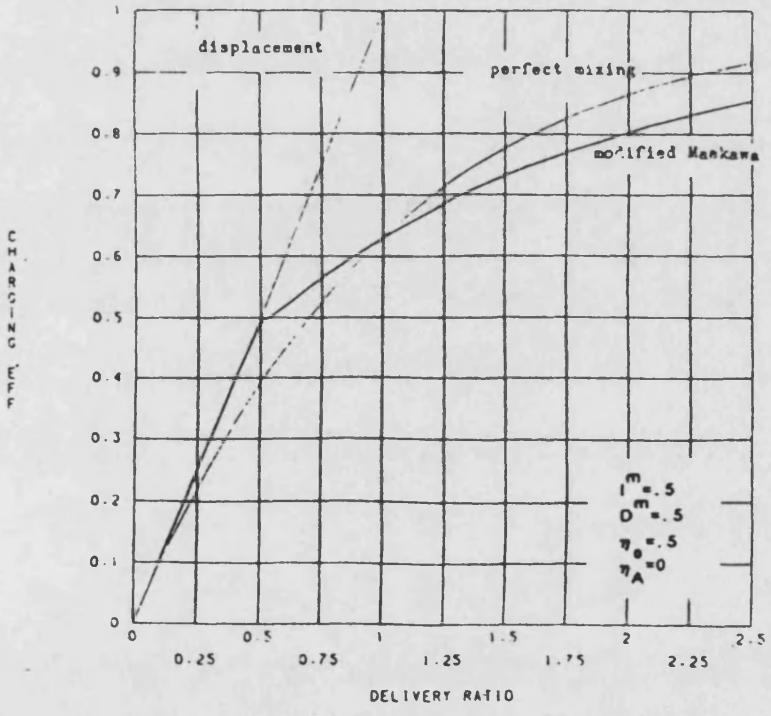

Formula of charging efficiency: from equations (2.56) to (2.84)

$$\eta_{ch} = \lambda \qquad (\lambda < \lambda_A = 1-\eta_o)$$

$$\eta_{ch} = 1 - \eta_o \exp\left(-\frac{D^m(\lambda-(1-\eta_o))}{D^m(1-\eta_o)+\eta_o}\right) \qquad (\lambda > \lambda_A)$$

Remarks: No "dead space" of residual gas

Isothermal idealization

2.6.7 BAUDEQUIN AND ROCHELLE'S MODEL[2.2]

Main hypothesis: Three zones

Two phases: phase A and phase B

Remaining residual gas

Isothermal process

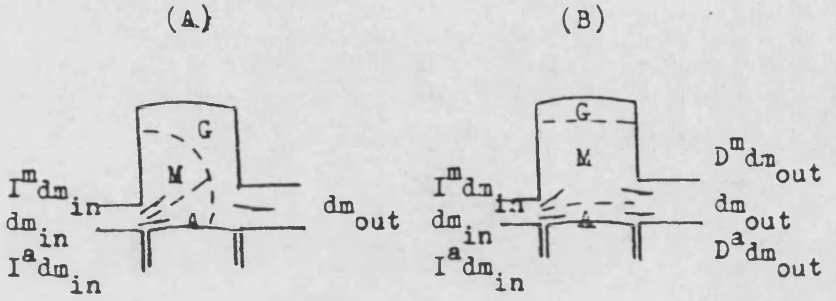

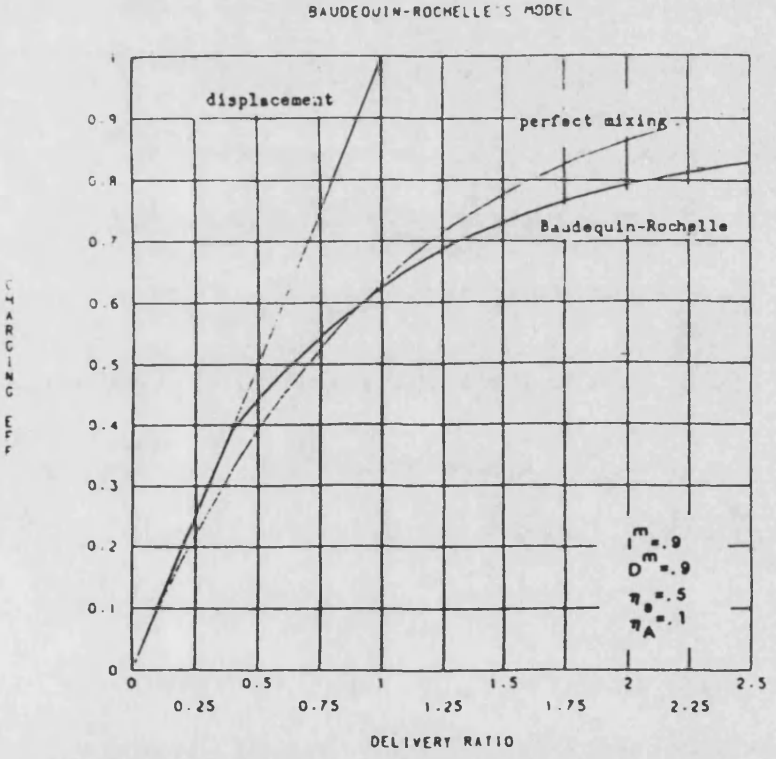

Formula of charging efficiency: from equation (2.56) and (2.84)

$$\eta_{ch} = \lambda \qquad (\lambda < \lambda_A = 1-\eta_o-\eta_A)$$

$$\eta_{ch} = (1-\eta_A) - \eta_o \exp\left(-\frac{D^m(\lambda-(1-\eta_o-\eta_A))}{D^m(1-\eta_o-\eta_A)+\eta_o}\right) \qquad (\lambda > \lambda_A)$$

Remarks: Isothermal idealization

2.7 CRITIQUE OF VARIOUS MODELS

Two groups of typical experimental results of charging efficiency for different scavenging systems by Schweitzer [1.1] and Fiat Co. [2.6] are shown in Figs. 2.5 and 2.6. It can be seen that the experimental curves of charging efficiency have the following characteristics.

(1). variability: the different curve for the different scavenging systems, even for the different running conditions.
(2). a straight-line section for the displacement scavenging phase.
(3). a monotonically increasing curve section for the mixing scavenging phase, which has gradually decreasing gradient, possibly intersects the perfect mixing curve, and with increase of delivery ratio approaches a limit of less than 1.

Hopkinson's model is the simplest one-zone model with the mixing zone and gives only one unique charging efficiency curve. This model includes only the mixing scavenging phase.

Benson's model is a two-zone model with the mixing and residual gas zones and gives a curve family of one parameter η_o which describes the effect of varying residual gas mass discharged during the displacement scavenging phase. This model includes the displacement scavenging phase, but does not include the short-circuiting of fresh air. Therefore, this model cannot explain the possible intersection of the experimental curve with the perfect mixing curve.

Maekawa's model is a two-zone model with the mixing and air zones and gives a curve family of two parameters I^m and D^m which describe the effect of varying exhaust history during the mixing phase. This model does not include the displacement scavenging phase. The curve family can intersect the perfect mixing curve, but displays a wrong intersection trend. When such intersection occurs, the charging efficiency curve should be first higher and then lower than the perfect mixing curve.

The synthesis of Benson and Maekawa's models is a three-zone model and gives a curve family of three parameters η_o, I^m and D^m. This model does not include either a residual gas "dead space" or the short-circuiting

of fresh air, and cannot express a very slow increase of charging efficiency at the side of high delivery ratio.

The modified Benson model is a two-zone model with mixing and gas zones and gives a curve family of two parameters η_o and η_A. Without short-circuiting of air, this model has a residual gas "dead space" of $\eta_A V_{cyl}$. The modified Maekawa model is a three-zone model and gives a curve family of two parameters η_o and D^m. Without "dead space" of residual gas, this model includes short-circuiting of air. Baudequin and Rochelle's model is a three-zone model and gives a curve family of three parameters η_o, η_A and D^m. This model includes both "dead space" of gas and short-circuiting of air. These three model can correctly express the intersection of the perfect mixing curve and the very slow increase of charging efficiency at high delivery ratio. The generalized model suggested in this chapter is a three-zone model and gives a five-parameter curve family. This model can precisely and flexibly represent all characteristics of the experimental charging efficiency curve, because its five parameters provide greater freedom for curve fitting.

Actually, this three-zone model can be further simplified as a two-zone model with air and gas zones and with variable coefficients of discharge proportion. In principle, this two-zone model can provide an exact curve for any scavenging process. However, unlike the three-zone model, the two-zone model cannot provide an analytical formula and requires the numerical method to solve it.

2.8 CONCLUSIONS

Because of its brevity, the model characterized by isobaric and isochoric process is apposite to assess scavenging performance for the ideal cycle simulation. If the parameters are chosen properly, this model can give a good estimation. The shortcomings of this model are its incapacity to give a step-by-step description of the scavenging process and requirement of an artificial history of the flow and concentration fields.

The model needs five parameters:

one of two coefficients of intake proportion of the air and mixing zones

two of three coefficients of discharge proportion of the air, gas and mixing zones
ratio of the initial gas zone volume to the cylinder volume
ratio of the remaining gas zone volume to the cylinder volume

Under the further assumption of constant coefficients of intake and discharge proportions, the analytical formulae for this model can be derived. And from it, all existing models with the assumption of isobaric and isochoric scavenging process can be deduced.

REFERENCES

[2.1] B. Hopkinson
"The Charging of Two-Cycle Engines"
Trans. N. E. Cst. Instn. Engrs. Shipbldrs, XXX, 1914

[2.2] F. Baudequin and P. Rochelle
"Some Scavenging Models For Two-Stroke Engines"
Proc. Instn. Mech. Engrs, 194, No. 12, 1980

[2.3] F. List
"The Charging Processes of Internal Combustion Engines"
Proc. Instn. Mech. Engrs Automobile Division, 1953-54

[2.4] R. S. Benson and P. T. Brandham
"A Method for Obtaining a Quantitative Assessment of the Influency on Two-Stroke Engine"
Int. J. Mech. Sci. No. 3, 1969

[2.5] T. Oka and S. Ishihara
"Relation between Scavenging Flow and its Efficiency of Two-Stroke Engine"
J. Soc. Mech. Engrs. Japan, No. 69, 1971

[2.6] G. Ciliberto
"Flat Research on Scavenging of 2-Stroke Large Bore Engines"
SAE 710146, 1971

Table 2.1 Parameters and Coefficients Used in Computations

type of scavenging system	initial volumetric ratio of mixing zone	volumetric ratio of displacement scavenging	volumetric ratio of remaining residual gas
uniflow	.55	.45	0.
loop	.60	.32	.08
cross	.63	.12	.25

type of scavenging system	coefficients of intake proportion		coefficients of exhaust proportion	
	air zone	mixing zone	air zone	mixing zone
uniflow	.58	.42	.10	.90
loop	.65	.35	.44	.56
cross	.65	.35	.41	.59

(a). Entrainment

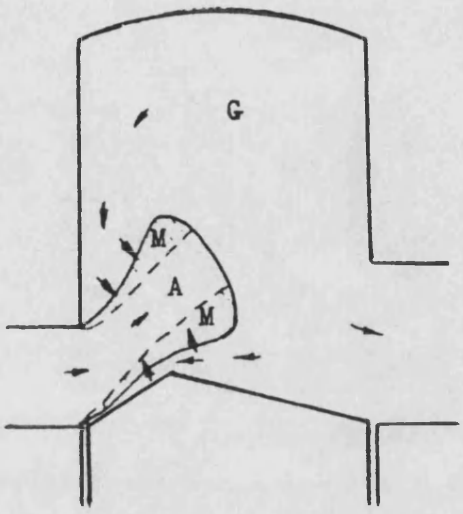

(b). Entrainment
and
Recirculation

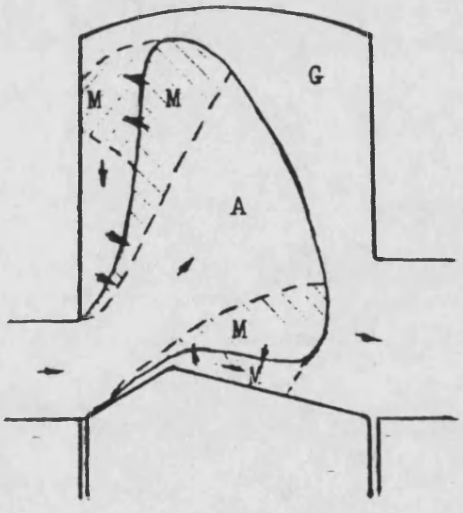

Fig. 2.1 Entrainment and Recirculation

(a). Displacement Scavenging

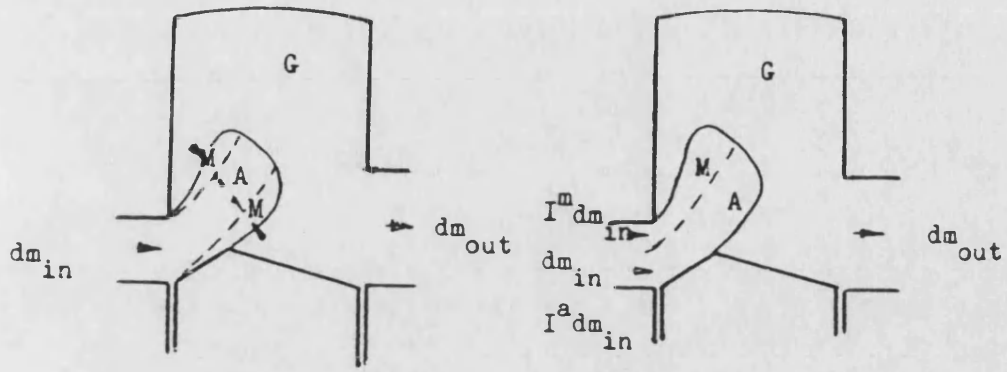

(b). Mixing Scavenging

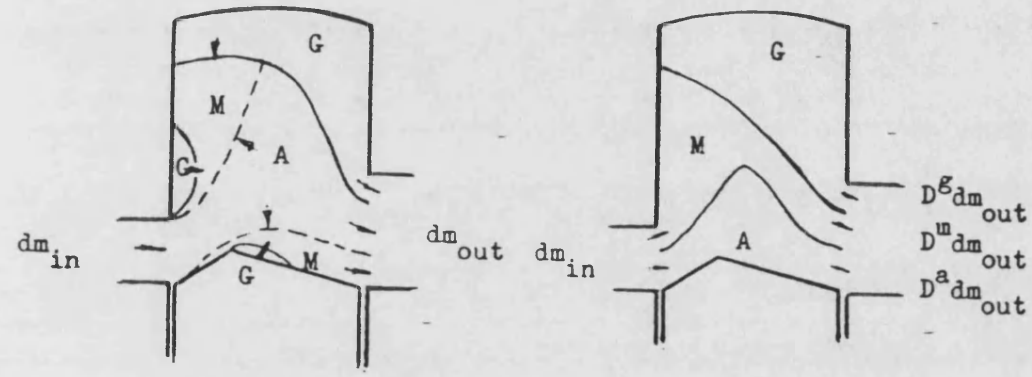

(c). Short-Circuiting

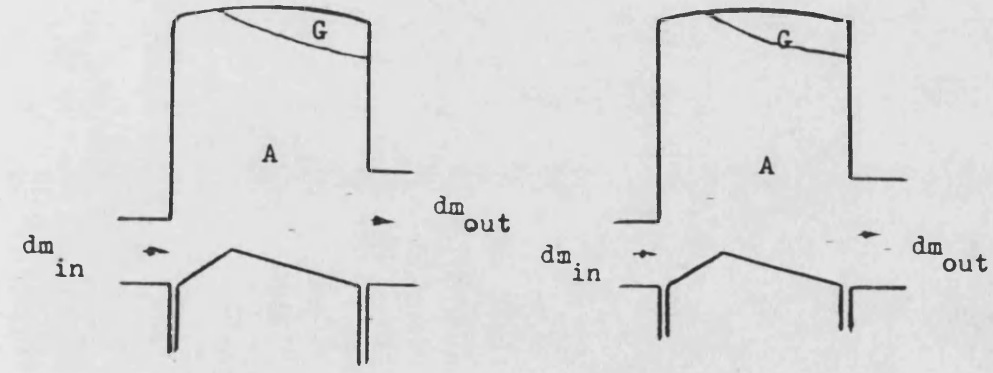

real process ideal process

Fig. 2.2 Idealization of Real Scavenging Process

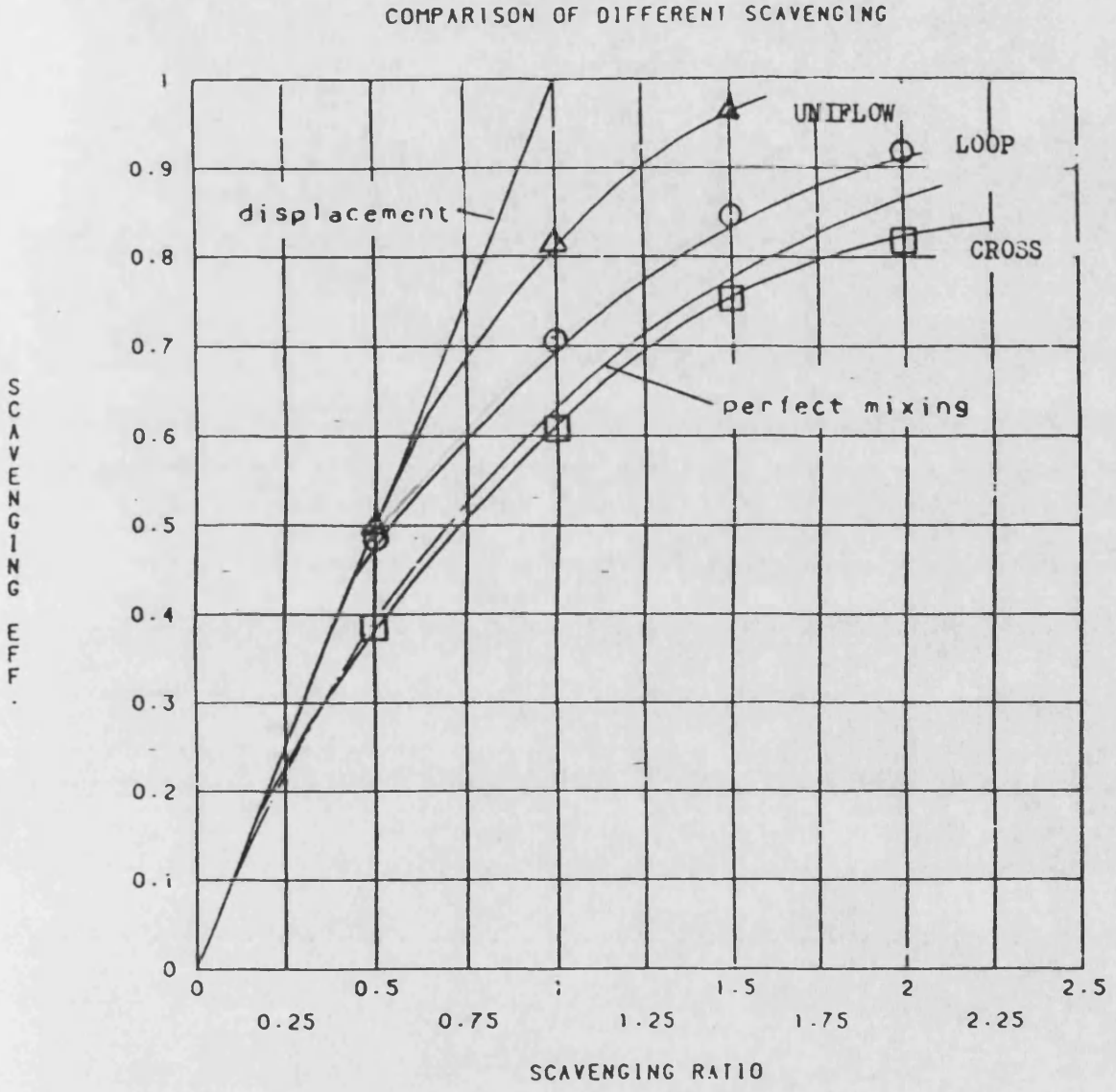

Experimental Results

△ —— Uniflow

○ —— Loop

□ —— Cross

Fig. 2.3 Comparison between Experimental and Computational Results Using Isobaric and Isochoric Model

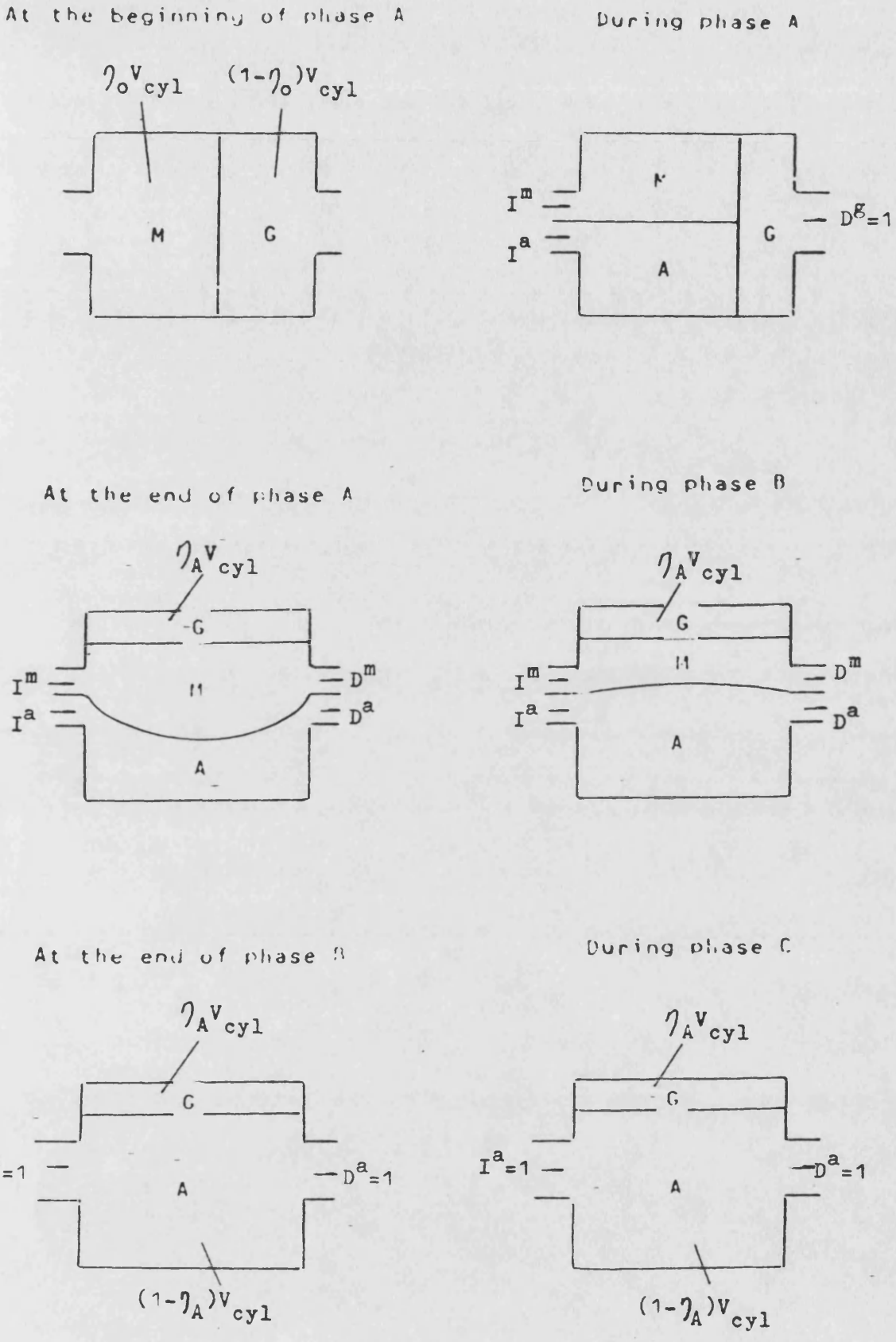

Fig. 2.4 The Simplified Anlalytical Model

Cross scavenging

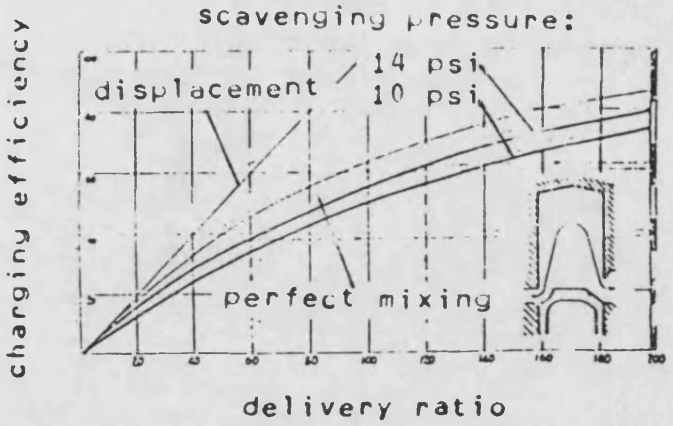

Loop Scavenging

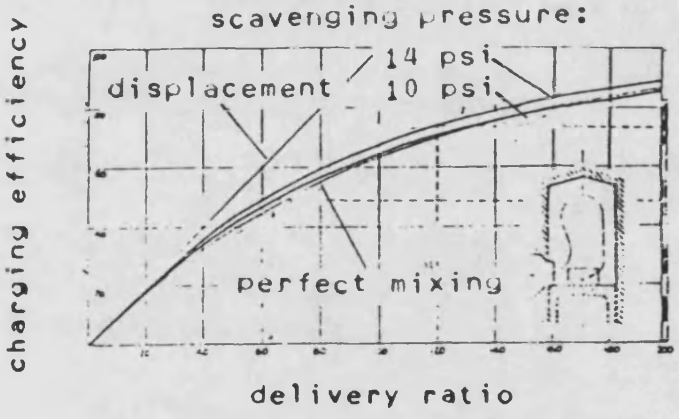

Uniflow scavenging

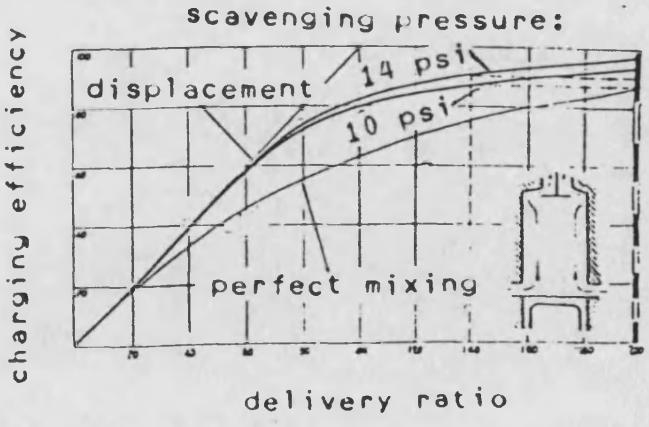

Fig. 2.5 Experimental Charging Curves by Schweitzer

Cross scavenging

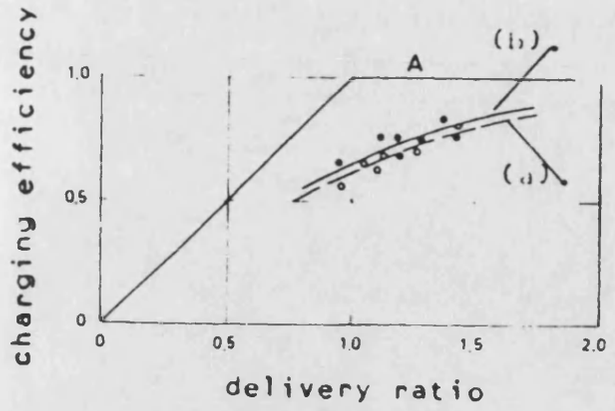

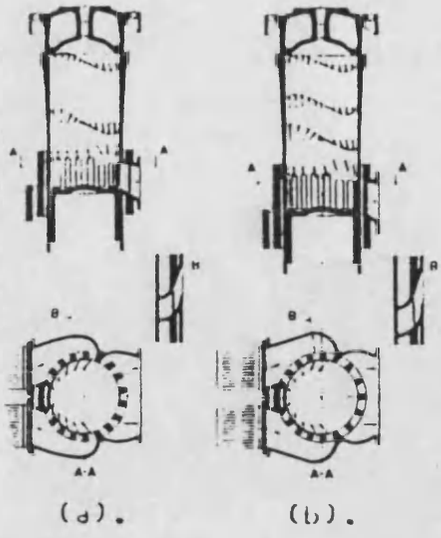

Loop Scavenging

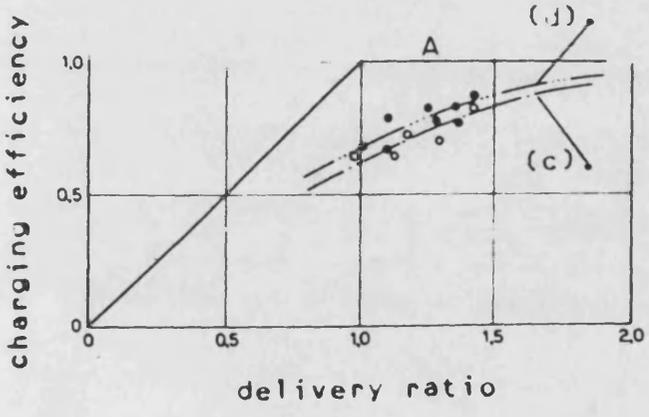

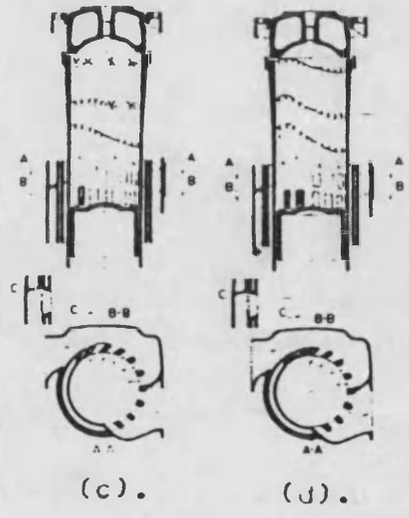

Uniflow scavenging

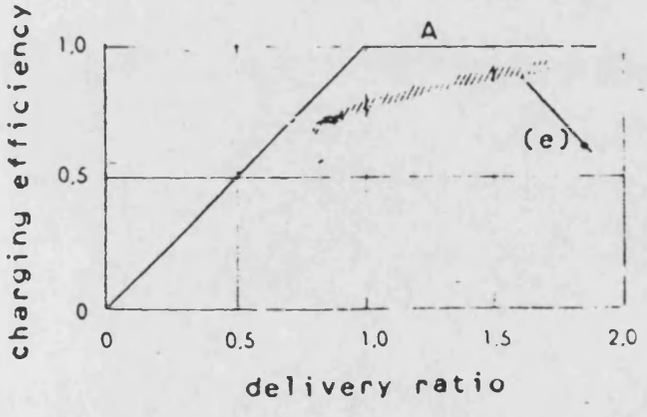

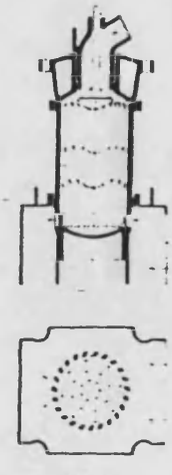

Fig. 2.6 Experimental Charging Curves by Fiat Co.

Chapter 3 STEP-BY-STEP THREE ZONE THERMODYNAMIC SCAVENGING MODEL

3.1 INTRODUCTION

In Chapter 2, the genaralized isobaric and isochoric thermodynamic model has been suggested. In that model it is assumed that the cylinder is subdivided into three zones: air, gas and mixing zones, and composition and temperature in each zone are homogeneuous.

As aforementioned, the model may provide a good approximation of the scavenging process. However, under the assumptions of constant pressure and volume the model fails to give a detailed description of varying pressure and volume during the scavenging process, and cannot determine the trapped pressure and mass based on the running condition. On the other hand, step-by-step numerical calculations of the scavenging process are of particular importance for optimizing port timing and matching a supercharger.

This chapter is aiming at developing a step-by-step thermodynamic model with variable cylinder pressure and volume following the previous idea that the cylinder space is divided into the three zones in which composition and temperature are homogeneous respectively.

3.2 PHYSICAL DESCRIPTION

The scavenging process including the inlet, in-cylinder and exhaust flow processes is of considerable complexity. These processes are unsteady. However, it has been shown by several investigators [3.1], [3.2] and [3.3] that these unsteady flow processes can be analyzed on a quasi-steady basis. "Quasi-steady" state here means that there are no local pressure differences in the cylinder and in the inlet and exhaust manifolds, i.e. the pressures are only functions of time, and that the mass rate flowing through the valves and ports at all time obeys the steady-state discharge equation, see Fig. 3.1.

As above mentioned, owing to the entrainment the air jet flowing into the

cylinder becomes two zones: the mixing and air zones. And in virtue of the recirculation, a mixing zone is separated from the residual gas zone. Thus, the cylinder is actually divided into three zones. Among three zones, only the composition of the mixing zone is temporally and spatially variable.

The scavenging process may be composed of the following phases: displacement scavenging, mixing scavenging and short-circuiting. Following the same idea as in Chapter 2, specifying the initial volume of the mixing zone, "dead volume" of the residual gas zone and coefficients of intake and discharge proportions within the three zones during different phases provides an artificial history of flow and concentraton during the scavenging process. The simplifying assumptions made in this chapter are as follows

(1). uniform pressure within the cylinder
(2). dividing the cylinder into three zones: the air, gas and mixing zones
(3). homogeneous temperature and composition within each zone
(4). heat transfer between zones and walls using Woschni's correlation on the basis of a bulk average temperature
(5). neglect of mass, momentum and energy transfer between zones
(6). specifying an initial volume of the mixing zone, if necessary, a "dead volume" of the residual gas zone and an artificial history of intake proportions within the air and mixing zones, and of discharge proportions within the air, gas and mixing zones.

3.3 MATHEMATICAL TREATMENT

3.3.1 GOVERNING EQUATIONS

3.3.1.1 Conservation of mass

For the general zone i,

$$\Delta m^{i} = \Delta m^{i}_{in} - \Delta m^{i}_{out} \qquad (3.1)$$

change of mass in the zone = mass flowing into the zone − mass flowing out of the zone

where, as above, the superscript i may be taken as a, g and m which

represent the air, gas and mixing zones respectively.

3.3.1.2 Composition equation

Instead of air mass concentration, in this model, the equivalence ratio is used indirectly as a parameter of composition, because it can be conveniently used for calculating thermodynamic properties of air, gas and their gas mixture.

For the general zone i,

$$F^i = \frac{m_f^i}{f_s m_s^i} = \frac{m_{f,o}^i + m_{f,in}^i - m_{f,out}^i}{f_s (m_{s,o}^i + m_{s,in}^i - m_{s,out}^i)} \qquad (3.2)$$

and

$$m^i = m_f^i + m_s^i$$

where the superscript i retains the previous significance,

m_f^i is the mass of burnt fuel within the zone i,

m_s^i is the sum of air mass and the air mass consumed in the combustion of the fuel m_f^i.

fs is stoichiometric fuel-air ratio,

the subscripts o, in and out represent the initial, inflowing and outflowing amount respectively.

Under the assumption of complete combustion, the mass of residual gas is

$$m_g^i = \left(1 + \frac{1}{f_s}\right) m_f^i \qquad (3.3)$$

and the actual mass of fresh air is

$$m_a^i = m^i - m_g^i \qquad (3.4)$$

3.3.1.3 Conservation of energy

For the general zone i,

$$\Delta(m^i u^i) = \sum(\Delta m^i_{in} h^i_{in}) - \sum(\Delta m^i_{out} h^i_{out}) - \Delta Q^i - P\Delta V^i \qquad (3.5)$$

change of internal energy in the zone = enthalpy flowing into the zone − enthalpy flowing out of the zone − heat transfer from the zone − external work done by the zone

where h^i_{in} is the specific absolute enthalpy within the upstream zone

Similarly, the superscripts a, g and m are substituted for i to stand for the air, gas and mixing zones.

The equilibrium thermodynamic properties of the products of combustion of CnH2n and air are calculated from cylinder pressure, local temperature and equivalence ratio within each zone based on the mathematical expressions for the internal energy and gas constant by Newhall and Starkman [3.4].

Woschni's correlation is adopted to calculate heat transfer [3.5]

$$\Delta Q_w = \alpha A_w (T_{cyl} - T_w)\Delta t \qquad (3.6)$$

where α is the heat transfer coefficient,

$$\alpha = C \cdot D^{-0.2} \cdot P^{0.8} \cdot T^{-0.53} \left(C_1 V_m + C_2 \frac{V_s T_{tr}}{P_{tr} V_{tr}} (P - P_o)\right)^{0.8} \qquad (3.7)$$

where the bulk average temperature is defined by

$$T_{cyl} = \frac{m^a T^a + m^m T^m + m^g T^g}{m^a + m^m + m^g} \qquad (3.8)$$

and

D is the cylinder bore

V_m is the mean piston speed

V_s is the swept volume

P is the cylinder pressure

P_{tr}, V_{tr}, T_{tr} are the trapped pressure, volume and temperature.

$P-P_o$ is the difference between cylinder pressure with combustion and cylinder pressure at the same point in the cycle for the same conditions except for the absence of any combustion.

The total heat transfer from the cylinder is composed of three portion: heat transfer from the cylinder head, liner and piston for which the subscripts h, l and p represent respectively. Thus, the total heat transfer is

$$\Delta Q_{cyl} = \Delta Q_h + \Delta Q_l + \Delta Q_p \qquad (3.9)$$

The heat transfers in the various zones are allocated in relation to their mass and temperatures, i.e.

$$\Delta Q^i = \frac{m^i T^i}{m^a T^a + m^m T^m + m^g T^g} \Delta Q_{cyl} \qquad (3.10)$$

where the letter i may be taken as a, g and m for the air, gas and mixing zones respectively.

Heat transfer between the zones is ignored.

3.3.1.4 Equation of state

Using local properties, the equation of state is used for each zone

$$PV^i = m^i R T^i \qquad (3.11)$$

3.3.1.5 Mass constraint

The present trapped mass is equal to the sum of the previous trapped mass, inflowing and outflowing mass

$$m = m_o + \Delta m_{in} - \Delta m_{out} \qquad (3.12)$$

3.3.1.6 Volume constraint

The volumes of the air, gas and mixing zones add up to the total volume of cylinder.

$$V^a + V^g + V^m = V_{cyl} \qquad (3.13)$$

The instantaneous cylinder volume and its derivative in respect of crank angle can be calculated based on the piston-crank mechanism. The kinetic analysis of a horizontal opposed piston engine, which this thesis emphasizes, is attached in Appendix I.

3.3.2 BOUNDARY CONDITIONS

The mass flowing through the inlet or exhaust ports is determined from the compressible flow equation

$$\Delta m = C_d A \frac{P_u}{\sqrt{R_u T_u}} \Psi_m \Delta t \qquad (3.14)$$

where

$$\Psi_m = \sqrt{\frac{2\gamma}{\gamma-1}\left(\Pi^{\frac{2}{\gamma}} - \Pi^{\frac{\gamma+1}{\gamma}}\right)} \qquad (3.15)$$

for

$$\Pi = \frac{P_d}{P_u} > \Pi_{cr} = \gamma\left(\frac{2}{\gamma+1}\right)^{\frac{\gamma}{\gamma-1}}$$

and

$$\Psi_m = \Psi_{m,cr} = \sqrt{\gamma\left(\frac{2}{\gamma+1}\right)^{\frac{\gamma+1}{\gamma-1}}} \qquad (3.16)$$

for

$$\Pi < \Pi_{cr}$$

where Δm is the mass flowing through the inlet or exhaust ports

$\prod$ is the pressure ratio

A is the geometric flow area

C_d is the coefficient of discharge

P_u, R_u, T_u are the stagnation pressure, specific gas constant, stagnation temperature, all at the upstream condition

P_d is the pressure downstream

γ is the specific heat ratio based on the upstream conditions

The coefficient of discharge C_d in equation (3.14) is defined as the quotient of the actual and the theoretical mass flow rates based on the geometric area. The coefficient of discharge is quoted from a published correlation [3.6], which, from dimensional analysis, is established between the coefficient of discharge and the following variables: the cylinder pressure, port opening and temperature. Actually, it has been shown [3.7] that constant coefficients of discharge render rather good results.

For the general zone i,

the definitions of the coefficients of intake and discharge proportion are the same as in Chapter 2

$$I^i = \frac{\Delta m^i_{in}}{\Delta m_{in}} \qquad (3.17)$$

$$D^i = \frac{\Delta m^i_{out}}{\Delta m_{out}} \qquad (3.18)$$

It is noted that the following equations are valid

$$I^a + I^m = 1 \qquad (3.19)$$

$$D^a + D^g + D^m = 1 \qquad (3.20)$$

The equation of energy conservation (3.5) becomes

$$\Delta(m^i u^i) = I^i \Delta m_{in} h^i_{in} - D^i \Delta m_{out} h^i_{out} - \Delta Q^i - P\Delta V_i \qquad (3.21)$$

It is noted that with the equations of mass and volume constraints, (3.12) and (3.13), the equations of energy conservations of all the three zones (3.21) may be added to give the following overall energy balance equation

$$\Delta(mu) = \Delta m_{in} h_{in} - \Delta m_{out} h_{out} - \Delta Q_{cyl} - P\Delta V_{cyl} \qquad (3.22)$$

change of internal energy = enthalpy flowing into the cylinder − enthalpy flowing out of the cylinder − heat transfer from the cylinder − external work done

In summary, for each zone equations (3.1), (3.2), (3.21), (3.14), (3.10) and (3.11) constitute a system of governing equations, and for all the three zones the equations of mass and volume constraints, (3.12) and (3.13), must be satisfied. The simultaneous equations are non-linear. When the coefficients of intake and discharge proportions, I and D, are given, the system is solvable.

3.4 COMPUTATIONAL PROCEDURE AND RESULTS

The flow chart for computation is shown in Fig. 3.2. The simultaneous system is solved by a stepwise integration method. With the compressible flow equation (3.14), equations (3.1) and (3.2) can be explicitly solved for mass and composition. However, equations (3.21), (3.10) and (3.11) are coupled for pressure, temperature and volume to satisfy the constraint equations (3.12) and (3.13). A triple iteration loop is used for solution. The outer iteration loop ensures the volumes of the air, gas and mixing zones to satisfy the equation of volume constraint, and thereby verifies the conjecture of the cylinder pressure. The intermediate iteration loop makes the temperature and volume with each zone to satisfy the equation of state (3.11). The reason for the introduction of the inner iteration loop is that the calculation from thermodynamic properties to temperature requires the inverse function of the internal energy polynomial, whose analytic form, however, is difficult to obtain. The program is incorporated in a step-by-step cycle simulation propram as an optional part to describe a scavenging process. The increment is 1° crank angle.

For the sake of estimating the difference resulting from the isobaric and

isochoric assumptions in the previous model in Chapter 2, the same experimental work for the uniflow, loop and cross scavenging systems by List [2.3] is used again. The computations use the varying pressure and volume model suggested in this chapter. Because the original paper by List did not provide the details of the tested engines, these computations have been done based on a supposed engine with the same size and port timing, but with the different scavenging systems, whose characteristics are summarized in Table 3.1. It is assumed that for the loop and cross scavenging systems the unsymmetric timing is realized by auxiliary scavenging valve The coefficients of intake and discharge proportions are the same as in Chapter 2, as listed in Tab. 2.1. The comparison between the computational results from these two models shows that the discrepancy remains within 5%. Thus, the isobaric and isochoric model gives a good approximation, as shown in Fig. 3.3. Pressures, temperatures, equivalence ratios and mass during the scavenging processes of the uniflow, loop and cross systems are illustrated in Figs. 3.4 to 3.6, respectively. From these figures, it is obvious that under the same running conditions, among three scavenging systems the uniflow scavenging system traps the largest and purest charge, and achieves the best scavenging quality, the cross system traps the smallest and least pure, and the loop system situates between the previous two systems.

3.5 COMPARISON OF DIFFERENT STEP-BY-STEP MODELS

In a real scavenging process, the air flowing into the cylinder first enters the air zone exclusively and then entrains gas within the gas zone and forms the mixing zone, in other words, air and gas from the air and gas zones respectively flow into the mixing zone.

From the equations of mass constraint (3.12), overall energy balance (3.22) and compressible flow (3.14), it is evident that under given conditions of inlet and exhaust manifolds, the history of overall exhaust composition, i.e. the upstream condition before exhaust ports, dominates the scavenging process. On the other hand, different combinations of different compositions and coefficients of intake and discharge proportions within the three zones may lead to identical histories of overall exhaust composition.

The models suggested in Chapter 2 and this chapter both consider that a part of air injected through the inlet ports directly mixes with a given amount of residual gas and forms the mixing zone. On the basis of the previous analysis, provided the correct exhaust history is specified these models are always able to give an approximate description of the real scavenging process.

3.5.1 STREIT AND BORMAN'S MODEL [3.8]

3.5.1.1 Main points (Fig. 3.7)

Two zones:

zone 1 connected to the inlet ports
zone 2 connected to the exhaust ports

Two phases:

displacement scavenging
mixing scavenging

Mass transfer:

During the displacement scavenging phase, there is no mass transfer between these two zones, i.e. zone 1 is the air zone and zone 2 is the gas zone.

During the mixing scavenging phase, both mass transfer rates from zone 1 to zone 2 and from zone 2 to zone 1 increase with time, i.e. both zones 1 and 2 become the mixing zones with different compositions. However, with increase of time, the compositions within zones 1 and 2 approach the same concentration.

3.5.1.2 Analogous description based on the model suggested in this chapter

Two zones:

the gas zone and the mixing zone

Two phases:

displacement scavenging
mixing scavenging

Coefficients of intake and discharge proportions:

Throughout the scavenging process all the air entering the cylinder flows into the mixing zone, i.e. $l_m = 1$.
During the displacement scavenging phase, only the gas within the gas zone flows out of the cylinder.
During the mixing scavenging phase, with increase of time the coefficient of discharge proportion from the gas zone decrease, and the coefficient of discharge proportion from the mixing zone increase. When the coefficient of discharge proportion from the gas zone decreases to zero, the scavenging process becomes a completely mixing scavenging process.

3.5.2 BENSON'S MODEL [3.9]

3.5.2.1 Main points (Fig. 3.8)

Three zones:

the air, gas and mixing zones.
Throughout the scavenging process the air zone is always adjacent to the inlet ports.

Three phases:

displacement scavenging phase
short-circuiting
mixing scavenging phase
During the scavenging process, the gas, air and mixing zones are adjacent to the exhaust ports in the displacement scavenging, short-circuiting and mixing scavenging phases respectively.

Mass transfer:

The air entering the mixing zone at any instant of time is a fixed proportion of the instantaneous air flow rate entering the cylinder. The gas entering the mixing zone is treated as follows:

treatment 1 : At any instant of time the proportions of gas and air entering the mixing zone are constant, i.e. a fixed gas entrainment ratio.
treatment 2 : The mass of gas in the gas zone is reduced linearly with time.

3.5.2.2 Analogous decription based on the model suggested in this chapter

Three zones and three phases are the same as above mentioned.

Coefficients of intake and discharge proportion:

Throughout the scavenging process, the ratio of coefficients of intake proportion into the mixing and air zones is equal to the same fixed ratio as in Benson's model, i.e. I^m/I^a=const.

During the displacement scavenging phase, only the gas within the gas zone discharges from the cylinder, i.e. $D^g=1$.

During the short-circuiting phase, only the air within the air zone flows out of the cylinder, i.e. $D^a=1$.

For the mixing scavenging phase, choosing an initial volume of residual gas for the mixing zone and coefficients of discharge proportion from the gas and mixing zones is equivalent to obtaining virtually the same overall exhaust composition as that in Benson's model. It is obvious that for treatment 1 the coefficient of discharge proportion from the gas zone is variable in order to get the same history of exhaust composition with in Benson's model, while for treatment 2 the coefficient of discharge proportion from the gas zone is fixed so as to give an linear reduction of the mass in the gas zone with the lapse of time.

3.5.3 HEESCHEN'S MODEL [3.10]

3.5.3.1 Main points (Fig 3.9)

Three zones:

the air, gas and mixing zones.
Throughout the scavenging process the air zone is always connected with the inlet ports.

Three phases:

displacement scavenging
mixing scavenging
short-cirtuiting

Mass transfer:

During the displacement scavenging phase, only the gas zone is connected to the exhaust ports.
During the mixing scavenging phase, only the mixing zone is connected to the exhaust ports. The mixing scavenging phase continues until the mixing zone disappears.
During the short-circuiting phase, only the air zone is connected to the exhaust ports.
Throughout the scavenging process, both air and residual gas from the air and gas zones respectively enter the mixing zone in a fixed proportion which is dependent on power output.

3.5.3.2 Analogous description based on the model suggested in this chapter

Three zones and three phases are the same as above.
Coefficients of intake and discharge proportion:

During the displacement scavenging phase, only the gas in the gas zone discharges from the cylinder, i.e. $D^g=1$.
During the displacement and mixing scavenging phases, the ratio of coefficients of intake proportion into the mixing and air zones is the same as in Heeschen's model.

Similarly, for the mixing scavenging, fitting an initial volume of residual gas for the mixing zone and coefficients of discharge proportion from the gas and mixing zones is to maintain the same history of overall exhaust composition as in Heeschen's model.
During the short-circuiting phase, only the air in the air zone flows into and out of the cylinder, i.e. $I^a=1$ and $D^a=1$.

3.6 CONCLUSIONS

The present model characterized by varying pressure and volume is able to give a step-by-step description of the scavenging process. This model, like any other thermodynamic model, requires an artificial history of the flow and concentration fields.
The model needs five parameters:

one of two coefficients of intake proportion of the air and mixing zones
two of three coefficients of discharge proportion of the air, gas and mixing zones
ratio of the initial gas zone volume to the cylinder volume
ratio of the remaining gas zone volume to the cylinder volume

Properly selecting the previous parameters, the generalized step-by-step three zone model can represent any one of the various scavenging models discussed in this chapter.

REFERENCES

[3.1] H. List and G. Reyl

"Der Ladungswechsel der Verbrenbnungskraftmaschine Part 1: Grundlagen"

Springer Verlag, Vienna, 1949

[3.2] K.J. McAulay, T. Wu, S. K. Chen, G.L. Borman, P.S. Myers and O.A. Uyehara

"Development and Evaluation of the Simulation of the Compression-Ignition Engine"

SAE 650451, 1965

[3.3] M. Ryti

"A Computer Programme for the Gas Exchange Process in Turbocharged Diesel Engines"

The Brown Boveri Review, Aug. 1968

[3.4] H.K. Newhall and E.S. Starkman

"Thermodynamic Properties of Octane and Air for Engine Performance"

SAE 633G, 1963

[3.5] G. Woschni

"A Universally Applicable Equation for the Instantaneous Heat Transfer Coefficient in the Internal Combustion Engine"

SAE 670931, 1967

[3.6] F.J. Wallace and R.W.S. Mitchell

"Wave Action Following the Sudden Release of Air Through an Engine Port System"

Proc. Instn. Mech. Engrs. (B) Vol. 1B, No. 8, 1952-53

[3.7] R.S. Benson

"The Influence of Exhaust Belt Design on the Discharge Process of a Two-Stroke Cycle Engine"

Proc. Instn. Mech. Engrs. 174, 713, 1960

[3.8] E.E. Streit and G.L. Borman

"Mathematical Simulation of a Large Turbocharged Two-Stroke Diesel Engine"
SAE 710176, 1971

[3.9] R.S. Benson
"A New Gas Dynamic Model for the Gas Exchange Process in Two Stroke Loop and Cross Scavenged Engines"
Int.J.Mech.Sci. vol. 19, No. 12, 1977

[3.10] K. Heeschen
"Beitrag zur Berechnung des Betriebsverhaltens gleichstromgespulter Zweitakt-Schiffsdieselmotoren"
MTZ 45, 9, 1985

Table 3.1 Characteristics of the Supposed Engine

Number of cylinders	3
Bore	82.55 mm
Stroke	203.2 mm
Swept volume	3.261 l
Nominal compression ratio	14/1
Rated power output	78 kw
Exhaust port open	66 BBDC
Inlet port open	43 BBDC
Exhaust port close	53 ABDC
Inlet port close	56 ABDC
Two-stroke cycle	
Compression ignition	
Scavenging system	optional

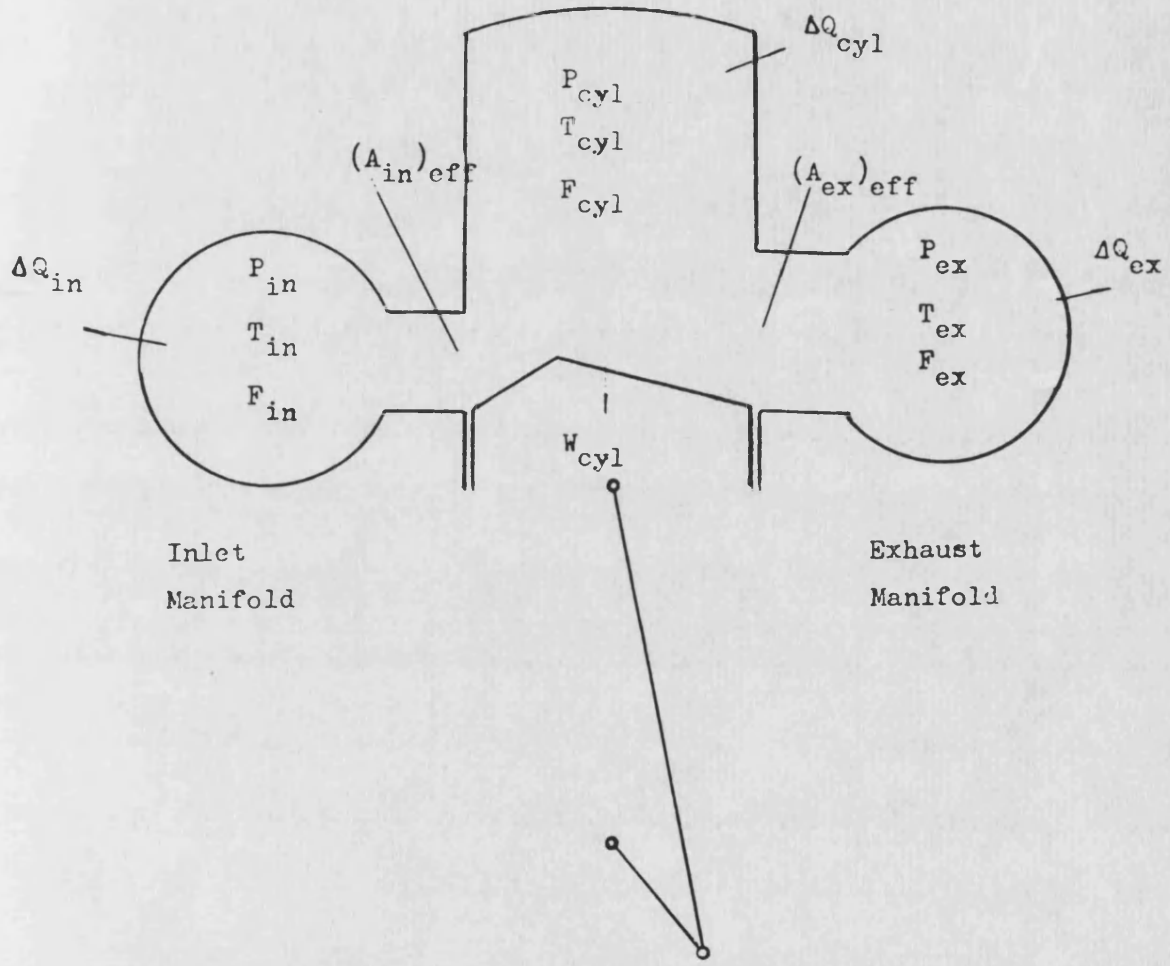

Fig. 3.1 Thermodynamic System during Scavenging Process

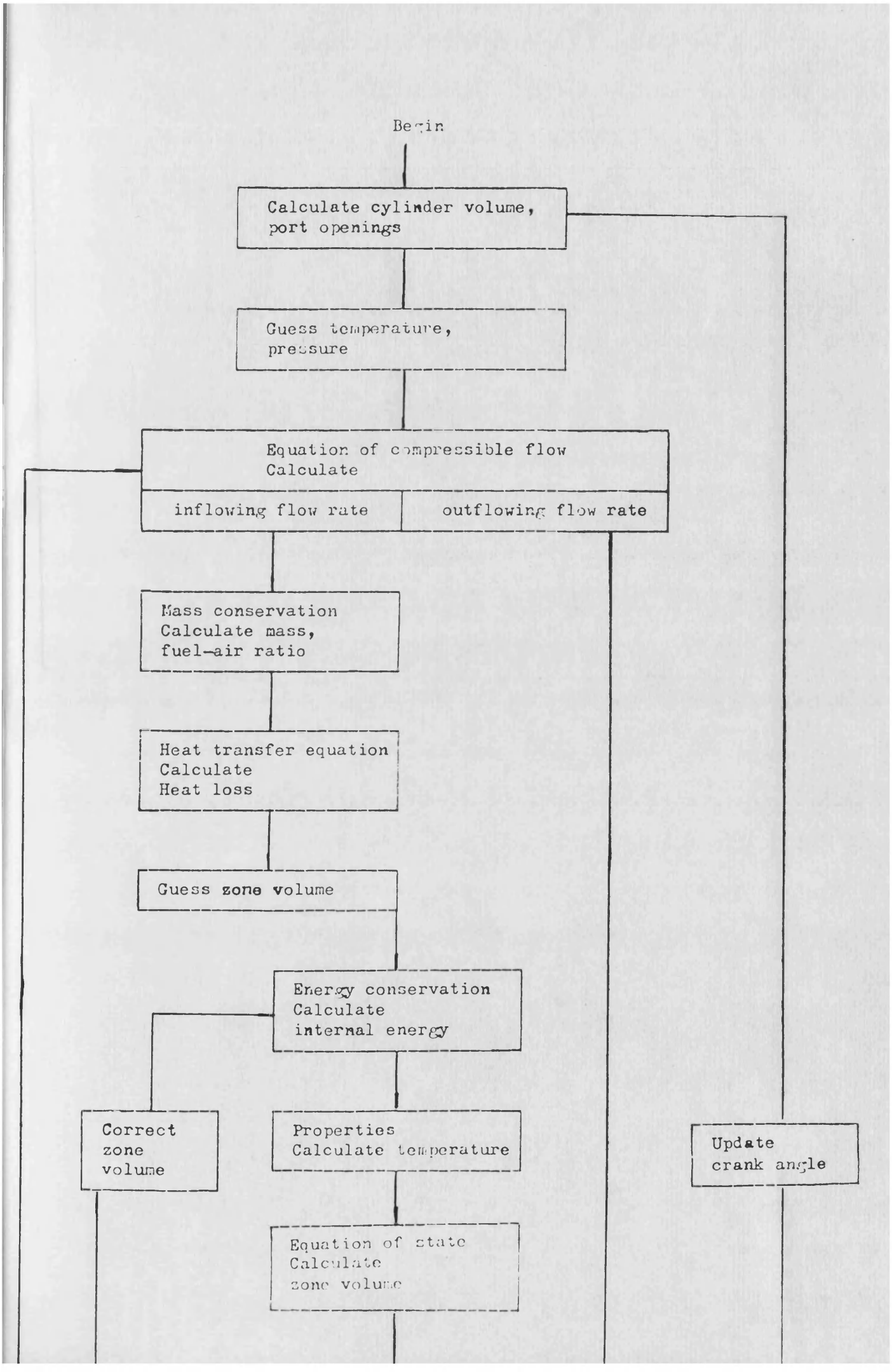
Begin
Calculate cylinder volume, port openings
Guess temperature, pressure
Equation of compressible flow Calculate
inflowing flow rate
outflowing flow rate
Mass conservation Calculate mass, fuel-air ratio
Heat transfer equation Calculate Heat loss
Guess zone volume
Energy conservation Calculate internal energy
Correct zone volume
Properties Calculate temperature
Update crank angle
Equation of state Calculate zone volume

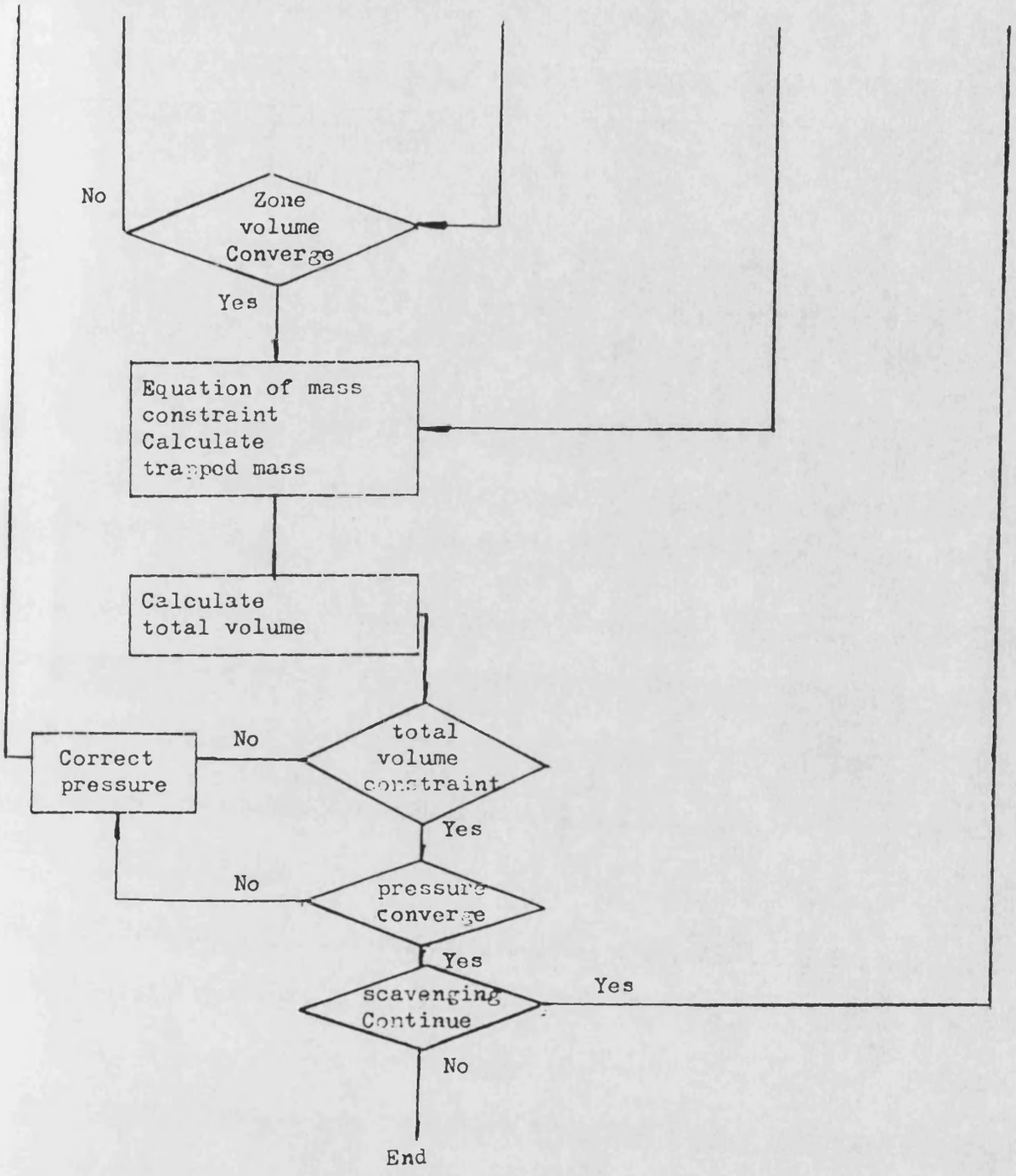

Fig. 3.2 Flow Chart for Three Zone Model Calculation

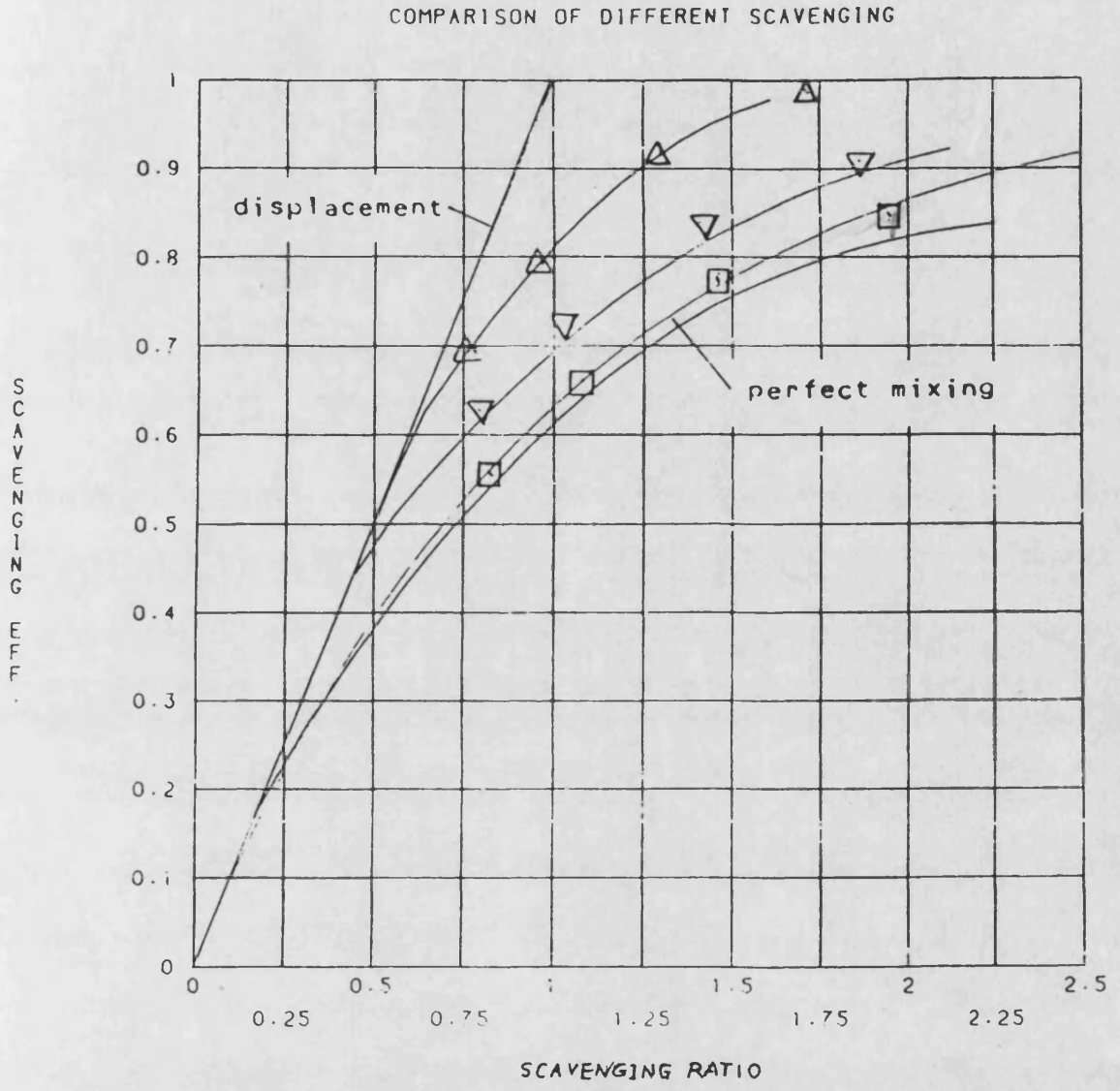

Theoretical Results

△ —— Uniflow

▽ —— Loop

□ —— Cross

Fig. 3.3 Comparison between Experimental and Computational Results Using Three Zone model

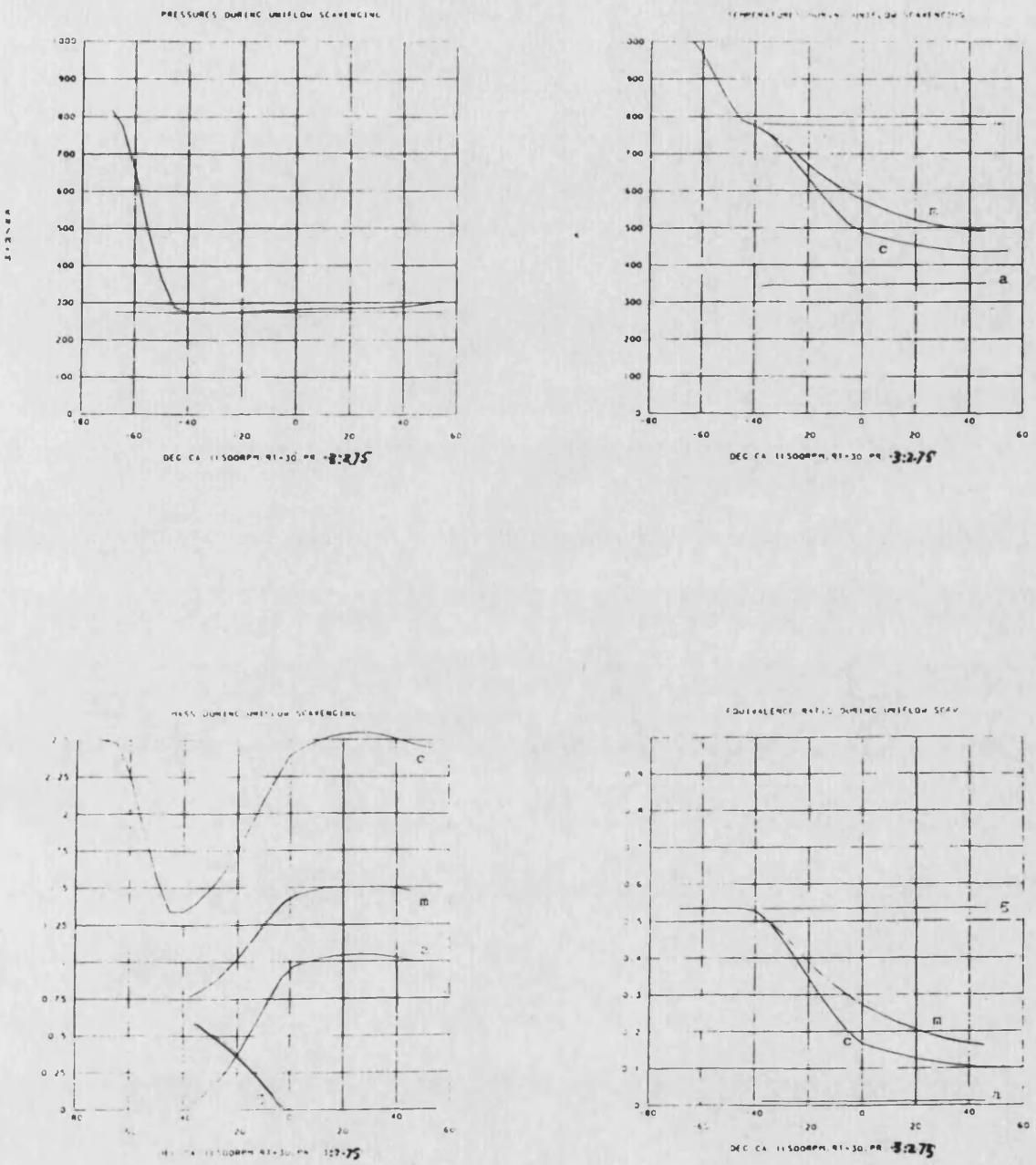

c— cylinder
a— air zone
m— mixing zone
r— residual gas zone

Fig. 3.4 Pressure, Temperature, Mass and Equivalence Ratio during Uniflow Scavenging Process

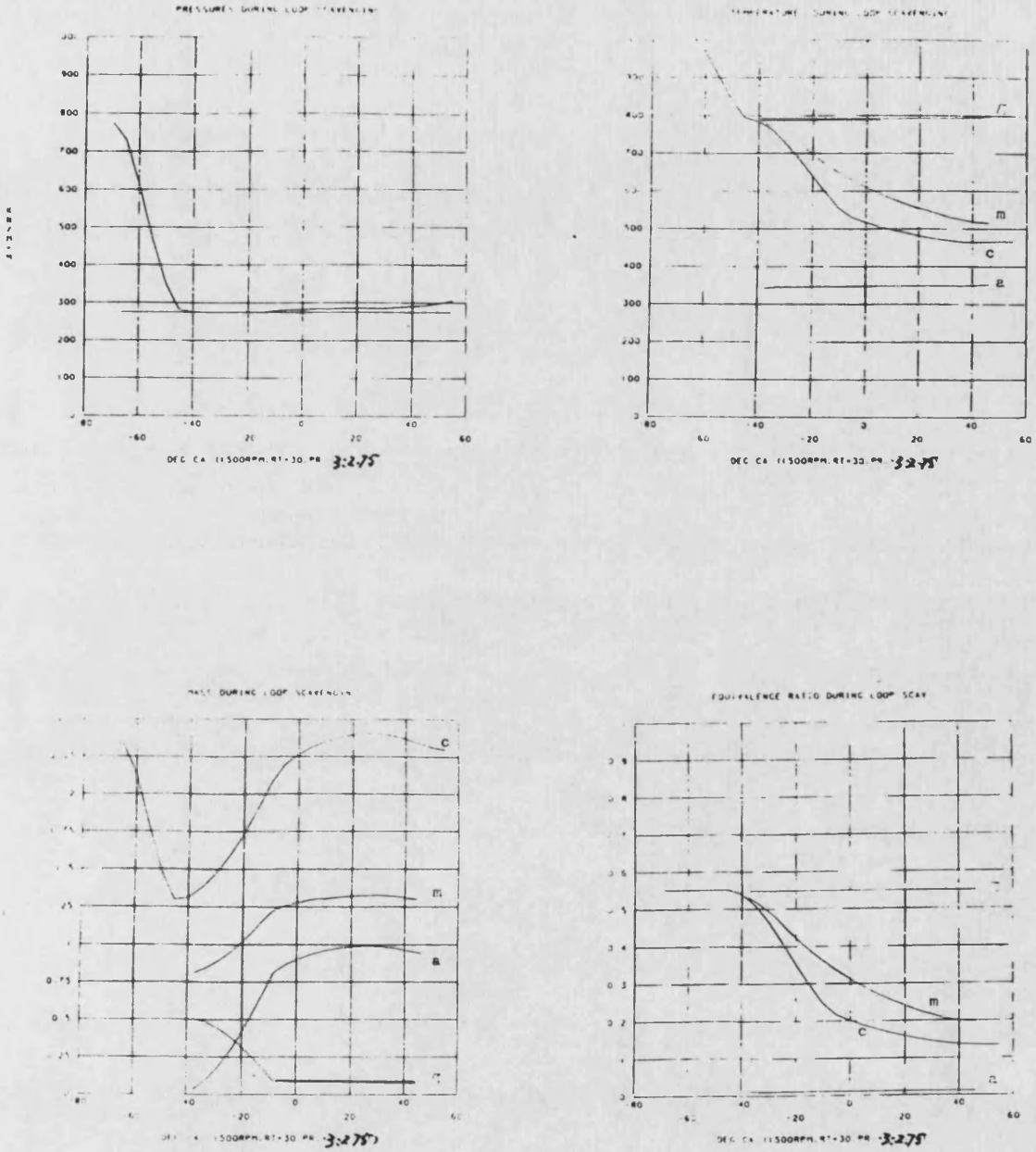

c— cylinder
a— air zone
m— mixing zone
r— residual gas zone

Fig. 3.5 Pressure, Temperature, Mass and Equivalence Ratio during Loop Scavenging Process

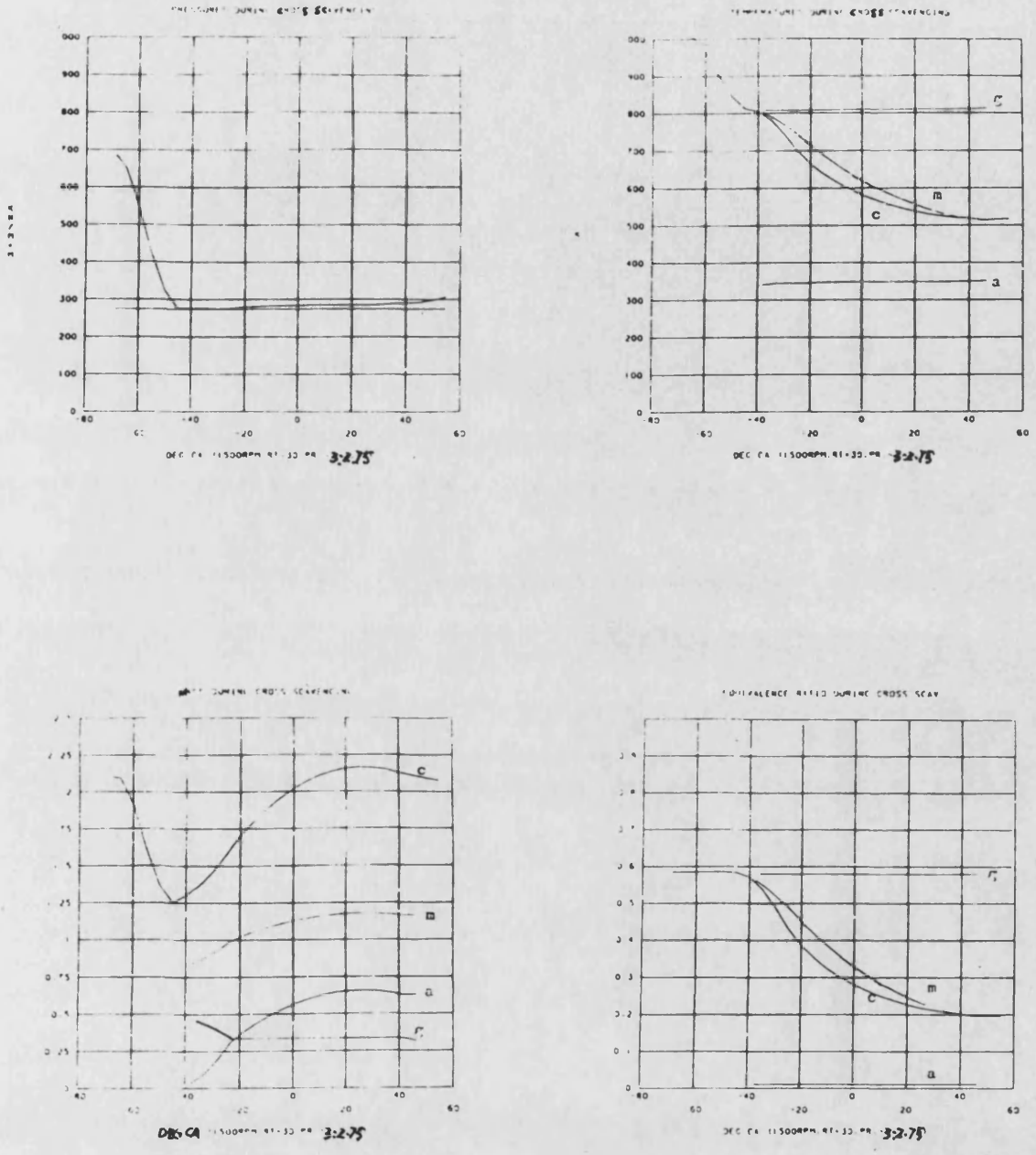

c-- cylinder
m-- mixing zone
a— air zone
r— residual gas zone

Fig. 3.6 Pressure, Temperature, Mass and Equivalence Ratio during Cross Scavenging Process

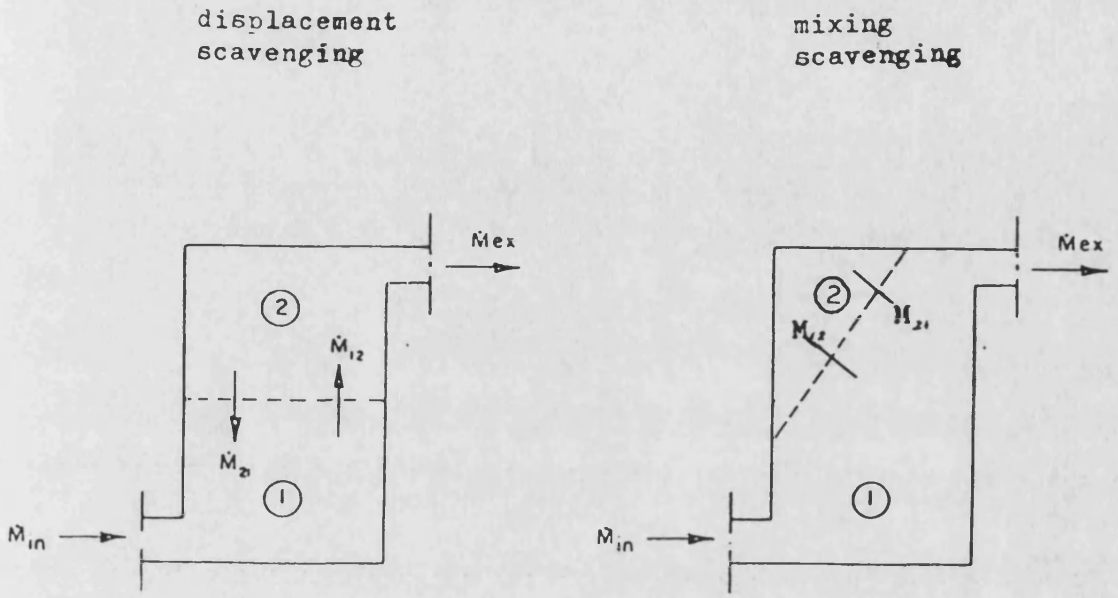

M_{12} — mass flow rate from system 1 into system 2

M_{21} — mass flow rate from system 2 into system 1

M_{in} — mass flow rate through the inlet ports

M_{ex} — mass flow rate through the exhaust ports

Fig. 3.7 Streit and Borman's Model

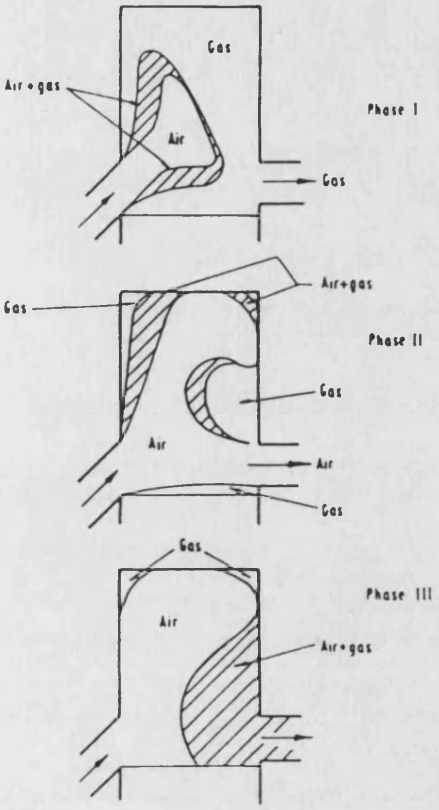

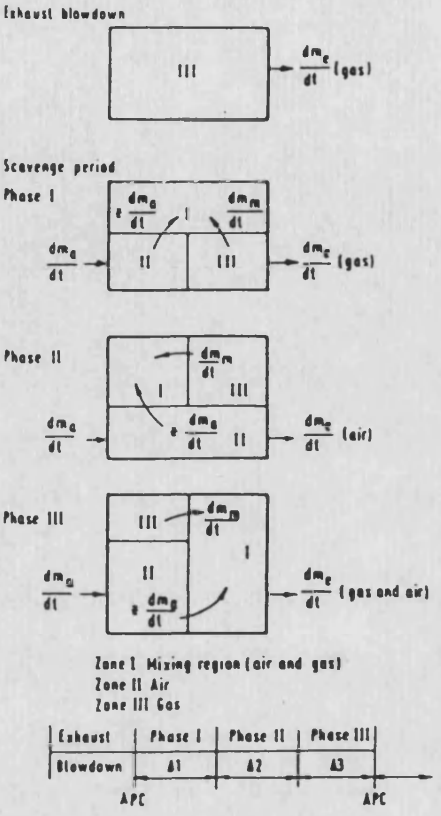

Variation of gas zone volume III vs. crank angle— Version 2

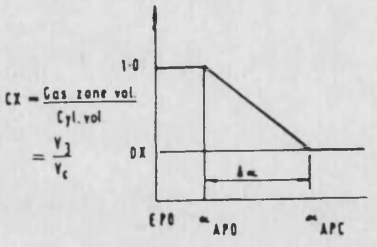

Fig. 3.8 Benson's Model

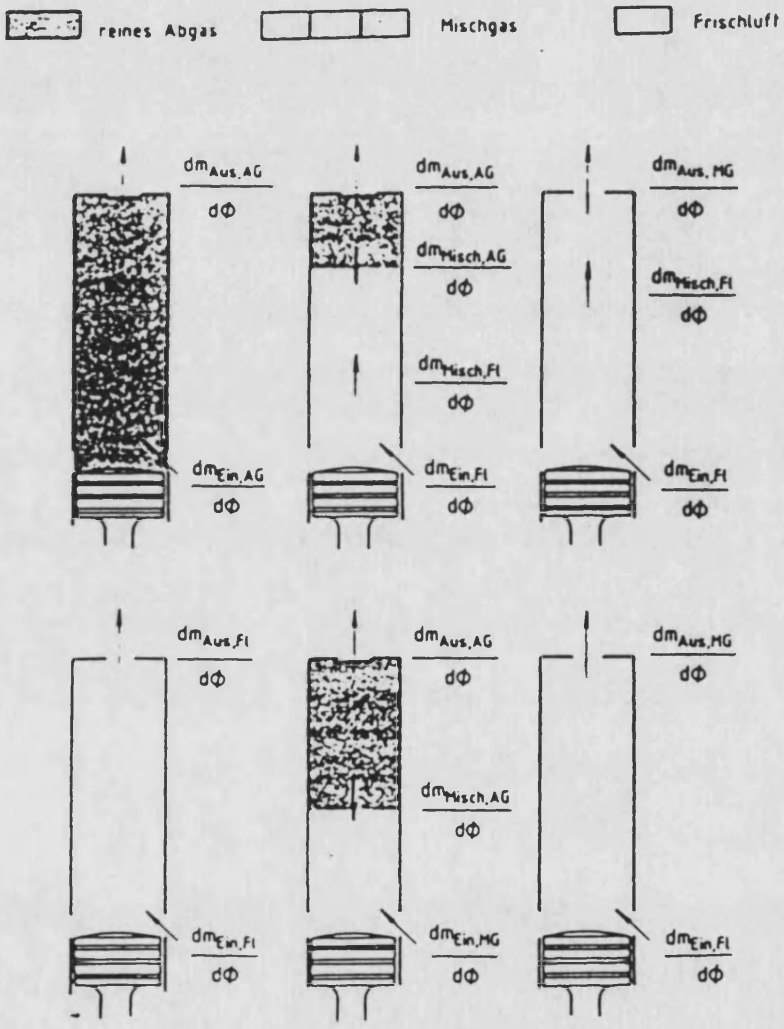

Fig. 3.9 Heeschen's Model

Chapter 4 PHENOMENOLOGICAL FLUID DYNAMIC MODELS BASED ON JET MIXING FOR UNIFLOW SCAVENGING

4.1 INTRODUCTION

A number of models have been developed over many years to describe the scavenging process. The essential nature of the previous models is thermodynamic, although some recent models have begun to take some gas dynamic characteristics into consideration. All these models require an artificial description of the history of the transport process in the cylinder in order to bridge the information gap which the omission of details of the transport process incurs.

The behaviour of turbulent jet flow in the scavenging process was first investigated many years ago [4.1]. Nevertheless, the complexity of the phenomenon precludes a comprehensive model. Fortunately, the axisymmetry of the uniflow scavenging process, which achieves the best scavenging quality, alleviates the difficulty of the problem.

The aim of this chapter is to develop two simplified and practical fluid dynamic models for uniflow scavenging. Under the simplifying assumptions, such as uniform cylinder pressure and simple profiles of velocity and composition, the models in this chapter quickly and easily give a phenomenological description with a temporal and spatial resolution of flow and concentration fields.

Firstly, this chapter outlines the fundamental features of the transport phenomena in the scavenging process.

Secondly, following a conventional idea, this chapter introduces a steady jet model. This model assumes that the scavenging process is composed of two periods:

(1). the blowdown period based on compressible flow with varying pressure: and
(2). the scavenge period based on incompressible flow with constant pressure and opening of the inlet and exhaust ports.

The model retains the original advantages of simplicity and the ability to design the exhaust belt and approximately determine air flow rate [4.2], and furthermore, has the merit of providing a better physical description of the scavenging process than the earlier thermodynamic models.

Finally, this chapter suggests a multi-zone model based on unsteady jet theory. The model treats the scavenging process as compressible flow with varying pressures and variable opening of the inlet and exhaust ports. This model has two versions:

version 1 based on mass entrainment rate, in which the jet is considered as an entity;
version 2 based on eddy diffusivity theory, in which the jet is further divided into several strips.

The model has all the capacities possessed by the steady jet model, and gives a better temporal and spatial resolution of the transport process.

4.2 TRANSFER PHENOMENA IN THE SCAVENGING PROCESS

The scavenging process involves the transfer of momentum, energy and mass induced by forced convection. For convective flow, momentum transfer assumes a dominant role over those of energy and mass transfer, although these three transfers actually interact.

When air emerges from the inlet ports, it interacts with gas from the surroundings to form a jet. The jet separates from the ports. Immediately downstream from the ports, there is a region, the potential core, within which the velocity and concentration of air remain unchanged. As a consequence of momentum exchange between the jet and surroundings, fluid is entrained from the surroundings perpendicular to the direction of flow. Outside the potential core a free shear layer develops. Entrainment is due to shear action as represented by an exchange coefficient and the transverse velocity gradient. The turbulent exchange coefficient is several orders of magnitude higher than the molecular exchange coefficient.

Because the jet is confined by the cylinder wall, cylinder head and piston, the void in the surroundings left by jet entrainment must be replenished from

the part near the void. On the other hand, because of entrainment, the jetting region expands and decelerates with propagation. When the jet has developed sufficiently to block the supply of the void from the surroundings themselves, the void must be filled up directly from the jetting region. A recirculating flow is set up. Entrainment causes the gas in the surrounding region to flow into the jetting region. By contrast, the recirculation causes the air in the jetting region to flow into the surrounding region, as shown in Fig. 4.1.

In some scavenging systems, intake swirl is used as a means of improving the scavenging quality. The tangentially directed inlet ports induce rotation in a stream of fluid. The jet flow has a tangential velocity component in addition to the axial and radial components of velocity encountered in non-swirling jets. The presence of the swirl results in the setting up of radial and axial pressure gradients which, in turn, influence the flow field. In swirling systems with weak swirl, the jet flows along the inner region and leaves a recirculating region in the outer portion of the jet. As the swirl intensity increases, a critical point is reached when the adverse pressure gradient along the jet cannot be further overcome by the kinetic energy of the fluid particles flowing in the axial direction, and a recirculating flow is set up in the central portion of the jet. The internal recirculation zone has the form of a toroidal vortex. The abrupt change of flow pattern is called vortex breakdown. [4.3] Thus, the flow in the cylinder has two patterns:

(1). inner jetting flow with weak swirl;
and
(2). outer jetting flow with strong swirl,

as shown in Fig. 4.2.

The angle of spread of the jet increases with increasing swirl intensity. In the case of vortex breakdown, with increase of swirl, the length of the central recirculation region decreases and its width increases. The entrainment increases, causing faster decay of the velocity and concentration of the jet with distance from the inlet ports.

For jet flow in the scavenging process, variation in density arises due to heterogeneities in temperature and composition. Density variation changes

local effective transport properties, buoyancy effects augment the transfer process, hence affect the flow. [4.4]

The quantitative description of the transfer phenomena is explained in Appendix II.

4.3 PHENOMENOLOGICAL STEADY JET MODEL

4.3.1 PHYSICAL DESCRIPTION

As aforementioned, a scavenging process can be subdivided into three distinct periods: (1) the blowdown period, (2) the scavenging period and (3) the charging period. In ordinary circumstances, however, the amount that can enter during the charging period is small because the time interval is very short and pressure in the cylinder during this period is rising rapidly, due to the upward movement of the piston. Therefore, the scavenging process is considered as a process of two periods: (1) the blowdown period and (2) the scavenge period. During the blowdown period period τ_b, the pressure in the cylinder falls to the trapped pressure which is between the inlet and exhaust manifold pressures. The blowdown period can end before or after the inlet ports or valves are open. During the scavenge period τ_s, the turbulent jet, with or without swirl, entrains and pushes the residual gas out of the cylinder through the exhaust ports or valves until they are closed. Owing to entrainment and recirculation, the cylinder space is divided into two regions: the jetting and recirculating regions. The flow patterns may be of two forms: either an inner jetting flow without or with only weak swirl, or an outer jetting flow with strong swirl. Actually, the jet flow is a very complicated unsteady flow. It includes sudden jet expansion, impingement and sudden contraction, shear layer, flow separation and reattachment, with superimposed pulsating effects due to varying pressure gradients in the cylinder and flapping effects due to the changing gap between the ports and the piston both of which exert an influence on the entrainment rate of the jet.

In the present model, the simplifying assumptions are as follows:

Throughout the scavenging process:

(1). constant pressure in the inlet and exhaust manifolds.
(2). uniform cylinder pressure.
(3). no heat transfer.
(4). no wall friction.

During the blowdown period:

(5). isentropic expansion of compressible gas from a constant volume cylinder through the exhaust ports or valves to the trapped pressure

During the scavenge period:

(6). the cylinder space is axisymmetrically subdivided into two regions: the jetting region and the recirculating region, and the velocities and concentrations are transversely homogeneous respectively in both regions.
(7). identical and uniform density of air and residual gas.
(8). quasi-steady imcompressible flow within the cylinder, constant volume flow rate through the inlet and exhaust ports or valves, focussing the previous effects on an apparent entrainment rate.

4.3.2 MATHEMATICAL TREATMENT

4.3.2.1 Determination of the blowdown period τ_b

In this model, the trapped pressure is considered to be equal to the arithmetic mean value of the inlet and exhaust manifold pressures. Under the previous assumptions, the process of exhaust gas flow through the exhaust ports has been investigated. [4.2], [4.5]

The pressure in the exhaust ports is equal to that in the exhaust manifold, Pe. The release pressure at the exhaust port opening is Pr. The cylinder pressure at any instant is Pcyl. The ratios of sonic velocities are:

$$X_r = \frac{a_e}{a_r} = \left(\frac{P_e}{P_r}\right)^{\frac{\gamma-1}{2\gamma}} \qquad (4.1)$$

$$X = \frac{a_e}{a_{cyl}} = \left(\frac{P_e}{P_{cyl}}\right)^{\frac{\gamma-1}{2\gamma}} \qquad (4.2)$$

The sonic velocity is

$$a = \sqrt{\gamma RT} \qquad (4.3)$$

For subsonic flow, the following equation can be obtained (cf. 7.114 [4.2])

$$\frac{X_r a_r}{V_{cyl}} \int A \, dt = b \int_{X_r}^{X} \frac{dx}{x^b (1-x^2)^{0.5}} \qquad (4.4)$$

where

$$b = \frac{2}{\gamma - 1}$$

The analytical solution of the right-hand side of equation (4.4) is

$$-\sqrt{b} \left(\frac{1}{(b-1)} \frac{(1-x^2)^{0.5}}{x^{b-1}} + \frac{(b-2)}{(b-1)} \int \sec^{b-2} \theta \, d\theta \right) \qquad (4.5)$$

where a new variable θ is defined as

$$x = \cos\theta$$

When $\gamma = 1.4$, i.e. $b = 5$, and equation (4.4) becomes:

$$\frac{X_r a_r}{V_{cyl}} \int A_e dt = -\frac{\sqrt{5}}{4} \left(\frac{1}{4} \frac{(1-x^2)^{0.5}}{x^4} + \frac{3}{2} \left(\frac{\sin\theta}{\cos^2\theta} + \ln \tan\left(\frac{\pi}{2} + \frac{\theta}{2}\right) \right) \right) \Bigg|_{X_r}^{X} \qquad (4.6)$$

For sonic flow, the following equation is valid (cf. 7.127 [4.2])

$$\frac{X_r a_r}{V_{cyl}} \int A_e \, dt = b \left(\frac{\gamma+1}{2} \right)^e (X' - X_r) \qquad (4.7)$$

where

$$e = \frac{(\gamma+1)}{2(\gamma-1)}$$

and

$$X' = \frac{a_e}{a'_{cyl}} = \left(\frac{P_e}{P'_{cyl}} \right)^{\frac{\gamma-1}{\gamma}}$$

where P'_{cyl} corresponds the cylinder pressure at which the choked flow ceases.

For the general case of sonic and then subsonic flow, both equations (4.4) and (4.7) must be used. These two equations can be generalized in the form

$$\frac{X_r a_r}{V_{cyi}} \int A_e \, dt = f(P_r, P_{cyl}) \qquad (4.8)$$

The critical pressure for sonic flow is

$$P_{cr} = P_e \left(\frac{\gamma+1}{2}\right)^{\frac{\gamma}{\gamma-1}} \qquad (4.9)$$

If the release pressure Pe at the exhaust port opening is lower than Pcr, only the subsonic flow proceeds during the blowdown period. If Pe is higher than Pcr, then the sonic and then subsonic flow occurs. The sonic flow begins at Pe, ends at Pcr, i.e. the ratio X' in equation (4.7) is

$$X' = \left(\frac{P_e}{P_{cr}}\right)^{\frac{\gamma-1}{2\gamma}} \qquad (4.10)$$

Then, the subsonic flow begins at Pcr, ends at Ptr, i.e. the ratio Xr in equation (4.4) is

$$X_r = \left(\frac{P_e}{P_{cr}}\right)^{\frac{\gamma-1}{2\gamma}} \qquad (4.11)$$

Considering the relation

$$\int A_e \, dt = \frac{1}{360N} \int A_e \, d\alpha \qquad (4.12)$$

equation (4.8) can be solved by numerical integration, giving the blowdown period τ_b

4.3.2.2 Determination of mass flow rate of scavenging air during the scavenge period

After the blowdown period, the scavenge period begins. It is easy to obtain the scavenge period τ_s from the blowdown period τ_b and the timing of

closing of ports or valves. Using the quasi-steady compressible flow equation, the mass flow rate of the scavenging air is

$$\dot{m} = C_d A_r P_s \sqrt{\frac{2\gamma}{(\gamma-1)RT_s}\left(\left(\frac{P_e}{P_s}\right)^{\frac{2}{\gamma}} - \left(\frac{P_e}{P_s}\right)^{\frac{\gamma+1}{\gamma}}\right)} \qquad (4.13)$$

where Ps is the pressure in the inlet manifold,

Pe is the pressure in the exhaust manifold,

C_d is the discharge coefficient

and the reduced area A_r is

$$A_r = \frac{1}{\tau_b}\int \frac{A_s A_e}{\sqrt{A_s^2 + A_e^2}}\,dt \qquad (4.14)$$

Hence, the overall mean velocity flowing through the inlet ports is

$$U_{in} = \frac{\dot{m}}{\rho_c A_{in}} \qquad (4.15)$$

where the mean area of the inlet ports, A_{in}, is

$$A_{in} = \frac{1}{\tau_b}\int A_s\,dt \qquad (4.16)$$

The velocity, furthermore, can be decomposed into a radial and a tangential component within the cylinder. As an approximate analysis, after the jets impinge, the radial velocity u_0 may be transformed into an equivalent axial velocity w_0. According to angular momentum conservation, the tangential port velocity v_0 changes into an azimuthal cylinder component, i.e. shapes a swirl. The swirl subsequently decays because of wall friction, which is beyond the scope of this model.

4.3.2.3 Description of in-cylinder flow during the scavenge period

This model considers that the uniflow scavenging process is composed of two phases:

(1). displacement scavenging,

and

(2). mixing scavenging.

Before the front of the jetting flow arrives at the exhaust ports or valves, the pure residual gas is discharged out of the cylinder, that is, the displacement scavenging phase is conducted, as shown in Fig. 4.2a and c. After its arrival, the gas mixture of air and residual gas is discharged from the exhaust ports, i.e. the mixing scavenging phase goes on, as shown in Fig. 4.2b and d. Meantime, the fresh air concentration within the cylinder becomes higher and higher. Using the analysis of quasi-steady flow, this model describes an approximate temporally and spatially ever-changing concentration field during the scavenging process. Focussing the various effects on an apparent entrainment spread rate, and neglecting the delicate construction of the field, this method avoids the difficulties of unsteady jet flow.

4.3.2.3.1 Initial condition

Vortex breakdown has been observed only in highly swirling flows. The second condition for the breakdown, under high swirl, is an adverse gradient of pressure in the axial direction. This implies that the downstream condition has an influence on vortex breakdown. But as a rule of thumb, the critical intake angle is taken. When the angle is greater than 40°, vortex breakdown occurs. [4.6]

From the analysis in the previous section, the initial effective flow area is

$$A_0 = A_{in} \cos\varphi \qquad (4.17)$$

where φ is intake angle of inlet ports, as shown in Fig. 4.3.

According to the criterion of vortex breakdown, the apparent initial jet radius can be obtained:

before vortex breakdown, i.e. for the inner jetting flow with weak swirl,

$$r_0 = \sqrt{\frac{A_0}{\pi}} \qquad (4.18)$$

after vortex breakdown, i.e. for the outer jetting flow with strong swirl

$$r_o = \sqrt{R^2 - \frac{A_o}{\pi}} \qquad (4.19)$$

where R is the cylinder radius.

4.3.2.3.2 Basic equations

When the jet spread rate $\frac{dr}{dz}$ is given, the model will be able to delimit the boundary between the jetting and recirculating regions.

For inner jetting flow, the jetting region expands from the central region to the outer region.

$$r_2 = r_0 + \int_0^z \frac{dr}{dz}\, dz \qquad (4.20)$$

for outer jetting flow, the jetting region expands from the outer region to the central region.

$$r_2 = r_0 - \int_0^z \frac{dr}{dz}\, dz \qquad (4.21)$$

When the radius of the jetting region becomes equal to the cylinder radius R or zero, respectively for the inner and outer jetting flow, the jet flow develops into a pipe flow.

Using the Eulerian approach, for inner jetting flow, neglecting the pressure gradient in the cylinder and the wall friction, the continuity and momentum equations can be written as

$$r_j^2 w_j + (R^2 - r_r^2) w_r = r_0^2 w_0 \qquad (4.22)$$

$$r_j^2 w_j^2 + (R^2 - r_r^2) w_r^2 = r_0^2 w_0^2 \qquad (4.23)$$

where r_0 is the apparent initial jet radius,
w_0 is the initial jet axial velocity,
w_j is the axial velocity in the jetting region
w_r is the axial velocity in the recirculating region.

Their solutions are

$$w_j = w_o\left(\frac{r_o}{R}\right)^2\left(1+\sqrt{\left(\left(\frac{R}{r}\right)^2-1\right)\left(\left(\frac{R}{r_o}\right)^2-1\right)}\right) \tag{4.24}$$

$$w_r = w_o\left(\frac{r_o}{R}\right)^2\left(1-\sqrt{\frac{\left(\frac{R}{r}\right)^2-1}{\left(\frac{R}{r_o}\right)^2-1}}\right) \tag{4.25}$$

Similarly, for outer jetting flow,

$$(R^2-r_j^2)w_j+r_r^2 w_r = (R^2-r_0^2)w_0 \tag{4.26}$$

$$(R^2-r_j^2)w_j^2+r_r^2 w_r^2 = (R^2-r_0^2)w_0^2 \tag{4.27}$$

and

$$w_j = w_o\left(1-\left(\frac{r_o}{R}\right)^2\right)\left(1+\frac{1}{\sqrt{\left(\left(\frac{R}{r}\right)^2-1\right)\left(\left(\frac{R}{r_o}\right)^2-1\right)}}\right) \tag{4.28}$$

$$w_r = w_o\left(1-\left(\frac{r_o}{R}\right)^2\right)\left(1-\sqrt{\frac{\left(\frac{R}{r}\right)^2-1}{\left(\frac{R}{r_o}\right)^2-1}}\right) \tag{4.29}$$

Because jetting region expands with jet distance, i.e. $r_2 > r_0$ for inner jetting flow and $r_2 < r_0$ for the outer jetting flow, from relations (4.25) and (4.29), the recirculating velocities w_r always take negative values. This means a backflow in the recirculating region. It is seen that the jetting flow is a decelerating flow along the axial direction.

As for convective velocities between the jetting and recirculating regions, the following equations can be achieved using a control volume of length dz in the jetting region based on mass conservation, as shown in Fig. 4.3.

For inner jetting flow,

$$d(w_j \pi r^2) = w_c 2\pi r dz \qquad (4.30)$$

i.e.

$$w_c = \frac{d(w_j r^2)}{2rdz} \qquad (4.31)$$

For outer jetting flow,

$$d[w_j \pi (R^2 - r_0^2)] = w_c 2\pi r dz \qquad (4.32)$$

i.e.

$$w_c = \frac{d(w_j (R^2 - r^2))}{2rdz} \qquad (4.33)$$

For the jetting region near the inlet ports, the convective velocities take positive values, that is, the jetting flow entrains gas from the adjacent recirculating region. But if the jetting flow expands sufficiently, w_c will become negative, i.e. the jetting flow discharges a part of gas into its neighbouring recirculating region. Under the assumption of steady jet flow, the jetting, recirculating and convective velocities on any cross-section maintain constant values throughout the scavenge period.

As for the concentrations in the jetting and recirculating regions, within a control volume in both the jetting and recirculating regions, based on composition conservation, the following equation can be obtained

$$\rho V_i \frac{dc_i}{dt} = \Sigma \dot{m}_{in} c_{in} - \Sigma \dot{m}_{out} c_{out} \qquad (4.34)$$

where V_i is the volume,

C_i is the air concentration of the volume,

C_{in} is the upstream air concentration flowing into the volume,

C_{out} is the air concentration flowing out of the volume.

The mass flow rate can be determined from the relevant jetting, recirculating and convective velocities and areas. Here, the concentrations are treated as temporally and spatially variable. At the beginning of the scavenge

period, the air concentration in the cylinder are set to zero throughout except at the inlet ports where it is set to 1.

The equation systems (4.20), (4.24), (4.25), (4.31), (4.33), (4.34) and (4.21), (4.28), (4.29), (4.31), (4.33), (4.34) are the basic systems respectively for the inner and outer jetting flows. Under the previous assumptions, an approximate steady flow is used to substitute for an unsteady flow. When the jet spread rate, initial effective flow area and pressures in the inlet and exhaust manifolds are given, the boundary between the jetting and recirculating regions and a constant velocity field in the cylinder can be determined. The temporally and axially variable concentrations in the jetting and recirculating regions describe a history of the scavenging process.

4.3.2.3.3 Jet spread rate

For a confined jet, between the jetting and surrounding regions there exists a shear boundary layer in which lateral gradients in the mean velocity are dissipated. The real transverse velocity profile is bell-shaped, not "top-hat" shaped. Under the assumptions of the uniform density and initial momentum-flux distribution, the jet spread rate is well correlated by, [4.7]

$$\frac{dr}{dz} = 0.0813 \qquad (4.35)$$

However, this steady jet model has left the following aspects out of consideration,

(1). the effect of variable densities and unsteadiness, including flapping and pulsating, during the scavenge period.
(2). the effect of jet boundary layer.
(3). the effect of supercharging due to the late inlet port closure during the charging period.

Thus, for improving the prediction of the scavenging process the model needs an apparent jet spread rate to compensate for the oversimplification. The experiments by Binder and Marinet [4.8] show that the unsteadiness of the jet evidently widens the jet spread angle in the early stages, and that with increase of the initial jetting velocity and swirl and with decrease of the

initial jetting area, the jet spread rate increases. On this basis, a phenomenological relation is introduced,

$$\frac{dr}{dz} = K_1 \frac{w_o^a}{A_o^b} (1 + K_2(\tan\varphi)^c) \qquad (4.36)$$

where the constants K_1, K_2, a, b, c reflect the effects of unsteadiness and configuration of the cylinder, inlet and exhaust ports on the jet spread rate. The constants K1, K2, a, b and c can be obtained from experiment.

4.3.3 COMPUTATIONAL PROCEDURE AND RESULTS

The flow chart for computation is illustrated in Fig. 4.4.

Firstly, from equation (4.8) the blowdown period is determined, and from equations (4.14) and (4.16) the reduced area and the mean inlet area are obtained based on numerical integration.

Secondly, the jet spread rate dr/dz is selected. From intake angle the flow pattern is decided. The radii of the jetting region are determined from equations (4.18) and (4.20) for inner jetting flow or from equations (4.19) and (4.21) for outer jetting flow.

Thirdly, the jetting and recirculating velocities from equations of (4.24) and (4.25), or (4.28) and (4.29), and the convective velocities from equation (4.31) or (4.33) can be obtained.

Fourthly, two non-dimensional arrays T and D are introduced. The time ratio T is used for the control volume and defined as the ratio of the time interval during which a fluid element enters and leaves the volume to the time step length, in other words, T is the step number the fluid element needs when it passes through the volume element,

$$T = \frac{\Delta L}{\Delta T / W_m} \qquad (4.37)$$

where ΔL is the axial mesh size,

W_m is the mean axial velocity flowing through the control volume.

The delay array D is used for the cross-sectional control surface in the jetting or the recirculating region, and defined as the step number in which the jet front arrives at the cross-sectional surface. It is notable that the jet front forwards propagates in the jetting region, and then is divided into two parts, a part continues the forward propagation and develops into pipe flow, another part is diverted to the recirculating region and propagates backwards to the inlet port end. Considering this time sequence, the delay array D can be determined based on the time ratio T.

Finally, using the upstream differencing scheme of the finite difference method the time-dependent constituent continuity equation (4.34) can be solved. For a control volume within the jetting or the recirculating region, the air concentration at the cross-sectional control surface first maintains the old value, and then is replaced by the new value when the flow with a higher air concentration arrives at the surface, while the air concentration at the longitudinally sectional control surface is equal to an average of the concentrations at the adjacent cross-sectional surfaces of the corresponding upstream control volume. From the arrays T and D, these time-dependent concentration values at the control surfaces can be determined, from equation (4.34) the new mean concentration of the control volume can be obtained. This procedure is repeated until the scavenging process ends, thus giving a description of the temporally and axially variable concentration, i.e. a history of the scavenging process.

The criterion of stability of this algorithm is that the time ratio must be greater than 1. This indicates that for each time step the flow in the jetting or the recirculating region should not penetrate a mesh. A comparison between the computational results for mesh numbers 8 and 32 respectively shows that the relative error of calculated scavenging efficiencies is within 1 %.

The computational results are compared with Taylor's experiments. [4.9] The engine tested was a CFR uniflow scavenged two-stroke engine, 3 1/4 in. bore by 4 1/2 in. stroke. The engine had rectangular inlet ports and two poppet exhaust valves in the cylinder head, without intake swirl, see Fig. 4.5. There were four configurations. The timing in configuration A

was symmetrical. Configurations D, E and F were the same as configuration A except that the exhaust-valve timings were set to 7, 14 and 21^{0}, respectively ahead of the symmetrical position, as summarized in Table 4.1. The discharge coefficient C_d is taken as 0.78.

At first, the fixed jet spread rate of equation (4.35) is used. Fig. 4.6 shows the comparison between the experimental and computational results. Compared with the perfect mixing model, this model improves the prediction of the scavenging efficiency. However, it fails to describe the effect of engine speed and exhaust timing on scavenging efficiency. Compared with the experimental results the discrepancy is up to 15 %. These shortcomings originate from the oversimplifications of the model.

And then, the apparent spread rate is selected as follows.

$$\frac{dr}{dz} = 4.38 \cdot 10^{-8} \left(\frac{w_o}{100}\right)^{1.8} / \left(\frac{r_o}{R}\right)^{16.8} \qquad (4.38)$$

Here, the term containinig intake angle φ in equation (4.36) disappears because the CFP engine has no swirl. Fig. 4.7 shows the comparison between the experimental and computational results. The comparison shows that this model can approximately reproduce the trend of the experimental results that with the increase of piston speed and with the advance of exhaust timing, the scavenging efficiency improves. The discrepancy is within 8 %.

Fig. 4.8 illustrates an example of flow field in the cylinder under a given running condition. This figure displays the velocities in the jetting and recirculating regions and the varying directions of the convective velocities. The convective and recirculating flows and a part of the jetting flow rotate around an eddy eye, and form the recirculation.

Fig. 4.9 shows a history of concentration in the cylinder. This figure indicates that with the lapse of time, hence with increase of delivery ratio, the space occupied by residual gas diminishes and the air concentration increases.

The equation of apparent jet spread rate (4.38) reflects the following effects.

(1). With increase of jet velocity, the jet entrainment rate increases, thus improving the scavenging efficiency.
(2). The thinner jet gains the better scavenging efficiency from strong entrainment and longer residence time in the cylinder.

It is worthwhile noting that the equation of apparent jet spread rate (4.38) is purely empirical, hence is applied only for the specific engines.

4.3.4 SUMMARY

The phenomenological model for the uniflow scavenging process in two-stroke engines can be characterized by a steady jet. This model describes the fixed velocity field and time-dependent history of concentration in the cylinder during the scavenging process.

This method allows the designer to estimate a history of concentration and to approximately predict the scavenging efficiency. The latter requires introducing a relationship of apparent jet spread rate. Because this model is oversimplified, it is difficult to obtain a universal relationship of apparent jet spread rate.

The finite difference algorithm for the composition conservation equation employs the following criterion of stability:

the time ratio T (4.36) greater than 1.

4.4 PHENONENOLOGICAL UNSTEADY JET MODEL

4.4.1 PHYSICAL DESCRIPTION

Compared with the previous thermodynamic methods, this new multi-zone model introduces the equations of momentum and moment of momentum conservations to give a description of the spatial and temporal history of mass, local temperature and concentration within every zone, hence to avoid an artificial history. In comparison with comprehensive computational fluid dynamics (CFD) models, this model considers that the pressure in the cylinder is uniform, i.e. it neglects the pressure term in the equations of momentum conservation. This indicates that the model ignores the details of conversion of kinetic and pressure potential energies, and considers that pressure relaxation is carried out without delay. This assumption lends the model effictiveness of computation, but makes it unable to predict the details of the conversion of mechanical energies. The conversion between kinetic and pressure potential energies plays an important role in cross and loop scavenged engines. Fortunately, in uniflow scavenged engines this conversion is less important except during jet impingement and, additionally with swirl, during vortex breakdown processes within the regions next to the inlet and exhaust ports. The present model neglects these processes, because their periods are relatively short compared with the total time a fluid particle takes from the inlet ports to the exhaust ports. Actually, the omission of these processes will have a minor influence on the whole temporal resolution of the scavenging process, especially for engines with long stroke. This model treats them as boundary condition.

The air jet flow and the residual gas within the cylinder are considered as two different regions. The jet portion entering the cylinder during a time step length makes up a new zone within the jetting region, Fig. 4.10. The temperature, concentration and velocity within each zone are uniform. Their varying profiles at different times and cross-sections describe the spatial and temporal history of the scavenging process. As the jet propagates, the jet zones entrain the recirculation zones, and the adjacent jet and recirculation zones transfer mass, momentum and energy mutually. The void left by the entrainment within the recirculation region is filled up by neighbouring zones. The zones near the exhaust end will be discharged out of the cylinder. If a later jet zone overtakes an earlier jet zone, the two zones

will merge. If the jet flow en route develops into pipe flow, the surplus part of that jet zone will become a part of the corresponding recirculation zone. Thus, this model gives a step-by-step description of the scavenging process.

The model makes the following assumptions:

(1). uniform pressure within the cylinder.
(2). quiescent surrounding region.
(3). homogeneous temperature, concentration and velocity within each zone individually.
(4). neglect of wall friction.
(5). heat transfer using Woschni's correlation based on a bulk average temperature.
(6). neglect of the distribution of radial velocity.

There are two different versions of profiles of velocity and concentration. fioff version 1: investigates the overall behaviour of the jet flow based on the turbulence model of entrainment and considers the jetting region as an entirety, i.e. provides a simple "top-hat" profile.
version 2: discusses the transverse distribution of the jet flow based on the turbulence model of eddy diffusivity and divides the jetting region into several strips, i.e. gives a detailed "step-shaped" profile.

4.4.2 MATHEMATICAL TREATMENT

4.4.2.1 Version 1: entrainment model

4.4.2.1.1 Boundary conditions

The flow rates of inflowing and outflowing gas mixture are determined from the compressible flow equation in which the discharge coefficient is quoted from the same correlation as in Chapter 3.

As previously, the intake angle is taken as a criterion of vortex breakdown. When the angle is greater than 40°, vortex breakdown occurs, i.e. outer jetting flow is initiated. When the angle is lower than the critical value, inner jetting flow occurs.

It is assumed that after the jet impingement the radial velocity component u eventually and equivalently becomes the axial component w and the tangential velocity component v achieves a radially proportional distribution based on moment of momentum conservation.

Before the scavenge period, the temperature and concentration throughout the cylinder are assumed to be uniform.

4.4.2.1.2 Governing equations

Using the Lagrangian approach, a large number of zones keeps track of the fluid elements respectively within the jet and recirculation regions.

The conservation equations are derived in generalized form, in which outflowing terms, for the jet zone, and inflowing terms, for the recirculation zone disappear. Figs. 4.10 and 4.11 show the subdivision of the unsteady flow field into axially advancing times I which are divided into transverse regions. Fig. 4.10 applies to version 1 in which the transverse distribution is limited to the jetting and recirculating regions only, whereas in version 2 the jet is transversely divided into several transverse regions of varying velocity and concentrations, as shown in Fig. 4.11.

4.4.2.1.2.1 conservation of mass

For the I-th zone within region m,

$$\Delta m^{m,I} = \Delta m^{m,I}_{in} - \Delta m^{m,I}_{out} \qquad (4.39)$$

change of mass in the zone = mass flowing into the zone − mass flowing out of the zone

where the superscript m is j for the jetting region, or, r for the recirculation region and the superscript I is the zone number.

4.4.2.1.2.2 composition equation

The equivalence ratio is used indirectly as a parameter of composition.
For the I-th zone within region m,

$$F^{m,l} = \frac{m_f^{m,l}}{f_s m_s^{m,l}} = \frac{m_{f,o}^{m,l} + m_{f,in}^{m,l} - m_{f,out}^{m,l}}{f_s (m_{s,o}^{m,l} + m_{s,in}^{m,l} - m_{s,out}^{m,l})} \qquad (4.40)$$

and $m^{m,l} = m_f^{m,l} + m_s^{m,l}$

where the superscripts m and l retain the previous significance.

$m_f^{m,l}$ is the mass of burnt fuel in the l-th zone within region m.

$m_s^{m,l}$ is the sum of the air mass trapped and the air mass consumed in the combustion of the fuel $m_f^{m,l}$.

fs is the stoichiometric fuel-air ratio.

the subscripts o, in and out represent the initial, inflowing and outflowing amount respectively.

Under the assumption of complete combustion, the mass of residual gas is

$$m_g^{m,l} = (1 + \frac{1}{f_s})\, m_f^{m,l} \qquad (4.41)$$

and the remaining mass of fresh air is

$$m_a^{m,l} = m^{m,l} - m_g^{m,l} \qquad (4.42)$$

4.4.2.1.2.3 conservation of axial momentum

Neglecting the pressure term,

$$\Delta(m^{m,l} w^{m,l}) = \Delta m_{in}^{m,l} w_{in}^{m,l} - \Delta m_{out}^{m,l} w_{out}^{m,l} \qquad (4.43)$$

change of momentum in the zone = momentum flowing into the zone − momentum flowing out of the zone

where $w_{in}^{m,l}$ is the axial velocity within the upstream zone of the l-th zone of region m.

$w_{out}^{m,l}$ is the axial velocity within the l-th zone of region m.

4.4.2.1.2.4 conservation of angular momentum about the centreline-axis

$$\Delta(m^{m,l}_{} r^{m,l}_{} v^{m,l}_{}) = \Delta m^{m,l}_{in} r^{m,l}_{in} v^{m,l}_{in} - \Delta m^{m,l}_{out} r^{m,l}_{out} v^{m,l}_{out} \qquad (4.44)$$

change of angular momentum in the zone = angular momentum flowing into the zone − angular momentum flowing out of the zone

where $v^{m,l}_{in}$ is the tangential velocity within the upstream zone of the l-th zone of region m.

$v^{m,l}_{out}$ is the tangential velocity within the l-th zone of region m.

4.4.2.1.2.5 conservation of energy

For the l-th zone of region m.

$$\Delta(m^{m,l}_{} e^{m,l}_{}) = \sum(\Delta m^{m,l}_{in} h^{m,l}_{in}) - \sum(\Delta m^{m,l}_{out} h^{m,l}_{out}) - \Delta Q^{m,l} - P\Delta V^{m,l} \qquad (4.45)$$

change of the total internal energy in the zone = total enthalpy flowing into the zone − total enthalpy flowing out of the zone − heat transfer from the zone − external work done by the zone

where $h^{m,l}_{in}$ is the specific absolute enthalpy within the upstream zone of the l-th zone of region m.

$h^{m,l}_{out}$ is the specific absolute enthalpy with the l-th zone of region m.

The equilibrium thermodynamic properties of the products of combustion of CnH2n and air are calculated from the cylinder pressure, local temperature and equivalence ratio within each zone based on the same mathematical expressions as in Chapter 3.

Woschni's correlation is adopted to calculate heat transfer again.

$$\Delta Q_w = \alpha A_w (T_{cyl} - T_w) \Delta t \qquad (4.46)$$

where A_w is the wall area,

α is the heat transfer coefficient,

$$\alpha = C \cdot D^{-0.2} \cdot P^{0.8} \cdot T^{-0.53} \left(C_1 V_m + C_2 \frac{V_s T_{tr}}{P_{tr} V_{tr}} (P - P_o) \right)^{0.8} \tag{4.47}$$

where the bulk average temperature is defined by

$$T_{cyl} = \frac{\sum_m \sum_l m^{m,l} T^{m,l}}{\sum_m \sum_l m^{m,l}} \tag{4.48}$$

and the other notations are the same as in Chapter 3.

The total heat transfer from the cylinder is composed of three portion: heat transfer from the cylinder head, liner and piston for which the subscripts h, l and p represent respectively. Thus, the total heat transfer is

$$\Delta Q_{cyl} = \Delta Q_h + \Delta Q_l + \Delta Q_p \tag{4.49}$$

The heat transfers in the various zones are allocated in relation to their mass and temperatures, i.e.

$$\Delta Q^{m,l} = \frac{m^{m,l} T^{m,l}}{\sum_l \sum_k m^{l,k} T^{l,k}} \Delta Q_{cyl} \tag{4.50}$$

where the superscripts l and m stand for the l-th zone in region m and the denominator with the superscripts l and k should be summed for all zones and regions.

Heat transfer between zones is ignored.

4.4.2.1.2.6 equation of state

Using local properties, the equation of state is used for each zone

$$PV^{m,l} = m^{m,l} R T^{m,l} \tag{4.51}$$

4.4.2.1.2.7 equation of entrainment

The entrainment equation is taken directly from the experimental results by Ricou and Spalding [4.10]

$$\Delta m = 0.28\, \rho_s^{\frac{1}{2}} F_0^{\frac{1}{2}} \Delta z \Delta t \qquad (4.52)$$

where Δz is the axial length of a given jet zone

ρ_s is the density of the surrounding fluid of the jet zone

the initial injected momentum flux at the inlet ports is

$$F_0 = \rho_0 U_0^2 A_{in} \qquad (4.53)$$

where ρ_0 is the initial jet density at the inlet ports.

U_0 is the initial jet velocity.

A_{in} is the opening area of the inlet ports.

The jet retains its "memory" of this flux and entrains its surrounding fluid in relation with the density of surrounding fluid.

4.4.2.1.2.8 coalescence of zones

When a later zone k catches up an earlier zone l in the jetting region, the coalescence of the zones is accomplished under an isobaric process.

$$mh = m^{m,l} h^{m,l} + m^{m,k} h^{m,k} \qquad (4.54)$$

total enthalpy of the merged zone = sum of enthalpies of the zones to be merged

$$mw = m^{m,l} w^{m,l} + m^{m,k} w^{m,k} \qquad (4.55)$$

axial momentum of the merged zone = sum of axial momentum of the zones to be merged

$$mrv = m^{m,l} r^{m,l} v^{m,l} + m^{m,k} r^{m,k} v^{m,k} \qquad (4.56)$$

angular momentum about centreline of the merged zone = sum of angular momentum about centreline of the zones to be merged

Under the assumption that the entrainment rate is not affected by the coalescence of zones, from equation (4.52), the following equation can be obtained

$$F_o = \left(\sqrt[N]{F_o^{m,l}} + \sqrt[N]{F_o^{m,k}} \right)^2 \qquad (4.57)$$

4.4.2.1.3 Mass constraint

The present trapped mass is equal to the sum of the previous trapped mass, inflowing and outflowing mass

$$m = m_0 + \Delta m_{in} - \Delta m_{out} \qquad (4.58)$$

4.4.2.1.4 Volume constraint

The calculated volumes of all zones trapped in the cylinder should be equal to the total volume of the combustion chamber.

$$\sum_m \sum_l V^{m,l} = V_{cyl} \qquad (4.59)$$

It is noted that with the constraint equations of mass and volume, the energy conservation equations (4.45) through (4.50) may be added to give the following overall energy balance equation.

$$\Delta(me) = \Delta m_{in}\, h_{in} - \Delta m_{out}\, h_{out} - P\Delta V_{cyl} - \Delta Q_{cyl} \qquad (4.60)$$

change of total internal energy of working fluid = total enthalpy flowing into the cylinder − total enthalpy flowing out of the cylinder − external work done − heat transfer from the cylinder

4.4.2.1.5 Configuration of jet flow

The flow pattern of the jet is determined from the criterion of vortex breakdown based on the intake angle. The velocities of every zone are obtained from the momentum and angular momentum conservations, and the displacements of the zones may be calculated from the axial velocities. The volumes of the zones are obtained by means of an iteration method based on the energy equation, the equation of state and the volume constraint. The cross-sectional area of the first zone next to the inlet ports equates to the area of the ports. From the axisymmetry of jet flow, the geometry of the first zone can be determined. The top area of the later zone equates to the bottom area of the adjacent former zone in the jet region. Following a similar procedure, these zones build up the jet region. With the entrainment and propagation, it is possible that some parts of jet zones exceed the cylinder boundary. The redundant volume of the jet zone beyond the boundary will become a part of the corresponding surrounding recirculation zone. After contouring the jet, the recirculation zones fill up the space left in the cylinder. The total mass and volume of all the zones in the cylinder should satisfy the mass and volume constraints.

4.4.2.2 Version 2: eddy diffusivity model

The boundary conditions and basic equations except the entrainment equation are the same in version 2 as in version 1. The important distinction between version 1 and version 2 is that version 2 divides the jetting region transversely into several strips.

Hence, the superscript m in the terms of the basic equations, such as in $m^{m,l}$, $w^{m,l}$ etc., represents all the different strips of the jetting region and the surrounding region, Fig. 4.11.

The equation of overall entrainment rate by Ricou and Spalding is no longer applicable. Instead, this model uses a synthetic eddy diffusivity hypothesis from Scheitz's [4.11] and Lilley's [4.12] models.

Firstly, this model follows Scheitz's idea to extend Prandtl's model of plain jet with constant density to plain jet with variable density. Here, plain jet means free jet without swirl. The model then imitates Lilley's model to generalise the plain jet model to a swirling jet model using an anisotropic eddy diffusivity model.

According to Prandtl's model of plain jet with constant density. [4.13] the eddy diffusivity ϵ_t is

$$\epsilon_t = -c\, b(U_{max} - U_{min}) \qquad (4.61)$$

where c is an empirical constant.

b is the jet width.

U is the mean velocity.

and the subscripts max and min denote the extreme values at a cross section.

Scheitz has extended the previous formula to free tubulence with variable density.

$$\rho\epsilon_t = -C_1 b\,((\rho U)_{max} - (\rho U)_{min}) \qquad (4.62)$$

where C_1 is a constant.

For eddy diffusivity model. the effective convection mass flux may be expressed as follows. (cf. Appendix II)

$$\dot{m}_c U = -\rho\epsilon_t \frac{\partial U}{\partial n} \qquad (4.63)$$

where $\dot{m}_c$ is the effective convection mass flux.

U is the total mean velocity.

ϵ_t is the eddy diffusivity.

$\frac{\partial U}{\partial n}$ is the deriviative of velocity U normal to the main flow.

For swirling jet. after substitution of equation (4.62). equation (4.63) is written in a cylindric polar coordinates system.

$$\dot{m}_c U = -\rho\epsilon_{rz}\frac{\partial W}{\partial r} + \rho\epsilon_{r\theta} r\frac{\partial}{\partial r}\left(\frac{V}{r}\right)$$

$$= -\rho\epsilon_{rz}\left(\frac{\partial W}{\partial r} + C_2 r\frac{\partial}{\partial r}\left(\frac{V}{r}\right)\right)$$

$$= -C_1 b\left((\rho W)_{max} - (\rho W)_{min}\right)\left(\frac{\partial W}{\partial r} + C_2 r\frac{\partial}{\partial r}\left(\frac{V}{r}\right)\right) \qquad (4.64)$$

where U is the total mean velocity.

V is the tangential mean velocity.

W is the axial mean velocity.

ϵ_{rz} is the rz- eddy diffusivity.

$\epsilon_{r\theta}$ is the rθ- eddy diffusivity.

$$C_2 = \frac{\epsilon_{r\theta}}{\epsilon_{rz}}$$

the factors C_1 and C_2 are functions of the swirl rate. This model leaves two parameters C_1 and C_2. which describe the entrainment and anisotropy of the jet respectively. and can be used to obtain a "best fit" with experiment. The results of this process by Scheitz and Lilley respectively are.

$$C_1 = 0.039$$

$$C_2 = 1+5.0\ S_z^{\frac{1}{3}}$$

where the initial swirl rate S_z is

$$S_z = \frac{G_\theta}{RG_z} = \frac{\int_0^R (Vr)\rho W \cdot 2\pi r dr}{R\int_0^R W\rho W \cdot 2\pi r dr} \qquad (4.65)$$

where R is the outer radius.

G_z is axial flux of linear momentum.

G_θ^z is axial flux of angular momentum.

Under the aforementioned assumptions of the axial and tangetial velocity distribution. that the swirl rate can be expressed as

$$S_z = \frac{2}{3}\tan\varphi \qquad (4.66)$$

where φ is the intake angle of the inlet ports.

From this. it is obvious that the entrained mass between adjacent zones is

$$\Delta m = -C_1 b \frac{((\rho W)_{max} - (\rho W)_{min})}{U}\left(\frac{\partial W}{\partial r} + C_2 r \frac{\partial}{\partial r}\left(\frac{V}{r}\right)\right) 2\pi r \Delta z \Delta t \qquad (4.67)$$

This relation reflects the influence of "local" behaviours of turbulent jets on the mass entrainment, whereas the entrainment equation (4.52) by Ricou and Spalding relates the entrained mass with the initial injected momentum flux.

The procedure of contouring the jet flow in version 2 is similar to that in version 1. Since version 2 has a multi-strip construction, the jetting region must be built up strip-by-strip and then the residual gas fills up the rest of the space in the cylinder.

4.4.3 COMPUTATIONAL PROCEDURE AND RESULTS

The flow chart for computation is illustrated in Fig. 4.12. The system of simultaneous first order differential equations is solved by a stepwise integration process. Combined with the entrainment equation (4.52) in version 1 or (4.67) in version 2, equations (4.39) through (4.44) can be explicitly solved for the mass, composition, axial momentum and angular momentum of all zones. However, equations (4.45) through (4.51) cannot be explicitly solved for the pressure, temperature and volume to satisfy the constraint equations (4.58) and (4.59). A triple iteration loop is used for solution. The program is incorporated in a step-by-step cycle simulation program as one of the available options to describe the scavenging process. [4.14] The time step length is 1 degree crankshaft angle. A graphics subroutine to draw timeline and contour velocity and concentration distribution is included in the program.

An experimental study of the scavenging process for validating the present analysis was conducted by Wallace et al. [4.15], [4.16] The experimental technique applied was the trace gas method. The engine was the Rootes TS-3, 3-cyl. opposed piston 2-stroke engines, as shown in Fig. 4.13. The characteristics of the engines are summarized in Table 4.2.

The varying parameters include engine speed, boost ratio, delivery ratio and air-fuel ratio. Eight of these tests are compared in detail with the two versions of the present model and listed in Table 4.3. The comparison shows that both versions 1 and 2 provide satisfactory predictions for the scavenging process in uniflow scavenged engines. Version 1 and version 2 give similar descriptions for the scavenging process, although version 1

uses an "overall" entrainment correlation whereas version 2 quotes a "local" eddy diffusivity hypothesis.

Using version 1, Fig. 4.14 gives a comparison of the charging efficiencies between the experimental and theoretical results at the different engine speeds and loads. Fig. 4.15 illustrates the effect of delivery ratio on trapping and charging efficiencies. Fig. 4.16 is an example of the cylinder pressure and mean temperature during the scavenging process.

For version 2, the multi-strip model, it is necessary to estimate the convergence of the algorithm. Table 4.4 shows that the algorithm of version 2 has a good convergence for modelling the scavenging process. It is recommended that the number of strips is taken as four as a compromise between precision and computation cost.

Fig. 4.17 shows a group of computed results for jet timelines, velocity and concentration distributions for version 1 and version 2 divided into four and six strips under the running condition listed in Table 4.4. The flow and concentration fields display a similar disposition, although the strip numbers in version 2 are different. This also verifies the stability of the algorithm of both two versions.

4.4.4 DISCUSSIONS

4.4.4.1 Verification of the multi-zone model

As was mentioned by Wallace [4.16], the trace gas method, due to the low temperature and little oxidation, underestimated the charging efficiency at high air-fuel ratio. An experimental result [4.17] also showed that the nearly complete combustion occurs at an air-fuel ratio of about 30. This indicates that the trace gas method at air-fuel ratios of about 30 should give good accuracy. The model simulation at about this ratio also displays a satisfactory agreement with the experimental results. Over the whole range, good agreement of air flow and output power provides further evidence of the validity of versions 1 and 2.

The present model simplifies the distribution of velocity and concentration as

a "top-hat" in version 1 or "step-shaped" profile in version 2, and uses the published entrainment rate or eddy diffusivity hypothesis. Thus the model gives a good description of average behaviours. It is unnecessary in either versions 1 or 2 of this model to calibrate coefficients at different running conditions. The good predictions implies that the model is successful.

4.4.4.2 Model prediction

From the viewpoints of mechanical integrity and port timing, the available range of opening areas in the inlet ports belt is limited. When the opening area is fixed, with increase of the intake angle, the cross-section area of the inlet ports decreases. When the intake angle is greater than the critical angle, vortex breakdown occurs. Fig. 4.18 shows an example of different flow patterns and distributions of velocity and concentration. Fig. 4.19 illustrates the relationship between delivery ratio and pressure drop in the inlet and exhaust manifolds at different intake angles. Fig. 4.19 also shows the effect of delivery ratio on trapping and charging efficiency.

It is evident that the increase of engine speed shortens the period available for the scavenging process, and hence lessens the delivery ratio at the same pressure drop, and that the increase of the intake angle narrows the effective passages of the inlet ports, therefore, dimishes the delivery ratio. On the other hand, it is also clear that the increase of swirl angle decreases the initial axial velocity of the jet flow, and defers the arrival of the jet at the exhaust ports. Hence, it depresses the trend of short-circuiting. Excessively high delivery ratios cannot improve the trapping efficiency, because they lead to pressure drops, and hence to excessive compressor work. From Fig. 4.19 , it is easy to understand that strong swirl at low engine speed is superior. However, weak swirl at high speed is advantageous. From considerations of both effectiveness and economy in the scavenging process variable geometry of the inlet ports is desirable.

4.4.5 SUMMARY

The good agreement between experimental and computational results indicates that the present multi-zone unsteady jet model, in both versions 1 and 2 based on fundamental physical principles, is successful.

The model predicts the effect of swirl strength on the effectiveness of the scavenging process and demonstrates the desirability of variable geometry of inlet ports from considerations of both effectiveness and economy in the scavenging process.

REFERENCES

[4.1] W. Rizk

"Experimental Studies of the Mixing Process and Flow Configurations in Two-Cycle Engine Scavenging"

Proc. Instn. Mech. Engrs. Vol. 172, pp. 417-437, 1958

[4.2] R.S. Benson and N.D. Whitehouse

"Internal Combustion Engines", Vols. 1 and 2

Pergamon Press, 1979

[4.3] J.H. Faler and S. Leibovich

"An Experimental Map of the Internal Structure of a Vortex Breakdown"

J. Fluid Mech. Vol. 86, Part 2, pp. 313-335, 1978

[4.4] P.A. Libby

"Studies in Variable-Density and Reacting Turbulent Shear Flows"

<<Studies in Convection>> Vol. 2

Academic Press, 1977

[4.5] R.S. Benson

"A Method for Calculating the Exhaust Port Area for Two-Stroke Cycle Engines"

J. of Royal Aeronaut. Soc. 61, 127, 1957

[4.6] M.G. Hall

"Vortex Breakdown"

Ann. Rev. Fluid Mech. 4, pp. 195-219, 1972

[4.7] H.A. Becker, H.C. Hottel and G.C. Williams

"Mixing and Flow in Ducted Turbulent Jets"

<Ninth Symposium (International) on Combustion>

Academic Press, 1963

[4.8] G. Binder and M.F. Marinet

"Some Characteristics of Pulsating or Flapping Jets"

<<Unsteady Turbulent Shear Flows IUTAM Symposium Toulouse/France 1981>>

[4.9] C.F. Taylor, A.R. Rogowski, A.L. Hagen and J.D. Koppernaes
"Loop Scavenging vs. Through Scavenging"
Transaction of SAE vol.66, p444, 1958

[4.10] F.P. Ricou and D.B. Spalding
"Measurement of Entrainment by Axi-Symmetrical Tuibulent Jets"
J. Fluid Mech. vol.11, pp21-32, 1961

[4.11] J.A. Scheitz
"Injection and Mixing in Turbulent Flow"
vol.68 Progress in astronautics and Aeronautics
American Institution of Aeronautics and Astronautics

[4.12] D.G. Lilley
"Prediction of Inert Turbulent Swirl Flows"
AIAA J. Vol.11 No. 7, 1977

[4.13] L. Prandtl
"Bemerkungen zur Theorie der freien Turbulenz"
ZAMM 22, pp 241-243, 1942

[4.14] M. Tarabad
"Diesel Engine Cycle Simulation"
The University of Bath, 1982

[4.15] F.J. Wallace and E.J. Wright
"Characteristics of a Two-Stroke Opposed-Piston Compression-Ignition Engine Operating at High Boost"
Proc. Instn. Mech. Engrs. Vol180, Parti, No. 7, 1965-66

[4.16] F.J. Wallace and P.R. Cave
"Experimental and Analytical Studies on a Two-Cycle Opposed-Piston Diesel Engine"
SAE 710175, 1971

[4.17] J.M. Perez and E.M. Landen
"Exhaust Emission Characteristics of Precombustion Chamber Engine"
SAE 680421, 1968

Table 4.1 Characteristics of the CFR engine

Number of cylinders	1
Bore	3.25 in (82.55 mm)
Stroke	4.50 in (124.3 mm)
Nominal compression ratio	5.8/1

Two-stroke cylinder with 2 poppet exhaust valves

Spark ignition

Port timing: 4 configurations

Timing	BBTC	BBTC	ABTC	ABTC
Configuration	IO	EO	IC	EC
A	57	88	57	88
D	57	95	57	81
E	57	102	57	74
F	57	109	57	67

Table 4.2 Characteristics of the Rootes TS3 Engine

Number of cylinders	3
Bore	3.25 in (82.55 mm)
Stroke	2*4.0 in (2*101.6 mm)
Swept volume	0.115 cub.ft(3.261 l)
Nominal compression ratio	16/1 , 14/1
Rated power output	78 kw

Opposed-piston

Two-stroke cycle

Compression ignition

Table 4.3 Comparison Between Experimental and Computational Results

Case No.	1	2	3	4
Operating conditions				
Engine Speed, rpm	1010.	1126.	1510.	1510.
Boost Pressure, bar	1.99	2.50	1.52	1.60
Exhaust Pressure, bar	1.84	2.26	1.39	1.38
Trapped Air-Fuel Ratio	30.5	39.2	30.5	29.8
Measured Values				
Output Power, kw	48.61	52.56	54.52	59.57
Brake Thermal Efficiency	0.381	0.398	0.391	0.398
Charging Efficiency	0.88	0.86	0.80	0.83
Air Mass Flow, kg/min	9.88	13.65	8.28	10.63
Calculated Values from Version 1				
Output Power, kw	48.24	53.22	52.77	60.06
Brake Thermal Efficiency	0.377	0.389	0.383	0.390
Charging Efficiency	0.87	0.87	0.77	0.83
Air Mass Flow, kg/min	10.31	14.26	8.53	11.14
Calculated Values from Version 2				
Output Power, kw	49.56	54.18	54.78	61.89
Brake Thermal Efficiency	0.380	0.391	0.387	0.393
Charging Efficiency	0.89	0.89	0.81	0.85
Air Mas Flow, kg/min	10.35	14.06	8.53	11.05

Case No.	5	6	7	8
Operating conditions				
Engine Speed, rpm	1505.	1515.	1500.	2010.
Boost Pressure, bar	1.99	2.50	3.00	1.99
Exhaust Pressure, bar	1.59	2.15	2.55	1.54
Trapped Air-Fuel Ratio	30.5	41.2	56.7	31.7
Measured Values				
Output Power, kw	74.85	68.88	58.86	94.03
Brake Thermal Efficiency	0.414	0.412	0.398	0.403
Charging Efficiency	0.85	0.78	0.72	0.82
Air Mass Flow, kg/min	16.66	17.96	21.53	17.83
Calculated Values from Version 1				
Output Power, kw	73.50	67.59	56.97	90.33
Brake Thermal Efficiency	0.397	0.400	0.393	0.404
Charging Efficiency	0.85	0.84	0.85	0.79
Air Mass Flow, kg/min	16.07	17.02	20.61	16.78
Calculated Values from Version 2				
Output Power, kw	74.19	68.52	58.20	92.64
Brake Thermal Efficiency	0.398	0.402	0.395	0.406
Charging Efficiency	0.86	0.86	0.86	0.81
Air Mass Flow, kg/min	15.93	16.99	20.36	16.79

Table 4.4 Convergence of Algorithm of Version 2 and Comparison with Version 1

Operating Condition

Engine Speed: 1530 rpm Trapped Air-Fuel Ratio: 43

Boost Pressure: 2.50 bar Exhaust Pressure: 2.29 bar

	Version 2				Version 1
No. of Strips	3	4	5	6	
Charging Eff.	0.7933	0.8122	0.8124	0.8126	0.7803
Trapping Eff.	0.6753	0.6967	0.6936	0.7004	0.6644
Air Flow, kg/min	13.568	13.566	13.530	13.402	13.567
Comp. Time Ratio	1.00	1.27	1.66	1.99	0.60

non-swirling
and weak swirling

strong swirling

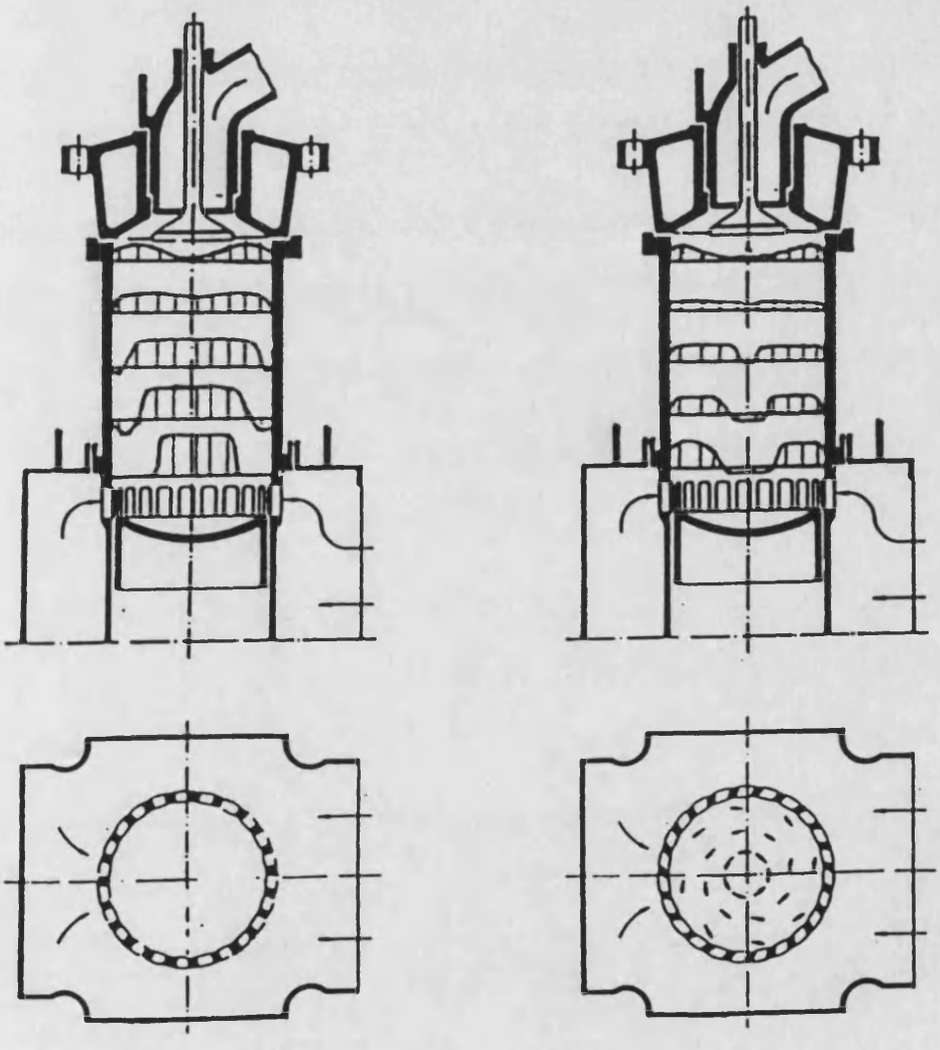

Inner Jet

Outer Jet

Fig. 4.1 Flow Patterns

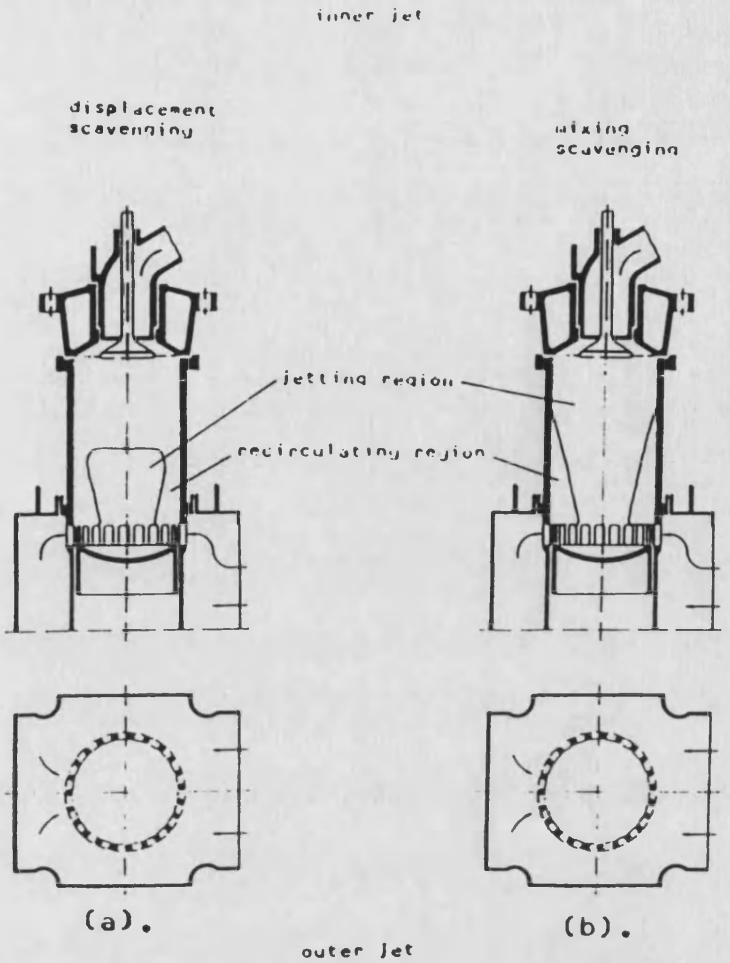

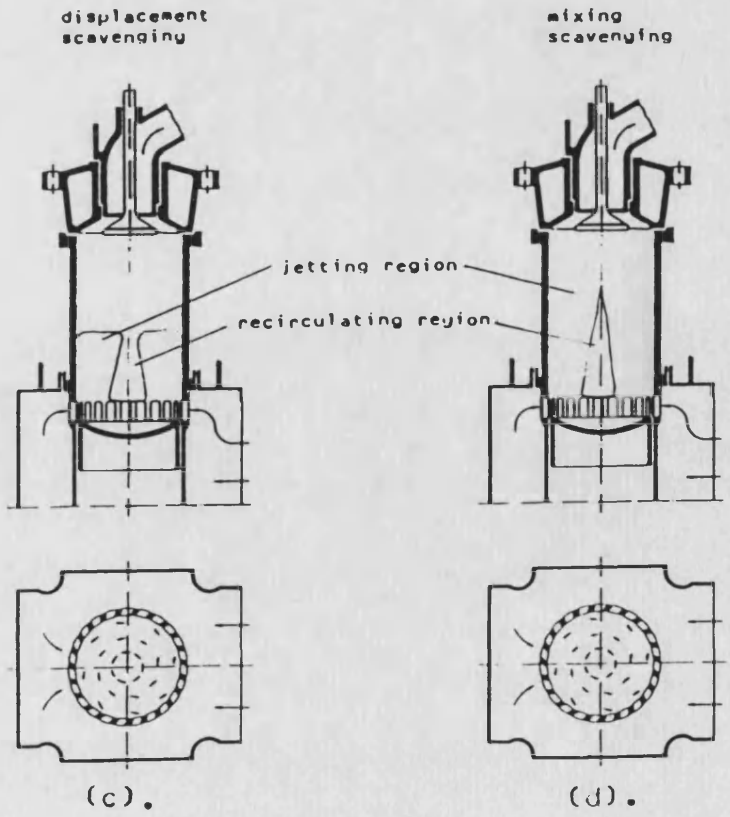

Fig. 4.2 Uniflow Scavenging Process

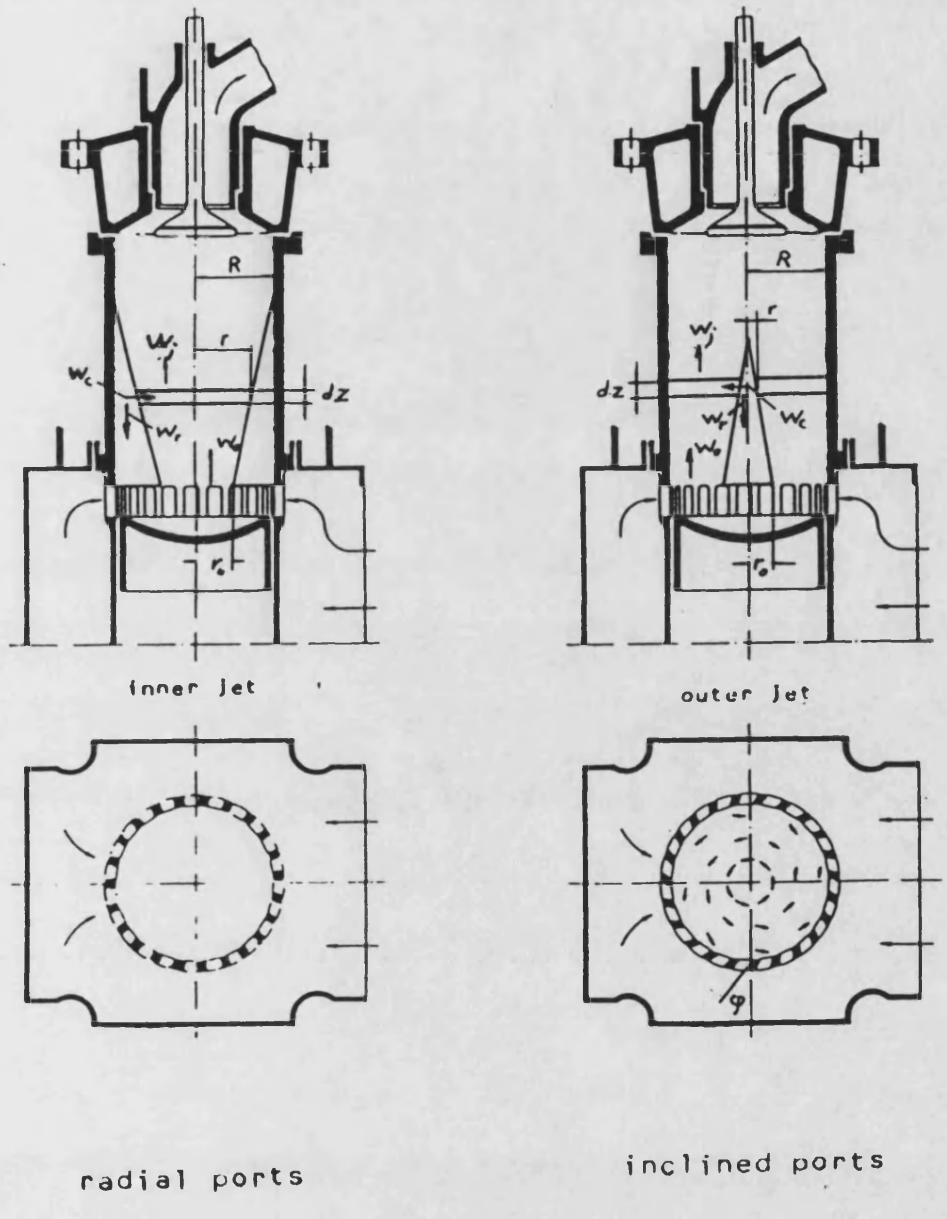

Fig. 4.3 Convection Between Jetting and Recirculating Regions

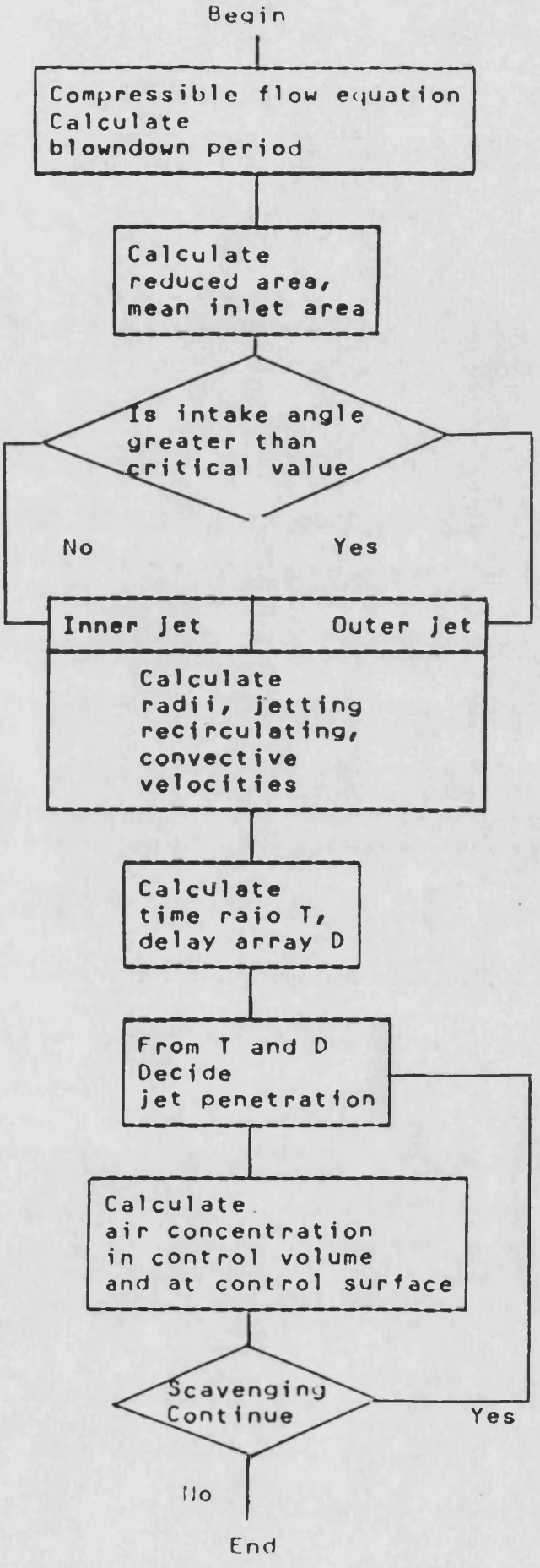

Fig. 4.4 Flow Chart for Steady Jet Model

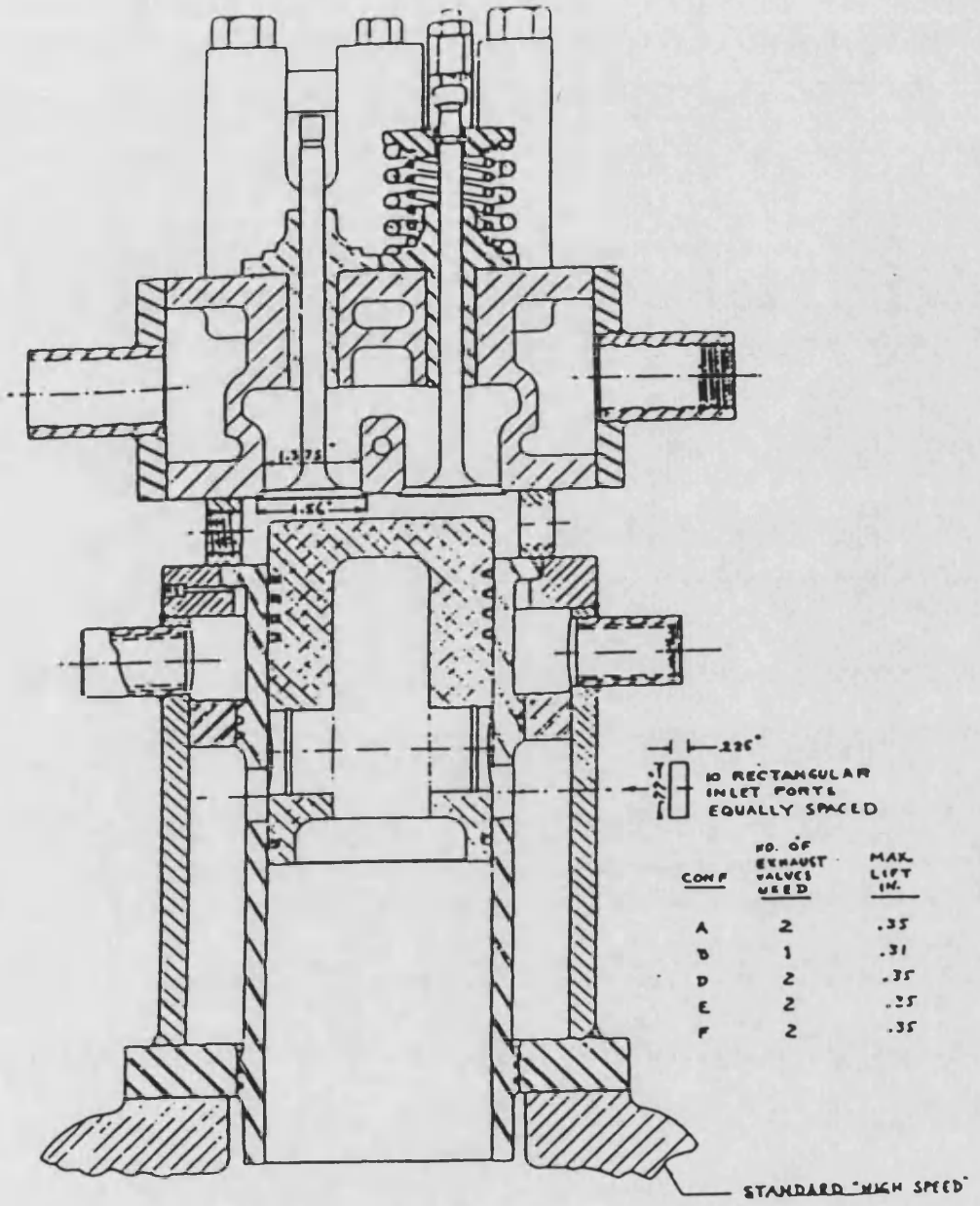

CONF	NO. OF EXHAUST VALVES USED	MAX. LIFT IN.
A	2	.35
B	1	.31
D	2	.35
E	2	.25
F	2	.35

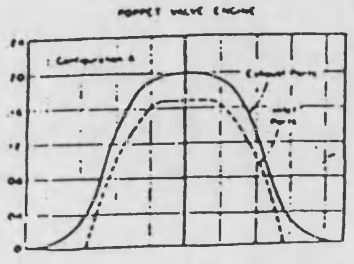

Poppet-Valve Exhaust Valves

Configuration	Number	Maximum lift, in.	Mass Flow Factor	Flow Factor Ratio*
A	2	0.35	0.050	1.29

Inlet ports, all configurations

Number	Maximum area, in.²	Flow Factor
10	1.73	0.039

* Flow factor ratio = Mass exhaust flow factor/mass inlet flow factor

Fig. 4.5 CFR Poppet-Valve Two-Stroke Cylinder

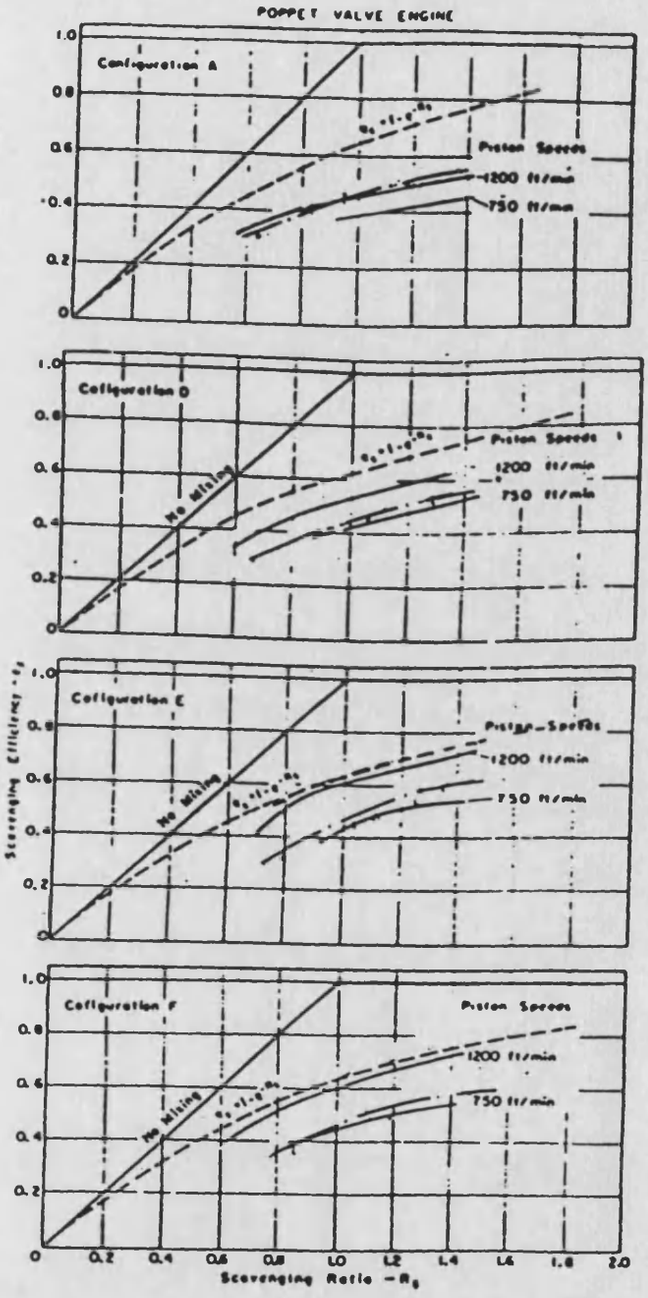

Fig. 4.6 Comparison between Experimental and Computational Results Using Steady Jet Model with Fixed Spread Rate

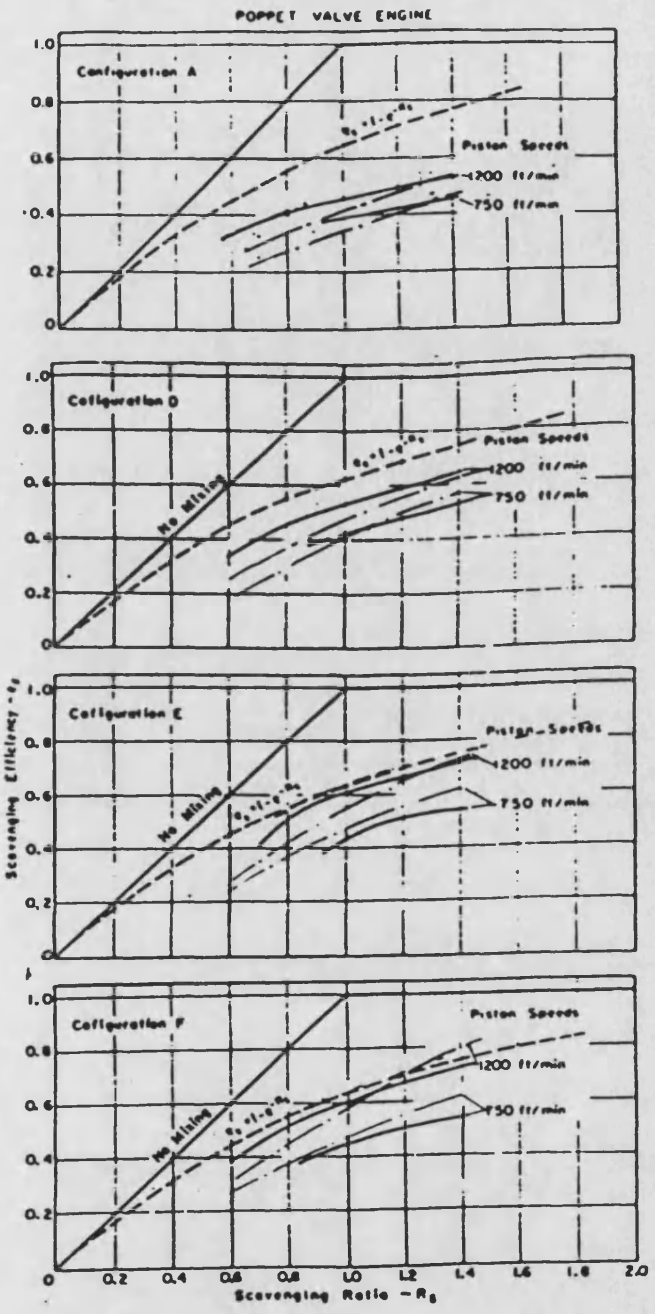

——— experimental results

—·——·— computational results

Fig. 4.7 Comparison between Experimental and Computational Results Using Steady Jet Model with Apparent Spread Rate

configuration: F boost/exhaust pressure ratio: 1.2/1.0

piston speed: 1500 ft/min scavenging ratio: 1.0

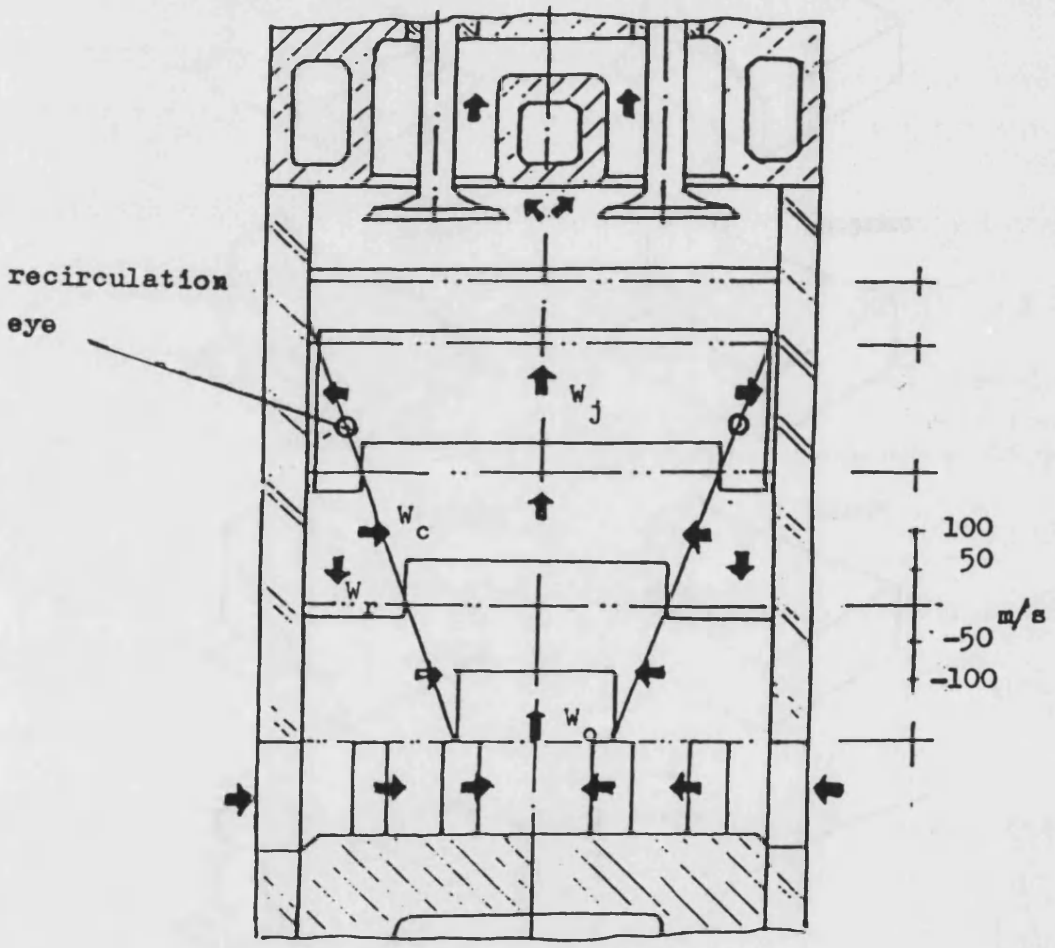

Fig. 4.8 Flow Field in the Cylinder

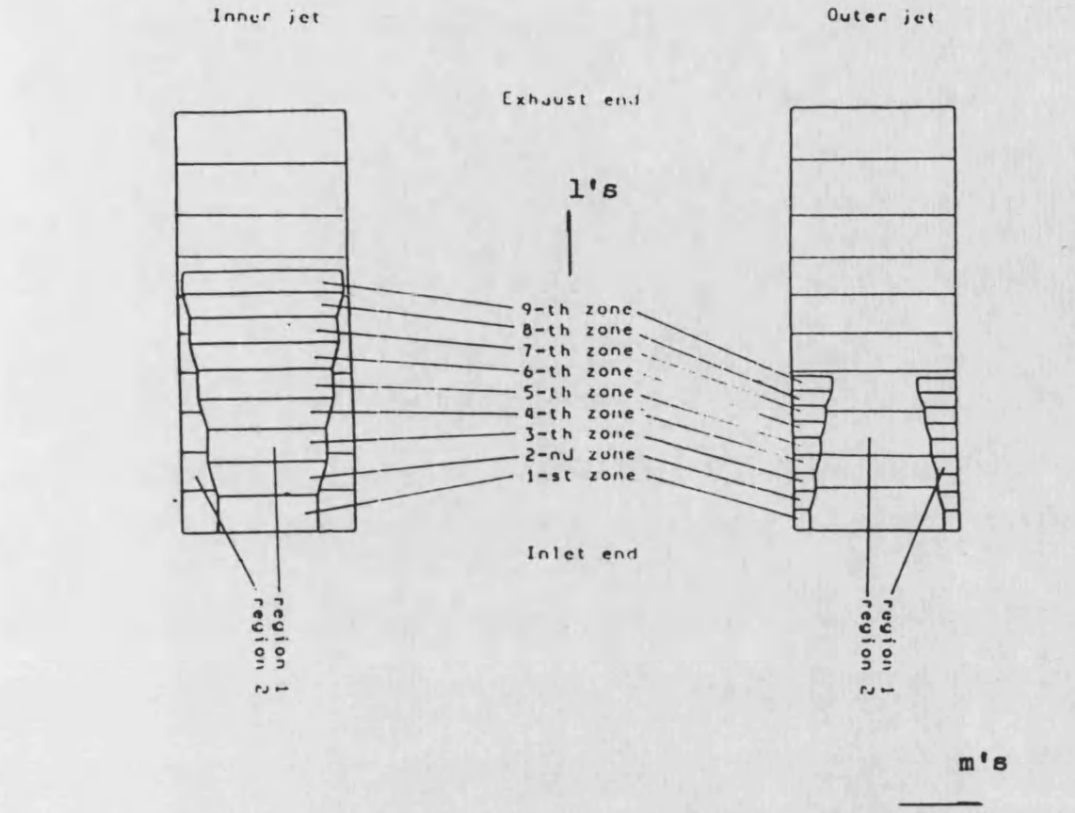

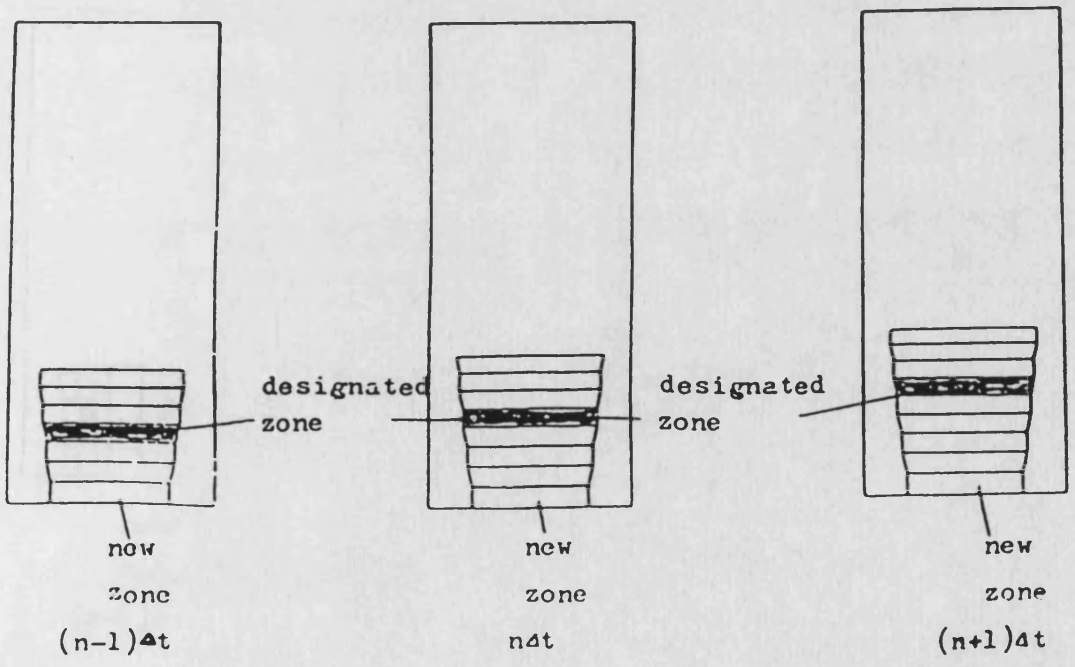

Fig. 4.10 Simplified Flow Patterns and Divided Jet Zones Version 1

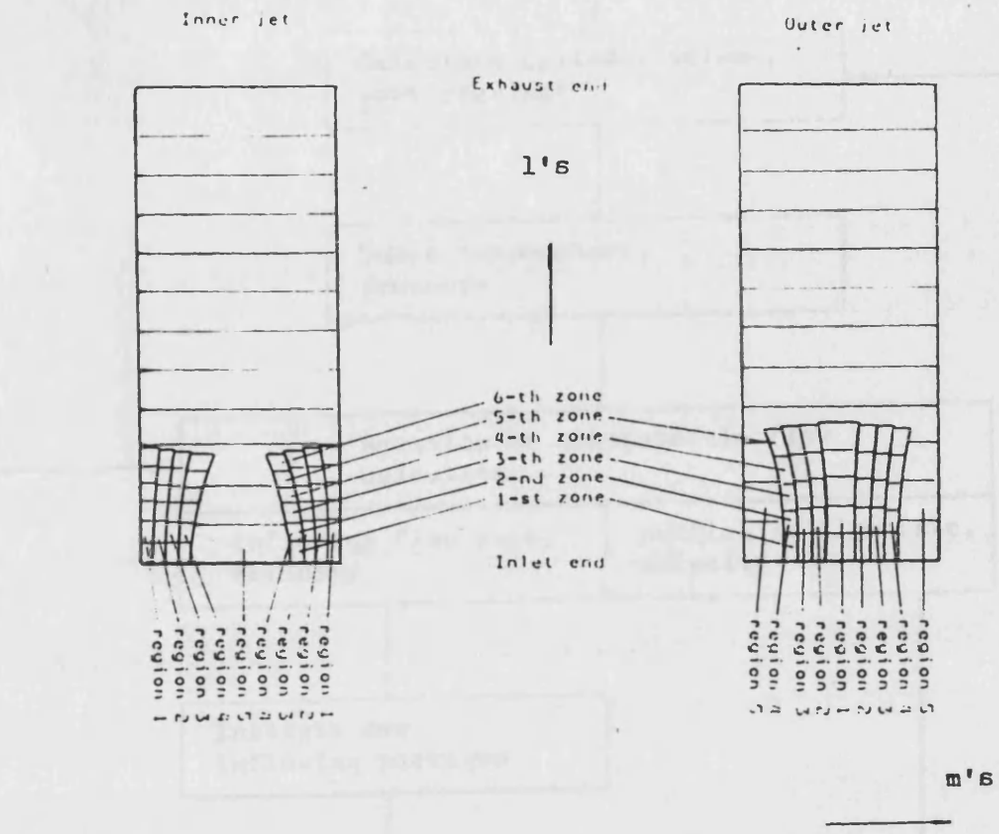

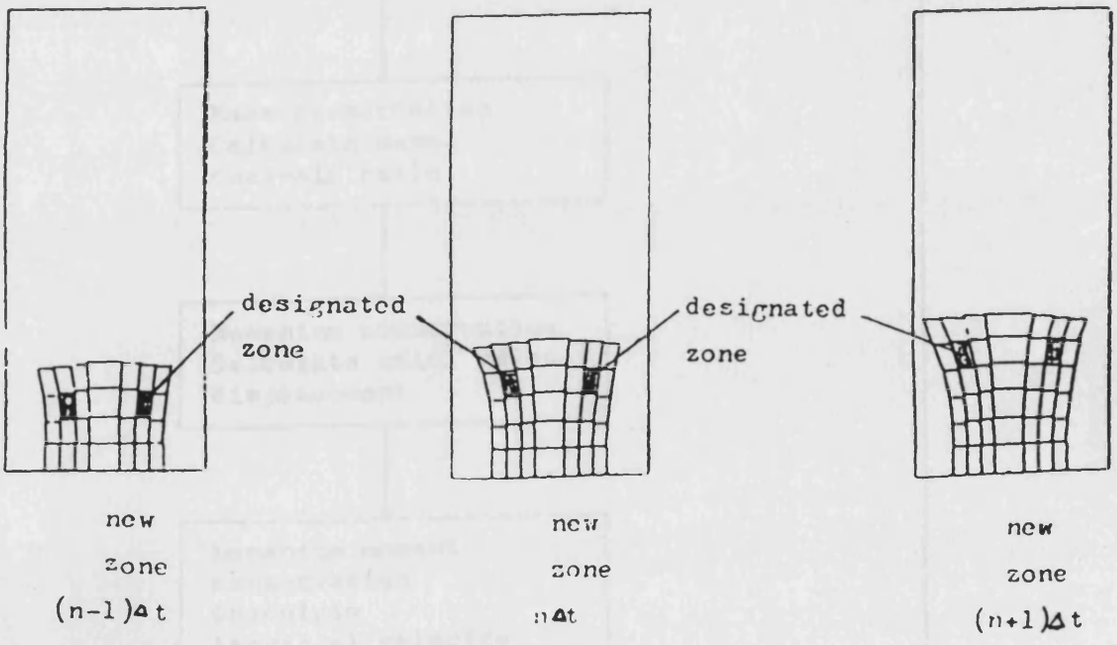

Fig. 4.11 Simplified Flow Patterns and Divided Jet Zones Version 2

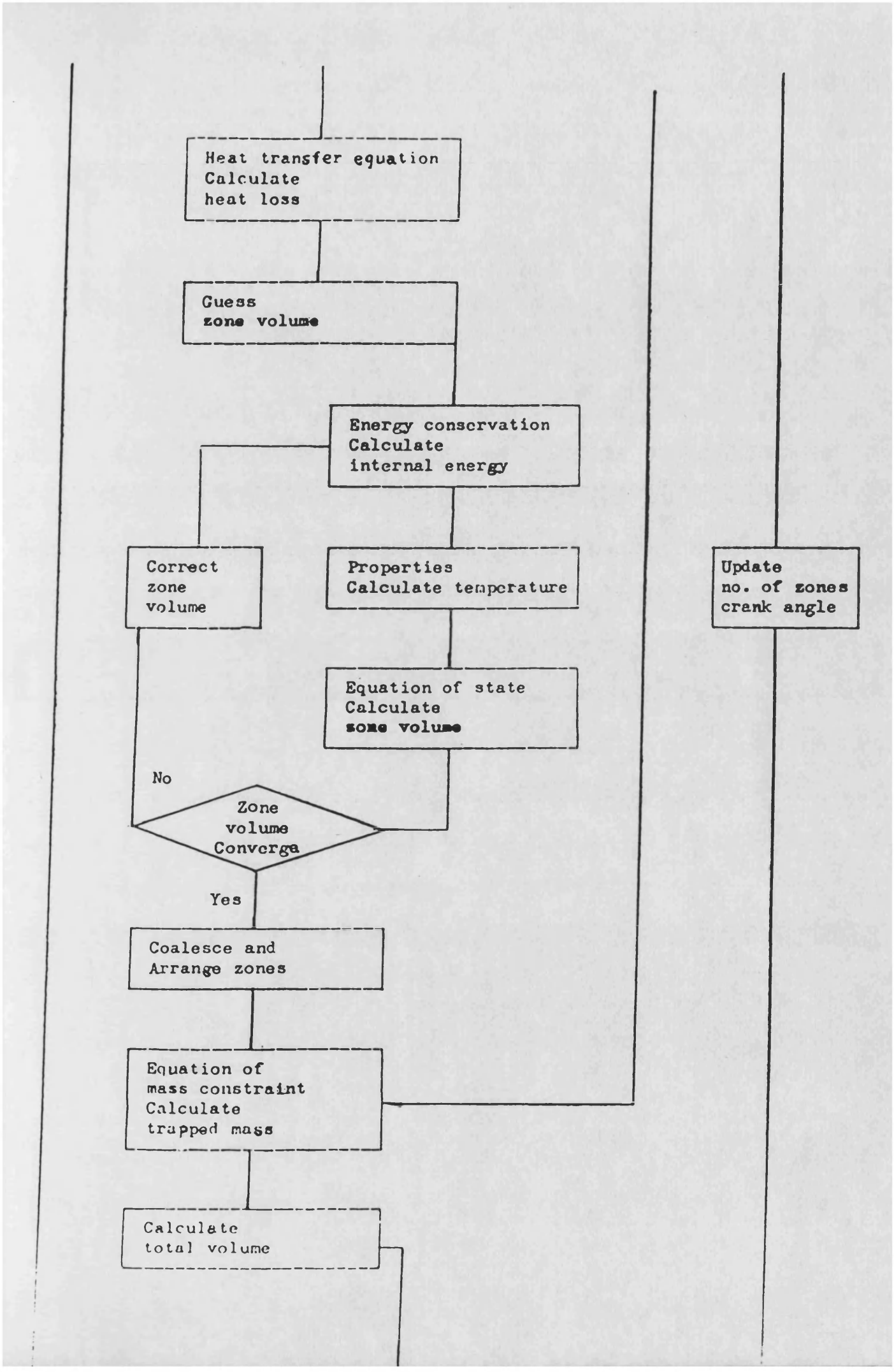
Heat transfer equation
Calculate
heat loss
Guess
zone volume
Energy conservation
Calculate
internal energy
Correct
zone
volume
Properties
Calculate temperature
Update
no. of zones
crank angle
Equation of state
Calculate
zone volume
No
Zone
volume
Converge
Yes
Coalesce and
Arrange zones
Equation of
mass constraint
Calculate
trapped mass
Calculate
total volume

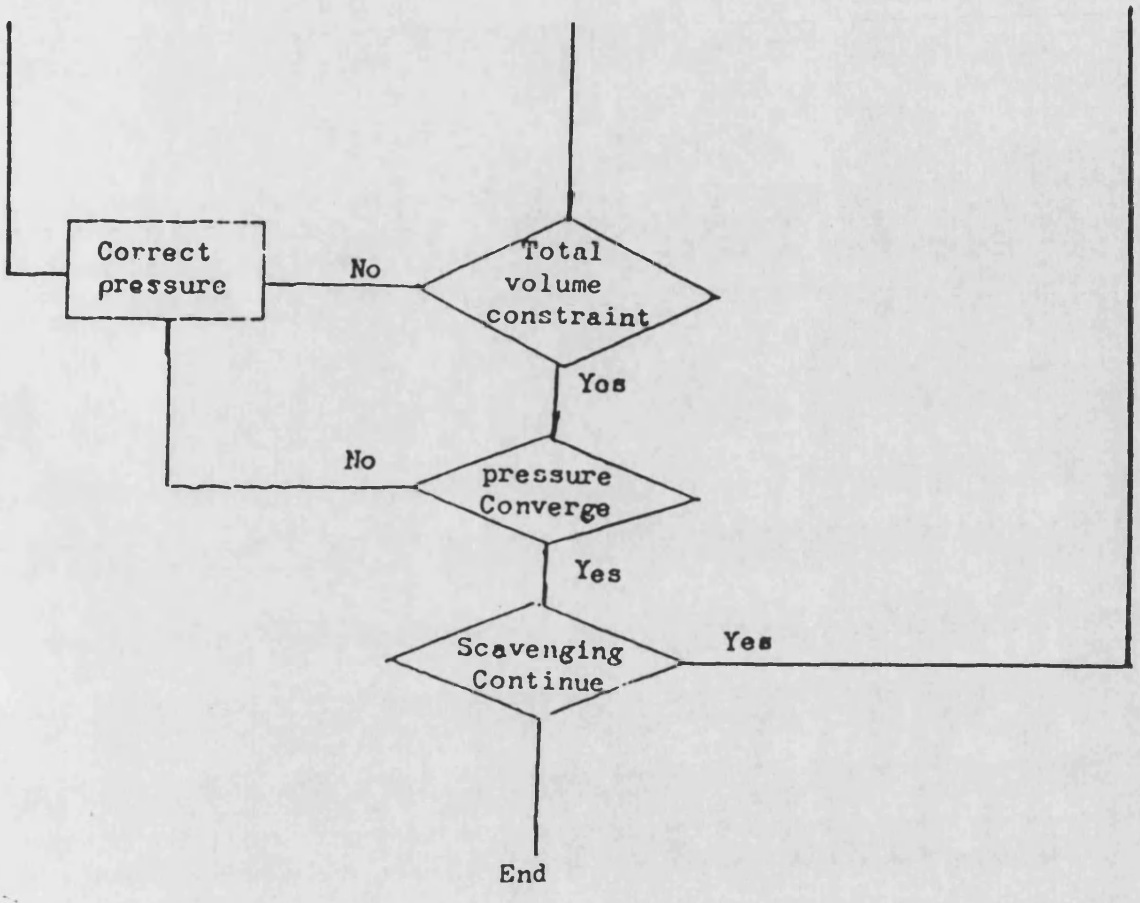

Fig. 4.12 Flow Chart of Multi-Zone Program

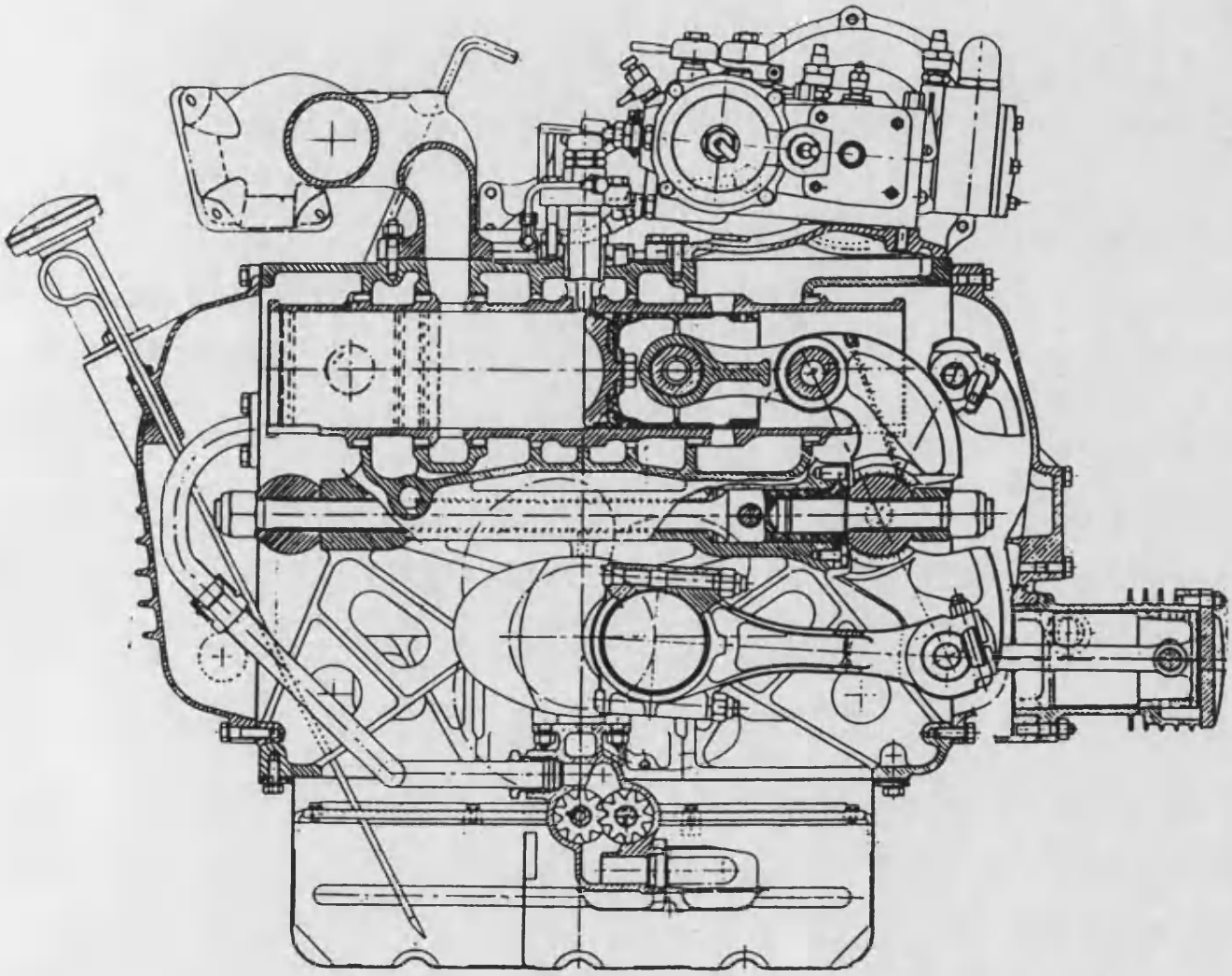

Fig. 4.13 Rootes Opposed Piston Two-Stroke Engine

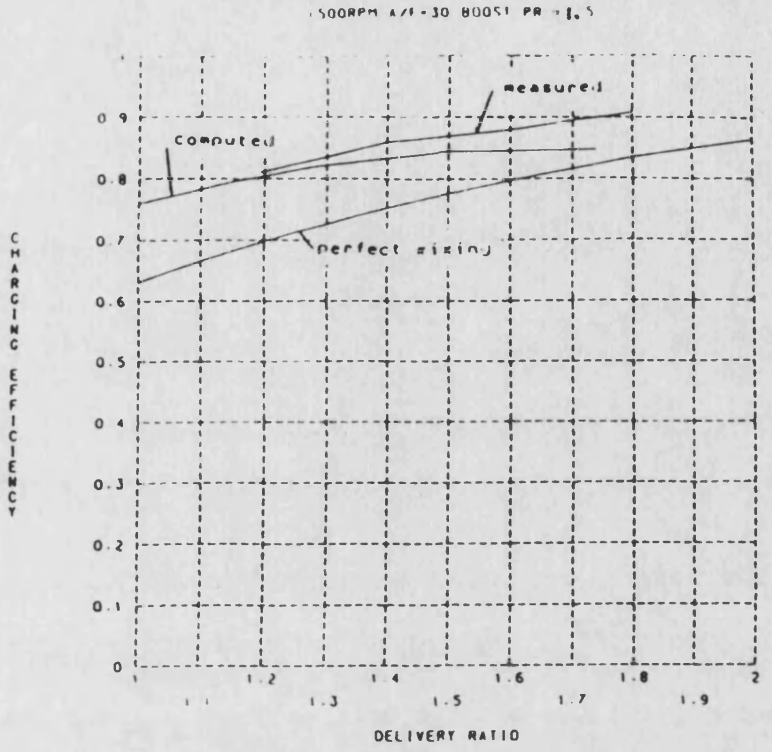

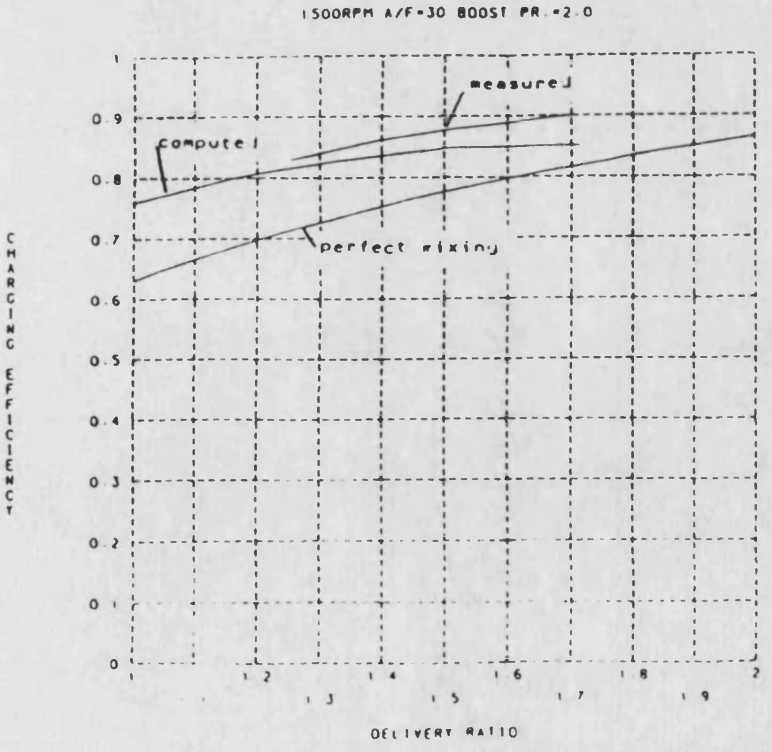

Fig. 4.14 Comparison of Charging Efficiency

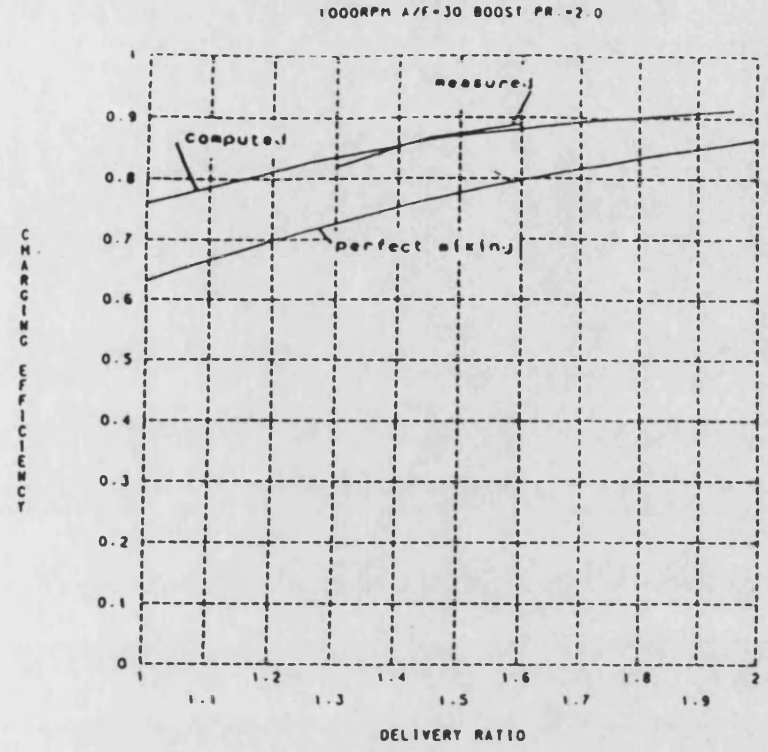
1000RPM A/F=30 BOOST PR.=2.0
measured
computed
perfect mixing
CHARGING EFFICIENCY
0
0.1
0.2
0.3
0.4
0.5
0.6
0.7
0.8
0.9
1
1.1
1.2
1.3
1.4
1.5
1.6
1.7
1.8
1.9
2
DELIVERY RATIO

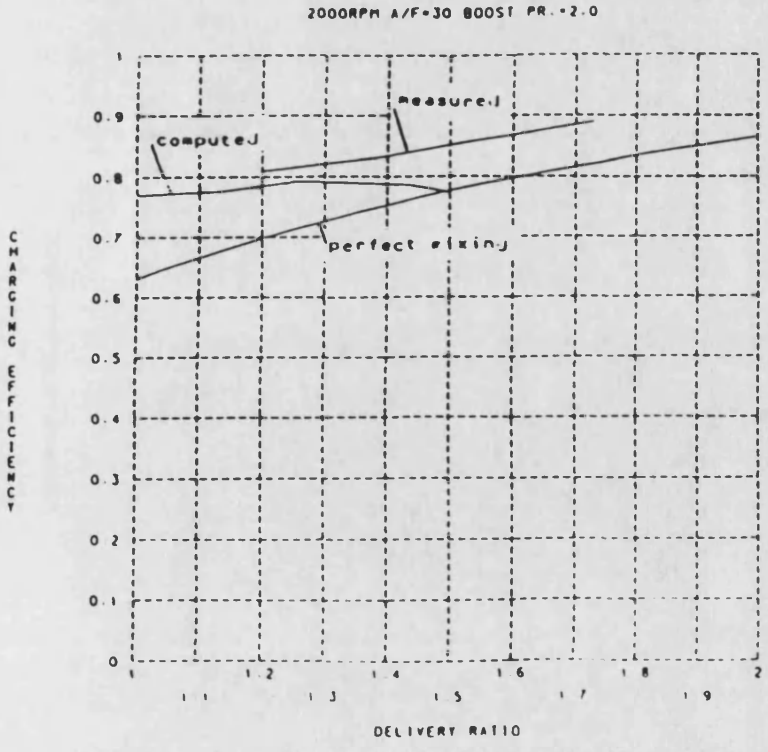
2000RPM A/F=30 BOOST PR.=2.0
measured
computed
perfect mixing
CHARGING EFFICIENCY
0
0.1
0.2
0.3
0.4
0.5
0.6
0.7
0.8
0.9
1
1.1
1.2
1.3
1.4
1.5
1.6
1.7
1.8
1.9
2
DELIVERY RATIO

Fig. 4.14 (cont.)

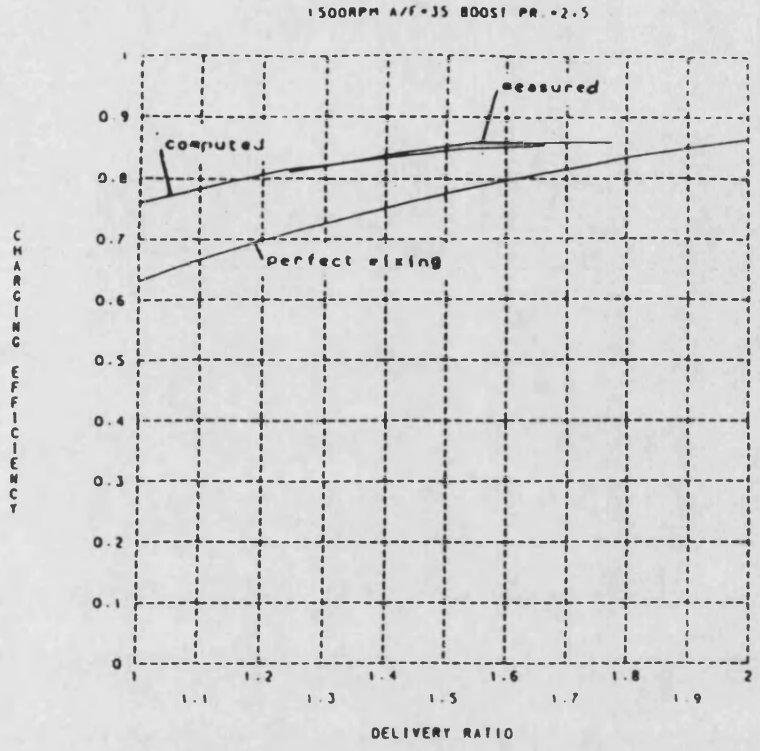
1500RPM A/F=35 BOOST PR.=2.5
measured
computed
perfect mixing
CHARGING EFFICIENCY
0
0.1
0.2
0.3
0.4
0.5
0.6
0.7
0.8
0.9
1
1
1.1
1.2
1.3
1.4
1.5
1.6
1.7
1.8
1.9
2
DELIVERY RATIO

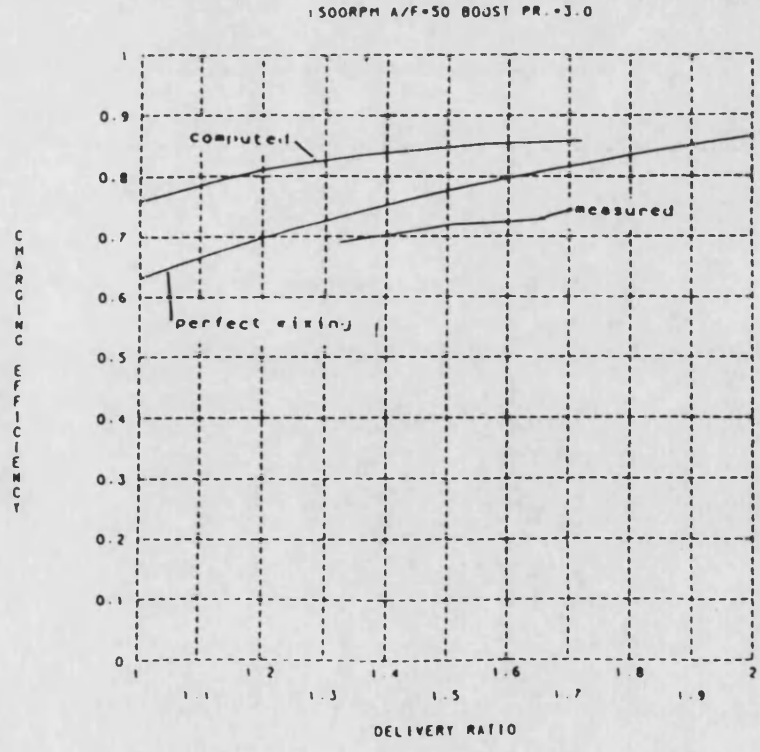
1500RPM A/F=50 BOOST PR.=3.0
computed
measured
perfect mixing
CHARGING EFFICIENCY
0
0.1
0.2
0.3
0.4
0.5
0.6
0.7
0.8
0.9
1
1
1.1
1.2
1.3
1.4
1.5
1.6
1.7
1.8
1.9
2
DELIVERY RATIO

Fig. 4.14 (cont.)

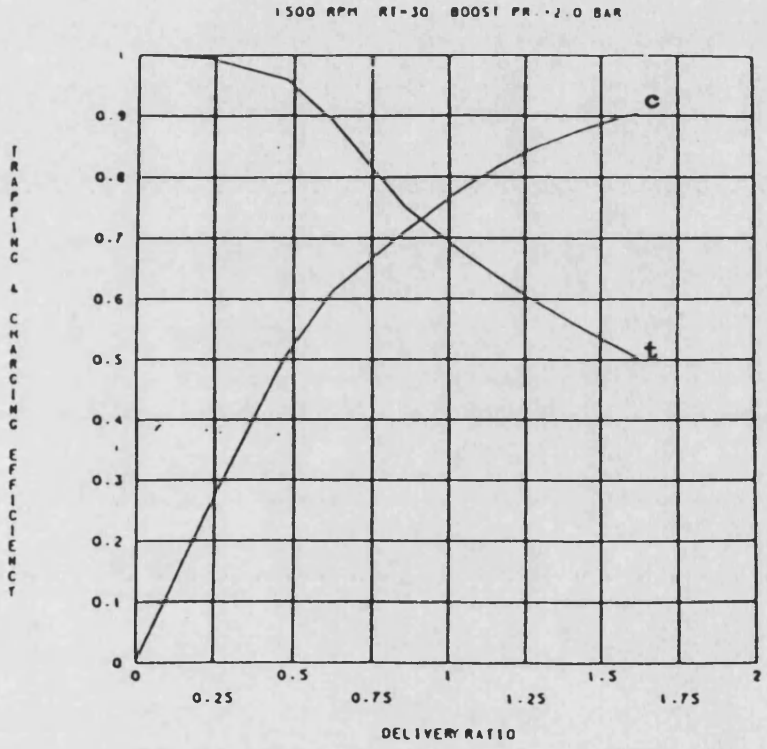

c— charging efficiency
t— trapping efficiency

Fig. 4.15 Effect of Delivery Ratio

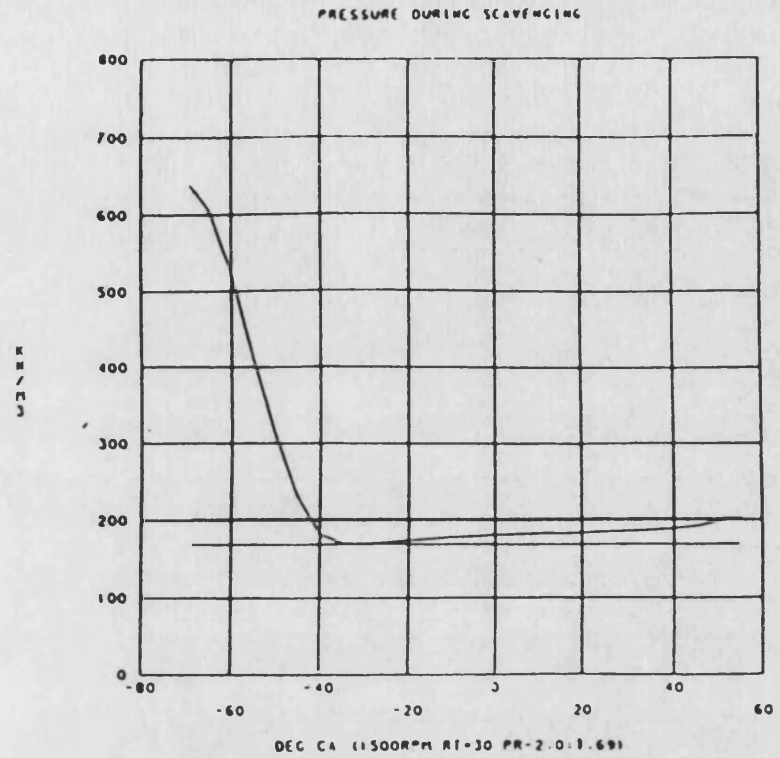

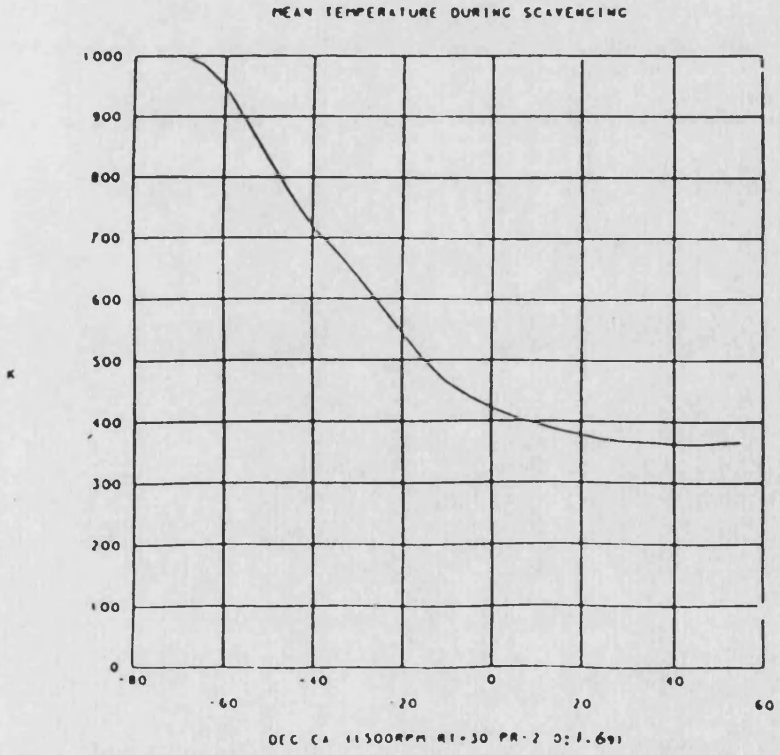

Fig. 4.16 Cylinder Pressure and Mean Temperature

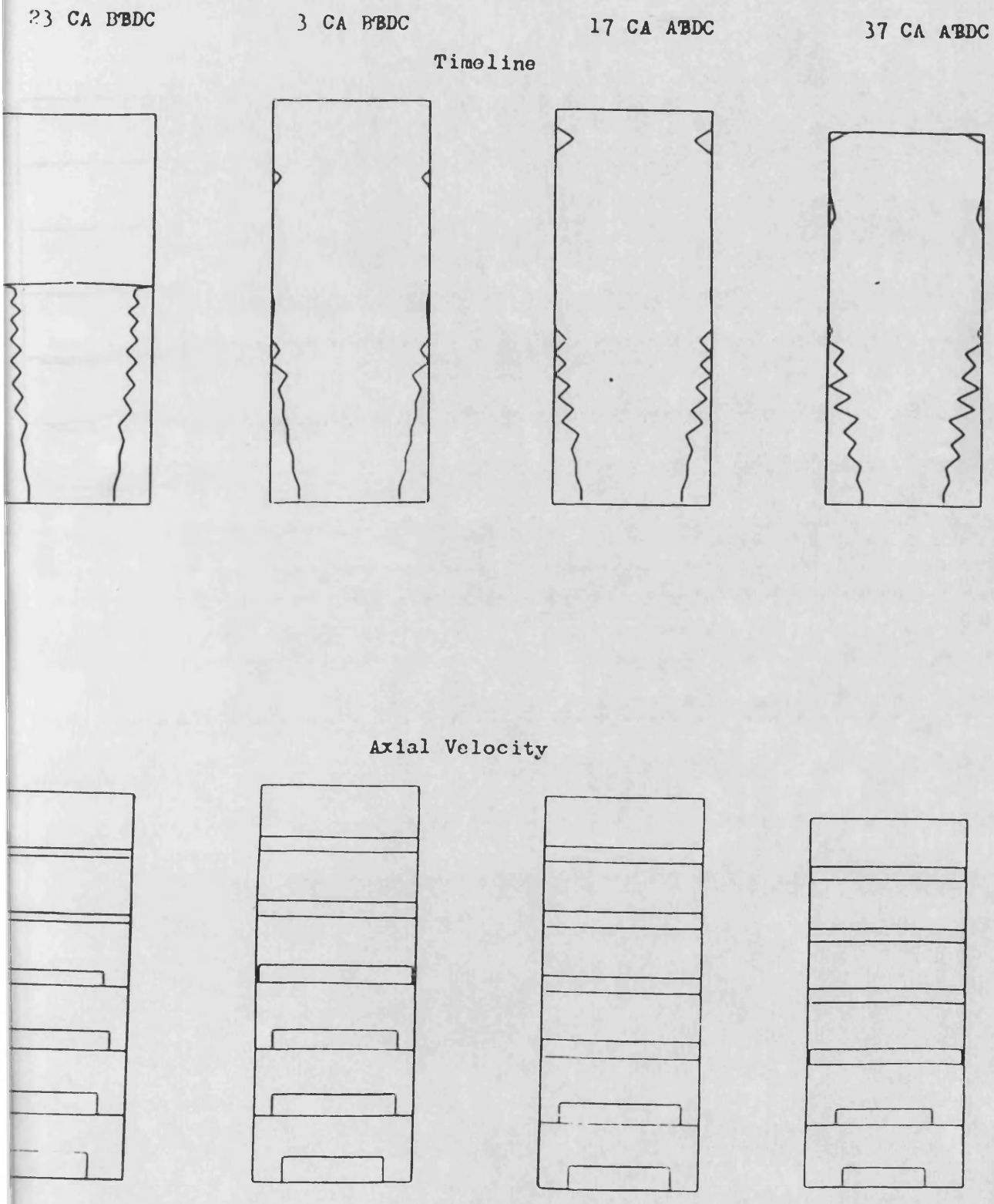

Fig. 4.17 A Group of Computational Results under a Given Running Condition

23 CA BTDC

3 CA BTDC

17 CA ATDC

37 CA ATDC

Tangetial Velocity

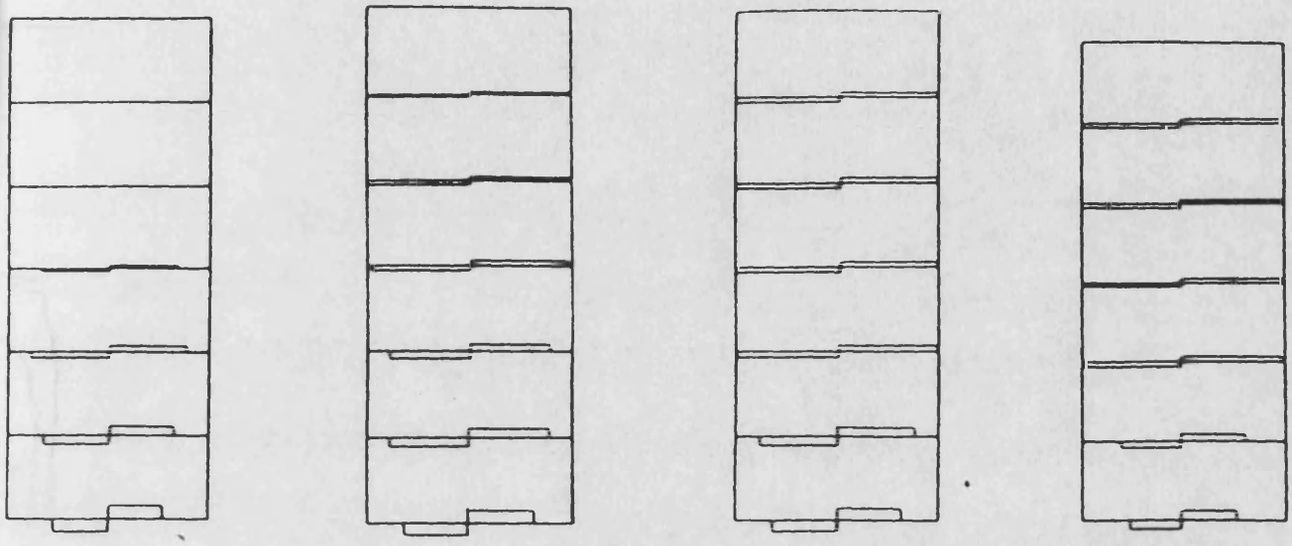

Concentration

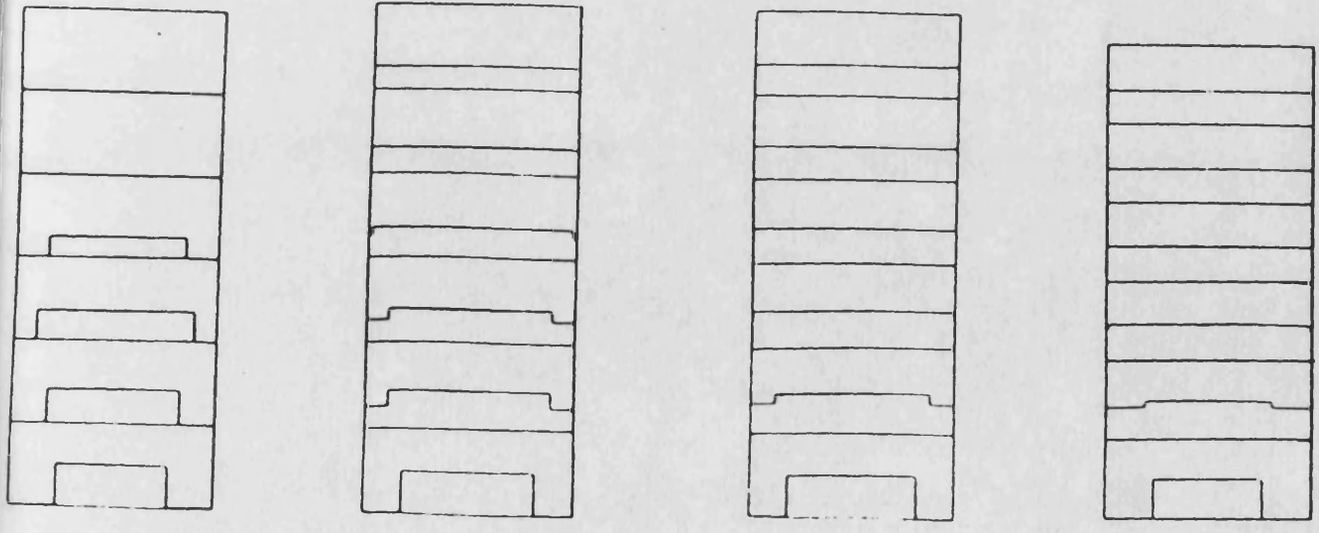

Version 1

Fig. 4.17 (cont.)

23 CA BTDC

3 CA BTDC

17 CA ATDC

37 CA ATDC

Timeline

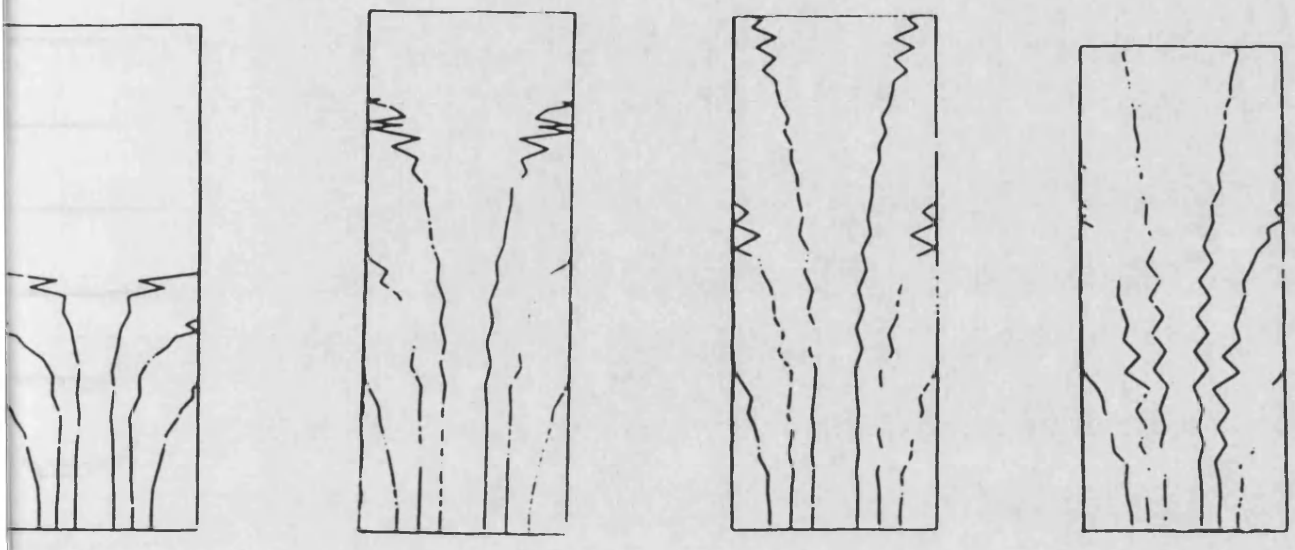

Axial Velocity

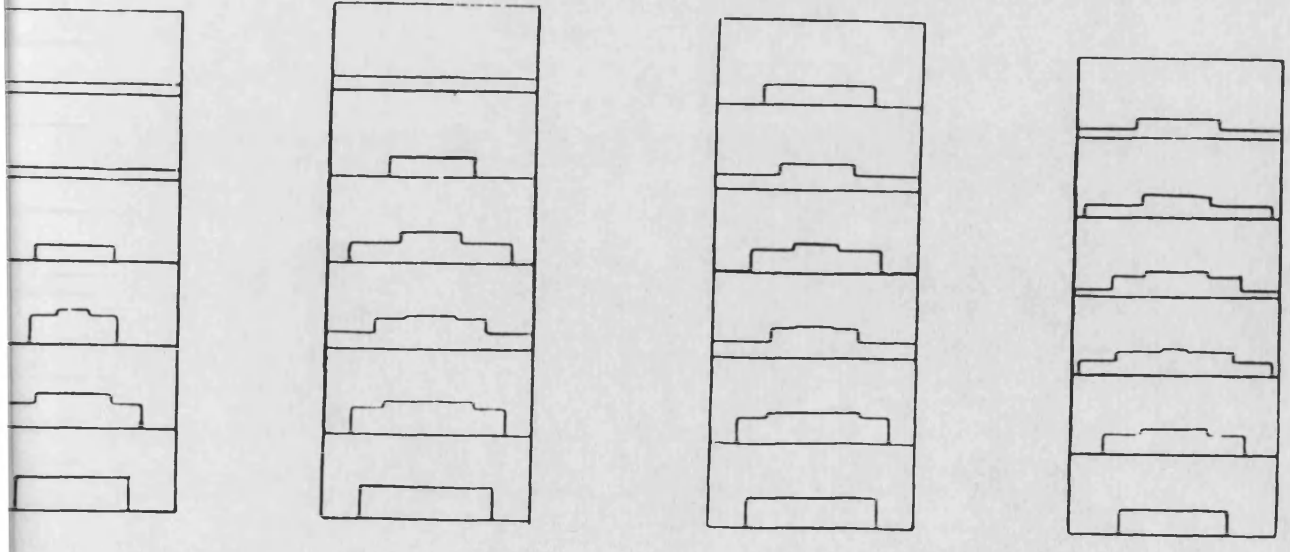

Version 2 — 4 strips

Fig. 4.17 (cont.)

23 CA ATDC

3 CA BTDC

17 CA ATDC

37 CA ATDC

Tangetial Velocity

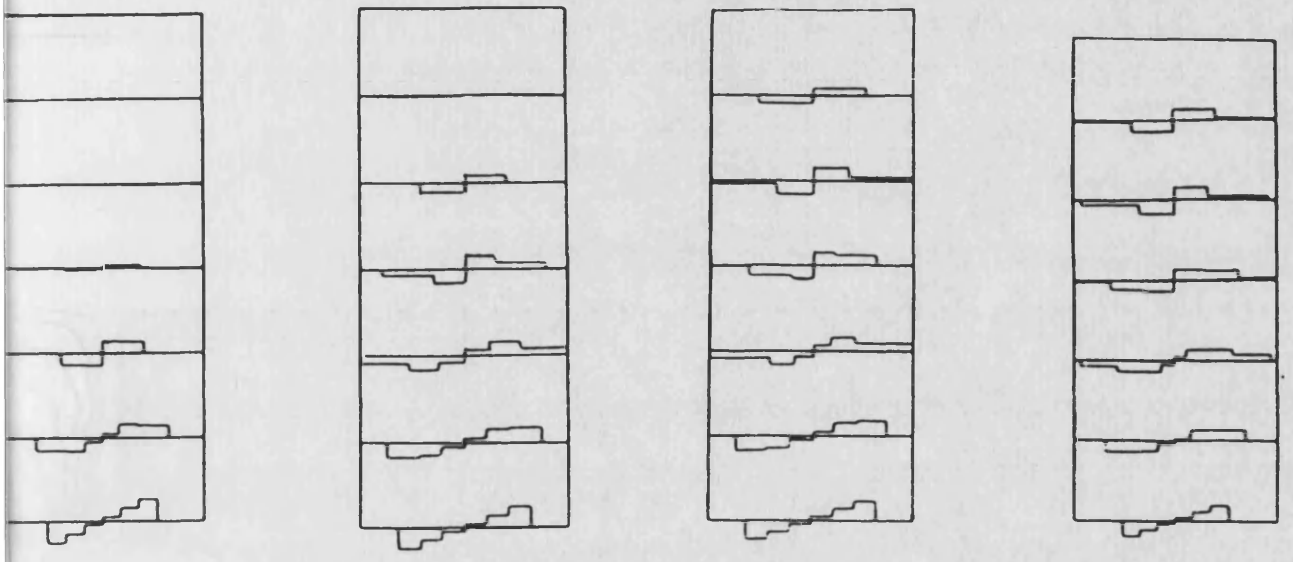

Concentration

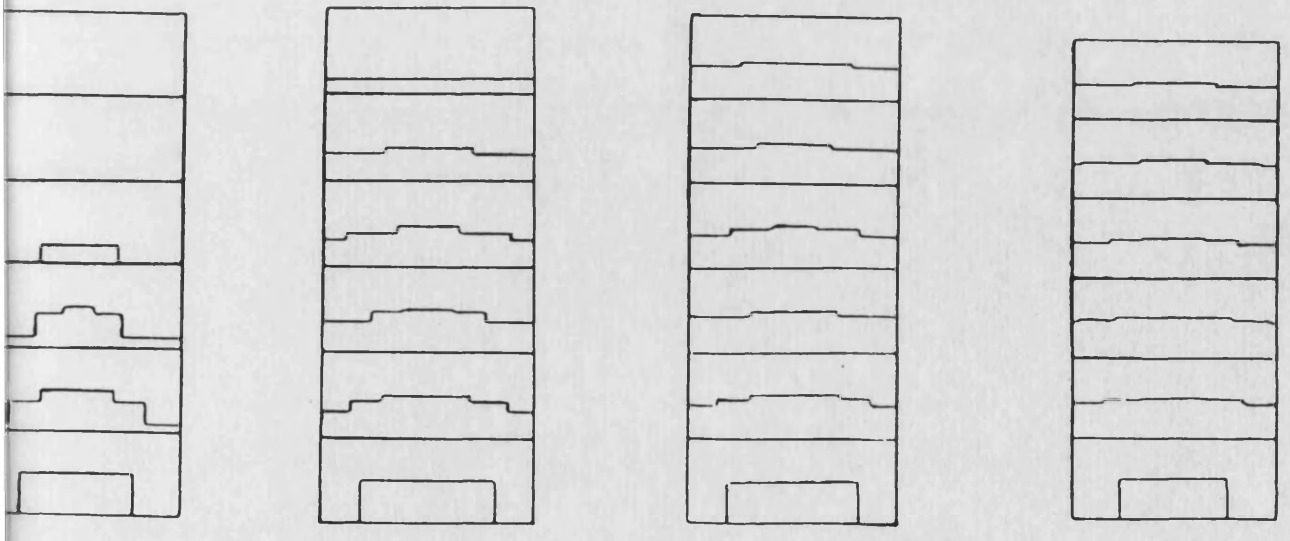

Version 2 -- 4 strips

Fig. 4.17 (cont.)

23 CA BTDC

3 CA BTDC

17 CA ATDC

37 CA ATDC

Timeline

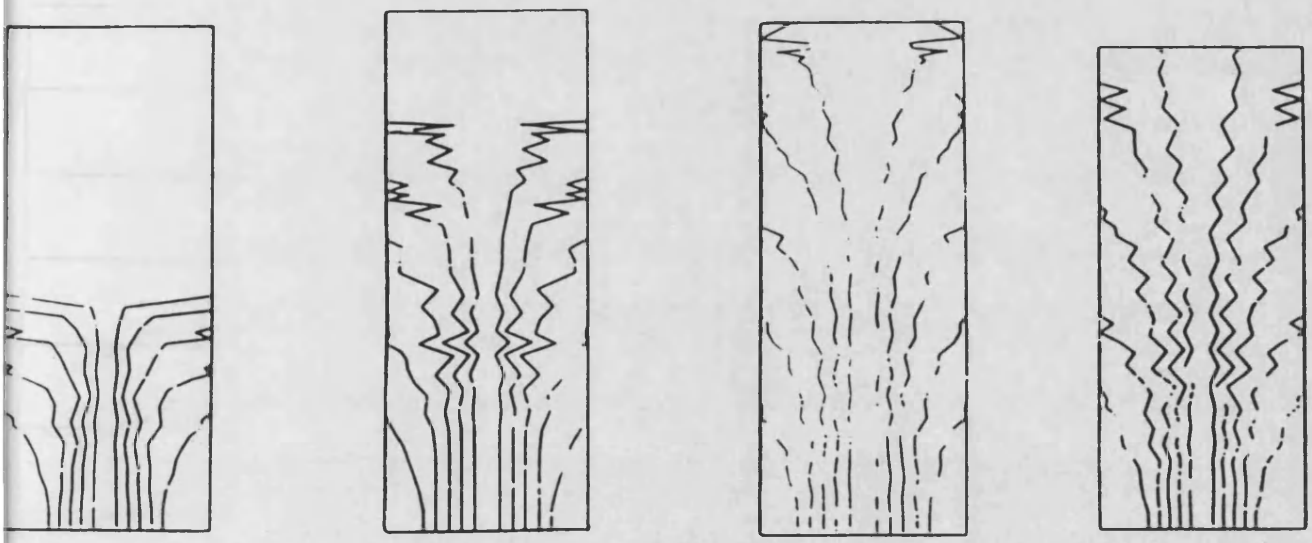

Axial Velocity

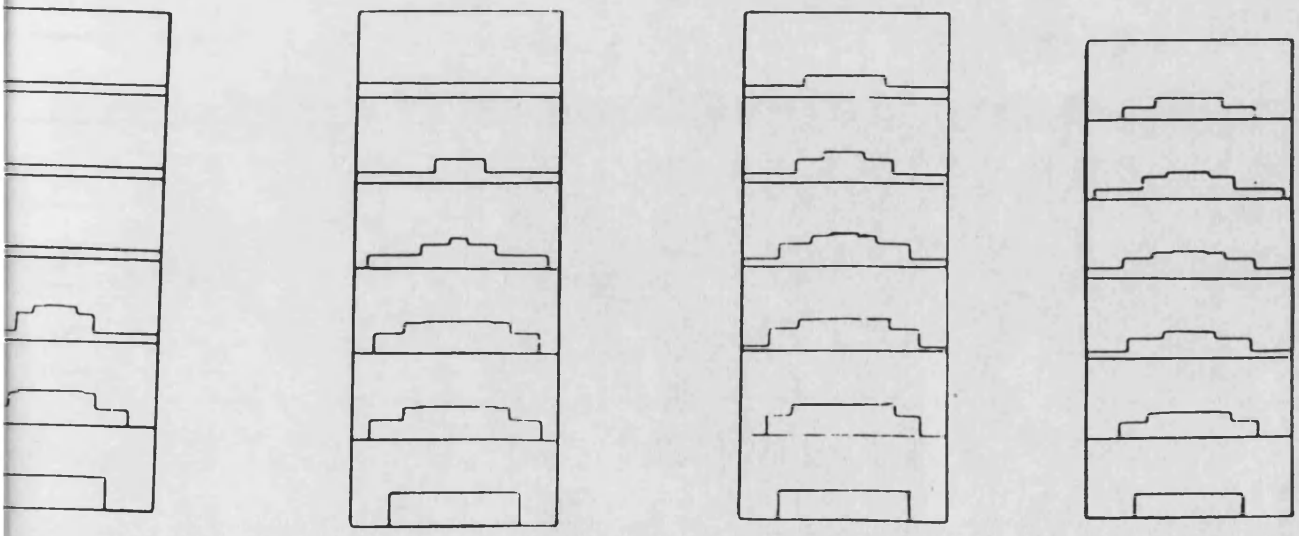

Version 2 — 6 strips

Fig. 4.17 (cont.)

23 CA BBDC

3 CA BBDC

17 CA ABDC

37 CA ABDC

Tangetial Velocity

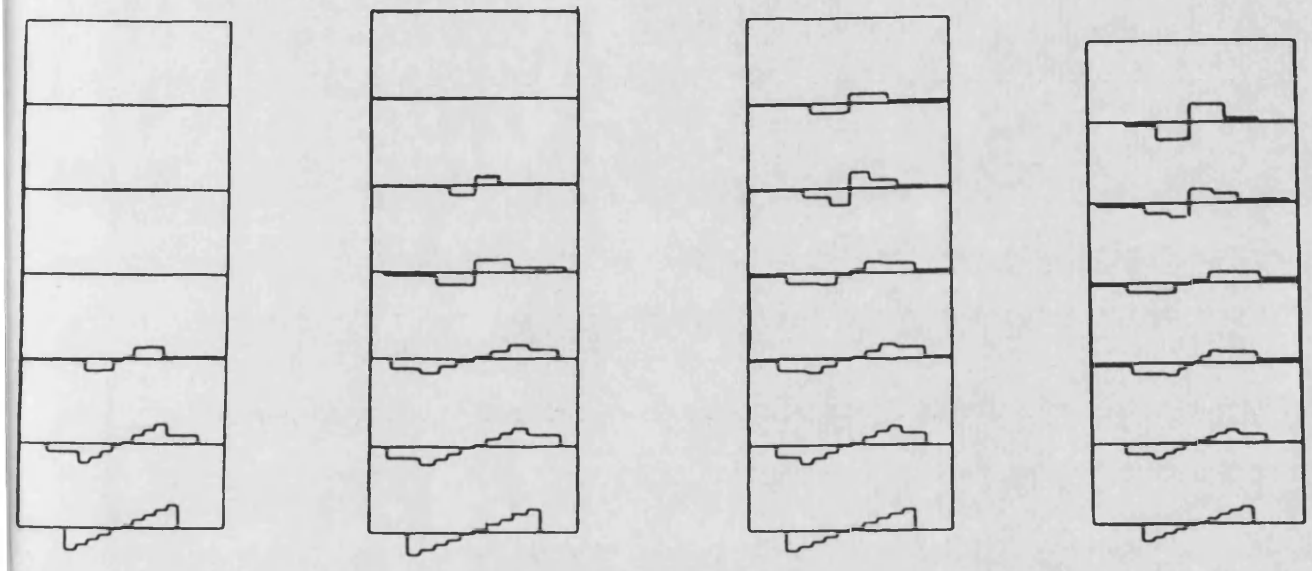

Concentration

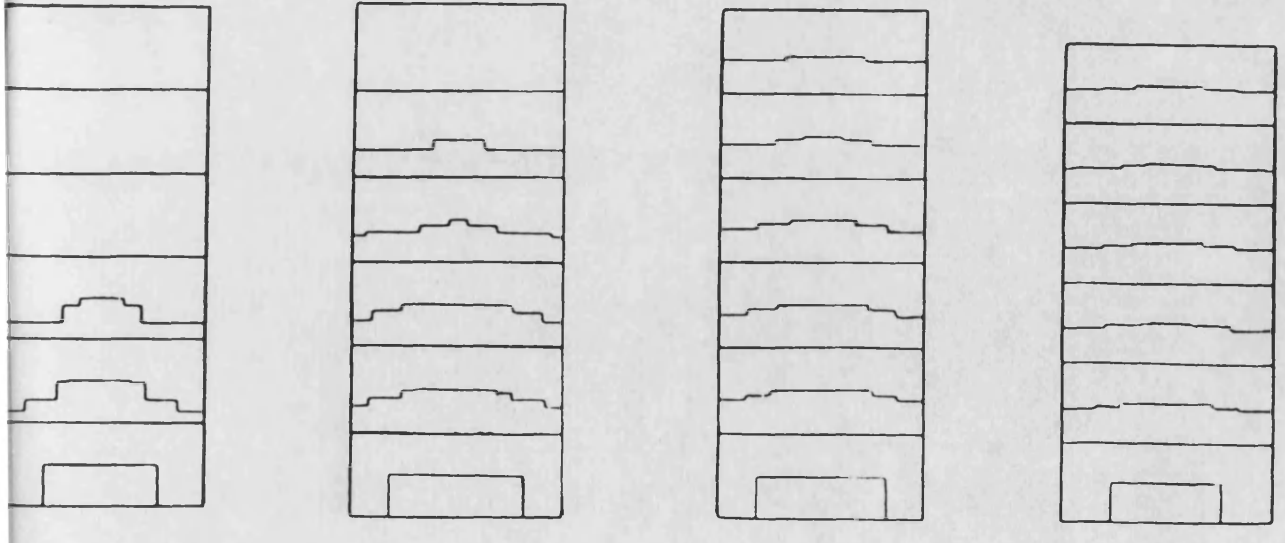

Version 2 — 6 strips

Fig. 4.17 (cont.)

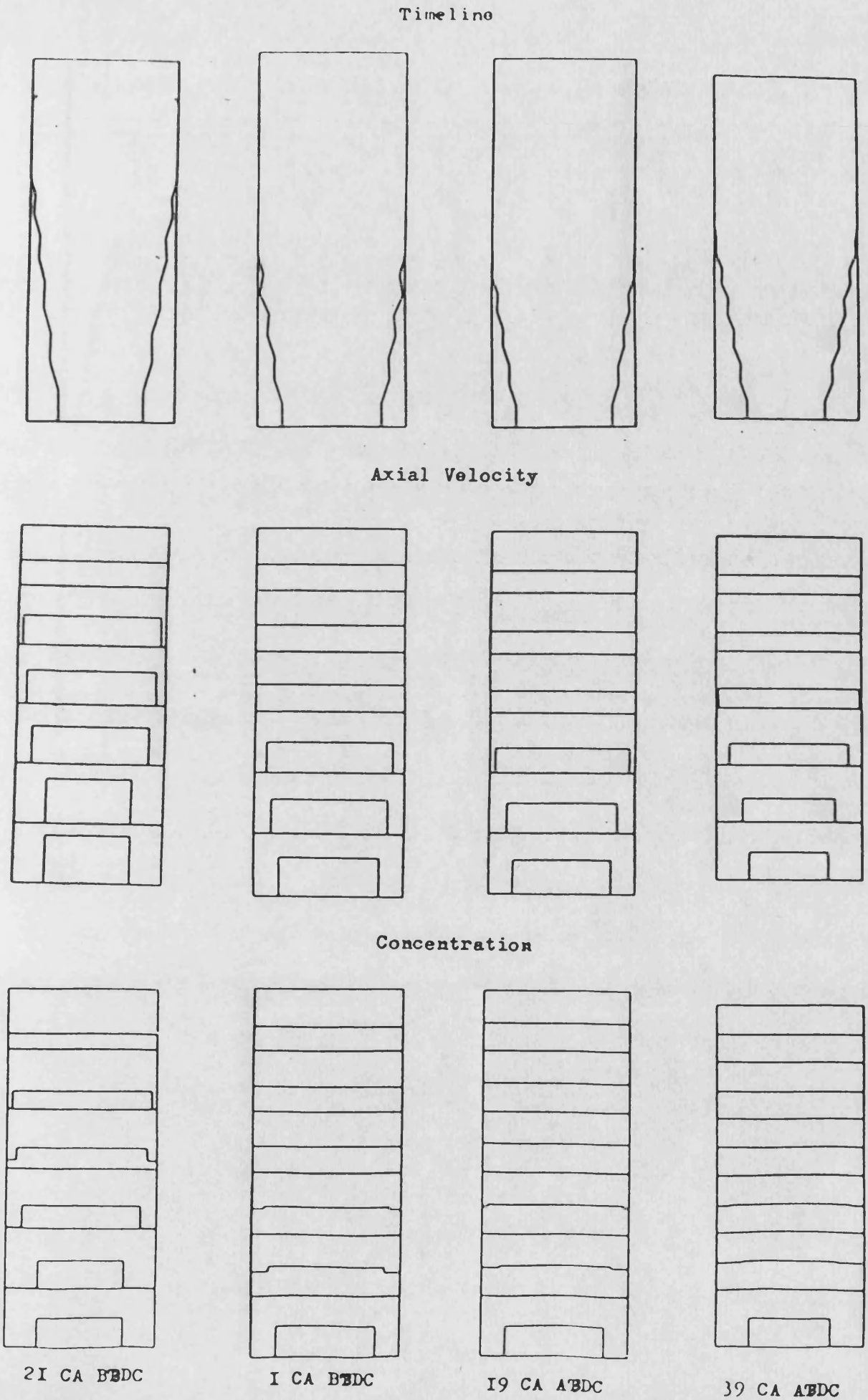

Fig. 4.18 Flow and Concentration Field
(0 deg. swirl angle)

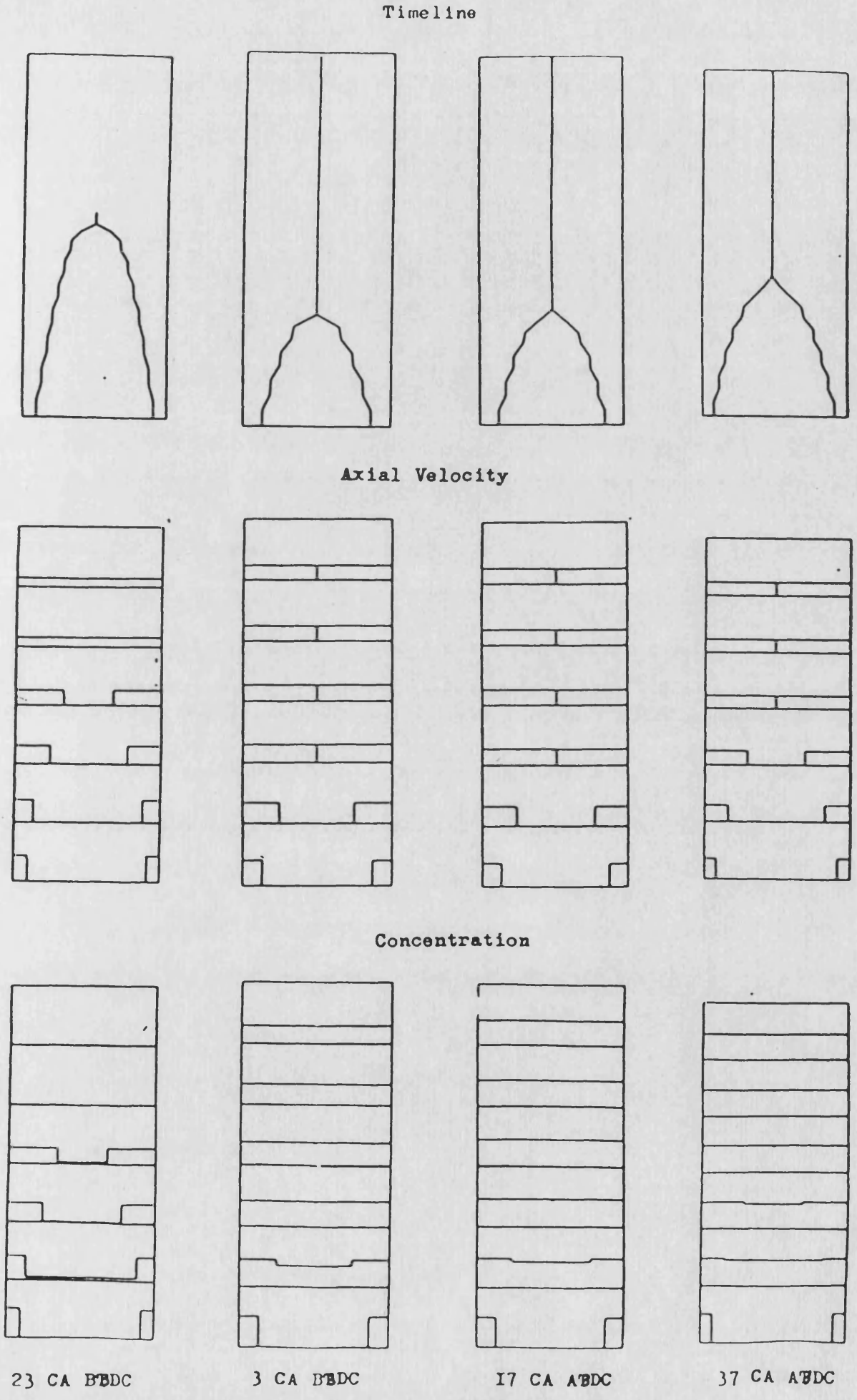

Fig. 4.18 Flow and Concentration Field
(60 deg. swirl angle)

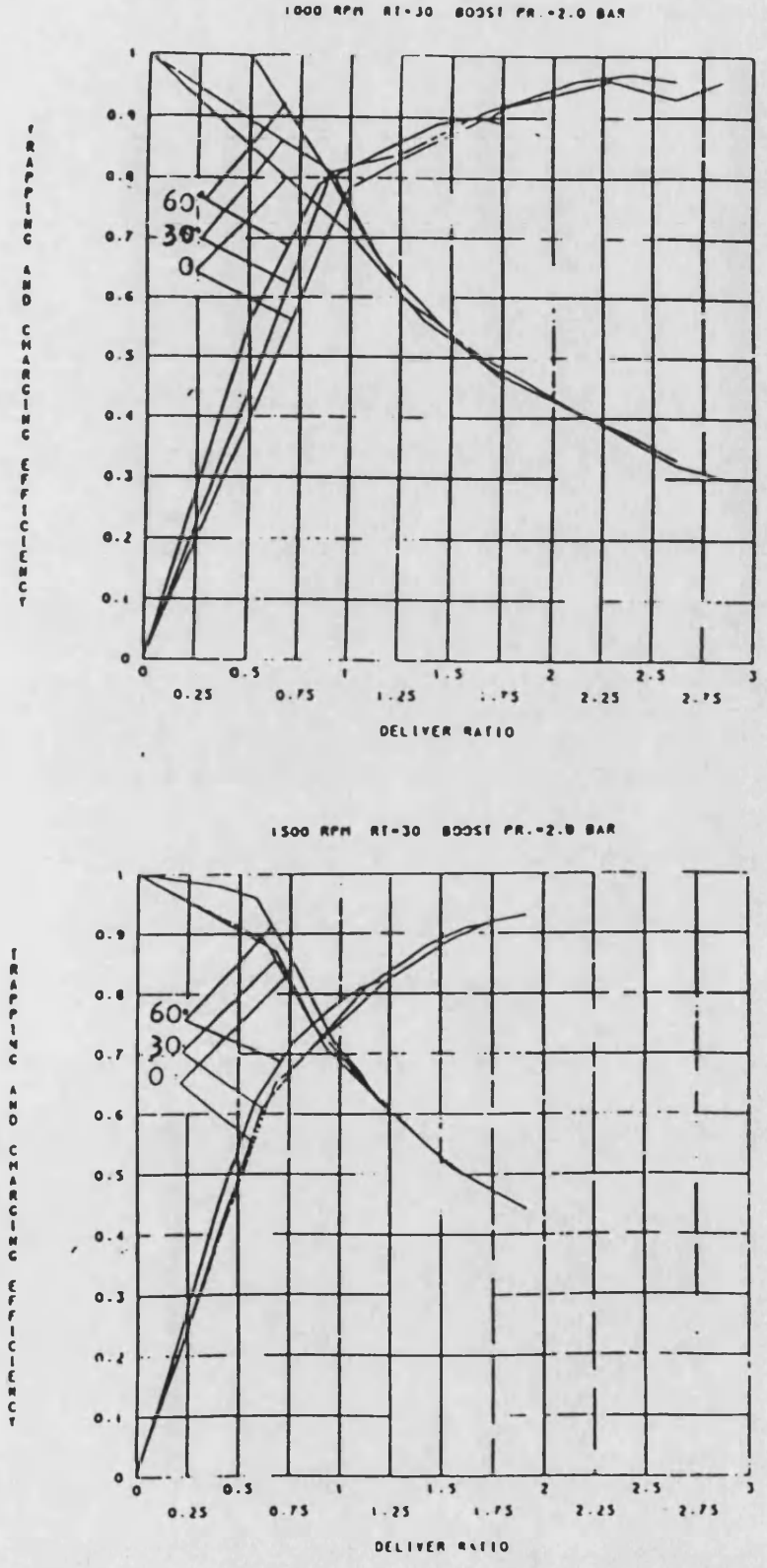

Fig. 4.19 Effect of Swirl Angle at Different Speeds

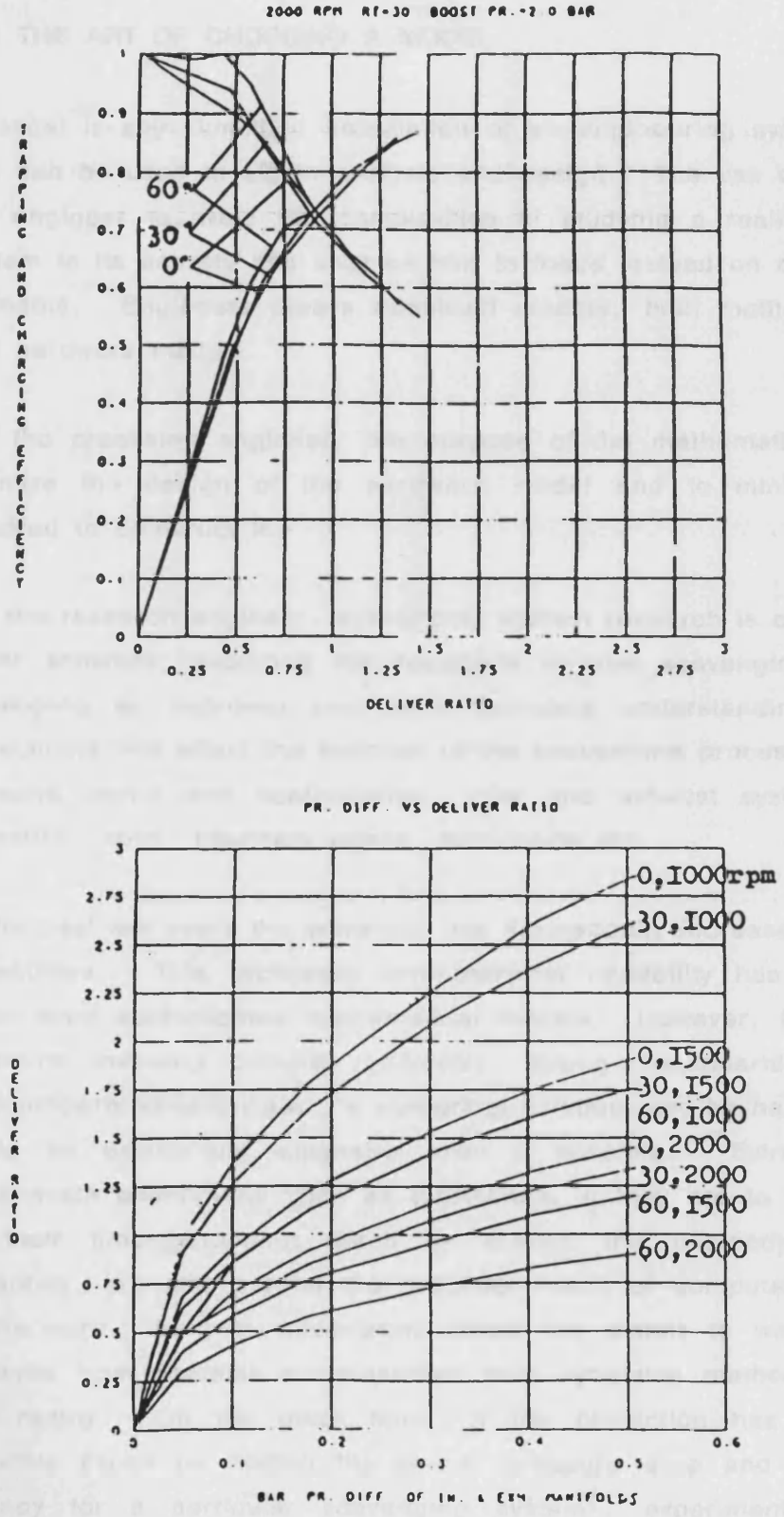
2000 RPM RF=30 BOOST PR.=2.0 BAR
TRAPPING AND CHARGING EFFICIENCY
60°
30°
0°
DELIVER RATIO
PR. DIFF. VS DELIVER RATIO
DELIVER RATIO
0,1000rpm
30,1000
0,1500
30,1500
60,1000
0,2000
30,2000
60,1500
60,2000
BAR PR. DIFF OF IN. & EXH MANIFOLDS

Fig. 4.19 (cont.)

Chapter 5 CRITICAL ASSESSMENT OF SCAVENGING MODELS

5.1 THE ART OF CHOOSING A MODEL

A model is any simplified description of an engineering system or process that can be used to aid in analysis and design. The use of models allows the engineer to avoid the complexities of studying a realistic engineering system in its entirety and enables him to focus instead on only its essential elements. Engineers always construct models, both mathematical models and hardware models.

For the practising engineer, the purpose of the mathematical model is to optimize the design of the hardware model and to minimize the effort required to construct it.

For the research engineer, scavenging system research is comprised of two major activities: exploring the feasibility of new scavenging systems and developing an improved and more complete understanding of important phenomena that affect the success of the scavenging process, such as port or valve layout and configuration, inlet and exhaust system tuning, jet formation, swirl, boundary layers, turbulence etc.

In the past few years the computer has dramatically increased our analytical capabilities. This increased computational capability has made possible much more sophisticated mathematical models. However, for such difficult problems involving complex geometry, strong nonlinearities sensitive to fluid-property variation etc., a numerical solution may be hard to obtain and would be excessively expensive even if possible. Extremely fast and small-scale phenomena such as turbulence, if they are to be computed in all their time-dependent detail by solving the unsteady Navier-Stokes equations, are still beyond the practical reach of computational methods. Furthermore, there is uncertainty about the extent to which the results obtained from complex computational fluid dynamics methods would agree with reality. On the other hand, if the prediction has a very limited objective (such as finding the overall pressure drop and the scavenging effiency for a particular scavenging system), experiment may be less expensive than computation.

Therefore, the appreciation of the strengths and weaknesses of different approaches is essential to the proper choice of the appropriate technique. There is no doubt that experiment is the only method for investigating a new basic phenomenon. In this sense, experiment leads and computation follows. It is in the synthesis of a number of known phenomena that the computation performs more efficiently. Even then, sufficient validation of the computed results by comparison with experimental data is required. On the other hand, preliminary computations are often helpful in the design of the hardware model and reduction of the amount of experimentation.

An optimum prediction effort should thus be a judicious combination of computation and experiment, and a correct choice of mathematical models. The judgment consists in arriving at a compromise between the objectives of the prediction and economic and other constraints, such as computer capacity etc.

5.2 FURTHER DETAILED CONSIDERATION

5.2.1 GENERAL

In the previous chapters, attention has been drawn to the general motion within the cylinder, entrainment and recirculation which decide the nature of the flow process. However, from the viewpoint of the scavenging process, turbulence and swirl have obvious influences on the motion, while the flow in the wall boundary layers partly controls exhaust emissions. From the viewpoint of a complete cycle, the turbulence and the boundary layer affect the combustion, the heat transfer and the pollution formation. Over a longer operating period, cycle-to-cycle variations of the scavenging efficiency induce performance oscillation. As the boundary conditions, the port or valve layout and configuration, the pressure distribution and the velocity and turbulent intensity profile all exert an effect on the scavenging process. Therefore, a comprehensive predictive capability requires a wide range of knowledge covering turbulence, swirl, boundary layer, cycle-to-cycle variations, information relating to inlet and exhaust manifolds.

The following qualitative picture of the flow features in a typical engine is based on experiments in motored and operating engines, and to a great extent, on other flows of similar character.

5.2.2 SWIRL

Swirling flows in cylinders exhibit a wide variety of flow features. At least three types of mean flow field can be identified. [5.1]

(1). no flow reversal.
(2). a central recirculation zone.
(3). a long backflow region or columnar flow.

as shown in Fig. 5.1.

A minimun flow Reynolds number is required for flow recirculation. Increasing swirl will cause a transition from type 1 to type 2, and with further swirl increase from type 2 to type 3.

It is now generally accepted that the transition from type 1 to 2, termed vortex breakdown, is a transition from supercritical to subcritical flow. In this context, the term "critical" refers to a flow for which long inertia waves are stationary with respect to the flow. If the flow is supercritical, such waves are swept downstream from the originating disturbance, while for subcritical flow these waves propagate upstream against the flow, carrying with them information about the nature of the downstream geometry and conditions.

From measurements with laser Doppler anemometers [5.2], it is shown that the vortex flow, in general, remains subcritical down to the exit with backflow evident throughout the cylinder, and that the entire flow field is strongly affected by the exit geometry. It is also shown that even a weak exit contraction has a significant influence on a flow which remains subcritical. However, a subcritical vortex flow in a cylinder of constant cross-section approaches the critical flow state in the downstream direction, and if the cylinder is sufficiently long, eventually goes through the critical state and becomes increasingly supercritical, mainly under the influence of viscous vortex-core thickening. In contrast, a strong contraction has practically no influence on a flow which becomes supercritical, as shown in Fig. 5.2.

Further complicating the picture is the frequent occurrence of flow

oscillations which depend in part on the entering velocity profiles and on flow geometry. [5.3] Slight asymmetry at the inlet section has major effect on axial asymmetry at downstream sections. The centre of swirl turns helically around the cylinder axis in the same direction as the swirl itself and its pitch depends only on the swirl intensity. The recirculation bubble undergoes oscillations in the axial direction.

5.2.3 BOUNDARY LAYER

Using flow visualization techniques, a vortex motion is observed at the corner between the piston face and cylinder wall as the piston moves in the cylinder. In this investigation two types of flows are observed. [5.4]

(1). a sink flow as the piston retreats downwards in the cylinder.
(2). a spiral vortex flow as the piston moves upwards.

as shown in Fig. 5.3. This indicates that during the expansion stroke a boundary layer is formed on the cylinder wall, while during the reverse stroke the fluid must be peeled off the cylinder wall, which gives rise to the formation of a larger vortex, so that quench layers formed at the walls during combustion are expelled at some point in the process. These complex events determine which fluid elements remain in the cylinder at the end of the exhaust process.

5.2.4 TURBULENCE

Turbulence generated in a cylinder is quite complex. During the intake process, flow passing the ports or valves separates, produces sharp shear layers off the edge of the ports or valves and results in a highly unsteady motion. These shear layers break down initially into ring-like vortices which merge to form larger-scale vortices. These larger-scale vortices in turn break down into three-dimensional turbulent motion. The turbulence increases from a moderate level in the jet core to a peak which coincides with the jet edge. [5.5] The resulting turbulent jet contains a broad spectrum of turbulence scales ranging from large eddies of the order of the jet thickness to small-scale eddies that dissipate the turbulent motion. The jet flow induces a general circulation in the cylinder, which may be compounded by intake swirl produced in the manifold. The separation of

the shear layers off the edge of the ports or valves sets up recirculation regions. The large-scale circulations probably induce smaller reverse circulation in the corner, as shown in Fig. 5.4. After bottom dead centre and after closure of the inlet and exhaust ports, the existing turbulence field is compressed first by the motion of the piston during the compression stroke and subsequently by expanding burned gases during combustion.

5.2.5 CYCLE-TO-CYCLE VARIATION

From an experimental study, [5.6] Fig. 5.5a plots the turbulence intensity versus engine speed and shows that repeated measurements at a given speed exhibit considerable variation; Fig. 5.5b depicts the turbulent flame velocity Ut versus speed and exhibits even larger variations between individual cycle at a given speed. The cycle-to-cycle variation derives from the turbulence phenomenon and non-repeatibility of the incoming flow during the intake process.

Recirculating flows of the above mentioned type are typically very sensitive to minor variations in the flow, and hence there probably are substantial cycle-to-cycle variations in the locations and sizes of the recirculation regions. It is known that high flow rates and strongly swirling-induced flow patterns lead to reduction of cyclic variability.

5.3 PREREQUISITES OF A COMPREHENSIVE AND PRECISE MODEL

5.3.1 ACCURATE BOUNDARY CONDITIONS

The inlet and exhaust boundary conditions play the dominant role in the generation of the mean flow and turbulence fields during the intake process. The observed sensitivity to the boundary conditions implies that accurate boundary conditions must be used for calculations. There is the danger that incorrect boundary conditions can by cancellation of errors result in apparently accurate flow calculations. The stipulation of boundary conditions involves dealing with the various and often complex shapes of practical chambers, associated induction and exhaust arrangements, pressure distribution and velocity profiles

5.3.2 DETAILED FLOW MODELLING

There is more than one mechanism for flow recirculation in the cylinder. In many cases, recirculation zone formation is an inviscid process only indirectly influenced by viscous and turbulent momentum transport. For instance, in terms of the inviscid flow theory, Benjamin successfully predicted the vortex breakdown phenomenon for swirling flow [5.7], and Meroney satisfactorily computed corner eddies for channel flow contractions [5.8]. Thus failure accurately to predict flow recirculation is most likely not the result of a poor turbulence model. On the other hand, waves and flow oscillation are frequently linked to flow recirculation, and it may prove necessary to incorporate explicitly their influence in models for such flows.

However, the influence of turbulence and turbulent transport on flow recirculation should not underestimated. Flow patterns in and around the recirculation zone are affected by turbulence. Furthermore, swirl affects turbulence levels and turbulent transport, and boundary layer separation complicates the flow configuration. The effect is greatly magnified in variable density flows where, depending on conditions, turbulence production can either be enhanced or suppressed by swirl.

5.3.3 PREDICTIBILITY OF CYCLIC VARIATION

Cycle-to-cycle variations are related to turbulence, and their inclusion in flow models has tended to be regarded as unique to engines where their effects are undoubtedly important.

Because the flows in the cylinder are not steady, conventional turbulence definitions based on time averaging are inappropriate. In periodic flows, an obvious alternative, namely phase averaging, cannot provide information about individual cycles, because cyclic variations of all origins are included as turbulence in this definition.

5.4 COMPUTATIONAL FLUID DYNAMICS METHODS (CFD METHODS)

5.4.1 STATISTICAL FLUX MODELS (SFM) AND LARGE-EDDY SIMULATION (LES)

The foundations of all existing computational fluid dynamics methods lie in the well-known differential equations expressing the conservation laws of

momentum (i.e. the Navier-Stokes equations), mass and energy. If they could be solved exactly, then all information required for the scavenging process would be accessible. However, this is not possible because the unresolvably small time and length scales of the turbulent flows lead to the need for some form of averaging and closure with inherent approximations and consequent inexactitude and loss of information. The averaging-closure process has been termed "turbulence modelling".

There are two main classes of models which seem suitable for engine applications, namely:

5.4.1.1 SFM (STATISTICAL FLUX MODELS) [5.9], [5.10]

The models employ the phase-averaging process to yield a new set of equations containing additional unknowns which have the significance of turbulent fluxes of the entity in question (e.g. the "Reynolds stress" in the case of the momentum equations). Closure of the equation set is then effected by deriving additional equations, of either algebraic or differential form, for the new unknowns, in which process certain approximations and assumptions necessarily enter, which render the results inexact. The success or failure of such methods, therefore, resides in the validity of the approximations which they embody.

5.4.1.2 LES (LARGE EDDY SIMULATION) [5.11]

The method uses spatial averaging in which the averaging is limited to the eddies below a certain scale which can be made of the same order of magnitude as the mesh size of computational grids for which numerical calculations are feasible. Motion larger than this are calculated in the normal way, i.e. as for laminar flow. The new unknowns arising from the averaging process (termed "subgrid-scale Reynolds stress" in the case of the momentum equations) are approximated by a SFM, but the small-scale turbulence is believed to possess certain regularities (e.g. isotropy) which should allow them to be modelled accurately in particularly simple laws.

5.4.2 COMPARISON BETWEEN SFM AND LES

In SFM, models are needed for various averages of turbulence quantities.

These models must reflect the contributions of all scales of turbulent motion. However, LES is an approach in which one actually calculates the large-scale three-dimensional time-dependent turbulence structure in a single cycle. Thus, only the small-scale turbulence need be modelled. The small-scale turbulence is much more isotropic than the large-scale turbulence, and is quite universal in character, and responds rapidly to changes in the large-scale field. This makes the modelling of the statistical fluxes associated with the small-scale motions a simple task compared to that faced in SFM, where the effects of large-scale turbulence must be included in the models.

An important difference between SFM and LES is in the definition of the "turbulence". In SFM, the "turbulence" is the deviation of the flow at any point at any instant from the average over many cycles of the flow. Thus, SFM "turbulence" contains some contribution from cycle-to-cycle variation, as shown in Fig. 5.6a.

On the other hand, the turbulence in LES is defined as the departure from a local average at a single instant in time. LES gives the precise definition of the large-scale velocity, pressure, density, temperature and concentration fields. These should represent a smoothing of the actual field, with the smoothing removing the small-scale fluctuation. Therefore, the large-scale field of a variable at a point, x, should be defined as some sort of a local average of the actual field at points near x. The deviation of the actual field from the local average field is then the small-scale "turbulence", that is, in LES the "turbulence" really is related to events in the current cycle, as shown in Fig. 5.6b. Hence, LES carried out over several cycles should reveal the magnitude of cycle-to-cycle variation, which cannot be found by SFM.

At present, the computer time requirements of LES calculations in engine-like system are such that they are beyond the capacities of most research groups. If one is limited by computer capacity to two-dimensional time-dependent calculations, then LES is not possible, and SFM is the only choice. However, if one has the computer capability to do a three-dimensional time-dependent calculation, then it might as well be LES as SFM, and LES is likely to give more accurate results. With projected computer development, it is possible that within a decade LES calculations

in engine-related system will become routine.

5.4.3 THE STATE OF THE ART OF LES

LES models have been subjected to limited evaluation for engine flow prediction, but only for two-dimensional calculation, which raises doubts about the validity of the comparison with experiments because the turbulence is always three-dimensional although the mean flow may be two-dimensional.

Even in the proper three-dimensional context, the following major problems still exist:

(1). the difficulty of posing realistic inflow boundary condition during induction.
(2). the necessity to accumulate statistics over many simulated engine cycles in order rigorously to compare with experiment.

Therefore, the LES approach is still in an early stage of development and is not yet ready for use in engine flow, but it may offer the best hope for soundly based, accurate flow calculations in practical engine systems.

5.4.4 THE STATE OF THE ART OF SFM

5.4.4.1 Critique of SFM

From evaluation studies, the SFM approach has been proven to be a positive one. [5.12] As errors from other sources such as uncertain boundary conditions and numerical approximations are systematically reduced, so the overall accuracy of prediction has improved to levels which may already be adequate for some purpose. The speed, flexibility and accuracy of the numerical methods have steadily improved to the stage where three-dimensional calculations for practical chambers are feasible, but costly and subject to limitation.

However, the following weaknesses of the methods still remain

(1). their inability to predict cycle-to-cycle variation.

(2). their discretization errors, which require the use of fine grids even with higher-order scheme.
(3). the problems of maintaining the required mesh connectivity properties during the scavenging process.
(4). the still large computing cost of three-dimensional calculations.
(5). the uncertain distributions of all the main dependent variables (i.e. the velocity, composition, pressure, temperature and turbulence parameters which depend on the upstream condition and cannot be deduced from knowledge of the chamber configuration alone).
(6). the lack of reliable boundary layer formulae for the circumstances of engine flows because in an engine the wall boundary layers do not have time to relax to local equilibrium, hence the indiscriminate application of an assumed "universal" wall layer formula, such as in pipe flow, is a potential source of error.
(7). the inadequacy of experimental data, so that the analyses of in-cylinder flow behaviour have been characteristically, but not uniquely, extrapolative in nature.

Hence, SFM has earned the status of being a useful tool for engine flow analysis including the scavenging process, but in view of the still rather limited amount of accuracy assessment, and the known limitations of the SFM, the results must be accepted with some caution. According to the turbulence model, SFM has further been classified into different versions.

5.4.4.2 Critique of turbulence models in SFM

Because of the appearance of the turbulent flux terms due to the averaging process, the mean-flow equations are not closed, and a turbulence model is neccessary to determine these turbulent transport terms before the equations can be solved.

5.4.4.2.1 Simple models

In the gradient diffusion approach, turbulent diffusion of any quantity is assumed proportional to the mean spatial gradient of that quantity. (cf. Appendix II) The coefficient of proportionality is an eddy "diffusivity". The first example of simple models is Prandtl's mixing-length hypothesis [5.13]. This hypothesis calculates the eddy diffusivity ϵ_t by the following equation.

$$\epsilon_t = l_m^2 \frac{\partial U}{\partial n} \qquad (5.1)$$

where $\frac{\partial U}{\partial n}$ is the local mean-velocity gradient.

l_m is a single unknown parameter, the mixing length, whose distribution over the flow field has to be prescribed empirically.

The mixing-length hypothesis is the simplest model.

The second example of simple models is another Prandtl model pertinent to free turbulence. [4.13] This theory assumes that the overall flow character with the mixing layer is determined by the dimensions of the layer and the greatest velocity difference across this layer, and that the eddy diffusivity is determined by,

$$\epsilon_t = c\, b(U_{max} - U_{min}) \qquad (5.2)$$

where c is a constant,

b is the width of the jet.

This model has been extended and used in version 2 of the phenomenological unsteady jet model suggested in Chapter 4.

The simple models have been used widely and with considerable success for calculations of simple shear layers, and a great amount of experience has been accumulated in the specification of the empirical constant in such flows. However, the simple models are not suitable whenever turbulence transport and history effects are important, because the gradient diffusion approach implies that generation and dissipation of turbulence energy are in balance everywhere, and the convection and diffusion of turbulence energy are ignored. [5.14] The simple models are of little use for flows more complex than shear layers because of the great difficulties in specifying the empirical constants in such flows.

5.4.4.2.2 One-equation models

One-equation models [5.15] employing a transport equation for the kinetic energy κ of turbulence account for transport and history effects. The

transport equation is a differential equation describing how the rate of κ is balanced by convective transport by the mean motion, diffusive transport by turbulent motion, production by interaction of turbulent stress and mean-velocity gradients, and destruction by dissipation. Therefore, these models are superior to the simple models for non-equilibrium shear layers where the length-scale distribution can be prescribed realistically. However, they are not very suitable for complex flows, such as in-cylinder flows, where an empirical length-scale determination is difficult.

The engine flow calculations performed to date have been based on two-equation models and stress-flux equation model.

5.4.4.2.3 Two equation models

Two-equation models employ an additional transport equation for the length scale. Among these, the $\kappa-\epsilon$ model [5.14] is the most popular one in which the turbulence kinetic energy κ and its dissipation rate ϵ are used to characterize turbulence. From eddy viscosity-diffusivity concept, the turbulent fluxes and stresses are represented by diffusion-like terms containing an isotropic eddy viscosity which is related to the two turbulence parameters. It has been shown to predict with a sufficient accuracy in-cylinder flows, including separating and complex three-dimensional flows.

However, the eddy viscosity concept itself, and more importantly, the use of the isotropic viscosity do not describe certain important flow phenomena in the cylinder because in the complex cylinder geometry, eddy viscosity and diffusivity will certainly depend on the stress or flux component considered. For the scavenging process with variable densities, turbulence is strongly influenced by buoyancy forces acting in a dominant direction.

5.4.4.2.4 Turbulent stress-flux equation models

Turbulent stress-flux equation models are more sophisticated models. In most general form, models of this type comprise seven simultaneous partial differential equations for the six stress components and the dissipation rate ϵ. These equations are derived in exact forms, but they contain higher-order correlations which have be approximated in order to obtain a closed system. A particular advantage of deriving the exact equations is

that terms accounting for buoyancy, rotation and other effects are introduced automatically. Among them, one relatively simple model is the Reynolds stress model (RSM) by Launder and his co-workers [5.16], which is the only other SFM that has seen application in engine calculations. In many instances, the computed results show a good quantitative agreement, but still remain some discrepancies between measurements and predictions. [5.17]

Compared with the $\kappa-\epsilon$ model, this type of model is rather complex and computationally expensive. However, it is undeniable that the RSM performs even better than the $\kappa-\epsilon$ model and, therefore, offers an alternative should the latter eventually prove to be inadequate.

5.5 PHENOMENOLOGICAL FLUID DYNAMIC MODELS

5.5.1 PHENOMENOLOGICAL STEADY AND UNSTEADY JET MODELS (SJM AND UJM)

In contrast to the computational fluid dynamics (CFD) models just discussed, the phenomenological scavenging models developed in Chapter 4 offer the advantages of greater simplicity and much shorter computation time, at the expenses of loss of detail.

The basis of UJM, as mentioned in Chapter 4, is still provided by the conservation equations of momentum, mass and energy, taken with assumptions, such as uniform cylinder pressure and assumed profiles of velocity and composition. Furthermore, it is assumed in the case of the SJM described in Chapter 4 that the process is isobaric and isochoric during the scavenge period, and that heat transfer is absent.

The real difficulty in the calculation of the velocity field in CFD models lies in the unkown pressure field. The pressure gradient forms a part of the source term for a momentum equation. There is no obvious equation for obtaining pressure. The assumption of uniform pressure greatly simplifies the computational work, but clearly does not reflect the real physical situation.

5.5.2 CRITIQUE OF UJM

The neglect of the pressure term in the equations of momentum conservation makes the model unable to predict the conversion from kinetic to pressure potential energy. In loop scavenged engines this conversion of mechanical energies dominates throughout the scavenging process, whereas in uniflow scavenged engines the conversion is unimportant except within the regions near the inlet and exhaust ports.

With the proper entrainment equation, the unsteady jet model can approximately depict the flow pattern and satisfactorily predict scavenging efficiency for uniflow scavenged engines.

5.5.3 CRITIQUE OF SJM

The model not only omits the pressure term in the equations of momentum conservation, i.e. the conversion of mechanical energies, but also replaces a time-dependent flow by a steady imcompressible flow with variable compositions.

These simplifications mean that the SJM is only able to provide a roughly approximate flow history of uniflow scavenged engines. Nevertheless, the model avoids the need for an artificial history during the scavenging process, as is the case with thermodynamic models.

5.6 THERMODYNAMIC MODELS

5.6.1 STEP-BY-STEP THERMODYNAMIC MODELS (STM) AND ISOBARIC AND ISOCHORIC THERMODYNAMIC MODELS (ITM)

Thermodynamic models take account of energy and mass conservations and neglect momentum conservations, i.e. omit any of the fluid dynamic behaviour. However, the neglect of momentum conservations produces the uncertainty of the flow and concentration fields. The models needs an artificial history of the flow and concentration fields. Based on this presupposition, the models can quickly and easily give a description of the thermodynamic properties.

One of the crucial tasks of the study of the scavenging process is to predict the history of the flow and concentration fields, i.e. the scavenging

effectiveness. The inability to predict this is an inherent drawback of thermodynamic models. On the other hand, arbitrary specifications of exhaust history make the models able to cover a wide spectrum of scavenging processes from short-circuiting to perfect displacement scavenging and to provide a thermodynamic description of any scavenging process.

Under the assumption of the cylinder being divided into several homogeneous zones, the STM can give a step-by-step desription of the scavenging process.

Under the further assumption of isobaric and isochoric processes, the ITM can provide a simple and direct relationship between mass flow rate and scavenging effectiveness.

5.6.2 CRITIQUE OF STM

The STM can provide an accurate and informative step-by-step description of the scavenging process, and hence estimate the influence of port timing, which is important for investigating the scavenging process and matching supercharging systems in STM. It is assumed that the cylinder is divided into two or three zones, viz. air, gas and mixing zones, composition and temperature in each zone being assumed homogeneous. Combined with a specification of an exhaust history, a model can give a thermodynamic description for a particular scavenging system. As already mentioned, Streit and Borman's model and Heeschen's model are applicable to uniflow scavenging systems, whereas Benson's model is limited to loop scavenging systems only.

The model suggested in Chapter 3 posesses the flexibility of specifying appropriate intake and exhaust proportions in different phases, and can thus provide a description for any type of scavenging system.

5.6.3 CRITIQUE OF ITM

The assumption of an isobaric and isochoric process approximates to the physical situation during the scavenging process and bestows simplicity on the models. In the ITM, it is assumed that the cylinder is either

represented as a mixing zone, or alternatively divided into two or three zones. With an exhaust history, the ITM gives a relationship between mass flow rate and scavenging effectiveness for the particular process. As above mentioned, given an exhaust history any such model can give simple algebraic relations for scavenging effeciency.

The ITM proposed in Chapter 2 displays this generality. With a set of variable intake and exhaust proportions the model can express any scavenging process. Furthermore, with a set of fixed intake and exhaust proportions respectively in different phases, the model gives a set of algebraic equations which apply with different numerical values to any of cases described.

5.7 SUMMARY

Briefly, the more comprehensive a model, the greater its complexity. Since the scavenging process in the engine is very complex, simplifications must be made for its modelling under the limitation of computation cost. Accuracy must be weighed against complexity and cost. Different applications need different level of predictive programs.

Characteristics, advantages and disadvantages of the different models are outlined in Table 5.1:

REFERENCE

[5.1] F.C. Gouldin, J.S. Depsky and S-L. Lee
"Velocity Field Characteristics of a Swirling Flow Combustion"
AIAA Journal Vol. 23, No. 1, pp 95-102, 1985

[5.2] M.P. Escudier and J.J Keller
"Recirculation in Swirling Flow: a Manifestation of Vortex Breakdown"
AIAA Journal Vol. 23, No. 1, pp 111-116, 1985

[5.3] S. Kito
"Axi-asymmetric Character of Turbulent Swirling Flow in a Straight Circular Pipe"
Bulletin of JSME Vol. 27, No. 226, 1984

[5.4] R.J. Tabaczynski, D.P. Hoult and J.C. Keck
"High Reynolds Number Flow in a Moving Center"
J. Fluid Mech. Vol. 42, pp 249-256, 1970

[5.5] A.P. Morse, J.H. Whitelaw and M. Yinneskis
"Turbulent Flow Measurements by Laser-Doppler Anemometry in Motered Piston-Cylinder Assemblies"
Transaction of the ASME Vol. 101, pp208-216, 1979

[5.6] R.G. Abdel-Gayed, K.J. Al-Khishali and D. Bradley
"Turbulent Burning Velocities and Flame Straining in Explosions"
Pro. R. Soc. Vol. A391, pp393-414, 1984

[5.7] T.B. Benjamin
"Theory of the Vortex Breakdown Phenomenon"
J. Fluid Mech. Vol. 14, pp 593-629, 1962

[5.8] R.N. Meroney
"Inviscid Shear Flow Analysis of Corner Eddies Ahead of a Channel Flow Contraction"
Transaction of the ASME Vol. 107, pp212-217, June, 1985

[5.9] R.S. Rogallo and P. Moin

"Numerical Simulation of Turbulent Flows"
Ann. Rev. Fluid Mech. Vol. 16, pp99-137, 1984

[5.10] A. D. Gosman, R. J. R. Johns and A. P. Watkins
"Development of Prediction Methods for In-Cylinder Process in Reciprocating Engines"
<Combustion Modeling in Reciprocating Engines>
Plenum Press

[5.11] P. O. E. Witze
"Comparison between Measurement and Analysis of Fluid Motion in Internal Combustion Engines"
Sandia National Laboratory Report SAND 81-8242, 1981

[5.12] A. D. Gosman
"Multimensional Modeling of Cold Flows and Turbulence in Reciprocating Engines"
SAE 850344, 1985

[5.13] L. Prandtl
"Uber die ausgebildete Turbulenz"
ZAMM, 5, p. 136, 1925

[5.14] W. Rodi and D. B. Spalding
"A Two-Parameter Model of Turbulence, and its Application to Free Jets"
Warme- und Stoffubertragung, 3, pp. 85-85, 1970

[5.15] W. Rodi
"Examples of turbulence Models for Incompressible Flows"
AIAA, vol. 20, No. 7, 1981

[5.16] B. E. Launder, G. J. Reece and W. Rodi
"Progress in the Development of a Reynolds Stress Turbulence Closure"
J. Fluid Mech. Vol. 16, pp99-137, 1984

[5.17] S. E. Tahry

"Application of a Reynolds Stress Model to Engine Flow Calculation"
<Flows in Internal Combustion Engines- II>
ASME. New York. pp39-46. 1984

Table 5.1 Summary of Various Models

method	ITM	STM	SJM
conservation law	mass and energy		mass, momentum and energy
thermodynamic characteristics	constant pressure and volume	variable pressure and volume	constant pressure and volume
turbulence model	none. artificial inlet and exhaust proportions instead		jet spread rate
predicti-bility	poor, depending on the specification of exhaust history		medium with a steady jet flow pattern
economy	excellent	very good	
application	all systems		uniflow only

method	UJM	SFM	LES
conservation law	mass, momentum and energy		
thermodynamic characteristics	variable pressure and volume	variable pressure gradient and geometry	
turbulence model	entrainment law, eddy diffusivity	2-equation models stress/flux model	large eddy simulation
predicti-bility	good with a unsteady flow pattern	very good with 3-D flow pattern exc.cyclic effect	excellent with 3-D flow pattern inc.cyclic effect
economy	good	medium	poor
application	uniflow only	all systems	

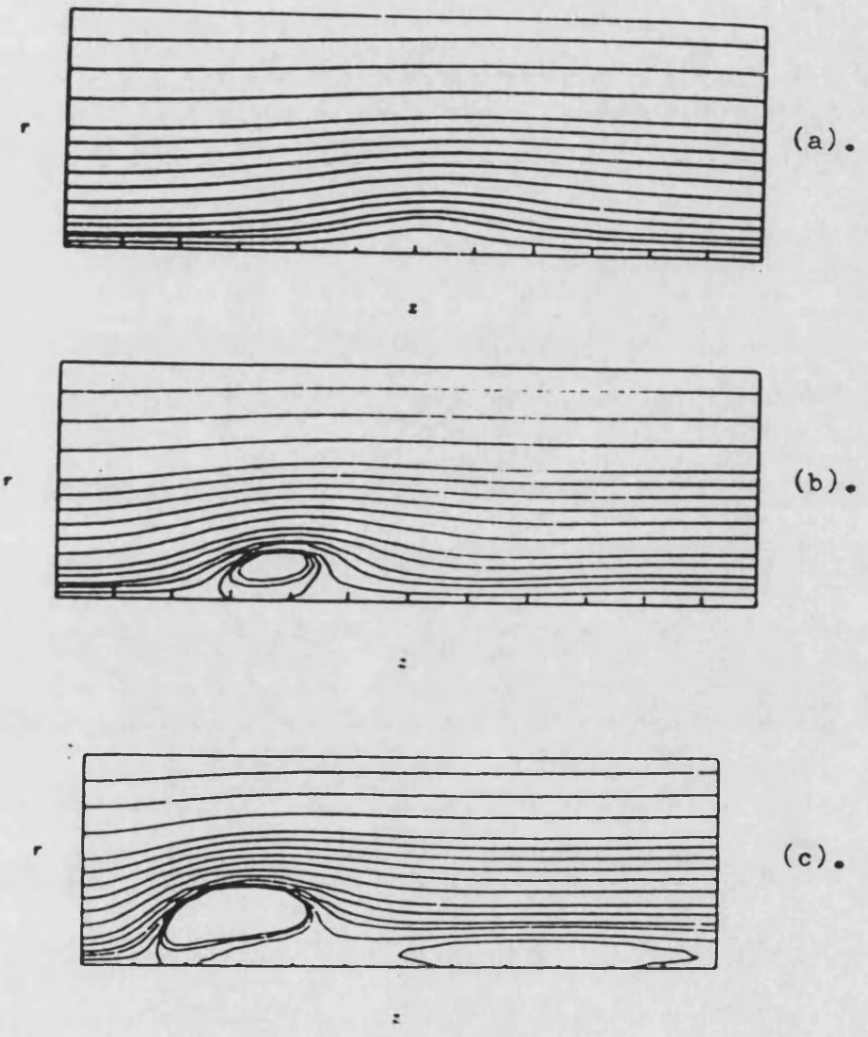

(a). flow without reversal,
(b). flow with a central recirculation,
(c). flow with a long backflow region.

Fig. 5.1 Swirling Flows

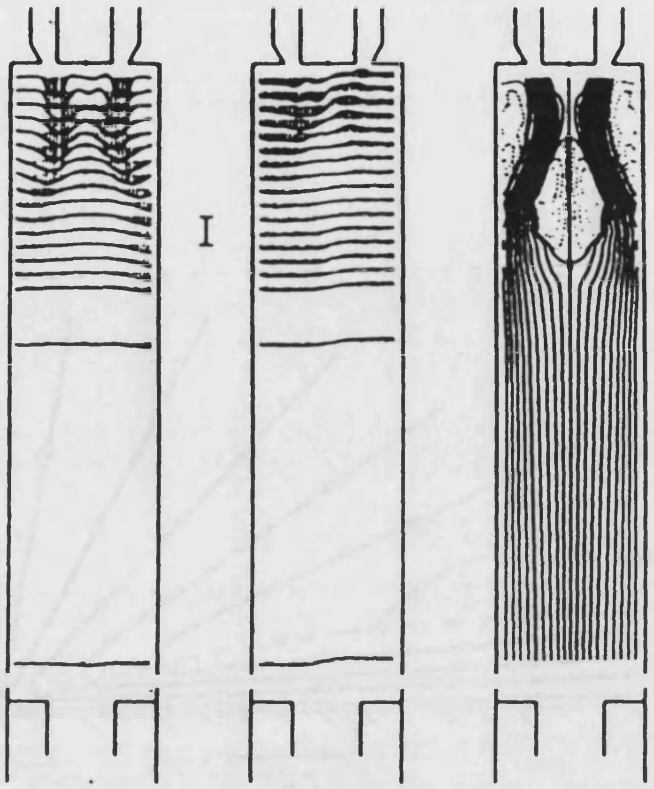

LDA measurements for a flow which recovers to supercritical after breakdown with 79% exit-area contraction ($D_E/D = 0.455$).

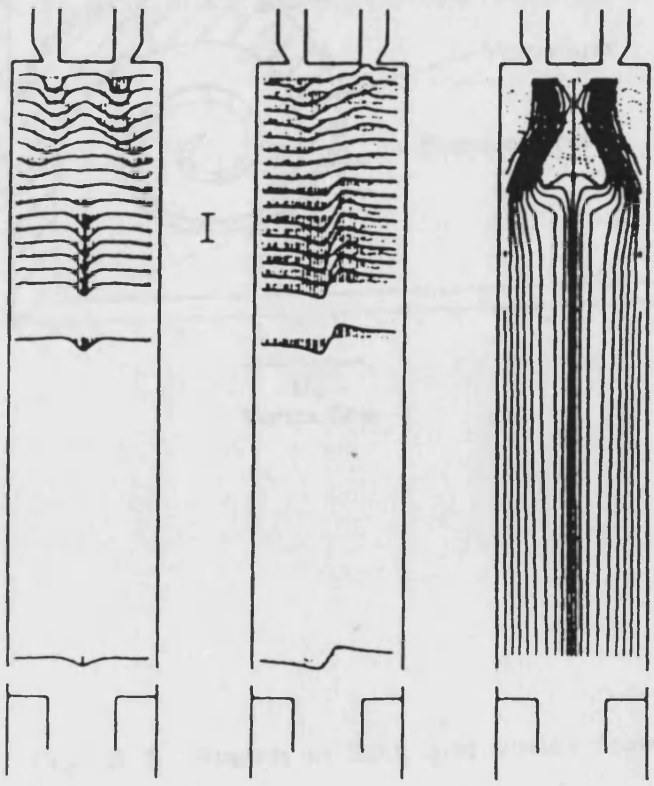

LDA measurements for a flow which remains subcritical after breakdown with 79% exit-area contraction ($D_E/D = 0.455$).

Fig. 5.2 Supercritical and Subcritical Flow

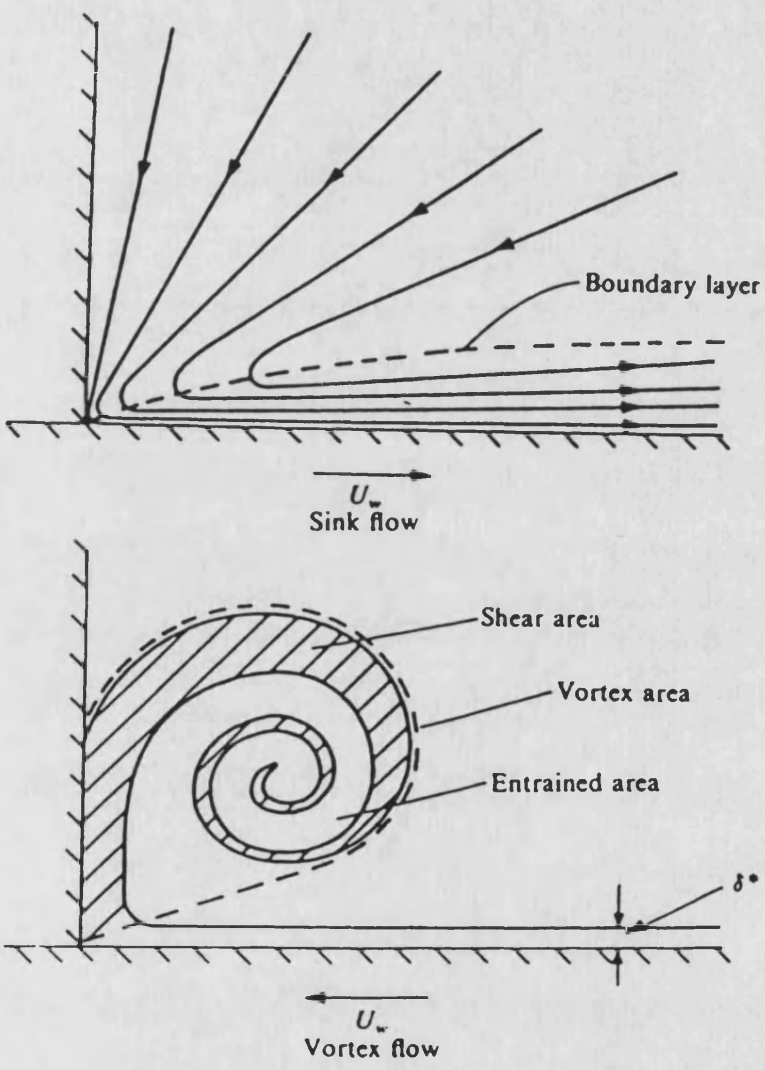

Fig. 5.3 Sketch of Sink and Vortex Flow

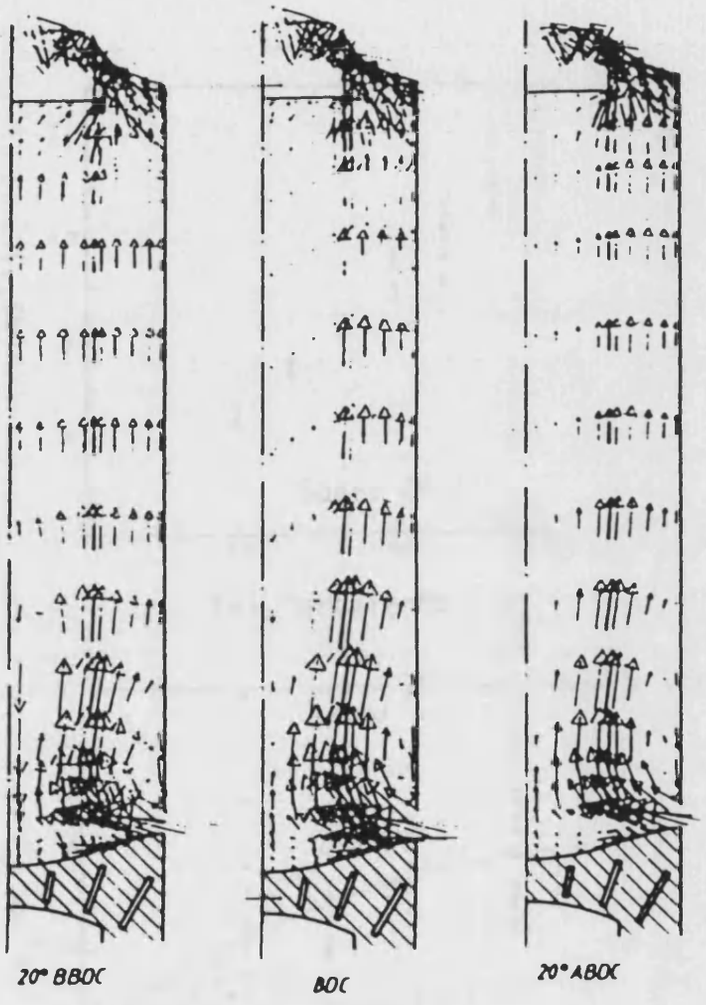

Fig. 5.4 Recirculation in the Cylinder

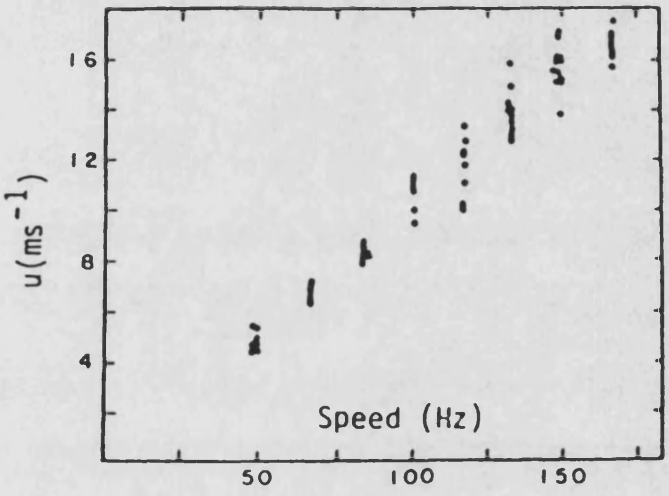

(a) Turbulence

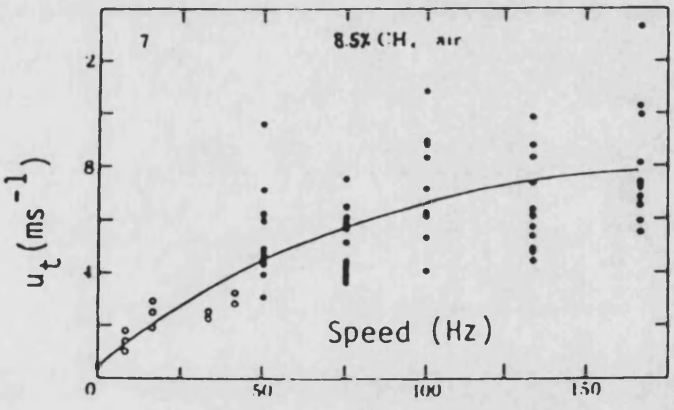

(b) Flame Velocity

Fig. 5.5 Measurements of Turbulence Intensity and Turbulent Flame Velocity

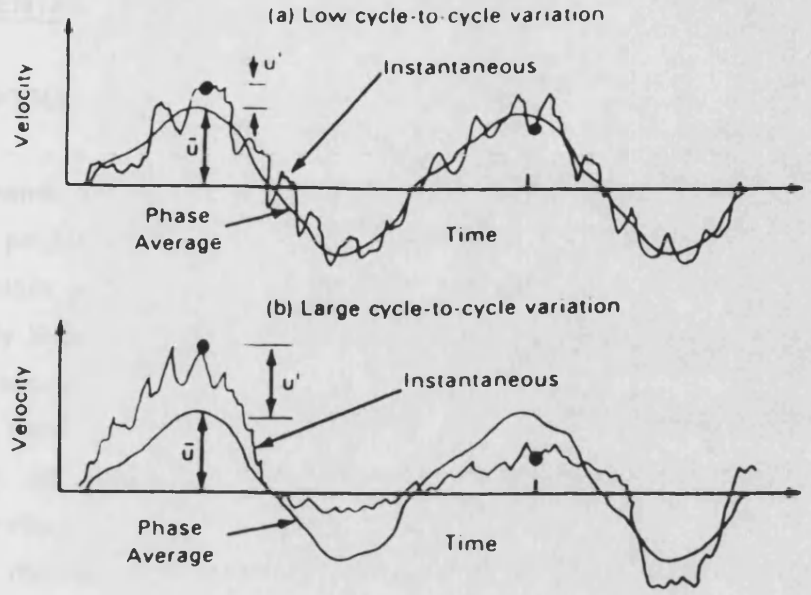

(a). SFM (phase averaging)

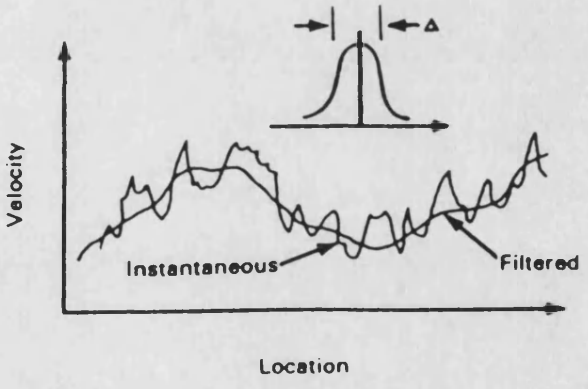

(b). LES (spatial averaging)

Fig. 5.6 Turbulence Definitions

Chapter 6 SCALE MODELLING OF THE SCAVENGING PROCESS AND EXPERIMENTAL RESULTS FROM HYDRAULIC ANALOGUE

6.1 INTRODUCTION

Improvements in scavenging effectiveness require an understanding of the physical processes taking place during the scavenging process. Both mathematical and hardware models are beneficial for the understanding. A completely theoretical approach of the flow processes during the scavenging process based on the differential equations of Navier-Stokes is unrealistic because solving these equations is beyond the present computational capability, as explained in Chapter 5. Any mathematical model, from simple to comprehensive, must be validated by reality, i.e. experiments on hardware model, prototype or scale model. Experimental investigations on real engines have provided information of overall, i.e. macroscopic, scavenging effectiveness [6.1], [2.6], [4.9], [4.16]. However, detailed or microscopic experimental studies of the scavenging process in engines involving flow and composition measurements are both tedious and difficult. In view of this, scale model testing possesses great advantages due to its simplicity and economy.

Some scavenging investigations have been conducted on the scale models reportedly for loop scavenging [6.2], [6.3]. However, these experiments did not aim at uniflow scavenging process and did not include any investigation of entrainment law. The object of the author is to build up a simple two-dimensional scale model for uniflow scavenging to validate the phenomenological unsteady jet model suggested in Chapter 4.

6.2 SCALE MODEL

6.2.1 GENERAL CONCEPT

A scale model can serve as a valid substitute for the prototype model, when all functional relations of the scale model are made similar to the corresponding relations of the prototype. The scaled transformation of all important prototype relations into the similar model relations involves the application of seven (or less, if less suffice) primary scale factors of basic

physical quantities: those of length, time, mass, temperature, electric current, luminous intensity and amount of substance, in which, usually, only the former four quatities are used in fluid dynamics. By scaling length, time, force (instead of mass) and temperature, all quantities (variables and constants) of the model can be scaled. Primary scale factors and their interrelations can be derived from the following fundamental requirement of the scale model:

model and prototype must be governed by the same physical laws.

Each of the governing laws can be converted into one relationship, i.e. model law, between various characteristic numbers which are dimensionless secondary scale factors taken with the form of power function of the previous primary scale factors. With order-of-magnitude analysis, neglect of "weak" characteristic numbers, the set of model laws can further be simplified.

6.2.2 MODEL LAWS IN THE SCAVENGING PROCESS

The integral forms of the conservation equations are used for deriving model laws, because the identification of the possible fluxes is most revealingly done. The physical meaning of the conservation equations is,

change of quantity accumulated in the control volume	=	increase of quantity by convection through the control surface	+	increase of quantity by diffusion through the control surface	+	production of quantity by source in the control volume	
		destruction of quantity by dissipation in the control volume	-				

(6.1)

There exist three physical quantities to be transported: material, momentum and energy. They must be considered independently because these quantities are different.

The phenomenon concerned is a transient behaviour of the confined jet entrainment and mixing during the scavenging process. The outer surface

of the jetting region is defined as a control surface S. The volume V bounded by S is called a control volume. The part of the cylinder space outside V is the residual gas region, as shown in Fig. 6.1.

6.2.2.1 Material fluxes

The equation of air species conservation is

$$\frac{d}{dt}\int_V \rho_j C_{ja}\, dV + \int_S \rho_r C_{ra}(U-v)\, dS + \int_S j_n\, dS = 0 \qquad (6.2)$$

$$\frac{\rho_j S b C_{ja}}{t} \qquad \rho_r S U C_{ra} \qquad \frac{D \rho_r S C_{ja}}{b}$$

$$\frac{\rho_j C_{ja} b}{\rho_r C_{ra} U t} \qquad 1 \qquad \frac{C_{ja} D}{C_{ra} U b}$$

$$\frac{\rho_j C_{ja}}{\rho_r C_{ra}} Sr \qquad 1 \qquad \frac{1}{Sc\ Re} \frac{C_{ja}}{C_{ra}}$$

$$O(1) \qquad O(1) \qquad O(10^{-5})$$

This most general form allows for a moving system boundary: each surface element dS moves with velocity component v normal to its plane.

Equation (6.2) is the sum of three fluxes. The importance of each of these are dependent on its ratio to the others. This relationship can be assessed by means of approximation.

The first term, the rate-of-accumulation term, is

$$\frac{d}{dt}\int_V \rho_j C_{ja}\, dV = \frac{\rho_j V C_{ja}}{t} = \frac{\rho_j S b C_{ja}}{t} \qquad (6.3)$$

where ρ_j is the density within the jetting region.

C_{ja} is the air concentration in terms of the mass fraction in the jetting region.

t is the process time, a typical time constant for the process.

b is the width of the jetting region.

The second term, the convection term, is

$$\int_S \rho_r C_{ra} (U-v)\, dS = \rho_r SUC_{ra} \qquad (6.4)$$

where the upstream is the residual gas region due to entrainment.

ρ_r is the density within the residual gas region.

C_{ra} is the air concentration in terms of the mass fraction in the residual gas region.

and the convective velocity is assumed approximately equal to the jet velocity U, because they should have the same order of magnitude.

From Fick's law, the third term, the diffusion term, is

$$\int_S j_n\, dS = \frac{D\rho_r SC_{ja}}{b} \qquad (6.5)$$

where j_n is the mass diffusion flux.

D is the mass diffusivity.

After substitution of equations (6.3) to (6.5) into equation (6.2), equation (6.2) becomes the form of the second line in expression (6.2). Being divided by $\rho_r SUC_{ra}$, the expression changes into the form of the third line in expression (6.2). Finally, from the definitions of the characteristic numbers, the equation becomes the form of the fourth line. Here, the characteristic numbers are:

Reynolds number, $Re=\frac{Ub}{\nu}$, the ratio of inertia to viscosity force.

Schmidt number, $Sc=\frac{\nu}{D}$, the ratio of molecular viscosity to mass diffusivity.

Strouhal number, $Sr=\frac{b}{Ut}$, the ratio of local to convective velocity, or the

ratio of piston to convective velocity, because the jet width has the same order of magnitude as the opening port height, or as the piston displacement during the scavenging process.

6.2.2.2 Momentum fluxes

The equation of the momentum conservation is

$$\frac{d}{dt}\int_V \rho_j U dV + \int_S \rho_r (U-v) U dS - \int_V g(\rho_j-\rho_r) dV + \int_S \delta_n P dS - \int_S \tau_n dS = 0 \qquad (6.6)$$

$$\frac{\rho_j SbU}{t} \qquad \rho_r SU^2 \qquad gSb(\rho_j-\rho_r) \qquad S\Delta P \qquad \frac{\mu SU}{b}$$

$$\frac{\rho_j}{\rho_r}\frac{b}{Ut} \qquad 1 \qquad \frac{gb}{U^2}\left(\frac{\rho_j}{\rho_r}-1\right) \qquad \frac{\Delta P}{\rho_r U^2} \qquad \frac{\mu}{\rho_r Ub}$$

$$\frac{\rho_j}{\rho_r}Sr \qquad 1 \qquad \frac{\rho_j}{\rho_r}Fr \qquad \frac{\rho_j}{\rho_r}Eu \qquad \frac{\rho_j}{\rho_r}\frac{1}{Re}$$

$$O(1) \qquad O(1) \qquad O(10^{-5}) \qquad O(1) \qquad O(10^{-5})$$

Equation (6.6) is the sum of five fluxes. The first term, the body inertia force term, is

$$\frac{d}{dt}\int_V \rho_j U dV = \frac{\rho_j VU}{t} = \frac{\rho_j SbU}{t} \qquad (6.7)$$

The second term, the convection term, is

$$\int_S \rho_r (U-v) U dS = \rho_r SU^2 \qquad (6.8)$$

where the upstream is the residual gas region.

The third term, the buoyancy term, is

$$\int_V g(\rho_j-\rho_r)dV = gSb(\rho_j-\rho_r) \qquad (6.9)$$

The fourth term, the dynamic pressure-area force term, is

$$-\int_S \delta_n P dS = S\Delta P \qquad (6.10)$$

where δ_n is the outward normal unit vector.

From Stoke's hypothesis for a Newtonian fluid, the fifth term, the momentum diffusion term, is

$$\int_S \tau_n dS = \frac{\mu SU}{b} \qquad (6.11)$$

where μ is the dynamic viscosity.

Similarly, being substituted by equations (6.7) to (6.11) and divided by $\rho_r SU^2$, expression (6.6) assumes dimensionless form, as shown in its fourth line. There, the new characteristic numbers are

Euler number, $Eu=\frac{\Delta P}{\rho_j U^2}$, the ratio of pressure to inertia force.

Froude number, $Fr=\frac{gb}{U^2}|(1-\frac{\rho_r}{\rho_j})$, the ratio of inertia to gravity force.

6.2.2.3 Energy fluxes

The equation of energy conservation is

$$\frac{d}{dt}\int_V \rho_j u dV + \int_S \rho_r h(U-v)dS + \int_S q_n dS - \int_V \rho_j e_v dV - V\frac{dP}{dt} = 0 \qquad (6.12)$$

$$\frac{\rho_j C_v \Delta TSb}{t} \qquad \rho_r C_p \Delta TUS \qquad \frac{\kappa \Delta TS}{b} \qquad \frac{\mu SU^2}{b} \qquad \frac{Sb\Delta P}{t}$$

$$\frac{1}{\gamma}\frac{\rho_j}{\rho_r}\frac{b}{Ut} \qquad 1 \qquad \frac{\alpha}{Ub} \qquad \frac{\rho_j}{\rho_r}\frac{\mu U}{\rho_r b C_p \Delta T} \qquad \frac{\rho_j}{\rho_r}\frac{b\Delta P}{\rho_j U t C_p \Delta T}$$

$$\frac{1}{\gamma}\frac{\rho_j}{\rho_r} \qquad 1 \qquad \frac{1}{PrRe} \qquad \frac{\rho_j}{\rho_r}\frac{Eu}{Re} \qquad \frac{\rho_j}{\rho_r}\,SrEuEc$$

$$O(1) \qquad O(1) \qquad O(10^{-5}) \qquad O(10^{-5}) \qquad O(1)$$

Equation (6.12) is the sum of five fluxes. The first term, the body internal energy term, is

$$\frac{d}{dt}\int_V \rho_j u dV = \frac{\rho_j C_v \Delta T V}{t} = \frac{\rho_j C_v \Delta T S b}{t} \qquad (6.13)$$

where C_v is the specific heat at constant volume.

The second term, the convection term, is

$$\int_S \rho_r h(U-v)\,dS = \rho_r C_p \Delta T U S \qquad (6.14)$$

where the upstream is the residual gas region.

C_p is the specific heat at constant pressure.

From Fourier's law, the third term, the thermal diffusion term, is

$$\int_S q_n dS = \frac{\kappa \Delta T S}{b} \qquad (6.15)$$

where q_n is the thermal enthalpy diffusion flux.

κ is the thermal conductivity.

Also from Stoke's hypothesis for a Newtonian fluid, the fourth term, the friction heating term, is

$$-\int_V \rho_f e_v dV = \frac{\mu SU2}{b} \qquad (6.16)$$

where e_v is the rate of generation of thermal energy by viscous dissipation of mechanical energy.

The fifth term is the compression heating term.

Similarly, the dimensionless form with characteristic numbers can be derived as in the fourth line of expression (6.12). During the transformation of expression (8.11) from the second to the third line, in the third term the following relation is used.

$$\alpha = \frac{\kappa}{\rho_r C_p} \qquad (6.17)$$

where α is the thermal diffusivity.

The two more new characteristic numbers are

Eckert number, $Ec = \frac{U^2}{C_p \Delta T}$, the ratio of kinetic energy convection to thermal enthalpy convection

Prandtl number, $Pr = \frac{\nu}{\alpha}$, the ratio of molecular viscosity to thermal diffusivity.

6.2.2.4 Similarity in the scavenging process

Incorporated with geometric similarity and the equation of state, the above mentioned conservation equations constitute a complete set of the physical laws governing the scavenging process, as follows.

the geometrical similarity

the equation of state

from equation (6.2)

$$f_m\left(Sr, \frac{C_{fa}}{C_{ra}}, \frac{\rho_f}{\rho_r}, Re, Sc\right) = 0 \qquad (6.18)$$

from equation (6.6)

$$f_{mv}\left(Sr, \frac{\rho_l}{\rho_r}, Eu, Re, Fr\right) = 0 \qquad (6.19)$$

from equation (6.12)

$$f_{e}\left(Sr, \frac{\rho_l}{\rho_r}, Eu, Ec, Pr\right) = 0 \qquad (6.20)$$

where subscripts m, mv and e denote the conservation laws of mass, momentum and energy respectively.

This means that the perfect similarity is a set of relationships between characteristic numbers Sr, $\rho l/\rho r$, Eu, Ec, Re, Fr and Pr.

The order-of-magnitude analysis can be used to omit weak terms and obtain a simple similarity. From the typical data in the scavenging process, the orders of magnitude of characteristic numbers are estimated, as follows.

$Sr = O(1)$

$$\frac{\rho_l}{\rho_r} = O(1)$$

$Eu = O(1)$

$Ec = O(1)$

$Re = O(10^{5})$

$Sc = O(1)$

$Fr = O(10^{-5})$

$Pr = O(1)$

By the estimation of order of magnitude of the characteristic numbers, the following reliable similarity can be derived from the dimensionless forms of the conservation equations (6.2), (6.6) and (6.12).

the geometrical similarity.

the equation of state.

$$f_m\left(Sr, \frac{C_{ja}}{C_{ra.}} \frac{\rho_j}{\rho_{r.}}\right) = 0 \qquad (6.21)$$

$$f_{mv}\left(Sr, \frac{\rho_j}{\rho_{r.}} Eu\right) = 0 \qquad (6.22)$$

$$f_e\left(Sr, \frac{\rho_j}{\rho_{r.}} EuEc\right) = 0 \qquad (6.23)$$

After the combination of the equation of state and the conservation equations (6.21), (6.22) and (6.23), the reliable similarity becomes as follows.

$$f\left(Sr, \frac{C_{ja}}{C_{ra.}} \frac{\rho_j}{\rho_{r.}} Eu, Ec\right) = 0 \qquad (6.24)$$

Here, the air concentration ratio Cja/Cra may be explained as a dimensionless parameter for the scavenging effectiveness:

Strouhal number Sr can be considered as a ratio of piston speed to jet speed:

Euler number Eu is a ratio of pressure drop to kinetic energy:

Eckert number Ec is a ratio of kinetic energy to heat transfer.

When Ec is assumed as much smaller than 1, the following isothermal similarity can be obtained

the geometrical similarity

$$f\left(Sr, \frac{C_{ja}}{C_{ra.}} \frac{\rho_j}{\rho_{r.}} Eu\right) = 0 \qquad (6.25)$$

Since heat transfer effects have been eliminated by omitting the Eckert number, so that the model cannot predict heat transfer effects.

Furthermore, isodensity is assumed in scale models, the simple similarity is

the geometrical similarity

$$f(Sr.\frac{C_{ja}}{C_{ra}}\ Eu) = 0 \qquad (6.26)$$

This equation expresses the model law the water model with a moving piston must obey. Under the condition of similar geometrical configuration, the scavenging effectiveness, denoted by Cja/Cra, is dependent on the Euler and Strouhal numbers, i.e. scavenging pressure and piston speed.

6.3 WATER SCALE MODEL

6.3.1 BACKGROUND

The water model technique is a very useful tool, simple and economic for studying jet entrainment and mixing phenomena, which has been used to investigate the fuel jet mixing in the diesel engine [6.4]. The use of water as a medium in model testing offers certain advantages such as slowing down the whole process many times, and hence providing feasibility of much simpler experimental techniques, for example, slow speed photography.

The object of this experiment is to validate the phenomenological unsteady jet model, suggested in Chapter 4, and estimate its precision in the case of planar imcompressible jet flow including jet impingement.

6.3.2 DESIGN OF WATER RIG

As a simplest scheme, the author has chosen a two-dimensional cylinder-like layout without a movable piston for modelling the uniflow scavenging process without swirl. Under this idea, the similarity of the scale model becomes the following simplest form

the geometrical similarity,

$$f(Sr.\frac{C_{ja}}{C_{ra}}) = 0 \qquad (6.27)$$

It is obvious that this model fails to identify the following effects:

(1). the effect of temperature and density variation on the scavenging effectiveness.
(2). the effect of piston movement on the scavenging effectiveness.
(3). the effect of intake swirl on the scavenging effectiveness.

The engine to be modelled is a medium speed opposed-piston two-stroke engine design developed by British Shipbuilders Co. which has a bore and stroke of 420 and 1000 mm respectively, a potential output of 1660 hp per cylinder at 360 rpm.

From the similarity, Strouhal number must be maintained constant.

$$(Sr)_m = (Sr)_e \qquad (6.28)$$

that is,

$$\frac{L_m}{U_m T_m} = \frac{L_e}{U_e T_e} \qquad (6.29)$$

or

$$\frac{R_l}{R_u R_t} = 1 \qquad (6.30)$$

where R_l, R_u and R_t are the scaling factors for length, velocity and time respectively.

For simplicity, the author has rebuilt the original water rig and used the existing injection pump, whose displacement volume is 0.5 litre. To obtain the geometrical similarity, the thickness δ is 0.25 times the width W and the length L is 2.38 times the width. Under the condition of the maximum delivery ratio 1.2, from

$$V_{pump} = \lambda \cdot V_m \qquad (6.31)$$

the model geometry can be determined

W = 89 mm

δ = 22 mm

L = 211 mm

The scaling factor of geometry is

$$R_l = \frac{L_m}{L_e} = \frac{89}{420} = 0.210$$

It is assumed that the scavenging process takes 100 degrees of crankshaft angle, the jet velocity is equal to 65 m/sec.. From these typical data of the engine, the following order-of-magnitude estimation can be achieved

$$Sr = \frac{L_e}{V_e t_e} = \frac{0.420}{65 \cdot 0.0463} = 0.1396$$

$$R_v = \frac{V_m}{V_e} = \frac{V_m}{65}$$

$$R_t = \frac{t_m}{t_e} = \frac{t_m}{0.0463}$$

hence

$$t_m = \frac{t_e R_l}{R_v} = \frac{0.6320}{V_m}$$

In this water rig, the jet velocity is equal to about 1 m/sec.. This means that the cine-camera with 64 frame/sec. can take about 41 frames which gives a rather good resolution.

6.3.3 LAYOUT OF WATER RIG

The schematic layout of the water rig is shown in Fig. 6.2. The water rig consists of the following components:

(1). a square tank sized by 22·89·211 mm. i.e. 0.41 litre, made of perpex with 2 inlet and 2 exhaust ports at two ends respectively, to represent the engine cylinder.

(2). an injection pump with capacity of 0.5 litre, made of stainless steel with a sealed piston and a filling plug.
(3). two plastic hoses which connect the injection pump with the square tank via two spring-loaded diaphragm check valves which prevent backflow from the tank to the pump, as shown in Figs. 6.3 and 6.4.
(4). a container which keeps the discharged water from the tank.
(5). a PH meter to measure the PH values of solutions, hence to determine scavenging effectiveness.
(6). a compressed air supply with a reservoir in which the air supply pressure is adjusted by a valve.
(7). a stablized power supply and a control console.

6.3.4 OPERATION

(1). prepare alkali solution with concentration of PH value about 10.
(2). drain all solution in the tank, container and hoses.
(3). set the injection pressure and amount to the required level.
(4). stir the alkali solution in a beaker to uniform.
(5). fill the alkali solution via the exhaust port into the tank with a proper height in the exhaust port tube.
(6). fill pure water via the filling plug into the hoses and the pump.
(7). switch on the current and actuate the pump.
(8). pour the solution within the container into a graduated glass.
(9). pour the solution within the tank into another graduated glass.
(10). use the PH meter and measure the PH values of the solution in the two graduated glasses and the beaker respectively.
(11). repeat the operation from procedure (3) to (10) until the experiment ends.

It is notable that the simultaneous measuring the PH values of the solutions in procedure (10) is to avoid the error effected by zero-shift of the PH meter.

6.3.5 CALCULATION

In essence, the previous testing process is a diluting process of alkali solution. From the definitions, the PH and POH values are,

$$PH = -\mathrm{Log}C_{H^+} \tag{6.32}$$

$$POH = -\mathrm{Log}C_{OH^-} \; . \tag{6.33}$$

where C_{H^+} is the H concentration.
C_{OH^-} is the OH concentration.

The PH and POH values of an aqueous solution are related by the ion product for water, which is approximately constant.

$$C_{H^+} \times C_{OH^-} = 10^{-14} \tag{6.34}$$

After the use of logarithms and rearrangement, the following relationship can be achieved.

$$PH = 14 - POH = 14 + \mathrm{Log}C_{OH^-} \tag{6.35}$$

The conservations of OH species are,

for the mass trapped in the tank,

$$m_{in} C_{in} = m_{j,in} C_j + m_{r,in} C_r \tag{6.36}$$

where m_{in} is the mass retained in the tank.
$m_{j,in}$ is the injected mass retained in the tank.
$m_{r,in}$ is the residual mass retained in the tank.
and C_{in}, C_j and C_r are the corresponding OH concentrations.

for the mass discharged from the tank,

$$m_{out} C_{out} = m_{j,out} C_j + m_{r,out} C_r \tag{6.37}$$

where m_{out} is the mass discharged from the tank.
$m_{j,out}$ is the injected mass discharged from the tank.
$m_{r,out}$ is the residual mass discharged from the tank.
and C_{out} is the OH concentration of the mass discharged from the tank.

And from imcompressibility, the mass conservations are,

for the injected mass.

$$m_j = m_{j.in} + m_{j.out} \quad (6.38)$$

injected mass = injected mass retained + injected mass discharged
in the tank from the tank

for the residual mass.

$$m_r = m_{r.in} + m_{r.out} \quad (6.39)$$

initial residual mass = residual mass retained + residual mass discharged
in the tank from the tank

and

$$m_r = m_{in} \quad (6.40)$$

initial residual mass = total mass retained in the tank

$$m_j = m_{out} \quad (6.41)$$

injected mass = total mass discharged from the tank

$$m_{j.in} = m_{r.out} \quad (6.42)$$

injected mass retained = residual mass discharged
in the tank from the tank

After substitution and rearrangement, the following relationship can be obtained.

$$m_{j.in} = m_{in} \frac{C_{in} - C_r}{C_j - C_r} \quad (6.43)$$

$$m_{j.out} = m_{out} \frac{C_{out} - C_r}{C_j - C_r} \quad (6.44)$$

From the definition of charging and trapping efficiencies, they are.

$$\eta_{ch} = \frac{C_{in} - C_r}{C_j - C_r} \qquad (6.45)$$

$$\eta_{tr} = \frac{C_{out} - C_j}{C_r - C_j} \qquad (6.46)$$

Because pure water is injected into the tank, the OH concentration of the injected water C_j can be neglected. Being substituted by the PH value definition, the previous formulae (6.45) and (6.46) become

$$\eta_{ch} = 1 - \frac{C_{in}}{C_r} = 1 - 10^{PH(in)-PH(r)} \qquad (6.47)$$

$$\eta_{tr} = \frac{C_{out}}{C_r} = 10^{PH(out)-PH(r)} \qquad (6.48)$$

Therefore, the PH values can be measured by PH meter, and the charging and trapping efficiencies can be obtained. Thus, the delivery ratio can be determined from

$$\lambda = \frac{\eta_{ch}}{\eta_{tr}} \qquad (6.49)$$

In this experiment, the injected water amount is used as a monitoring parameter, instead of a measured parameter, because it is difficult to precisely control the same remaining water mass in the tank before and after the injection.

6.4 EXPERIMENTAL RESULTS ON THE WATER SCALE MODEL

The experimental work has been conducted as follows.

(1). The gauge pressures of the compressed air reservoir are equal to 1.4 and 2.8 bar respectively.
(2). The displacements of the injection pump are equal to 100, 200, 300, 350, 400 and 430 mm respectively.
(3). At each running condition, the experiment includes the following two tests:
(a). the flow visualization.
(b). the scavenging test with the PH-meter method.

6.4.1 FLOW VISUALIZATION

In this test, potassium permanganate (KMnO4) is used as a colour indicator. The red-coloured water solution of KMnO4 is filled through the filling hole into the injection pump. The water without colour is filled through the exhaust port into the tank. After the injection pump has been actuated, a jet propagates, mixes with the surrouding water without colour and forms a red-coloured mixing region. Therefore, the whole red-coloured region is composed of the fresh charge and mixing zones, while the region without colour is the residual charge zone. These processes of the jet propagation are filmed by a cine-camera with 64 frame per second. From these photographs, the following phenomena can be seen.

(1). After entering the tank, the two jets from two inlet ports impinge and deflect their directions to axial. However, this impingement is a process of gradually deflecting, not straightly impacting and abruptly deflecting.
(2). After the impingement, the jet flow develops to an axial jet. Despite the tank layout is designed as symmetric, the jet is unsymmetric because of the deviation in manufacture and operation.
(3). The propagation of the jet flow arouses a recirculating flow in the surrounding region. The recirculating flow lasts a rather long time after the end of the scavenging process.
(4). If the amount of the injected water is less than a certain value, the red-coloured water of fresh charge and mixing regions never arrives at and discharges from the exhaust ports, i.e., only the displacement scavenging phase occurs.
(5). When the amount of the injected water is greater than a certain value, first only the water without colour discharges from the exhaust ports, and then the red-coloured water arrives at and discharges from the exhaust ports. This means that the displacement scavenging phase first occurs, and then the mixing scavenging phase follows.

Fig. 6.5 illustrates a group of typical photographs for the flow visualization of the scavenging process.

6.4.2 SCAVENGING TEST WITH THE PH-METER METHOD

Following the above operation procedures, described in Section 6.3.2, this

experiment has been done under the same operating conditions as those in the flow visualization test. The experimental results are shown in Fig. 6.6.

From the experimental results, it can be concluded that.

(1). in the scavenging process, always the displacement scavenging phase first occurs, and then the mixing scavenging phase follows.
(2). with increase of delivered amount of fresh charge the trapped amount of fresh charge, i.e. the charging efficiency increases, while the trapping efficiency decreases.

These quanlitative conclusions are consistent with those from the flow visualization. It is important to give an estimation of the precision for the phenomenological unsteady jet model suggested in Chapter 4 based on these experimental results.

6.5 VALIDATION OF THE PHENOMENOLOGICAL UNSTEADY JET MODEL

The program WATERRIG is rewritten based on the program of the phenomenological unsteady jet model (UJM), as described in Chapter 4. The program WATERRIG has the same idea and structure as those in UJM. Actually, program WATERRIG is a simplified version of version 1 of UJM for modelling imcompressible planar jet flow in a rectangular tank with constant flow section areas of inlet and exhaust ports because the entrainment law used in version 1 of UJM is valid also for planar flow, while the entrainment law in version 2 is used for cylindrical system. Like UJM, WATERRIG neglects the investigation of jet impingement.

In the real model rig, the inlet ports are fitted with diaphragm valves for preventing leakage of water from the injection pump into the tank before injection. However, the modelling with WATERRIG requires the flow areas of the inlet ports as the boundary conditions. Under the simplification of imcompressible quasi-steady flow, the following equation is evident.

$$m_{in} = \rho C_f A_{in} v_{in} T_{in} \qquad (6.50)$$

where m_{in} is the total mass flowing through the inlet ports,
ρ is the density,

C_f if the flow coefficient of the inlet port.
A_{in} is the area of the inlet ports.
v_{in} is the flow velocity at the inlet ports.
T_{in} is the duration of the jet flow.

Here, the total mass m_{in} can be measured, and the duration Tin and the velocity v_{in} can be approximately estimated from the photographs filmed in the flow visualization test. Therefore, the flow section area CfAin can be determined. For the sake of estimating the precision of the phenomenological unsteady jet model, the experiment at each operating point must be repeated twice, one with PH-meter method to obtain the charging and trapping efficiencies, another with flow visualization to determine the boundary conditions for computing.

A comparison between these experimental and computational results of the charging and trapping efficiencies is shown in Fig. 6.7. The discrepancy is within 5 %. Correspondingly, Fig. 6.8 illustrates a comparison between the jet penetration processes. The prediction of the arrival time of jet from inlet to exhaust end is satisfactory. Fig. 6.9 shows an example of computational results of concentration field.

From these comparisons, it can be concluded that under the condition of imcompressible flow without swirl the phenomenological unsteady jet model for uniflow scavenging process is satisfactory, and the entrainment law by Ricau and Spalding [4, 10] quoted in this model slightly underestimates mass entrainment rate. From the photographs from the flow visualization, for the jet confined within the cylinder-like space, the recirculation intensifies the entrainment and mixing process.

It is necessary in further experimental work to build a model in the form of a real cylinder with ports and a moving piston, and to carry out measurements with this model under operating conditions of variable density and swirl. In order to validate version 2 of the phenomenological unsteady jet model, it is required to measure the velocity and concentration fields, thus also establishing a new entrainment law for this kind of confined jet.

6.6 CONCLUSIONS

Scale modelling technique is beneficial for parametric and microscopic study of the scavenging process.

A group of model laws has been established. Generally speaking, the more accurate a modelling method, the more complicated the model rig and the measuring techniques for satisfying the more generalized model law and providing the more abundant information.

A series of scale model tests have been done on the simple water rig. These experiments combine the PH-meter method with the flow visualization. The experimental results have validated that for imcompressible jet flow without swirl the phenomenological unsteady jet model, suggested in Chapter 4, is satisfactory with error of less than 5 %.

REFERENCES

[6.1] K. Sato and K. Kido
"Simulation of the Gas Exchange process in a Small Two-Stroke Cycle Engine"
Bulletin of the JSME, Vol.26, No.217, 1983

[6.2] N. Dedeoglu
"Scavenging Model Solves Problems in Gas Burning Engine"
SAE 710579, 1971

[6.3] T. Oka and S. Ishihara
"Relation between Scavenging Flow and its Efficiency of a Two-Stroke Cycle Engine"
Bulletin of the JSME, Vol.14, No.69, 1971

[6.4] R.J.B. Way
"Investigation of Interaction between Swirl and Jets in Direct Injection Diesel Engines Using a Water Model"
SAE 770412, 1977

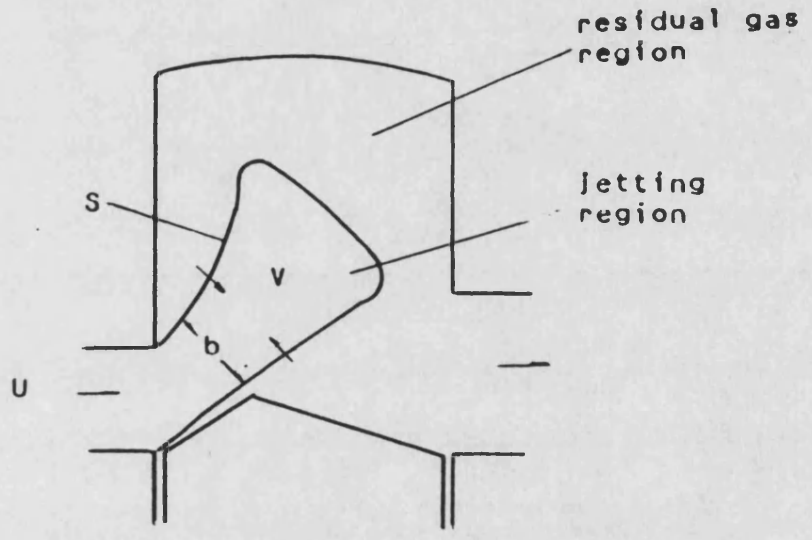

V control volume
S control surface
b jet width

Fig. 6.1 Confined Jet

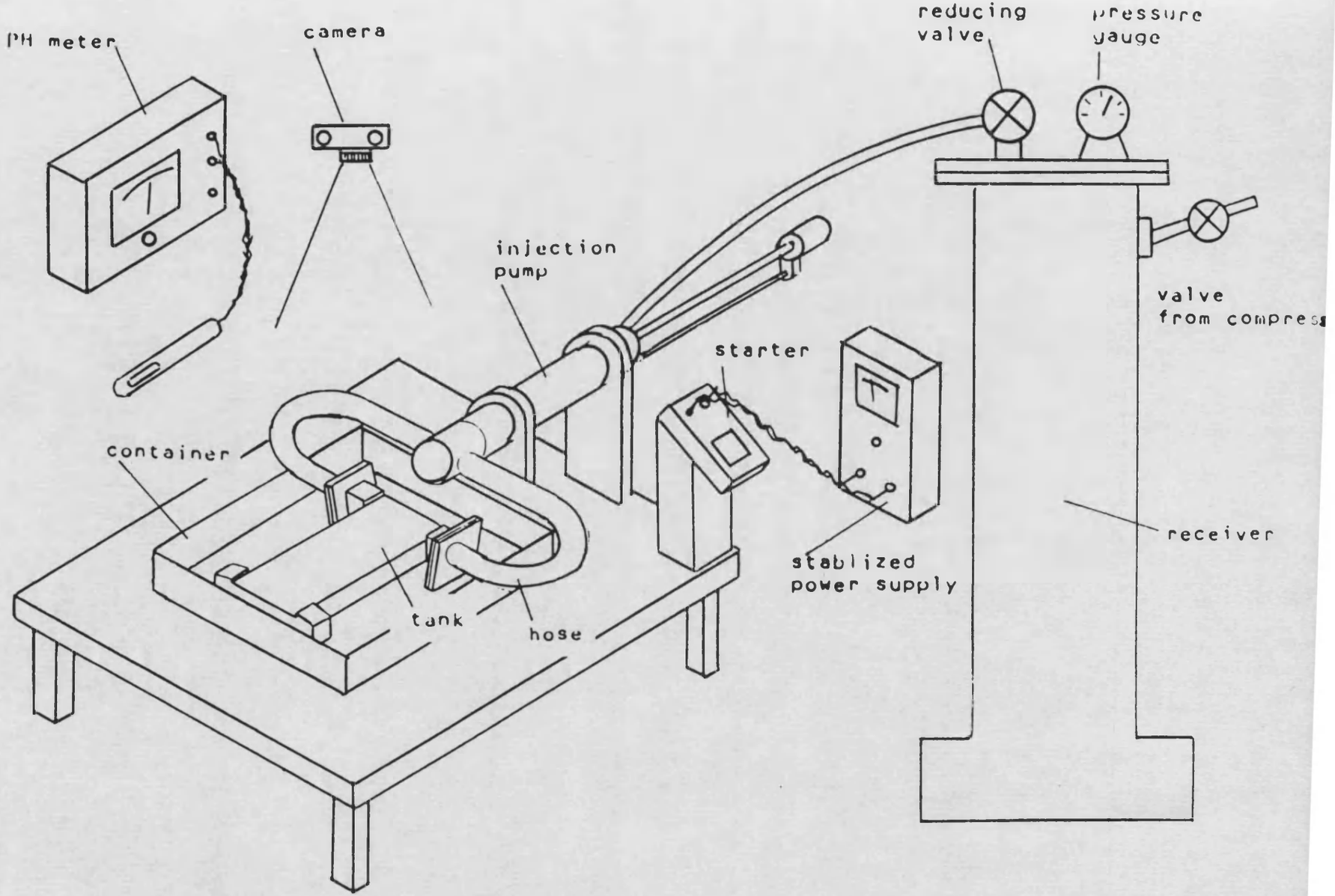

Fig. 6.2 Layout of Water Rig

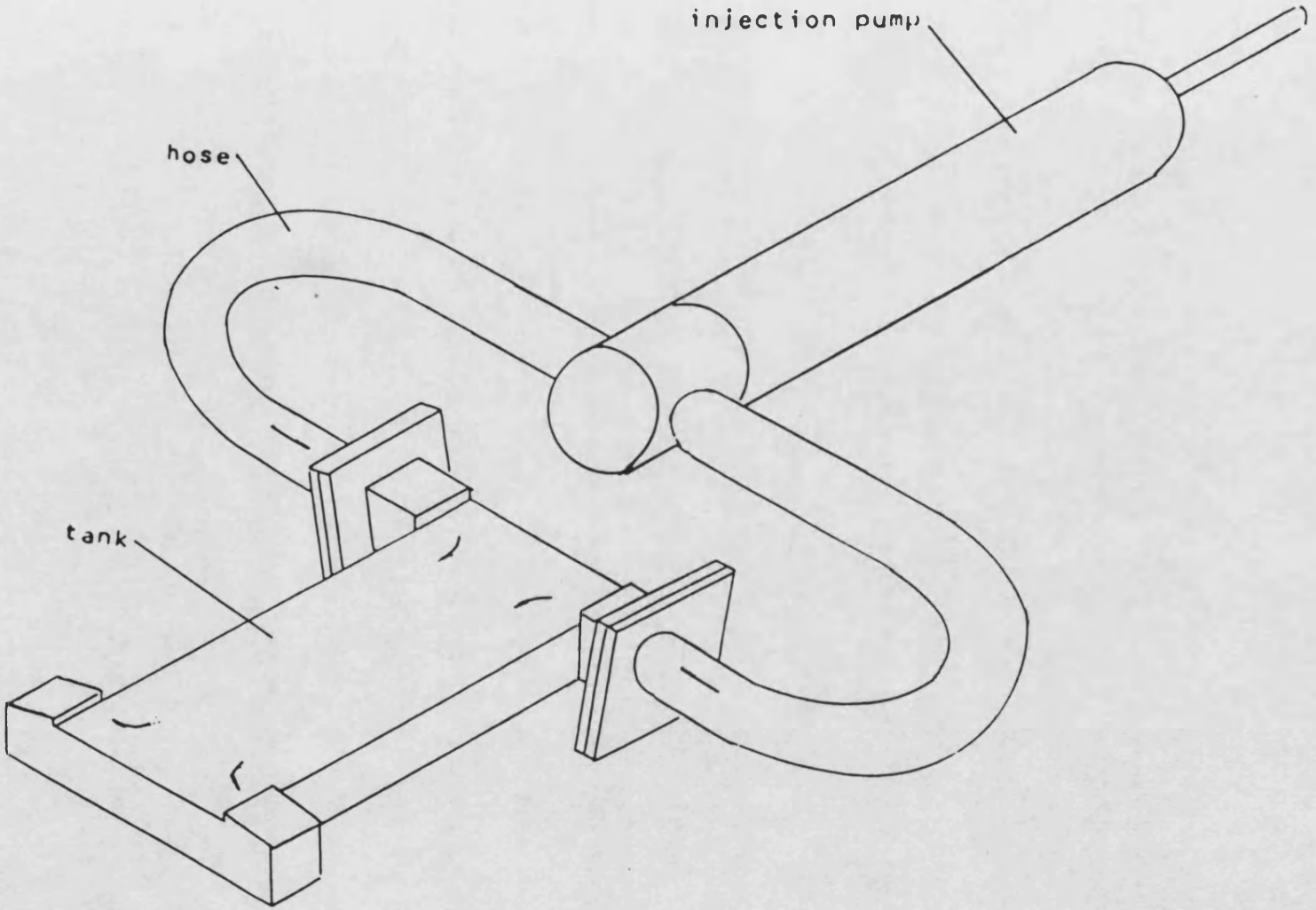

Fig. 6.3 Injection Pump and Tank

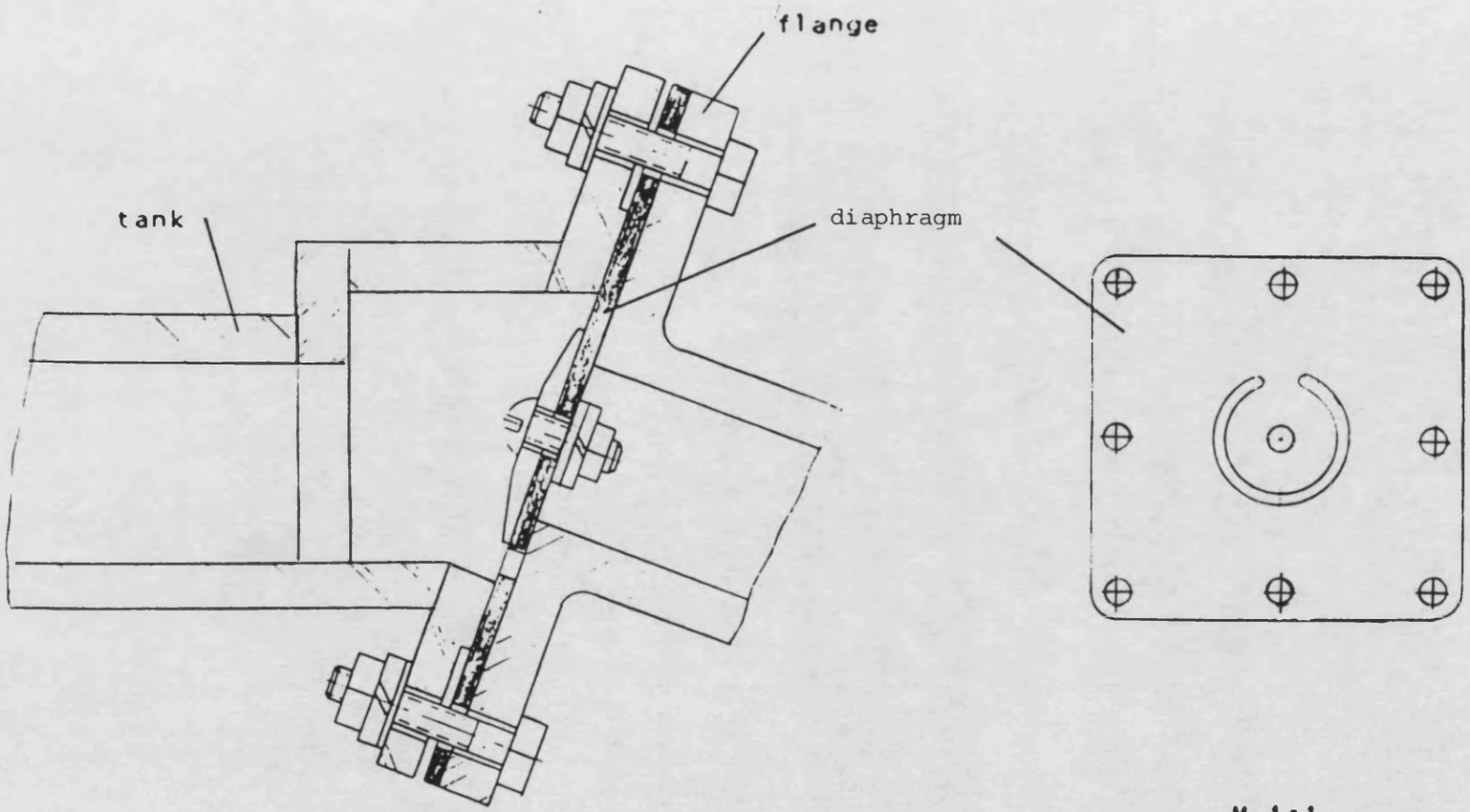

Fig. 6.4 Diaphranm Check Valve

injection pump displacement 400 mm gauge pressure 1.4 bar.

3/64 sec.

2/64 sec.

1/64 sec.

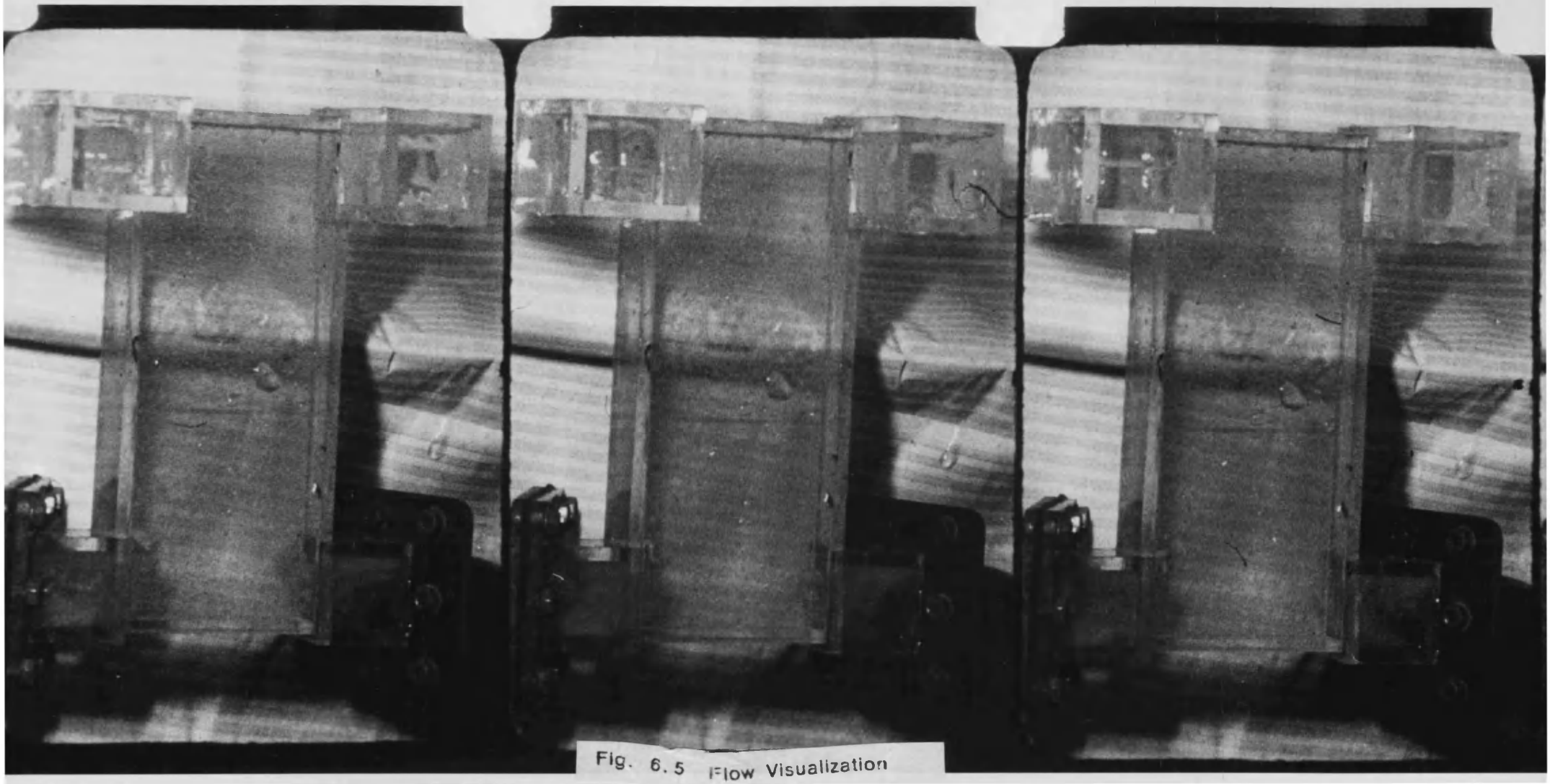

Fig. 6.5 Flow Visualization

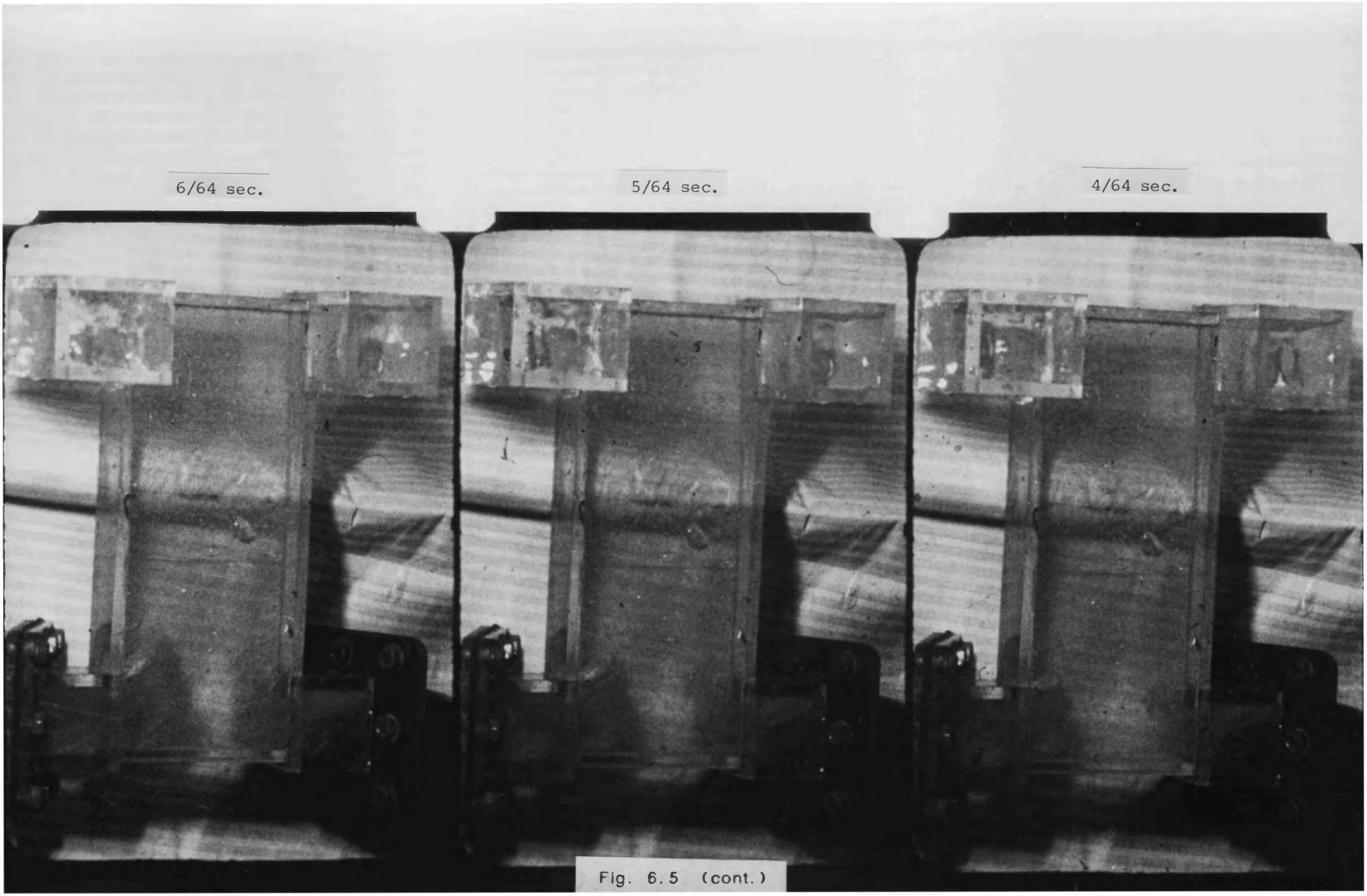

Fig. 6.5 (cont.)

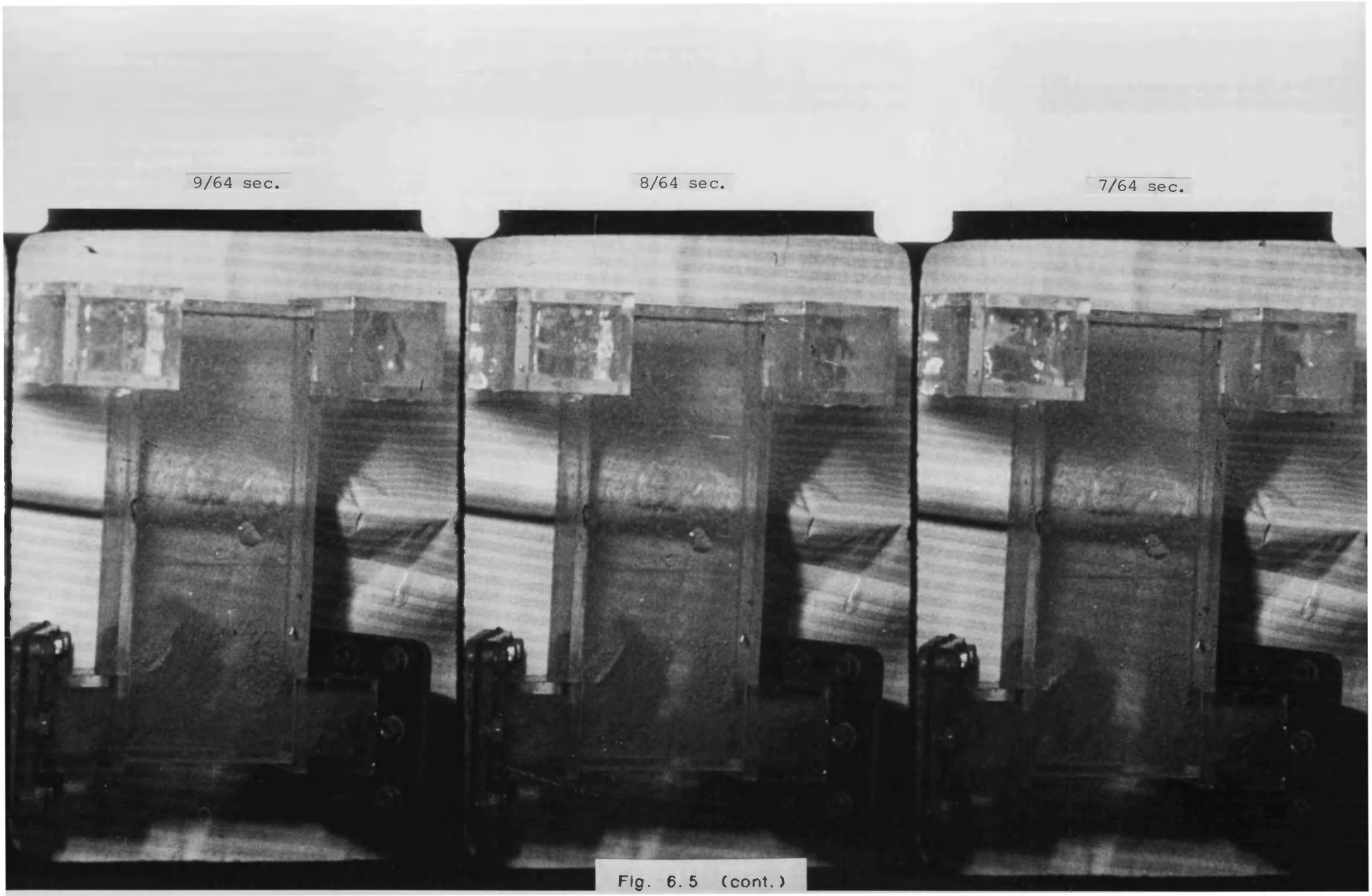

Fig. 6.5 (cont.)

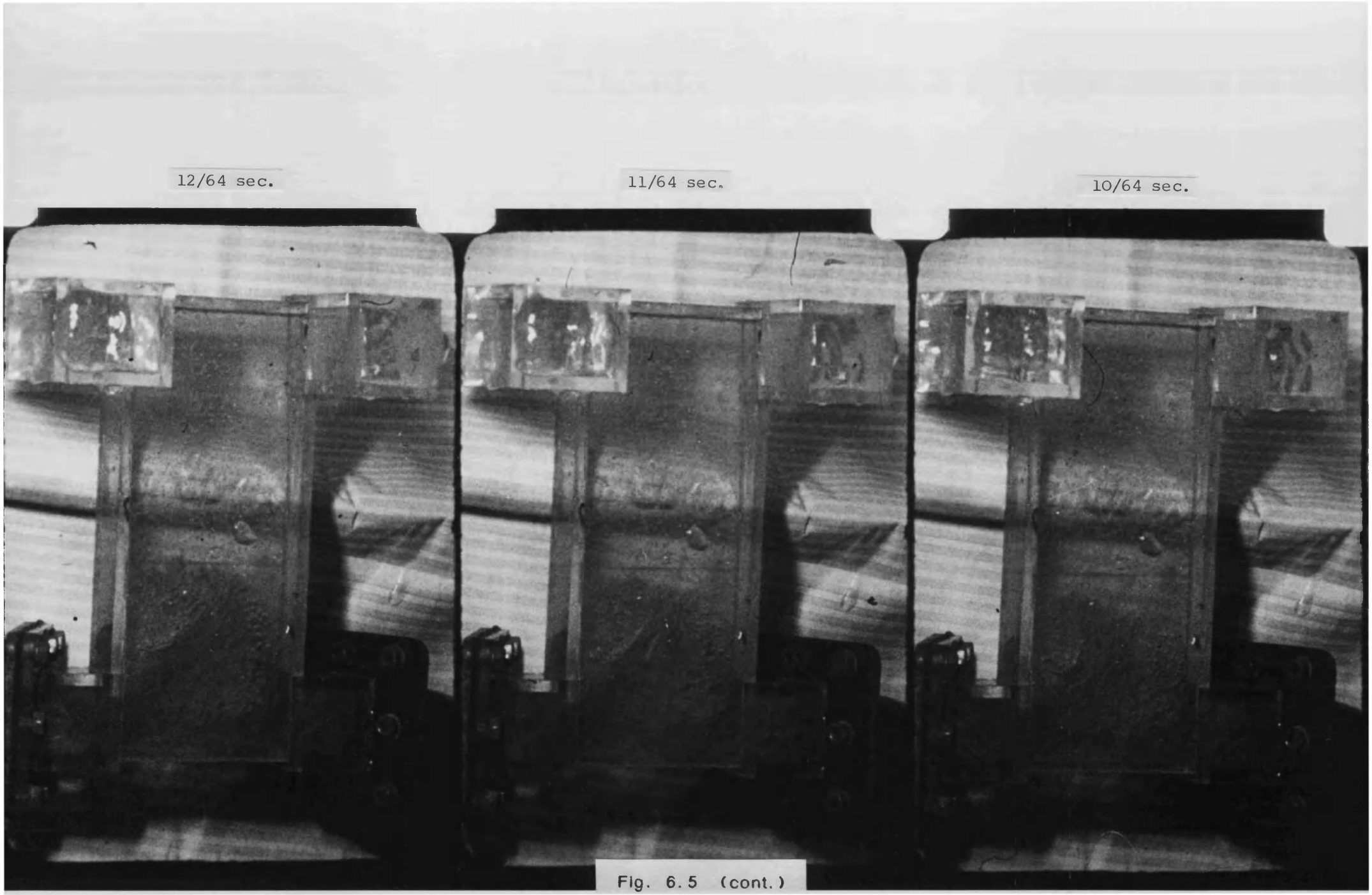

Fig. 6.5 (cont.)

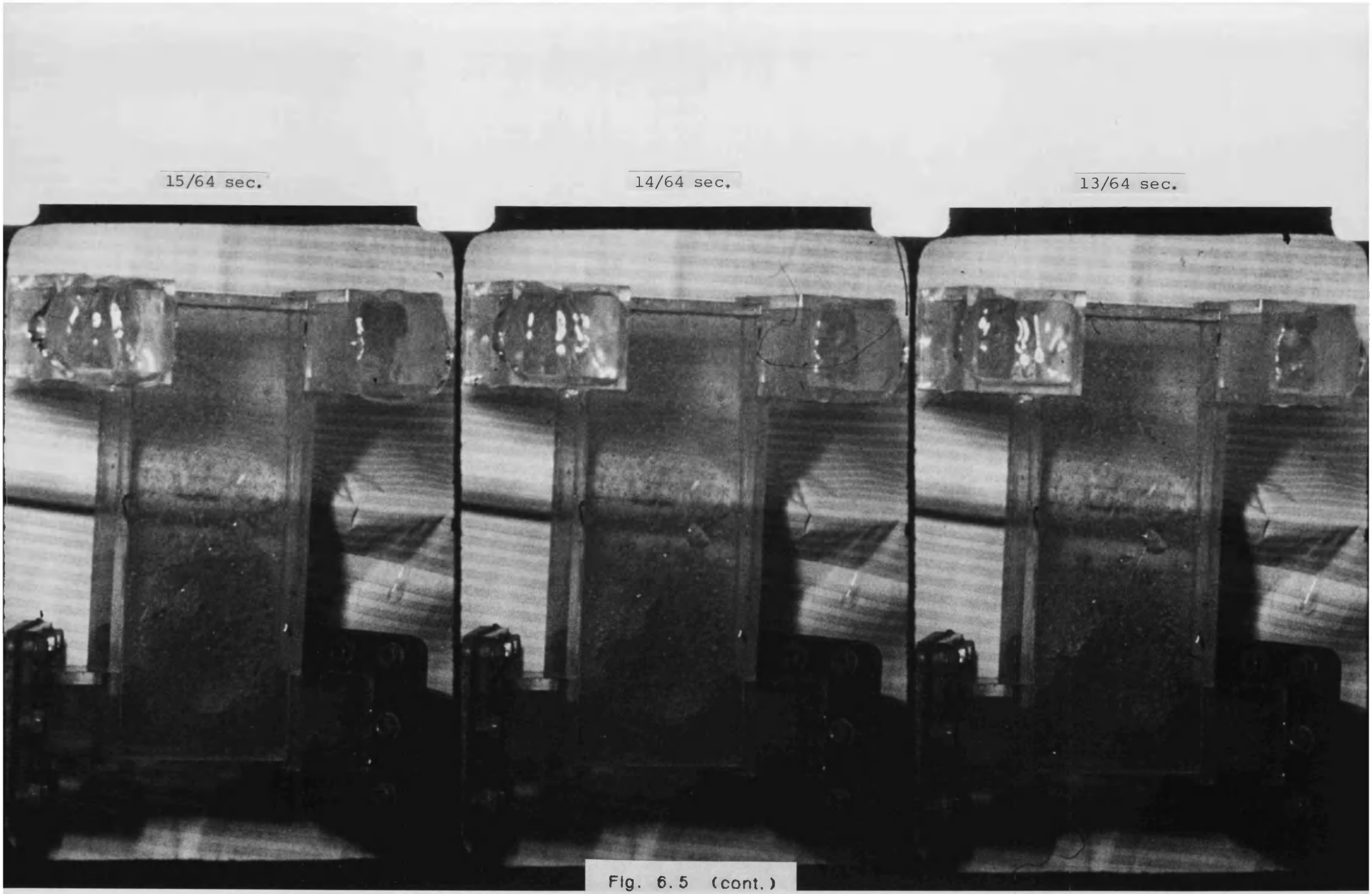

Fig. 6.5 (cont.)

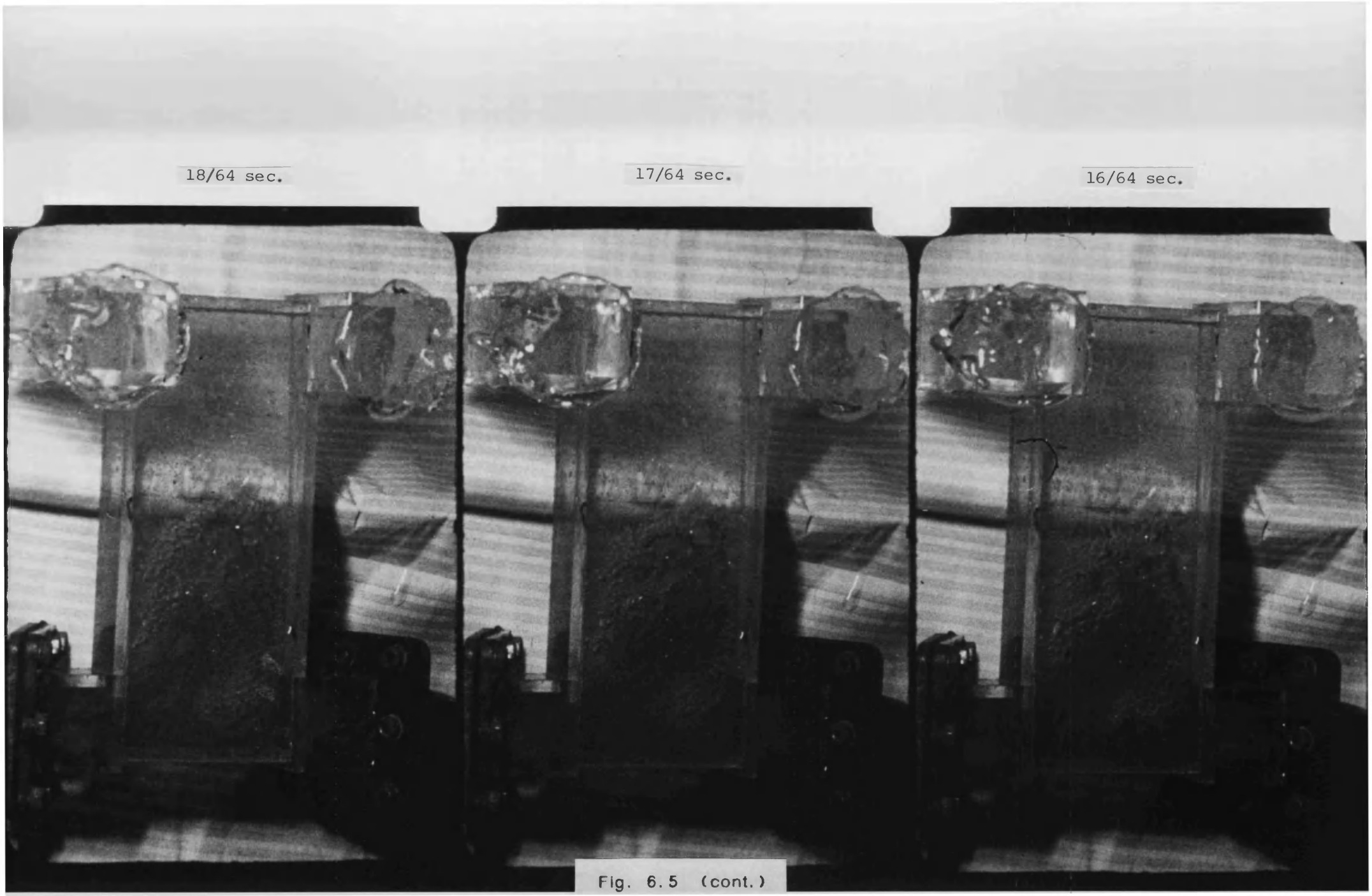

Fig. 6.5 (cont.)

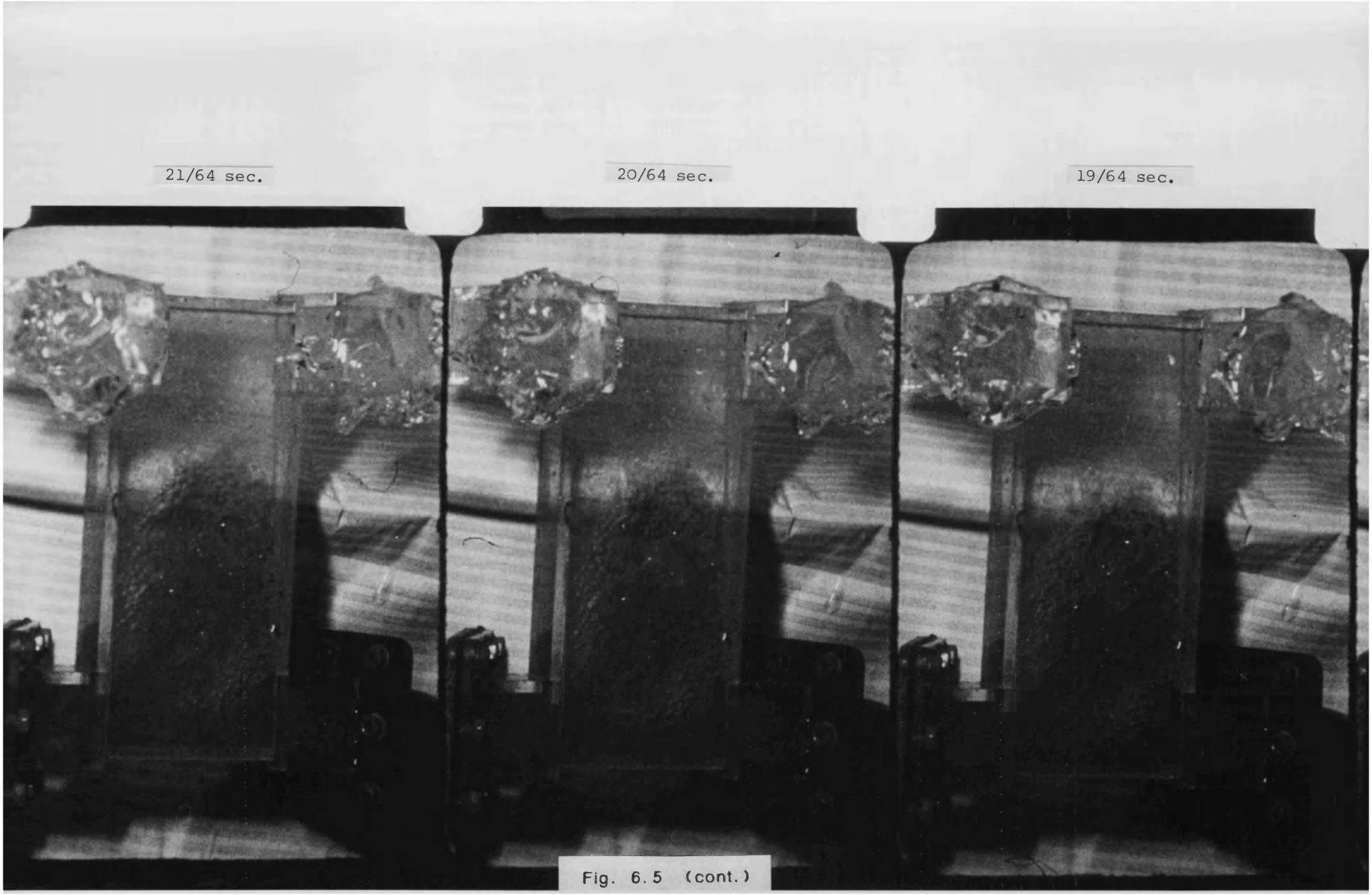

Fig. 6.5 (cont.)

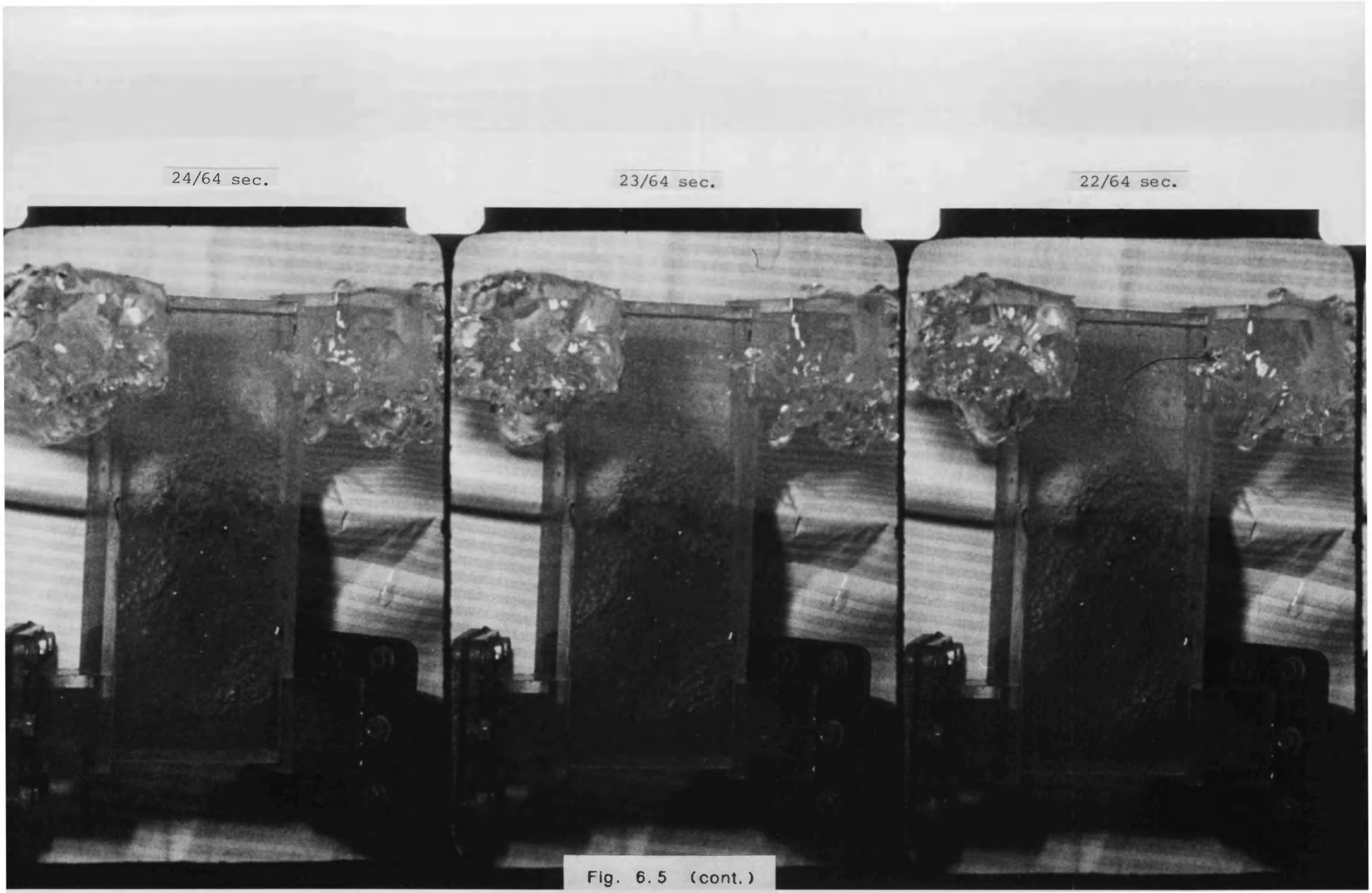

Fig. 6.5 (cont.)

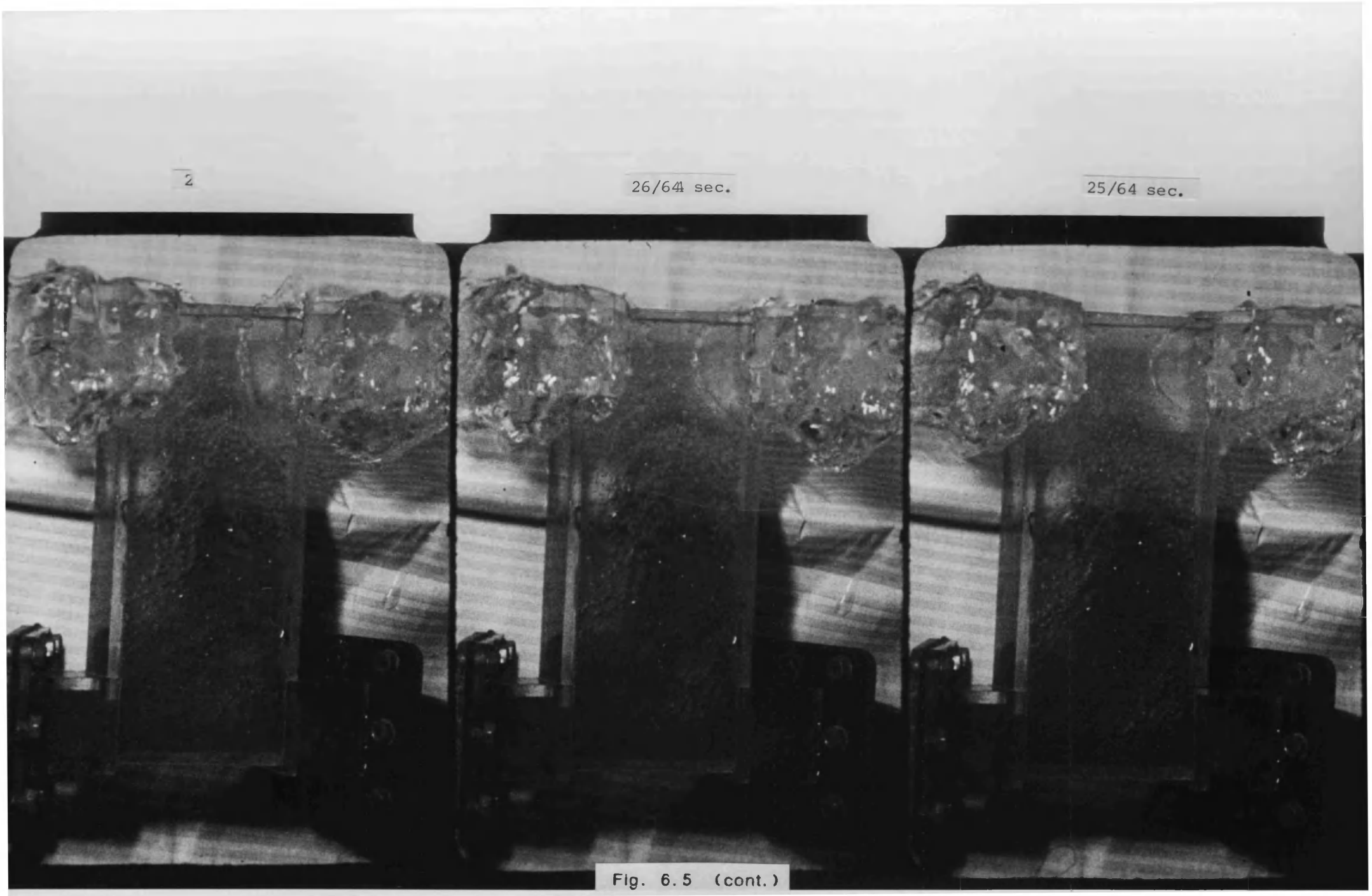

Fig. 6.5 (cont.)

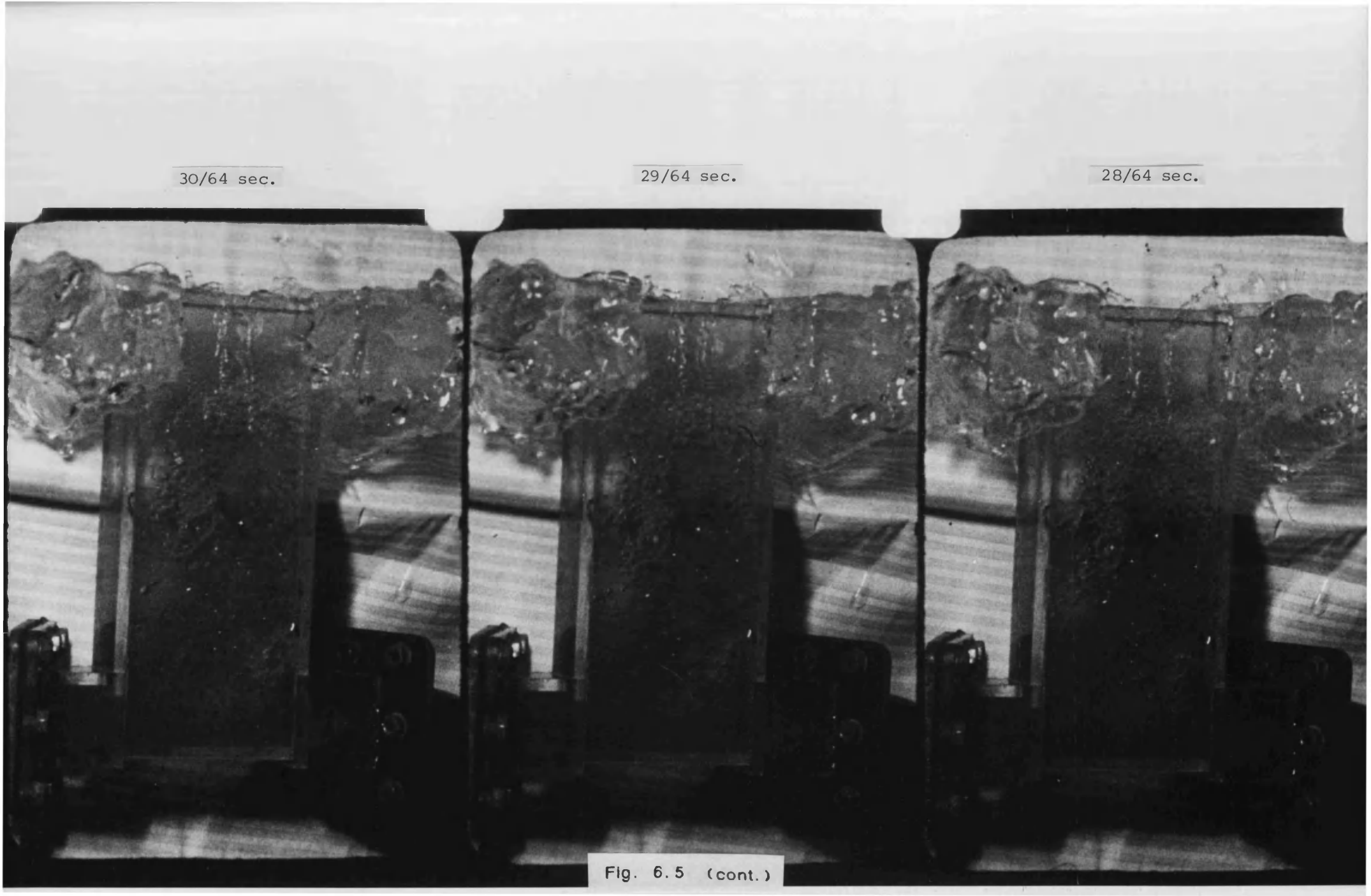

Fig. 6.5 (cont.)

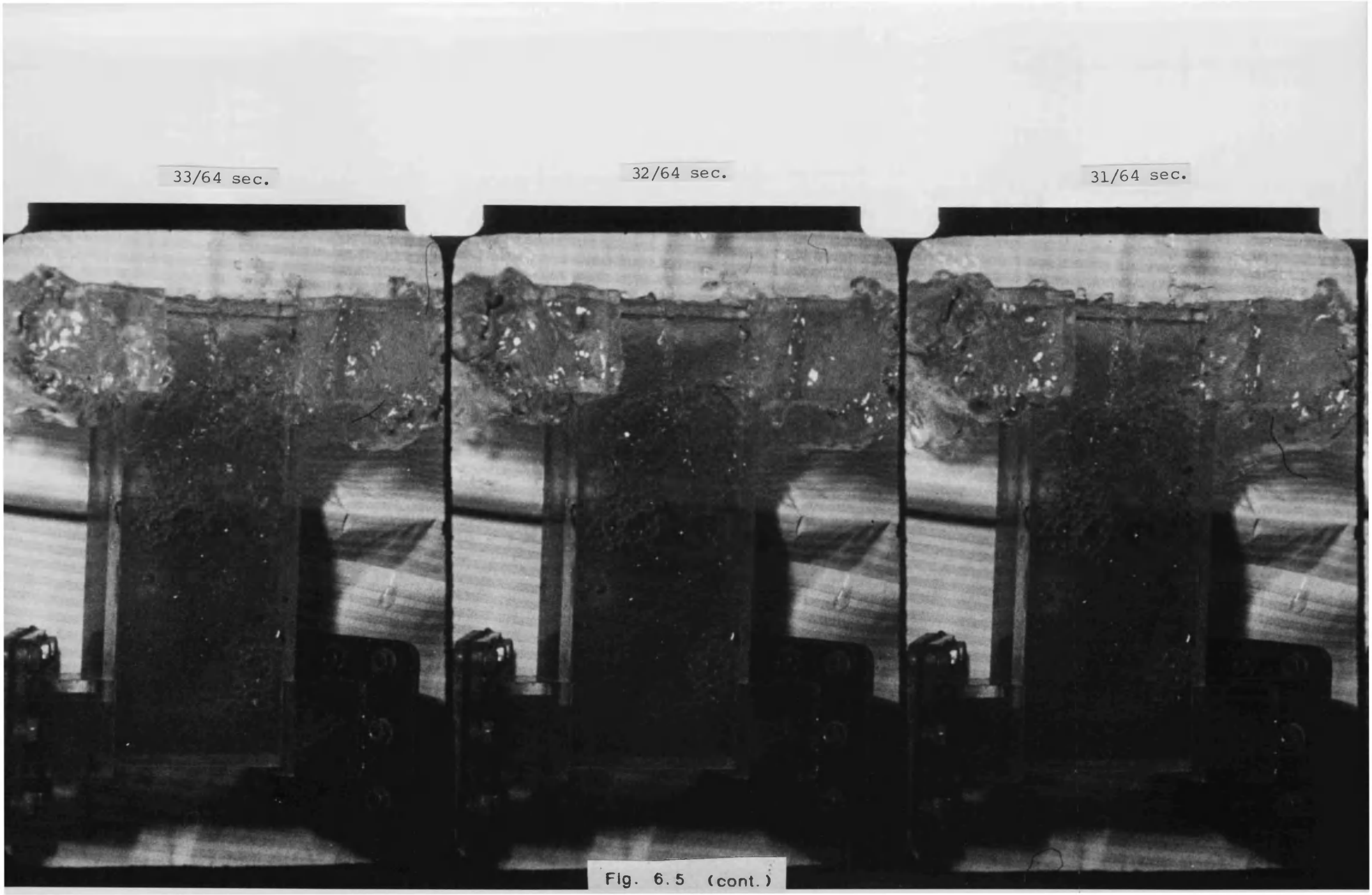

Fig. 6.5 (cont.)

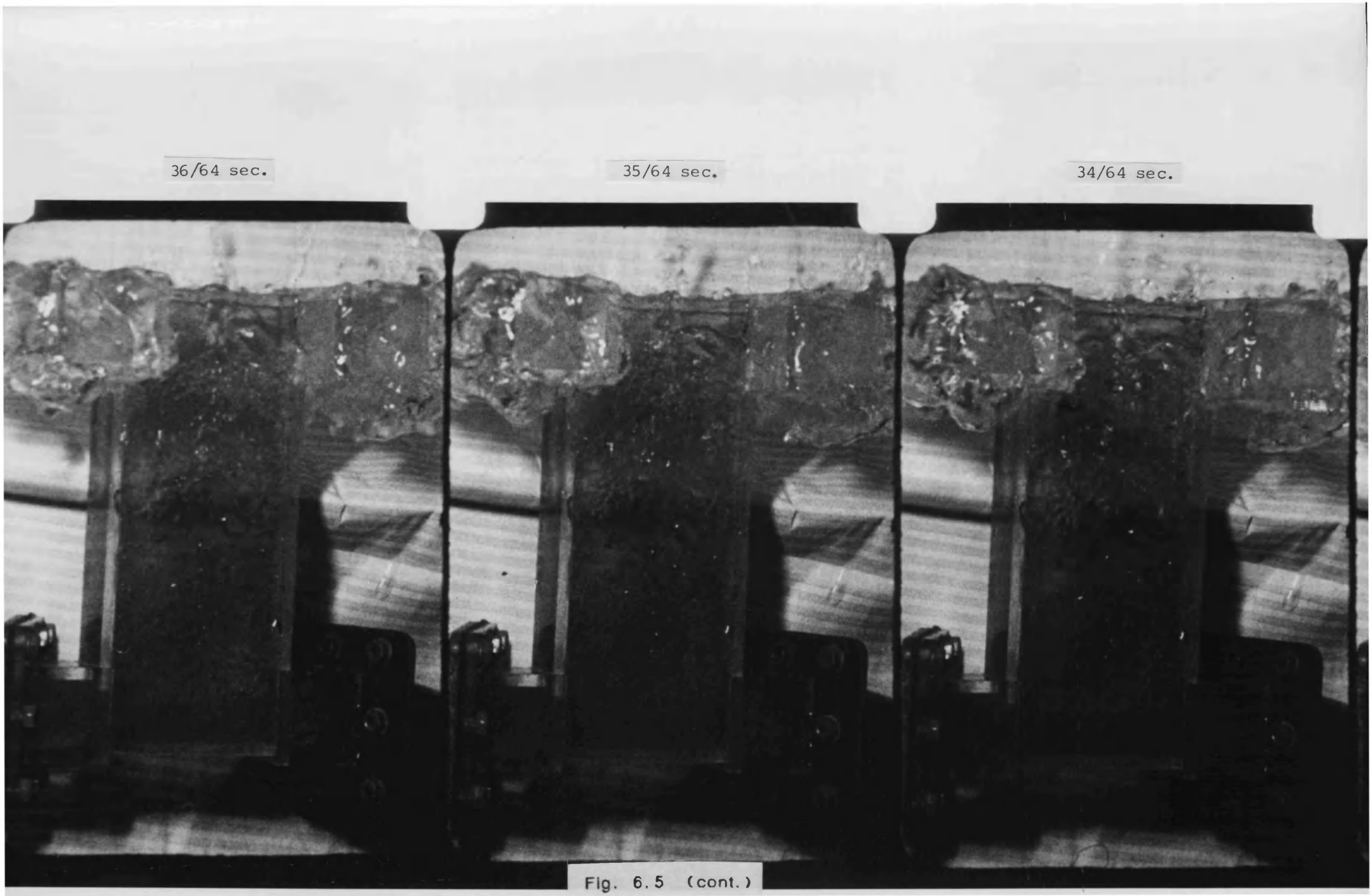

Fig. 6.5 (cont.)

gauge pressure 1.4 bar

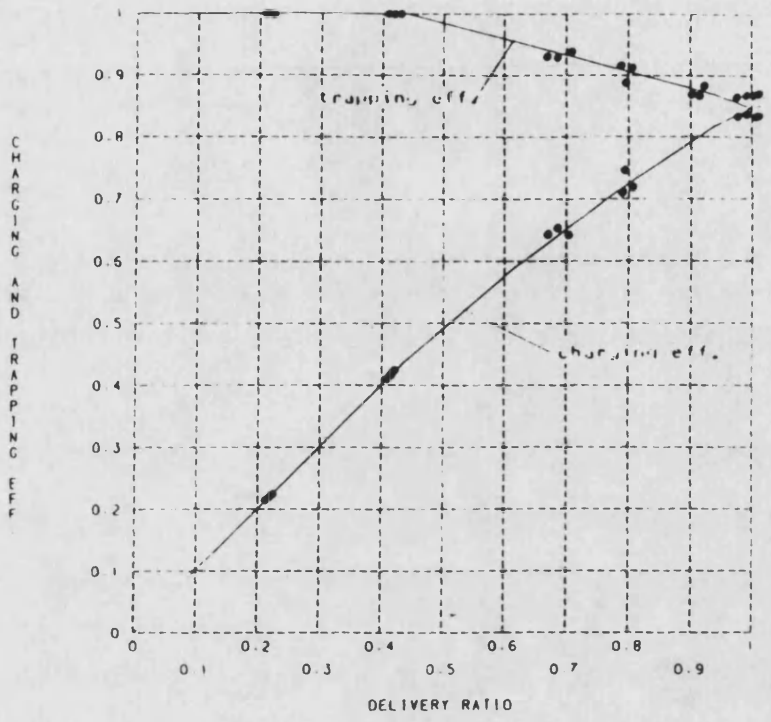

gauge pressure 2.8 bar

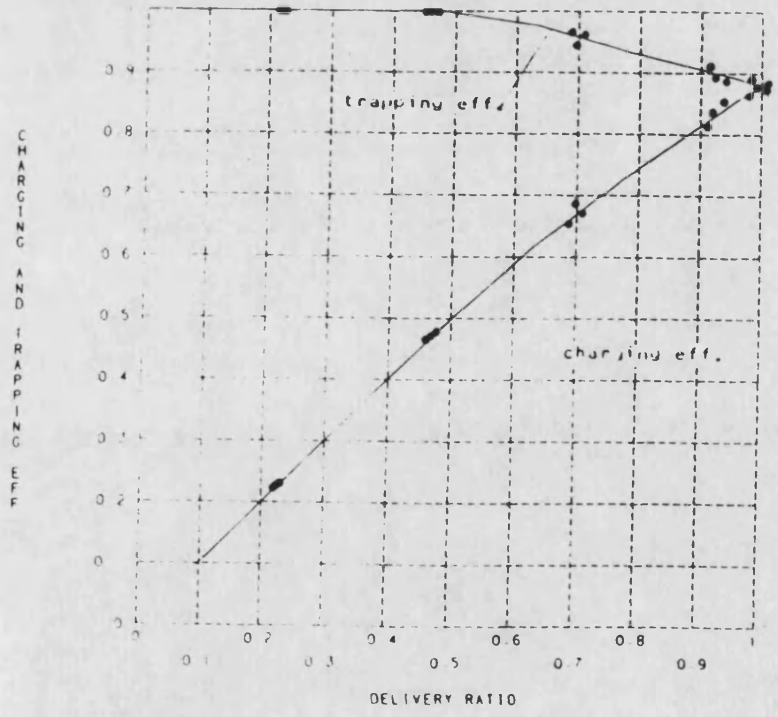

Fig. 6.6 Experimental Results on Water Rig

gauge pressure 1.4 bar

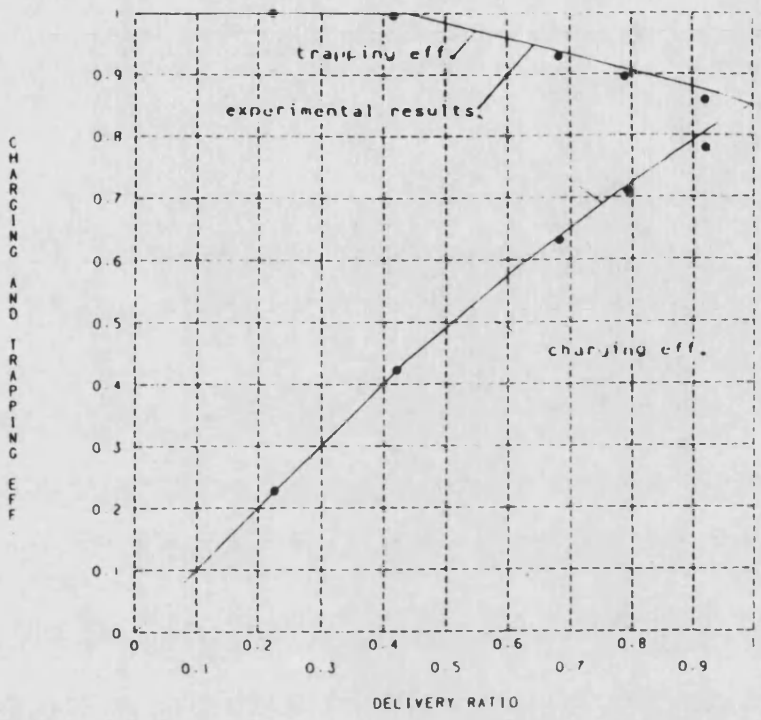

• computational results

gauge pressure 2.8 bar

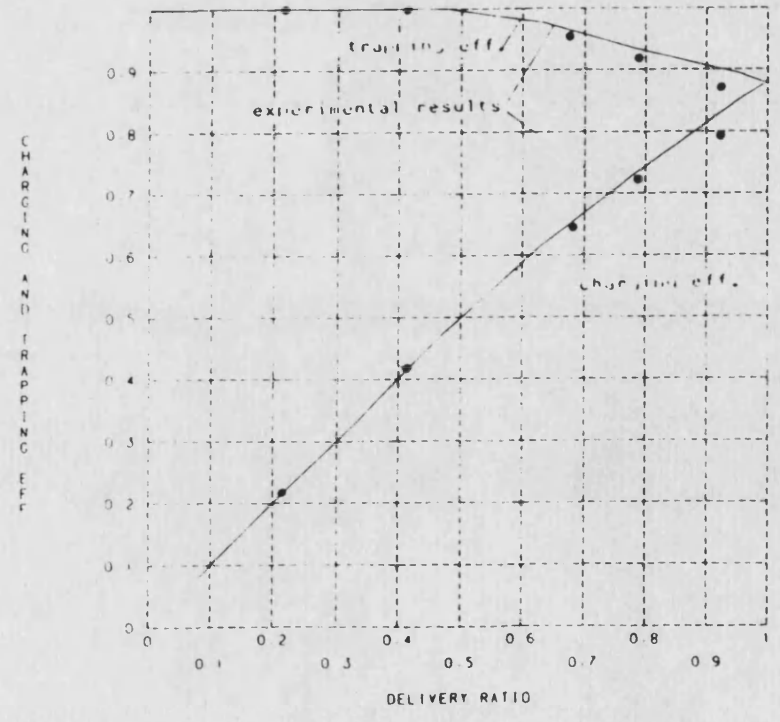

• computational results

Fig. 6.7 Comparison between Computational and Experimental Results on Water Rig

injection pump displacement 400 mm gauge pressure 1.4 bar

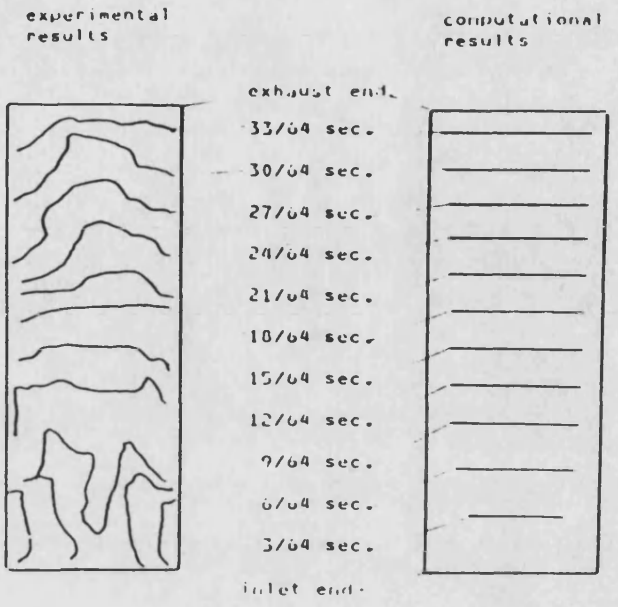

injection pump displacement 400 mm gauge pressure 2.8 bar

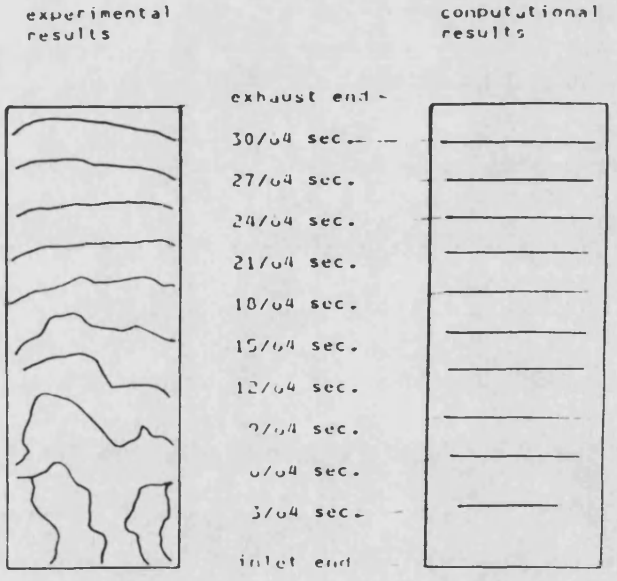

Fig. 6.8 Comparison of Jet Penetration

Timeline
injection pump displacement 400 mm gauge pressure 1.4 bar

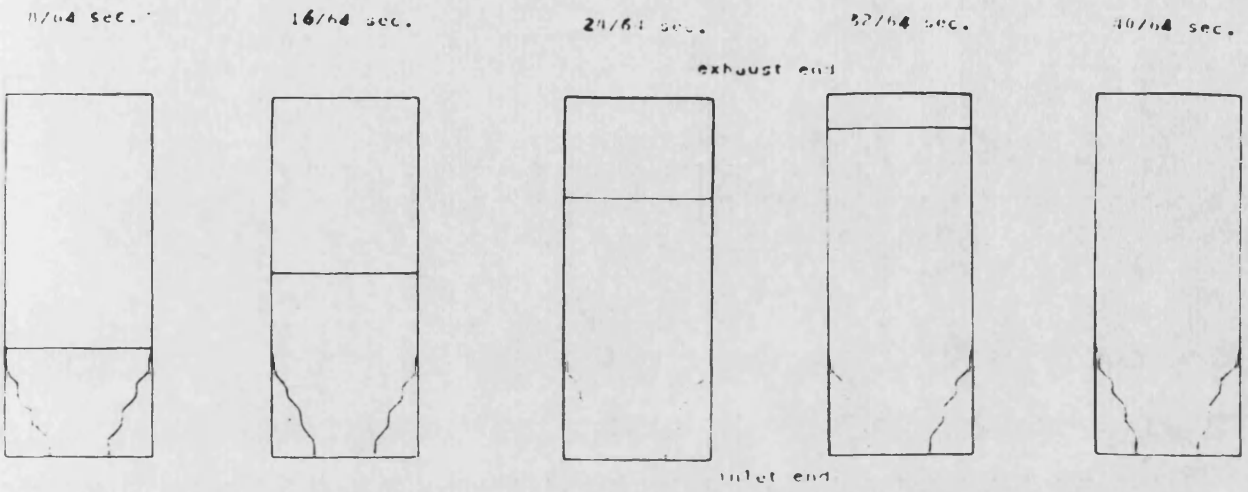

Concentration
injection pump displacement 400 mm gauge pressure 1.4 bar

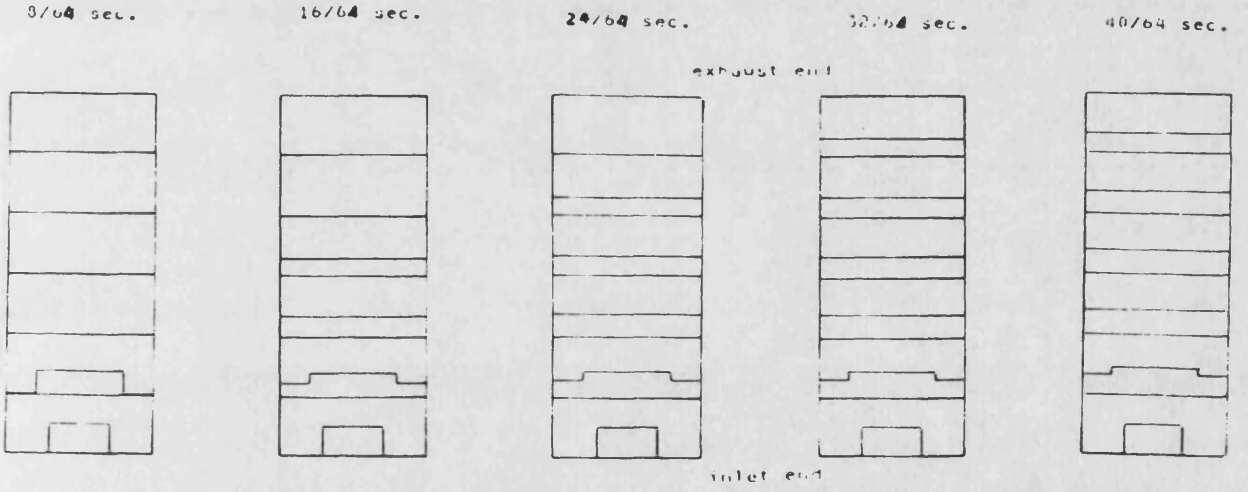

Fig. 6.9 A Group of Computational Results
for Expelments on Water Rig

Time line
injection pump displacement 400 mm gauge pressure 2.8 bar

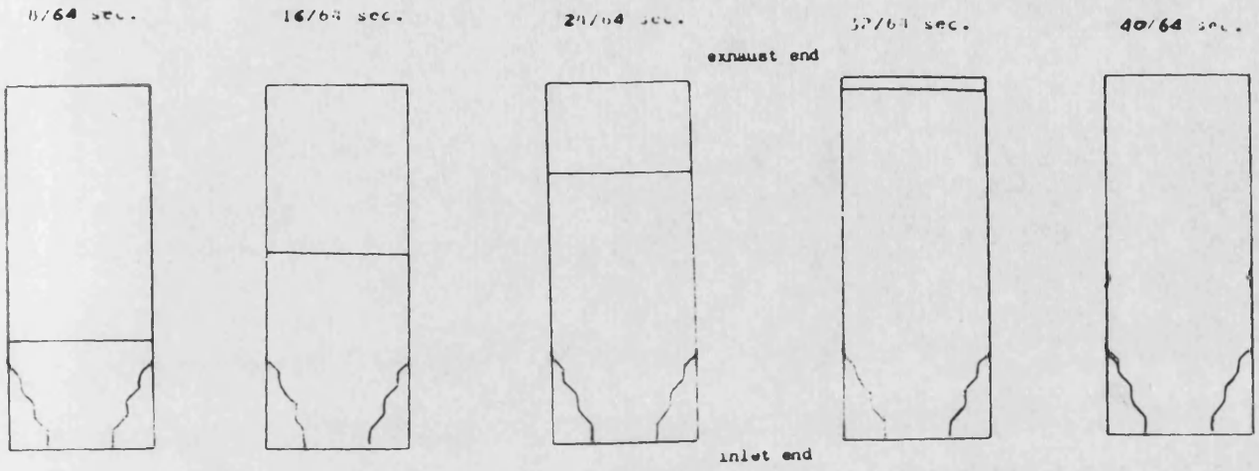

Concentration
injection pump displacement 400 mm gauge pressure 2.8 bar

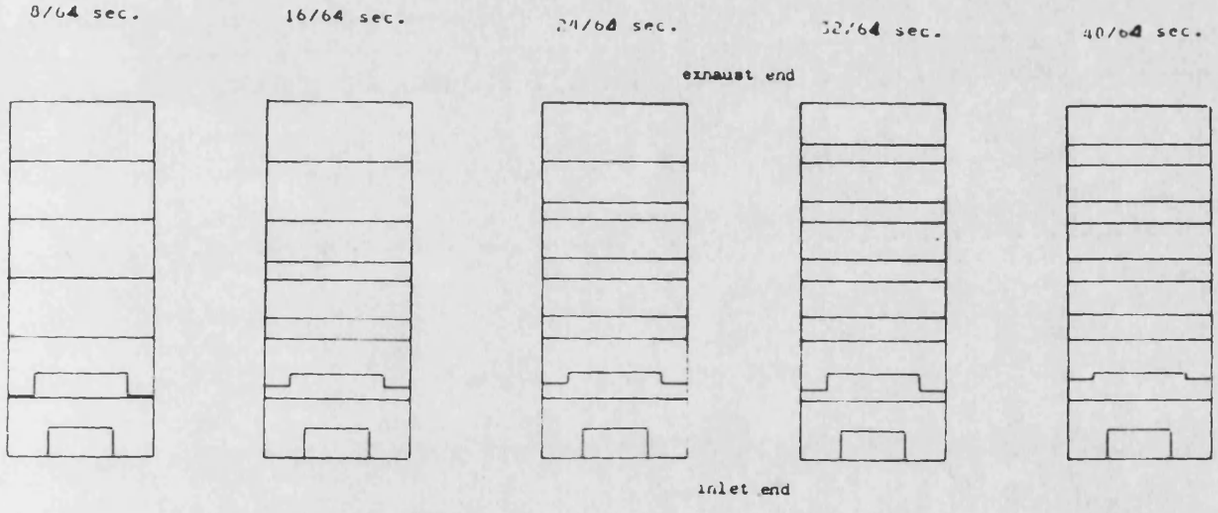

Fig. 6.9 (cont.)

Part 3 SUPERCHARGING AND COMPOUNDING

Chapter 7 TWO-STROKE DIESEL ENGINE MODELS

7.1 INTRODUCTION

The diesel engine, being the most efficient known power plant, has been used in many applications. The output, fuel consumption and exhaust emissions of any diesel engine are governed by the flow and movement of gas in the engine. The flow in turn depends on compression ratio, dimensions and configuration of the combustion chamber, inlet and exhaust port or valve layout, size and timing, swirl, squish, air-fuel ratio and injection system. Since all these parameters are variable, some over a very wide range, engine development or optimization of a basic design with an empirical approach would take a long and costly process. In recent years, the computer modelling techniques have been developed and used to simulate the diesel engine thermodynamic cycle and predict the performance satisfactorily.

The earliest air-standard models assumed air as the working fluid, [7.1] typically, but not certainly, assumed to be independent of temperature. After that, the fuel-air models used two separate charts for calculating the thermodynamic properties of a fuel-air mixture and the products of combustion of this mixture respectively [7.2]. An earlier five-point model developed by Way and Wallace [7.3] belongs to this group of models. These two groups of models both assumed that all engine processes are independent of time. This assumption simplifies the computation, but heavily damages the predictability. Then, thermodynamic rate models used time as a variable which represented a significant advance. [7.4] This type of model can predict the effect of valve timing, and the effect of injection timing. Recently the multi-dimensional models based on the computational fluid dynamics methods have been developed for predicting engine subprocesses such as in-cylinder flows, spray distribution and mixing. [7.5], [7.6] However, these models add markedly to the complexity of the model and the computer time required, and need the further experimental validations which are tedious and difficult.

The main uses of engine cycle simulation are as follows:

(1). to investigate major design options (for example, the performance

estimation of the thermally insulated engine).
(2). to optimize aspects of design via parametric studies (for example, the optimization of port timing).
(3). to predict cylinder pressure and hence mechanical loading.
(4). to predict component temperature and hence thermal loading.

Generally speaking, the more simple the model, the more limited the applicability, and consequently the more limited the information obtained from the model. Based on the compromise between model complexities and computer capability, the thermodynamic rate models should be suitable for the above applications. According to different applications, the following two engine models are suggested.

(1). a simple engine model with a large step length.
(2). a step-by-step model which has two versions with different scavenging models.

These three programs are:

CSPS: Cycle Simulation Program with the Simple models, which is composed of the simple engine model with the isobaric and isochoric thermodynamic scavenging model, in Chapter 2.

CSP3Z: Cycle Simulation Program with the 3 Zone scavenging model, which is composed of the step-by-step engine model with the three-zone thermodynamic scavenging model, in Chapter 3.

CSPMZ: Cycle Simulation Program with the Multi-Zone scavenging model, which is composed of the step-by-step engine model with the phenomenological multi-zone unsteady jet model, in Chapter 4.

The engine model is composed of the following submodels:

(1). piston-crank mechanism
(2). gas properties
(3). combustion
(4). gas exchange
(5). heat transfer

(6). engine friction

Some submodels have different versions with different complexity level. Different programs use different submodels in the light of various requirements.

7.2 SIMPLE ENGINE MODEL (PROGRAM CSPS)

7.2.1 SOME CONCEPTS

The simple engine model is composed of the simple submodels in order to shorten computing time. CSPS can only give a cycle-to-cycle description rather than a "degree-by-degree" description.

The simple engine model has been developed based on a polytropic process with variable exponent, combined with the heat release correlation by Watson, Marzouk and Pilly [7.7]. The cycle process in the combustion chamber is divided into the following three phases:

(1). compression
(2). combustion
(3). expansion

The combustion phase is, furthermore, subdivided into several steps. In each step, the burning fuel mass is computed based on Watson's correlation.

For a closed system, from the first law of thermodynamics, the non-flow energy equation is

$$Q_{12} - W_{12} = \Delta U_{12} \qquad (7.1)$$

For a cylinder, the volume is determined by its piston crank mechanism. Generally speaking, the process within the cylinder is a polytropic process with variable exponent, depending on the relationship of heat transferred to the system.

This model assumes that the polytropic exponents in the compression and

expansion phases and each step of the combustion phase remain constant. Therefore, the model uses large step length.

7.2.2 PISTON-CRANK MECHANISM

This submodel evaluates the distance of the piston from the top dead centre position, cylinder volume and rate of change of cylinder volume with crank angle. The submodel provides two options, for the conventional engine and opposed-piston engine layouts. The submodel for the former has been programmed and described in the work by Tarabad. [4.14] The submodel for the latter is described in Appendix I.

7.2.3 GAS PROPERTIES

In accordance with the requirement of quick and easy calculation, a set of relatively simple empirical polynomial relationship by Way and Wallace [7.3] are used in program CSPS for calculating the specific heat at constant pressure, ratio of specific heats and enthalpy of exhaust gas in diesel engines as functions of temperature and equivalence ratio, but not of pressure. The corresponding subroutine has been made by Way.

7.2.4 HEAT TRANSFER

The heat flow transferred to cooling water and cooling oil is computed based on the correlation by Wallace and Wright [4.15] which gives very good results, the error exceeding 5 per cent in very few instances for two-stroke opposed piston engines, and is a correlation between heat flow and running parameters:

$$Q_c = K(M_f)^{0.87} \left(\frac{No}{N}\right) r_c^{-0.6} \lambda^{-0.2} \qquad (7.2)$$

in which M_f is the fuel mass supplied to engine per minute

N is the engine speed in rev/min,

r_c is the boost pressure ratio,

λ is the delivery ratio

and coefficient K is determined by calibration with experimental results from the engine.

This correlation based on the running parameters is suitable for a simple model because it does not involve any calculation of thermodynamic process variables.

It is assumed that 10 per cent of the heat loss is allocated to the compression and expansion phases respectively, while 80 per cent is attributed to the combustion phase and is proportionally subtracted from the burning heat release. The transient heat flux experiments [7.8] support this approximate estimation of the heat loss distribution for conventional water-cooled engines.

7.2.5 COMBUSTION

To model the actual chemical combustion mechanism taking into consideration all the spatial and kinetic variables and so produce a time and space dependent heat release model is at present an extremely difficult task. However, the current alternative approach is to use experimentally determined heat release diagrams and obtain mathematical expressions that conform to these diagrams. Apparent heat release equations are thus achieved without detailing the combustion reaction kinetics. This method avoids true combustion modelling. It is purely an experimental approach with only limited fundamental theoretical support.

the ignition delay period is calculated based on the theory by Wolfer [7.9]

$$\delta(ms) = a_1 \exp\left(\frac{a2}{Tm}\right) P_m^{a3} \qquad (7.3)$$

from which ignition timing can be determined.

The apparent rate of fuel burning is determined from the correlation by Watson et. al. based on a form of Wiebe function. The accumulated amount of fuel burning is composed of the premix and the diffusion portions.

$$m_a = m_p + m_d \qquad (7.4)$$

Using the nominal burning duration Δ and the total quantity of fuel injected m_t, the equation is non-dimensionalized as

$$M_t(\tau) = \beta M_p(\tau) + (1-\beta) M_d(\tau) \qquad (7.5)$$

where M_p is the "pre-mixed" burning fraction,

M_d is the "diffusion" burning fraction,

β is the phase proportionality factor of pre-mixed to total burning mass.

$$\beta = \frac{m_p}{m_t}$$

and

$$\tau = (\theta - \theta_i)/\Delta$$

The best representation of the experimental data has been achieved using the following functions

$$M_p(\tau) = 1 - (1 - \tau^{Cp1})^{Cp2} \qquad (7.6)$$

$$M_d(\tau) = 1 - \exp(-Cd1\,\tau^{Cd2}) \qquad (7.7)$$

Furthermore, the correlation of the shape parameters Cp1, Cp2, Cd1 and Cd2 with the basic engine parameters of ignition delay δ, trapped equivalence ratio F_t and engine speed N_e may be established empirically or experimentally. This subroutine has been programmed by Tarabad.

7.2.6 VARIABLE POLYTROPIC EXPONENTS

From the previous relationships (7.5), (7.6) and (7.7), the burning fuel mass in each step within the combustion phase can be obtained. Combined with the heat loss flux, the heat quantity transferred into or out of the system in each phase and each step can be determined.

Thus, the following iteration procedures are used in each step in the combustion phase and in the compression and expansion phases.

(1). calculate the volume of the final state V_2.

(2). calculate the heat quantity Q_{12}, as explained before.

(3). guess a polytropic exponent n.

(4). determine the temperature of the final state T_2 from.

$$T_2 = T_1 \left(\frac{V_2}{V_1}\right)^{(1-n)}$$

(5). calculate the pressure of the final state P_2 from:

if $n \neq 1$

$$P_2 = P_1 \left(\frac{T_2}{T_1}\right)^{\frac{n}{n-1}}$$

if $n=1$

$$P_2 = \frac{P_1 V_1}{V_2}$$

(6). calculate the work along the process.

if $n \neq 1$

$$W_{12} = \frac{P_2 V_2 - P_1 V_1}{1-n}$$

if $n=1$

$$W_{12} = P_1 V_1 \, \mathrm{Log}\left(\frac{V_2}{V_1}\right)$$

(7). calculate the internal energy from the function of thermodynamic properties.

(8). examine the correctness of the supposed polytropic exponent from the first law.

$$f(n) = Q_{12} - W_{12} - \Delta U_{12} = 0$$

(9). If the error lies within a tolerance limit, the calculation in this step or phase ends.

(10). If the error exceeds the limit, correct the supposed polytropic exponent, repeat the calculation from the procedure (3)

These procedures are repeated from the compression, through the combustion, to the expansion phases. Thus, a series of polytropic

processes with constant exponents approximate the real process with continually variable exponents, as shown in Fig. 7.1.

7.2.7 ENGINE FRICTION

From the generated pressure - crank angle diagram, the cycle simulation programs are able to calculate the indicated work output. To determine the brake power output, the power loss due to friction must be calculated. Experimentally the most satisfactory method of determing the frictional power loss is to subtract the measured brake power from the indicated work. If no accurate pressure measuring device is available, the best alternatives are the Morse test and Willans line method.

From experimental tests, researchers have deduced empirical formulae for the frictional mean effective pressure (FMEP) as functions of engine speed and cylinder pressure. The formulae by S.K. Chen and Flynn [7.10] developed for turbocharged engines and by F.J. Wallace and Wright for the TS3 two-stroke opposed piston engine [4.15] are optional in programs.

$$FMEP = A + B \cdot P_{max} + C \cdot V_p \qquad (7.8)$$

where P_{max} is the maximum cylinder pressure
V_p is the mean piston velocity
and A, B and C are empirical constants for particular engines.

The FMEP is thus used to calculate the frictional power loss, due to all the the moving engine components. A fraction of this power loss is due to the sliding contact of the piston rings with the liner. The heat generated at the rings can therefore be estimated and used in the above mentioned heat transfer resistance network.

7.2.8 GAS EXCHANGE

In program CSPS, the flow characteristic of the engine is given in the form of a mapping which is obtained from the experiments.

The simplified analytical scavenging model is used in program CSPS. The

coefficients of intake and discharge proportions and the volumetric ratios of the initial mixing and remaining residual gas zones are determined either empirically or experimentally. This simplified treatment makes program CSPS particularly suitable for rapid cycle calculations, e.g. for parametric studies.

7.2.9 SUMMARY

This model combines simplicity and precision. Compared with the original five-point model [7.3], this model has improved the simulation precision, especially for the running conditions with predominantly premix combustion, because the five-point model only took diffusion combustion into consideration and neglected premix combustion. This model also discards the demand for a correcting engine diagram factor, whereas the five-point model needs the diagram factor to improve precision.

7.3 STEP-BY-STEP ENGINE MODELS (CSP3Z AND CSPMZ)

7.3.1 SOME CONCEPTS

These two programs can give a step-by-step description of cycle simulation. Programs CSP3Z and CSPMZ are based on the emptying and filling cencept [7.4] in which the inlet and exhaust manifolds and cylinders are treated as control volumes with simultaneous gaseous inflows and outflows. The manifolds are treated as simple receivers specified by their volumes alone with neglect of heat transfer. The cylinders are also treated as simple volumes, but with variable volumes and surface areas. The simplifyinging assumptions of the inlet and exhaust manifolds as mere receivers rather than a complex pipe system substantially reduce the complexity of the programs, and hence computing costs. However, these simplications mean that the pressures in each volume are spatially uniform and temporally variable. The models ignore the effect of pressure wave propagation.

Programs CSP3Z and CSPMZ have been developed on the basis of program CSP which is a program based on the "emptying and filling" method for four-stroke diesel engine by Tarabad [4.14]. In this thesis, the attention will be concentrated on author's own work. The equations of energy and mass conservations bave been introduced in Chapters 3 and 4. Their

detailed treatment in the programs has be described in the literature. [4.14]. [7.11] Programs CSP3Z and CSPMZ use the same submodels for piston-crank mechanism, combustion and engine friction as those in program CSP.

7.3.2 GAS PROPERTIES

The equibrium thermodynamic properties of the products of combustion of CnH2n and air were calculated by Newhall and Starkman [3.4], using the data from the JANAF table. These values were converted to reference temperature of 0 K by Krieger and Borman [7.12] to obtain mathematical expressions for the internal energy, gas constants and their partial derivatives as functions of temperature, pressure and equivalence ratio. The lean side formulation is in terms of normal interest in diesel engine practice. The rich side formulation is in terms of a single equation for each of a selected number of equivalence ratios. These relatively complex expressions are suitable for a step-by-step description in programs CSP3Z and CSPMZ for improving prediction accuracy.

7.3.3 HEAT TRANSFER

The heat flow path between the working gas and the engine coolant may be divided into three parts:

(1). gas to wall
(2). conduction through the wall
(3). wall to coolant

For the first part, the intermittent process inside the combustion chamber is very complex, involving rapidly varying gas pressure and temperature and local fluid velocities which are in turn functions of engine speed, load, injection characteristics and chamber design. In programs CSP3Z and CSPMZ, the Woschni bulk heat transfer correlation [3.5] is used to calculate the instantaneous convective heat transfer from gas to wall. For the third part, an empirical bulk heat transfer coefficient is used. For the second part, two-dimensional or three-dimensional heat flux models using the finite element method could be considered. However, the complexity and computing time and storage requirements of such models, in relation to the

rest of the simulation program, render their use impractical with a "single zone" combustion model, which implicitly ignores spatial variations in gas temperature. Hence, the concept of one-dimensional steady-state heat flux is used. In the one-dimensional model, increasing the number of surfaces will improve the definition of temperature distribution, but will add to the complexity of data input and increase the computer time. The equivalent network of thermal resistance used is a trade-off between these factors, as shown in Fig. 7.2.

This one-dimensional model assumes that at a specified running condition the wall surfaces of piston, cylinder and head operate with constant and uniform temperatures and heat transfer coefficients respectively since the heat capacity of the surface material is normally large enough to heavily dampen the temperature fluctuations. In the network in program CSP the piston is treated as a star element with fixed thermal resistances, while in CSP3z and CSPMZ the piston is treated as a Delta element with variable thermal resistances. In CSP, the determination of the thermal resistance of the star element, in principle, can be obtained by the finite element method, but, actually, is difficult especially for a range of piston surface temperatures, because with variation of surface temperatures the resistances are changed. The suggested treatment of the Delta element can embody the dependence of heat flux upon surface temperates.

The heat conduction in the piston is a three-dimensional problem with a complex configuration and boundary conditions. Therefore, it is necessary to make the following assumptions.

(1). A "most approximate" solid circular cylinder of finite length is used to simulate the real configuration.
(2). The temperatures of the piston gas, liner and oil side surfaces are different, but respectively constant and uniform.

This produces a simple steady state heat conduction problem with a cylindrical coordinate system. The solution of the general heat conduction problem gives a temperature distribution from which the net heat flux through each side surface can be determined. However, it is difficult to decide what the individual contributions of heat flux are. In other words, the net heat fluxes, Qg, Ql and Qo, can be determined easily, while the heat flux

contributions. Qgl. Qlo and Qgo. are difficult to determine. Therefore. the Delta element denoting the piston has three branches through which the net heat fluxes flow. as shown in Fig. 7.2.

There is a heat flux balance at each junction. From the three major junctions. under the specified flow directions shown in Fig. 7.2. the following equations can be obtained

for junction I.

$$Q_g = Q_{pg} \qquad (7.9)$$

for junction II.

$$Q_l + Q_{lw} = Q_{lg} + E_{fr} \qquad (7.10)$$

for junction III.

$$Q_o + Q_{co} = 0 \qquad (7.11)$$

where Q_g is the net heat flux through the piston gas side surface.
Q_l is the net heat flux through the piston liner side surface.
Q_o is the net heat flux through the piston oil side surface.
Q_{pg} is the convective heat flux through the piston gas side.
Q_{lg} is the heat flux through the liner gas side.
Q_{lw} is the heat flux through the liner into cooling water.
Q_{co} is the heat flux through the piston into cooling oil.
for these heat fluxes. the positive directions are specified as those shown in Fig. 7.2,
and E_{fr} is the heat loss due to friction between piston and liner.

After substitution of the resistances R1. R2 and R8. the set of equations (7.9). (7.10) and (7.11) become

$$Q_g = Q_{pg} \qquad (7.12)$$

$$Q_l + \frac{T_{lg} - T_{cw}}{R_1 + R_2} = Q_{lg} + E_{fr} \qquad (7.13)$$

$$Q_o + \frac{T_{po} - T_{co}}{R_8} = 0 \qquad (7.14)$$

Using cyclic integration, the total convective heat flux transferred per cycle, Q_{pg} and Q_{lg}, can be calculated for each wall of the combustion chamber. And the heat loss flux due to friction between ring and liner is a certain fraction of the friction work loss. The model treats the thermal resistances from wall to coolant as constant. Thus, to solve the previous set of three non-linear equations needs the knowledge of the relationship between net heat fluxes and surface temperatures in the piston.

Under the above simplifying assumptions, when the temperatures of all the piston side surfaces are given, the temperature distribution throughout the piston can be determined by a solution of the heat conduction equation using the separation method in the form of Bessel's function. Then from the Fourier law of heat conduction the net heat fluxes through all the side surfaces Q_g, Q_l and Q_o can be obtained. The details of the solution of the heat conduction equation are explained in Appendix III.

Summarizing, the procedures for heat transfer are as follows.

(1). estimate the temperatures of the combustion chamber.
(2). calculate the cycle average convective heat transfer rates to each wall of the combustion chamber.
(3). guess the temperatures of the three side surfaces of the piston.
(4). calculate the net heat fluxes through the piston side surfaces, Qg, Ql and Qo.
(5). solve the equation system (7.12), (7.13) and (7.14) to obtain the temperatures of each element.
(6). if the temperature errors are within the limit, the iteration of the inner loop ends, continue procedure (8).
(7). if the temperature errors are beyond the limit, correct the temperatures and repeat the iteration of the inner loop from procedure(4).
(8). update the temperatures, repeat the iteration of the outer loop from procedure (2) until the calculation converges.

In the inner loop in program CSP3Z and CSPMZ, the Gauss-Seidel iteration method is used for solving the set of non-linear equations.

The other thermal resistances in the network are determined by component dimensions and material properties, or boundary conditions of the cooling system. [7.11] The suggested resistance network describes the dependence of heat flux on surface temperatures of the piston. Thus, this heat transfer model can directly give an estimation of the heat flux and component temperatures for various engines, including thermally insulated engines.

7.3.4 GAS EXCHANGE

In programs CSP3Z and CSPMZ, the flow characteristics of the engine are calculated based on the compressible fluid equations in which the discharge coefficient correlation by Wallace and Mitchell [3.6] is quoted.

The step-by-step three-zone thermodynamic scavenging model in Chapter 3 is used in program CSP3Z. This scavenging model makes program CSP3Z able to provide a step-by-step description and to simulate all the scavenging processes: uniflow, loop and cross scavenging systems subject to the proper and empirical choice of the flow and concentration field parameters.

The multi-zone unsteady jet model in Chapter 4 is used in program CSPMZ. This scavenging model allows program CSPMZ to predict the performance only for uniflow scavenging system and at the expense of computation cost.

7.4 CRITIQUE OF PROGRAM CSPS, CSP3Z AND CSPMZ

The author has developed these three programs, from simple to complex, CSPS, CSP3Z and CSPMZ. In these programs, there is a rather balanced level of sophistication in the calculation for the various individual processes: gas exchange, heat transfer and combustion.

The simple program CSPS is composed of three simple submodels: the combustion model with large step length based on variable polytropic exponents, the scavenging model based on the analytical isobaric and isochoric thermodynamic process and the heat transfer model based on an empirical correlation. This simplicity allows program CSPS to give a quick

and easy calculation suitable for predicting the overall performance of a compound engine system over all the operating range. The precision of the prediction relies on the choice of the scavenging parameters. The simple heat transfer model for the water-cooled engine in CSPS makes this program unable to predict the performance in thermally insulated engines. Improvements in predicting the scavenging and heat transfer processes are dependent on experiments and advanced analytical models.

The middle-level program CSP3Z is composed of submodels with middle-level complexity: the step-by-step description of all processes, the three-zone thermodynamic scavenging model and the heat transfer model with variable thermal resistance of the piston. The step-by-step method can predict the effect of port timing on supercharging. The three-zone scavenging model enables program CSP3Z to predict performance for the different scavenging systems, including cross, loop and uniflow systems, provided the proper parameters of the exhaust history are chosen. The heat transfer model can estimate the heat flux and temperature in each element for conventional and insulated engines.

Instead of the three-zone scavenging model, the complex program CSPMZ uses the complex multi-zone unsteady jet scavenging model. This scavenging model allows program CSPMZ to fully predict the uniflow scavenging process.

A comparison between the computational results with programs CSP3Z, CSPS and the five-point engine model [7.3] has been conducted for estimating their precision. The computed engine is the differential compound engine using a two-stroke opposed piston engine as an alternative for the present DCE with a four-stroke engine. The only difference of the latter two cases is that in the engine programs, one uses the engine model of variable polytropic exponents above described, the other uses the five-point engine model. Tables 7.1 to 7.3 list the computed results with these programs. For CSPS and the five-point engine model, the engine diagram factor is set to 1. Compared with the results from CSP3Z, the discrepancy of the results of the output power and efficiency from CSPS is within 4 %, whereas from the five-point engine model is within 8 %, which originates from the oversimplified combustion submodel. For the exhaust temperature, the maximum difference from CSPS is 130 K, while from the five-point engine

model is 230 K.

7.5 CONCLUSIONS

It is notable that the more complex the model, the more computation time the program needs. The computation time per cycle program CSP3Z requires is about one order of magnitude higher than CSPS, and the computation time with CSPMZ is a further order of magnitude higher than CSP3Z.

Each of the three programs is suitable for particular applications, depending on the compromise which is to be made between the ability to predict the process in detail and computation time.

Program CSPS is suitable for predicting overall performances of an engine compounding system. The behaviour of heat transfer is based either on experiments or on the results of simulation using program CSP3Z.

Program CSP3Z is appropriate for estimating the effect of port timing on supercharging and predicting heat transfer for conventional and insulated engines. The performance of the scavenging process is estimated based on either experiment or simulation with CSPMZ.

Program CSPMZ in a single cylinder version is suitable for predicting the scavenging performance of a uniflow scavenging system in detail.

REFERENCES

[7.1]. C.F. Hirshfeld and W.N. Barnard
"Elements of Heat Power Engineering"
John Willey and Sons, 1915

[7.2]. R.L. Hersey, J.E. Eberhardt and H.C. Hottel
"Thermodynamic Properties of the Working Fluid in Internal Combustion Engines"
SAE Transactions, 31, 409, 1936

[7.3]. R.J.B. Way and F.J. Wallace
"Notes on Engine Performance Analysis"
School of Engineering, University of Bath, 1977

[7.4]. K.J. McAulay, T.C. Wu, S. Chen, G.L. Borman, O.A. Uyehara and P.S. Myers
"Development and Evaluation of the Simulation of the Compression Ignition Engines"
SAE Transaction, 1966

[7.5]. A.D. Gosman, Y.Y. Tsui and A.P. Watkins
"Calculation of Three-Dimensional Air Motion in Model Engines"
SAE 840229, 1984

[7.6]. T.W. Kuo and R.C. Yu
"Modelling of Transient Evapovating Spray Mixing Process - Effects of Injection Characteristics"
SAE 840226, 1984

[7.7]. N. Watson, M. Marzouk and A.D. Pilley
"A Combustion Correlation for diesel Engine Simulation"
SAE 800029, 'diesel Combustion and Emissions' SP86, 1980

[7.8]. N.D. Whitehouse
"Heat Transfer in a Quiscent diesel Engine"
Proc. I. Mech. E. Vol. 185, 1970-71

[7.9]. H.H. Wolfer
"Der Zunderzug im diesel Motor"
CDI Forschungsheft 392, 15-24, 1938

[7.10]. S.K. Chen and P.F. Flynn
"Development of a single Cylinder Compression ignition Research Engines"
SAE 650733, 1965

[7.11]. A.C. Cole
"diesel Engine Thermal Insulation"
Ph.D. Thesis, Unidersity of Bath, 1986

[7.12]. R.B. Krieger and G.L. Borman
"The Computation of Apparent Heat Release for Internal Combustion Engines"
ASME 66-WA/DGP-4, 1966

Table 7.1 Computed Results Based on Step-by-Step Three Zone Model

ROOTES TS3 DCE

number of cylinders	3.0	bore (m.m.)	94.98	stroke (m.m.)	33 88 56 24			233.53
con-rod length (m.m.)	109.55	inlet valve closing (degs)	55.6	compressor scale factor				1.15
ambient temperature (deg k)	294.4	ambient pressure (bar)	0.99	cooler effectiveness				0.8320
compression ratio	14.00	engine diagram factor	1.0000	turbine flow loss factor				0.8000
engine speed(r.p.m)	2522.00	2178.00	2230.00	1738.00	1925.00	1087.00	1533.00	778.00
boost pressure ratio	3.110	2.070	3.300	1.890	3.490	1.950	4.830	2.070
trapped air to fuel ratio	25.350	22.020	26.450	23.080	27.370	31.170	25.710	36.290
delivery ratio	0.691	0.536	0.801	0.532	1.004	1.085	1.218	1.700
manifold temp (deg k)	343.000	331.000	345.000	331.000	347.000	328.000	365.000	329.000
engine power (k w.)	271.24	144.41	270.51	97.26	258.94	69.53	301.27	55.82
engine torque (n.m.))	1027.00	633.20	1158.50	534.40	1284.50	610.70	1876.20	685.40
b.m.e.p (bar)	13.0200	8.0200	14.6800	6.7700	16.2800	7.7400	23.7800	8.6900
s.f.c. (kg/kw hr)	0.211	0.231	0.208	0.242	0.208	0.226	0.211	0.225
b.thermal eff.	0.3983	0.3636	0.4045	0.3482	0.4038	0.3719	0.3993	0.3733
fuel / rev / cyl (g.)	0.133	0.085	0.140	0.076	0.156	0.080	0.223	0.090
max cyl pressure (bar .)	138.13	98.70	158.21	93.74	128.76	94.71	162.45	106.13
exhaust temperature(deg k)	789.00	843.00	740.00	796.00	724.00	606.00	746.00	483.00
mass flow (kg/s)	0.462	0.209	0.512	0.154	0.562	0.213	0.803	0.255
compressor speed (r.p.m.)	5429.0	2773.0	5980.0	2209.0	6510.0	2808.0	9131.0	3232.0
compressor pressure ratio	3.210	2.100	3.450	1.910	3.620	1.980	5.050	2.120
compressor power (kw.)	74.69	24.23	93.60	16.30	109.24	22.75	229.32	28.86
compressor torque (n.m)	131.37	93.44	149.46	70.47	160.22	77.36	239.81	85.26
compressor efficiency	0.721	0.601	0.683	0.567	0.673	0.596	0.604	0.622
by pass valve area (sq.cm.)	0.000	0.000	0.000	0.000	0.000	0.000	0.000	0.000
turbine speed (r.p.m)	47500.0	38250.0	46000.0	29000.0	43500.0	25000.0	41500.0	17000.0
turbine pressure ratio	2.630	1.940	2.760	1.830	2.840	1.980	3.790	1.870
mass flow (kg/s)	0.486	0.228	0.540	0.154	0.562	0.190	0.776	0.247
turbine power (kw)	73.37	27.02	79.30	16.17	83.23	13.26	143.56	11.86
turbine torque (n.m)	14.75	6.75	16.46	5.32	18.27	5.07	33.04	6.66
inlet temperature (deg k)	789.00	843.00	740.00	796.00	724.00	606.00	746.00	483.00
turbine efficiency	0.734	0.750	0.753	0.718	0.760	0.722	0.751	0.622
output shaft speed (rpm)	2500.00	2500.00	2000.00	2000.00	1500.00	1000.00	500.00	500.00
output shaft power (kw)	259.20	143.60	246.50	95.30	220.30	47.80	203.70	36.40
output shaft torque (n./m)	990.00	549.00	1177.00	455.00	1403.00	552.00	3890.00	696.00
output thermal efficiency	0.3806	0.3617	0.3687	0.3411	0.3436	0.3091	0.2700	0.2437
dynamic injection(degree ca)	165.0	160.1	163.7	158.0	175.0	166.8	179.5	168.4
turbine gear ratio	19.00	15.30	23.00	14.50	29.00	25.00	83.00	34.00
output shaft gear ratio	1.388	1.388	1.388	1.388	1.388	1.388	1.388	1.388
charging efficiency	0.634	0.534	0.699	0.530	0.792	0.757	0.849	0.998

1

Table 7.2 Computed Results Based on Variable Polytropic Exponent Model

0ROOTES TS3 DCE

						33	88	56	24
0number of cylinders	3.0	bore (m.m.)	94.98	stroke (m.m.)	233.53				
con-rod length (m.m.)	109.55	inlet valve closing (degs)	55.6	compressor scale factor	1.15				
ambient temperature (deg k)	294.4	ambient pressure (bar)	0.99	cooler effectiveness	0.8320				
compression ratio	14.00	engine diagram factor	1.0000	turbine flow loss factor	0.8000				
0engine speed(r.p.m)	2522.00	2178.00	2230.00	1738.00	1925.00	1087.00	1533.00	778.00	
boost pressure ratio	3.088	2.052	3.304	1.916	3.542	2.021	4.767	2.207	
trapped air to fuel ratio	24.797	20.482	27.268	21.092	28.273	35.706	29.681	44.464	
delivery ratio	0.634	0.485	0.749	0.485	0.880	0.952	1.253	1.454	
manifold temp (deg k)	324.059	304.347	328.987	312.792	333.560	304.137	359.843	306.166	
engine power (k w.)	272.89	142.53	272.33	96.04	257.31	68.78	300.07	55.17	
engine torque (n.m.))	1026.34	631.80	1157.85	534.19	1283.94	611.47	1876.43	684.68	
b.m.e.p (bar)	13.0780	7.9095	14.7603	6.6789	16.1559	7.6480	23.6586	8.5703	
s.f.c. (kg/kw hr)	0.209	0.246	0.199	0.257	0.206	0.226	0.205	0.220	
b.thermal eff.	0.3983	0.3392	0.4188	0.3248	0.4043	0.3683	0.4059	0.3794	
fuel / rev / cyl (g.)	0.126	0.089	0.135	0.079	0.153	0.080	0.223	0.087	
max cyl pressure (bar .)	138.14	88.64	158.71	81.92	138.24	90.74	170.23	102.78	
exhaust temperature(deg k)	895.43	966.45	812.57	897.67	793.03	553.18	763.23	460.83	
mass flow (kg/s)	0.436	0.204	0.480	0.148	0.515	0.197	0.729	0.233	
percentage heat to coolant	12.41	19.04	12.26	22.99	12.20	25.51	10.33	26.69	
0compressor speed (r.p.m.)	5429.2	2836.0	5944.5	2235.6	6361.9	2761.2	8839.9	3148.4	
compressor pressure ratio	3.295	2.119	3.550	1.952	3.817	2.083	5.267	2.288	
mass flow (kg/s)	0.436	0.204	0.480	0.148	0.515	0.197	0.729	0.233	
compressor power (kw.)	75.36	24.04	93.42	16.40	110.95	22.87	225.58	29.26	
compressor torque (n.m)	132.50	80.90	150.01	70.04	166.47	79.04	243.58	88.72	
delivery temperature (deg k)	466.08	411.87	487.45	405.09	507.82	410.20	598.83	419.25	
compressor efficiency	0.695	0.601	0.663	0.562	0.640	0.594	0.579	0.630	
by pass valve area (sq.cm.)	0.000	0.000	0.000	0.000	0.000	0.000	0.000	0.000	
0turbine speed (r.p.m)	47500.0	38250.0	46000.0	29000.0	43500.0	25000.0	41500.0	17000.0	
turbine pressure ratio	2.690	1.943	2.743	1.853	2.888	1.899	3.708	2.026	
mass flow (kg/s)	0.452	0.214	0.495	0.155	0.530	0.201	0.746	0.237	
turbine power (kw)	77.45	26.80	78.19	16.01	85.54	13.48	137.20	12.85	
turbine torque (n.m)	15.56	6.69	16.22	5.27	18.77	5.15	31.56	7.22	
inlet temperature (deg k)	895.43	966.45	812.57	897.67	793.03	553.18	763.23	460.83	
turbine nozzle angle	8.868	6.189	9.059	4.465	9.073	4.424	9.753	4.360	
turbine efficiency	0.756	0.732	0.757	0.698	0.760	0.714	0.753	0.637	
output shaft speed (rpm)	2500.00	2500.00	2000.00	2000.00	1500.00	1000.00	500.00	500.00	
output shaft power (kw)	256.15	136.01	239.49	89.30	218.66	55.47	195.99	36.13	
output shaft torque (n./m)	978.01	519.30	1143.02	426.22	1391.43	529.50	3741.63	689.82	
output shaft sfc (kg/kw.hr)	0.223	0.258	0.226	0.276	0.243	0.281	0.315	0.336	
output thermal efficiency	0.3739	0.3237	0.3683	0.3020	0.3436	0.2971	0.2651	0.2485	
engine fuel flow (kg/s)	0.952	0.584	0.904	0.411	0.885	0.260	1.028	0.202	
dynamic injection(degree ca)	165.0	160.1	163.7	158.0	175.0	166.8	179.5	168.4	
duration of injection	0.0	0.0	0.0	0.0	0.0	0.0	0.0	0.0	
turbine gear ratio	19.00	15.30	23.00	14.50	29.00	25.00	83.00	34.00	
output shaft gear ratio	1.388	1.388	1.388	1.388	1.388	1.388	1.388	1.388	
charging efficiency	0.572	0.474	0.641	0.474	0.713	0.747	0.875	0.933	

1

Table 7.3 Computed Results Based on Five-Point Diesel Cycle Model

0ROOTES TS3 DCE

0number of cylinders	3.0	bore (m.m.)	94.98			35 81 87 24 stroke (m.m.)			233.53
con-rod length (m.m.)	109.55	inlet valve closing (degs)	55.6			compressor scale factor			1.00
ambient temperature (deg k)	294.4	ambient pressure (bar)	0.99			cooler effectiveness			0.8235
compression ratio	14.00	engine diagram factor	1.0000			turbine flow loss factor			0.8000
0engine speed(r.p.m)	2522.00	2178.00	2230.00	1738.00	1925.00	1087.00	1533.00	778.00	
boost pressure ratio	3.061	1.695	3.272	1.564	3.510	1.950	4.740	2.126	
trapped air to fuel ratio	25.114	18.297	28.011	21.820	29.977	24.930	31.579	29.343	
delivery ratio	0.611	0.530	0.739	0.537	0.884	0.975	1.304	1.549	
manifold temp (deg k)	322.051	299.588	327.134	299.524	331.460	302.878	360.590	305.983	
engine power (k w.)	273.00	111.38	272.33	71.28	260.38	68.91	300.12	55.16	
engine torque (n.m.))	1026.34	496.22	1157.85	398.61	1283.94	611.47	1876.43	684.68	
b.m.e.p (bar)	13.0834	6.1810	14.7604	4.9570	16.3486	7.6618	23.6621	8.5687	
s.f.c. (kg/kw hr)	0.201	0.315	0.191	0.307	0.192	0.319	0.195	0.329	
b.thermal eff.	0.4150	0.2649	0.4356	0.2720	0.4340	0.2613	0.4271	0.2532	
fuel / rev / cyl (g.)	0.121	0.089	0.130	0.070	0.144	0.112	0.212	0.130	
max cyl pressure (bar .)	171.98	99.32	195.57	84.98	150.76	118.13	167.40	132.13	
exhaust temperature(deg k)	870.52	1070.47	782.28	863.69	739.01	749.74	719.03	615.13	
mass flow (kg/s)	0.419	0.187	0.472	0.140	0.516	0.195	0.752	0.240	
percentage heat to coolant	12.63	20.97	12.43	25.83	12.35	24.80	10.36	25.57	
0compressor speed (r.p.m.)	5912.6	2877.5	6604.0	2263.2	7180.8	3055.0	10257.6	3596.4	
compressor pressure ratio	3.253	1.757	3.508	1.601	3.783	2.013	5.270	2.212	
mass flow (kg/s)	0.419	0.187	0.472	0.140	0.516	0.195	0.752	0.240	
compressor power (kw.)	69.36	16.14	87.94	10.14	106.15	21.27	222.36	28.22	
compressor torque (n.m)	111.98	53.53	127.10	42.78	141.11	66.45	206.92	74.90	
delivery temperature (deg k)	458.75	380.50	479.24	366.96	498.43	402.88	585.47	411.66	
compressor efficiency	0.717	0.600	0.685	0.587	0.664	0.602	0.607	0.641	
by pass valve area (sq.cm.)	0.000	0.000	0.000	0.000	0.000	0.000	0.000	0.000	
0turbine speed (r.p.m)	47500.0	38250.0	46000.0	29000.0	43500.0	25000.0	41500.0	17000.0	
turbine pressure ratio	2.702	1.582	2.733	1.506	2.857	1.828	3.634	1.938	
mass flow (kg/s)	0.435	0.197	0.487	0.146	0.530	0.202	0.769	0.245	
turbine power (kw)	72.36	19.28	73.33	10.23	78.75	16.83	132.64	15.93	
turbine torque (n.m)	14.54	4.81	15.22	3.37	17.28	6.42	30.51	8.94	
inlet temperature (deg k)	870.52	1070.47	782.28	863.69	739.01	749.74	719.03	615.13	
turbine nozzle angle	8.370	8.288	8.771	5.714	8.841	5.377	9.943	5.475	
turbine efficiency	0.753	0.729	0.753	0.724	0.759	0.691	0.761	0.605	
output shaft speed (rpm)	2500.00	2500.00	2000.00	2000.00	1500.00	1000.00	500.00	500.00	
output shaft power (kw)	230.84	80.64	219.05	44.83	200.79	49.50	188.51	34.53	
output shaft torque (n./m)	881.38	307.89	1045.45	213.95	1277.72	472.53	3598.70	659.19	
output shaft sfc (kg/kw.hr)	0.238	0.435	0.238	0.488	0.249	0.444	0.311	0.526	
output thermal efficiency	0.3509	0.1918	0.3504	0.1711	0.3347	0.1878	0.2682	0.1585	
engine fuel flow (kg/s)	0.915	0.585	0.869	0.364	0.834	0.367	0.977	0.303	
dynamic injection(degree ca)	165.0	160.1	163.7	158.0	175.0	166.8	179.5	168.4	
duration of injection	13.0	7.9	11.7	6.0	13.0	4.8	14.5	4.4	
turbine gear ratio	19.00	15.30	23.00	14.50	29.00	25.00	83.00	34.00	
output shaft gear ratio	1.350	1.350	1.350	1.350	1.350	1.350	1.350	1.350	
charging efficiency	0.558	0.505	0.636	0.510	0.714	0.760	0.892	0.957	

1

boost ratio = 3.0878 exhaust ratio = 2.6901
fuel mass (g/cyl/cycle) = 0.1256 heat loss percentage = 0.1241

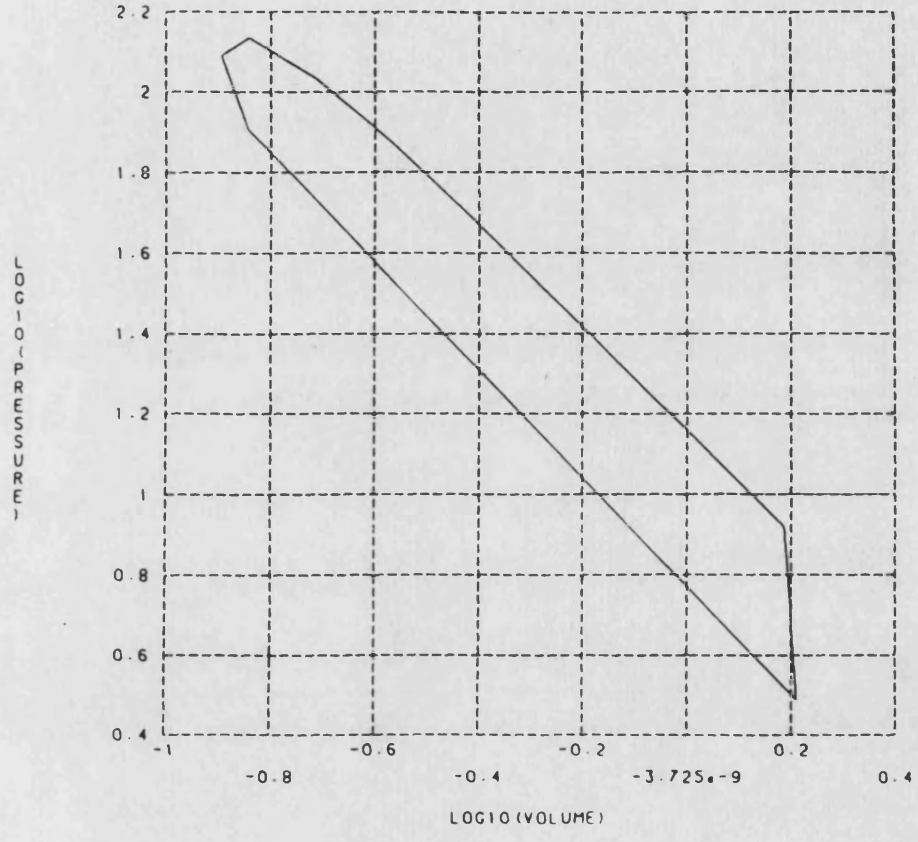

cyl. vol (lit.)	pres. (bar)	temp. (K)	poly. index	heat rel. rate
1.6268	3.0665	443.6357	1.3477	-0.0124
0.1628	68.2047	987.5500	1.3477	0.0000
0.1431	81.1759	1032.9161	3.6237	0.2280
0.1273	124.0980	1404.5327	-0.8551	0.3202
0.1436	137.6022	1757.3360	0.8020	0.2110
0.1921	108.9668	1861.5360	1.0901	0.0964
0.2709	74.9261	1804.7985	1.1993	0.0335
0.3761	50.5354	1690.4441	1.2482	0.0092
0.5023	35.2245	1573.3830	1.2683	0.0020
0.6423	25.7854	1472.9079	1.2994	-0.0124
1.5367	8.3007	1134.3351	1.2994	0.0000

Fig. 7.1 Logarithmic PV Diagram

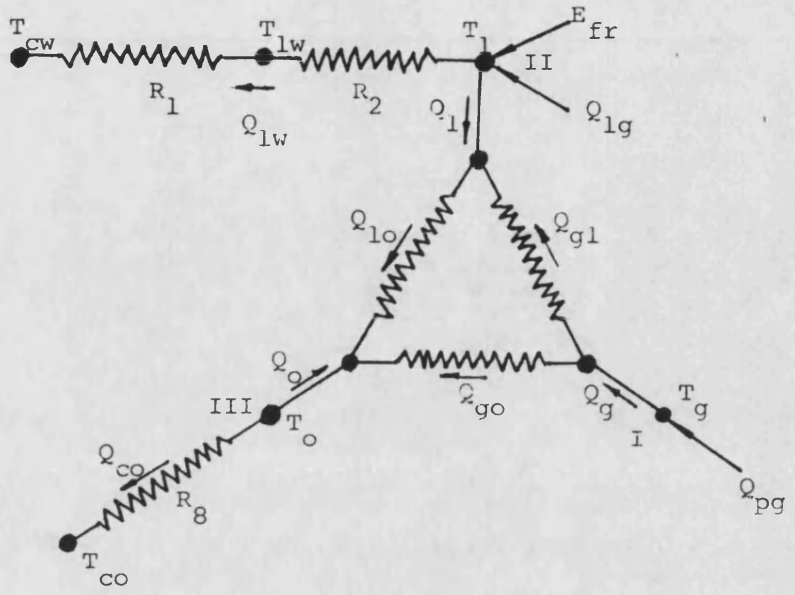

Suffices as used with temperature (T) and heat flux (Q)

g	piston, gas side surface,
l	piston, liner side surface,
o	piston, oil side surface,
co	cooling oil,
cw	cooling water,
fr	friction between piston and liner,
gl	piston, from gas to liner side surface,
go	piston, from gas to oil side surface,
lo	piston, from liner to oil side surface,
lg	liner, gas side surface,
lw	liner, cooling water side surface,
pg	piston, gas side surface.

Fig. 7.2 Thermal Resistance Network

Chapter 8 APPLICATIONS OF THE TWO-STROKE DIESEL ENGINE MODELS

8.1 INTRODUCTION

In a conventional diesel engine, approximately one-third of the total fuel input energy is converted to useful work. A major part of the energy is rejected with the exhaust gases which are discharged at high temperature. Another major part of the energy is lost in the form of heat via the cooling system. For the conventional diesel engine, if only its cooling system is moved away, the wall temperature will rise, thus still a considerable amount of energy may be lost through the walls. To depress the heat loss, the walls must be thermally insulated. Therefore, limited cooled or uncooled insulated engines have been proposed.

It is expected that the thermally insulated engines possess the following advantages.

(1). improved engine efficiency: Such designs can reduce the parasitic losses associated with the cooling system. Due to the thermal insulation of the engine extra energy will be available at the exhaust which can be recovered through a compounding system.
(2). reduced engine-package volume: This is attributed to the elimination or at least the reduction of the size of the radiator and cooling system.

However, the thermal insulation will further increase the temperature of the walls due to the hot combustion gases. During the scavenging process the wall temperature is now considerably greater than that of the air charge which is expected to be detrimental to the engine volumetric efficiency due to the increased wall-to-charge heat transfer.

Compared with the four-stroke engines, the heat flow rate through the combustion chamber walls of the two-stroke engines is much greater, because in the two-stroke engines the injected fuel mass is almost twice of that in the same sized four-stroke engines running at the same boost, air-fuel ratio and speed. Therefore, the same insulation measure will reduce much more heat loss for the two-stroke engines than that for the four-stroke engines. [8.1] Correspondingly, the component temperatures are also substantially higher. But the geometry of the wholly ported two-stroke engine lends itself substantially better to ceramic material than the valved

engines. On the other hand, it is expected that compared with the four-stroke engine the two-stroke engine has a shorter gas exchange period, i.e. the shorter duration of wall-to-charge heat transfer, which lessens the influence of the hot walls on the volumetric efficiency, and that compared with two-stroke engines with other scavenging systems the uniflow scavenging system should have a better volumetric efficiency, because this system considerably reduces the "dead space" in which the charge heated by the hot wall is reduced to a low density at a given scavenging pressure.

The majority of the research work on insulated engines has been concentrated on the four-stroke engine, [8.2], [8.3], [8.4], [8.5], while the Ford Co. has been developing a ceramic uncooled two-stroke opposed-piston diesel engine. The performance predictions have been made mainly for four-stroke engines. The thermodynamic rate engine models have been successfully used for the optimization of the valve timing for four-stroke engines [7.3], but not satisfactorily for the optimization of the port timing. The reason is that for a four-stroke engine the scavenging period is short and the scavenging process occurs near the top dead centre at which the cylinder volume is a minimum, hence the four-stroke engine is not sensitive to the scavenging model, whilst for a two-stroke engine the scavenging process occurs near the bottom dead centre at which the cylinder volume is a maximum, hence the two-stroke engine is sensitive to the scavenging model. Therefore, the optimization of the port timing for the two-stroke engines needs a scavenging model with predictably. The phenomenological unsteady jet model provides the possibility for the uniflow scavenged two-stroke engines.

The objects of this chapter are to predict the performance of the Ford ceramic two-stroke opposed-piston diesel engine and to optimize the port timing. It is notable that according to the requirement of the Ford Co. the definitions of delivery ratio λ and charging efficiency η_{ch} use the SAE terminology:

$$\lambda = \frac{\text{Mass of delivered air}}{\text{Displaced volume} \cdot \text{ ambient density}} \qquad (8.1)$$

$$\eta_{ch} = \frac{\text{Mass of delivered air retained}}{\text{Displaced volume} \cdot \text{ ambient density}} \qquad (8.2)$$

8.2 PERFORMANCE PREDICTION OF THE CERAMIC UNCOOLED ENGINE

8.2.1 ENGINE SPECIFICATIONS

The Ford newly designed engine is a small partially thermally insulated single-cylinder diesel engine.

The major characteristics of the engine are:

two-stroke opposed piston engine layout, as shown in Fig. 8.1.

bore= 58 mm
stroke= 124.8 mm
compression ratio= 22
displacement= 0.33 litre
uncooled system with monolithic pistons and cylinder of silicon nitride with thermal conductivity of 12 W/m·K.

port timing- exhaust port opening 75 BBDC
inlet port opening 44 BBDC
exhaust port closing 50 ABDC
inlet port closing 67 ABDC

8.2.2 METHOD OF PREDICTING PERFORMANCE

The performance prediction is based on calculation and comparison with the baseline engine. The baseline engine is a water-cooled engine with the same size and configuration, and at the same running conditions.

The heat transfer coefficient suggested by the Ford Co., as shown in the Fig. 8.2, is used for calculating the heat transfer from wall to coolant of the uncooled engine, whereas the correlation by Howarth [8.6] is used for calculating the heat transfer from wall to water of the water-cooled engine. The calculation of heat conduction through the wall is based on the heat conductivity of material.

The uncooled friction correlation for ringless piston by the Ford Co. is used for the uncooled engine.

fmep= -12.07 + 0.0471*Ne

where friction mean effective pressure, fmep, is in Kn/m2

engine speed, Ne, in rpm.

The friction formula from Wallace's experiments on the TS-3 two-stroke opposed piston engine, which operates in the speed range from 500 to 2000 rpm, is used for the water-cooled engine.

fmep= 27.0 + 0.005*Pmax + 0.025*Ne

where Pmax is the maximum cylinder pressure,
fmep and Pmax in Kn/m2,
Ne in rpm.

Version 1 of program CSPMZ is used for predicting the performance of the uniflow scavenged engine.

8.2.3 IDENTIFICATION OF COMPUTATION CONDITIONS

Both the uncooled and the water-cooled engines have the same running conditions.

The injection rate is set to 12 c.c. per degree of crankshaft angle per cubic metre of cylinder displacement. The start of combustion is at TDC, as required, for compromising fuel economy and NOx emission reduction.

Full load is defined, as suggested: Air/Fuel ratio= 22, delivery ratio= 1.2
Hence, part loads are defined as
2/3 load: Air/Fuel ratio= 33, delivery ratio= 1.2
1/3 load: Air/Fuel ratio= 66, delivery ratio= 1.2.

The flow characteristics of the engine are computed respectively at delivery ratio= 0.8, 1.0 and 1.2.

The mean surface temperatures of cylinder and pistons are obtained from the calculations themselves.

8.2.4 UNCOOLED ENGINE CALCULATIONS

8.2.4.1 Scavenging performance

With increase of engine speed the ratio of inlet to exhaust pressures, hence

the air flow rate, increases at the same delivery ratio, as shown in Figs. 8.3 and 8.4.

With increase of delivery ratio the charging efficiency improves and the trapping efficiency deteriorates, as shown in Figs. 8.5 to 8.8. Figs. 8.5 and 8.6 show that engine speed has evident influence on charging efficiency and trapping efficiency. The higher the engine speed, the more efficient the scavenging process at the same delivery ratio. The experiments by Taylor et. al. have clearly validated this effect [4.9]. In the phenomenological unsteady jet model the explanation of this effect is as follows. With increase of engine speed the difference between the inlet manifold and the cylinder pressures increases, thus the air flow velocity at the inlet ports increases and after entering the cylinder the air jet expands to a larger section area. The faster jet entrains more residual gas because of the increasing velocity gradient within the shearing layer. And like a larger "air piston", the wider air jet purges residual gas more efficiently. The faster and wider jet flow reflects the increase of the jet initial momentum flux in the entrainment equation by Ricou and Spalding, [4.10] as described in Chapter 4. In the range of delivery ratio from 0.8 to 1.2, the curve family of charging efficiency for this scavenging process just intersect the charging efficiency curve for the perfect mixing scavenging process, as shown in Fig. 8.5. Figs. 8.7 and 8.8 show that the increase of injected fuel only improves the charging and trapping efficiencies slightly.

8.2.4.2 Engine performance

Fig. 8.9 shows the brake horsepower (BHP) under full load. Correspondingly, the brake specific fuel consumption (BSFC) is shown in Fig. 8.10. The brake thermal efficiency (BTE) is mapped in Fig. 8.11. Figs. 8.12 and 8.13 show the increases of the maximum cylinder pressure and mean exhaust gas temperature with increase of engine speed.

Figs. 8.14 and 8.15 depict the increases of mean liner and piston surface temperatures.

The heat balance at full load is shown in Fig. 8.16. It is obvious that with the increase of engine speed the portion of heat loss to liner and pistons decreases, whereas the portion of heat loss to exhaust increases.

8.2.5 WATER-COOLED ENGINE CALCULATIONS

8.2.5.1 Scavenging performance

The water-cooled engine has almost the same air flow characteristics as the uncooled engine. However, because of relatively low trapped temperature, the water-cooled engine has better charging and trapping efficiencies than those of the uncooled engine, as shown in Figs. 8.17 and 8.18.

8.2.5.2 Engine performance

Figs. 8.19 and 8.20 are BHP and BSFC under full load. Fig. 8.21 shows the contours of BTE. Figs. 8.22 to 8.25 are the maximum cylinder pressure, mean exhaust gas, liner and piston surface temperatures.

Fig. 8.26 shows the heat balance at full load.

8.2.6 UNCOOLED ENGINE PREDICTIONS

Compared with the baseline water-cooled engine, the uncooled engine suffers losses from 0.5 to 3 % in charging efficiency due to elevated trapped temperature. The lower the engine speed and delivery ratio, the larger the loss in charging efficiency.

The degree of heat insulation is a function of engine speed and load. With increase of engine speed, degree of heat insulation increases. And the leaner the mixture, the more rapidly the degree of heat insulation increases, as shown in Fig. 8.27. Here, the degree of heat insulation (DHI) is define as,

$$DHI = 1 - \frac{\text{Heat rejection with insulation}}{\text{Heat rejection without insulation}} \qquad (8.3)$$

It is expected that the uncooled engine improves BSFC by an arithmetic mean of 13 %. However, the comparison of BSFC or BTE is uncertain because of the extrapolated engine speed in the friction formula used in the water-cooled engine. Therefore, a comparison of indicated thermal efficiency (ITE) is conducted, as shown in Fig. 8.28. The improvement of the uncooled engine in ITE is in the range from 3 to 6 %, but is not proportional to rate of heat insulation. The explanation is that with increasing engine speed the uncooled engine gains from more efficient reduction of heat losses to pistons and cylinder, and meanwhile, suffers losses from irreversible compression work increasing with piston and liner

surface temperatures.

As a result of the increased charge heating during the intake process and compression stroke, the ignition delays of the uncooled engine is reduced by approximately 10% relative to the water-cooled engine, as shown in Fig. 8.29. The reduction in the amount of premixed combustion implies lower HC and NOx emissions.

The increase in mean exhaust temperature in the uncooled engine varies in the range from 20 to 25 K at full load, and the exhaust gas energy increases by 3 % of the total energy input.

8.2.7 DISCUSSION

The Ford Co. used the perfect displacement and complete mixing scavenging models (program TWOSIM) for the performance prediction of the ceramic uncooled engine. Table 8.1 illustrates a comparison of the computed results. The comparison shows a satisfactory agreement except for exhaust temperatures. It is noted that for the delivery ratio ranging from 0.8 to 1.2 the scavenging efficiency obtained from CSPMZ is located between the scavenging efficiencies of the perfect displacement and complete mixing models from TWOSIM.

For the naturally aspirated four-stroke insulated engine the low volumetric efficiencies are clearly unacceptable (e.g. a typical reduction of the efficiency is 7 % at air-fuel ratio 22:1 and 1000 rpm compared with the baseline water-cooled engine [7.11]), while for the uniflow scavenged two-stroke engine, from the computed results the charging efficiency is reduced by 3 %. It is expected that the uniflow scavenged engine should have this advantage in volumetric efficiency because the inlet air is heated by the hot wall for a shorter time.

8.2.8 SUMMARY

The thermal insulation reduces the heat loss to coolant, increases the exhaust temperature, and generally improves the indicated thermal efficiency. The increased exhaust temperature will increase the useful energy to the turbine. The temperature of the insulated walls rises, and the cylinder pressure slightly increases. The high wall temperature reduces the volumetric efficiency because of heating the incoming charge. The

temperature of the walls during the scavenging and compression processes also affects the ignition delay of the injected fuel. Shorter delay may result in quieter combustion and decrease of the thermal efficiency.

Compared with the four-stroke engine and the two-stroke engine with other scavenging systems, the uniflow scavenged engine is expected to give a better volumetric efficiency because of the shorter time for heating the charge and the smaller "dead space" heated by the hot walls. For a given insulated engine, the degree of heat insulation is dependent on engine speed. The lower the speed, the less the degree of heat insulation because the time of heat transfer to coolant becomes longer. The modified thermal resistance network suggested in Chapter 7 can give an estimation of the component temperature.

8.3 OPTIMIZATION OF PORT DESIGN

8.3.1 ESSENCE OF PORT DESIGN

The objective of port design is to efficiently scavenge residual gas, that is, to trap as much fresh air as possible for combustion with the least loss of useful work, i.e. minimising loss of effective stroke and compressor work. The essence of this task is to provide sufficient port area at the right time with an optimum pressure difference across the ports.

The blowdown period must be long enough to permit residual gas to be expanded to a pressure level which is less than the pressure in the inlet manifold, lest exhaust gases be blown into the inlet manifold. The scavenge period must be long enough to purge the cylinder with fresh air. The charging period must be proper to reach the desired supercharge.

The correct selection of scavenging pressure is important for a scavenging system design. When the scavenging pressure is too low, the longer scavenging duration reduces the effective stroke, hence the engine output. When the scavenging pressure is too high, more power to drive the compressor is expended to produce the higher scavenging pressure. Thus, there exists an optimum timing and a level of scavenging pressure to give the maximum output shaft efficiency.

The optimization of port design is to reconcile these requirements, i.e. to allocate the working and scavenging durations and to fully utilise the limited

scavenging duration at the least expense of useful work.

The mathematical meaning of this optimization is to find a scheme, which has the best output shaft efficiency among all the schemes with various combinations of port shape, port timing and scavenging pressures. The following procedures are used for optimizing port design.

(1). choice of port shape.
(2). optimization of port timing.
(3). size of exhaust port height.
(4). estimation of the effect of inlet port intake angle.

All the configurations used in this optimization are listed in Table 8.2. In all the following predictions, the exhaust manifold pressure is equal to 1.05 bar.

8.3.2 OPTIMIZATION OF PORT DESIGN

8.3.2.1 Choice of engine running condition

For an optimization study, a thorough treatment covering the complete range of speed and load needs a huge volume of computing work. The simplifying treatment for a critical running condition is reasonable and useful. Once a design of opposed-piston engine has been fixed the characteristics of flow sectional area versus crankangle are fixed. With increase of engine speed the time for scavenging is reduced in inverse proportion. Therefore, the problem of output power reduction due to insufficient port areas first occurs at the rated speed of 4000 rpm. With increase of engine load the pressure at the beginning of the blowdown period rises. Therefore, the problem of exhaust backflow into the inlet manifold due to short exhaust lead first happens at full load (air-fuel ratio 22) and rated speed.

Thus, during the optimization, it is stipulated that the engine operates at the full load of air-fuel ratio 22 and rated speed of 4000 rpm, the harshest running condition, which requires the engine to possess the longest exhaust lead and the highest flow capacity.

8.3.2.2 Compressor power

In the previous section, the power to drive the compressor has not been

subtracted from the engine brake power. However, it is necessary for the optimization of port design to take it into consideration, i.e. to give net output shaft thermal efficiency.

The compressor power can be expressed as

$$W_c = \frac{1}{\eta_c} mh_{ad\,c}$$

$$= \frac{1}{\eta_c} mT_{in} R \frac{\gamma}{\gamma-1} \left[\left(\frac{P_{out}}{P_{in}}\right)^{\frac{\gamma-1}{\gamma}} - 1\right] \qquad (8.4)$$

where the compressor efficiency, η_c, is equal to 0.7.

8.3.2.3 Choice of port shape

The inlet and exhaust ports should take a rectangular shape with as large a total width as possible in order to achieve sufficient area for the least scavenging duration.

In the new designs, the total widths of the inlet and exhaust ports are equal to their maximums of 75 and 70 per cent of the circumference respectively. For a specified total port width, the selection of port number implies a bridge width. A perfect theoretical study should based on thermal and stress analysis. As a simple estimation, it is helpful to list the following statistics of similar engines:

bridge width = 3.7 mm for GM 71 engine having 107.95 mm bore.
bridge width = 6.5 mm for TS3 engine having 82.55 mm bore.

The port number of 8 to 10 gives bridge widths of 5.7 and 4.5 mm which are coincident with the above statistics. In the case of angularly directed inlet ports, the effective cross-section width should be multiplied by the cosine of the flow intake angle to the radial. The total width of the exhaust ports is made slightly narrower than that of the inlet ports because of the thermal strain.

Compared with the original configuration O, the modified configuration I, as summarized, together with other configurations in Table 8.2, uses rectangular ports without intake swirl and has the same port timing. The calculated results indicate that configuration I ,i.e. rectangular ports,

provides ample port area, improves the flow capacity, as shown in Fig. 8.30, and increases the trapped air mass, as shown in Fig. 8.31. The increase of the output shaft power, see Fig. 8.32, prevails over the increase of the compressor power, see Fig. 8.33. Consequently, the output shaft efficiency of configuration I improves by 2 %, see Fig. 8.34. From the viewpoint of the relationship between delivery ratio and charging effiiency, the original design is better than configuration I, see Fig. 8.35.

8.3.2.4 Optimization of port timing

Optimizing port timing is to

(1) determine blowdown period,
(2) determine charging period,
(3) determine scavenge period.

8.3.2.4.1 Determination of blowdown period

In all the modified configurations, the exhaust ports have taken the widest rectangular shape, as above described. Therefore, based on the previous step-by-step computational results, the blowdown period, or the exhaust lead, can be determined. From the step-by-step cylinder pressure description of configuration I, it is seen that for the exhaust ports with total width of 0.7 times circumference and height of greater than 9.5 mm the exhaust blowdown takes about 25 degrees. Afterwards, the model results for all configurations II to XI have proven that this exhaust lead is adequate.

8.3.2.4.2 Determination of charging period

Determination of the charging period is not purely theoretical. Table 8.3 below shows the effect of the charging period. From Table 8.3, it is seen that with decrease of speed the trend of charge backflow into the inlet manifold rises, and that compared with the Ford initial design, the optimum scheme with a shorter charging period evidently improves the charging process, but does not avoid a small charge mass backflow into the manifold. Because the emptying and filling method neglected the effect of inertia of intake air flow, the shorter charging period of 5 degrees was used to take it into consideration. With reference to similar opposed piston two-stroke engines, such as the Junkers Jumo 207 and Rootes TS3, 3 to 5 degrees of crank angle should be considered as an ideal charging period.

8.3.2.4.3 Determination of scavenge period

After the determination of blowdown and charging periods, once the scavenge period is decided, the port timing will be determined. Optimising the scavenge period is to minimise engine and compressor losses. The engine power output is affected by both the effective compression and expansion strokes. If the effective compression stroke is shortened, the trapped volume is reduced, thus decreasing the total charge, hence the power output. With decrease of the effective expansion stroke, the energy absorbed by engine is reduced, and the energy loss to exhaust gas rises. Therefore, the improvement of engine power output needs a longer effective stroke. On the contrary, the decrease of compressor power loss requires higher ports, that is, to shorten effective stroke.

The scavenge period can be determined through the comparison of computational results of a group of schemes, configurations II to V, with various scavenging pressures and port timings to find the optimum scheme with best output shaft efficiency.

According to the principle of the least modification in the original design, at first, the trials for restricting the physical variation to port location and size were done. However, under such restriction, it is impossible to obtain the flexibility for changing port timing. The reason is that for a given opposed piston - crank mechanism, the port opening and closing both at the same time are determined by the top edge of the ports. Therefore, adjustment of port positions and dimensions cannot concurrently satisfy the requirements that the blowdown, scavenge and charging period should each vary independently. For example, it cannot extend the blowdown period and shorten the charging period simultaneously. Therefore, the new schemes have changed only the following four elements of the crank piston linkage to obtain the above mentioned blowdown and charging periods and to vary the scavenge period, as in Fig. 8.54.

(1). lower connecting arm length, B.
(2). lower rocker arm length, C.
(3). distance from the crank vertical centre line to the inner edge of the inlet ports, F.
(4). distance from the crank vertical centre line to the inner edge of the exhaust ports, G.

Table 8.2 lists the port timings of configurations II to V with increasing scavenge period. With the increase of scavenge period, the flow capacity, the trapped air mass and hence the output shaft power increase, see Figs. 8.36 to 8.38. However, at a given scavenging pressure high flow capacity means high compressor power, as shown in Fig. 8.39, and with the increase of scavenge period the loss of effective stroke concurrently increases. Thus, the maximum output shaft efficiency will occurs at an intermediate port timing. Fig. 8.40 illustrates the variation of output shaft efficiency with the increase of scavenge period. The output shaft efficiency of configuration II is relatively poor because it has too short scavenge period to efficiently purge the cylinder with fresh air. The efficiency of configuration V also becomes poor because it has too long scavenge period, thus suffering a loss of effective stroke. Compared with the original configuration O, configuration III and IV improve the output shaft efficiency by 6 %.

Fig. 8.41 shows that with the increase of scavenge period the charging efficiency deteriorates.

Here configuration III has been chosen as a start for optimizing designs, because the slightly shorter scavenge period in configuration III is good for the mid and low speed running conditions. A slightly shorter scavenging period implies a slightly longer effective stroke. With decrease of speed, the time for scavenging is longer, the flow capacity becomes relatively more ample, thus increasing power output.

8.3.2.5 Sizing of port height

As high an inlet port as possible is always beneficial for improving flow capacity. Therefore, in all the the modified schemes, the inlet port heights have been taken at their possible maximum. When port heights are changed, the piston-crank mechanism and the port top edges always are fixed, hence the port timings are fixed, while the bottom edges shift, but are not set by the extreme outer piston position.

Now, it is necessary to estimate the effects of exhaust port height.

These estimations were conducted on a group of configurations III, VI and VII, which have the same port timing and decreasing exhaust port heights and operate at an air-fuel ratio of 22 and 4000 rpm.

Figs. 8.42 to 8.47 show the computational results with decrease of exhaust port height from 13 via 11.5 to 9.5 mm. With the decrease of exhaust port height, the flow capacity deteriorates, see Fig. 8.42, the trapped air mass, hence the output shaft power decrease, see Figs. 8.43 and 8.44. Meanwhile, the compressor power at the given inlet manifold pressures also decreases, see Fig. 8.45. Fig. 8.46 shows that the output shaft efficiencies of this group of configurations remain almost at the same level because with the decrease of exhaust port area the reduction of compressor power and the loss of engine output power cancel each other.

Here it is notable that 9.5 mm is the minimum exhaust port height which ensures the neccesary area for the above described blowdown period.

Fig. 8.47 shows that with the decrease of exhaust port height, the charging efficiency becomes relatively poor.

The configuration VI has been taken as a new start for continuing this optimization, because too high exhaust ports may prevent the cylinder pressure to build up toward the inlet pressure near the end of the scavenging process, thus harming trapping of scavenging air mass for mid and low speed running conditions.

8.3.2.6 Sizing of intake angle of inlet port

Swirl exerts an influence not only on the scavenging process but also on the combustion process. However, Watson's correlation of apparent rate of burned fuel used in the program cannot predict the effect of swirl on combustion. [7.6]

Is was assumed that the combustion process is not affected by swirl. The computational results of a group of configurations VI, VIII, IX, X and XI with intake angles of 0, 10, 20, 30 and 40 deg. respectively, give an estimation of the effect of swirl on the engine performance, as shown in Figs. 8.48 to 8.53. With the increase of inlet port intake angle, the effective flow section area, i.e. flow capacity, and the trapped air mass decrease, see Figs. 8.48 to 8.49. Consequently the output shaft power and the compressor power decrease, as shown in Figs. 8.50 and 8.51. At the same time, the charging efficiency improves marginally because of swirl, see Fig. 8.52.

The output shaft efficiencies stay almost at the same level with the increase of intake angle from 0 to 40 deg., as shown in Fig. 8.53. It is seen that even though the design with radial inlet ports used the same combustion correlation as the design with 30 degree intake angle, the increase of thermal efficiency was only 1 %. If the effect of swirl on combustion had been taken into consideration and a proper combination of air swirl and fuel spray had been realized, it could be expected that configuration X will give a satisfactory output shaft efficiency. Actually the Rootes TS3 has used the intake angle of 30 degrees and achieved a satisfactory combustion process.

Therefore, configuration X should be recommended as the optimum design.

8.3.3 PERFORMANCE PREDICTION OF OPTIMUM SCHEME

Compared with the original design, the following modifications have been made in the optimum scheme:

(1). lower connecting arm length B = 131.40 mm.
(2). lower rocker arm length C = 151.00 mm.
(3). distance from the crank vertical centre line to the inner edge of the inlet ports F = 57.00 mm.
(4). distance from the crank vertical centre line to the inner edge of the exhaust ports G = 52.00 mm.
(5). rectangular inlet ports: height = 11.00 mm, total width = 136.65 mm, set at 30 deg. angle with respect to the cylinder radius.
(6). rectangular exhaust ports: height = 11.50 mm, total width = 127.54 mm, radial.
(7). piston bowl volume = 6.0657 cu. cm to keep the compression ratio of 22.00.

conseqently,

(8). stroke = 133.51 mm.
(9). displacement = 0.35 litre.
(10). minimum piston separation = 1.777 mm.
(11). port timing- exhaust port opening 71 BBDC
inlet port opening 43 BBDC
exhaust port closing 53 ABDC
inlet port closing 58 ABDC

The rest of the geometry and the characteristics are the same as in the original design. The linkage geometry of the optimum scheme is shown in Fig. 8.54. Its porting diagram is shown in Fig. 8.55. The piston displacements and the port areas are listed in Table 8.4.

8.3.3.1 Performance prediction for optimum delivery ratio

As aforementioned, realization of the best performance relies on the combination of optimum configuration and optimum scavenging pressure. A series of numerical tests show that the optimum scavenging pressures vary with engine speed and are slightly affected by engine load. Fig. 8.56 shows the relationship between engine speed and optimum delivery ratio. With increase of engine speed the optimum delivery ratio decreases from about 2.0 at 500 rpm to about 1.1 at 4000 rpm. Fig. 8.57 illustrates the scavenging pressures in the neighbourhood of the optimum delivery ratio. Figs. 8.58 to 8.60 show the corresponding air flow rate, output shaft power and specific fuel consumption under full load. Fig. 8.61 shows the contours of the output shaft thermal efficiency. It is worthwhile noting that the compressor power has been subtracted in all these brake output predictions in this section. However, it has not been taken into consideration in the brake output predictions of Section 8.2. Even so, the output shaft thermal efficiency of the optimum scheme achieves almost the same peak value of 37 % as the original design. After the power to drive the compressor has been subtracted from the engine output of the original design, the optimum scheme improves the output shaft efficiency by approximately 5 %, and enhances the output shaft torque at the full load of A/F ratio 22 in the range of from 9 % at 4000 rpm to 29 % at 500 rpm.

Figs. 8.62 to 8.65 give the maximum cylinder pressure, mean exhaust gas, liner and piston surface temperatures.

The sensitivity of the optimum scheme to scavenging pressure is summed up in Table 8.5. It can be seen that under the high speed and load running conditions the sensitivity of output shaft efficiency to scavenging pressure increases.

However, the realization of varying delivery ratio implies the use of a continuously variable transmission (CVT) between the engine and the compressor. Therefore, it is necessary to predict the performance of the optimum scheme running at a fixed delivery ratio.

8.3.3.2 Performance prediction for fixed delivery ratio

The delivery ratios are varied in the range of from 0.8 to 1.2, correspondingly the ratio of inlet to exhaust pressures, air flow rate, charging and trapping efficiencies are illustrated in Figs. 8.66 to 8.69.

In the following calculations the fixed delivery ratio is equal to 1.2 which is not only the choice for the original design, but also a good compromise between performances at low and high speeds for the optimum design.

The output shaft power and specific fuel consumption are shown in Figs. 8.70 and 8.71. The contours of the output shaft efficiency are drawn in Fig. 8.72. Compared with the optimum scheme for the optimum delivery ratios, at the high speed side the area of high efficiency for the fixed delivery ratio contracts slightly, the output shaft efficiency is reduced by an arithmetic mean of 2.5 %. The output shaft torque varies from an increase by 1 % at 4000 rpm to a decrease by 13 % at 500 rpm. Compared with the original design the output shaft efficiency running at the delivery ratio of 1.2 improves by 2.5 %, and the output torque at full load enhances in the range between 10 % at 4000 rpm and 16 % at 500 rpm, see Fig. 8.61.

Figs. 8.73 and 8.74 show the maximum cylinder pressure and mean exhaust temperature. Figs. 8.75 and 8.76 illustrate the mean liner and piston temperatures. Fig. 8.77 is the heat balance at full load.

The comparison between the performances of the optimum scheme running at the optimum and fixed ratios are summed up in Table 8.6.

8.3.3.3 Estimation of feasibility for compressor CVT

In the previous calculations for the optimum delivery ratio, the mechanical loss of the compressor CVT has not been taken account. Here the efficiency of the CVT is equal to 0.9. After the loss of the CVT has been subtracted, compared with the original design the output shaft efficiency virtually improves by 4 % and the output shaft torque by 8 % at 4000 rpm and 15 % at 500 rpm.

8.3.4 SUMMARY

The phenimenological unsteady jet model is used for optimizing the port

design. The optimum scheme obtained evidently improves the engine performance. The following drawbacks of the Ford initial design have been pinpointed.

(1). bad port shape: circular ports cannot fully utilise the limited port zone.
(2). wrong port timing: the charging period is too long.

The optimization procedures are suitable for any uniflow scavenged engine. For an optimum scheme, there exist a group of optimum delivery ratio varied with engine speed. However, the realization of variable delivery ratio implies the use of a CVT on the compressor shaft.

REFERENCES

[8.1] F.J. Wallace, T.K. Kao, M. Tarabad, W.D. Alexander and A. Cole
"Thermally Insulated Diesel Engines"
Proc. Instn. Mech. Engrs., vol. 198A, No. 5, 1984

[8.2] R. Kamo and W. Bryzik
"Adiabatic Turbocompound Engine Performance Prediction"
SAE 780068, 1978

[8.3] W.J. Griffiths
"Thermodynamic Simulation of the Diesel Engine Cycle to Show the Effect of Increasing the Combustion Chamber Wall Temperatures on Thermal Efficiency and Heat Rejection"
Wellworthy Topics, No. 63, 1967-7

[8.4] F.J. Wallace, R.J.B. Way and H. Vollmert
"Effect of Partial Suppression of Heat Loss to Coolant on the High Output Diesel Engine Cycle"
SAE 790823, 1979

[8.5] N. Watson, N.P. Kyrtatos and K. Holmes
"The Performance Potential of Limited Cooled Diesel Engines"
Proc. Instn. Mech. Engrs. vol. 197A, 45, 1983

[8.6] M.H. Howarth
"The Design of High Speed Diesel Engines"
Constable and Co. 1966

Table 8.1 Comparison of the Computed Results from CSPMZ and TWOSIM

	CSPMZ			TWOSIM: P. Mixing			TWOSIM: P. Scavenging		
Engine speed (rpm)	1000	1000	1000	1000	1000	1000	1000	1000	1000
Bhp (hp)	0.78	0.76	0.76	0.77	0.77	0.77	0.77	0.77	0.76
Bmep (psi)	15.2	15.1	14.9	14.8	14.8	14.8	14.7	14.8	14.6
Bsfc (lbm/hp-hr)	0.522	0.523	0.524	0.516	0.517	0.521	0.521	0.522	0.529
A/F trapped	70.2	75.8	81.7	63.4	68.9	74.4	86.0	89.0	92.0
Delivery ratio	0.799	1.002	1.196	0.798	1.004	1.199	0.808	1.005	1.199
Manifold delta P (in Hg)	0.29	0.43	0.60	0.40	0.48	0.66	0.40	0.48	0.66
Trapping efficiency	0.679	0.577	0.523	0.588	0.511	0.466	0.795	0.664	0.574
Scavenging efficiency	0.737	0.771	0.816	0.695	0.744	0.792	0.964	0.969	0.974
Exhaust temp (K)	451	442	434	383	375	368	389	376	367
Peak combustion temp (K)	1147	1134	1124	1330	1315	1306	1356	1329	1303
Peak combustion P (psi)	856	862	871	922	931	949	931	942	953
Engine speed (rpm)	1250	1250	1250	1250	1250	1250	1250	1250	1250
Bhp (hp)	2.39	2.36	2.36	2.44	2.38	2.38	2.39	2.38	2.38
Bmep (psi)	37.6	37.1	37.1	37.5	36.6	36.6	36.7	36.5	36.5
Bsfc (lbm/hp-hr)	0.406	0.403	0.400	0.390	0.389	0.389	0.393	0.392	0.392
A/F trapped	38.32	41.91	44.86	32.00	36.90	40.40	42.90	46.00	48.00
Delivery ratio	0.795	0.997	1.196	0.804	0.998	1.201	0.804	0.999	1.201
Manifold delta P (in Hg)	0.42	0.63	0.88	0.48	0.72	0.99	0.48	0.72	0.99
Trapping efficiency	0.708	0.617	0.546	0.565	0.512	0.466	0.748	0.639	0.554
Scavenging efficiency	0.812	0.850	0.876	0.741	0.788	0.830	0.982	0.987	0.988
Exhaust temp (K)	602	579	563	488	455	435	485	456	436
Peak combustion temp (K)	1362	1327	1304	1677	1616	1584	1687	1632	1595
Peak combustion P (psi)	905	931	948	1001	1027	1054	1009	1038	1059
Engine speed (rpm)	1700	1700	1700	1700	1700	1700	1700	1700	1700
Bhp (hp)	6.53	6.54	6.52		6.50	6.61	6.48	6.48	6.57
Bmep (psi)	75.6	75.9	75.4		73.4	74.6	73.2	73.2	74.2
Bsfc (lbm/hp-hr)	0.385	0.376	0.370		0.361	0.357	0.369	0.361	0.357
A/F trapped	20.25	22.54	24.66		19.90	21.90	20.90	23.40	24.90
Delivery ratio	0.804	1.002	1.198		0.998	1.198	0.796	0.998	1.197
Manifold delta P (in Hg)	0.73	1.10	1.55		1.23	1.74	0.81	1.23	1.74
Trapping efficiency	0.710	0.630	0.563		0.515	0.472	0.692	0.603	0.536
Scavenging efficiency	0.876	0.903	0.921		0.845	0.875	0.995	0.994	0.996
Exhaust temp (K)	897	839	796		637	590	718	637	590
Peak combustion temp (K)	1899	1814	1749		2061	1998	2205	2080	2013
Peak combustion P (psi)	886	919	965		1041	1089	983	1047	1093
Exhaust mfld P (kn/m/m)	105.0			104.7			104.7		
Friction mep (psi)	5.08/6.79/9.86			5.2/6.8/9.8			5.2/6.8/9.8		

Table 8.2 Summary of Configurations for Optimizing Port Design

configuration no.	0	I	II	III	IV	V
port shape	circular	rectangular				
ex. port open BBDC	75		68	71	73	75
in. port open BBDC	44		41	43	45	47
ex. port close ABDC	50		51	53	55	57
in. port close ABDC	67		55	58	61	63
in.port height/stroke ratio	0.095		0.075	0.082	0.090	0.097
eff.in.port width/circum.ratio	0.653	0.750				
in.port intake angle deg.	25	0				
ex.port height/stroke ratio	0.119		0.090	0.097	0.105	0.112
ex.port width/circum.ratio	0.812	0.700				
comment	original design	for shaping port	for port timing			

configuration no.	VI	VII	VIII	IX	X	XI
port shape	rectangular					
ex. port open BBDC	71					
in. port open BBDC	43					
ex. port close ABDC	53					
in. port close ABDC	58					
in. port height/stroke ratio	0.082					
eff.in.port width/circum.ratio	0.750		0.739	0.705	0.650	0.575
in.port intake angle deg.	0		10	20	30	40
ex.port height/stroke ratio	0.086	0.071	0.086			
ex. port width/circum.ratio	0.700					
comment	for sizing exhaust port height		for determining inlet port intake angle			

Table 8.3 The Effect of the Charging Period

	Ford initial design EPC = 50 ABDC IPC = 67 ABDC charging period = 17 deg.			Optimum scheme (configuration X) EPC = 53 ABDC IPC = 58 ABDC charging period = 5 deg.		
engine speed (rpm)	trapped mass at EPC (g)	trapped mass at IPC (g)	extra charging mass (g)	trapped mass at EPC (g)	trapped mass at IPC (g)	extra charging mass (g)
500.	0.307	0.276	-0.031	0.320	0.317	-0.003
1000.	0.304	0.278	-0.026	0.320	0.317	-0.003
2000.	0.311	0.289	-0.022	0.325	0.323	-0.002
3000.	0.318	0.296	-0.022	0.335	0.332	-0.003
4000.	0.332	0.314	-0.018	0.345	0.343	-0.002

comment: delivery ratio =1.2 air-fuel ratio = 22.0

Table 8.4 Piston Displacement and Port Areas of the Optimum Scheme

CA	in.p.displ. (mm)	ex.p.displ. (mm)	in.port area (sq.cm)	ex.port area (sq.cm)	cyl.vol. (lit.)
-300.	56.6287	38.8365	0.0000	0.0000	0.2907
-298.	55.3577	37.6735	0.0000	0.0000	0.2857
-296.	55.0691	36.5196	0.0000	0.0000	0.2805
-294.	54.2594	35.3766	0.0000	0.0000	0.2753
-292.	53.4238	34.1562	0.0000	0.0000	0.2700
-290.	52.5779	32.9500	0.0000	0.0000	0.2645
-288.	51.7070	31.7298	0.0000	0.0000	0.2590
-286.	50.8166	30.4974	0.0000	0.0000	0.2534
-284.	49.9070	29.2546	0.0000	0.0000	0.2477
-282.	48.9738	28.0033	0.0000	0.0000	0.2420
-280.	48.0325	26.7452	0.0000	0.0000	0.2361
-278.	47.0635	25.4822	0.0000	0.0000	0.2302
-276.	46.0875	24.2162	0.0000	0.0000	0.2243
-274.	45.0900	22.9490	0.0000	0.0000	0.2183
-272.	44.0767	21.6824	0.0000	0.0000	0.2123
-270.	43.0481	20.4183	0.0000	0.0000	0.2062
-268.	42.0051	19.1586	0.0000	0.0000	0.2002
-266.	40.9484	17.9049	0.0000	0.0000	0.1941
-264.	39.8737	16.6593	0.0000	0.0000	0.1879
-262.	38.7970	15.4234	0.0000	0.0000	0.1818
-260.	37.7041	14.1990	0.0000	0.0000	0.1757
-258.	36.6010	12.9879	0.0000	0.0000	0.1696
-256.	35.4887	11.7917	0.0000	0.0000	0.1635
-254.	34.3683	10.6124	0.0000	0.0000	0.1574
-252.	33.2409	9.4514	0.0000	0.0000	0.1514
-250.	32.1078	8.3104	0.0000	0.0000	0.1454
-248.	30.9701	7.1911	0.0000	0.0000	0.1394
-246.	29.8292	6.0951	0.0000	0.0000	0.1335
-244.	28.6865	5.0239	0.0000	0.0000	0.1276
-242.	27.5433	3.9789	0.0000	0.0000	0.1219
-240.	26.4012	2.9618	0.0000	0.0000	0.1161
-238.	25.2617	1.9739	0.0000	0.0000	0.1105
-236.	24.1265	1.0167	0.0000	0.0000	0.1050
-234.	22.9970	0.0914	0.0000	0.0000	0.0996
-232.	21.8751	-0.1994	0.0000	0.0000	0.0942
-230.	20.7623	-0.3420	0.0000	0.0000	0.0890
-228.	19.6606	-0.5204	0.0000	0.0000	0.0840
-226.	18.5716	-0.7357	0.0000	0.0000	0.0790
-224.	17.4972	-0.9892	0.0000	0.0000	0.0742
-222.	16.4391	-1.2817	0.0000	0.0000	0.0695
-220.	15.3992	-1.6145	0.0000	0.0000	0.0650
-218.	14.3794	-1.9884	0.0000	0.0000	0.0607
-216.	13.3813	-2.4044	0.0000	0.0000	0.0565
-214.	12.4070	-2.8633	0.0000	0.0000	0.0525
-212.	11.4580	-3.3659	0.0000	0.0000	0.0487
-210.	10.5362	-3.9130	0.0000	0.0000	0.0450
-208.	9.6433	-4.5053	0.0000	0.0000	0.0416
-206.	8.7809	-5.1434	0.0000	0.0000	0.0384
-204.	7.9508	-5.8278	0.0000	0.0000	0.0353
-202.	7.1544	-6.5591	0.0000	0.0000	0.0325
-200.	6.3933	-7.3376	0.0000	0.0000	0.0299
-198.	5.6689	-8.1638	0.0000	0.0000	0.0276
-196.	4.9825	-9.0379	0.0000	0.0000	0.0254
-194.	4.3356	-9.9598	0.0000	0.0000	0.0235
-192.	3.7292	-10.9293	0.0000	0.0000	0.0218
-190.	3.1646	-11.9463	0.0000	0.0000	0.0204
-188.	2.6427	-13.0100	0.0000	0.0000	0.0192
-186.	2.1645	-14.1195	0.0000	0.0000	0.0182
-184.	1.7309	-15.2741	0.0000	0.0000	0.0175

-182.	1.3427	0.5075	0.0000	0.0000	0.0170
-180.	1.0005	0.7664	0.0000	0.0000	0.0164
-178.	0.7049	1.0724	0.0000	0.0000	0.0168
-176.	0.4565	1.4240	0.0000	0.0000	0.0171
-174.	0.2557	1.8232	0.0000	0.0000	0.0176
-172.	0.1027	2.2667	0.0000	0.0000	0.0184
-170.	-0.0021	2.7547	0.0000	0.0000	0.0194
-168.	-0.0587	3.2861	0.0000	0.0000	0.0207
-166.	-0.0669	3.8691	0.0000	0.0000	0.0222
-164.	-0.0268	4.4756	0.0000	0.0000	0.0239
-162.	0.0617	5.1314	0.0000	0.0000	0.0259
-160.	0.1982	5.8263	0.0000	0.0000	0.0281
-158.	0.3826	6.5589	0.0000	0.0000	0.0305
-156.	0.6146	7.3280	0.0000	0.0000	0.0331
-154.	0.8938	8.1320	0.0000	0.0000	0.0360
-152.	1.2197	8.9695	0.0000	0.0000	0.0391
-150.	1.5918	9.8387	0.0000	0.0000	0.0423
-148.	2.0096	10.7382	0.0000	0.0000	0.0458
-146.	2.4724	11.6662	0.0000	0.0000	0.0495
-144.	2.9795	12.6209	0.0000	0.0000	0.0534
-142.	3.5302	13.6007	0.0000	0.0000	0.0574
-140.	4.1237	14.6037	0.0000	0.0000	0.0616
-138.	4.7590	15.6282	0.0000	0.0000	0.0660
-136.	5.4352	16.6723	0.0000	0.0000	0.0706
-134.	6.1514	17.7341	0.0000	0.0000	0.0753
-132.	6.9065	18.8119	0.0000	0.0000	0.0801
-130.	7.6995	19.9039	0.0000	0.0000	0.0851
-128.	8.5291	21.0082	0.0000	0.0000	0.0902
-126.	9.3943	22.1231	0.0000	0.0000	0.0954
-124.	10.2938	23.2469	0.0000	0.0000	0.1008
-122.	11.2263	24.3779	0.0000	0.0000	0.1062
-120.	12.1904	25.5142	0.0000	0.0000	0.1118
-118.	13.1849	26.6544	0.0000	0.0000	0.1174
-116.	14.2083	27.7963	0.0000	0.0000	0.1231
-114.	15.2592	28.9400	0.0000	0.0000	0.1289
-112.	16.3361	30.0825	0.0000	0.0000	0.1348
-110.	17.4374	31.2228	0.0000	0.0000	0.1407
-108.	18.5616	32.3595	0.0000	0.0000	0.1467
-106.	19.7072	33.4915	0.0000	0.0000	0.1527
-104.	20.8724	34.6174	0.0000	0.0000	0.1588
-102.	22.0556	35.7361	0.0000	0.0000	0.1648
-100.	23.2552	36.8465	0.0000	0.0000	0.1709
-98.	24.4694	37.9474	0.0000	0.0000	0.1771
-96.	25.6965	39.0379	0.0000	0.0000	0.1832
-94.	26.9348	40.1170	0.0000	0.0000	0.1893
-92.	28.1823	41.1839	0.0000	0.0000	0.1954
-90.	29.4375	42.2376	0.0000	0.0000	0.2015
-88.	30.6984	43.2775	0.0000	0.0000	0.2076
-86.	31.9632	44.3027	0.0000	0.0000	0.2136
-84.	33.2300	45.3126	0.0000	0.0000	0.2197
-82.	34.4971	46.3065	0.0000	0.0000	0.2256
-80.	35.7626	47.2838	0.0000	0.0000	0.2316
-78.	37.0247	48.2439	0.0000	0.0000	0.2374
-76.	38.2814	49.1863	0.0000	0.0000	0.2432
-74.	39.5310	50.1104	0.0000	0.0000	0.2490
-72.	40.7717	51.0157	0.0000	0.0000	0.2547
-70.	42.0015	51.9019	0.0000	0.0000	0.2602
-68.	43.2187	52.7684	0.0000	0.9800	0.2657
-66.	44.4216	53.6148	0.0000	2.0595	0.2712
-64.	45.6084	54.4408	0.0000	3.1129	0.2765

-62.	46.7773	55.2458	[illegible]	4.1397	0.2817
-60.	47.9266	56.0297	[illegible]	5.1794	0.2868
-58.	49.0548	56.7918	[illegible]	6.1115	[illegible]
-56.	50.1632	57.5329	[illegible]	7.0556	0.2967
-54.	51.2413	58.2399	[illegible]	7.9711	0.3014
-52.	52.2965	58.9350	0.0000	8.8576	0.3061
-50.	53.3244	59.6170	0.0000	9.7147	0.3105
-48.	54.3237	60.2655	0.0000	10.5419	0.3149
-46.	55.2931	60.8902	0.0000	11.3386	0.3191
-44.	56.2313	61.4907	0.0000	12.1045	0.3232
-42.	57.1371	62.0666	0.1623	12.8398	0.3271
-40.	58.0096	62.6176	1.1948	13.5416	0.3308
-38.	58.8477	63.1439	2.1866	14.2118	0.3345
-36.	59.6506	63.6427	3.1367	14.6671	0.3379
-34.	60.4173	64.1161	4.0441	14.6671	0.3412
-32.	61.1473	64.5623	4.9080	14.6671	0.3443
-30.	61.8400	64.9823	5.7277	14.6671	0.3472
-28.	62.4947	65.3742	6.5025	14.6671	0.3500
-26.	63.1110	65.7379	7.2319	14.6671	0.3526
-24.	63.6887	66.0729	7.9155	14.6671	0.3550
-22.	64.2275	66.3788	8.5531	14.6671	0.3572
-20.	64.7272	66.6550	9.1444	14.6671	0.3593
-18.	65.1877	66.9010	9.6894	14.6671	0.3611
-16.	65.6090	67.1161	10.1881	14.6671	0.3628
-14.	65.9913	67.2998	10.6405	14.6671	0.3643
-12.	66.3347	67.4516	11.0468	14.6671	0.3656
-10.	66.6394	67.5709	11.4074	14.6671	0.3667
-8.	66.9056	67.6571	11.7224	14.6671	0.3677
-6.	67.1337	67.7095	11.9924	14.6671	0.3684
-4.	67.3242	67.7277	12.2178	14.6671	0.3690
-2.	67.4773	67.7110	12.3990	14.6671	0.3693
0.	67.5936	67.6590	12.5367	14.6671	0.3695
2.	67.6736	67.5710	12.6313	14.6671	0.3695
4.	67.7177	67.4466	12.6836	14.6671	0.3693
6.	67.7266	67.2852	12.6941	14.6671	0.3689
8.	67.7008	67.0864	12.6635	14.6671	0.3683
10.	67.6408	66.8499	12.5926	14.6671	0.3675
12.	67.5473	66.5752	12.4819	14.6671	0.3665
14.	67.4208	66.2619	12.3321	14.6671	0.3653
16.	67.2619	65.9100	12.1441	14.6671	0.3640
18.	67.0711	65.5190	11.9183	14.6671	0.3625
20.	66.8491	65.0890	11.6556	14.6671	0.3607
22.	66.5964	64.6198	11.3566	14.6671	0.3588
24.	66.3136	64.1114	11.0219	14.6671	0.3567
26.	66.0012	63.5640	10.6522	14.6671	0.3545
28.	65.6597	62.9777	10.2481	14.0010	0.3520
30.	65.2897	62.3529	9.8102	13.2040	0.3494
32.	64.8917	61.6897	9.3392	12.3583	0.3466
34.	64.4661	60.9883	8.8355	11.4643	0.3436
36.	64.0135	60.2505	8.2999	10.5227	0.3405
38.	63.5342	59.4757	7.7327	9.5345	0.3371
40.	63.0288	58.6650	7.1346	8.5005	0.3337
42.	62.4976	57.8192	6.5060	7.4218	0.3300
44.	61.9412	56.9392	5.8474	6.2995	0.3262
46.	61.3598	56.0261	5.1594	5.1349	0.3223
48.	60.7539	55.0809	4.4424	3.9294	0.3182
50.	60.1238	54.1048	3.6968	2.6845	0.3139
52.	59.4701	53.0990	2.9231	1.4017	0.3096
54.	58.7929	52.0649	2.1217	0.0828	0.3050
56.	58.0927	51.0038	1.2931	0.0000	0.3004

98.	57.3699	49.9173	0.4378	0.0000	0.2956

ex.port open	-70.55cad
in.port open	-43.09cad
ex.port close	53.35cad
in.port close	58.22cad
CA at t.d.c.	100.00cad
CA at b.d.c.	0.00cad

	--	optimum	++	--	optimum	++			
A/F ratio	22	22	22	33	33	33	66	66	66
engine speed = 500 rpm									
in. manifold pr. (bar)	1.060	1.062	1.064	1.059	1.061	1.063	1.058	1.060	1.062
delivery ratio	1.9185	2.1030	2.2728	1.7995	2.0000	2.1733	1.6680	1.8718	2.0599
charging eff.	0.7849	0.7973	0.8069	0.7742	0.7928	0.8016	0.7534	0.7767	0.7894
trapping eff.	0.4091	0.3791	0.3550	0.4312	0.3964	0.3689	0.4517	0.4149	0.3822
B.M.E.P (bar)	5.70	5.80	5.87	3.68	3.75	3.79	1.45	1.53	1.50
output shaft power (KW)	1.68	1.71	1.73	1.09	1.11	1.12	0.43	0.45	0.45
output shaft eff.	0.314	0.315	0.314	0.307	0.307	0.306	0.249	0.256	0.247
compressor power (KW)	0.05	0.06	0.06	0.05	0.05	0.06	0.04	0.05	0.06
engine speed = 1000 rpm									
in. manifold pr. (bar)	1.075	1.085	1.095	1.075	1.085	1.095	1.075	1.085	1.095
delivery ratio	1.5314	1.8092	2.0519	1.5216	1.7994	2.0394	1.4954	1.7705	2.0168
charging eff.	0.7579	0.7922	0.8139	0.7614	0.7929	0.8143	0.7446	0.7826	0.8101
trapping eff.	0.4949	0.4379	0.3967	0.5004	0.4406	0.3995	0.4979	0.4420	0.4017
B.M.E.P. (bar)	6.38	6.65	6.82	4.20	4.39	4.46	1.70	1.80	1.81
output shaft power (KW)	3.75	3.91	4.01	2.47	2.58	2.62	1.00	1.06	1.06
output shaft eff.	0.363	0.363	0.362	0.359	0.359	0.356	0.296	0.296	0.291
compressor power (KW)	0.10	0.13	0.17	0.10	0.13	0.17	0.10	0.13	0.17
engine speed = 2000 rpm									
in. manifold pr. (bar)	1.120	1.140	1.160	1.120	1.140	1.160	1.120	1.140	1.160
delivery ratio	1.3020	1.4768	1.6313	1.2890	1.4643	1.6170	1.2676	1.4445	1.5940
charging eff.	0.7454	0.7777	0.8002	0.7337	0.7744	0.8000	0.7276	0.7664	0.7924
trapping eff.	0.5725	0.5226	0.4905	0.5692	0.5289	0.4947	0.5740	0.5305	0.4971
B.M.E.P. (bar)	6.36	6.67	6.86	4.08	4.29	4.37	1.44	1.53	1.54
output shaft power (KW)	7.47	7.85	8.06	4.80	5.05	5.14	1.69	1.81	1.80
output shaft eff.	0.371	0.372	0.369	0.357	0.358	0.354	0.257	0.259	0.252
compressor power (KW)	0.27	0.36	0.45	0.27	0.36	0.45	0.26	0.35	0.44
engine speed = 3000 rpm									
in. manifold pr. (bar)	1.160	1.190	1.220	1.160	1.190	1.220	1.160	1.1884	1.220
delivery ratio	1.1056	1.2439	1.3669	1.0907	1.2301	1.3540	1.0702	1.2034	1.3331
charging eff.	0.7265	0.7552	0.7794	0.7179	0.7547	0.7776	0.7098	0.7473	0.7753
trapping eff.	0.6571	0.6071	0.5702	0.6599	0.6135	0.5743	0.6633	0.6210	0.5816
B.M.E.P. (bar)	5.84	6.21	6.37	3.63	3.80	3.90	1.01	1.08	1.08
output shaft power (KW)	10.29	10.97	11.22	6.39	6.70	6.89	1.77	1.90	1.91
output shaft eff.	0.354	0.356	0.353	0.327	0.328	0.325	0.185	0.187	0.182
compressor power (KW)	0.46	0.62	0.78	0.45	0.61	0.78	0.45	0.59	0.76
engine speed = 4000 rpm									
in. manifold pr. (bar)	1.190	1.230	1.270	1.210	1.250	1.290	1.230	1.270	1.310
delivery ratio	0.9434	1.0517	1.1650	0.9971	1.1130	1.2115	1.0389	1.1502	1.2497
charging eff.	0.6803	0.7497	0.7709	0.7102	0.7363	0.7668	0.7249	0.7591	0.7776
trapping eff.	0.7211	0.7128	0.6617	0.7123	0.6615	0.6329	0.6978	0.6600	0.6222
B.M.E.P. (bar)	5.15	5.83	5.83	3.14	3.24	3.36	0.58	0.60	0.55
output shaft power (KW)	12.11	13.71	13.71	7.39	7.63	7.92	1.34	1.43	1.27
output shaft eff.	0.327	0.336	0.331	0.286	0.286	0.284	0.103	0.104	0.09
compressor power (KW)	0.62	0.84	1.02	0.73	0.97	1.22	0.83	1.08	1.34

	Optimum	Fixed	Optimum	Fixed	Optimum	Fixed
A/F ratio	22	22	33	33	66	66
engine speed = 500 rpm						
in. manifold pr. (bar)	1.0620	1.0540	1.0610	1.0541	1.0600	1.0543
delivery ratio	2.1030	1.1964	2.0000	1.2052	1.8718	1.2109
charging eff.	0.7973	0.6972	0.7928	0.6878	0.7767	0.6839
trapping eff.	0.3791	0.5828	0.3964	0.5707	0.4149	0.5648
B.M.E.P. (bar)	5.80	5.06	3.75	3.27	1.53	1.38
output shaft power (KW)	1.71	1.49	1.11	0.96	0.45	0.41
output shaft eff.	0.315	0.313	0.307	0.306	0.256	0.254
compressor power (KW)	0.06	0.03	0.05	0.03	0.05	0.03
engine speed = 1000 rpm						
in. manifold pr. (bar)	1.0850	1.0657	1.0850	1.0657	1.0850	1.0665
delivery ratio	1.8092	1.2118	1.7994	1.1954	1.7705	1.2090
charging eff.	0.7922	0.7022	0.7929	0.7041	0.7826	0.6958
trapping eff.	0.4379	0.5795	0.4406	0.5890	0.4420	0.5755
B.M.E.P. (bar)	6.65	6.05	4.39	3.84	1.80	1.58
output shaft power (KW)	3.91	3.56	2.58	2.26	1.06	0.93
output shaft eff.	0.363	0.363	0.359	0.356	0.296	0.294
compressor power (KW)	0.13	0.07	0.13	0.07	0.13	0.07
engine speed = 2000 rpm						
in. manifold pr. (bar)	1.1400	1.1104	1.1400	1.1119	1.1400	1.1134
delivery ratio	1.4763	1.2095	1.4643	1.2101	1.4445	1.2045
charging eff.	0.7777	0.7169	0.7744	0.7230	0.7664	0.7146
trapping eff.	0.5226	0.5927	0.5289	0.5974	0.5305	0.5933
B.M.E.P. (bar)	6.67	6.13	4.29	3.94	1.53	1.39
output shaft power (KW)	7.85	7.21	5.05	4.64	1.81	1.64
output shaft eff.	0.372	0.370	0.358	0.356	0.259	0.255
compressor power (KW)	0.36	0.23	0.36	0.24	0.35	0.24
engine speed = 3000 rpm						
in. manifold pr. (bar)	1.1900	1.1816	1.1900	1.1847	1.1844	1.1884
delivery ratio	1.2439	1.2039	1.2301	1.2050	1.2034	1.2034
charging eff.	0.7552	0.7403	0.7547	0.7446	0.7473	0.7473
trapping eff.	0.6071	0.6148	0.6135	0.6180	0.6210	0.6210
B.M.E.P. (bar)	6.21	6.07	3.80	3.76	1.08	1.08
output shaft power (KW)	10.97	10.71	6.70	6.63	1.90	1.90
output shaft eff.	0.356	0.354	0.328	0.327	0.187	0.187
compressor power (KW)	0.62	0.57	0.61	0.58	0.59	0.59
engine speed = 4000 rpm						
in. manifold pr. (bar)	1.2300	1.2787	1.2500	1.2837	1.2700	1.2874
delivery ratio	1.0517	1.1932	1.1130	1.1948	1.1502	1.1935
charging eff.	0.7497	0.7665	0.7363	0.7634	0.7591	0.7622
trapping eff.	0.7128	0.6424	0.6615	0.6389	0.6600	0.6386
B.M.E.P. (bar)	5.83	5.87	3.24	3.35	0.60	0.55
output shaft power (KW)	13.71	13.80	7.63	7.87	1.43	1.29
output shaft eff.	0.336	0.331	0.286	0.284	0.104	0.094
compressor power (KW)	0.84	1.15	0.97	1.18	1.08	1.19

TWO-STROKE OPPOSED PISTON ENGINE
ROCKER ARM CONFIGURATION

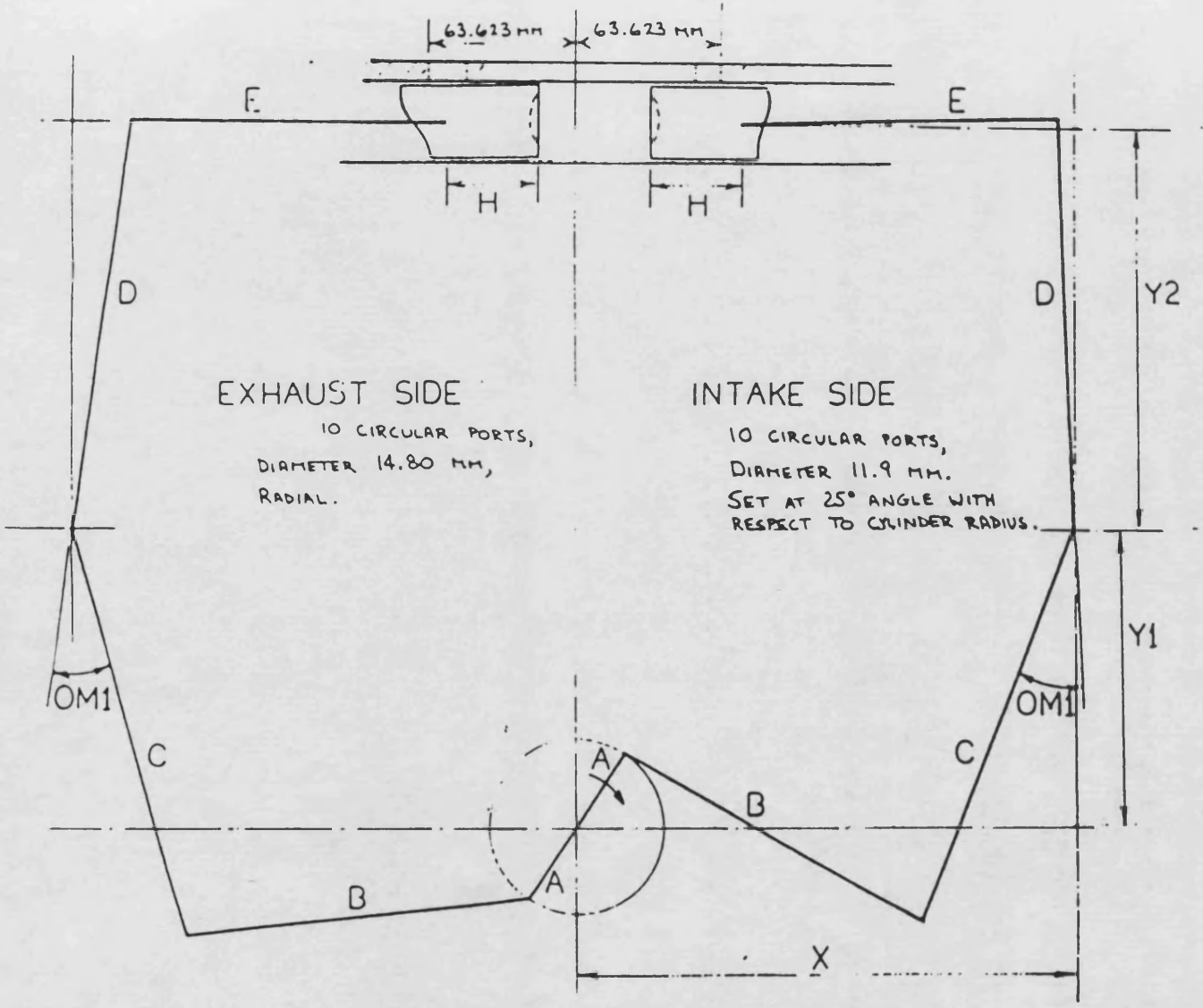

CHOSEN CONSTRAINTS:

- STROKE = TWICE CRANK RADIU
- VMAX/VMIN = 22.0
- MINIMUM PISTON SEPARATION = 0.07 INCHES
- SYMMETRY OF UPPER ROCKER ARM MOTION
- SYMMETRY OF PISTON ROD MOTION

FORD DIMENSIONS:

A = 32.00 mm
B = 131.94 mm
C = 157.35 mm
D = 154.33 mm
E = 121.89 mm
H = 36.50 mm
X = 190.00 mm
Y1 = 112.35 mm
Y2 = 152.65 mm
OM1 = 23.507 DEGREES
PISTON BOWL VOLUME = 0.33571 CU. IN.
CYLINDER BORE = 58.0 mm
CYLINDER WALL = 16.00 mm

Fig. 8.1 Ford Engine Configuration

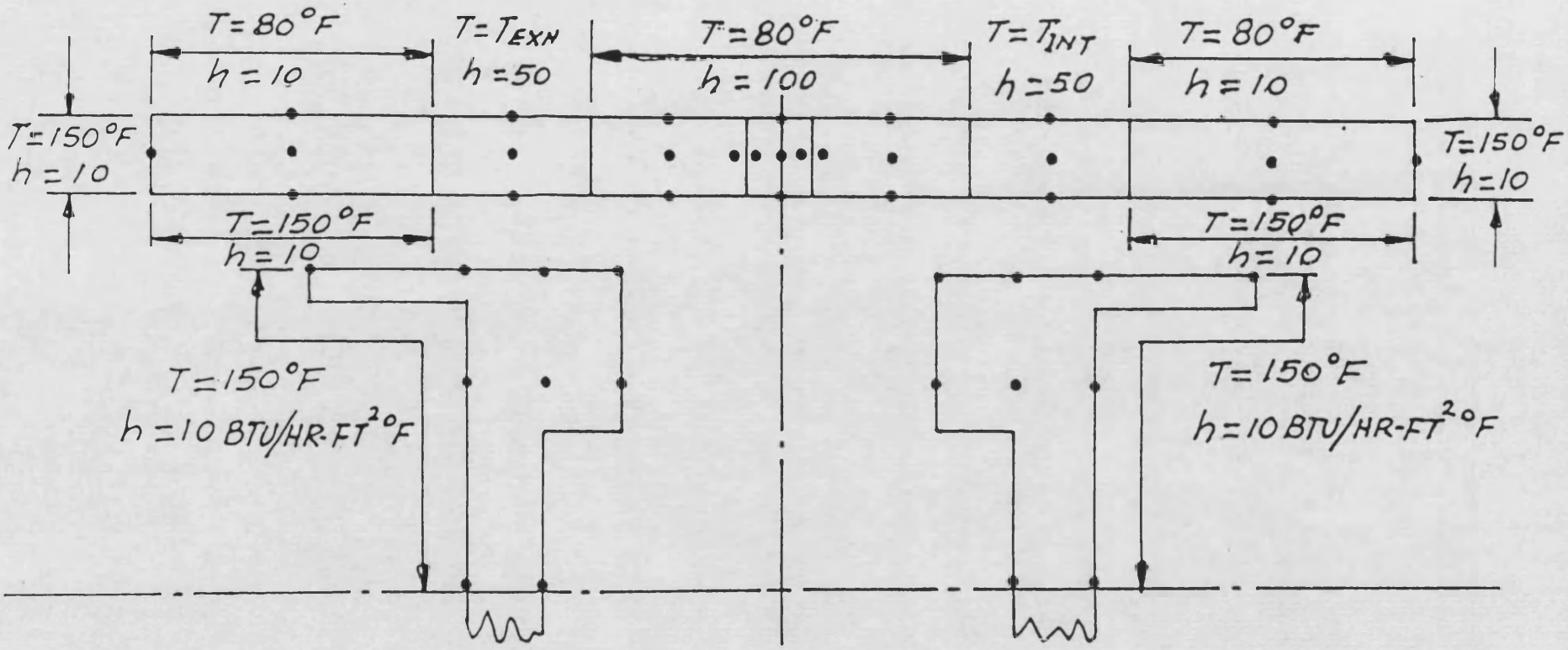

Fig. 8.2 Uncooled Boundary Conditions

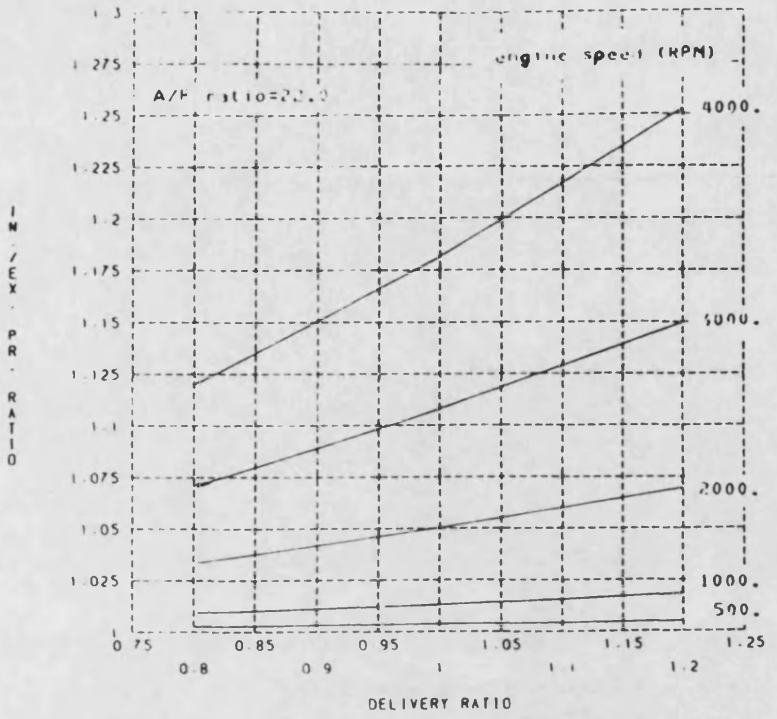

Fig. 8.3 Delivery Ratio versus Inlet/Exhaust Pressure Ratio

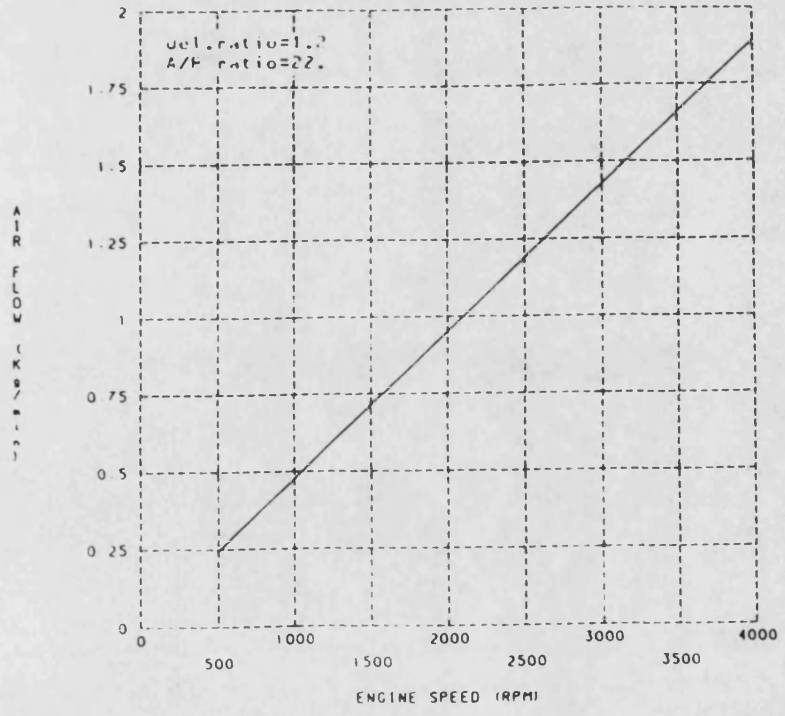

Fig. 8.4 Air Flow Rate

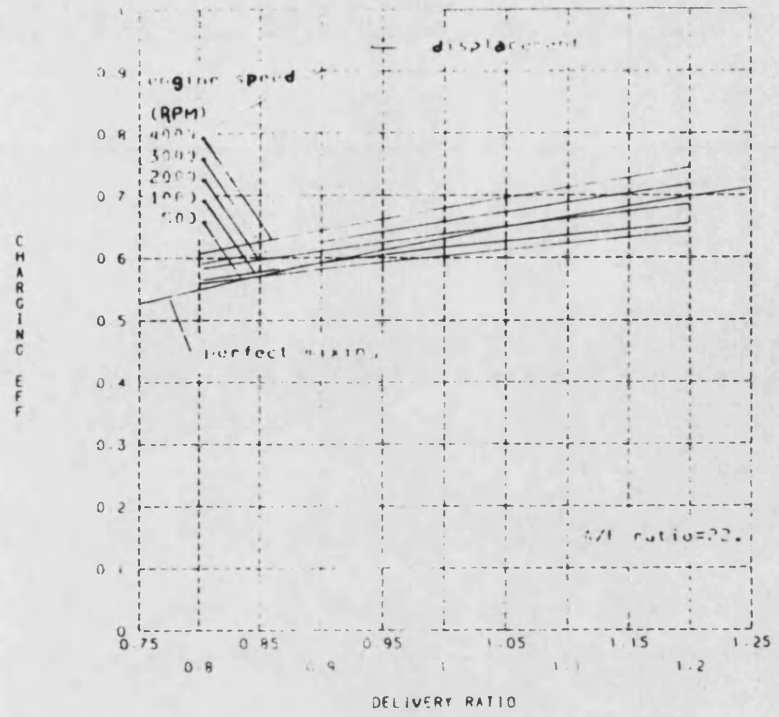

Fig. 8.5 Effect of Uncooled Engine Speed on Charging Efficiency

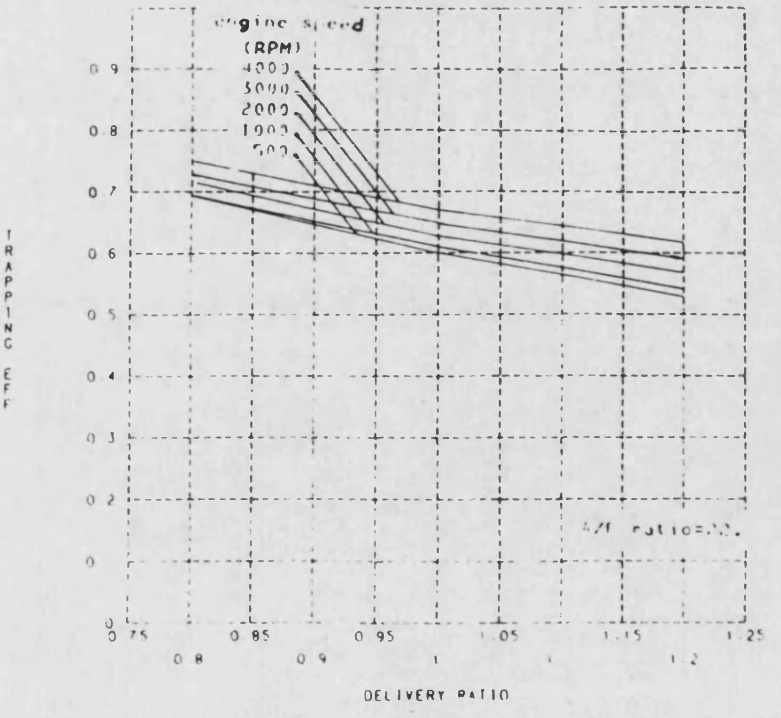

Fig. 8.6 Effect of Uncooled Engine Speed on Trapping Efficiency

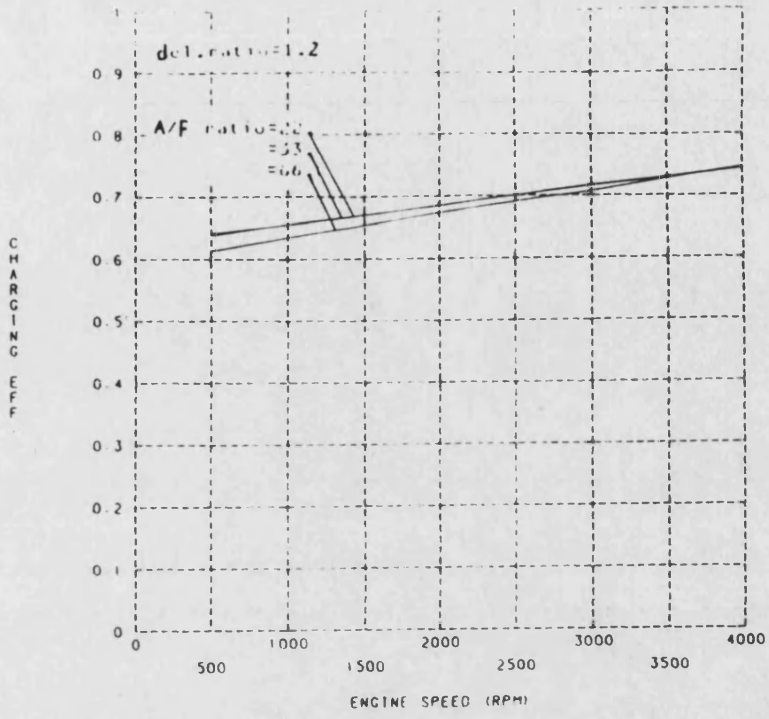

Fig. 8.7 Effect of Engine Load on Charging Efficiency

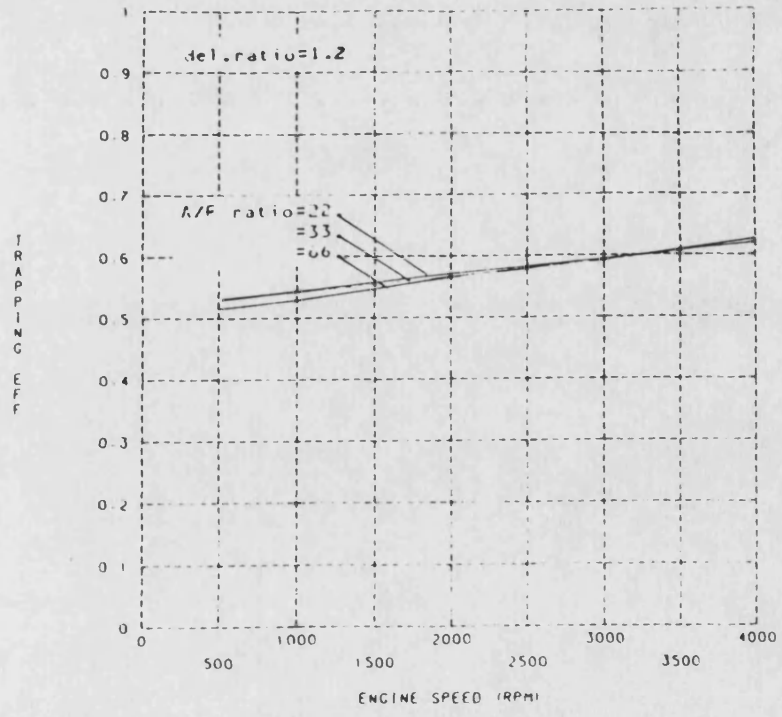

Fig. 8.8 Effect of Engine Load on Trapping Efficiency

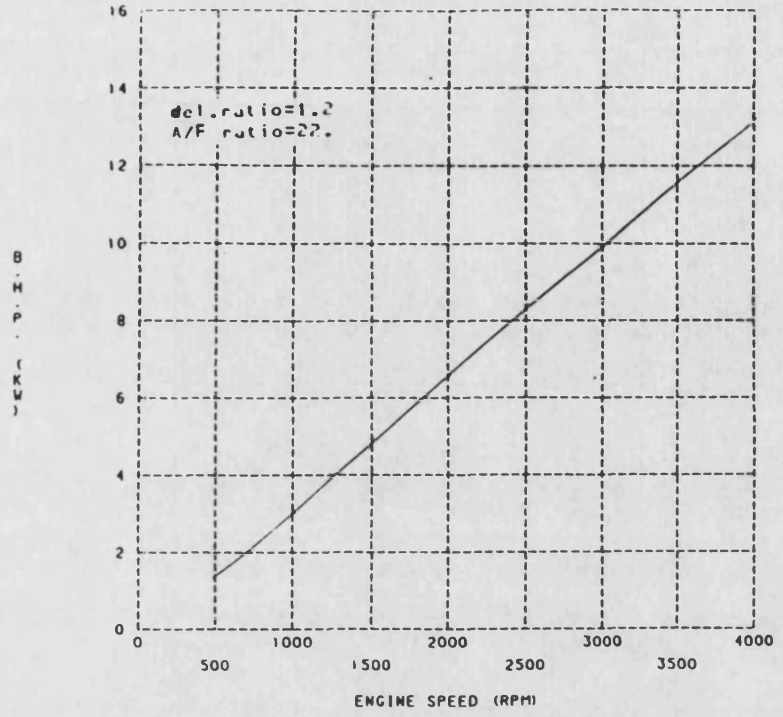

Fig. 8.9 Brake Horsepower of Uncooled Engine

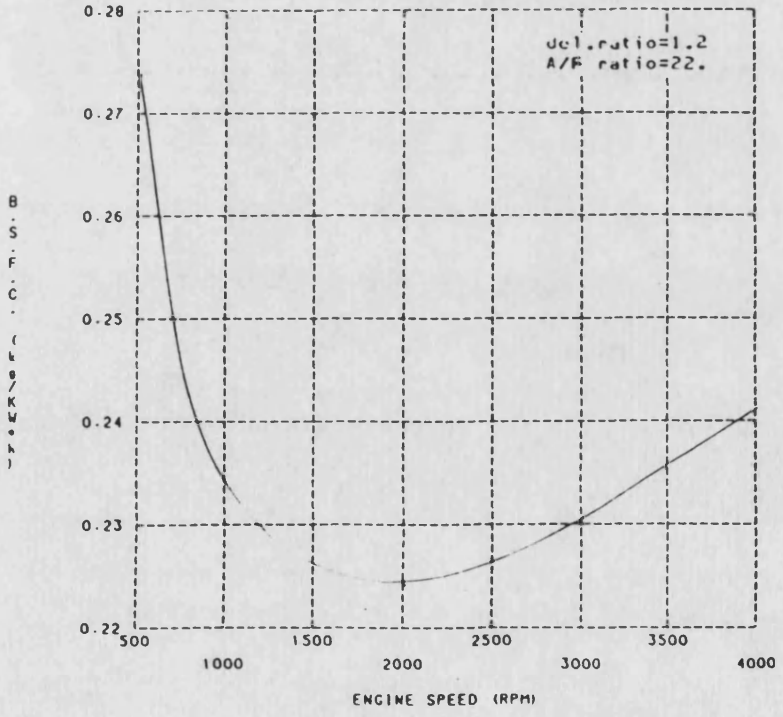

Fig. 8.10 Brake Specific Fuel Consumption of Uncooled Engine

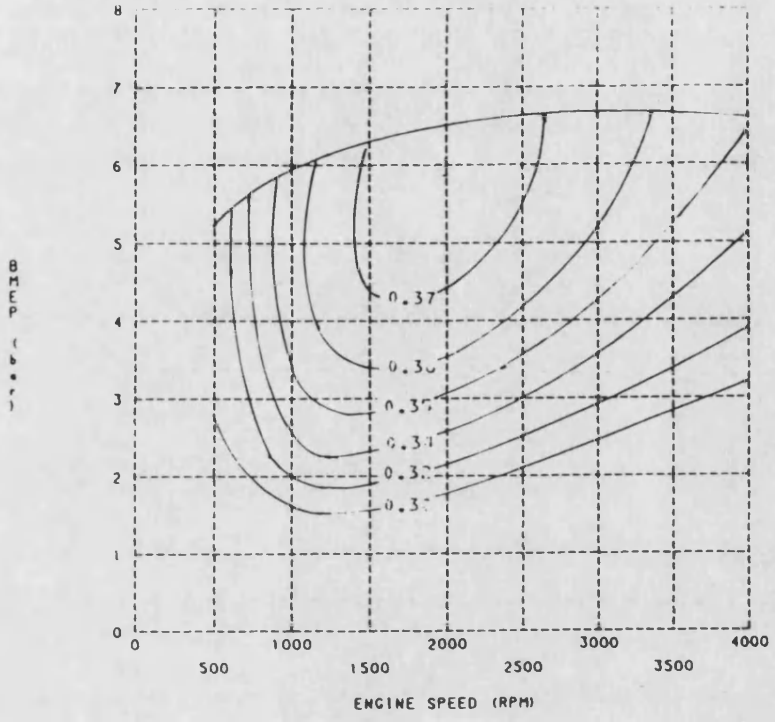

Fig. 8.11 Brake Thermal Efficiency of Uncooled Engine

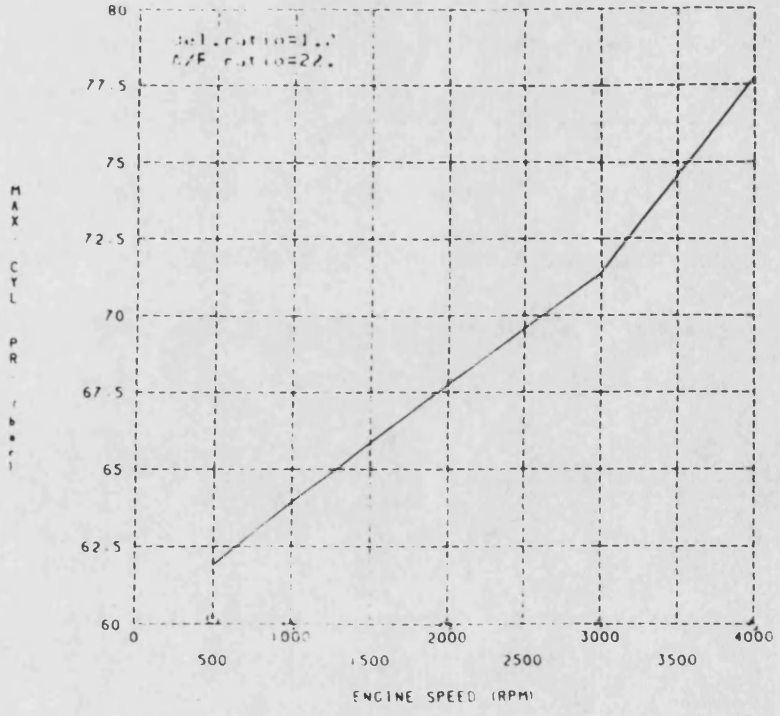

Fig. 8.12 Maximum Cylinder Pressure of Uncooled Engine

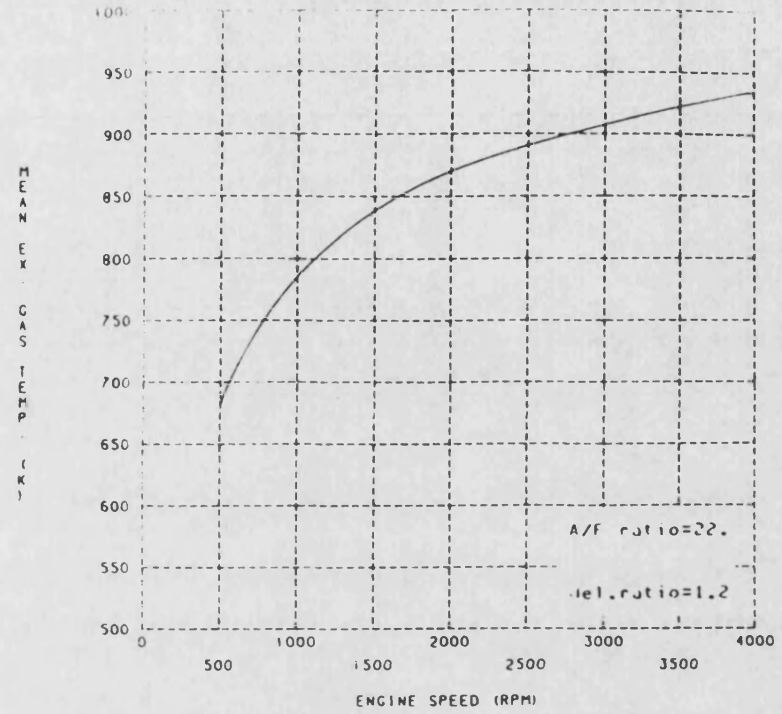

Fig. 8.13 Mean Exhaust Gas Temperature of Uncooled Engine

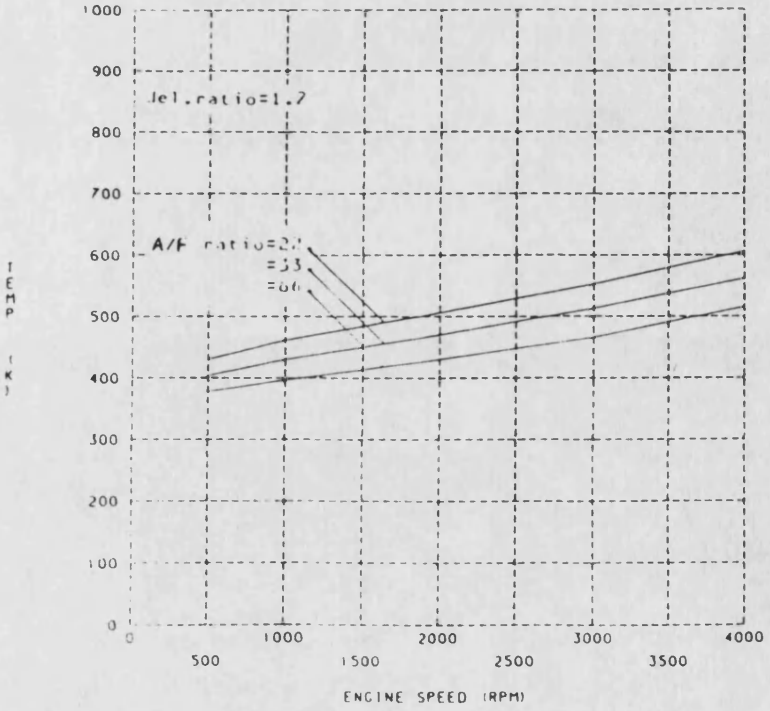

Fig. 8.14 Mean Liner Surface Temperature of Uncooled Engine

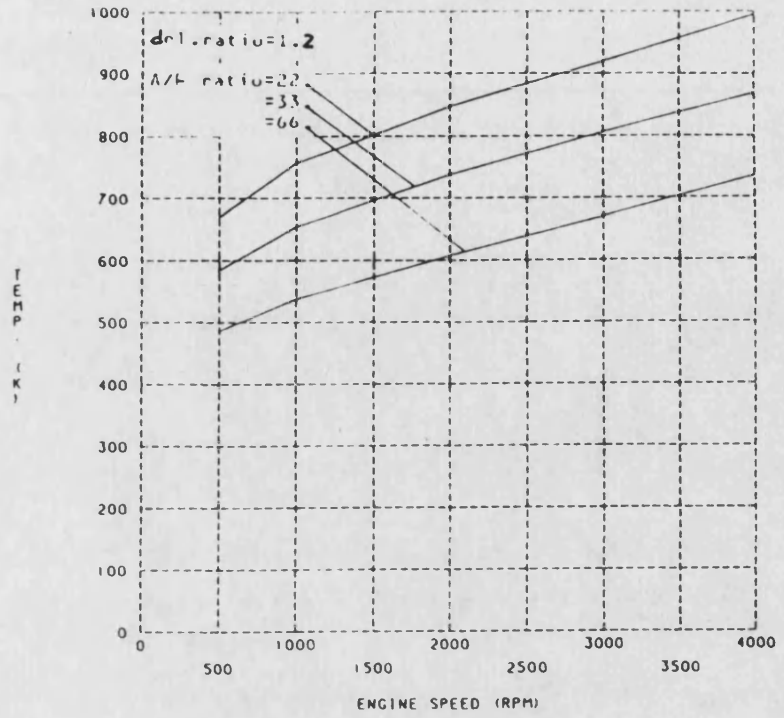

Fig. 8.15 Mean Piston Surface Temperature of Uncooled Engine

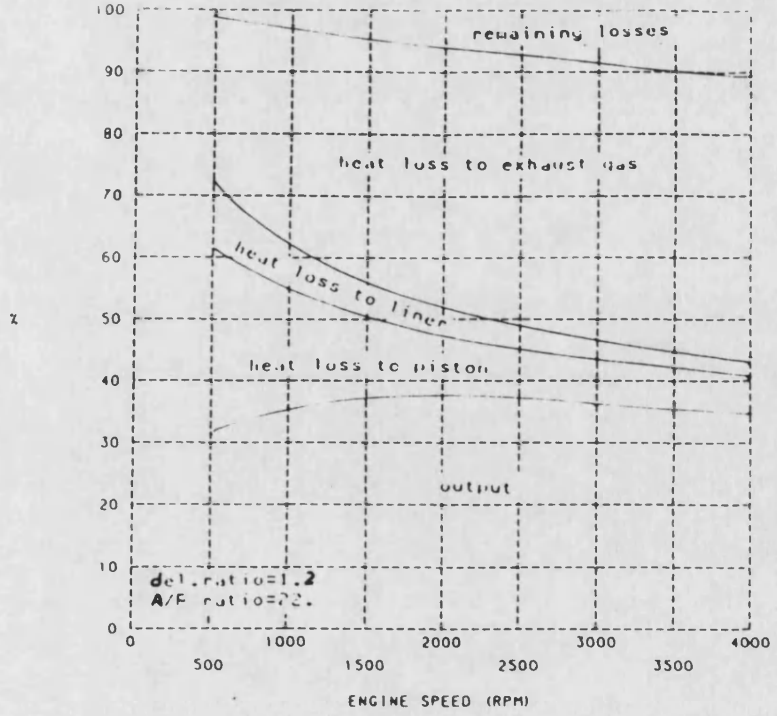

Fig. 8.16 Heat Balance of Uncooled Engine

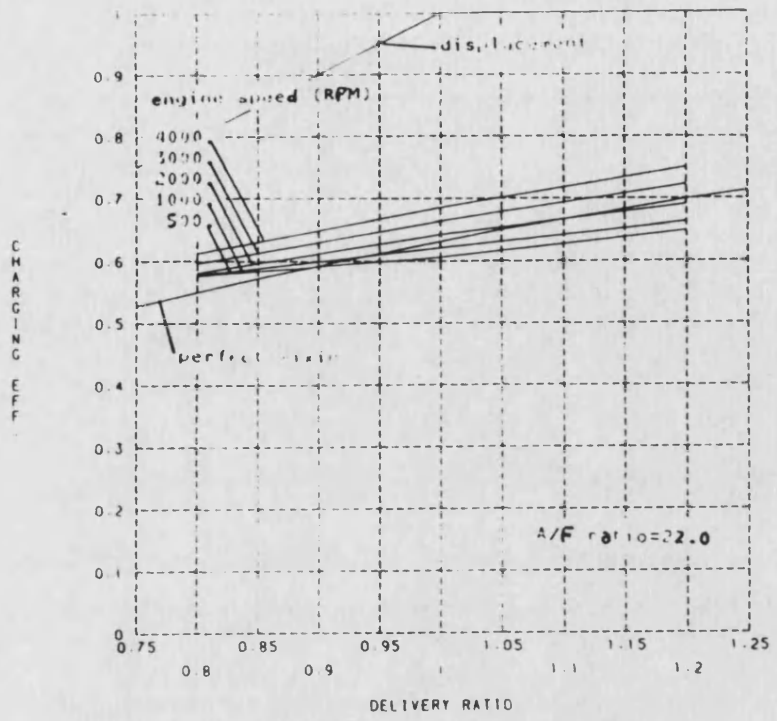

Fig. 8.17 Effect of Water-Cooled Engine Speed on Charging Efficiency

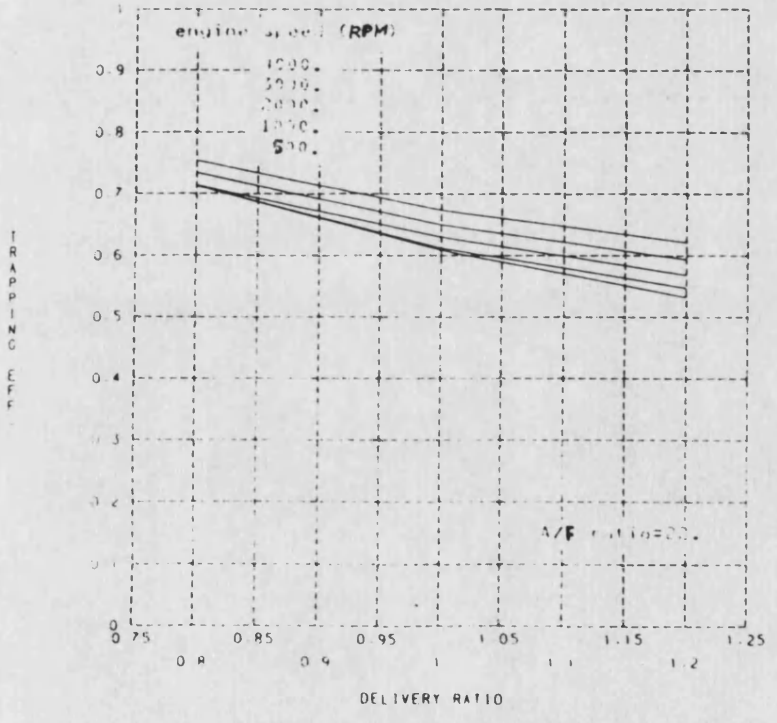

Fig. 8.18 Effect of Water-Cooled Engine Speed on Trapping Efficiency

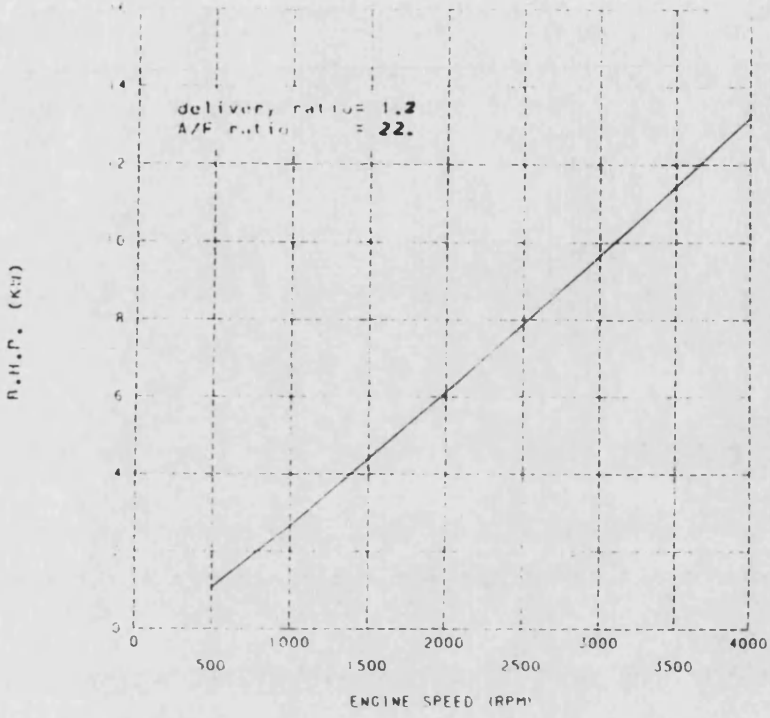

Fig. 8.19 Brake Horsepower of Water-Cooled Engine

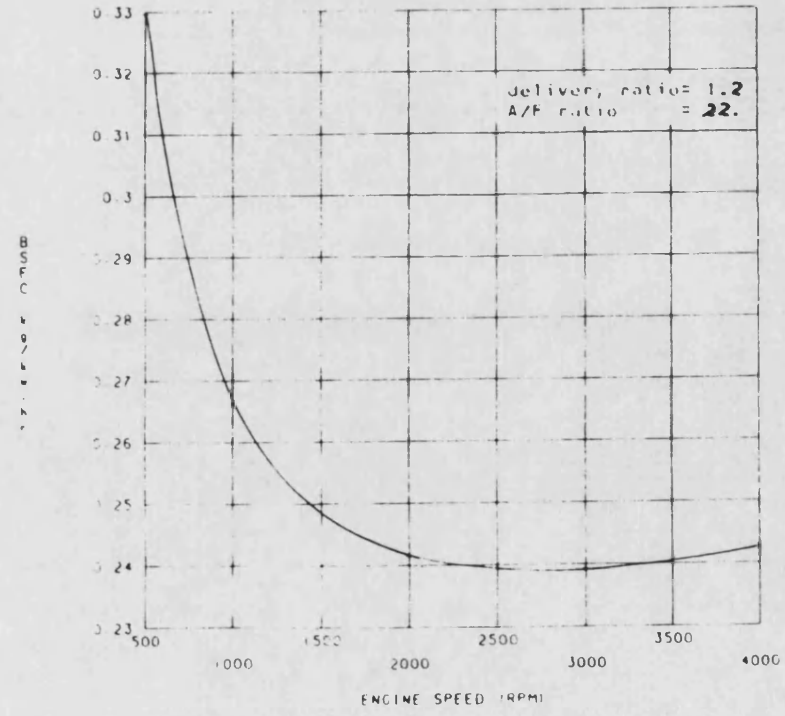

Fig. 8.20 Brake Specific Fuel Consumption of Water-Cooled Engine

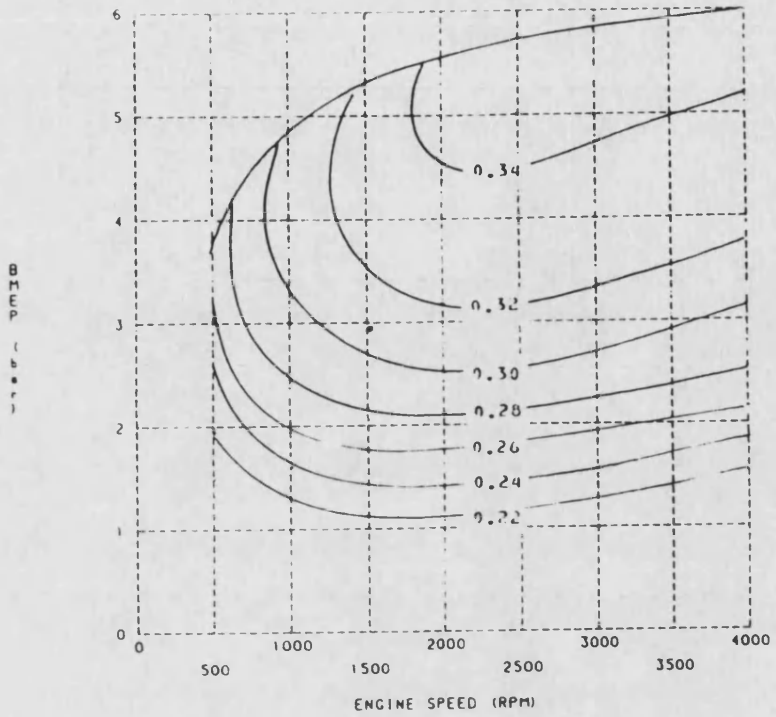

Fig. 8.21 Brake Thermal Efficiency of Water-Cooled Engine

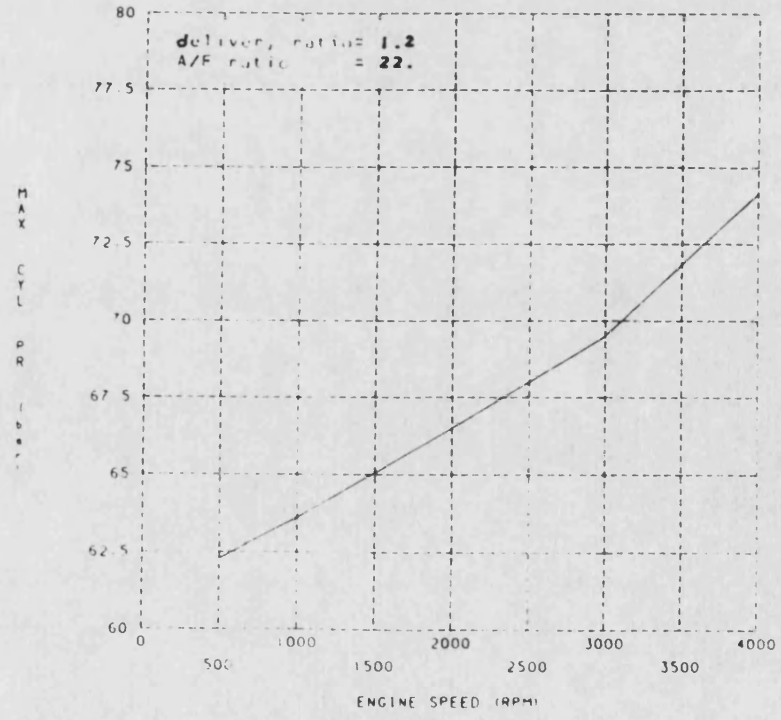

Fig. 8.22 Maximum Cylinder Pressure of Water-Cooled Engine

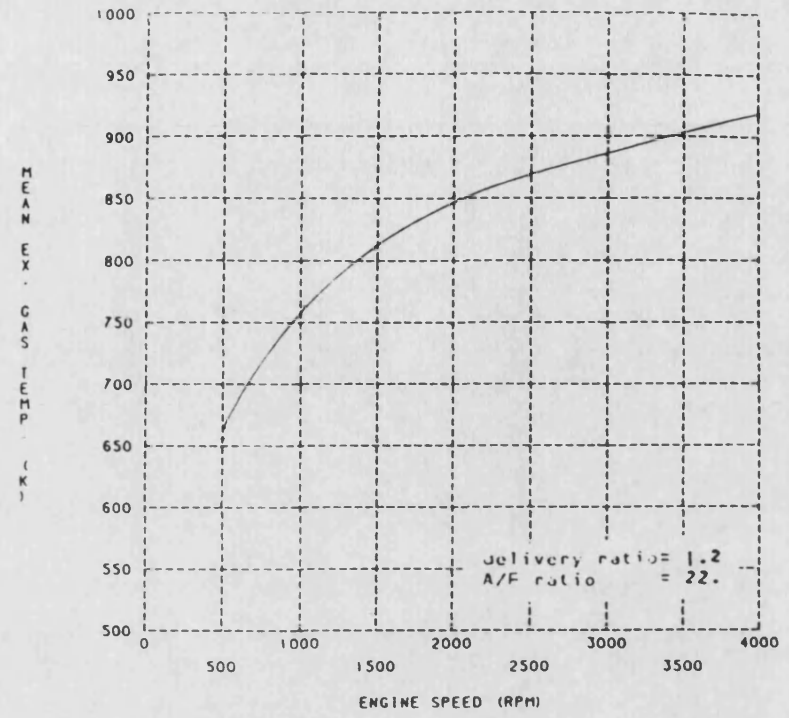

Fig. 8.23 Mean Exhaust Gas Temperature of Water-Cooled Engine

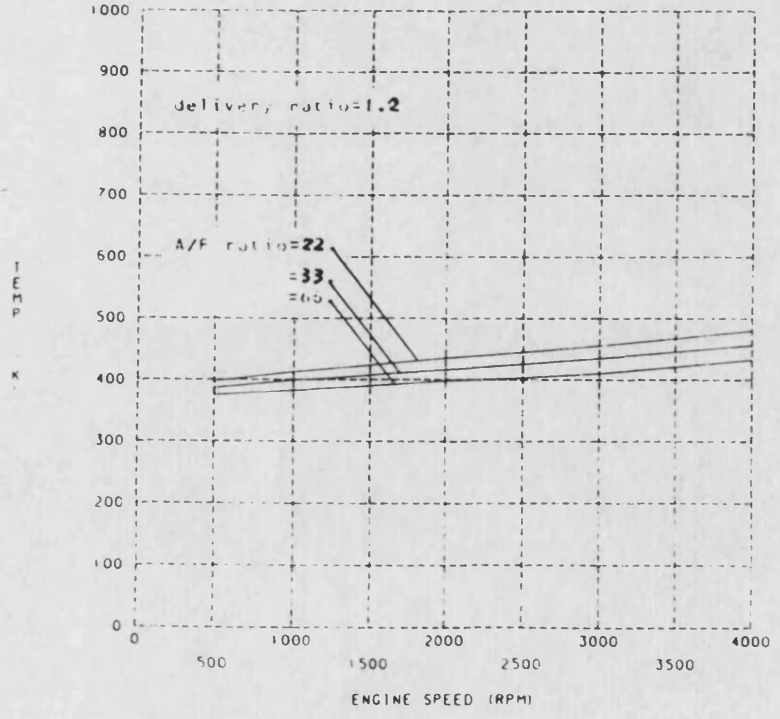

Fig. 8.24 Mean Liner Surface Temperature of Water-Cooled Engine

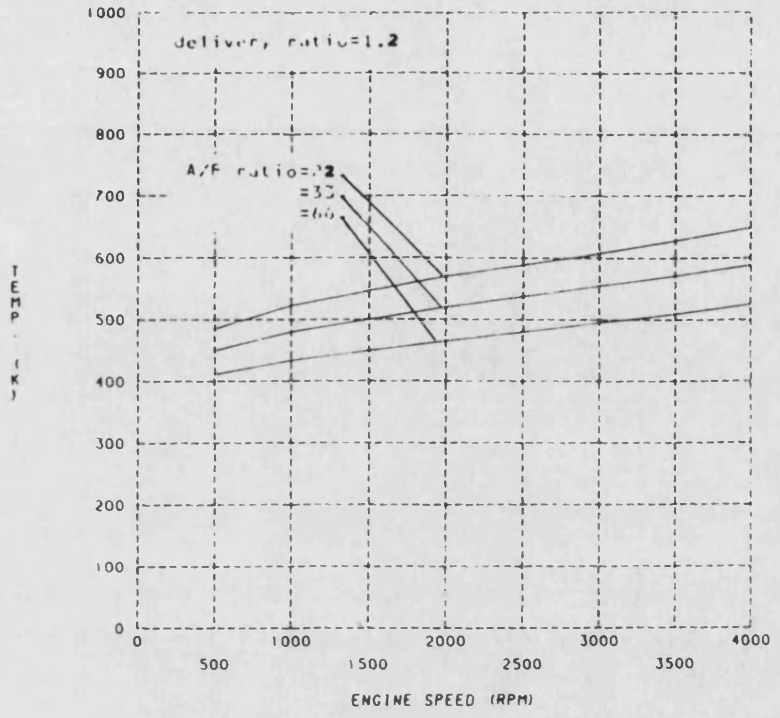

Fig. 8.25 Mean Piston Surface Temperature of Water-Cooled Engine

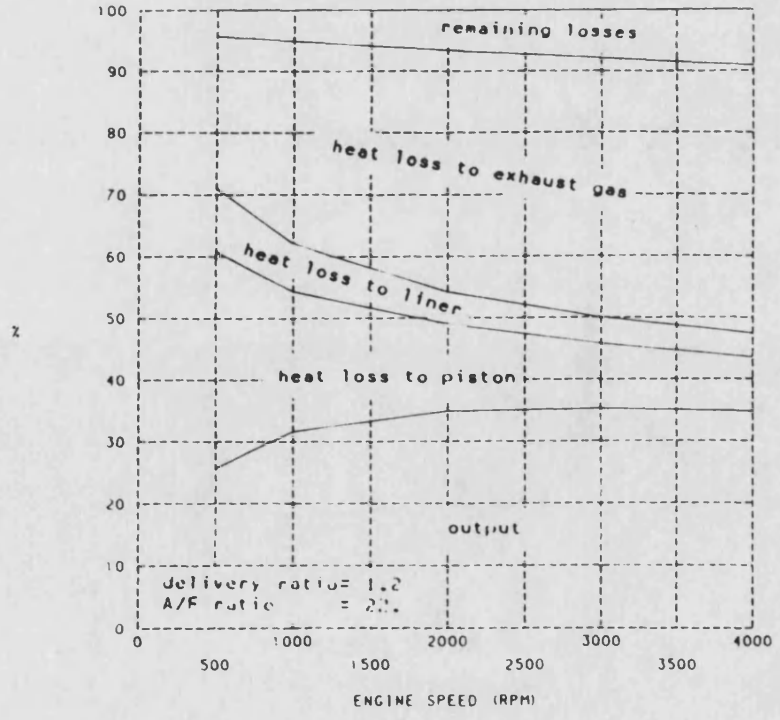

Fig. 8.26 Heat Balance of Water-Cooled Engine

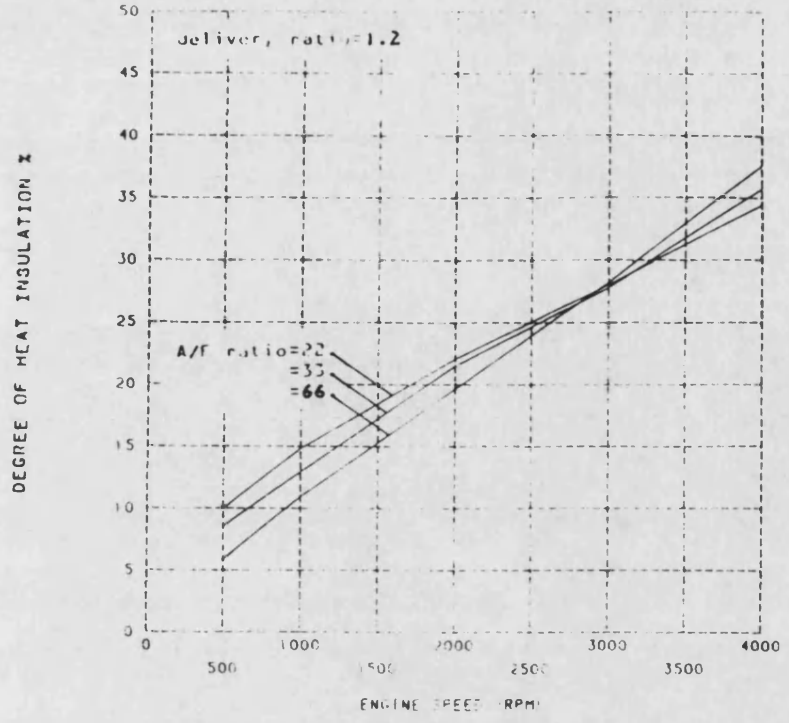

Fig. 8.27 Degree of Heat Insulation

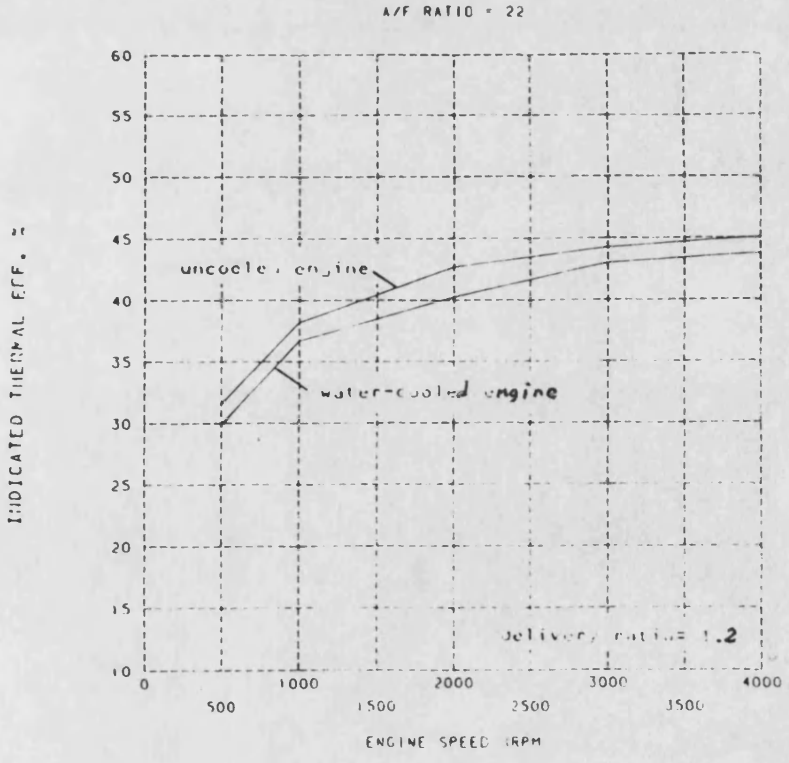

Fig. 8.28 Comparison of Indicated Thermal Efficiency

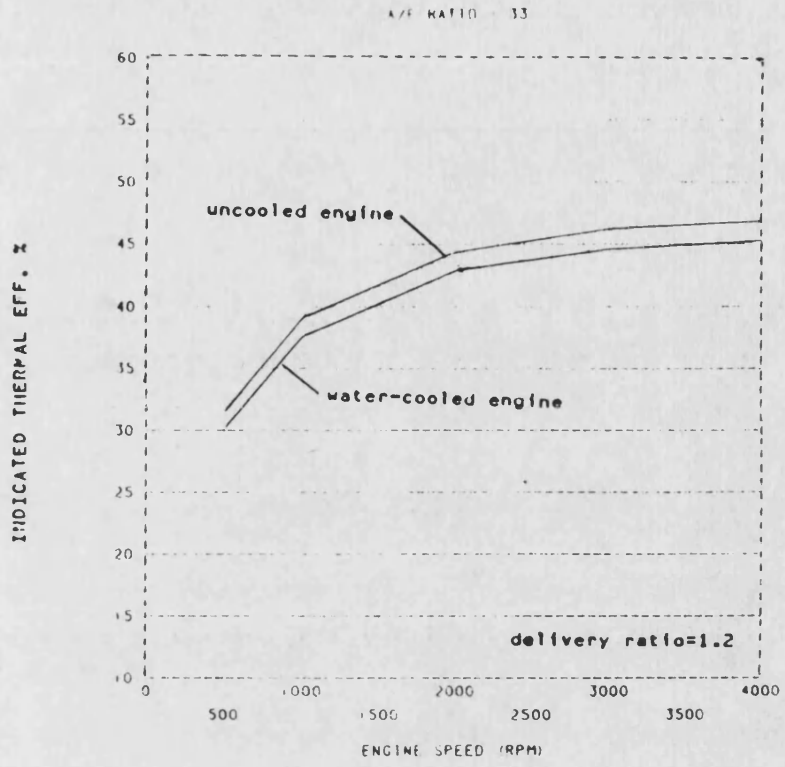
A/F RATIO = 33
INDICATED THERMAL EFF. %
60
55
50
45
40
35
30
25
20
15
10
uncooled engine
water-cooled engine
delivery ratio=1.2
0
1000
2000
3000
4000
500
1500
2500
3500
ENGINE SPEED (RPM)

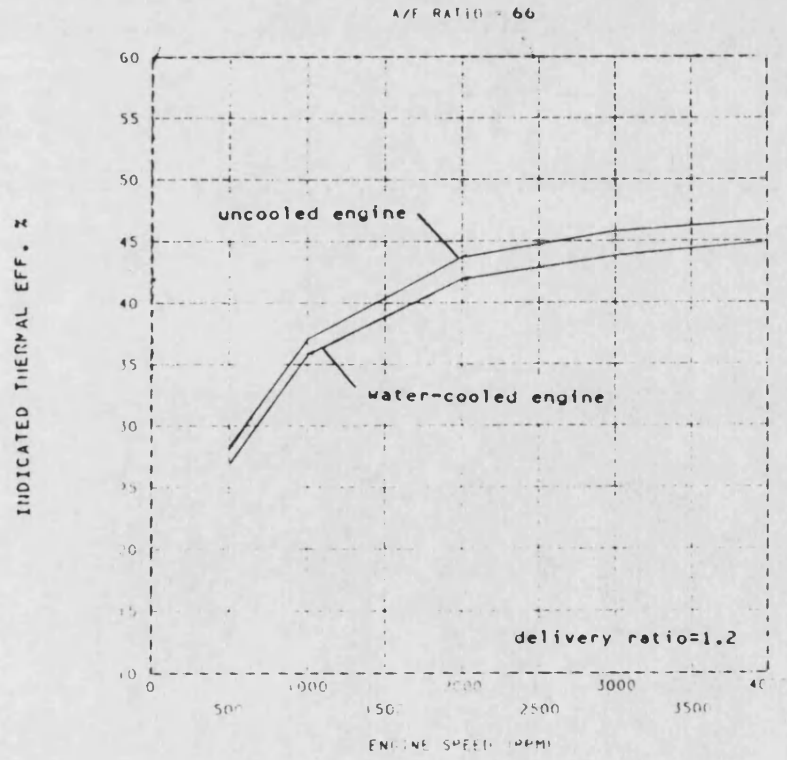
A/F RATIO = 66
INDICATED THERMAL EFF. %
60
55
50
45
40
35
30
uncooled engine
water-cooled engine
delivery ratio=1.2
0
3000
2500
3500
ENGINE SPEED (RPM)

Fig. 8.28 (cont.)

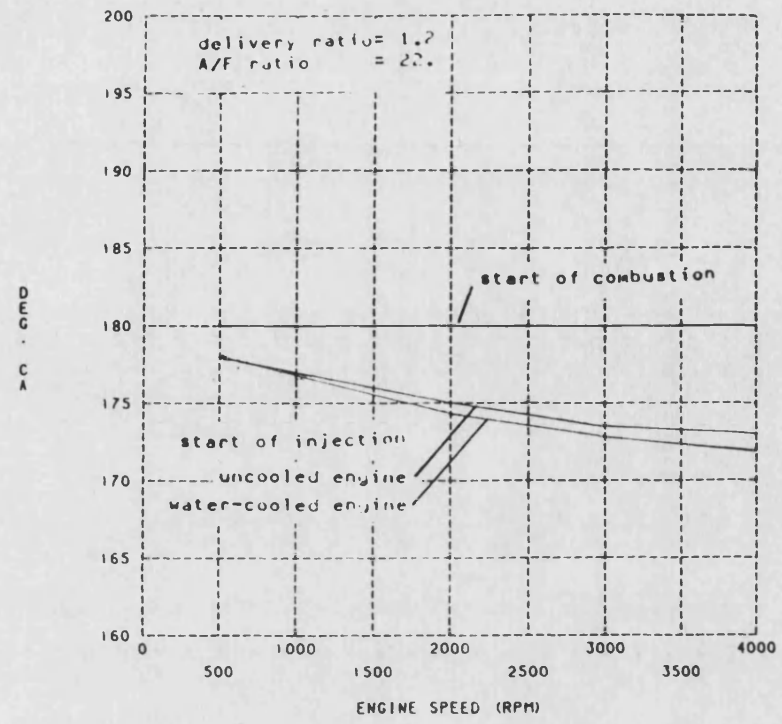

Fig. 8.29 Comparison of Ignition Delay

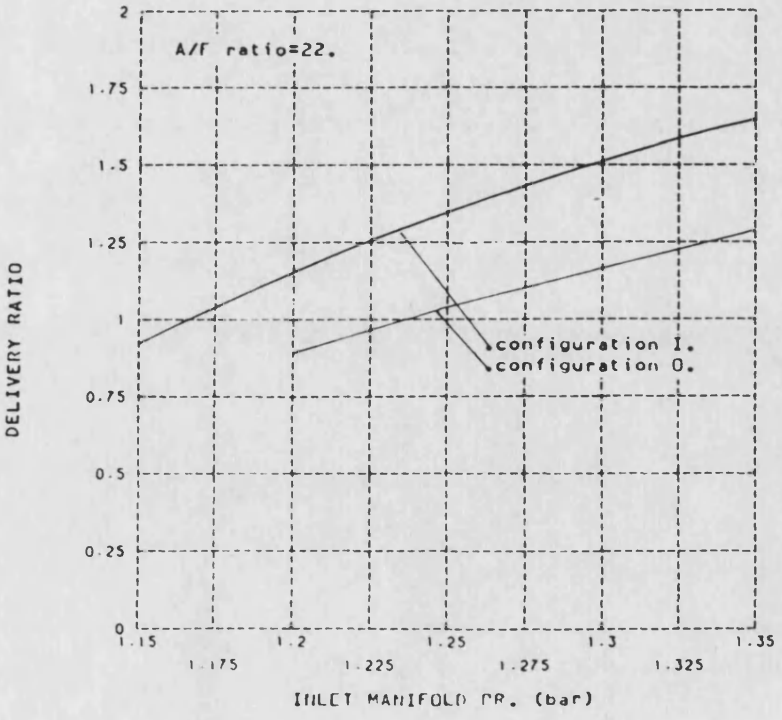

Fig. 8.30 Effect of Port Shape on Delivery Ratio

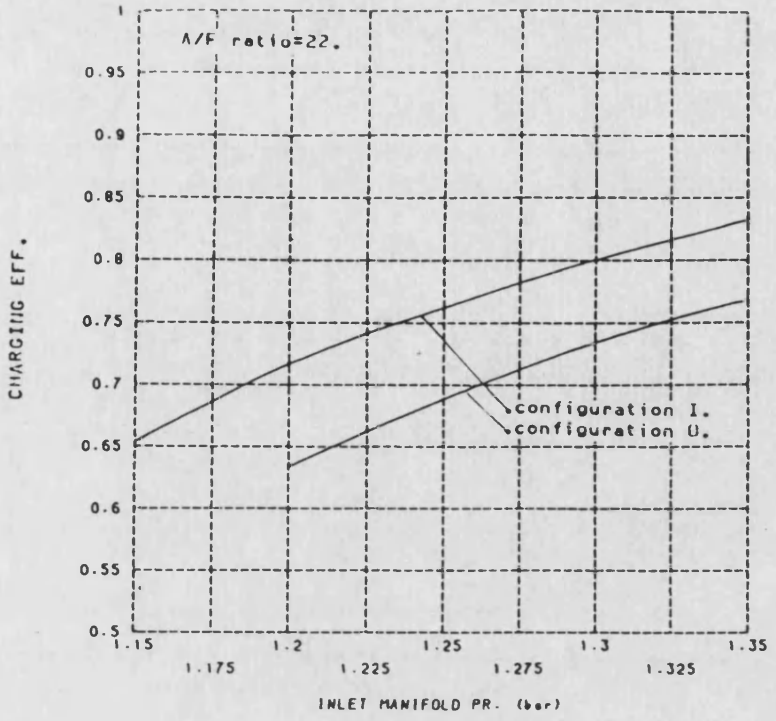

Fig. 8.31 Effect of Port Shape on Trapped Air Mass

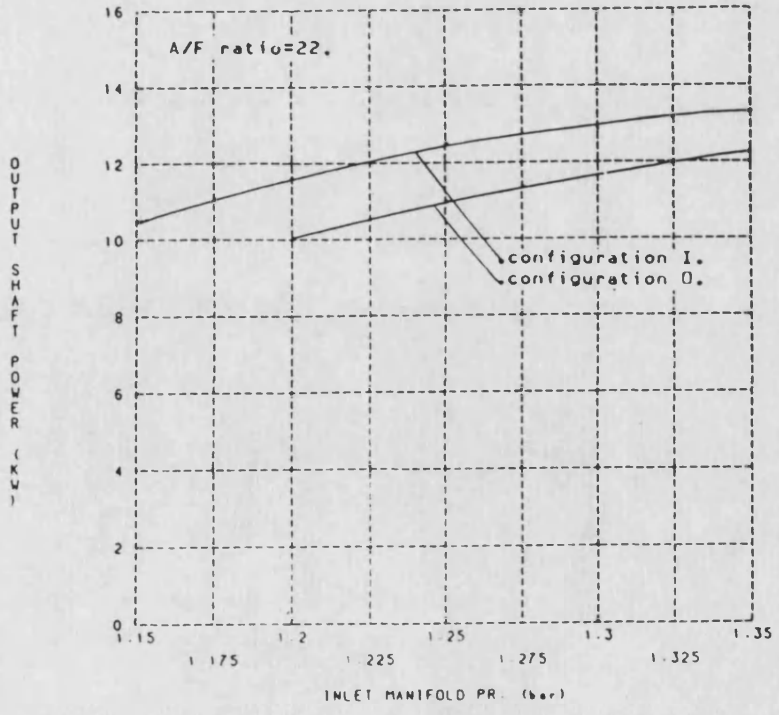

Fig. 8.32 Effect of Port Shape on Output Shaft Power

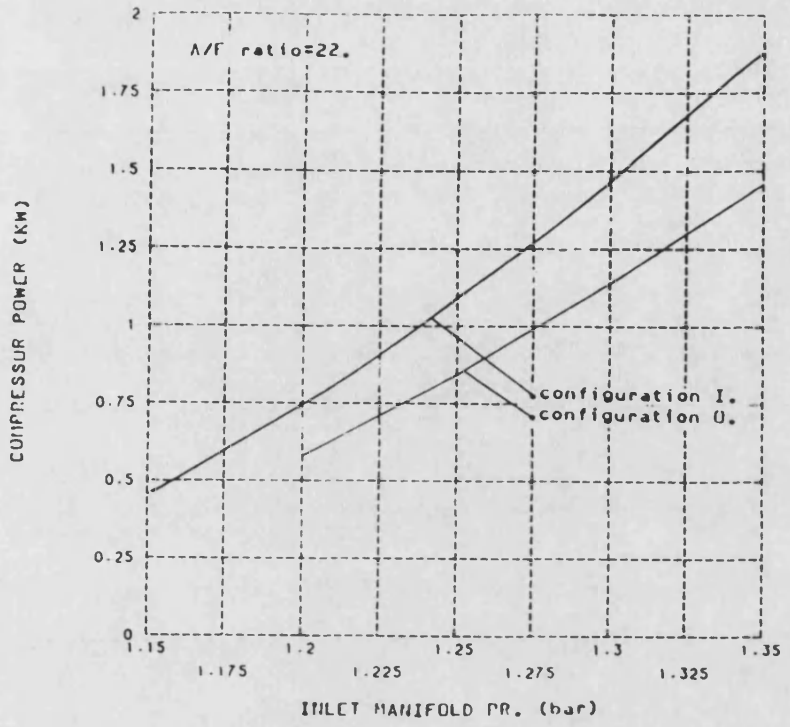

Fig. 8.33 Effect of Port Shape on Compressor Power

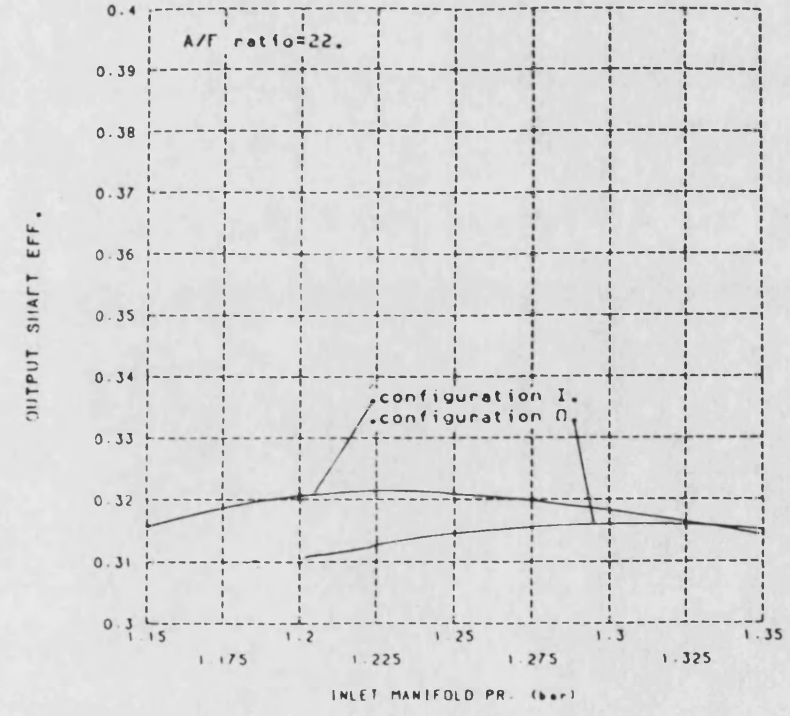

Fig. 8.34 Effect of Port Shape on Output Shaft Efficiency

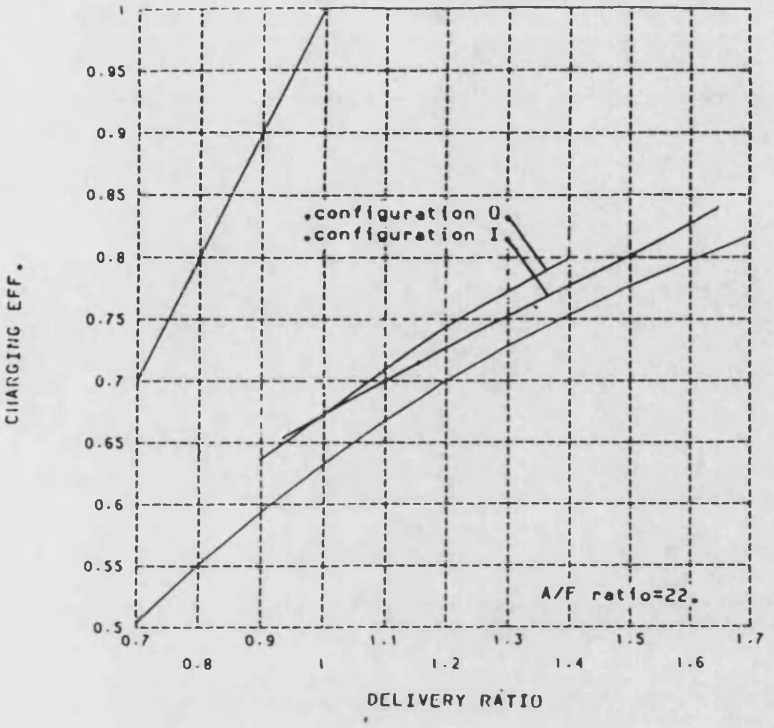

Fig. 8.35 Effect of Port Shape on Charging Efficiency

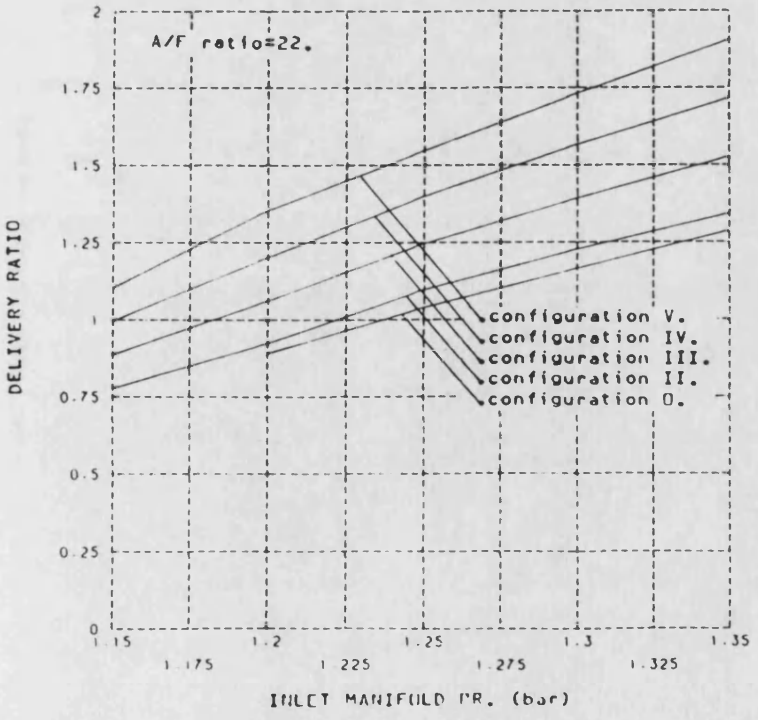

Fig. 8.36 Effect of Port Timing on Delivery Ratio

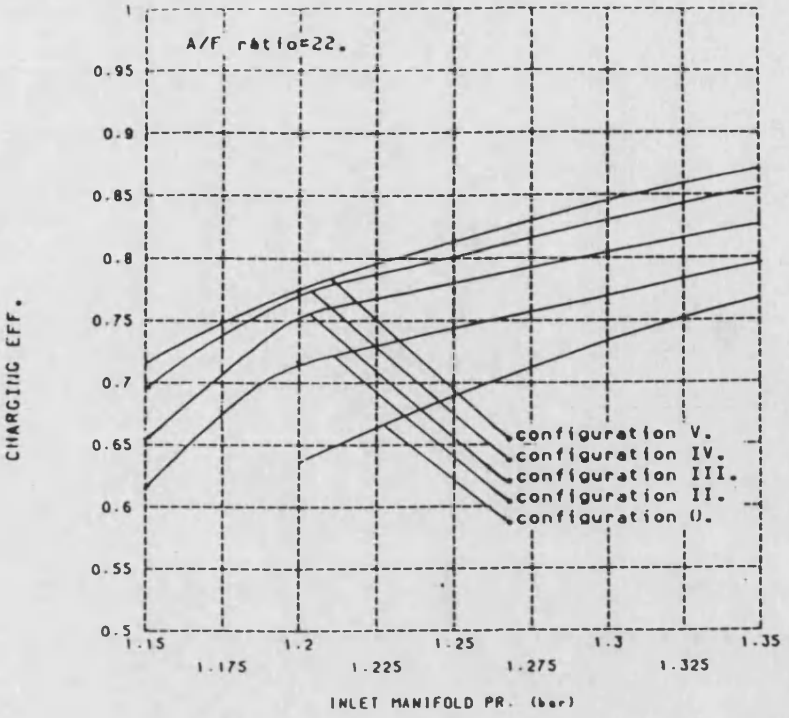

Fig. 8.37 Effect of Port Timing on Trapped Air Mass

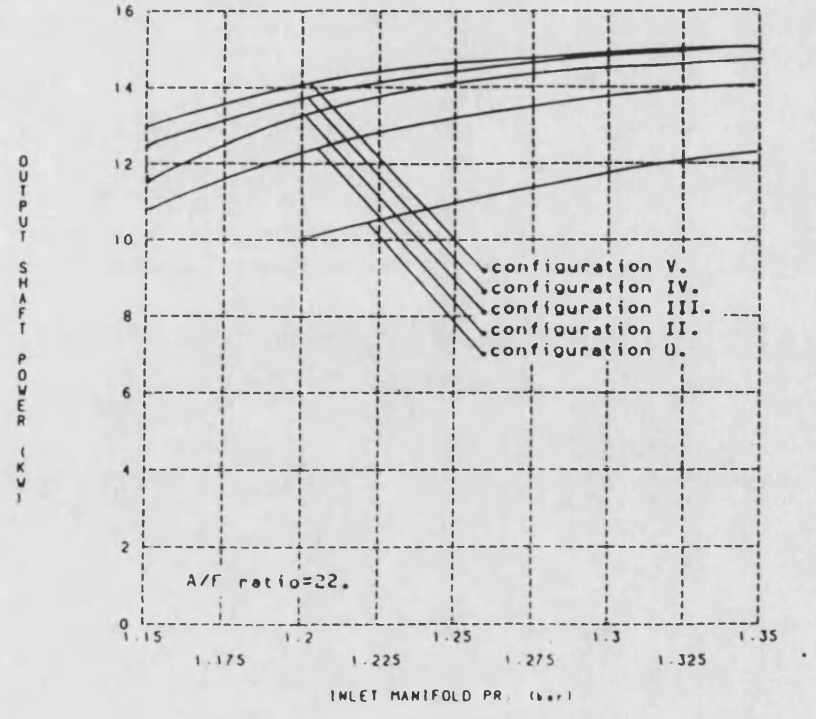

Fig. 8.38 Effect of Port Timing on Output Shaft Power

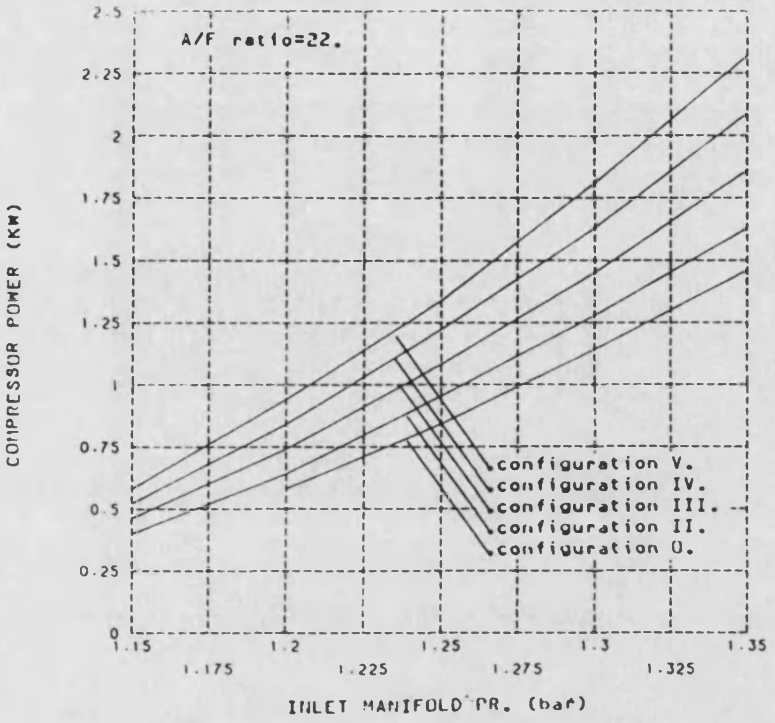

Fig. 8.39 Effect of Port Timing on Compressor Power

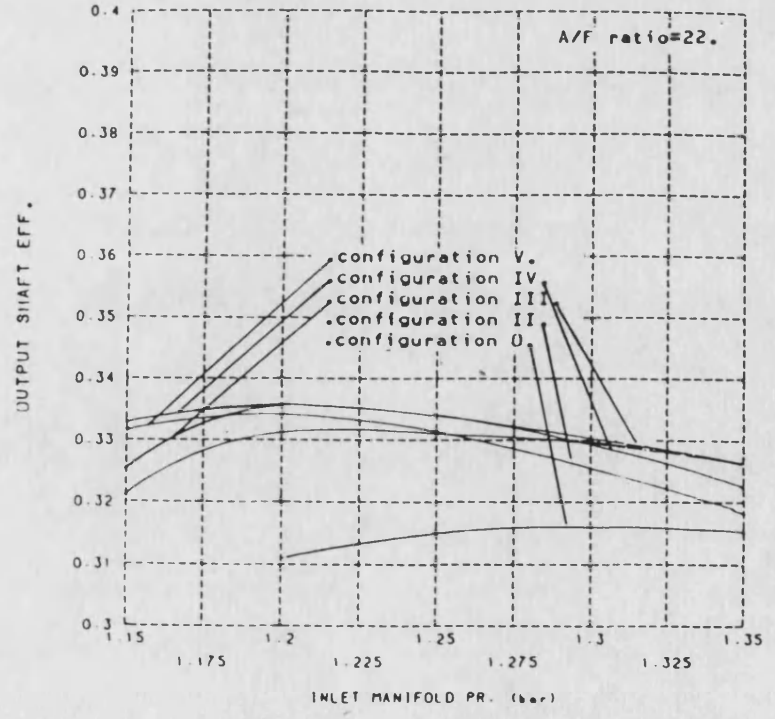

Fig. 8.40 Effect of Port Timing on Output Shaft Efficiency

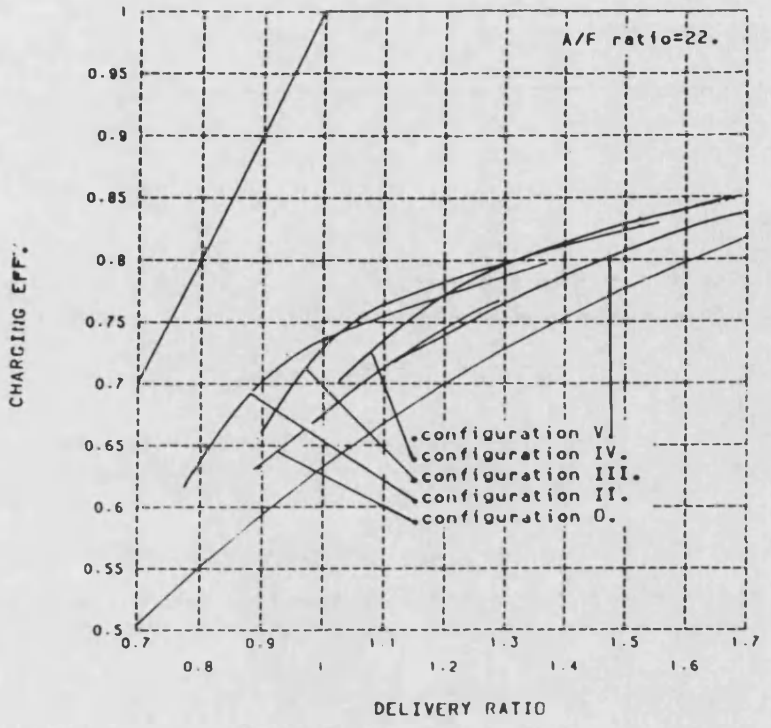

Fig. 8.41 Effect of Port Timing on Charging Efficiency

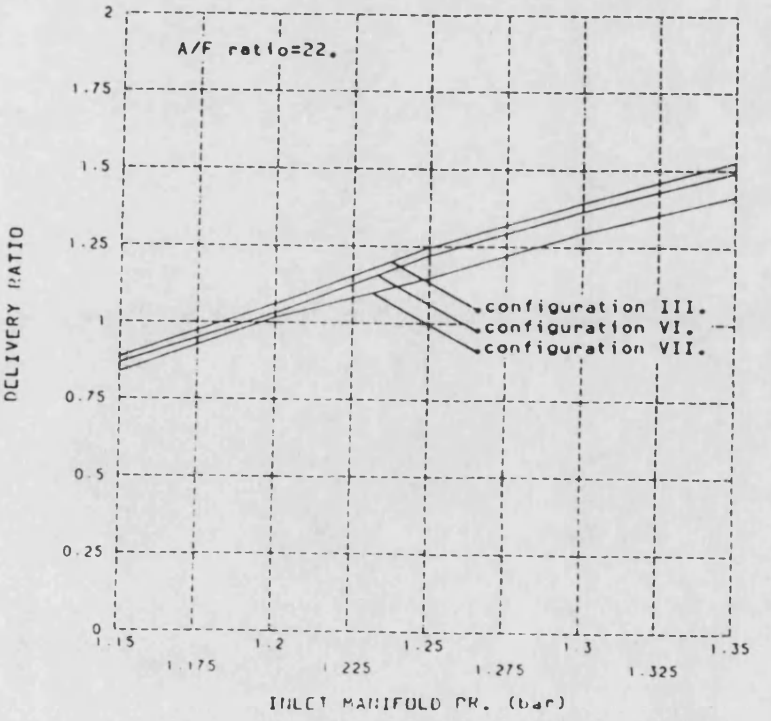

Fig. 8.42 Effect of Exhaust Port Height on Delivery Ratio

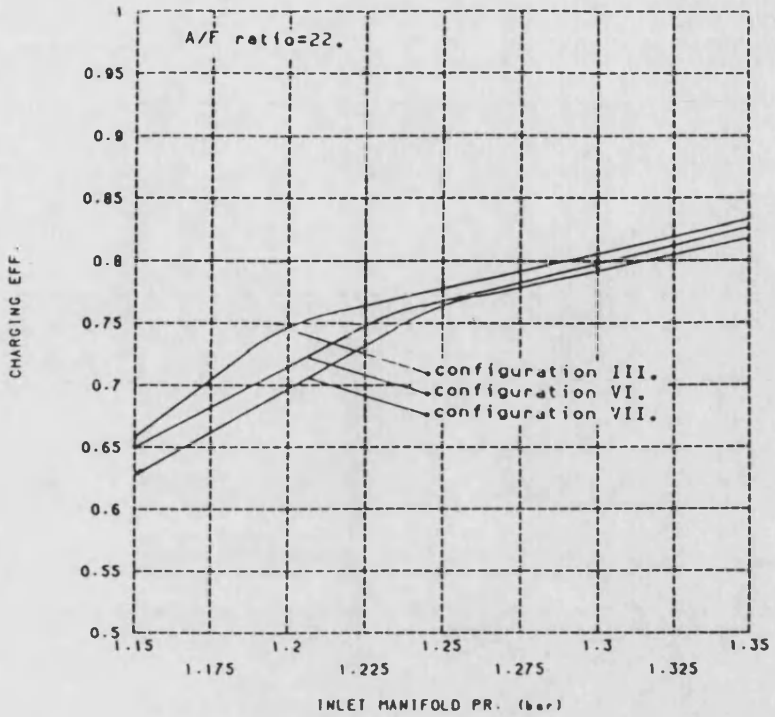

Fig. 8.43 Effect of Exhaust Port Height on Trapped Air Mass

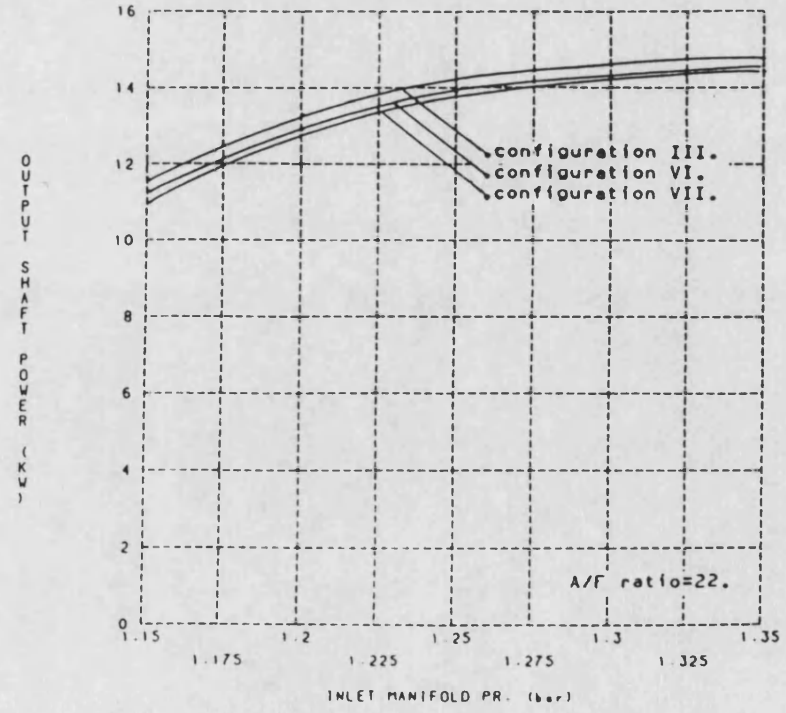

Fig. 8.44 Effect of Exhaust Port Height on Output Shaft Power

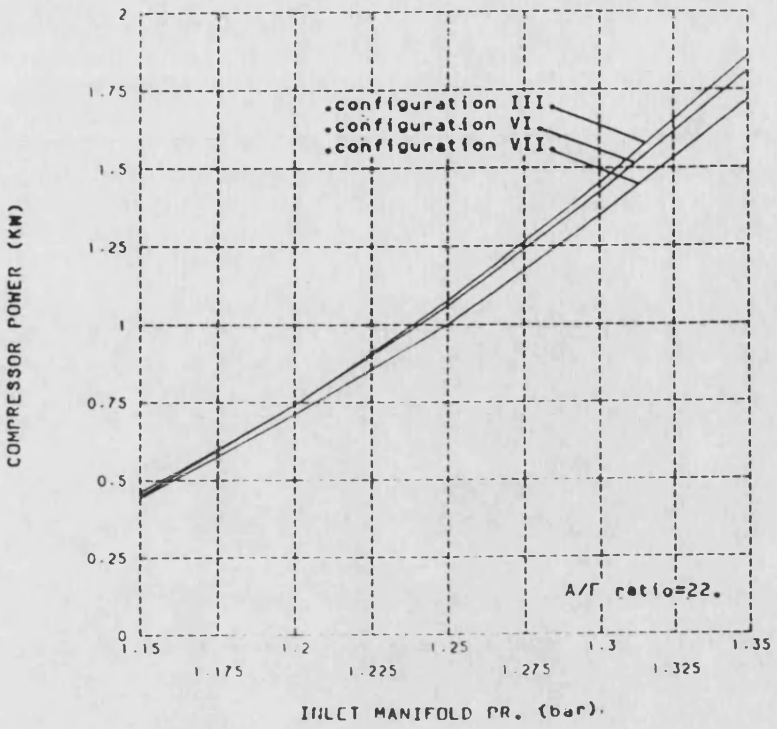

Fig. 8.45 Effect of Exhaust Port Height on Compressor Power

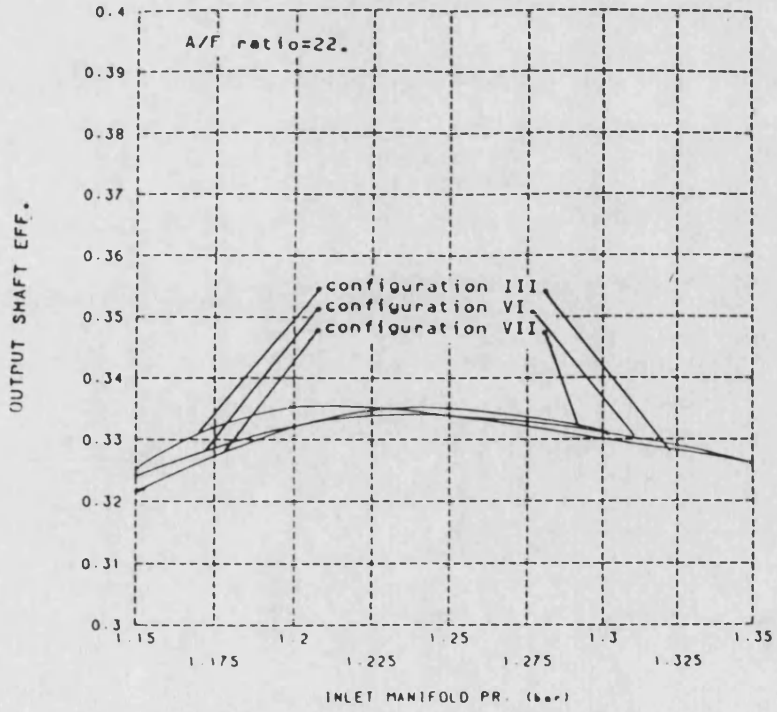

Fig. 8.46 Effect of Exhaust Port Height on Output Shaft Efficiency

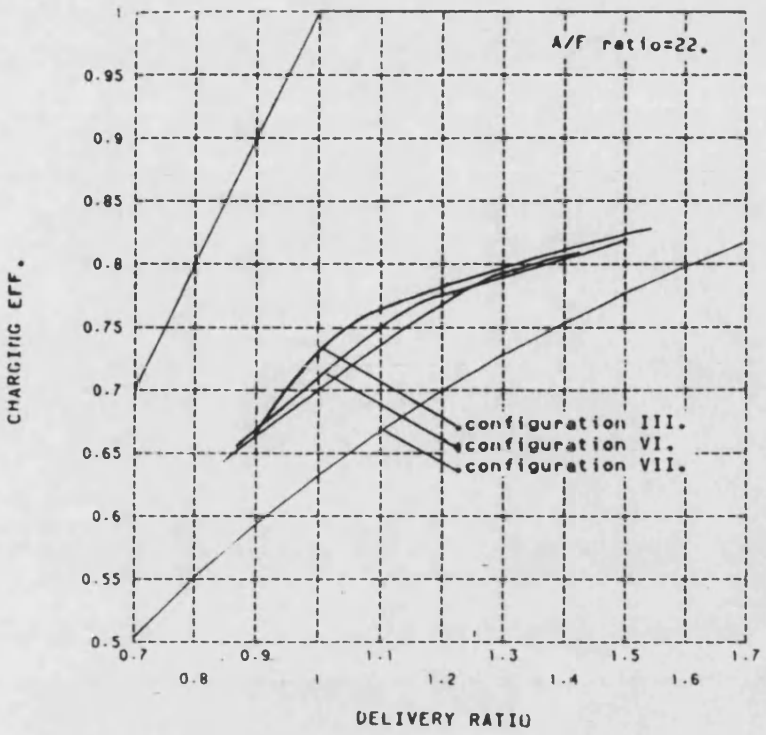

Fig. 8.47 Effect of Exhaust Port Height on Charging Efficiency

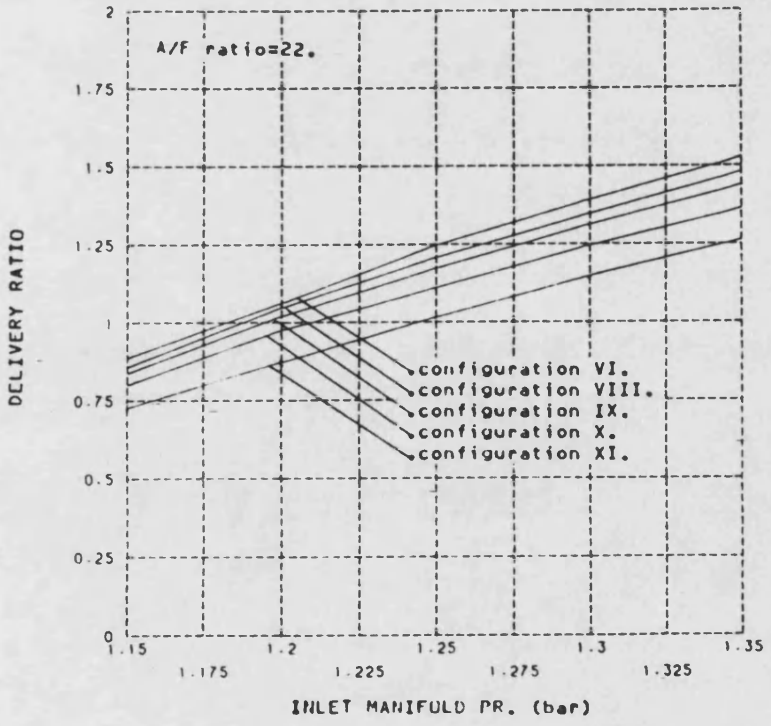

Fig. 8.48 Effect of Inlet Port Intake Angle on Delivery Ratio

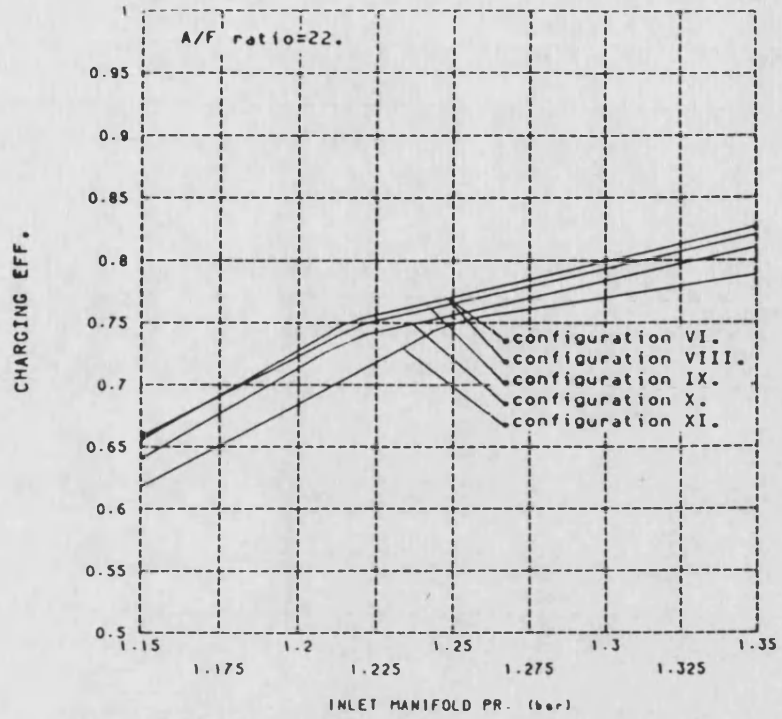

Fig. 8.49 Effect of Inlet Port Intake Angle on Trapped Air Mass

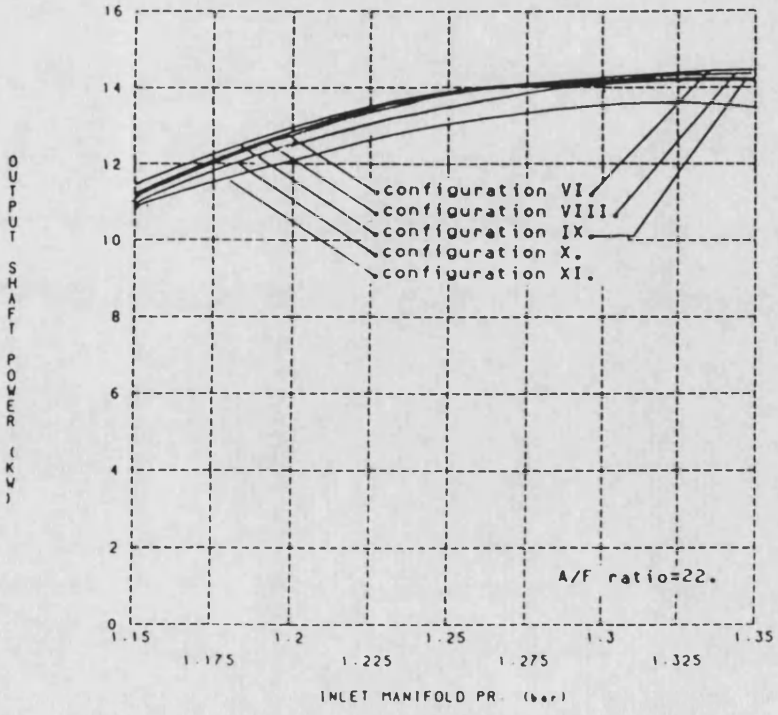

Fig. 8.50 Effect of Inlet Port Intake Angle on Output Shaft Power

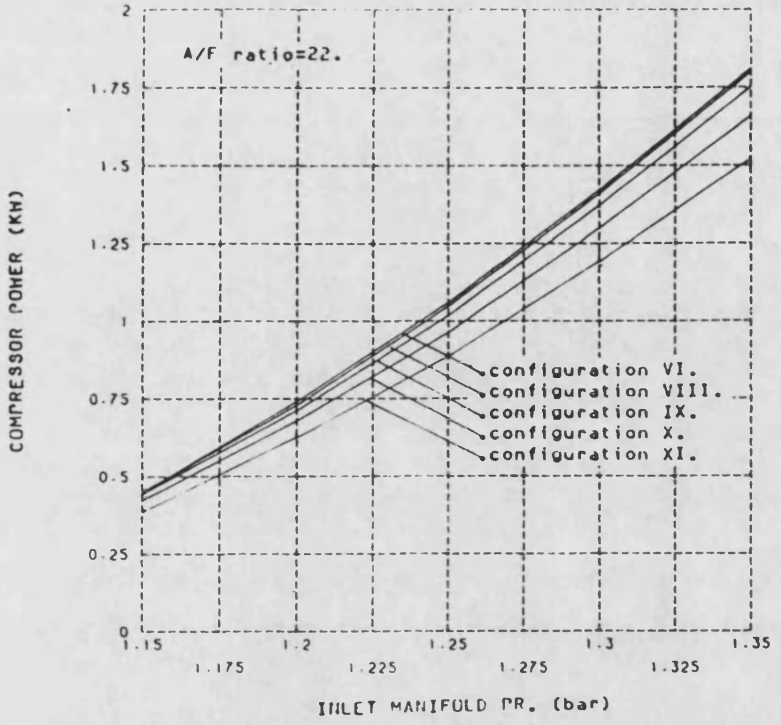

Fig. 8.51 Effect of Inlet Port Intake Angle on Compressor Power

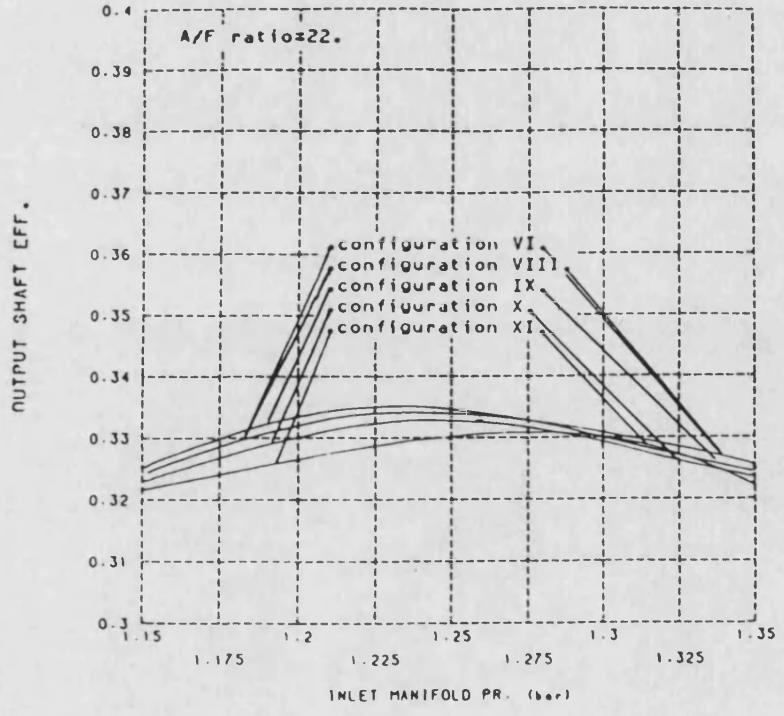

Fig. 8.52 Effect of Inlet Port Intake Angle on Output Shaft Efficiency

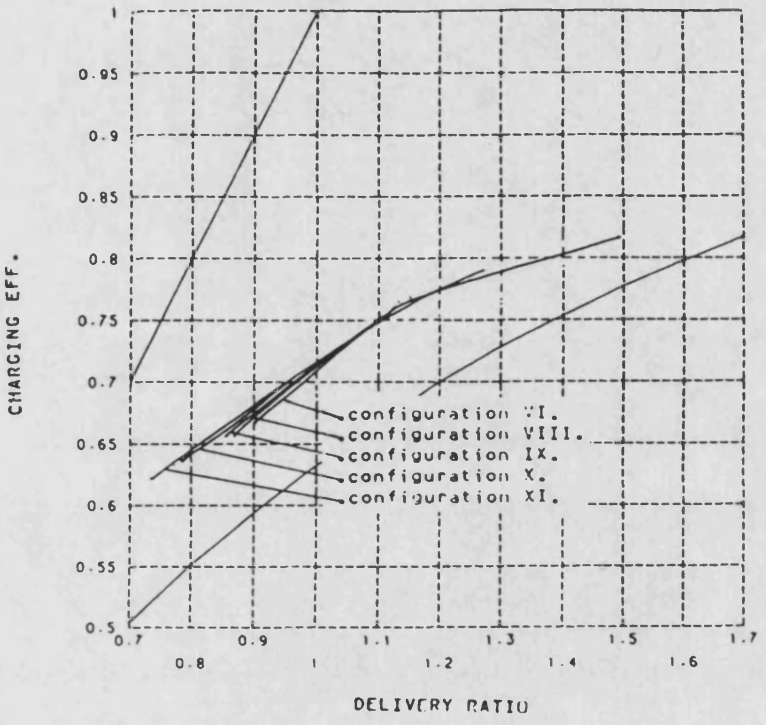

Fig. 8.53 Effect of Inlet Port Intake Angle on Charging Efficiency

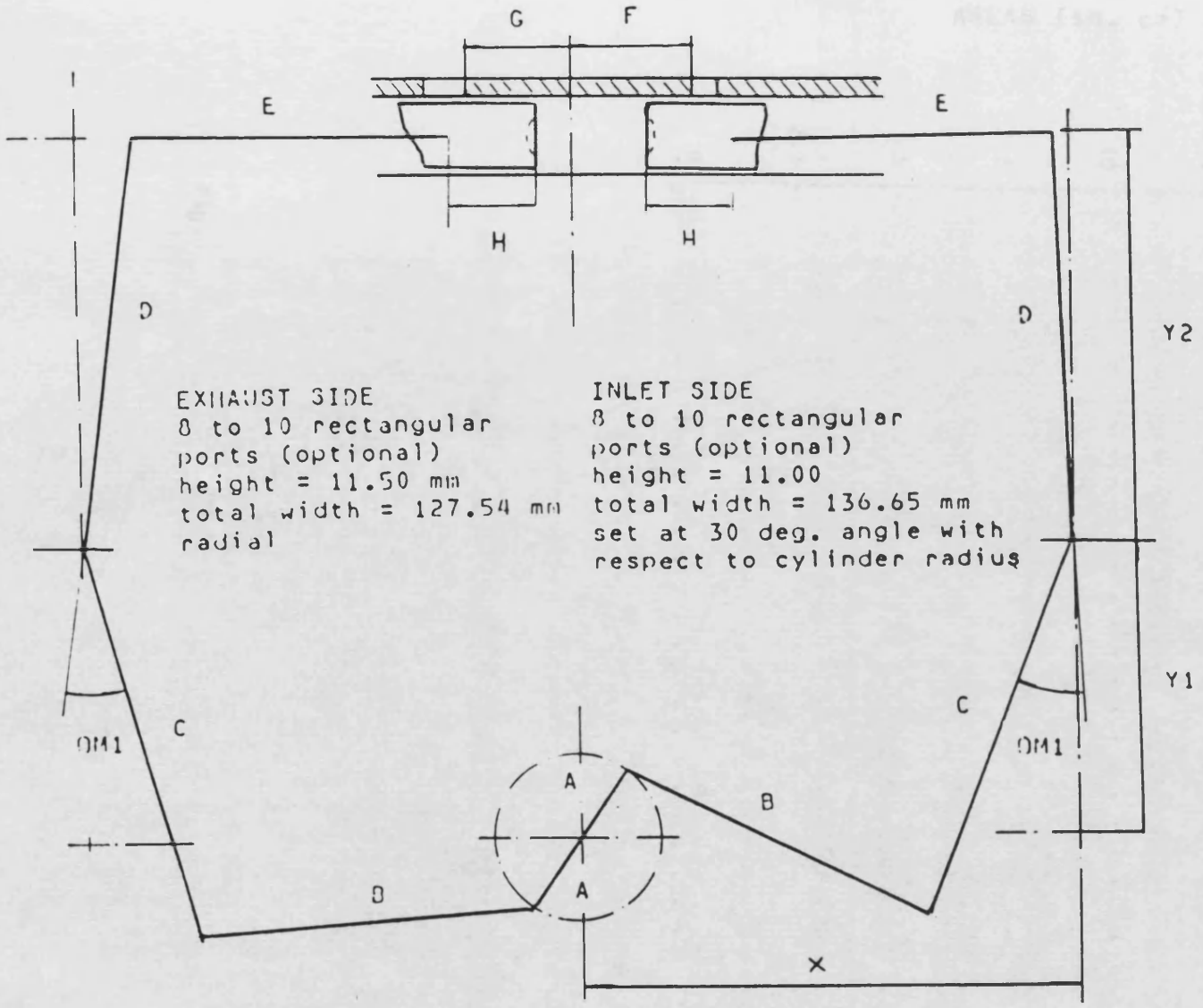

DIMENSIONS OF NEW SCHEME
A = 32.00 mm
B = 131.40 mm
C = 151.00 mm
D = 154.33 mm
E = 121.89 mm
F = 57.00 mm
G = 52.00 mm
H = 36.50 mm
X = 190.00 mm
Y1 = 112.35 mm
Y2 = 152.65 mm
OM1 = 23.507 mm
CYLINDER BORE = 53.00 mm
CYLINDER WALL = 16.00 mm
Vmax/Vmin = 22.00
STROKE = 133.51 mm
MINIMUM PISTON
SEPARATION = 1.777 mm
PISTON BOWL
VOLUME = 6.0657 cu. cm

Fig. 8.54 Linkage Geometry of Optimum Design

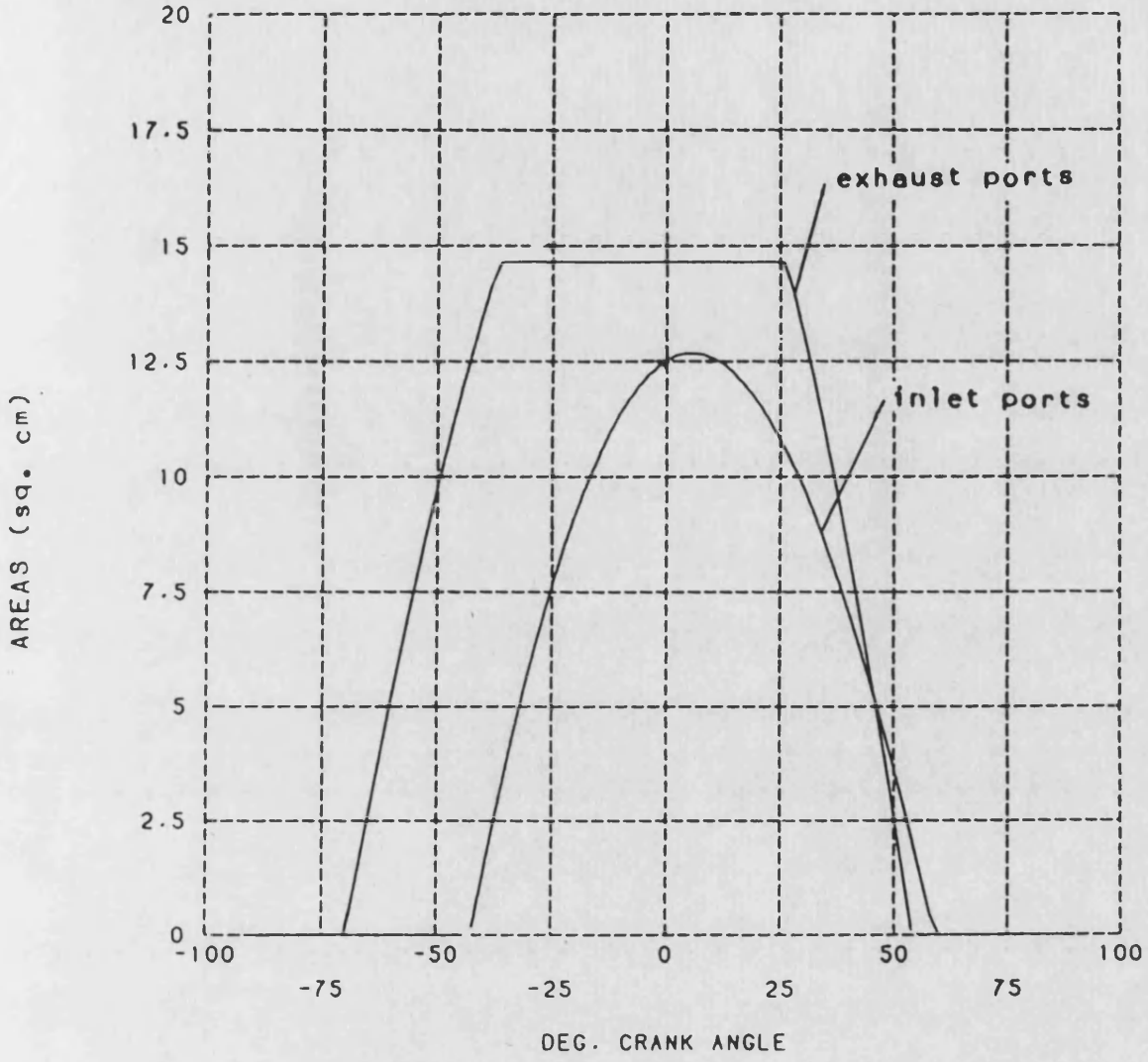

Fig. 8.55 Porting Diagram of Optimum Design

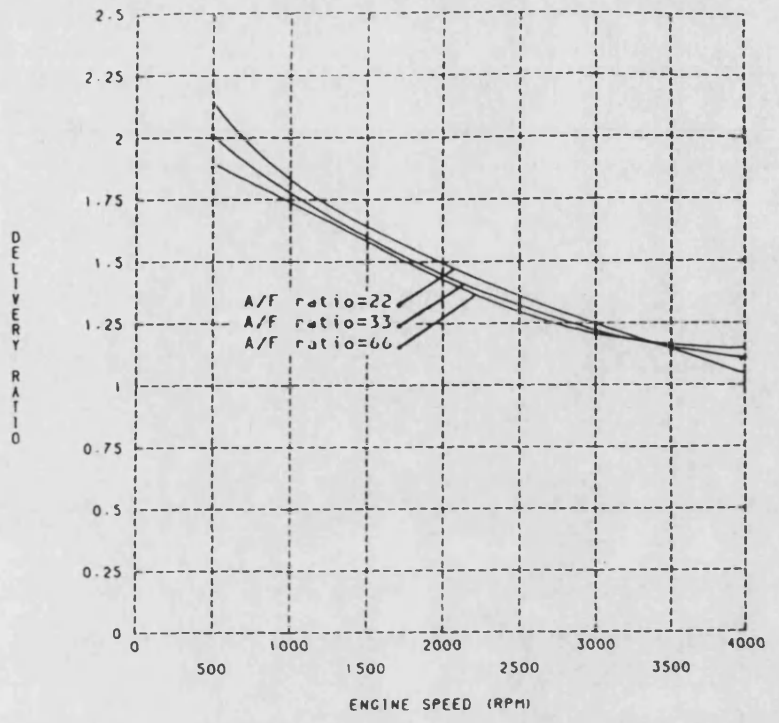

Fig. 8.56 Optimum Delivery Ratio

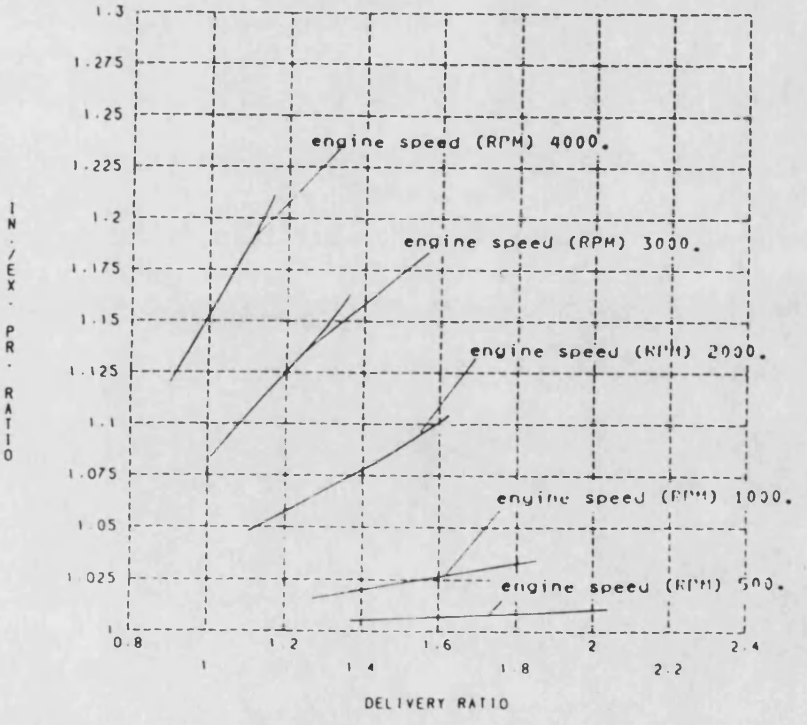

Fig. 8.57 Delivery Ratio versus Inlet/Exhaust Pressure Ratio in the Neibourhood of Optimum Delivery Ratio

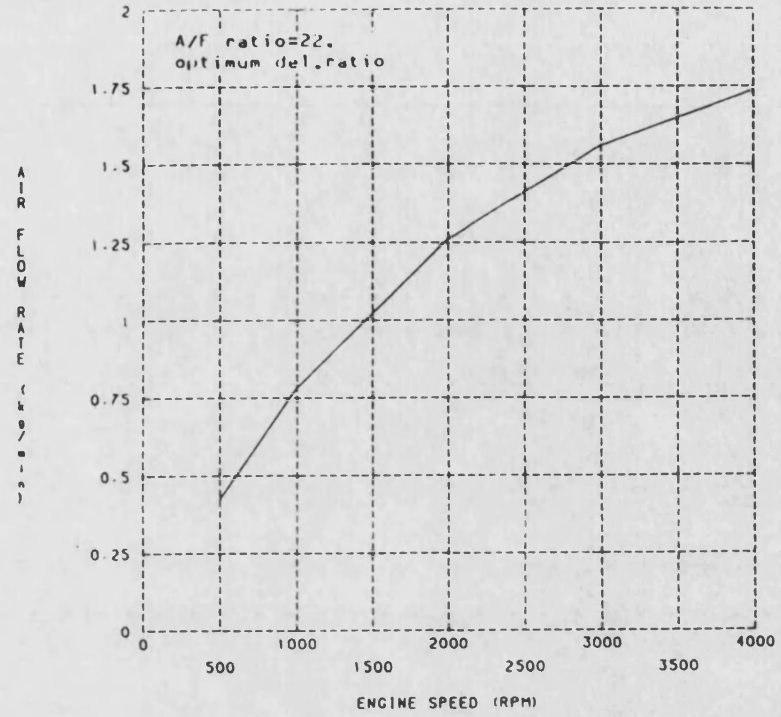

Fig. 8.58 Air Flow Rate of Optimum Scheme Running at Optimum Delivery Ratio

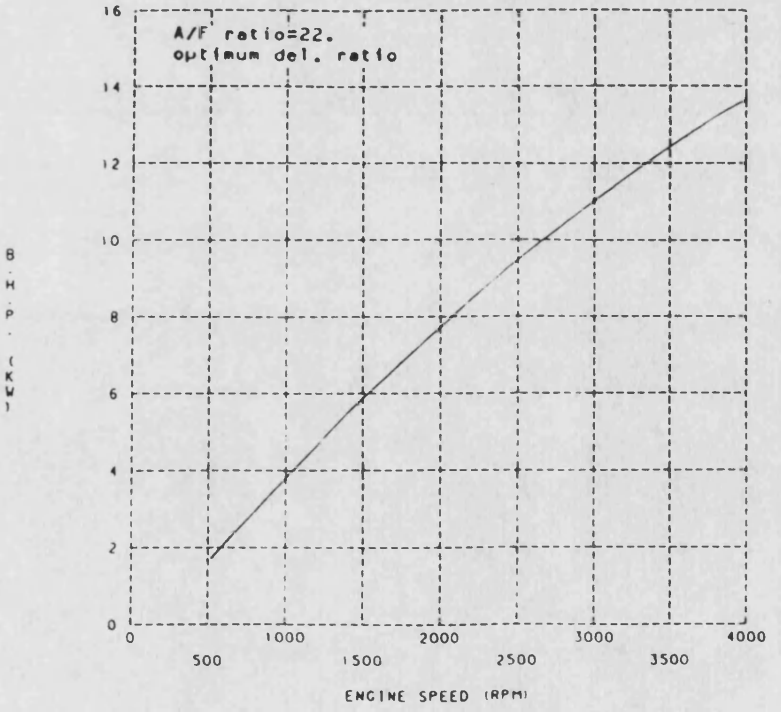

Fig. 8.59 Output Shaft Horsepower of Optimum Scheme Running at Optimum Delivery Ratio

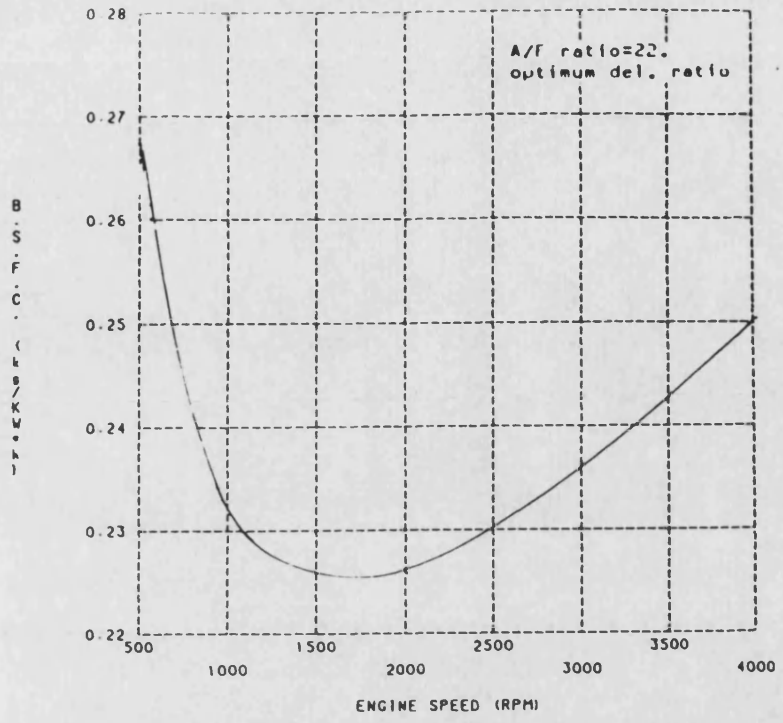

Fig. 8.60 Output Shaft Specific Fuel Consumption of Optimum Scheme Running at Optimum Delivery Ratio

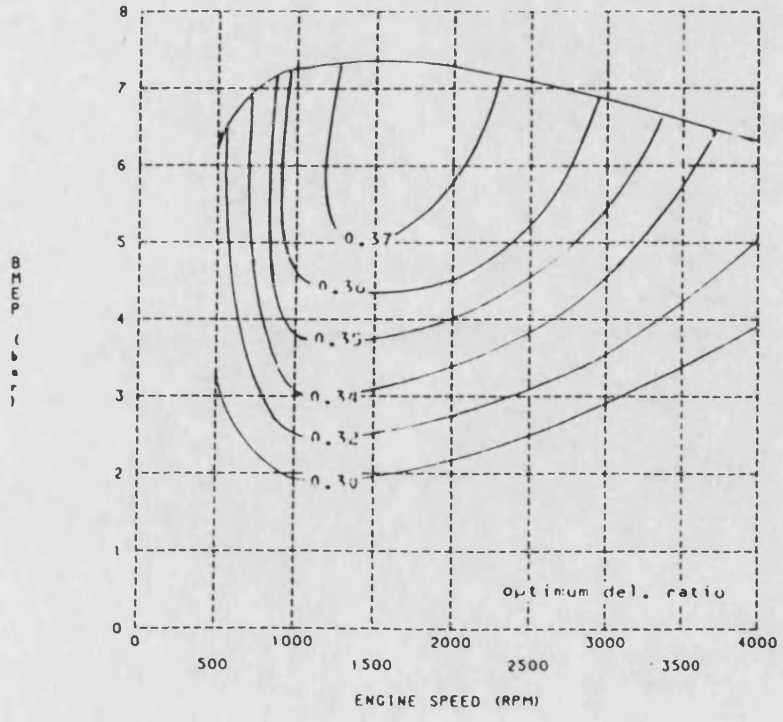

Fig. 8.61 Output Shaft Thermal Efficiency of Optimum Scheme Running at Optimum Delivery Ratio

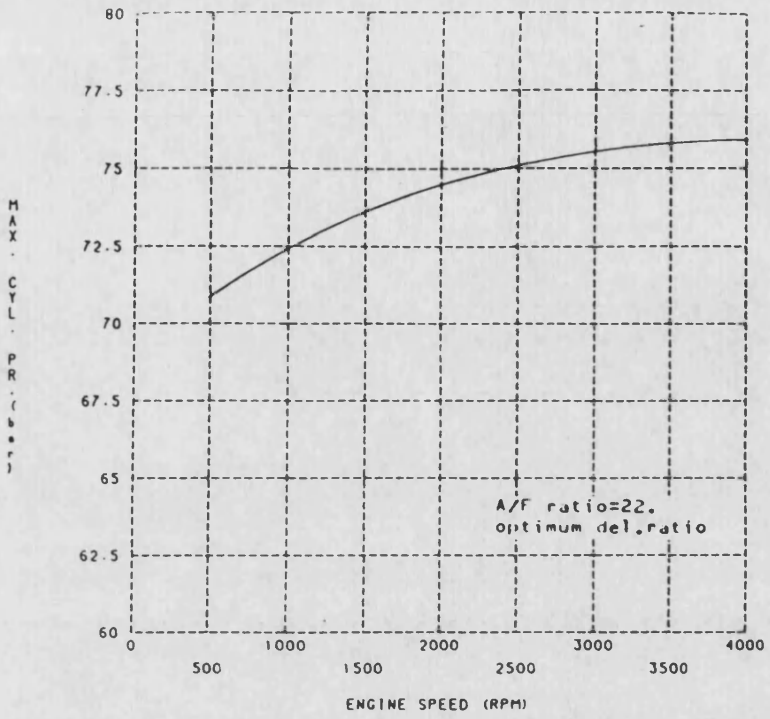

Fig. 8.62 Maximum Cylinder Pressure of Optimum Scheme Running at Optimum Delivery Ratio

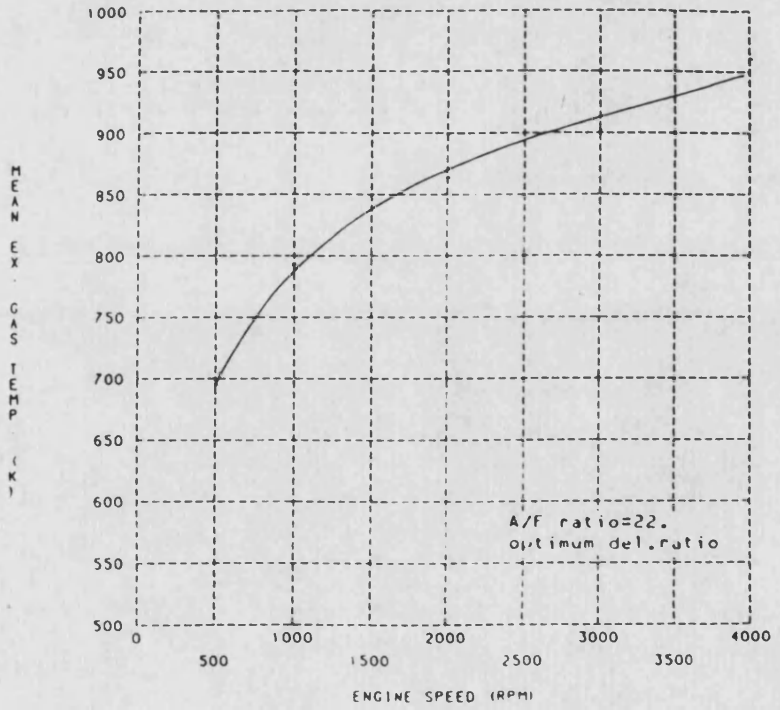

Fig. 8.63 Mean Exhaust Temperature of Optimum Scheme Running at Optimum Delivery Ratio

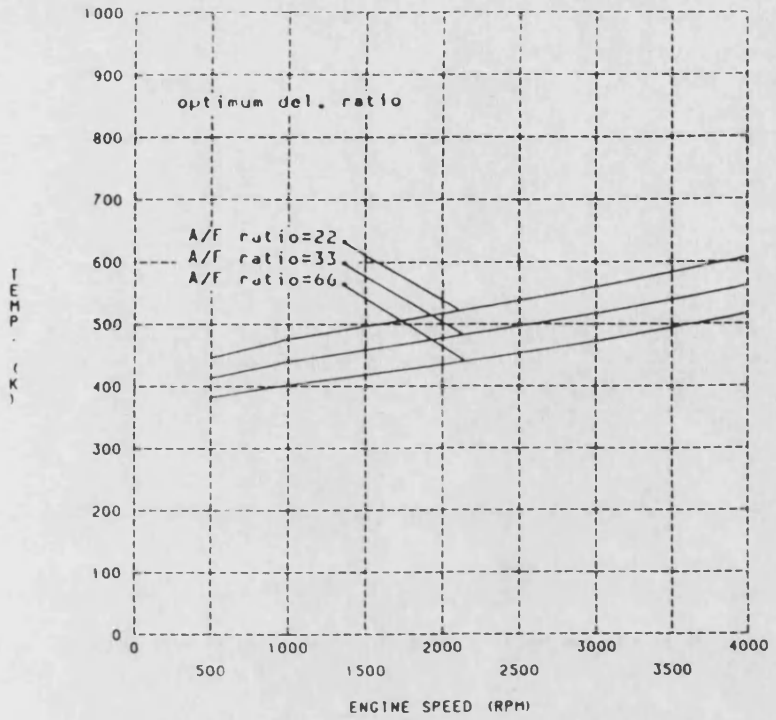

Fig. 8.64 Mean Liner Surface Temperature of Optimum Scheme Running at Optimum Delivery Ratio

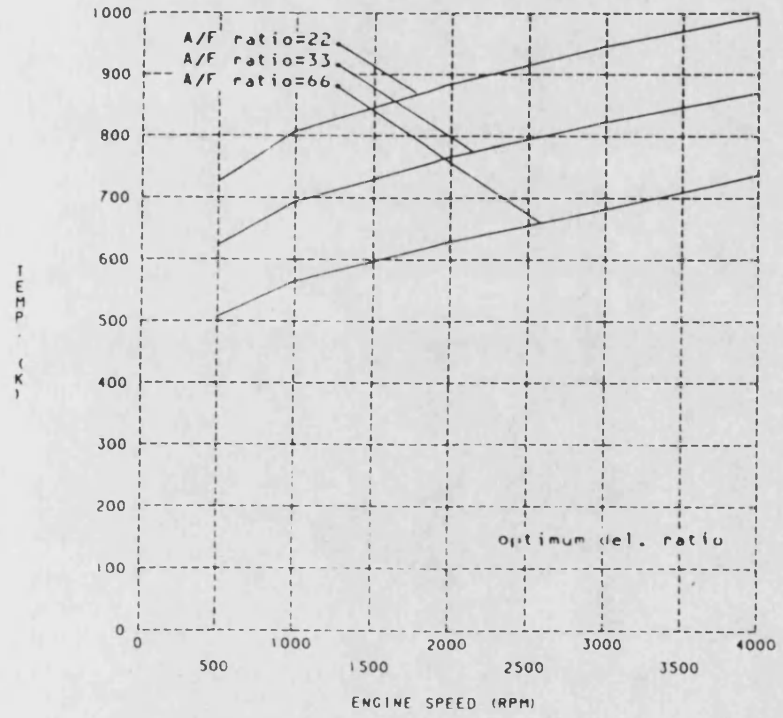

Fig. 8.65 Mean Piston Surface Temperature of Optimum Scheme Running at Optimum Delivery Ratio

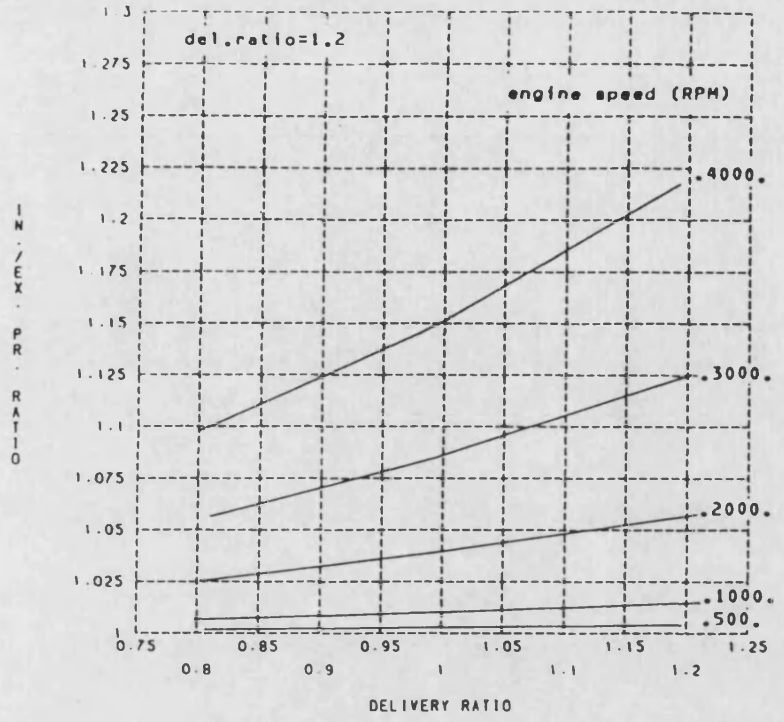

Fig. 8.66 Delivery Ratio versus Inlet/Exhaust Pressure Ratio (Delivery Ratio= 0.8 to 1.2)

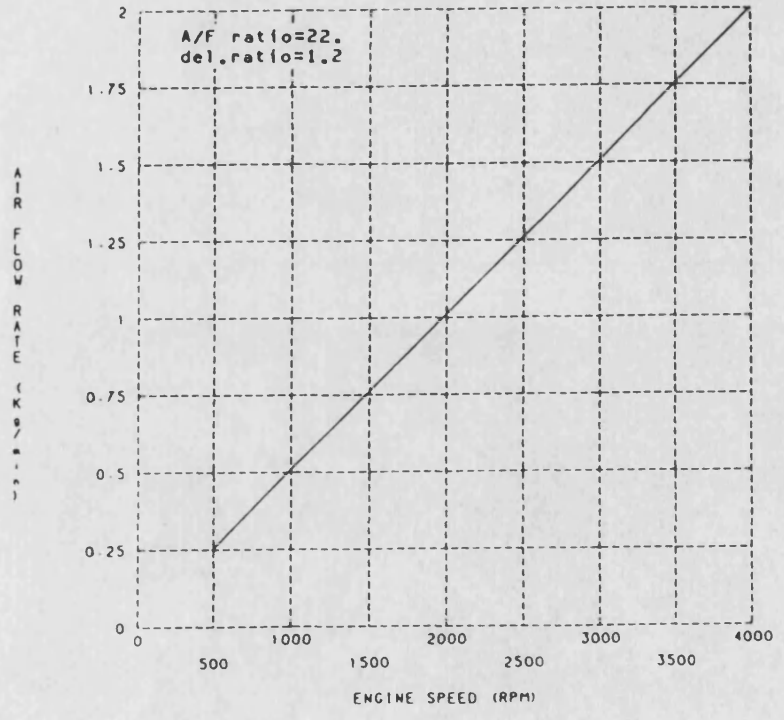

Fig. 8.67 Air Flow Rate of Optimum Scheme Running at Delivery Ratio of 1.2

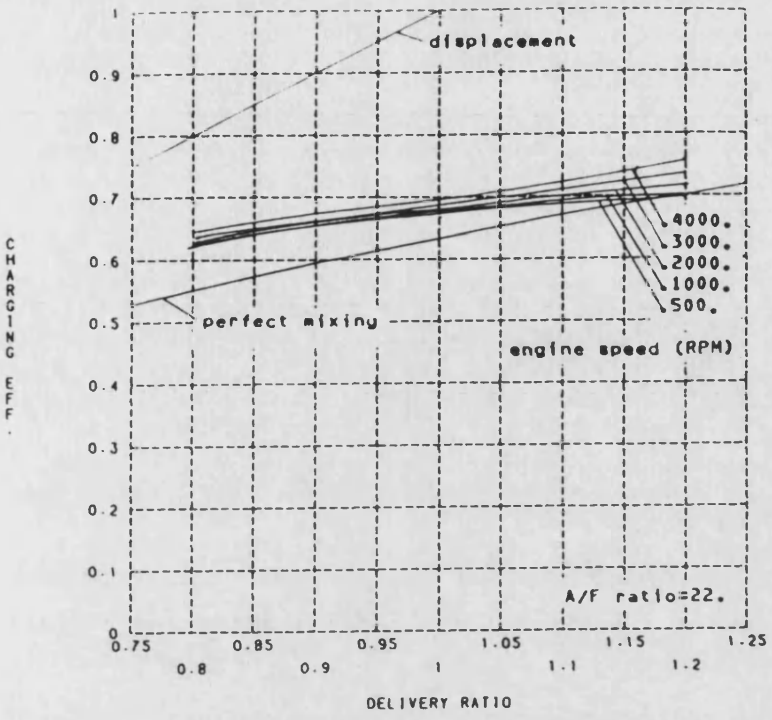

Fig. 8.68 Charging Efficiency of Optimum Scheme Running at Delivery Ratio from 0.8 to 1.2

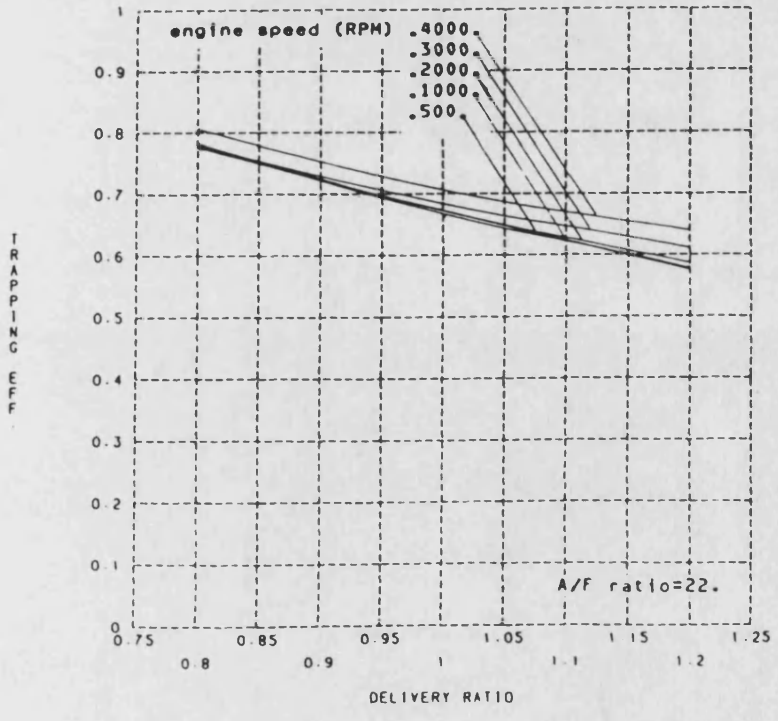

Fig. 8.69 Trapping Efficiency of Optimum Scheme Running at Delivery Ratio from 0.8 to 1.2

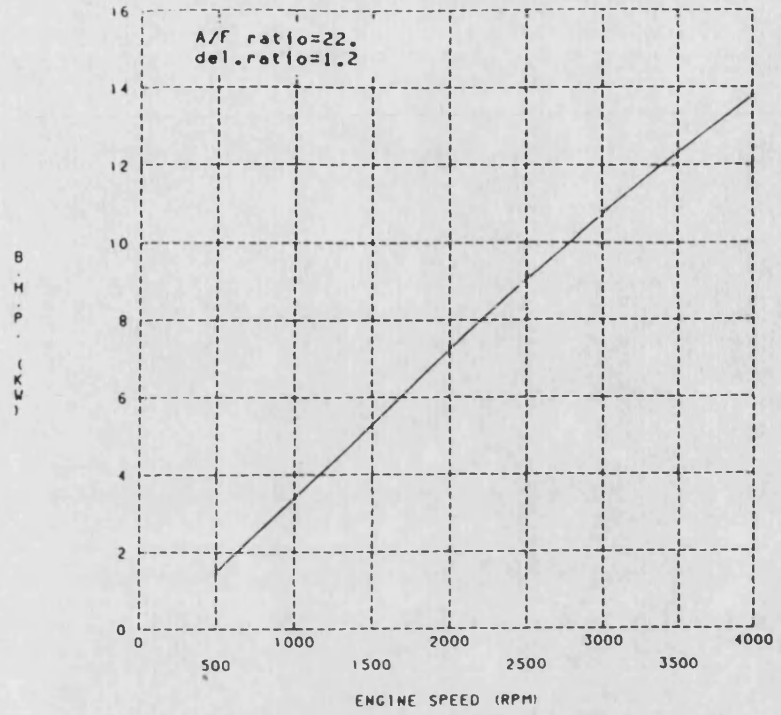

Fig. 8.70 Output Shaft Horsepower of Optimum Scheme Running at Delivery Ratio of 1.2

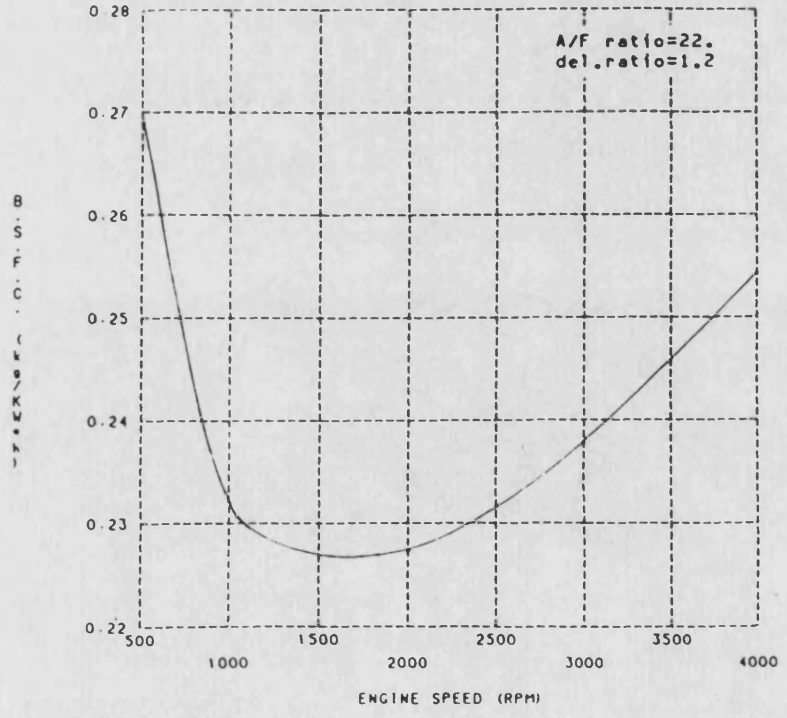

Fig. 8.71 Output Shaft Specific Fuel Consumption of Optimum Scheme Running at Delivery Ratio of 1.2

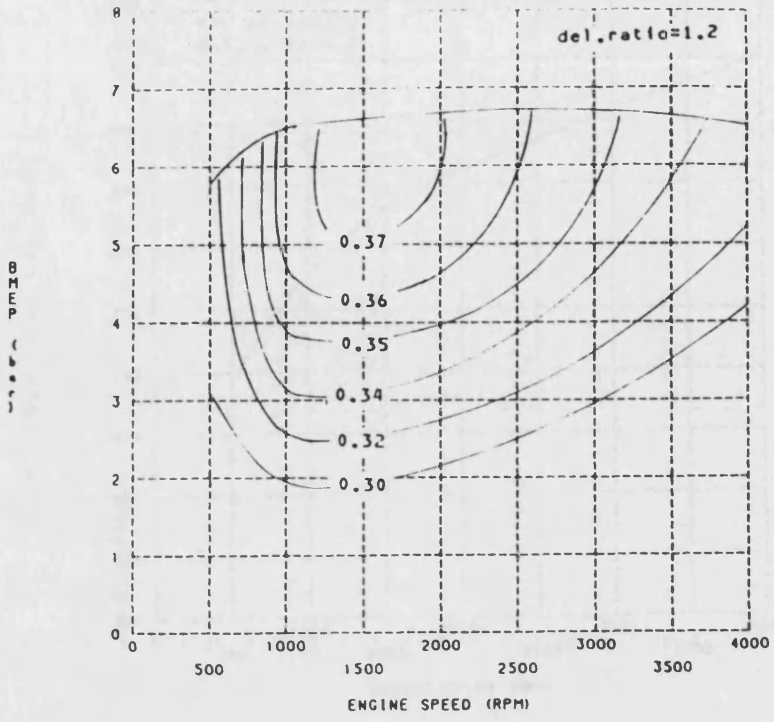

Fig. 8.72 Output Shaft Thermal Efficiency of Optimum Scheme Running at Delivery Ratio of 1.2

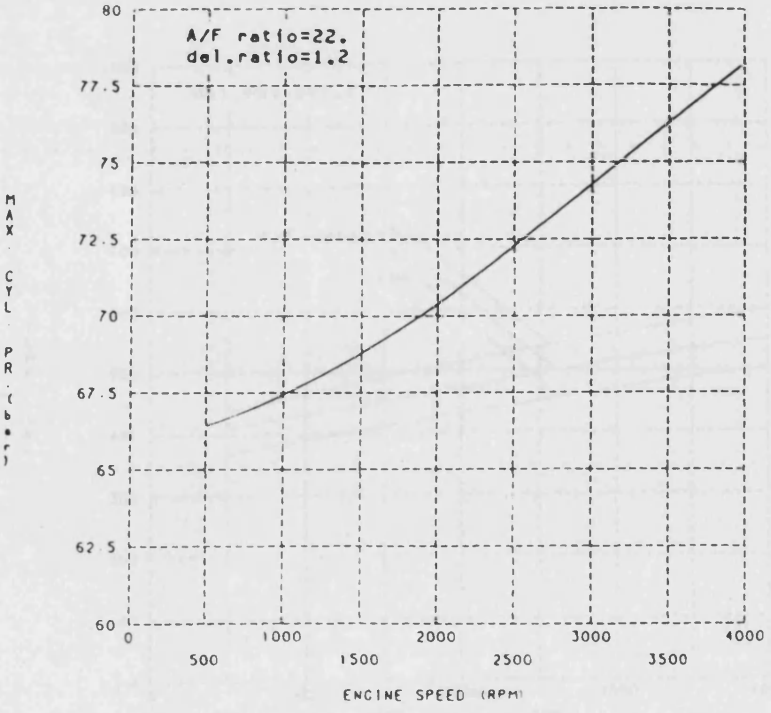

Fig. 8.73 Maximum Cylinder Pressure of Optimum Scheme Running at Delivery Ratio of 1.2

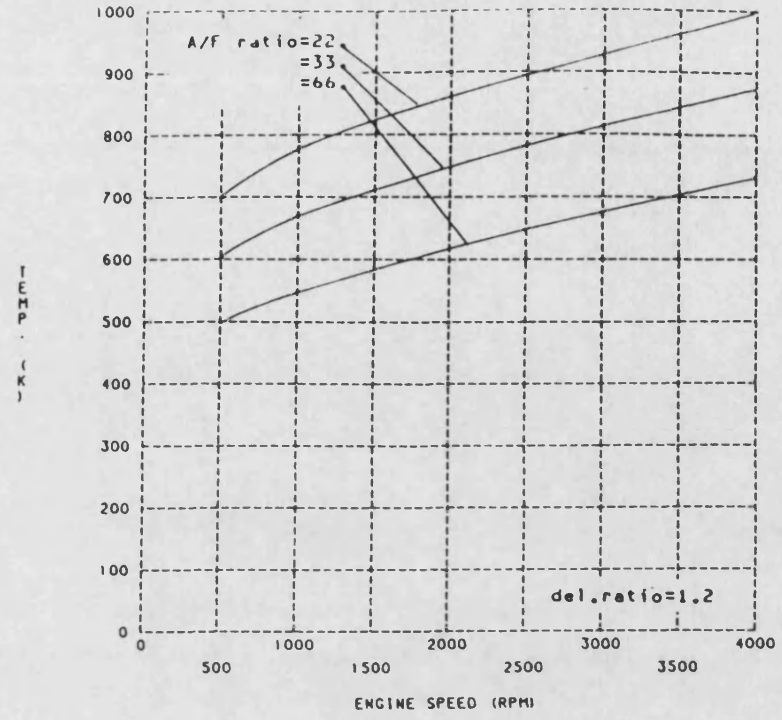

Fig. 8.76 Mean Piston Surface Temperature of Optimum Scheme Running at Delivery Ratio of 1.2

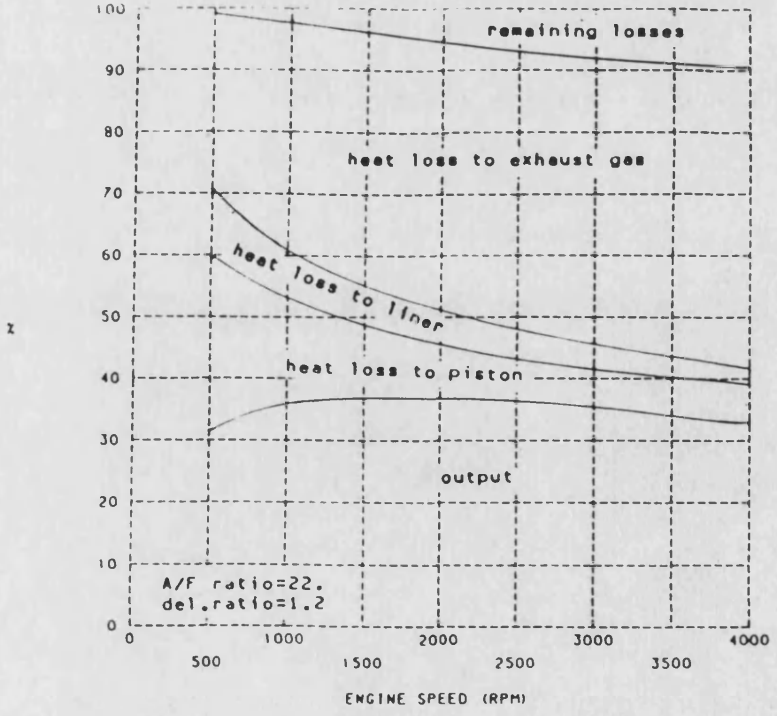

Fig. 8.77 Heat Balance of Optimum Scheme Running at Delivery Ratio of 1.2

Chapter 9 TWO-STROKE ENGINE SYSTEM MODELLING

9.1 INTRODUCTION

The two-stroke engine has no complete intake and exhaust stroke, is not self- aspirating and self- exhausting. It is necessary to use a compressor to help force out residual gases and fill in fresh charge. The compressor can be driven by the engine crankshaft or a turbine driven by the exhaust gases. The useful energy of the exhaust gases can be recovered by the turbine or a positive displacement expander, or used directly to drive a Comprex supercharger, or used as a heat source for a bottoming cycle. For improving thermal efficiency and power performance, many engine systems have been developed.

The system would be improved with the thermally insulated engine, leading to excellent economy due to reduction of heat loss and relaxation of cetane number requirements under "hot wall" condition. Furthermore, the system would be more compact with the two-stroke engine, in principle, doubling the output power within almost the same volume as that of the four-stroke engine.

To obtain optimum overall efficiency with such a sophisticated system, it is necessary to consider the performance of the total system rather than the efficiency of each component individually. There is, therefore, a pressing need for developing mathematical models to investigate the interaction of the various components and to improve the operating behaviour for the total system. For the two-stroke engines, the requirement of a positive pressure drop for scavenging and the tendency of low temperature of the diluted exhaust gases by the scavenging air add extra difficulties to the engine systems.

Designing an engine system is to devise a system layout and to select the components. Optimizing the engine system is to choose the component parameters and to determine the control policy. Modelling the system is to determine the distribution and balances of constituent, mass and energy from the mechanical, pneumatic and thermal connections based on the conservation laws.

9.2 SYSTEM MODELS

Different engine systems are aimed at different applications, use different layouts and components. This thesis will focus its attention on the following two-stroke engine systems.

(1). turbocharged engine without a blower.
(2). turbocharged engine with a blower.
(3). Wallace's differential compound enging (DCE).
(4). compound engine system withe 3 continuously variable transmissions (CVT).

For these systems, the system models include the following submodels.

(1). engine.
(2). compressor.
(3). turbine.
(4). transmission.

As explained in Chapter 7, the engine models have been made into three programs CSP, CSP3Z and CSPMZ. Being extended, these three programs can model Wallace's DCE. Based on the engine program CSP3Z, program CSP3ZTC is made for modelling a two-stage turbocharging scheme in which the high-pressure stage can be coupled to the engine crankshaft, and each compressor and turbine can be included or omitted at will. Thus, the following common turbocharging schemes can be simulated.

(1). single-stage turbocharging without a blower.
(2). single-stage turbocharging with a blower.
(3). two-stage turbocharging.

Program CSP3ZTC can deal with up to two turbochargers at each pressure stage.

9.2.1 COMPRESSOR MODEL

Both positive displacement and centrifugal compressors can be used in the system for boosting the inlet pressure. For centrifugal compressors, the

work completed by Whitfield, Patel and Wallace [9.1] has shown that the complex nature of the flow configuration makes an analytical model of acceptable accuracy too elaborate to be used for a matching program. As a result, manifacturer's compressor performance maps are used in the programs in the form of 3-dimensional numerical arrays. The simplified approach greatly reduces computing time compared with the more complex analytical approach.

A scaling factor method is used for considering the effect of compressor size. From similarity of turbomachinery, the following non-dimensional relationship is valid

$$\frac{\dot{m}\sqrt{RT_{01}}}{P_{01}D^2} \cdot \eta \cdot \frac{\Delta T_0}{T_{01}} = F\left(\frac{ND}{\sqrt{RT_{01}}}, \frac{P_{02}}{P_{01}}\right) \qquad (9.1)$$

where $\dot{m}$ is the mass flow rate,

R is the gas constant,

D is the diameter,

η is the efficiency,

N is the rotational speed,

$\Delta T_0 = T_{02} - T_{01}$ is the temperature difference,

the suffices 01 and 02 used with T and P denote the stagnation temperature and pressure at the inlet and outlet respectively.

This indicates that under the condition of geometric similarity the mass flow rate is proportional to the square of the diameter and the speed is inversely proportional to the diameter. Based on the diameter scaling factor the performance maps of a compressor with varying diameter can be represented. Furthermore, the sectional area scaling factor is introduced to take account of the effect of varying flow cross-sectional area in different trims of the compressor. Therefore, the virtual mass flow scaling factor is

$$f_m = f_d^2 f_a \qquad (9.2)$$

For positive displacement compressors, although the theoretical model has been built up, the performance maps are used in the programs. [9.2] Only

a mass flow scaling factor is used for considering the effect of size.

9.2.2 TURBINE MODEL

The turbine is used for recovering the exhaust available energy to drive the compressor, the engine crankshaft or the powerplant output shaft. The analysis of turbine performance is simpler than in the case of compressor, partly due to the simpler flow configuration and to the generally accelerating flow which presents less serious problems. The one-dimensional theory by Wallace [9.3] provides a successful analytical solution to both design and off-design conditions. The extended work by Wallace, Cave and Miles [9.4] includes an allowance for nozzle and rotor losses and variable nozzle angle. The investigation by Way [9.5] accomplishes the representation of a nozzleless turbine by assuming conservation of angular momentum within the turbine casing and radial entry to the turbine.

In the programs, this theoretical model is used for modelling variable geometry turbines, while the performance maps are used for modelling fixed nozzle turbines. Because turbines obey the same similarity law as that for centrifugal compressors, the same scaling factor method is used for considering the effect of turbine size on the performance.

9.2.3 TRAMSMISSION

9.2.3.1 Epicyclic gearbox model

In the systems, the epicyclic gear train is used as a differential transmission as in Wallace's DCE, or a power turbine reduction gear train. The model developed by Myers [9.6] is used to simulate dynamic performance of the total system including the epicyclic gearbox, the power output shaft and the load. Bearing and tooth load losses computed in the manner proposed by Magi [9.7] are incorporated in this model, which when used with relevant data could be used to represent any epicyclic gearbox train.

9.2.3.2 CVT model

For an engine, a compressor or a turbine, the operation with high efficiency occurs only over a relatively narrow range of speed and load. For an engine

system running over an wide range of speed and load. It is impossible for a fixed ratio transmission to obtain an optimum operation over the complete range. Therefore, the CVTs are used to adjust the transmission ratio to achieve the optimum matching. CVT transmission loss is complex and dependent on CVT type, speed ratio and load. However, the following simple model gives a good approximation.

It is assumed that the transmission loss is divided into two parts:

(1). constant friction torque τ_f
(2). constant dynamic loss ratio η_0 proportional to the output power.

From power balance, the following equation is evident

$$\tau_{out}\omega_{out} = \eta_0(\tau_{in}\omega_{in} - \tau_f\omega_{out}) \qquad (9.3)$$

i.e.

$$\tau_{out} = \eta_0(\tau_{in}r - \tau_f) \qquad (9.4)$$

where r is the speed ratio

τ_{in} is the input torque

τ_{out} is the output torque.

Compared with the experimental results tested on the Dutch Van Doorne CVT TS165 by Vahabzadeh [9.8], the coincidence between test and calculation is satisfactory, in which τ_f is 60 lb-in and ω_0 is 0.95, as listed in Table 9.1. Here, the traction coefficient is defined as,

$$\text{Tr. co.} = \frac{\text{Output speed} \cdot \text{output torque}}{\text{Input speed} \cdot \text{Input torque}} \qquad (9.5)$$

9.3 MODELLING TWO-STROKE TURBOCHARGED ENGINES

9.3.1 MODELLING THE TURBOCHARGED ENGINE WITHOUT A BLOWER

9.3.1.1 Some concepts

Matching a turbocharger to an automotive engine is difficult due to the wide speed and load variations encountered. The circumstances of the two-stroke engine aggravate the matching problems. The two-stroke engines require more scavenging air and a positive pressure drop from the intake to exhaust manifolds for scavenging, while the exhaust temperature is lower due to dilution of the exhaust gas with short-circuited air, which causes a decrease in the exhaust available energy to drive the turbine. Especially for low speed and load running conditions, the turbocharger will stall when the exhaust available energy is too low to drive it.

Few makes of automotive two-stroke engine are produced. The layout of turbocharged two-stroke engines with a blower is the only successful scheme. In this scheme normally a Roots blower is used, placed in series after the turbocharger compressor. The Roots blower provides most of the boost pressure at low speed and load, yet a reducing proportion of the total as speed and load rises. The Roots blower absorbs power from the crankshaft of the engine. The larger the capacity of Roots blower, the greater the loss in engine power output.

It will be expected that for a thermally insulated two-stroke engine the increased exhaust energy alleviates the above problem in matching of the turbocharger. The question is whether the turbocharged thermally insulated two-stroke engine can jettison the auxiliary blower or not. This section is to estimate the performance of the Ford turbocharged ceramic diesel engine without any blower and cooler and the effect of a waste gate on the performance.

9.3.1.2 Main specifications

The layout of the turbocharged engine is shown in Fig. 9.1. The system is composed of an engine and a turbocharger without or with a waste gate. There is no cooler and auxiliary blower in this scheme.

The engine is the Ford initial design of the ceramic 3-cylinder two-stroke opposed piston diesel engine. The engine characteristics have been listed in Chapter 8.

A Holset turbocharger for automotive diesel engines is used as the baseline

turbocharger. The turbine is the Holset 4 LG-T2/2.6 T/F radial flow turbine. The compressor is the Holset 4 LEK-255 radial flow compressor. The performance maps of the turbocharger used in these calculations are produced from the baseline turbocharger map multiplied by scaling factors.

9.3.1.3 Prediction method

Program CSP3ZTC is used for modelling the Ford turbocharged engine. This program uses the three-zone thermodynamic scavenging model, as explained in Chapter 3. For a turbocharged two-stroke engine there exists a possibility that backflow occurs. In this model the backflow from the exhaust manifold mingles with the residual gas zone during the displacement phase and with the mixing zone during the mixing phase, and the backflow from the cylinder to the inlet manifold comes from the air and mixing zones with the same ratio as the intake proportion.

For a given supercharged engine, when the boost ratio is varied its scavenging efficiency displays a relatively stable relationship with the delivery ratio with reference to cylinder trapping condition. The proper selection of the initial volume of the residual gas and the coefficients of intake and discharge proportions can allow this model to provide an approximate description for any scavenging system.

The complete turbocharger characteristics are used as boundary condition at the manifold "control volume". The compressor and turbine performance maps are produced using non-dimensional representation based on the baseline turbocharger map.

9.3.1.4 Identification of computation condition

The injection rate is still set to 12 c.c. per degree of crank shaft angle per cubic metre of cylinder displacement. The start of combustion is adjusted to TDC. Full load is defined as air-fuel ratio = 22.0. In the context of the turbocharged engine, delivery ratio is automatically determined from matching calculation. The volumes of the inlet and exhaust manifolds both are equal to 1 litre.

The relationship between scavenging efficiency and delivery ratio with reference to cylinder trapping condition is specified by the following

parameters, based on the TS3 engine test of Wallace and Cave, [4.16]

the ratio of the initial volume of the mixing zone to the cylinder volume at the beginning of the scavenging process = 0.42
the ratio of the dead space of the residual gas zone to the cylinder volume = 0.
the coefficient of intake proportion of the air zone = 0.63
the coefficient of intake proportion of the mixing zone = 0.37
the coefficient of discharge proportion of the air zone during the mixing scavenging phase = 0.50
the coefficient of discharge proportion of the mixing zone during the mixing scavenging phase = 0.50

Without any backflow, the three-zone thermodynamic model with these parameters gives the curve of scavenging efficiency versus delivery ratio with reference to cylinder trapping condition, as shown in Fig. 9.2.

9.3.1.5 Optimization of turbocharger matching

The criteria of correct selection of a turbocharger are:

(1). increase in output power,
(2). improvement in output shaft efficiency,
(3). wide operating region,
(4). easy starting-up
(5). protection from turbocharger overspeeding,
(6). protection from compressor surge

which may be contradictory.

For a given two-stroke engine, both compressor and turbine have an influence on the turbocharged engine performance. Therefore, the essence of turbocharger matching is a problem of two-parameter optimization. The optimization procedures can be divided into two stages.

(1). compressor-turbine matching: in which the size of compressor is changed gradually, for a given compressor a proper turbine is selected to satisfactorily meet the previous criteria based on the performances at the rated speed and load, thus both compressor and turbine are initially optimized for rated conditions only.

(2). turbocharger-engine matching: in which a comparison between performance of this group of initially optimized turbochargers is conducted based on the computational results over the complete range of speed and load. thus an ideal matching can be achieved.

In this report. firstly the matching of turbocharger without a waste gate is carried out. Secondly. the matching of turbocharger with a waste gate is conducted.

9.3.1.6 The performance of turbocharged engine without a waste gate

The design variables for a group of turbochargers having geometric similarity are size and sectional area. Because the air flow rate of the Ford turbocharged engine is approximately equal to half the flow rate of the baseline compressor. for simplicity. here the size is fixed to 0.7 times of the baseline turbocharger. thus the only variable is sectional area.

It is supposed that the cast compressor impeller can run at the maximum tip speed of 430 m/s. For the impeller of diameter of 63 mm it means that the turbocharger speed should be lower than 136000 rpm.

The numerical tests are conducted based on four different sized compressors fitted with various turbines. Their main characteristics are listed in Table 9.2. Correspondingly. the predicted performances at the rated speed and load are illustrated in Table 9.2 and the running points on compressor characteristics are shown in Fig. 9.3.

From these results. it can be seen that for a given sized compressor with decrease of turbine sectional area specific available energy at the turbine and pressure at the exhaust manifold increase. thus increasing turbocharger speed and boost. Air flow rate is affected by two opposite effects: the increased boost ratio tends to increase the air flow rate. while the decreased turbine sectional area tends to restrict and reduce it. therefore the air flow rate changes slightly. Possibly there exists a maximum flow rate. as shown in Fig. 9.3.

A correct turbocharger matching should increase output power and efficiency. ensure a sufficient surge margin. a safe overspeed margin and a wide and stable operating region.

From Fig. 9.3 it is evident that the top points in these four curves, i.e. Matches 4, 8, 12 and 16, produce their maximum output power and efficiency, and they are under the overspeed limitation of 136000 rpm and that with the decrease of compressor sectional area the matching points move away from the surge line and finally shift to the region of low compressor efficiency. Thus, Match 8 and 12 should be selected as the optimum schemes.

Under the circumstance of the two-stroke engine, for a given turbocharger engine match and a specified air-fuel ratio the increased scavenging air short-circuiting through the inlet and exhaust ports decreases specific exhaust energy at the turbine inlet. With increase of trapped air-fuel ratio the leaner combustion further decreases specific available energy. When engine speed and load decrease, the turbocharger will shift to an operating point with relatively low air flow rate, boost pressure and speed. Eventually, when the engine runs at low speed and load, the turbocharger possibly will stall, thus the engine without an auxiliary blower cannot operate any further. Therefore, it is important for a turbocharged two-stroke engine without a blower to estimate the stable operating range.

From computational results of Match 8, it is seen that it gives excellent output power and efficiency at high speed and load, as shown in Fig. 9.4. However, the turbocharger can operate only within a narrow region at high speed and load, as shown in Fig. 9.5. Its explanation can be obtained from Figs. 9.6 to 9.8 which are contours of exhaust temperature, boost pressure and delivery ratio respectively. With decrease of engine load and speed, declining exhaust temperature results in decrease of boost pressure, hence delivery ratio. The engine running lines with varying air-fuel ratio on compressor characteristics illustrate analogy of flow through a two-stroke engine to flow through an orifice, and also comfirm the conclusion of dramatic decline of boost ratio with the decrease of engine load and speed, as shown in Fig. 9.9. The corresponding turbine flow rate and efficiency are illustrated in Figs. 9.10 and 9.11. Compared with the initial scheme with an engine driven compressor, the turbocharged scheme increases output power by 90 % and efficiency by 15 %. However, the turbocharged engine provides an unfavourable increasing torque curve, as shown in Fig. 9.12. The pressure diagrams in the cylinder, inlet and exhaust manifolds at the rated speed and load are shown in Fig. 9.13.

9.3.1.7 The performance of turbocharged engine with a waste gate

The turbocharged engine fitted with a conventional fixed geometry turbine has encountered problems such as narrow operating range, insufficient torque backup, overspeeding and overboosting. A simple approach of avoiding these problems is to by-pass some of the exhaust gas around the turbine at high speed and load. A small turbocharger is fitted to achieve good low speed boost and extend the operating range to the low speed side. The waste gate can discharge part of the exhaust gas, thus reducing the exhaust pressure and coping with overspeeding and overboosting.

Based on the similar optimization procedures, described in the previous section, the optimum schemes Matches 17 and 18, for matching the turbocharger with a waste gate, can be obtained, and their main characteristics are listed in Table 9.3.

The waste gate characteristics of opening area versus exhaust pressure are illustrated in Fig. 9.14. It is supposed that the opening area is proportional to exhaust pressure and the waste gate is actuated at 2.8 bar and achieves its full opening of 10 sq. cm at 3.8 bar. Here, the high exhaust pressure is exploited for widening the operating range.

Matches 17 and 18, Fig. 9.15, show that, compared with the results without a waste gate, the operating range is widened with an "ideal" torque backup of 60 % at the expense of high speed power and torque. The engine global performances of Match 18 are summarized as follows. The contours of engine efficiency, turbocharger speed, exhaust temperature, boost pressure and delivery ratio are drawn in Figs. 9.16 to 9.20. The engine operating lines with varying air-fuel ratio on compressor characteristics are shown in Fig. 9.21. The corresponding turbine flow rate and efficiency are shown in Figs. 9.22 and 23. The pressure diagrams in the cylinder, inlet and exhaust manifolds at the rated speed and load are illustrated in Fig. 9.24. It is worth noting that the turbocharger with the waste gate greatly widens the turbocharger operating range, unfortunately it has left a stall region around the corner of low speed and load (Figs. 9.16 to 9.20).

9.3.1.8 Discussions

For a fixed geometry turbocharger with a waste gate, a formidable disadvantage is the turbocharger stall at low speed and load which not only makes the engine unable to operate at idle regimes, also indicates that it is difficult for the engine to start-up.

A naturally aspirated scavenging system by utilization of wave effects in the exhaust and induction system without a blower is not suitable for multi-cylinder engines running at variable speed because of the interference of exhaust waves between different cylinders. Especially when the engine operates at low speed regime, a relatively slow exhaust opening hinders the utilization of wave effects. [1.1]

The possible approaches for coping with these problems are as follows

(1). the turbocharged scheme with a variable geometry turbocharger.
(2). the turbocharged scheme with an engine-driven auxiliary blower.
(3). the supercharged scheme with a power turbine coupled with the engine.

9.3.1.9 Summary

(1). The turbocharged scheme without a waste gate can evidently improve the rated output power and efficiency. However, there exists a large region of turbocharger stall.
(2). At some sacrifice of rated output power the turbocharged scheme with the waste gate can evidently improve the output power and efficiency at mid speed and load and achieve an "ideal" torque backup of 60 %. However, there still exists a region of turbocharger stall in the region of low speed and load which indicates the inability of the engine to operate at idle regimes and the difficulty in starting-up.
(3). Three possible approaches for coping with these problems are suggested, as above.

9.3.2 MODELLING THE TURBOCHARGED ENGINE WITH A BLOWER

9.3.2.1 Some concepts

The existing successful scheme of the turbocharged two-stroke engines is a turbocharged layout with a blower, as shown is Fig. 9.25. In this scheme, the blower is driven by the engine, placed in series after the turbocharger compressor. Usually, a Roots compressor is used as this blower, because there is no surge, no choke and no friction in the working chamber, hence it can run at high speeds with minimal noise and vibration.

Coupled with the engine by a fixed ratio transmission, the blower takes

power from the engine and provides part of the boost pressure. even the total boost when the turbocharger stalls. As engine speed and load rises. the increasing available exhaust energy at the turbine inlet allows the turbine to provide most of the total boost. Sometimes. it is possible that at high speeds and loads the turbocharger supplies more air than the blower can take in; as a result. the pressure after the blower exit is lower than the pressure before the blower inlet. Thus. a mismatch between the compressor and the blower occurs. As for the engine performance over the complete range of load and speed. if the blower is too small. it cannot provide sufficient air flow at low speeds and loads; if the blower is too large. it will waste too much engine power at high speeds and loads. This means a conflict between performance at high and low speeds. The wide range of engine speed further aggravates the matching problems.

This section is to predict the performance of the Ford turbocharged engine with blower coupled by a fixed ratio transmission and to analysize the interaction between the compressor and blower and the effects of the compressor and blower capacity and the waste gate actuating pressure on the engine performance.

9.3.2.2 Main specification

The layout of the turbocharged engine is shown in Fig. 9.25. The system is composed of an engine. a blower and a turbocharger with a waste gate. Here. the compressor of the turbocharger is used as a low compression stage compressor. and the blower is engine-driven via a fixed ratio transmission. and used as a high compression stage. There is no cooler in this scheme.

The engine is the Ford initial design of the ceramic two-stroke opposed piston diesel engine. The engine characteristics have been listed in Section 9.3.2. The same Holset turbocharger is used as the baseline turbocharger. The turbine is the Holset 4LG-T2/2.6T/F radial flow turbine. The compressor is the Holset 4 LEK-255 radial flow compressor.

The 0.7 L helical Roots Blower is used as the baseline blower. Its performance maps are shown in Fig. 9.26. [9.9]

9.3.2.3 Prediction method

Also, program CSP3ZTC is used for predicting the performance. The only difference is that there are the two inlet manifolds: the low and high pressure inlet manifolds in the intake system. When the turbocharger stalls, the turbine and compressor of the turbocharger both are treated as orifices respectively.

The performance maps of the turbocharger and the blower are produced from the maps of the baseline turbocharger and blower based on the scaling factor method. The blower is of displacement type of compressor. Its performance map can be produced only by a mass flow scaling factor.

All computation conditions are identical with those in the previous section. Full load is defined as trapped air-fuel ratio of 22.

9.3.2.4 The performance of supercharged engine with a blower

Before the performance prediction of the Ford turbocharged engine with a blower commences, it is beneficial to investigate the performance of the supercharged engine with the Roots blower, because it provides a datum for the performance comparison. The engine is fitted with two different sized blowers, as listed in Table 9.4.

A relatively larger Roots blower is used in Match 1. The contours of delivery ratio, inlet manifold pressure and thermal efficiency of Matches 1 and 2 are shown in Figs. 9.27 to 9.29 and 9.30 to 9.32 respectively.

Using a fixed blower transmission ratio of 2, the blower mass flow rate is dependent on engine speed, while engine load has little influence on it. Therefore, the delivery ratio and inlet manifold pressure in Match 1 are higher than those in Match 2. Match 1 has a slightly better efficiency at low and mid speeds than Match 2.

9.3.2.5 The performance of turbocharged engine with a blower

The turbocharged scheme with blower, Match 3, is composed of the purely turbocharged engine with the waste gate (Match 18 in Section 9.3.2) and the Roots blower with a mass flow scaling factor of 0.8. Its main characteristics are summarized in Table 9.5.

The contours of thermal efficiency, turbocharger speed, exhaust

temperature, delivery ratio, inlet manifold pressure, turbocharger compressor and blower boost ratios are shown in Figs. 9.33 to 9.39. Compared with Figs. 9.16 to 9.20 of the purely turbocharged engine with the waste gate, the turbocharged engine with a blower can run over all speeds and loads, with greatly extended turbocharger operating range. However, the thermal efficiency deteriorates within the common operating range. The larger efficiency loss occurs at high speeds because the blower absorbs more power from the engine, as shown in Fig. 9.33. The maximum torque curve becomes unfavourable, the peak torque decreases and shifts to the high speed side, as shown in Fig. 9.33. The explanation is as follows. In Fig. 9.39, there exists a region at high loads, low and mid speeds where the boost ratio of the blower is lower than 1, i.e. the pressure after the blower is lower than the pressure before it. The reason is that the air flow rate of the blower is dependent on blower speed, if with increase of engine load the air flow rate of the turbocharger increases and surpasses the intake capacity of the blower, thus the blower virtually becomes a restriction in the intake system, as a result, a pressure drop occurs at the blower. Therefore, the maximum engine torque at low speeds decreases. The boost pressure rises with speed and load. Due to the installation of the blower the variation of the delivery ratio over the complete operating range is reduced, as shown in Fig. 9.36.

Fig. 9.40 shows the engine operation area superimposed on the compressor map. It is seen that the blower augments the air flow rate through the intake system, and with increase of engine speed the operating points enter the region of low compressor efficiency.

9.3.2.6 The effect of blower capacity

Match 4 is introduced together with Match 3 to construct a group for analysizing the effect of blower capacity on the performance. The main characteristics of Match 4 are summarized in Table 9.5. Match 4 is the same as Match 3 except that Match 4 uses a smaller blower having a mass flow scaling factor of 0.6. Actually, this capacity of the Roots blower has already achieved the margin for acceptable performance at low speeds.

Figs. 9.41 and 9.42 illustrate the comparisons between output torque and specific fuel consumption of Matches 3 and 4 at full load. The contours of thermal efficiency, turbocharger speed, exhaust temperature, delivery ratio, inlet manifold pressure, compressor and blower boost ratios for Match 4 are

shown in Figs. 9.33 to 9.49. Compared with those figures of Match 3, it is seen that the turbocharged engine with a larger blower, Match 3, has a better performance at low speeds, while the turbocharged engine with a smaller blower, Match 4, has a better performance at high speeds. If the Roots blower is too small, scavenging at low speeds will be poor. If it is too large, then power will be wasted in developing an excessive boost pressure at high speeds, where the turbocharger alone could provide sufficient boost. For Match 4, the delivery ratio and inlet manifold pressure is reduced, and the region, where the blower boost is lower than 1, is enlarged, as shown in Figs. 9.46, 9.47 and 9.49 respectively.

Fig. 9.50 shows the engine operation area on the compressor map. Like Match 3, as engine speed rises, the operating points in Match 4 enter the low efficiency region of the compressor. It is worthwhile noting that the engine operating points at high loads, low and mid speeds move towards the surge line because the mismatched blower blocks the compressor air flow, the air flow through the compressor reduces, but the turbine work is maintained due to a hotter exhaust as the total air-fuel ratio gets richer, thus the operating points shift to a point of smaller flow rate and higher pressure (refer Fig. 9.21).

9.3.2.7 The effect of turbocharger capacity

Matches 5 and 6 are introduced together with Match 3 to constitute a group for investigating the effect of turbocharger capacity on the performance. Matches 3, 5 and 6 use the same blower, but increasingly sized turbochargers, with same size scaling factor applied to both compressor and turbine. Their characteristics are summarized in Table 9.5.

Figs. 9.51 and 9.52 show the comparisons between output torque and specific fuel consumption of this group at full load. With increase of turbocharger size the thermal efficiency at low speeds deteriorates because the enlarged turbine area decreases the turbocharger boost ratio, but the efficiency at high speeds improves because the larger turbine area reduces the power loss for compressing scavenging air. With increase of the turbocharger size, the engine torque curve becomes worse, the peak torque moves towards high speed side, the maximum torque curve, eventually, becomes monotonically increasing curve with engine speed. Match 6 gives a poor torque characteristic.

Figs. 9.53 to 9.59 show the contours of thermal efficiency , turbocharger speed, exhaust temperature, delivery ratio, exhaust temperature, inlet manifold pressure, compressor and blower boost ratio for Match 6. Compared with those contours of Match 3, Match 6 evidently improves the thermal efficiency and output torque at high speeds, but both deteriorate at low speeds. With increase of the turbocharger size the inlet manifold pressure, turbocharger speed, the peak values of the compressor and blower boost ratios decrease.

Fig. 9.60 illustrates the engine operation area on the compressor map. It can be observed that compared with Match 3, Match 6 improves the matching at high speeds which coincides with the improvement of the engine efficiency at high speeds.

9.3.2.8 The effect of waste gate actuating pressure

Matches 7 and 8 are combinations of Match 3 with decreasing waste gate actuating pressures of 2.8, 2.5 and 2.2 bar respectively, as listed in Table 9.5.

With decrease of waste gate actuating pressure, the flow rate of exhaust gases discharged through the waste gate increases, as a result, the compressor boost ratio, delivery ratio, hence engine maximum torque and power decline, as summarized in Table 9.6. The maximum torque curves and the specific fuel consumptions at full load are shown in Figs. 9.61 and 9.62. The maximum torque decreases and the specific fuel consumption deteriorates with decrease of waste gate actuating pressure because the exhaust energy has not been fully exploited by the turbocharger.

9.3.2.9 Discussions

(1). variable ratio transmission of blower

The air mass flow rate of the blower is dependent on the blower speed, while the mass flow rate of the compressor is dependent mainly on the available exhaust energy at the turbine inlet. Therefore, the interaction between the turbocharger and the blower coupled via a fixed ratio transmission is inevitable. Sometimes, the blower boost ratio is less than 1, i.e. the mismatch occurs when the exhaust energy is high but the blower speed is too low.

From Figs. 9.39 and 9.49, it can be observed that the disadvantage of the fixed ratio transmission is that at high engine speeds the blower speed is too high: it provides too high a boost ratio and wastes too much engine power. On the contrary, sometimes, at high loads, low and mid engine speeds the blower speed is relatively low, the blower cannot intake as much air as the compressor supplies: thus a pressure drop at the blower will occur, which hinders the increase of the maximum torque. It is expected that the installation of a variable ratio blower transmission can improve the engine performance over the complete range of load and speed.

(2). switch-off machanism of blower transmission

Incorporated with another air passage between the high and low pressure inlet manifolds and an appropriate valve before the blower, an installation of a clutch on the blower transmission can cope with the above matching problems. When the turbocharger alone can provide sufficient scavenging air, the clutch is disengaged and the valve to the blower is cut-off, virtually, the system switches to a purely turbocharged scheme. With the switch-off mechanism, the system can use a blower with sufficient capacity for good scavenging at low engine speeds and loads, and switch off the blower and operate the engine only with the turbocharger to avoid wasting the engine power in driving the blower at high speeds and loads.

(3). variable geometry turbocharger

The above analysis of the effect of turbocharger capacity in Section 9.3.2.7 has the implication that the smaller housing turbocharger is beneficial for the performance at low speeds, and the larger housing is good for the performance at high speeds. Potentially, a variable geometry system could produce the characteristics of both small and large housing turbochargers. Therefore, it is expected that incorporated with a correct selected blower, the variable geometry turbocharger can improve the performance over the complete load and speed range.

9.3.2.10 Summary

(1). The installation of the blower placed in series after the turbocharger compressor greatly widens the operating region and allows the engine running over the complete range of load and speed.

(2). The turbocharged engine with a blower coupled via a fixed ratio transmission encounters the difficulty in compatibility of good performance both at high and low speeds. The turbocharged engine with the larger blower improves scavenging at low speeds, but at high speeds any scavenging benefit obtained by fitting the larger blower is marginal, and is not offset by its extra power requirements.

(3). Three possible approches for further improving the global performance are recommended, as above. However, the improvement in the performance is realized at the expense of complicated design.

9.4 MODELLING THE COMPOUND TWO-STROKE ENGINE SYSTEMS

9.4.1 MODELLING WALLACE'S DIFFERENTIAL COMPOUND ENGINE

9.4.1.1 Some concepts

The concept of the differential compound engine (DCE) has been developed over 20 years in University of Bath. Its layout is shown in Fig. 9.63. It is regarded as a means of achieving the following objectives, all particularly relevant in the context of traction prime movers.

(1). high unit output,
(2). high torque backup,
(3). fuel economy,
(4). dynamic response,
(5). low pollution emission.

The present experimental unit is equipped with a conventional 6-cylinder four-stroke DI engine for heavy truck and off-highway applications.

The task of this section is to predict the performances of the DCE with a two-stroke engine as a substitute for the four-stroke engine to enhance the advantage in high unit output and compactness.

9.4.1.2 Major components

9.4.1.2.1 Engine

The engine is a hypothetical high output two-stroke 3-cylinder DI engine

operating at high boost and BMEP conditions. Actually, the engine is an enlarged Rootes TS3 opposed piston two-stroke engine with a scaling factor of 1.15 and with a rating of 270 KW at 2500 rev/min. at boost pressure ratio 3/1. At this stage, no provision has been made for the incorporation of insulating components. The fuel pump is electronically all-speed governed, engine control constituting part of the overall control scheme.

9.4.1.2.2 Fully floating epicyclic gearbox

The epicyclic gearbox provides the continuously variable link between the engine and the output shaft, with the supercharging compressor being driven differentially. The engine drives the ring gear of the epicyclic gearbox. The planet carrier is geared to the output shaft. The supercharging compressor is driven by the sun gear.

Annulus to sun ratio: 3.074,
Sungear to compressor- step up ratio: 3.452,
Planet carrier to output shaft- step up ratio: 1.953.

9.4.1.2.3 Supercharging compressor

The compressor is the same rotary positive displacement type as that used in the DCE with the four-stroke engine. The only difference is the compressor with scaling factor 1.15 to satisfy the scavenging demand. The somewhat bulkier compressor has substantial advantages in the DCE with its large compressor speed range, associated with the differential drive, and the resultant wide mass flow range. This type of compressor has no surge and no choke.

9.4.1.2.4 Turbine

Also the same inward radial flow turbine is used in the present DCE. Its robustness, good efficiency and high pressure ratio capability have been proven fully. Variable nozzles of swivelling type confer a wide flow range and permit continuous adjustment for specific fuel consumption optimization and improved transient response.

9.4.1.2.5 Turbine CVT

The implementation of the turbine CVT is to improve overall efficiency and

output torque in the mid and low output shaft speed regimes, since the use of the turbine CVT allows the turbine to operate at maximum efficiency under all conditions.

9.4.1.2.6 Bypass valve

This device provides an alternative air path under low output shaft speed conditions when compressor speed, hence compressed air flow, is high. Under transient conditions the short-circuited air flow through the bypass valve can enhance engine fuel-air ratio and hence transient response. In the context of two-stroke engines, proper air flow through the bypass valve can increase the pressure in the exhaust manifolds, hence the trapped air mass in the cylinder under mid and low output shaft speed regime.

9.4.1.3 Control of the CVT

Control of the unit is through four simultaneous "inputs", namely

(1). fuel-rack setting, controlling power.
(2). turbine-nozzle setting, controlling boost pressure ratio.
(3). turbine CVT ratio setting, controlling the CVT ratio to optimize the turbine efficiency.
(4). bypass valve setting, controlling opening of the bypass valve to optimize the scavenging air flow through the cylinder.

9.4.1.4 Prediction of steady-state characteristics

9.4.1.4.1 General

Program CSPS is used for predicting overall performance, because it is a quick and easy program suitable for computations over a wide range of running conditions. In the simulation, the mass flow rate through the cylinders and the charging efficiency are based on the experimental results of Rootes TS3 two-stroke engine by Wallace and Wright [4.15].

9.4.1.4.2 Operating characteristics without a bypass valve

The steady-state performances are shown in Figs. 9.64 to 9.68 and in Table 9.7. In Figs. 9.69 to 9.72, two limiting torque curves (LTC) are illustrated. The torque backup of the upper LTC is approximately equal to

that of the DCE with the four-stroke engine [9.10], while in the region under the lower LTC the engine operates without exceeding the maximum cylinder pressure 150 bar. Table 9.8 shows the operating characteristics of the rated and "stall" conditions of the DCE with the two-stroke engine. Compared with those of the DCE with the four-stroke engine, it is evident that the DCE with the two-stroke engine requires a wide speed and flow range of the compressor imposed by the differential gearing and higher boost ratio for scavenging, which is not easily satisfied with current centrifugal compressors with higher efficiency levels.

Figs. 9.64 to 9.68 give the output shaft torque-speed envelopes with contours of overall thermal efficiency, engine brake mean effective pressure (BMEP), engine speed, boost pressure ratio and CVT ratio respectively, all at optimized conditions. Fig. 9.64 shows the remarkably high overall efficiencies achievable. From Figs. 9.65 and 9.66 it is obvious that the very high torque backup is obtained with gradually rising engine BMEP and decreasing engine speed. Torque multiplications over the output shaft speed range 2500> $N_{o/s}$ >500 rev/min. are 3.76 and 1.82 for the upper and the lower LTC respectively. BMEP also increase from 13.08 bar to 23.86 and 14.58 bar respectively. Fig. 9.67 gives boost pressure contours, this varies from 3.09 under the rated condition to 4.77 and 3.29 at the maximum torque condition for the upper and lower LTC respectively. For the upper LTC, the maximum cylinder pressure at the 'stall' output speed rises to 209 bar. Fig. 9.68 shows the overall turbine gear ratio for turbine best efficiency.

Close inspection of the performance prediction in Table 9.7 for output shaft speeds of 2500, 2000, 1500, 1000 and 500 rev/min., each at 4 or 5 power levels, highlights the benefits of compounding, particularly at high output shaft speeds when compressor speeds are relatively low.

From Table 9.7, under the rated condition (No/s = 2500 rev/min. and Wo/s = 256 kw), the work split among engine, compressor turbine and output shaft may be expressed as

$$W_{o/s} = W_e + W_t - W_c - W_{gear\ loss} \qquad (9.6)$$

that is,

$$256.0 = 272.9 + 77.3 - 75.4 - W_{\text{gear loss}}$$

where $W_{\text{gear loss}}$ = 18.8 KW (including CVT loss). From this, the estimation of total transmission losses would be safe.

9.4.1.4.3 Operating characteristics with a bypass valve

It is essential for the scavenging process in a two-stroke engine to retain the positive pressure drop between the inlet and exhaust manifolds, because in most of the scavenging process both the inlet and exhaust ports are open. In the network of air path in the DCE, the cylinder and turbine are connected in series. When the air flow through the cylinder increases, the pressure drop also increases. When the pressure in the exhaust manifold is too low, the trapped pressure in the cylinder also is too low, which impairs the scavenging effectiveness. Implementation of a bypass valve, i.e. a parallel connection of the cylinder and the bypass valve in the network, will be able to improve the scavenging effectiveness, since the proper opening of the bypass valve may increase the pressure in the exhaust manifold, i.e. the trapped pressure, at the same time reduce the excessive loss of the compressor work, which occurs when the opening of the bypass valve is too wide. Fig. 9.69 shows the relationship between optimum valve opening and output shaft speed and torques. The optimization of bypass valve openings increases the trapped mass in the cylinder, and incurs only a slight increase in the inlet pressure, as shown in Fig. 9.70. The improvement of the trapping efficiency, in turn, enhances the increase in the output BMEP and efficiency. From Figs. 9.71 and 9.72, it is obvious that the improvements occur at the mid and low output shaft speed range, at which the excessive air flow rate, and hence pressure drop, also occur. In these figures, also two LTC are illustrated. The upper LTC is an approximate curve of that for the DCE with the four-stroke engine, while the lower LTC is the curve without exceeding the maximum cylinder pressure 150 bar. Torque multiplications are 4.10 and 1.96 for the upper and lower LTC. BMEP increases from 13.08 bar at the rated condition to 23.66 and 14.58 at the "stall" condition. Boost ratio varies from 3.09 to 4.96 and 3.38. For the upper LTC, the maximum cylinder pressure reaches 214 bar. The computed results are listed in Table 9.9.

9.4.1.4.4 Operating characteristics with a CVT on output shaft

In the DCE, the engine, compressor and output shaft are geared by a

epicyclic train. With this linkage, the ratio of engine torque to compressor torque always maintains fixed. When output shaft speed decreases, the ratio of compressor speed to engine speed increases, which confers the DCE an excellent torque backup. Meanwhile, an excessive air mass rate flows through the DCE, which wastes extra compressor work. On the other hand, for low load running conditions, the engine operates under low boost pressure ratio and shows the inefficiency. The DCE without a change speed transmission will be confined from further improving the cruising performance. It is important to make the DCE operate the engine at optimum boost pressure ratio to achieve the best efficiency and maintain a proper ratio of compressor speed to engine speed to avoid excessive air flow rate.

The author suggests the following scheme:

The DCE is fitted with a CVT on the output shaft, which allows the compressor operate at proper speeds, i.e. supply optimum scaveging air flow rates.

Fig. 9.73 shows the optimum transmission ratio of the output shaft CVT. The corresponding engine and compressor speeds are shown in Figs. 9.74 and 9.75, at which the excessive scavenging air flows are avoided. Fig. 9.76 shows the optimum transmission ratios of the turbine CVT which give best efficiency. The size of the turbine is reduced to 0.8 of that in the previous DCE scheme. The scheme with an output shaft CVT manifests itself in a better efficiency at the mid and high mid load range, although its maximum of overall efficiency decreases slightly owing to the loss due to the output shaft CVT, as shown in Fig. 9.77. And it shows a worse efficiency only at the low load range, because the gain from the ouput shaft CVT cannot compensate the transmission loss due to the CVT. From the computed results, as listed in Table 9.10, it is seen that the output CVT greately extends the region of true compounding, i.e. excess of turbine over compressor power. In Figs. 9.73 to 9.76, only one LTC is shown. Under this LTC, the maximum cylinder pressure is lower than 150 bar. With decrease of output speed from 2500 to 500 rpm, torque rises 5.11 times, which is the desired constant horsepower characteristic. Boost ratio and BMEP maintain at the same levels of 3.2 and 12.6 bar.

From the above, the ideal DCE should be equipped with an output shaft CVT. When the power unit is accelerating, the output shaft CVT is switched

off to obtain the maximum torque backup, i.e. the best accelerating performance. When the unit is cruising, the output shaft CVT is switched on to achieve the best efficiency.

9.4.2 MODELLING THE COMPOUND ENGINE SYSTEM WITH THREE CVTS ON OUTPUT, COMPRESSOR AND TURBINE

9.4.2.1 Some concepts

The author puts forward the new concept of the compound engine system (CES) with three CVTs. The new compounding scheme would be able to satisfy all the requirements of traction prime movers.

The layout of the scheme is simple, as shown in Fig. 9.78. The engine drives the output shaft and the compressor via two CVTs respectively. The useful energy of the exhaust gases is recovered by the turbine, and the work is extraced by the turbine, in turn, is imposed on the output shaft through another CVT. The compounding scheme has eliminated the epicyclic gear train and bypass valve.

The other major components are the same as those in the DCE. The engine is the same 3-cylinder opposed piston two-stroke engine with scaling factor 1.15. The compressor is the same rotary positive displacement type. The turbine also is the same inward radial flow turbine with variable nozzles. The similar CVTs are fitted on the output, compressor and turbine shafts.

9.4.2.2 Control of CES with three CVTs

The following five simultaneous input variables are imposed on the unit

(1). fuel-rack setting, controlling power,
(2). turbine-nozzle setting, controlling boost pressure ratio,
(3). output shaft CVT setting,
(4). compressor CVT setting,
(5). turbine CVT setting.

Similarly, control of the turbine nozzles and CVT settings would be implemented via a microprocessor in conjuction with appropriate actuators, with overriding function to ensure operation within safe limits of all parameters.

The control should possess two modes of function:

(1). "economy" mode for cruising.
(2). "sport" mode for accelerating.

Optimization could presumably be established via microprocessor with stored multi-dimensional maps representing optimum control schedules for boost and CVT ratio, and actuators operating the turbine nozzles and the CVT's line pressures.

9.4.2.3 Steady-state performance

Program CSPSCVT, a modified version based on program CSPS, is used for predicting steady-state performances of the CES with three CVTs.

The strategy of optimization is to keep the engine running at fuel-efficient boost pressure and fuel-air ratios, say about 3:1 and 25:1 respectively, at which the engine and the compressor display their peak efficiencies.

Firstly, choosing the compressor CVT ratio is to obtain an optimum air flow rate for scavenging.
Secondly, adjusting the nozzle angle is to achieve an ideal boost pressure ratio.
Thirdly, optimizing the output shaft ratio is to ensure the engine running at the most efficient fuel-air ratio and to keep power balance at given output shaft torque and speed.
Finally, selecting the turbine CVT ratio is to obtain the best turbine efficiency.

Figs. 9.79 to 9.81 show the contours of optimum CVT ratios versus output shaft speed and torque. The corresponding overall output shaft efficiency is shown in Fig. 9.82, which displays a wide area of excellent overall efficiency, even marginally better than the DCE scheme with output shaft CVT owing to the omission of the epicyclic gearbox at the mid and high load regimes and a narrow area of worse efficiency at the low load regimes due to CVT's inefficiency. In Figs. 9.79 to 9.81, only one LTC is shown. Under this LTC, the maximum cylinder pressure is lower than 150 bar. From the computed results, listed in Table 9.11, it is seen that the region of true compounding is extended. Torque increases from 905 Nm at 2500 rpm to 4577 Nm at 500 rpm, i.e. 5 time, which is the ideal hyperbolic

characteristic.

From the above analysis, the CES with three CVTs would be considered as a promising scheme integrated with efficiency, flexibility and compactness.

9.4.3 DISCUSSIONS OF THE COMPOUND ENGINE SYSTEMS

For a 30-48 ton truck with the engine power from 200 to 350 KW designed to start on a gradient of 25 %, the satisfactory output torque characteristics should increase approximately 12 times from the rated output speed No/smax to output shaft stall. [9.11] The "gap" between output shaft stall and 1/5(No/smax) is bridged in vehicle application by an output torque converter with ratio 3.6. For the truck application, the output torque should have an increase of 3.31 times from No/smax to 1/5(No/smax). The torque backup of Wallace' DCE with the upper LTC, DCE with CVT on output shaft and CES with 3 CVTs all exceeed this required value. Hence, without a gearbox they can achieve a satisfactory climbing performance. However, the torque backup of DCE with lower LTC is 1.82 times, i.e. lower than the desired value. Hence it needs a 2-speed gearbox to obtain the requirement of driveability.

In the DCE, the CES with three CVTs and other schemes [9.12], [1.19], a power turbine extracts useful energy from exhaust gases directly to the engine, thus obviating the necessity for the thermodynamically wasteful condition of power balance between compressor and turbine in the purely turbocharged engine. The variable nozzles fitted in the power turbine further enhance improvements in thermal efficiency over all turbine running conditions.

For traction purposes, both the DCE and the CES with three CVTs schemes display excellent torque-speed characteristics. In the DCE scheme, this is achieved by coupling the engine, the compressor and the output shaft through the medium of epicyclic gearing. The mechanical connection permits the DCE to supply ample compressed air flow, i.e. high and reliable torque backup, at the low output shaft speeds.

In the CES with three CVTs, the ideal torque-speed characteristics are realized by linking the engine and the output shaft through a CVT, thus avoiding the excessive loading in the engine. The coupling of the engine and the compressor via a CVT permits the compressor to optimize its air

flow rate, thus eliminating excessive air flow and reverse of the compressor. The realization of the CES with three CVTs relies on the highly efficient and high rated CVT controlled by a microprocessor. The recent developments of such CVTs have made the CES with three CVTs promising. [9. 13], [9. 14], [9. 15]

The essentials of programs CSPS, CSP3Z, CSPMZ and CSP3ZTC are listed in Appendix IV.

REFERENCE

[9.1]. A. Whitfield, M.H. Patel and F.J. Wallace
"Design and Testing of Two Radial Flow Backward Swept Turbocharger Compressors"
I. Mech. E. Conference 'Turbocharging and Turbochargers' C74/78

[9.2]. S.C. Sorenson
"Simulation of a Positive Displacement Supercharger"
SAE 840244, 1984

[9.3]. F.J. Wallace
"Theoretical Assesssment of Performance Characteristics of Inward Radial Flow Turbines"
Proc. Instn. Mech. Engrs. Vol. 172 No. 33, 1959

[9.4]. F.J. Wallace, P.R. Cave and J. Miles
"Performance of Inward Radial Flow Turbines under Steady Flow Conditions with Special Reference to High Pressure Ratios and Partial Admission"
Proc. Instn. Mech. Engrs. Vol. 184, 19690

[9.5]. R.J.B. Way
"Notes on Modelling of Radial Inflow Turbines"
School of Engineering, University of Bath, 19

[9.6]. J.M. Myers
"Computer Modelling Techniques for Heavy Vehicle Power Train Systems"
Ph.D. Thesis, University of Bath, 1978

[9.7]. M. Magi
"On Effeciencies of Mech. Coplanar Shaft Power Transmission"
Report from Div. of Machine Elements, Chalmers University of Tech, 1974

[9.8]. H. Vahabzadeh
"Computer Controlled Four Square Dynamometer for Transient and Cycle Testing of Continuosly Variable Transmission"

Ph. D. Thesis, University of Wisconsin-Madison, 1982

[9.9] D. A. Singer
"Comparison of a Supercharger vs. a Turbocharger in a Small Displacement Gasoline Engine Application"
SAE 850244, 1985

[9.10]. F. J. Wallace
"The Differential Compound Engine as an Advanced Integrated Engine-Transmission System for Trucks and Off-Highway Applications"
School of Engineering, University of Bath, 1983

[9.11] F. J. Wallace and M. Tarabad
"Engine Transmission Systems for the Heavy Goods Vehicle and Passenger Carrying Bus"
Proc. Instn. Mech. Engrs. Vol. 197A, April, 1983

[9.12]. Anon
"Napier's Nomad Engine"
Aeroplane, 1954, 30th April

[9.13]. E. L. Kumm and T. C. Kraver
"Development of a Flat-Belt Contonuously-Variable Transmission"
SAE 850488, 1985

[9.14]. D. Scott
"CVTs Loom on European Horizon"
Automotive Engineering, Vol. 91, No. 12, 1983

[9.15]. C. Chan, T. Volz, D. Breitweiser, A. Frank and F. S. Jamzadeh
"System Design and Control Cosiderations of Automotive Continuously Variable Transmissions"
SAE 840048, 1984

Table 9.1 CVT Steady Test Results and Calculated Results

Nin rpm	Nout rpm	Torque in lb-in	Speed ratio	Test Results Torq.out	Tr.co. %	Calc. Results Torq.out	Tr.co. %
1319	2592	122	0.508	16	25.7	2	3.2
1308	2559	496	0.510	214	84.4	183	72.2
1309	2550	836	0.513	362	84.3	350	81.6
1348	1351	36	0.997	-26	-72.3	-22	-61.2
1385	1339	242	0.997	178	73.7	172	71.3
1282	1258	730	1.020	702	94.3	650	87.4
1319	675	58	1.950	2	1.7	50	44.1
1333	690	228	1.930	324	73.5	361	82.0
1312	685	554	1.910	952	89.7	948	89.3

Table 9.2 Main Characteristics and Performance of the Turbocharged Engine without Waste Gate

	Match 1	Match 2	Match 3	Match 4
compressor size scaling factor	0.70	0.70	0.70	0.70
compressor sectional area factor	1.00	1.00	1.00	1.00
turbine size scaling factor	0.70	0.70	0.70	0.70
turbine sectional area factor	0.80	0.75	0.70	0.65
engine speed (rpm)	4000.	4000.	4000.	4000.
air-fuel ratio	22.0	22.0	22.0	22.0
brake power (kw)	59.5	63.2	71.2	74.5
B.M.E.P (bar)	9.02	9.85	10.79	11.34
brake thermal efficiency	0.411	0.414	0.419	0.421
inlet manifold pressure (bar)	2.10	2.28	2.67	2.94
exhaust manifold pressure (bar)	1.82	1.97	2.31	2.57
exhaust manifold temperature (k)	798.	808.	832.	847.
air flow rate (kg/s)	0.112	0.119	0.134	0.140
density ratio	1.6	1.6	1.8	1.9
turbocharger speed (rpm)	95225.	100752.	114309.	118508.
delivery ratio	1.44	1.53	1.71	1.79
charging efficiency	0.95	1.00	1.12	1.17

	Match 5	Match 6	Match 7	Match 8
compressor size scaling factor	0.70	0.70	0.70	0.70
compressor sectional area factor	0.90	0.90	0.90	0.90
turbine size scaling factor	0.70	0.70	0.70	0.70
turbine sectional area factor	0.75	0.70	0.65	0.60
engine speed (rpm)	4000.	4000.	4000.	4000.
air-fuel ratio	22.0	22.0	22.0	22.0
brake power (kw)	62.1	69.5	73.1	75.7
B.M.E.P (bar)	9.42	10.52	11.08	11.49
brake thermal efficiency	0.413	0.418	0.419	0.420
inlet manifold pressure (bar)	2.25	2.61	2.88	3.14
exhaust manifold pressure (bar)	1.96	2.27	2.53	2.80
exhaust manifold temperature (k)	810.	832.	849.	867.
air flow rate (kg/s)	0.116	0.130	0.136	0.138
density ratio	1.6	1.8	1.9	2.0
turbocharger speed (rpm)	102314.	115133.	120093.	124108.
delivery ratio	1.49	1.67	1.74	1.78
charging efficiency	0.98	1.09	1.14	1.18

Table 9.2 Main Characteristics and Performance of the Turbocharged Engine Without Waste Gate

	Match 9	Match 10	Match 11	Match 12
compressor size scaling factor	0.70	0.70	0.70	0.70
compressor sectional area factor	0.80	0.80	0.80	0.80
turbine size scaling factor	0.70	0.70	0.70	0.70
turbine sectional area factor	0.70	0.65	0.60	0.55
engine speed (rpm)	4000.	4000.	4000.	4000.
air-fuel ratio	22.0	22.0	22.0	22.0
brake power (kw)	63.5	69.1	71.7	73.0
B.M.E.P (bar)	9.63	10.48	10.88	11.07
brake thermal efficiency	0.413	0.416	0.417	0.417
inlet manifold pressure (bar)	2.39	2.73	2.96	3.22
exhaust manifold pressure (bar)	2.09	2.40	2.66	2.92
exhaust manifold temperature (k)	827.	846.	864.	888.
air flow rate (kg/s)	0.118	0.128	0.130	0.128
density ratio	1.7	1.8	1.9	2.0
turbocharger speed (rpm)	110049.	119206.	124077.	128941.
delivery ratio	1.50	1.64	1.67	1.65
charging efficiency	1.01	1.09	1.13	1.15

	Match 13	Match 14	Match 15	Match 16
compressor size scaling factor	0.70	0.70	0.70	0.70
compressor sectional area factor	0.70	0.70	0.70	0.70
turbine size scaling factor	0.70	0.70	0.70	0.70
turbine sectional area factor	0.65	0.60	0.55	0.50
engine speed (rpm)	4000.	4000.	4000.	4000.
air-fuel ratio	22.0	22.0	22.0	22.0
brake power (kw)	62.1	65.7	67.5	68.3
B.M.E.P (bar)	9.41	9.96	10.24	10.36
brake thermal efficiency	0.410	0.412	0.410	0.409
inlet manifold pressure (bar)	2.44	2.72	2.98	3.12
exhaust manifold pressure (bar)	2.17	2.44	2.72	2.97
exhaust manifold temperature (k)	839.	857.	883.	907.
air flow rate (kg/s)	0.113	0.118	0.119	0.117
density ratio	1.7	1.8	1.9	1.9
turbocharger speed (rpm)	113786.	121184.	127049.	131497.
delivery ratio	1.46	1.52	1.53	1.49
charging efficiency	0.99	1.05	1.08	1.05

Table 9.3 Characteristics of Turbocharger with Waste Gate

	Match 17	Match 18
compressor size scaling factor	0.55	0.50
compressor sectional area factor	0.90	0.90
turbine size scaling factor	0.55	0.50
turbine sectional area factor	0.50	0.50
impeller diameter (mm)	49.5	45.0
maximum turbocharger speed (rpm)	173000.	190000.

Table 9.4 Characteristics of the Blower Supercharged Engines

	Match 1	Match 2
turbocharger	none	none
blower mass flow scaling factor	1.0	0.8

Table 9.5 Characteristics of the Turbocharged Engines with a Blower

	Match3	Match4	Match5	Match6	Match7	Match8
blower mass flow scaling factor	0.8	0.6	0.8	0.8	0.8	0.8
compressor size scaling factor	0.5	0.5	0.6	0.7	0.5	0.5
compressor sectional area scaling factor	0.9	0.9	0.9	0.9	0.9	0.9
turbine size scaling factor	0.5	0.5	0.6	0.7	0.5	0.5
turbine sectional area scaling factor	0.5	0.5	0.55	0.6	0.5	0.5
impeller diameter (mm)	45.0	45.0	54.0	63.0	45.0	45.0
maximum turbocharger speed (10000*rpm)	19.0	19.0	15.8	13.6	19.0	19.0
waste gate actuating pressure (bar)	2.8	2.8	2.8	2.8	2.5	2.2

Table 9.6 Performance of Matches 3, 7 and 8 at Rated Regimes

	Match 3	Match 7	Match 8
engine speed (rpm)	4000.	4000.	4000.
trapped air-fuel ratio	22.0	22.0	22.0
engine power (KW)	46.6	42.6	39.9
engine torque (NM)	111.	102.	95.
brake thermal efficiency	0.329	0.321	0.320
waste gate actuating pressure (bar)	2.8	2.5	2.2
flow rate through compressor (Kg/S)	0.092	0.089	0.084
flow rate through waste gate (Kg/S)	0.035	0.033	0.034
turbocharger speed (rpm)	183581.	149664.	133126.
turbocharger power (KW)	10.66	9.31	7.04
inlet manifold pressure (bar)	3.10	2.79	2.49
exhaust manifold pressure (bar)	2.90	2.60	2.32
exhaust temperature (K)	955.	942.	919.
compressor boost ratio	2.05	1.92	1.73
blower boost ratio	1.51	1.45	1.44
delivery ratio	1.18	1.13	1.07

Table 9.7 Computed Results of DCE without a Bypass Valve

ROOTES TS3 DCE						37 83 52 24		
number of cylinders	3.0	bore (m.m.)	94.98	stroke (m.m.)	233.53			
con-rod length (m.m.)	109.55	inlet valve closing (degs)	55.6	compressor scale factor	1.15			
ambient temperature (deg k)	294.4	ambient pressure (bar)	0.99	cooler effectiveness	0.7916			
compression ratio	14.00	engine diagram factor	1.0000	turbine flow loss factor	0.8000			
engine speed(r.p.m)	2522.00	2438.00	2298.00	2178.00	2021.00	2230.00	2167.00	2002.00
boost pressure ratio	3.088	2.960	2.401	2.052	1.926	3.304	3.043	2.577
trapped air to fuel ratio	24.841	24.789	22.807	20.236	16.000	26.950	29.161	26.706
delivery ratio	0.634	0.586	0.565	0.485	0.315	0.749	0.754	0.702
manifold temp (deg k)	324.059	319.087	311.500	304.347	378.863	328.987	323.114	316.241
engine power (k w.)	272.80	237.72	186.55	142.69	104.39	272.11	227.73	177.20
engine torque (n.m.))	1026.34	924.66	767.38	631.80	498.93	1157.85	996.51	841.95
b.m.e.p (bar)	13.0773	11.7852	9.8118	7.9182	6.2431	14.7481	12.7016	10.6981
s.f.c. (kg/kw hr)	0.209	0.214	0.227	0.249	0.399	0.202	0.208	0.218
b.thermal eff.	0.3991	0.3891	0.3680	0.3355	0.2092	0.4135	0.4091	0.3825
fuel / rev / cyl (g.)	0.126	0.116	0.102	0.090	0.114	0.137	0.119	0.107
max cyl pressure (bar .)	137.60	128.79	104.13	84.39	66.83	149.44	132.52	106.55
exhaust temperature(deg k)	893.71	897.52	914.76	978.64	1935.91	823.17	772.74	800.88
mass flow (kg/s)	0.436	0.380	0.287	0.204	0.093	0.480	0.441	0.328
percentage heat to coolant	12.41	13.32	16.01	19.01	21.80	12.24	13.30	15.82
compressor speed (r.p.m.)	5429.2	4796.0	3740.6	2836.0	1652.4	5944.5	5469.6	4225.8
compressor pressure ratio	3.295	3.122	2.512	2.119	1.931	3.550	3.256	2.713
mass flow (kg/s)	0.436	0.380	0.287	0.204	0.093	0.480	0.441	0.328
compressor power (kw.)	75.36	60.24	38.94	24.04	11.15	93.42	74.07	48.42
compressor torque (n.m)	132.50	119.90	99.36	80.90	64.44	150.01	129.26	109.37
delivery temperature (deg k)	466.08	452.12	429.65	411.87	414.26	487.45	461.42	441.25
compressor efficiency	0.695	0.717	0.656	0.601	0.509	0.663	0.706	0.662
by pass valve area (sq.cm.)	0.000	0.000	0.000	0.000	0.000	0.000	0.000	0.000
turbine speed (r.p.m)	47500.0	46250.0	41750.0	40500.0	51500.0	44800.0	41800.0	40000.0
turbine pressure ratio	2.690	2.657	2.193	1.943	1.877	2.743	2.543	2.287
mass flow (kg/s)	0.452	0.394	0.298	0.214	0.104	0.495	0.454	0.339
turbine power (kw)	77.27	66.57	41.82	27.22	24.88	79.47	63.37	43.56
turbine torque (n.m)	15.53	13.74	9.56	6.42	4.61	16.93	14.47	10.39
inlet temperature (deg k)	893.71	897.52	914.76	978.64	1935.91	823.17	772.74	800.88
turbine nozzle angle	8.859	7.824	7.343	6.288	4.483	9.114	8.725	7.424
turbine efficiency	0.756	0.752	0.744	0.734	0.720	0.759	0.755	0.746
output shaft speed (rpm)	2500.00	2500.00	2500.00	2500.00	2500.00	2000.00	2000.00	2000.00
output shaft power (kw)	255.98	227.21	175.08	136.41	109.65	240.68	201.82	160.50
output shaft torque (n./m)	977.38	867.51	668.48	520.81	418.64	1148.70	963.21	766.02
output shaft sfc (kg/kw.hr)	0.223	0.224	0.241	0.260	0.380	0.228	0.230	0.241
output thermal efficiency	0.3743	0.3719	0.3454	0.3207	0.2197	0.3658	0.3625	0.3465
engine fuel flow (kg/s)	0.951	0.849	0.705	0.591	0.694	0.915	0.774	0.644
dynamic injection(degree ca)	165.2	164.6	164.2	163.7	161.1	167.3	166.7	170.0
duration of injection	24.5	22.2	19.2	16.8	18.2	22.4	19.9	17.3
turbine gear ratio	19.00	18.50	16.70	16.20	20.60	22.40	20.90	20.00
output shaft gear ratio	1.388	1.388	1.388	1.388	1.388	1.388	1.388	1.388
charging efficiency	0.572	0.542	0.528	0.474	0.315	0.641	0.644	0.614

Table 9.7 Computed Results of DCE without a Bypass Valve

0ROOTES TS3 DCE						33 79 47 24		
0number of cylinders	3.0	bore (m.m.)	94.98	stroke (m.m.)	233.53			
con-rod length (m.m.)	109.55	inlet valve closing (degs)	55.6	compressor scale factor	1.15			
ambient temperature (deg k)	294.4	ambient pressure (bar)	0.99	cooler effectiveness	0.7647			
compression ratio	14.00	engine diagram factor	1.0000	turbine flow loss factor	0.8000			
0engine speed(r.p.m)	1901.00	1738.00	1925.00	1888.00	1650.00	1493.00	1330.00	1769.00
boost pressure ratio	2.335	1.916	3.542	3.241	2.473	2.030	1.756	4.180
trapped air to fuel ratio	25.366	19.072	29.002	31.435	32.156	30.128	23.192	30.348
delivery ratio	0.638	0.485	0.880	0.924	0.908	0.808	0.570	1.066
manifold temp (deg k)	308.749	312.792	333.560	327.915	316.270	305.514	321.513	347.852
engine power (k w.)	145.03	95.90	260.53	225.51	140.67	97.24	60.08	297.09
engine torque (n.m.))	736.20	534.19	1283.94	1132.09	810.77	627.74	439.28	1610.69
b.m.e.p (bar)	9.2209	6.6693	16.3582	14.4367	10.3041	7.8722	5.4599	20.2984
s.f.c. (kg/kw hr)	0.231	0.284	0.199	0.199	0.214	0.235	0.286	0.195
b.thermal eff.	0.3604	0.2933	0.4200	0.4186	0.3906	0.3548	0.2920	0.4286
fuel / rev / cyl (g.)	0.098	0.087	0.149	0.132	0.101	0.085	0.072	0.182
max cyl pressure (bar .)	90.80	65.43	158.52	142.82	102.46	77.97	56.16	186.04
exhaust temperature(deg k)	820.63	996.84	767.97	715.85	670.60	671.18	793.16	745.69
mass flow (kg/s)	0.263	0.148	0.515	0.494	0.336	0.229	0.119	0.649
percentage heat to coolant	17.83	22.69	12.24	13.13	17.36	21.68	27.72	10.92
0compressor speed (r.p.m.)	3464.4	2235.6	6361.9	6083.0	4288.8	3105.3	1876.5	7902.5
compressor pressure ratio	2.432	1.952	3.817	3.505	2.618	2.112	1.778	4.598
mass flow (kg/s)	0.263	0.148	0.515	0.494	0.336	0.229	0.119	0.649
compressor power (kw.)	34.53	16.40	110.95	93.55	47.43	26.41	11.16	173.02
compressor torque (n.m)	95.14	70.04	166.47	146.80	105.56	81.19	56.78	208.98
delivery temperature (deg k)	425.36	405.09	507.82	482.37	435.04	409.14	388.30	557.51
compressor efficiency	0.651	0.562	0.640	0.673	0.663	0.612	0.562	0.605
by pass valve area (sq.cm.)	0.000	0.000	0.000	0.000	0.000	0.000	0.000	0.000
0turbine speed (r.p.m)	39400.0	38600.0	43800.0	40800.0	34500.0	32100.0	31050.0	45000.0
turbine pressure ratio	2.173	1.853	2.838	2.611	2.100	1.864	1.697	3.270
mass flow (kg/s)	0.272	0.155	0.529	0.506	0.344	0.236	0.123	0.665
turbine power (kw)	33.52	18.58	82.71	67.25	33.37	19.20	10.04	111.89
turbine torque (n.m)	8.12	4.59	18.02	15.73	9.23	5.71	3.09	23.73
inlet temperature (deg k)	820.63	996.84	767.97	715.85	670.60	671.18	793.16	745.69
turbine nozzle angle	6.387	4.869	8.915	9.115	7.572	6.010	3.843	9.747
turbine efficiency	0.739	0.725	0.760	0.758	0.744	0.733	0.718	0.768
output shaft speed (rpm)	2000.00	2000.00	1500.00	1500.00	1500.00	1500.00	1500.00	1000.00
output shaft power (kw)	135.50	91.70	216.02	184.77	117.57	84.06	54.62	221.03
output shaft torque (n./m)	646.70	437.65	1374.65	1175.81	748.14	534.94	347.56	2109.77
output shaft sfc (kg/kw.hr)	0.248	0.297	0.240	0.243	0.256	0.272	0.314	0.262
output thermal efficiency	0.3367	0.2804	0.3482	0.3429	0.3264	0.3068	0.2654	0.3189
engine fuel flow (kg/s)	0.559	0.455	0.862	0.749	0.501	0.381	0.286	0.964
dynamic injection(degree ca)	171.1	172.4	169.5	170.5	172.7	174.5	176.1	171.2
duration of injection	15.5	13.3	21.3	19.2	14.3	11.9	10.0	23.7
turbine gear ratio	19.70	19.30	29.20	27.20	23.00	21.40	20.70	45.00
output shaft gear ratio	1.388	1.388	1.388	1.388	1.388	1.388	1.388	1.388
charging efficiency	0.575	0.474	0.713	0.735	0.727	0.670	0.573	0.801

Table 9.7 Computed Results of DCE without a Bypass Valve

number of cylinders	3.0	bore (m.m.)	94.98	stroke (m.m.)	233.53			
con-rod length (m.m.)	109.55	inlet valve closing (degs)	55.6	compressor scale factor	1.15			
ambient temperature (deg k)	294.4	ambient pressure (bar)	0.99	cooler effectiveness	0.8320			
compression ratio	14.00	engine diagram factor	1.0000	turbine flow loss factor	0.8000			
engine speed(r.p.m)	1569.00	1470.00	1087.00	1533.00	1345.00	1184.00	977.00	778.00
boost pressure ratio	3.407	3.013	2.021	4.767	3.926	3.289	2.871	2.207
trapped air to fuel ratio	34.634	38.895	34.385	31.137	35.733	40.250	44.325	42.809
delivery ratio	1.126	1.164	0.952	1.253	1.375	1.489	1.452	1.454
manifold temp (deg k)	331.235	322.674	304.137	359.843	342.126	328.947	317.958	306.166
engine power (k w.)	201.87	153.03	68.82	302.61	208.50	142.85	91.88	55.21
engine torque (n.m.))	1221.58	987.02	611.47	1876.43	1487.31	1159.21	904.32	684.68
b.m.e.p (bar)	15.5510	12.5823	7.6522	23.8587	18.7361	14.5824	11.3670	8.5769
s.f.c. (kg/kw hr)	0.196	0.200	0.235	0.194	0.195	0.200	0.208	0.228
b.thermal eff.	0.4249	0.4178	0.3548	0.4295	0.4280	0.4171	0.4006	0.3655
fuel / rev / cyl (g.)	0.140	0.115	0.083	0.213	0.168	0.134	0.109	0.090
max cyl pressure (bar .)	154.19	131.51	80.83	209.88	175.92	142.13	119.30	91.53
exhaust temperature(deg k)	652.00	593.90	572.39	727.39	630.93	560.70	512.53	473.70
mass flow (kg/s)	0.520	0.458	0.197	0.729	0.608	0.505	0.367	0.233
percentage heat to coolant	13.54	15.42	25.39	10.40	12.76	15.48	19.40	26.56
compressor speed (r.p.m.)	6394.8	5648.4	2761.2	8839.9	7422.7	6209.0	4648.5	3148.4
compressor pressure ratio	3.694	3.244	2.083	5.267	4.300	3.564	3.026	2.288
mass flow (kg/s)	0.520	0.458	0.197	0.729	0.608	0.505	0.367	0.233
compressor power (kw.)	106.15	75.89	22.87	225.58	150.11	97.85	56.63	29.26
compressor torque (n.m)	158.44	123.25	79.04	243.58	193.04	150.43	116.29	88.72
delivery temperature (deg k)	496.71	459.19	410.20	598.83	538.49	486.70	447.97	419.25
compressor efficiency	0.650	0.713	0.594	0.579	0.619	0.668	0.713	0.630
by pass valve area (sq.cm.)	0.000	0.000	0.000	0.000	0.000	0.000	0.000	0.000
turbine speed (r.p.m)	39000.0	36000.0	30000.0	47000.0	41000.0	37000.0	34000.0	28000.0
turbine pressure ratio	2.728	2.440	1.899	3.708	3.110	2.762	2.586	2.026
mass flow (kg/s)	0.531	0.466	0.201	0.745	0.619	0.513	0.372	0.237
turbine power (kw)	66.65	47.61	14.19	133.64	83.98	55.43	34.05	15.09
turbine torque (n.m)	16.31	12.62	4.51	27.14	19.55	14.30	9.56	5.15
inlet temperature (deg k)	652.00	593.90	572.39	727.39	630.93	560.70	512.53	473.70
turbine nozzle angle	8.699	8.176	4.612	9.500	8.742	7.667	5.674	4.536
turbine efficiency	0.758	0.752	0.725	0.771	0.763	0.754	0.741	0.727
output shaft speed (rpm)	1000.00	1000.00	1000.00	500.00	500.00	500.00	500.00	500.00
output shaft power (kw)	150.12	115.03	56.13	192.68	132.05	93.33	64.00	38.22
output shaft torque (n./m)	1432.90	1098.03	535.77	3678.32	2520.93	1781.81	1221.78	729.68
output shaft sfc (kg/kw.hr)	0.264	0.266	0.288	0.305	0.308	0.306	0.299	0.330
output thermal efficiency	0.3160	0.3140	0.2894	0.2735	0.2711	0.2725	0.2791	0.2531
engine fuel flow (kg/s)	0.660	0.509	0.270	0.979	0.677	0.476	0.319	0.210
dynamic injection(degree ca)	170.6	171.9	174.3	172.4	172.0	173.8	175.2	176.1
duration of injection	17.7	14.6	9.9	24.4	18.3	14.2	11.1	8.8
turbine gear ratio	39.00	36.00	30.00	94.00	82.00	74.00	68.00	56.00
output shaft gear ratio	1.388	1.388	1.388	1.388	1.388	1.388	1.388	1.388
charging efficiency	0.825	0.840	0.748	0.875	0.913	0.943	0.933	0.933

Table 9.8 Summary of DCE Rated and 'Stall' Conditions

	rated	stall upper LTC	stall lower LTC
Engine			
(3 cyl., 4.96 l., 2 stroke opposed piston, compression ratio 14:1)			
Speed (rpm)	2522.	1533.	1184.
Boost pressure ratio	3.09	4.77	3.29
Trapped air-fuel ratio	24.8	31.1	40.3
Engine power (KW)	272.9	302.6	142.9
BMEP (bar)	13.08	23.86	14.58
s.f.c. (Kg/KW h)	0.209	0.194	0.200
Brake thermal efficiency	39.9	42.9	41.7
Max. cylinder pressure (bar)	137.6	209.9	142.1
Exhaust temperature (K)	621.	727.	561.
Compressor			
(Rotary positive disp. type)			
Speed (rpm)	5429.	8840.	6209.
Pressure ratio	3.30	5.26	3.29
Comp. power (KW)	75.4	225.6	97.9
Comp. efficiency	69.5	57.9	68.8
Mass flow (Kg/Min)	26.2	43.7	30.3
Turbine			
(Radial inflow)			
Speed (rpm)	47500.	47000.	37000.
Pressure ratio	2.69	3.71	2.76
Turbine power (KW)	77.4	133.6	55.4
Turbine efficiency	75.6	75.1	75.4
Output shaft condition			
Output shaft speed (rpm)	2500.	500.	500.
Output shaft torque (Nm)	977.	3678.	1782.
Output shaft power (KW)	256.0	192.7	93.3
Output shaft s.f.c. (Kg/KW h)	0.223	0.305	0.306
Output shaft efficiency	37.4	27.4	27.3

Table 9.9 Computed Results of DCE with a Bypass Valve

```
1
0PROUTES T53 DCE                                                    37   84   47   24
0number of cylinders          3.0      bore              ( m.m.)   94.98   stroke              ( m.m.)   233.53
 con-rod length      ( m.m.) 109.55     inlet valve closing ( degs ) 55.6   compressor scale factor        1.15
 ambient temperature ( deg k ) 294.4    ambient pressure    ( bar )   0.99   cooler effectiveness           0.8109
 compression ratio            14.00     engine diagram factor         1.0000 turbine flow loss factor       0.8000
0engine speed(r.p.m)          2522.00   2438.00   2298.00   2178.00   2021.00   2230.00   2167.00   2002.00
 boost  pressure ratio           3.088     2.960     2.401     2.052     1.926     3.364     3.084     2.596
 trapped air to fuel ratio      24.841    24.789    22.807    20.236    16.000    24.048    26.442    24.905
 delivery ratio                  0.634     0.586     0.565     0.485     0.315     0.636     0.665     0.634
 manifold tem       ( deg k)   324.059   319.087   311.500   304.347   378.863   326.744   321.361   313.204
 engine power       ( k w.  )  272.80    237.72    186.55    142.69    104.39    268.65    227.67    175.09
 engine torque      ( n.m. ))  1026.34   924.66    767.38    631.80    498.93    1157.85   996.51    841.95
 b.m.e.p            ( bar )     13.0778   11.7852    9.8118    7.9182    6.2431   14.5611   12.6985   10.5706
 s.f.c.        ( kg/kw hr )      0.209     0.214     0.227     0.249     0.399     0.210     0.210     0.224
 b.thermal eff.                  0.3991    0.3891    0.3680    0.3355    0.2092    0.3972    0.3962    0.3718
 fuel / rev / cyl   (  g.   )    0.126     0.116     0.102     0.090     0.114     0.141     0.123     0.109
 max cyl pressure   ( bar  .)  137.60    128.79    104.13     84.39     66.83    147.40    130.38    104.31
 exhaust temperature(deg k )   893.71    897.52    914.76    978.64   1935.91    912.75    840.21    851.31
 mass flow  (kg/s)               0.436     0.380     0.287     0.204     0.093     0.418     0.396     0.301
 percentage heat to coolant     12.41     13.32     16.01     19.01     21.80     12.47     13.47     16.04
0compressor speed (r.p.m.)     5429.2    4796.0    3740.6    2836.0    1652.4    5944.5    5469.6    4225.8
 compressor pressure ratio       3.295     3.122     2.512     2.119     1.931     3.550     3.256     2.713
 mass flow  (kg/s)               0.436     0.380     0.287     0.204     0.093     0.480     0.441     0.326
 compressor power   ( kw.   )   75.36     60.24     38.94     24.04     11.15     93.42     74.07     48.42
 compressor torque (n.m)       132.50    119.90     99.36     80.90     64.44    150.01    129.26    109.37
 delivery temperature ( deg k) 466.08    452.12    429.65    411.87    414.26    487.45    461.42    441.25
 compressor efficiency           0.695     0.717     0.656     0.601     0.509     0.663     0.706     0.662
 by pass valve area (sq.cm.)     0.000     0.000     0.000     0.000     0.000     1.290     0.968     0.774
0turbine speed    (r.p.m)     47500.0   46250.0   41750.0   40500.0   51500.0   44800.0   41800.0   40000.0
 turbine pressure ratio          2.690     2.657     2.193     1.943     1.877     2.992     2.722     2.383
 mass flow (kg/s)                0.452     0.394     0.298     0.214     0.104     0.496     0.454     0.339
 turbine power    (kw)          77.27     66.57     41.82     27.22     24.88     89.53     70.23     46.61
 turbine torque (n.m)           15.53     13.74      9.56      6.42      4.61     19.07     16.04     11.12
 inlet temperature (deg k)     893.71    897.52    914.76    978.64   1935.91    863.98    805.84    821.49
 turbine nozzle angle            8.859     7.824     7.343     6.288     4.483     8.567     8.316     7.181
 turbine efficiency              0.756     0.752     0.744     0.734     0.720     0.757     0.753     0.744
 output shaft speed (rpm)     2500.00   2500.00   2500.00   2500.00   2500.00   2000.00   2000.00   2000.00
 output shaft power (kw)       255.98    227.21    175.08    136.41    109.65    250.05    208.21    163.35
 output shaft torque (n./m)    977.38    867.51    668.48    520.81    418.64   1193.40    993.70    779.60
 output shaft sfc (kg/kw.hr)     0.223     0.224     0.241     0.260     0.380     0.226     0.230     0.240
 output thermal efficiency       0.3743    0.3719    0.3454    0.3207    0.2197    0.3697    0.3624    0.3469
 engine fuel flow (kg/s)         0.951     0.849     0.705     0.591     0.694     0.940     0.799     0.655
 dynamic injection(degree ca)  165.2     164.6     164.2     163.7     161.1     167.0     168.4     169.9
 duration of injection          24.5      22.2      19.2      16.8      18.2      22.8      20.3      17.5
 turbine gear ratio            19.00     18.50     16.70     16.20     20.60     22.40     20.90     20.00
 output shaft gear ratio        1.388     1.388     1.388     1.388     1.388     1.388     1.388     1.388
 charging efficiency            0.572     0.542     0.528     0.474     0.315     0.574     0.591     0.572
1
```

Table 9.9 Computed Results of DCE with a Bypass Valve

```
1
OUTPUTS FOR DCE                                                    33   88   65   24
Number of cylinders          3.0     bore                ( m.m.)  94.98   stroke              ( m.m.)  233.53
con-rod length       ( m.m.) 109.55  inlet valve closing  ( degs )  55.6   compressor scale factor       1.15
ambient temperature  ( deg k ) 294.4 ambient pressure     ( bar )    0.99   cooler effectiveness          0.8105
compression ratio            14.00   engine diagram factor          1.0000 turbine flow loss factor      0.8000
Engine speed(r.p.m)          1901.00  1738.30  1925.00  1888.00  1650.00  1493.00  1330.00  1769.00
 boost  pressure ratio          2.335    1.916    3.633    3.321    2.499    2.035    1.756    4.399
 trapped air to fuel ratio     25.366   19.072   24.760   27.653   29.806   29.227   23.192   23.200
 delivery ratio                 0.638    0.485    0.693    0.753    0.797    0.774    0.570    0.684
 manifold temp        ( deg k) 308.749  312.792  329.158  325.710  313.020  304.688  321.513  335.297
 engine power         ( k w.  ) 145.03   95.90   257.65   222.54   138.75    96.98    60.08   297.19
 engine torque        ( n.m. )) 736.20   534.19  1283.94  1132.09   810.77   627.74   439.28  1610.69
 b.m.e.p              ( bar )    9.2209   6.6693  16.1772  14.2469  10.1636   7.8509   5.4599  20.3051
 s.f.c.          ( kg/kw hr )    0.231    0.284    0.209    0.207    0.219    0.237    0.286    0.209
 b.thermal eff.                 0.3604   0.2933   0.3994   0.4020   0.3802   0.3513   0.2920   0.3985
 fuel / rev / cyl     ( g.    ) 0.098    0.087    0.135    0.136    0.102    0.086    0.072    0.195
 max cyl pressure     ( bar   .) 90.89    65.43   156.58   139.69   100.32    77.32    56.16   187.83
 exhaust temperature(deg k )   820.63   796.84   802.83   801.67   713.91   686.85   793.16   943.15
 mass flow  (kg/s)              0.263    0.148    0.422    0.415    0.301    0.221    0.119    0.455
 percentage heat to coolant    17.83    22.69    12.58    13.44    17.67    21.82    27.72    11.46
Compressor speed (r.p.m.)     3464.4   2235.6   6361.9   6083.0   4288.8   3105.3   1876.5   7902.5
 compressor pressure ratio      2.432    1.952    3.817    3.505    2.618    2.112    1.778    4.598
 mass flow  (kg/s)              0.263    0.148    0.515    0.494    0.336    0.229    0.119    0.649
 compressor power     ( kw.   ) 34.53    16.40   110.95    93.55    47.43    26.41    11.16   173.02
 compressor torque (n.m)       95.14    70.04   166.47   146.80   105.56    81.19    56.78   208.98
 delivery temperature (deg k)  425.36   405.09   507.82   482.37   435.04   409.14   388.30   557.51
 compressor efficiency          0.651    0.562    0.640    0.673    0.663    0.612    0.562    0.605
 by pass valve area (sq.cm.)    0.000    0.000    1.935    1.613    0.968    0.323    0.000    3.871
Turbine speed   (r.p.m)      39400.0  38600.0  43800.0  40800.0  34500.0  32100.0  31050.0  45000.0
 turbine pressure ratio         2.173    1.853    3.208    2.928    2.251    1.889    1.697    4.094
 mass flow (kg/s)               0.272    0.155    0.530    0.507    0.344    0.236    0.123    0.666
 turbine power   (kw)          33.52    18.58    97.12    77.98    36.89    19.77    10.04   143.09
 turbine torque (n.m)           8.12     4.59    21.16    18.24    10.21     5.88     3.09    30.35
 inlet temperature (deg k)    820.63   996.84   821.66   755.42   687.45   677.45   793.16   838.35
 turbine nozzle angle           6.387    4.869    8.113    8.339    7.051    5.918    3.843    8.273
 turbine efficiency             0.739    0.725    0.753    0.753    0.740    0.732    0.718    0.751
 output shaft speed (rpm)    2000.00  2000.00  1500.00  1500.00  1500.00  1500.00  1500.00  1000.00
 output shaft power (kw)      135.50   91.70   229.44   194.77   120.85    84.59    54.62   250.08
 output shaft torque (n./m)   646.70   437.65  1460.03  1239.41   769.03   538.30   347.56  2387.07
 output shaft sfc (kg/kw.hr)    0.248    0.297    0.235    0.237    0.252    0.272    0.314    0.249
 output thermal efficiency      0.3367   0.2804   0.3557   0.3518   0.3312   0.3064   0.2654   0.3354
 engine fuel flow (kg/s)        0.559    0.455    0.897    0.770    0.507    0.384    0.286    1.037
 dynamic injection(degree ca)   171.1    172.4    169.1    170.2    172.6    174.5    176.1    170.3
 duration of injection           15.5     13.3     22.0     19.6     14.4     12.0     10.0     25.2
 turbine gear ratio             19.70    19.30    29.20    27.20    23.00    21.40    20.70    45.00
 output shaft gear ratio        1.388    1.388    1.388    1.388    1.388    1.388    1.388    1.388
 charging efficiency            0.575    0.474    0.609    0.644    0.668    0.655    0.532    0.603
```

Table 9.9 Computed Results of DCE with a Bypass Valve

0ROOTES TS3 DCE						38 107 62 24		
0number of cylinders	3.0	bore (m.m.)	94.98	stroke (m.m.)	233.53			
con-rod length (m.m.)	109.55	inlet valve closing (degs)	55.6	compressor scale factor	1.15			
ambient temperature (deg k)	294.1	ambient pressure (bar)	0.99	cooler effectiveness	0.8265			
compression ratio	14.00	engine diagram factor	1.0000	turbine flow loss factor	0.8000			
0engine speed(r.p.m)	1569.00	1470.00	1087.00	1533.00	1345.00	1184.00	977.00	778.00
boost pressure ratio	3.541	3.107	2.021	4.760	4.062	3.382	2.919	2.228
trapped air to fuel ratio	27.833	32.938	34.383	28.231	32.234	36.867	40.195	39.221
delivery ratio	0.768	0.846	0.952	0.960	1.074	1.177	1.132	1.231
manifold temp (deg k)	322.695	316.228	304.137	352.865	338.754	326.053	310.897	306.917
engine power (k w.)	199.67	150.83	68.83	300.07	208.66	142.84	91.74	55.25
engine torque (n.m.))	1221.58	987.02	611.47	1876.43	1487.31	1159.21	904.32	684.68
b.m.e.p (bar)	15.3811	12.4013	7.6535	23.6503	18.7508	14.5813	11.3494	8.5830
s.f.c. (kg/kw hr)	0.208	0.208	0.235	0.197	0.199	0.203	0.212	0.232
b.thermal eff.	0.4003	0.4012	0.3547	0.4226	0.4198	0.4106	0.3935	0.3590
fuel / rev / cyl (g.)	0.147	0.119	0.083	0.215	0.171	0.136	0.111	0.092
max cyl pressure (bar .)	149.85	128.66	80.83	214.26	176.41	142.57	118.71	90.65
exhaust temperature(deg k)	783.65	678.02	572.37	801.68	696.28	609.36	550.01	503.36
mass flow (kg/s)	0.379	0.350	0.197	0.592	0.496	0.414	0.297	0.199
percentage heat to coolant	14.19	16.08	25.39	10.70	13.10	15.93	20.14	27.23
0compressor speed (r.p.m.)	6394.8	5648.4	2761.2	8839.9	7422.7	6209.0	4648.5	3148.4
compressor pressure ratio	3.694	3.244	2.033	5.267	4.300	3.564	3.026	2.288
mass flow (kg/s)	0.520	0.458	0.197	0.729	0.608	0.505	0.367	0.233
compressor power (kw.)	106.15	75.69	22.87	225.58	150.11	97.85	56.63	29.26
compressor torque (n.m)	158.44	128.25	79.04	243.58	193.04	150.43	116.29	88.72
delivery temperature (deg k)	496.71	459.19	410.20	598.83	538.49	486.70	447.97	419.25
compressor efficiency	0.656	0.713	0.594	0.579	0.619	0.668	0.713	0.630
by pass valve area (sq.cm.)	3.226	2.581	0.645	1.935	1.935	1.935	1.935	1.290
0turbine speed (r.p.m)	39000.0	36000.0	30000.0	47000.0	41000.0	37000.0	34000.0	28000.0
turbine pressure ratio	3.263	2.826	1.899	4.219	3.550	3.045	2.714	2.080
mass flow (kg/s)	0.532	0.466	0.201	0.745	0.619	0.513	0.372	0.237
turbine power (kw)	82.62	57.20	14.19	151.83	97.31	62.78	36.86	16.20
turbine torque (n.m)	20.22	15.17	4.51	30.84	22.65	16.20	10.35	5.52
inlet temperature (deg k)	711.39	629.58	572.37	766.40	668.92	588.31	531.48	491.49
turbine nozzle angle	7.604	7.229	4.612	8.571	7.886	7.123	5.499	4.462
turbine efficiency	0.746	0.745	0.725	0.768	0.758	0.751	0.740	0.727
output shaft speed (rpm)	1000.00	1000.00	1000.00	500.00	500.00	500.00	500.00	500.00
output shaft power (kw)	164.99	123.96	56.13	209.62	144.46	100.17	66.61	39.25
output shaft torque (n./m)	1574.85	1183.22	535.76	4001.74	2757.75	1912.40	1271.70	749.32
output shaft sfc (kg/kw.hr)	0.252	0.253	0.288	0.282	0.287	0.290	0.292	0.327
output thermal efficiency	0.3312	0.3297	0.2894	0.2953	0.2906	0.2880	0.2857	0.2550
engine fuel flow (kg/s)	0.693	0.523	0.270	0.987	0.691	0.484	0.324	0.214
dynamic injection(degree cu)	170.2	171.7	174.3	172.3	171.8	173.6	175.0	176.0
duration of injection	18.4	14.9	9.9	24.6	18.6	14.4	11.2	8.9
turbine gear ratio	39.00	36.00	30.00	94.00	82.00	74.00	68.00	56.00
output shaft gear ratio	1.388	1.388	1.388	1.388	1.388	1.388	1.388	1.388
charging efficiency	0.652	0.694	0.748	0.753	0.804	0.845	0.827	0.865

1

Table 9.10 Computed Results of DCE with a Output Shaft CVT

```
ORDUTLS TS3 DCE
0number of cylinders                3.0      bore                    ( m.m.)   94.98      stroke                    ( m.m.)   233.53
 con-rod length          ( m.m.)  109.55     inlet valve closing     ( degs )  55.6       compressor scale factor             1.15
 ambient temperature     ( deg k ) 294.4     ambient pressure        ( bar )    0.99      cooler effectiveness                0.8375
 compression ratio                 14.00     engine diagram factor              1.0000    turbine flow loss factor            0.8000
0engine speed(r.p.m)              2500.00    2500.00    2500.00    2500.00    2500.00    2000.00    2000.00    2000.00
 boost  pressure ratio               3.160      3.160      3.160      3.160      3.160      3.180      3.180      3.180
 trapped air to fuel ratio          25.361     25.361     25.361     25.361     25.361     25.332     25.332     25.332
 delivery ratio                      0.594      0.594      0.594      0.594      0.594      0.586      0.586      0.586
 manifold temp           ( deg k)  320.030    320.030    320.030    320.030    320.030    313.213    313.213    313.213
 engine power            ( k w.  ) 261.01     261.01     261.01     261.01     261.01     205.93     205.93     205.93
 engine torque           ( n.m. )) 989.73     989.73     989.73     989.73     989.73     989.73     989.73     989.73
 b.m.e.p                 ( bar )    12.6187    12.6187    12.6187    12.6187    12.6187    12.4450    12.4450    12.4450
 s.f.c.          ( kg/kw hr )        0.210      0.210      0.210      0.210      0.210      0.217      0.217      0.217
 b.thermal eff.                      0.3966     0.3966     0.3966     0.3966     0.3966     0.3840     0.3840     0.3840
 fuel / rev / cyl  ( g.    )         0.122      0.122      0.122      0.122      0.122      0.124      0.124      0.124
 max cyl pressure  ( bar  .)       137.04     137.04     137.04     137.04     137.04     129.07     129.07     129.07
 exhaust temperature(deg k )       890.72     890.72     890.72     890.72     890.72     872.62     872.62     872.62
 mass flow  (kg/s)                   0.420      0.420      0.420      0.420      0.420      0.340      0.340      0.340
 percentage heat to coolant         12.51      12.51      12.51      12.51      12.51      14.19      14.19      14.19
0compressor speed (r.p.m.)         5250.0     5250.0     5250.0     5250.0     5250.0     4400.0     4400.0     4400.0
 compressor pressure ratio           3.243      3.243      3.243      3.243      3.243      3.239      3.239      3.239
 mass flow  (kg/s)                   0.420      0.420      0.420      0.420      0.420      0.340      0.340      0.340
 compressor power  ( kw.   )        70.60      70.60      70.60      70.60      70.60      59.24      59.24      59.24
 compressor torque (n.m)           128.37     128.37     128.37     128.37     128.37     128.51     128.51     128.51
 delivery temperature (deg k)      461.34     461.34     461.34     461.34     461.34     467.23     467.23     467.23
 compressor efficiency               0.704      0.704      0.704      0.704      0.704      0.678      0.678      0.678
 by pass valve area (sq.cm.)         0.000      0.000      0.000      0.000      0.000      0.000      0.000      0.000
0turbine speed   (r.p.m)          60000.0    60000.0    60000.0    61000.0    59500.0    62500.0    64000.0    63000.0
 turbine pressure ratio              2.817      2.817      2.817      2.817      2.817      2.973      2.973      2.973
 mass flow (kg/s)                    0.436      0.436      0.436      0.436      0.436      0.353      0.353      0.353
 turbine power   (kw)               79.25      79.25      79.25      79.33      79.19      65.81      65.86      65.85
 turbine torque (n.m)               12.61      12.61      12.61      12.41      12.70      10.05       9.83       9.98
 inlet temperature (deg k)         890.72     890.72     890.72     890.72     890.72     872.62     872.62     872.62
 turbine nozzle angle               16.762     16.762     16.762     16.762     16.762     12.654     12.654     12.654
 turbine efficiency                  0.776      0.776      0.776      0.777      0.775      0.777      0.777      0.777
 output shaft speed (rpm)        2500.00    2000.00    1500.00    1000.00     500.00    2500.00    2000.00    1500.00
 output shaft power (kw)          230.23     231.57     232.91     234.32     235.52     182.70     184.10     185.40
 output shaft torque (n.m)        879.06    1105.20    1482.11    2236.68    4096.31     697.57     878.64    1179.82
 output shaft sfc (kg/kw.hr)         0.239      0.237      0.236      0.234      0.233      0.245      0.243      0.241
 output thermal efficiency           0.3493     0.3519     0.3539     0.3560     0.3579     0.3407     0.3433     0.3458
 engine fuel flow (kg/s)             0.915      0.915      0.915      0.915      0.915      0.745      0.745      0.745
 dynamic injection(degree cs)      165.4      165.4      165.4      165.4      165.4      168.9      168.9      168.9
 duration of injection              23.7       23.7       23.7       23.7       23.7       19.1       19.1       19.1
 turbine gear ratio                24.00      30.00      40.00      61.00     119.00      25.00      32.00      42.00
 output shaft gear ratio            1.386      1.109      0.832      0.554      0.277      1.765      1.412      1.059
 charging efficiency                0.547      0.547      0.547      0.547      0.547      0.542      0.542      0.542
1
```

Table 9.10 Computed Results of DCE with a Output Shaft CVT

```
1
ORIGILS 153 DCE                                                                    48  115  136   24
0number of cylinders              3.0      bore                    ( m.m.)   94.98      stroke                  ( m.m.)   233.53
 con-rod length       ( m.m.)   109.55     inlet valve closing     ( degs )  55.6       compressor scale factor            1.15
 ambient temperature  ( deg k ) 294.4      ambient pressure        ( bar )    0.99      cooler effectiveness               0.9535
 compression ratio                14.00    engine diagram factor              1.0000    turbine flow loss factor           0.8000
0engine speed(r.p.m)             1000.00    1000.00    1000.00     500.00     500.00     500.00     500.00     500.00
 boost  pressure ratio              3.203      3.203      3.203      3.206      3.206      3.206      3.206      3.206
 trapped air to fuel ratio         26.524     26.524     26.524     30.749     30.749     30.749     30.749     30.749
 delivery ratio                     0.622      0.622      0.622      0.830      0.830      0.830      0.830      0.830
 manifold temp        ( deg k)    299.361    299.361    299.361    294.185    294.185    294.185    294.185    294.185
 engine power         ( k w.  )   102.97     102.97     102.97      52.15      52.15      52.15      52.15      52.15
 engine torque        ( n.m. ))   989.73     989.73     989.73     989.73     989.73     989.73     989.73     989.73
 b.m.e.p              ( bar )      12.4452    12.4452    12.4452    12.6074    12.6074    12.6074    12.6074    12.6074
 s.f.c.          ( kg/kw hr )      0.228      0.228      0.228      0.240      0.240      0.240      0.240      0.240
 b.thermal eff.                    0.3661     0.3661     0.3661     0.3475     0.3475     0.3475     0.3475     0.3475
 fuel / rev / cyl  ( g.   )        0.130      0.130      0.130      0.139      0.139      0.139      0.139      0.139
 max cyl pressure  ( bar  .)     126.14     126.14     126.14     124.82     124.82     124.82     124.82     124.82
 exhaust temperature(deg k )     745.29     745.29     745.29     570.53     570.53     570.53     570.53     570.53
 mass flow  (kg/s)                 0.190      0.190      0.190      0.129      0.129      0.129      0.129      0.129
 percentage heat to coolant       20.74      20.74      20.74      29.00      29.00      29.00      29.00      29.00
0compressor speed (r.p.m.)       2800.0     2800.0     2800.0     2150.0     2150.0     2150.0     2150.0     2150.0
 compressor pressure ratio          3.227      3.227      3.227      3.219      3.219      3.219      3.219      3.219
 mass flow  (kg/s)                 0.190      0.190      0.190      0.129      0.129      0.129      0.129      0.129
 compressor power  ( kw.   )      37.80      37.80      37.80      29.07      29.07      29.07      29.07      29.07
 compressor torque (n.m)         128.85     128.85     128.85     129.04     129.04     129.04     129.04     129.04
 delivery temperature (deg k)    491.21     491.21     491.21     516.64     516.64     516.64     516.64     516.64
 compressor efficiency,            0.592      0.592      0.592      0.522      0.522      0.522      0.522      0.522
 by pass valve area (sq.cm.)       0.000      0.000      0.000      0.000      0.000      0.000      0.000      0.000
0turbine speed   (r.p.m)        64500.0    64500.0    64500.0    62500.0    64000.0    63000.0    64000.0    63500.0
 turbine pressure ratio             3.103      3.103      3.103      3.094      3.094      3.094      3.094      3.094
 mass flow (kg/s)                  0.197      0.197      0.197      0.133      0.133      0.133      0.133      0.133
 turbine power   (kw)             31.28      31.25      31.25      15.14      14.96      15.08      14.96      15.02
 turbine torque (n.m)              4.67       4.63       4.63       2.31       2.23       2.29       2.23       2.26
 inlet temperature (deg k)       745.29     745.29     745.29     570.53     570.53     570.53     570.53     570.53
 turbine nozzle angle              6.197      6.197      6.197      3.654      3.660      3.656      3.660      3.658
 turbine efficiency                0.752      0.752      0.752      0.711      0.703      0.708      0.703      0.705
 output shaft speed (rpm)       3000.00    1500.00     500.00    2500.00    2000.00    1500.00    1000.00     500.00
 output shaft power (kw)          90.64      81.95      84.62      26.84      28.01      29.46      30.69      32.08
 output shaft torque (n./m)      330.85     521.46    1615.39     102.49     133.70     187.50     292.91     612.40
 output shaft sfc (kg/kw.hr)       0.291      0.286      0.277      0.466      0.447      0.425      0.408      0.390
 output thermal efficiency,      0.2867     0.2913     0.3008     0.1788     0.1866     0.1963     0.2044     0.2137
 engine fuel flow (kg/s)           0.391      0.391      0.391      0.209      0.209      0.209      0.209      0.209
 dynamic injection(degree ca)    171.4      171.4      171.4      175.1      175.1      175.1      175.1      175.1
 duration of injection            12.6       12.6       12.6        9.4        9.4        9.4        9.4        9.4
 turbine gear ratio               32.00      43.00     129.00      25.00      32.00      42.00      64.00     127.00
 output shaft gear ratio          9.132      2.386      0.795     11.639      9.311      6.983      4.656      2.328
 charging efficiency,             0.564      0.564      0.564      0.686      0.686      0.686      0.686      0.686
1
```

Table 9.11 Computed Results of CES with 3 CVTs

ROOTES TS3 DCE						0 96 19 24		
number of cylinders	3.0	bore (m.m.)	94.98	stroke (m.m.)	255.53			
con-rod length (m.m.)	109.55	inlet valve closing (degs)	55.6	compressor scale factor	1.15			
ambient temperature (deg k)	294.4	ambient pressure (bar)	0.99	cooler effectiveness	0.8375			
compression ratio	14.00	engine diagram factor	1.0000	turbine flow loss factor	0.8000			
engine speed(r.p.m)	2500.00	2500.00	2500.00	2500.00	2500.00	2000.00	2000.00	2000.00
boost pressure ratio	3.160	3.160	3.160	3.160	3.160	3.180	3.180	3.180
trapped air to fuel ratio	25.360	25.360	25.360	25.360	25.360	25.332	25.332	25.332
delivery ratio	0.595	0.595	0.595	0.595	0.595	0.586	0.586	0.586
manifold temp (deg k)	320.024	320.024	320.024	320.024	320.024	313.210	313.210	313.210
engine power (k w.)	261.02	261.02	261.02	261.02	261.02	205.94	205.94	205.94
engine torque (n.m.))	989.73	989.73	989.73	989.73	989.73	989.73	989.73	989.73
b.m.e.p (bar)	12.6192	12.6192	12.6192	12.6192	12.6192	12.4454	12.4454	12.4454
s.f.c. (kg/kw hr)	0.210	0.210	0.210	0.210	0.210	0.217	0.217	0.217
b.thermal eff.	0.3966	0.3966	0.3966	0.3966	0.3966	0.3841	0.3841	0.3841
fuel / rev / cyl (g.)	0.122	0.122	0.122	0.122	0.122	0.124	0.124	0.124
max cyl pressure (bar .)	137.03	137.03	137.03	137.03	137.03	129.07	129.07	129.07
exhaust temperature(deg k)	890.71	890.71	890.71	890.71	890.71	872.59	872.59	872.59
mass flow (kg/s)	0.420	0.420	0.420	0.420	0.420	0.340	0.340	0.340
percentage heat to coolant	12.51	12.51	12.51	12.51	12.51	14.19	14.19	14.19
compressor speed (r.p.m.)	5250.0	5250.0	5250.0	5250.0	5250.0	4400.0	4400.0	4400.0
compressor pressure ratio	3.243	3.243	3.243	3.243	3.243	3.239	3.239	3.239
mass flow (kg/s)	0.420	0.420	0.420	0.420	0.420	0.340	0.340	0.340
compressor power (kw.)	70.58	70.58	70.58	70.58	70.58	59.23	59.23	59.23
compressor torque (n.m)	128.33	128.33	128.33	128.33	128.33	128.49	128.49	128.49
delivery temperature (deg k)	461.29	461.29	461.29	461.29	461.29	467.21	467.21	467.21
compressor efficiency	0.704	0.704	0.704	0.704	0.704	0.679	0.679	0.679
by pass valve area (sq.cm.)	0.000	0.000	0.000	0.000	0.000	0.000	0.000	0.000
turbine speed (r.p.m)	60000.0	60000.0	60000.0	61000.0	59500.0	62500.0	64000.0	63000.0
turbine pressure ratio	2.816	2.816	2.816	2.816	2.816	2.973	2.973	2.973
mass flow (kg/s)	0.436	0.436	0.436	0.436	0.436	0.353	0.353	0.353
turbine power (kw)	79.23	79.23	79.23	79.32	79.18	65.81	65.87	65.84
turbine torque (n.m)	12.61	12.61	12.61	12.41	12.70	10.05	9.82	9.98
inlet temperature (deg k)	890.71	890.71	890.71	890.71	890.71	872.59	872.59	872.59
turbine nozzle angle	16.766	16.766	16.766	16.766	16.766	12.655	12.655	12.655
turbine efficiency	0.776	0.776	0.776	0.777	0.775	0.777	0.777	0.777
output shaft speed (rpm)	2500.00	2000.00	1500.00	1000.00	500.00	2500.00	2000.00	1500.00
output shaft power (kw)	237.12	237.79	238.47	239.22	239.76	188.28	189.02	189.66
output shaft torque (n./m)	905.34	1134.90	1517.49	2283.46	4577.21	718.89	902.14	1206.94
output shaft sfc (kg/kw.hr)	0.232	0.231	0.230	0.229	0.229	0.238	0.237	0.236
output thermal efficiency	0.3603	0.3613	0.3623	0.3635	0.3643	0.3511	0.3525	0.3537
engine fuel flow (kg/s)	0.915	0.915	0.915	0.915	0.915	0.745	0.745	0.745
dynamic injection(degree ca)	165.4	165.4	165.4	165.4	165.4	168.9	168.9	168.9
duration of injection	23.7	23.7	23.7	23.7	23.7	19.1	19.1	19.1
turbine gear ratio	24.00	30.00	40.00	61.00	119.00	25.00	32.00	42.00
output shaft gear ratio	1.000	0.800	0.600	0.400	0.200	1.250	1.000	0.750
compressor shaft gear ratio	2.100	2.100	2.100	2.100	2.100	2.200	2.200	2.200
charging efficiency	0.547	0.547	0.547	0.547	0.547	0.542	0.542	0.542

Table 9.11 Computed Results of CES with 3 CVTs

1								
0200TLS 153 DCF								
0number of cylinders	3.0	bore (m.m.)	94.98			0 119 27 24		
conrod length (m.m.)	199.55	inlet valve closing (degs)	55.6	stroke (m.m.)	233.53			
ambient temperature (deg k)	294.4	ambient pressure (bar)	0.99	compressor scale factor	1.15			
compression ratio	14.00	engine diagram factor	1.0000	cooler effectiveness	0.9229			
0engine speed(r.p.m)	2000.00	2000.00	1500.00	1500.00	1500.00	turbine flow loss factor	0.8000	
boost pressure ratio	3.180	3.180	3.194	3.194	3.194	3.194	3.194	3.203
trapped air to fuel ratio	25.332	25.332	25.461	25.461	25.461	25.461	25.461	26.524
delivery ratio	0.586	0.586	0.592	0.592	0.592	0.592	0.592	0.621
manifold temp (deg k)	313.210	313.210	306.262	306.262	306.262	306.262	306.262	299.362
engine power (k w.)	205.94	205.94	154.34	154.34	154.34	154.34	154.34	102.97
engine torque (n.m.))	989.73	989.73	989.73	989.73	989.73	989.73	989.73	989.73
b.m.e.p (bar)	12.4454	12.4454	12.4362	12.4362	12.4362	12.4362	12.4362	12.4451
s.f.c. (kg/kw hr)	0.217	0.217	0.224	0.224	0.224	0.224	0.224	0.228
b.thermal eff.	0.3841	0.3841	0.3724	0.3724	0.3724	0.3724	0.3724	0.3661
fuel / rev / cyl (n.)	0.124	0.124	0.128	0.128	0.128	0.128	0.128	0.130
max cyl pressure (bar .)	129.07	129.07	123.40	123.40	123.40	123.40	123.40	126.14
exhaust temperature(deg k)	872.59	872.59	834.18	834.18	834.18	834.18	834.18	745.30
mass flow (kg/s)	0.340	0.340	0.265	0.265	0.265	0.265	0.265	0.190
percentage heat to coolant	14.19	14.19	16.62	16.62	16.62	16.62	16.62	20.74
0compressor speed (r.p.m.)	4400.0	4400.0	3600.0	3600.0	3600.0	3600.0	3600.0	2800.0
compressor pressure ratio	3.239	3.239	3.234	3.234	3.234	3.234	3.234	3.227
mass flow (kg/s)	0.340	0.340	0.265	0.265	0.265	0.265	0.265	0.190
compressor power (kw.)	59.23	59.23	48.53	48.53	48.53	48.53	48.53	37.80
compressor torque (n.m)	128.49	128.49	128.67	128.67	128.67	128.67	128.67	128.86
delivery temperature (deg k)	467.21	467.21	475.90	475.90	475.90	475.90	475.90	491.24
compressor efficiency	0.679	0.679	0.645	0.645	0.645	0.645	0.645	0.592
by pass valve area (sq.cm.)	0.000	0.000	0.000	0.000	0.000	0.000	0.000	0.000
0turbine speed (r.p.m)	66000.0	66000.0	65000.0	66000.0	64500.0	65000.0	63500.0	65000.0
turbine pressure ratio	2.973	2.973	3.072	3.072	3.072	3.072	3.072	3.103
mass flow (kg/s)	0.353	0.353	0.275	0.275	0.275	0.275	0.275	0.197
turbine power (kw)	65.82	65.71	49.76	49.73	49.76	49.76	49.74	31.22
turbine torque (n.m)	9.52	10.20	7.31	7.19	7.36	7.31	7.46	4.58
inlet temperature (deg k)	872.59	872.59	834.18	834.18	834.18	834.18	834.18	745.30
turbine nozzle angle	12.655	12.655	9.288	9.288	9.288	9.288	9.288	6.196
turbine efficiency	0.777	0.776	0.769	0.769	0.769	0.769	0.769	0.751
output shaft speed (rpm)	1000.00	500.00	2500.00	2000.00	1500.00	1000.00	500.00	2500.00
output shaft power (kw)	199.32	190.89	136.24	136.89	137.59	138.27	138.92	81.66
output shaft torque (n./m)	1816.63	3644.30	520.18	653.34	875.57	1319.78	2652.15	312.56
output shaft sfc (kg/kw.hr)	0.235	0.234	0.254	0.253	0.251	0.250	0.249	0.287
output thermal efficiency	0.3549	0.3560	0.3287	0.3303	0.3320	0.3336	0.3352	0.2910
engine fuel flow (kg/s)	0.745	0.745	0.576	0.576	0.576	0.576	0.576	0.391
dynamic injection(degree ca)	168.9	168.9	171.6	171.6	171.6	171.6	171.6	171.4
duration of injection	19.1	19.1	16.0	16.0	16.0	16.0	16.0	12.0
turbine gear ratio	66.00	123.00	26.00	33.00	43.00	65.00	127.00	26.00
output shaft gear ratio	0.500	0.250	1.667	1.333	1.000	0.667	0.333	2.500
compressor shaft gear ratio	2.200	2.200	2.400	2.400	2.400	2.400	2.400	2.800
charging efficiency	0.542	0.542	0.546	0.546	0.546	0.546	0.546	0.564

Table 9 11 Computed Results of CES with 3 CVTs

```
1
ORDOTES TS3 DCE                                                                    0  115   27   24
Onumber of cylinders          3.0      bore                    ( m.m.)    94.98    stroke                  ( m.m.)   233.53
 con-rod length      ( m.m.) 109.55    inlet valve closing     ( degs )   55.6     compressor scale factor          1.15
 ambient temperature ( deg k ) 294.4   ambient pressure        ( bar )     0.99    cooler effectiveness             0.9535
 compression ratio            14.00    engine diagram factor               1.0000  turbine flow loss factor         0.8000
Oengine speed(r.p.m)          1000.00   1000.00   1000.00    500.00    500.00    500.00    500.00    500.00
 boost  pressure ratio           3.203     3.203     3.203     3.206     3.206     3.206     3.206     3.206
 trapped air to fuel ratio      26.524    26.524    26.524    31.152    31.152    31.152    31.152    31.152
 delivery ratio                  0.621     0.621     0.621     0.830     0.830     0.830     0.830     0.830
 manifold temp       ( deg k)  299.362   299.362   299.362   294.182   294.182   294.182   294.182   294.182
 engine power        ( k w.  ) 102.97    102.97    102.97     51.49     51.49     51.49     51.49     51.49
 engine torque       (  n.m. )) 989.73   989.73    989.73    989.73    989.73    989.73    989.73    989.73
 b.m.e.p             ( bar )    12.4451   12.4451   12.4451   12.4469   12.4469   12.4469   12.4469   12.4469
 s.f.c.          ( kg/kw hr )    0.228     0.228     0.228     0.240     0.240     0.240     0.240     0.240
 b.thermal eff.                  0.3661    0.3661    0.3661    0.3476    0.3476    0.3476    0.3476    0.3476
 fuel / rev / cyl  (  g.   )     0.130     0.130     0.130     0.137     0.137     0.137     0.137     0.137
 max cyl pressure  ( bar  .)   126.14    126.14    126.14    124.24    124.24    124.24    124.24    124.24
 exhaust temperature(deg k )   745.30    745.30    745.30    566.58    566.58    566.58    566.58    566.58
 mass flow  (kg/s)               0.190     0.190     0.190     0.129     0.129     0.129     0.129     0.129
 percentage heat to coolant     20.74     20.74     20.74     29.05     29.05     29.05     29.05     29.05
Ocompressor speed (r.p.m.)    2800.0    2800.0    2800.0    2150.0    2150.0    2150.0    2150.0    2150.0
 compressor pressure ratio       3.227     3.227     3.227     3.219     3.219     3.219     3.219     3.219
 mass flow  (kg/s)               0.190     0.190     0.190     0.129     0.129     0.129     0.129     0.129
 compressor power  ( kw.   )    37.80     37.80     37.80     29.05     29.05     29.05     29.05     29.05
 compressor torque (n.m)       128.86    128.86    128.86    128.99    128.99    128.99    128.99    128.99
 delivery temperature (deg k)  491.24    491.24    491.24    516.53    516.53    516.53    516.53    516.53
 compressor efficiency           0.592     0.592     0.592     0.523     0.523     0.523     0.523     0.523
 by pass valve area (sq.cm.)     0.000     0.000     0.000     0.000     0.000     0.000     0.000     0.000
Oturbine speed   (r.p.m)      64000.0   64500.0   64500.0   62500.0   64000.0   63000.0   64000.0   63500.0
 turbine pressure ratio          3.103     3.103     3.103     3.094     3.094     3.094     3.094     3.094
 mass flow (kg/s)                0.197     0.197     0.197     0.133     0.133     0.133     0.133     0.133
 turbine power    (kw)          31.29     31.26     31.26     15.00     14.82     14.94     14.82     14.88
 turbine torque (n.m)            4.67      4.63      4.63      2.29      2.21      2.26      2.21      2.24
 inlet temperature ( deg k)    745.30    745.30    745.30    566.58    566.58    566.58    566.58    566.58
 turbine nozzle angle            6.176     6.176     6.176     3.641     3.648     3.643     3.648     3.646
 turbine efficiency              0.752     0.752     0.752     0.710     0.701     0.707     0.701     0.704
 output shaft speed (rpm.)    2000.00   1500.00    500.00   2500.00   2000.00   1500.00   1000.00    500.00
 output shaft power (kw)        82.60     83.24     84.59     27.50     28.00     28.79     29.35     30.08
 output shaft torque (n./m)    394.21    529.73   1614.95    104.99    133.63    183.23    280.14    574.31
 output shaft sfc (kg/kw.hr)     0.284     0.282     0.277     0.449     0.441     0.429     0.421     0.411
 output thermal efficiency       0.2937    0.2960    0.3007    0.1856    0.1890    0.1944    0.1981    0.2031
 engine fuel flow (kg/s)         0.391     0.391     0.391     0.206     0.206     0.206     0.206     0.206
 dynamic injection(degree ca)  171.4     171.4     171.4     175.3     175.3     175.3     175.3     175.3
 duration of injection          12.6      12.6      12.6       9.3       9.3       9.3       9.3       9.3
 turbine gear ratio            32.00     43.00    129.00     25.00     32.00     42.00     64.00    127.00
 output shaft gear ratio        2.000     1.500     0.500     5.000     4.000     3.000     2.000     1.000
 compressor shaft gear ratio    2.800     2.800     2.800     4.300     4.300     4.300     4.300     4.300
 charging efficiency            0.564     0.564     0.564     0.686     0.686     0.686     0.686     0.686
1
```

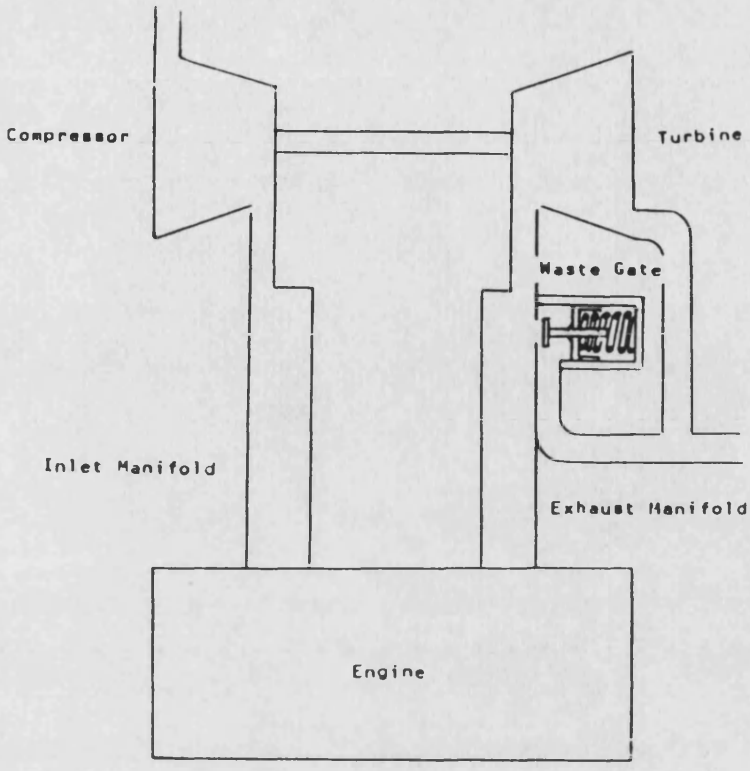

Fig. 9.1 Layout of Turbocharged Engine

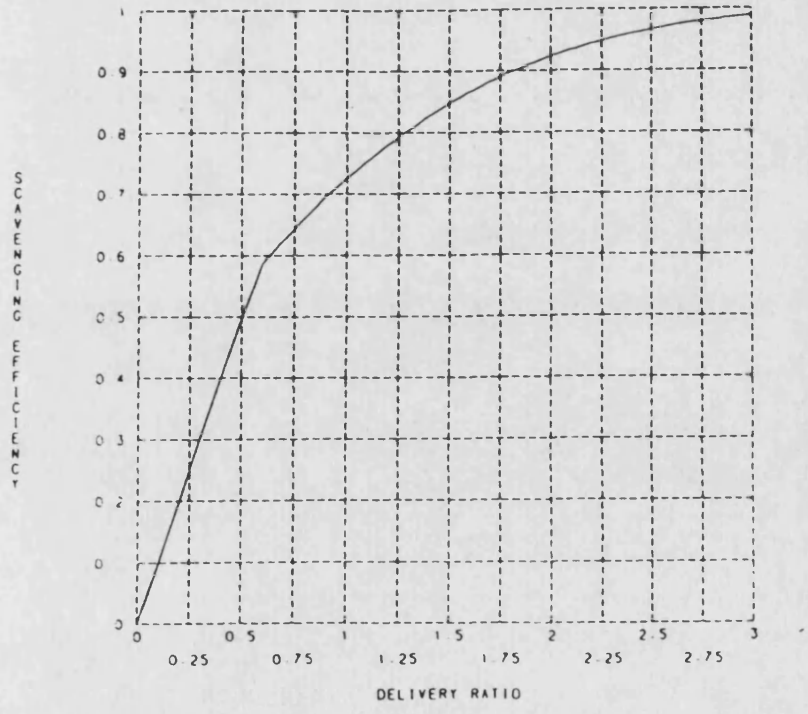

Fig. 9.2 Scavenging Efficiency versus Dolivery Ratio with Reference to Cylindor Trapping Condition

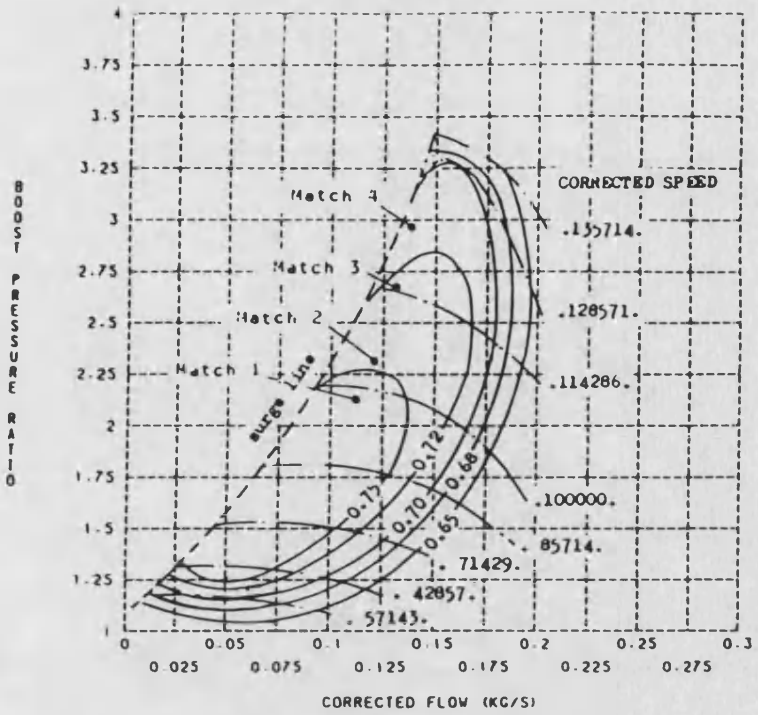

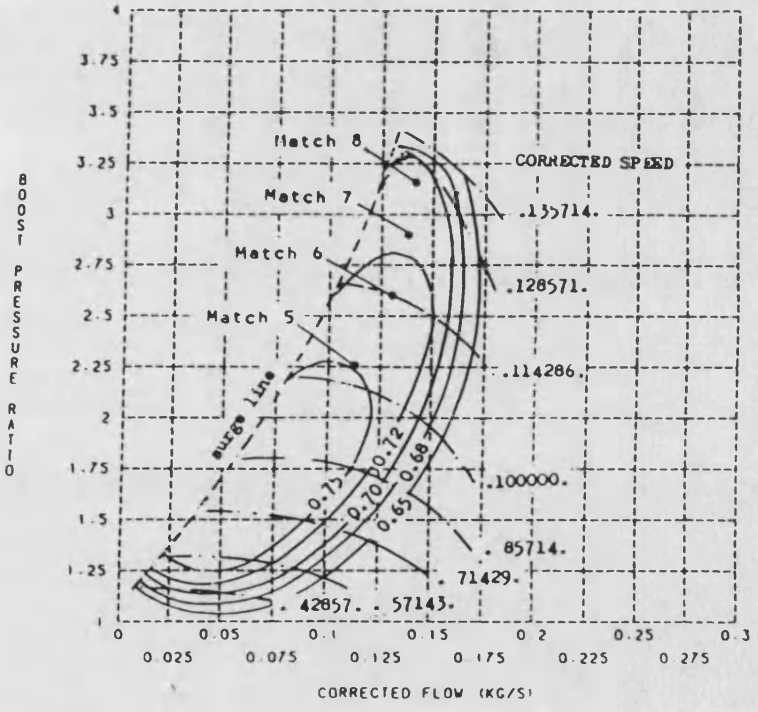

Fig. 9.3 Compressor Matching for Turbocharged Engine without Waste Gate

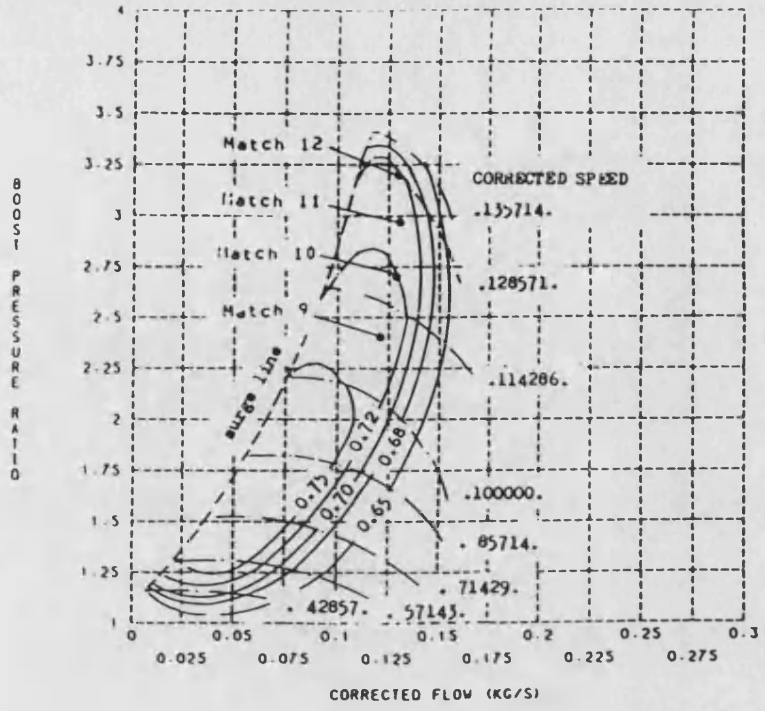
BOOST PRESSURE RATIO
Match 12
Match 11
Match 10
Match 9
CORRECTED SPEED
.135714.
.128571.
.114286.
.100000.
. 85714.
. 71429.
. 57143.
. 42857.
surge line
0.72
0.68
0.73
0.70
0.65
4
3.75
3.5
3.25
3
2.75
2.5
2.25
2
1.75
1.5
1.25
1
0
0.05
0.1
0.15
0.2
0.25
0.3
0.025
0.075
0.125
0.175
0.225
0.275
CORRECTED FLOW (KG/S)

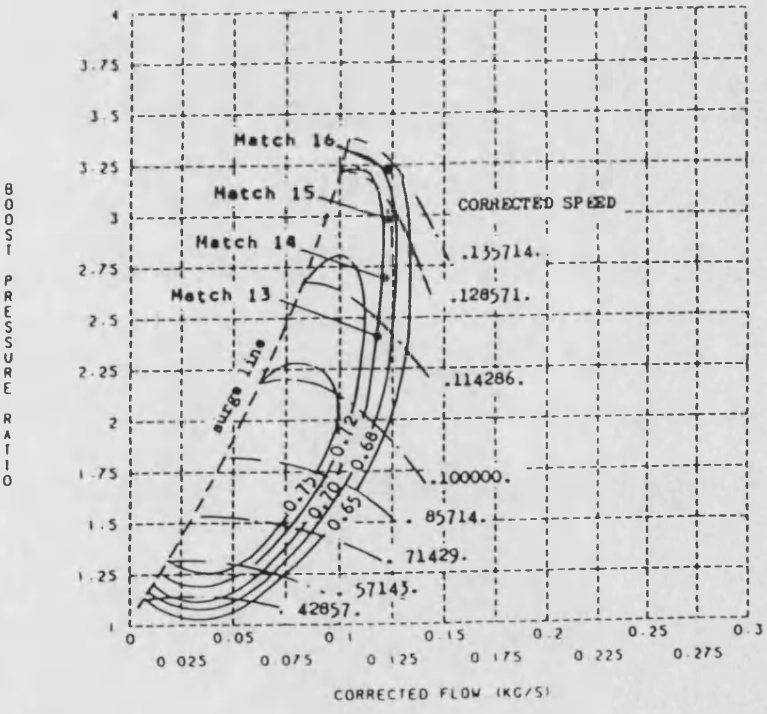
BOOST PRESSURE RATIO
Match 16
Match 15
Match 14
Match 13
CORRECTED SPEED
.135714.
.128571.
.114286.
.100000.
. 85714.
. 71429.
. 57143.
. 42857.
surge line
0.72
0.68
0.73
0.70
0.65
4
3.75
3.5
3.25
3
2.75
2.5
2.25
2
1.75
1.5
1.25
1
0
0.05
0.1
0.15
0.2
0.25
0.3
0.025
0.075
0.125
0.175
0.225
0.275
CORRECTED FLOW (KG/S)

Fig. 9.3 (cont.)

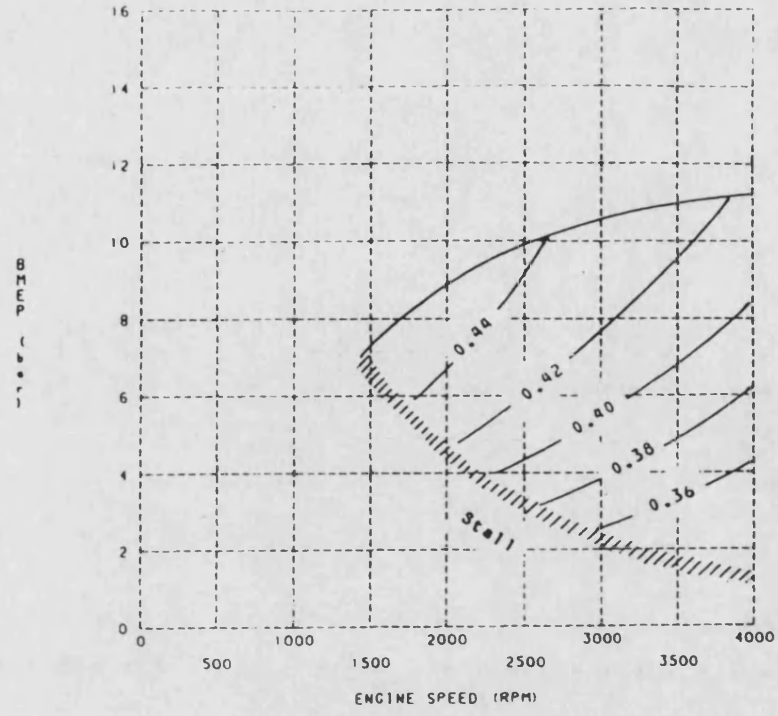

Fig. 9.4 Engine Efficiency Contours For Match 8

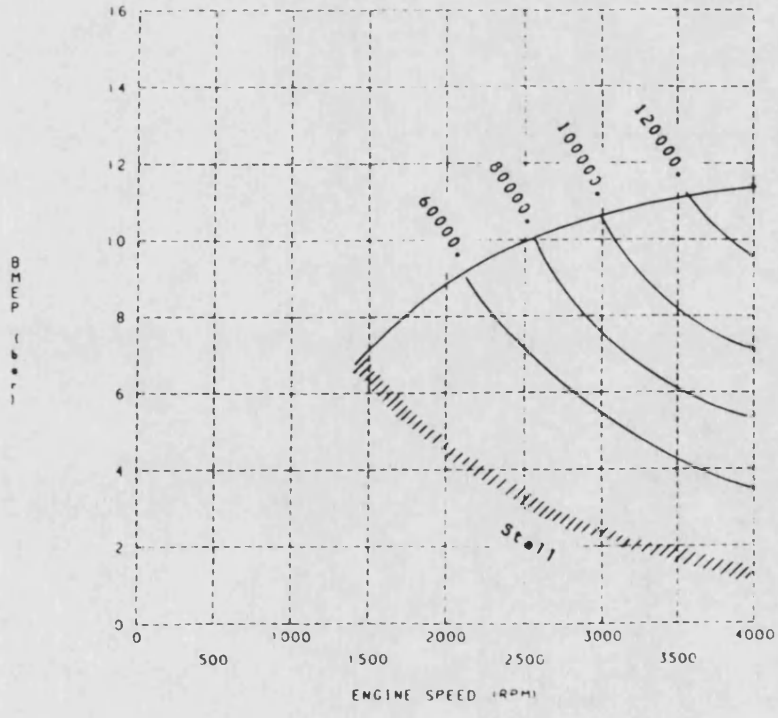

Fig. 9.5 Turbocharger Speed Contours for Match 8

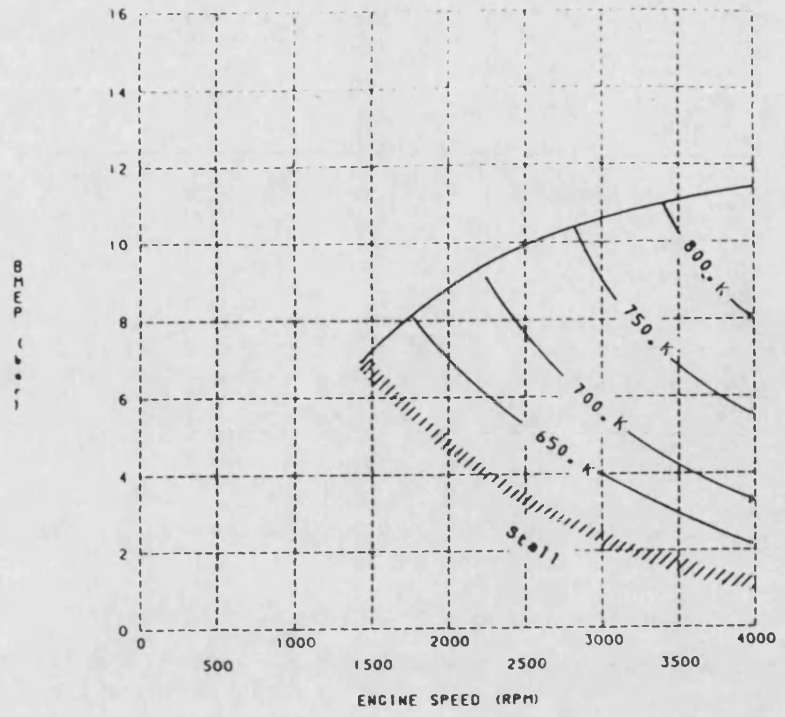

Fig. 9.6 Exhaust Temperature Contours for Match 8

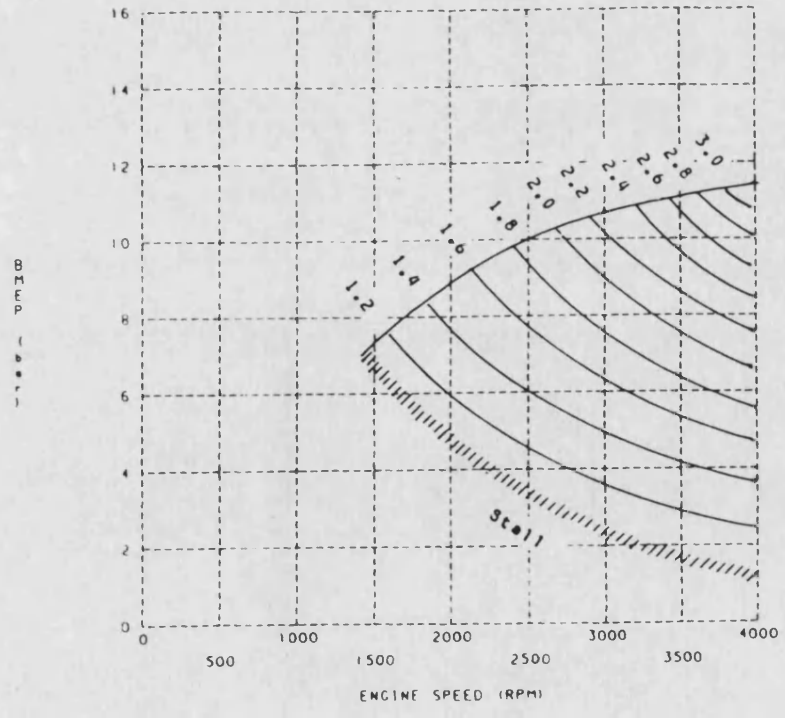

Fig. 9.7 Boost Pressure Contours for Match 8

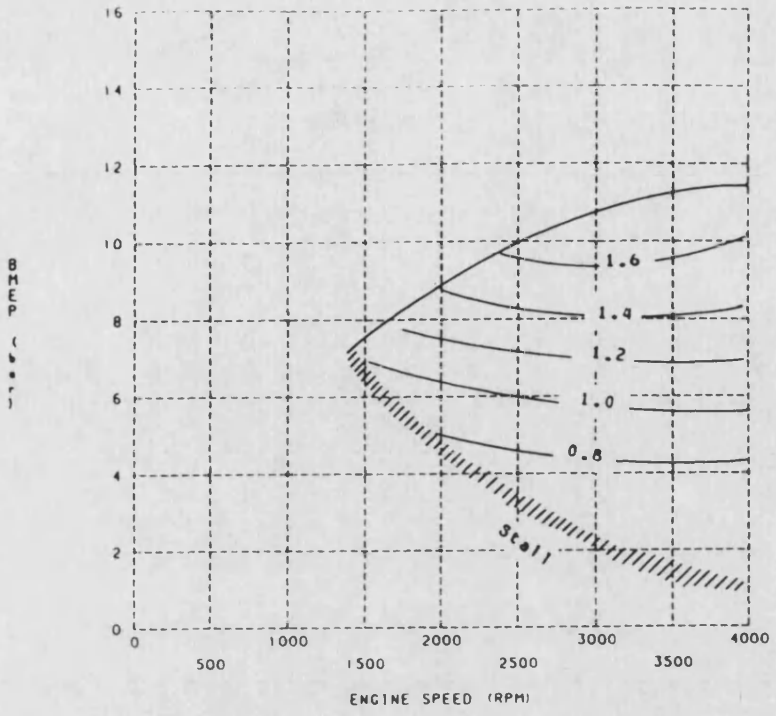

Fig. 9.8 Delivery Ratio Contours for Match 8

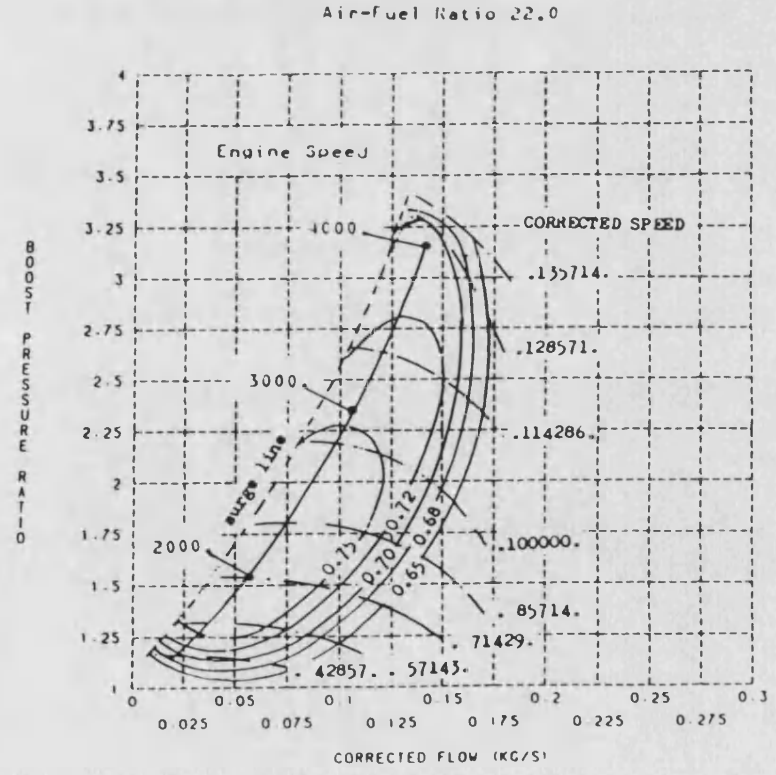

Fig. 9.9 Compressor Matching for Match 8

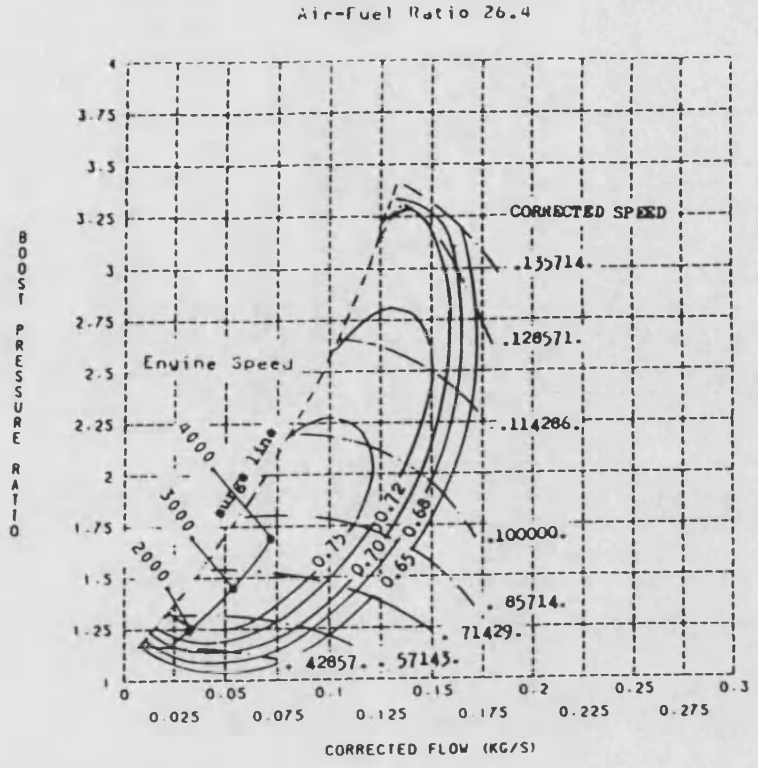
Air-Fuel Ratio 26.4
BOOST PRESSURE RATIO
CORRECTED FLOW (KG/S)
CORRECTED SPEED
.135714.
.128571.
.114286.
.100000.
. 85714.
. 71429.
. 57143.
. 42857.
Engine Speed
4000
3000
2000
surge line
0.75
0.72
0.70
0.68
0.65
4
3.75
3.5
3.25
3
2.75
2.5
2.25
2
1.75
1.5
1.25
1
0
0.05
0.1
0.15
0.2
0.25
0.3
0.025
0.075
0.125
0.175
0.225
0.275

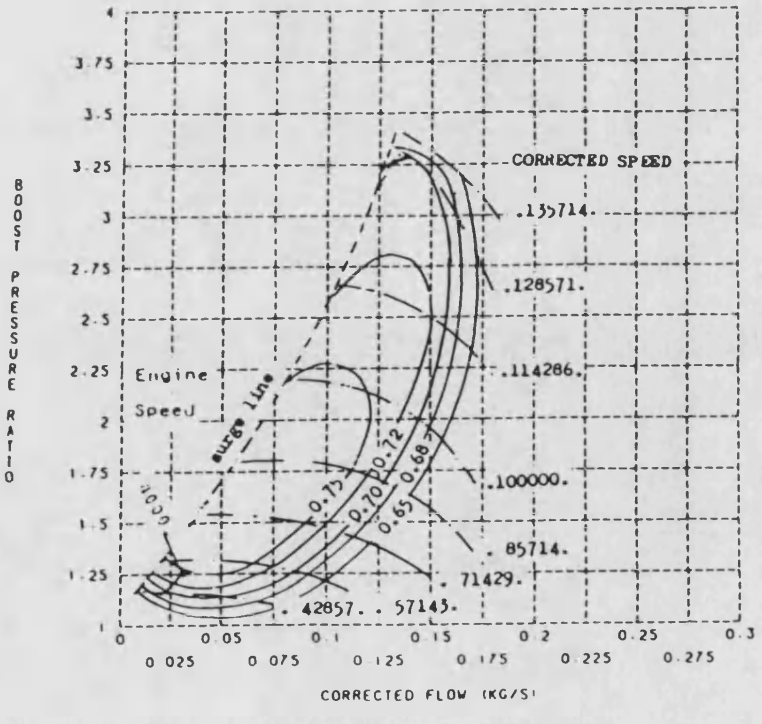
Air-Fuel Ratio 33.0
BOOST PRESSURE RATIO
CORRECTED FLOW (KG/S)
CORRECTED SPEED
.135714.
.128571.
.114286.
.100000.
. 85714.
. 71429.
. 57143.
. 42857.
Engine
Speed
surge line
0.75
0.72
0.70
0.68
0.65
4
3.75
3.5
3.25
3
2.75
2.5
2.25
2
1.75
1.5
1.25
1
0
0.05
0.1
0.15
0.2
0.25
0.3
0.025
0.075
0.125
0.175
0.225
0.275

Fig. 9.9 (cont.)

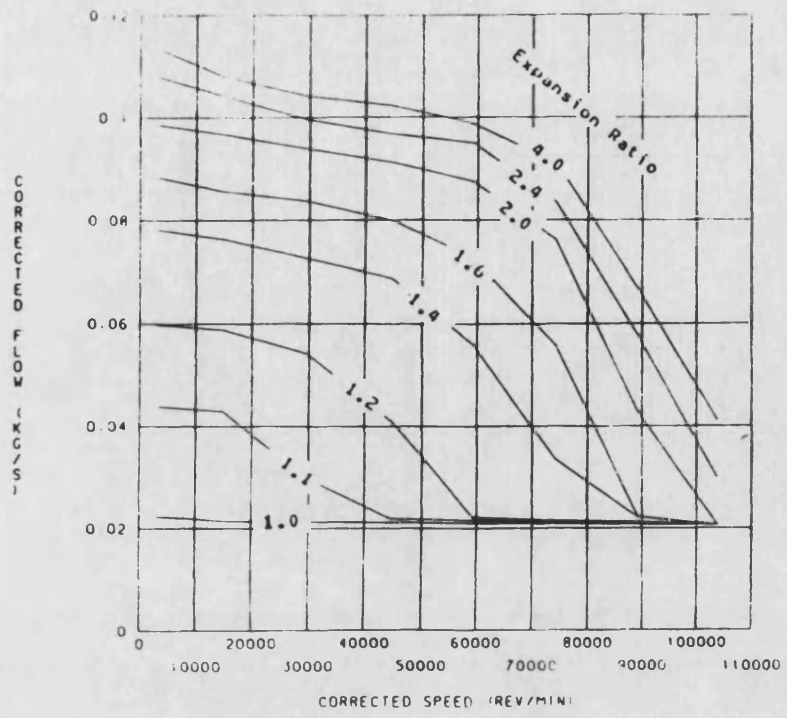

Fig. 9.10 Turbine Flow Rate for Match 8

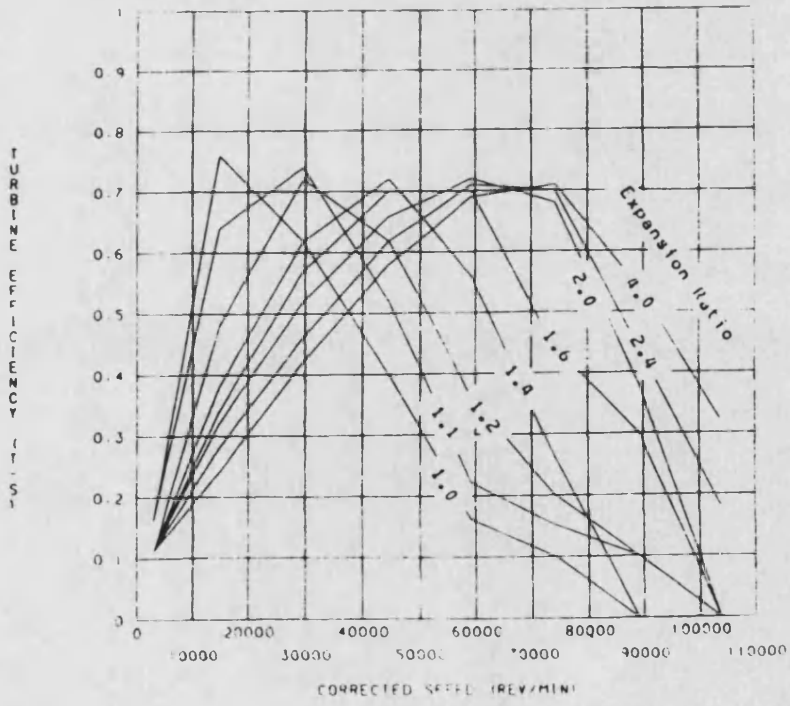

Fig. 9.11 Turbine Efficiency for Match 8

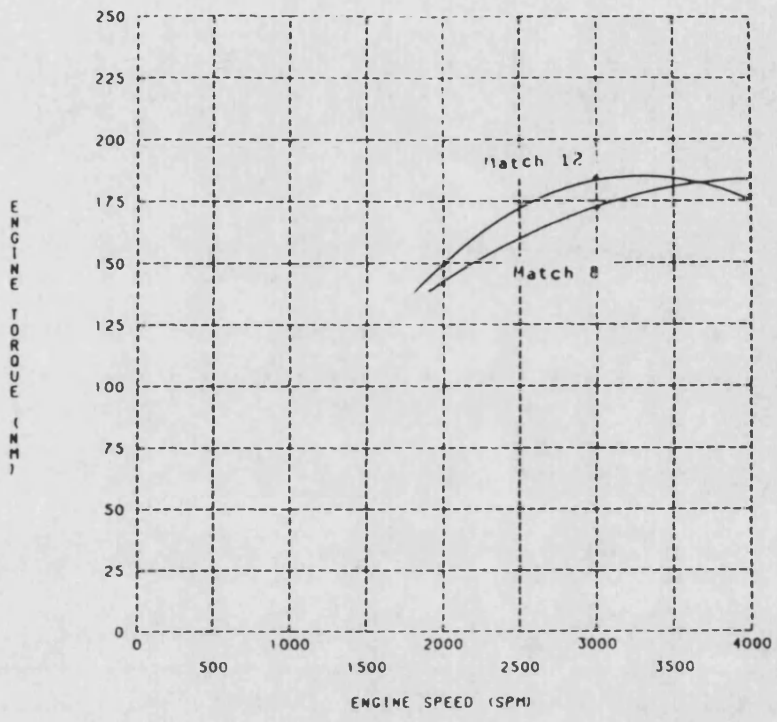

Fig. 9.12 Engine Torque Curves for Matches 8 and 12

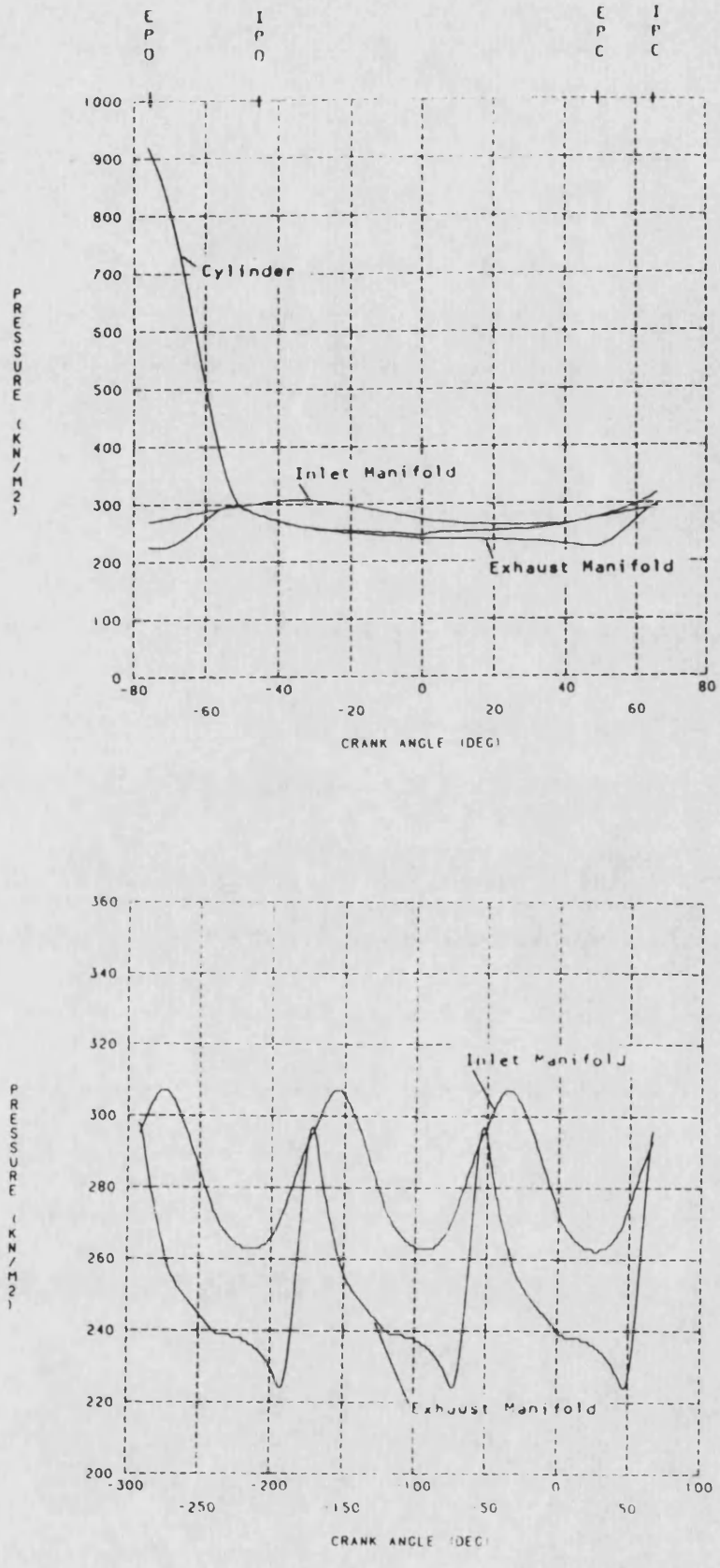

Fig. 9.13 Pressure Diagrams for Match 8 at Rated Regime

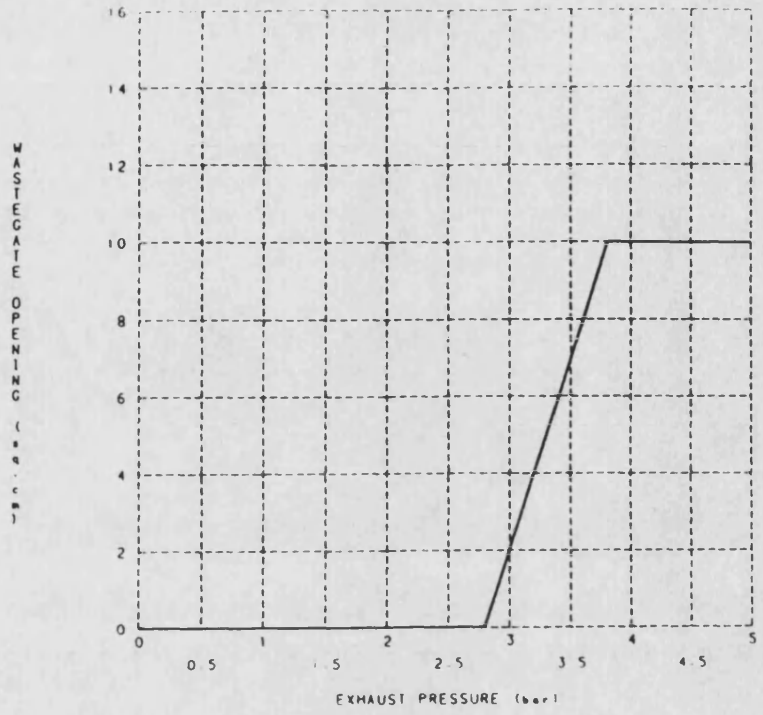

Fig. 9.14 Waste Gate Characteristics

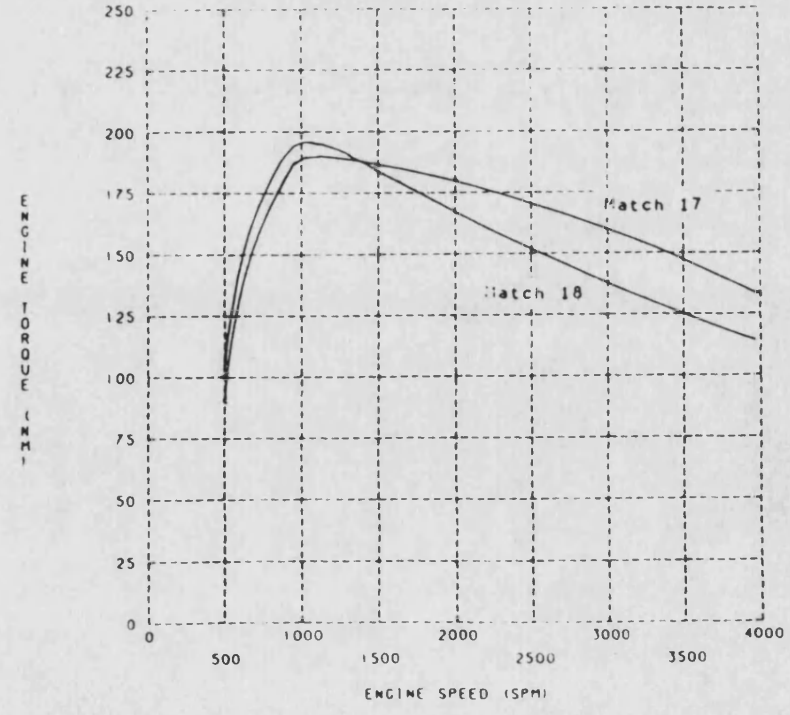

Fig. 9.15 Engine Torque Curves For Matches 17 and 18

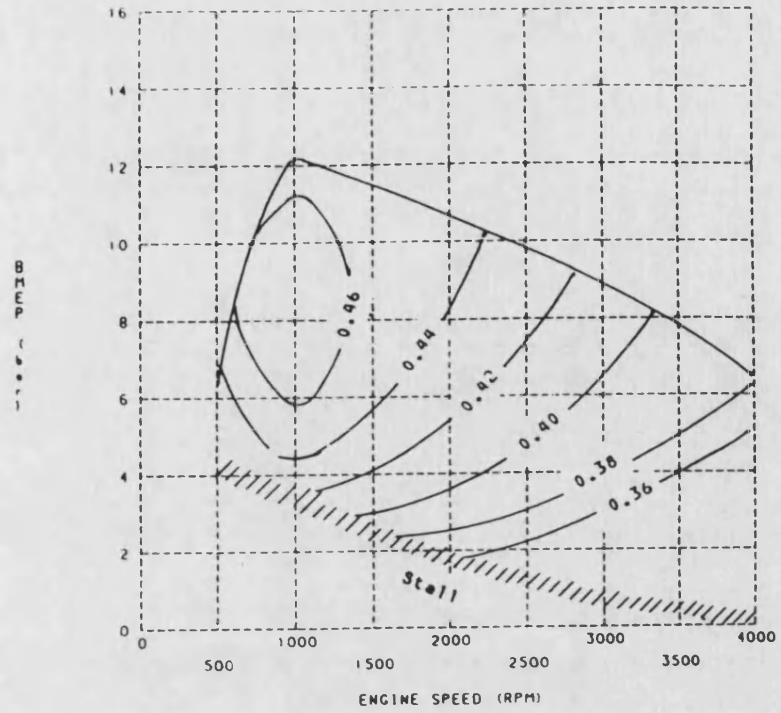

Fig. 9.16 Engine Efficiency Contours for Match 18

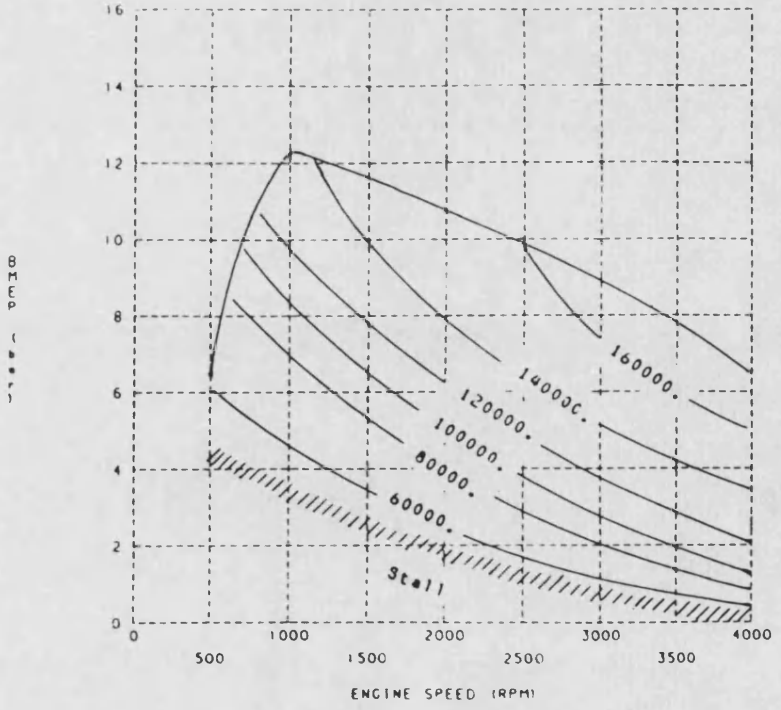

Fig. 9.17 Turbocharger Speed Contours for Match 18

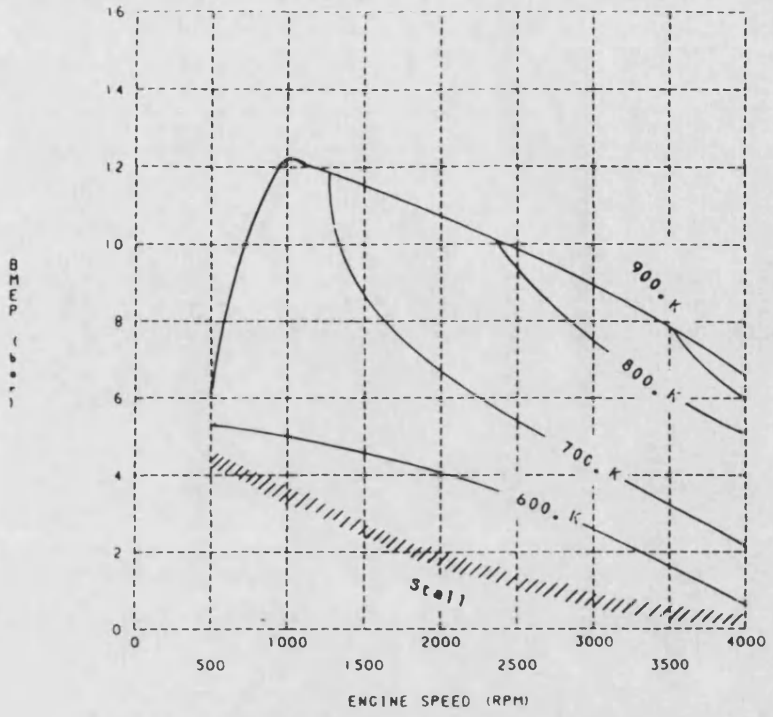

Fig. 9.18 Exhaust Temperature Contours for Match 18

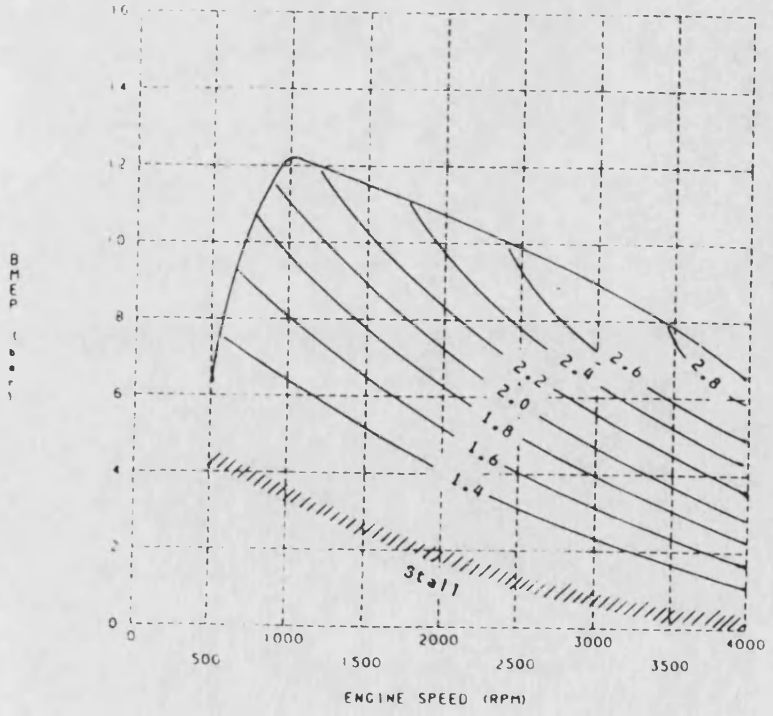

Fig. 9.19 Boost Pressure Contours for Match 18

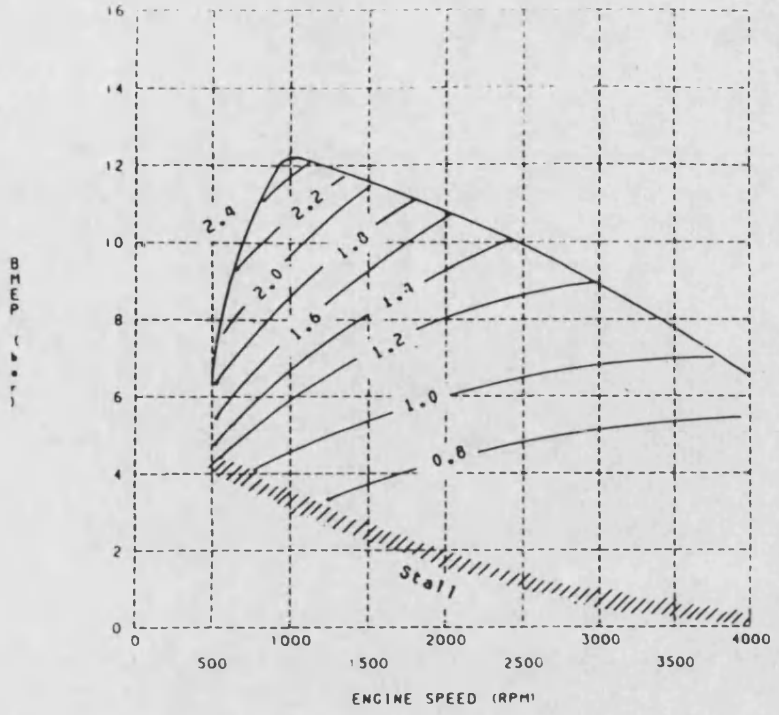

Fig. 9.20 Delivery Ratio Contours for Match 18

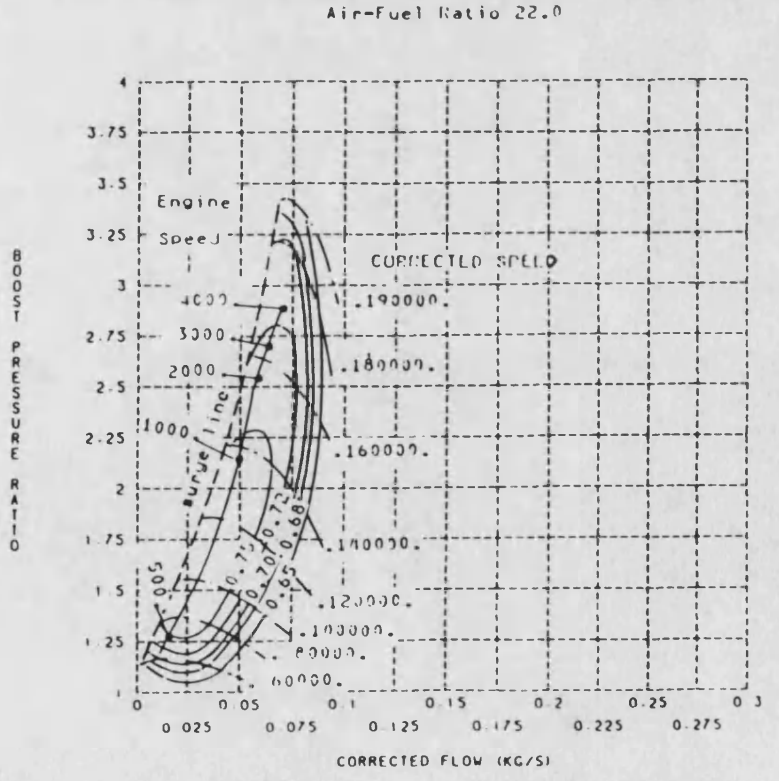

Fig. 9.21 Compressor Matching for Match 18

Air-Fuel Ratio 26.4

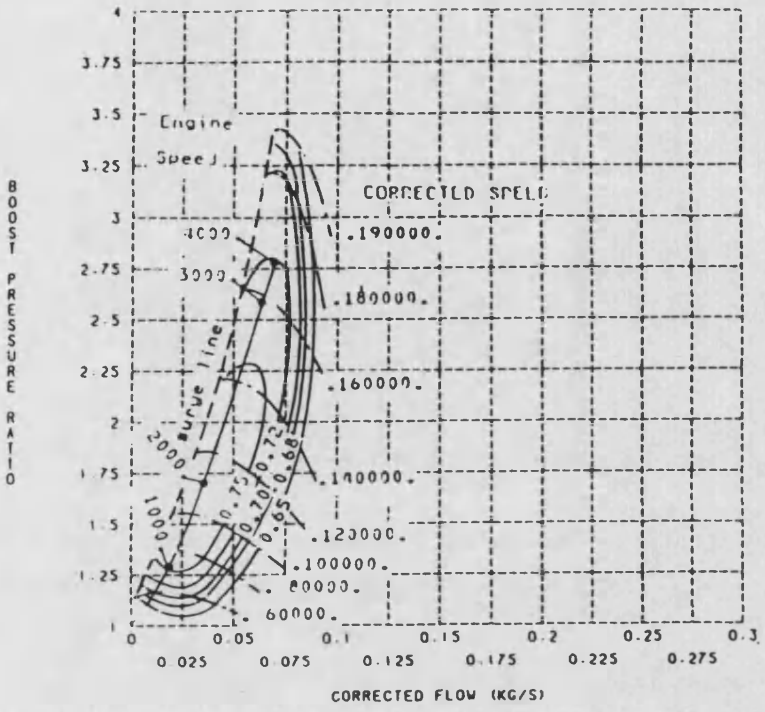

Air-Fuel Ratio 33.0

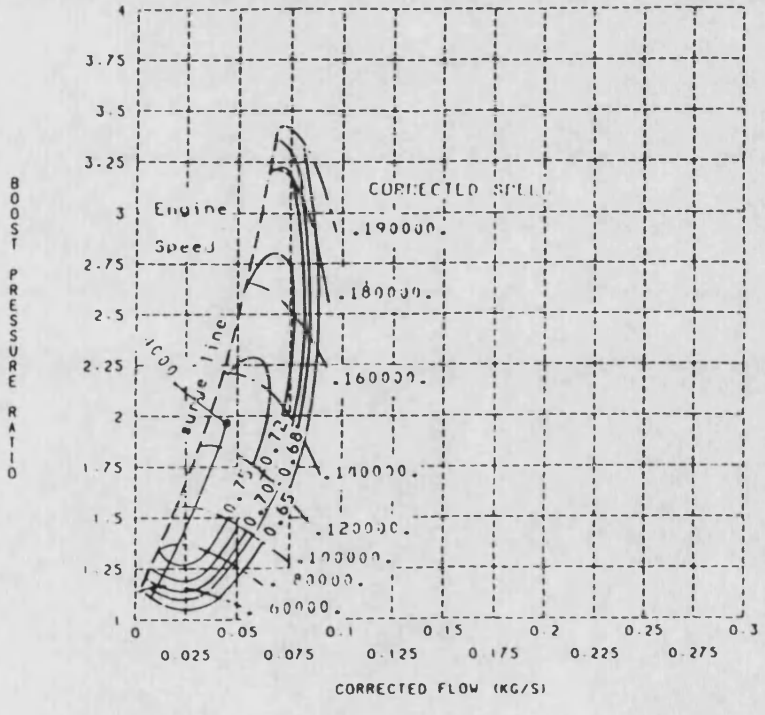

Fig. 9.21 (cont.)

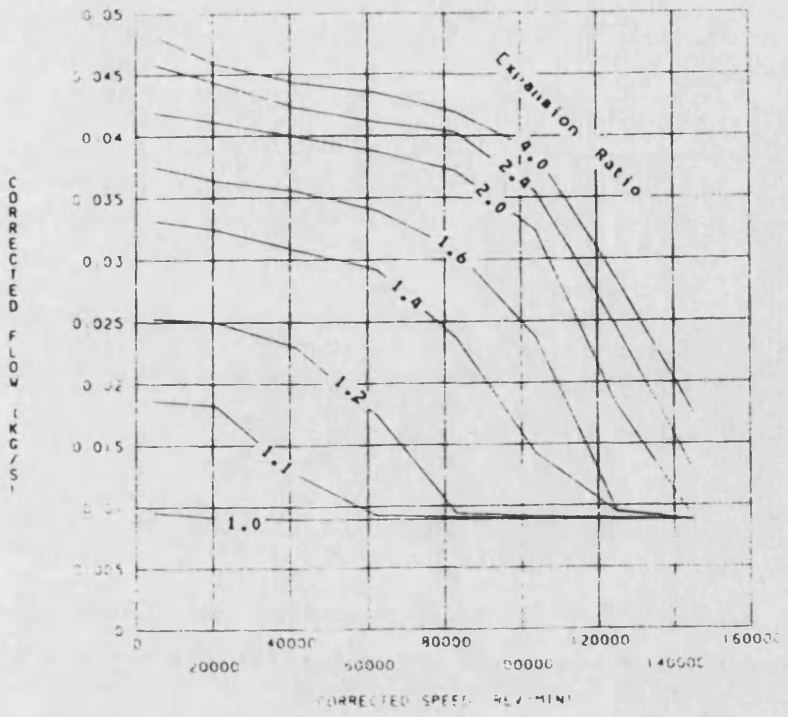

Fig. 9.22 Turbine Flow Rate for Match 18

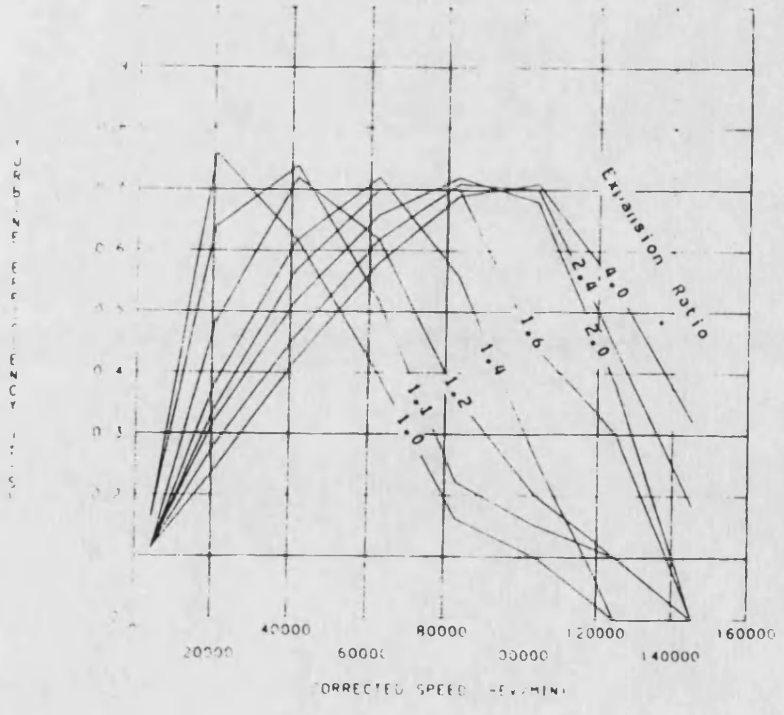

Fig. 9.23 Turbine Efficiency for Match 18

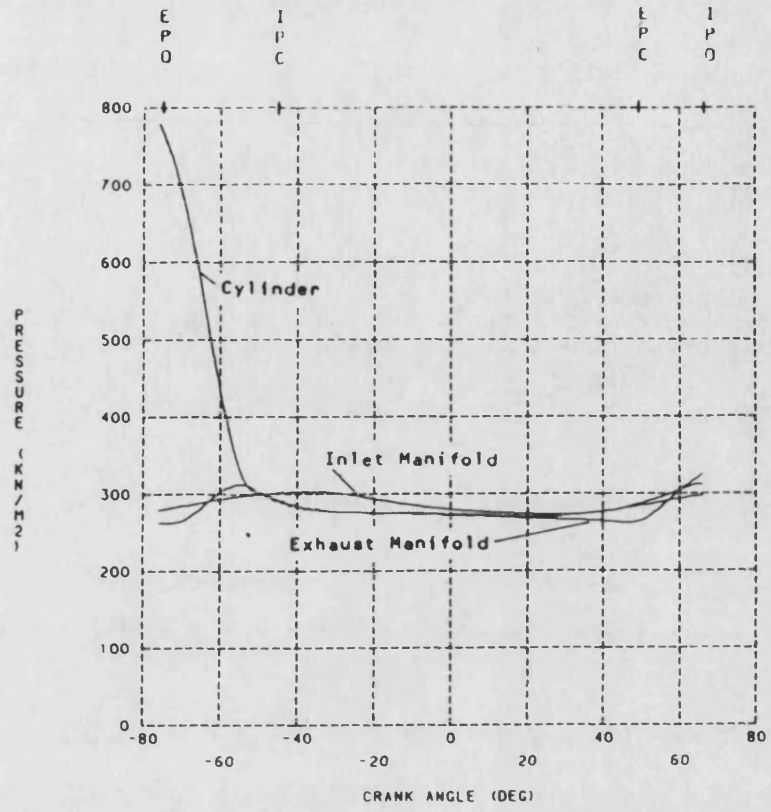

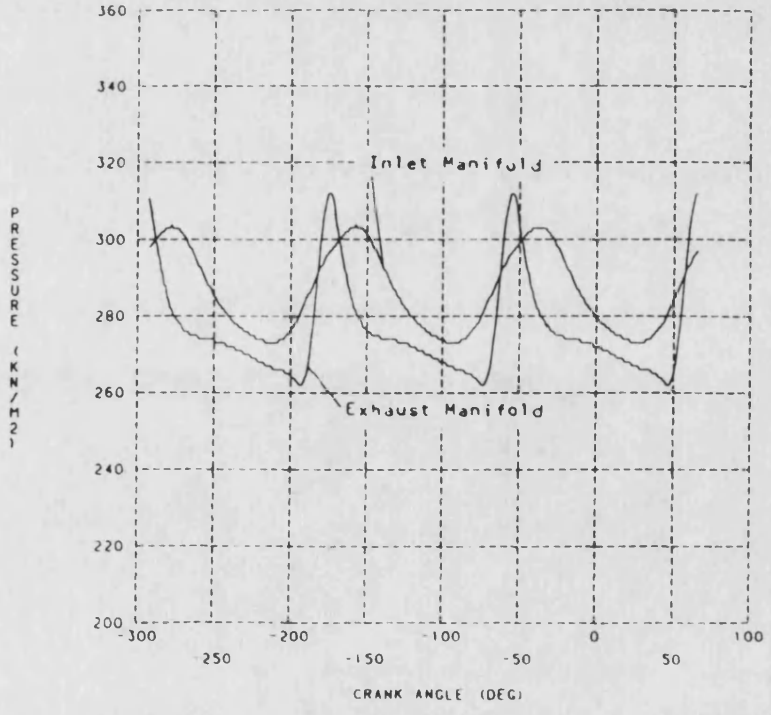

Fig. 9.24 Pressure Diagrams for Match 18 at Rated Regime

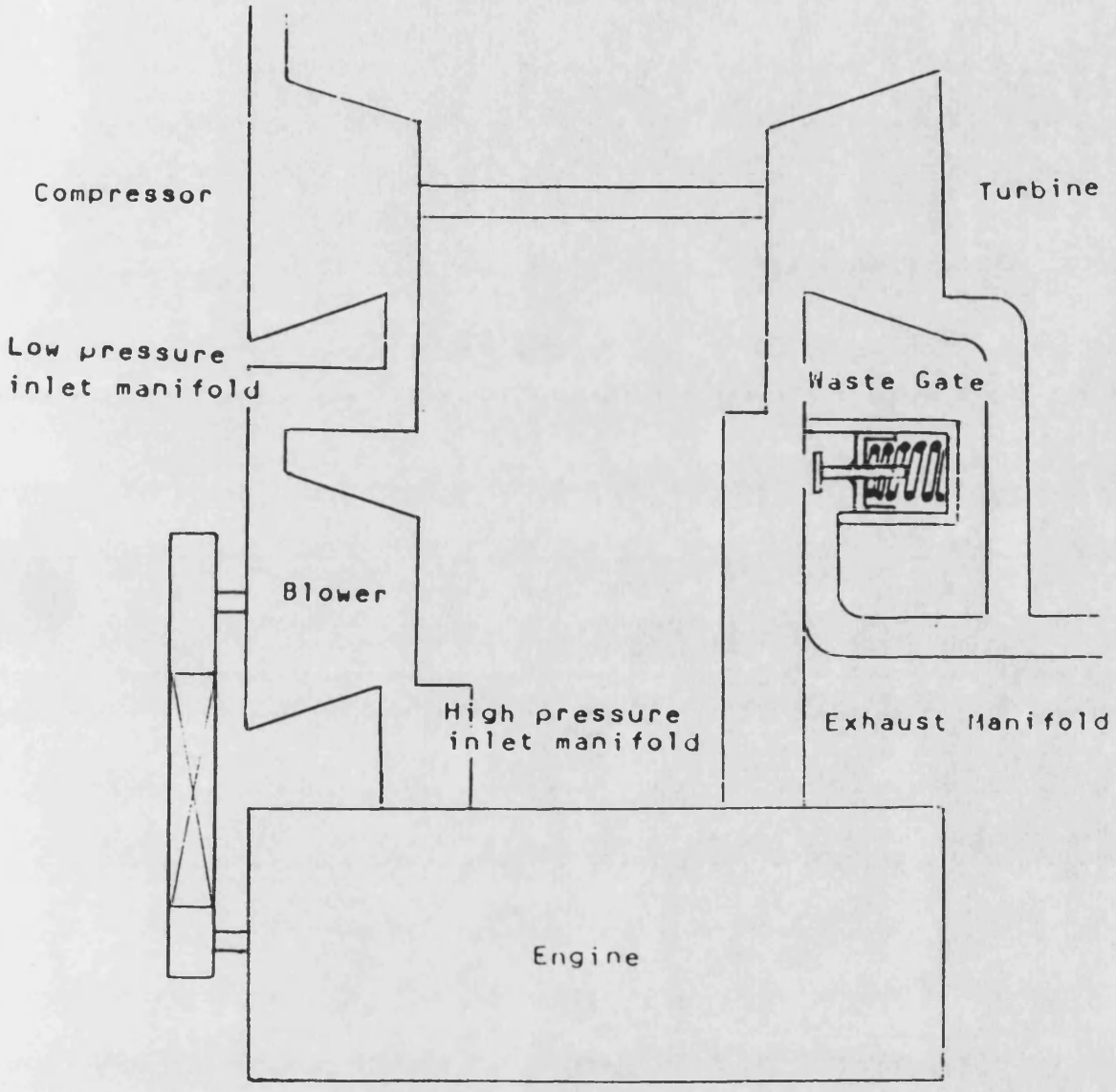

Fig. 9.25 Layout of Turbocharged Engine with Blower

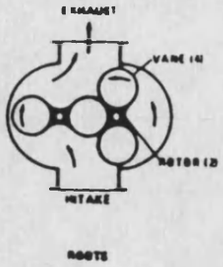

ROOTS

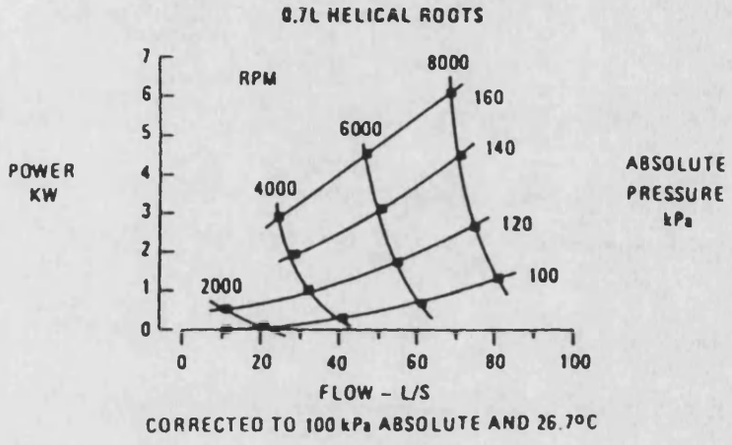

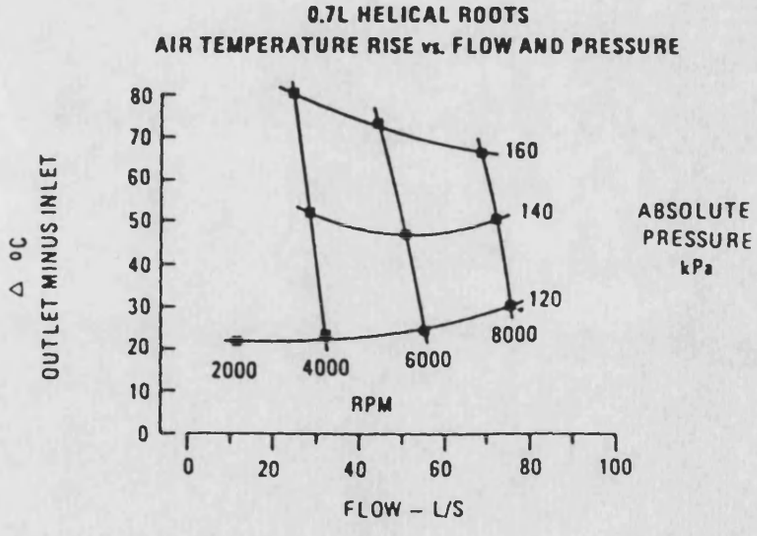

Fig. 9.26 Performance Maps of 0.7 L Helical Roots Blower

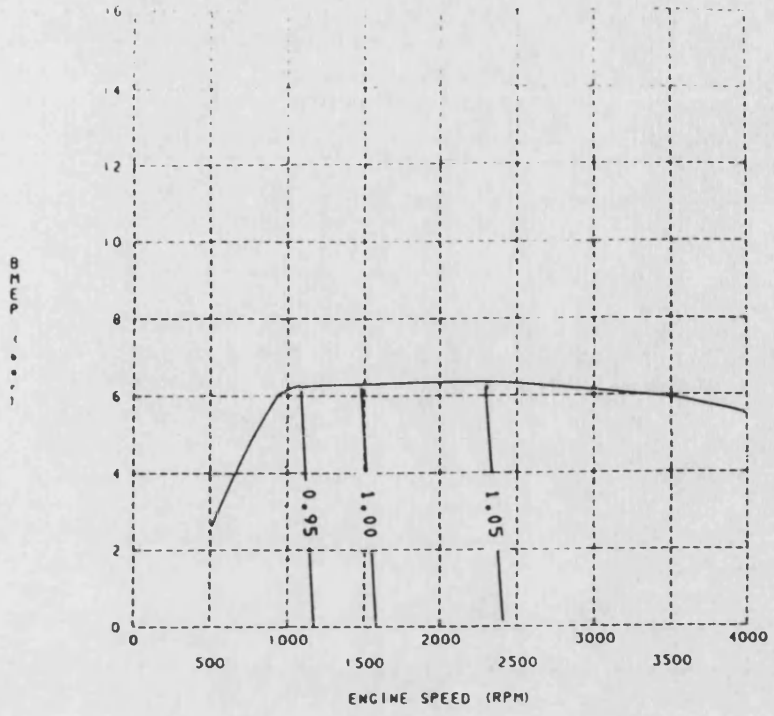

Fig. 9.27 Delivery Ratio Contours for Match 1

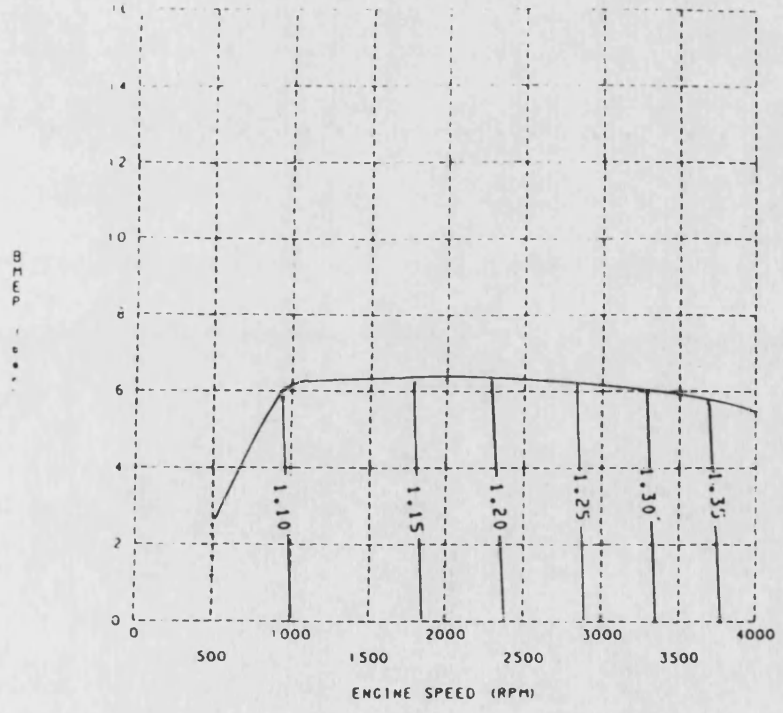

Fig. 9.28 Inlet Manifold Pressure Contours for Match 1

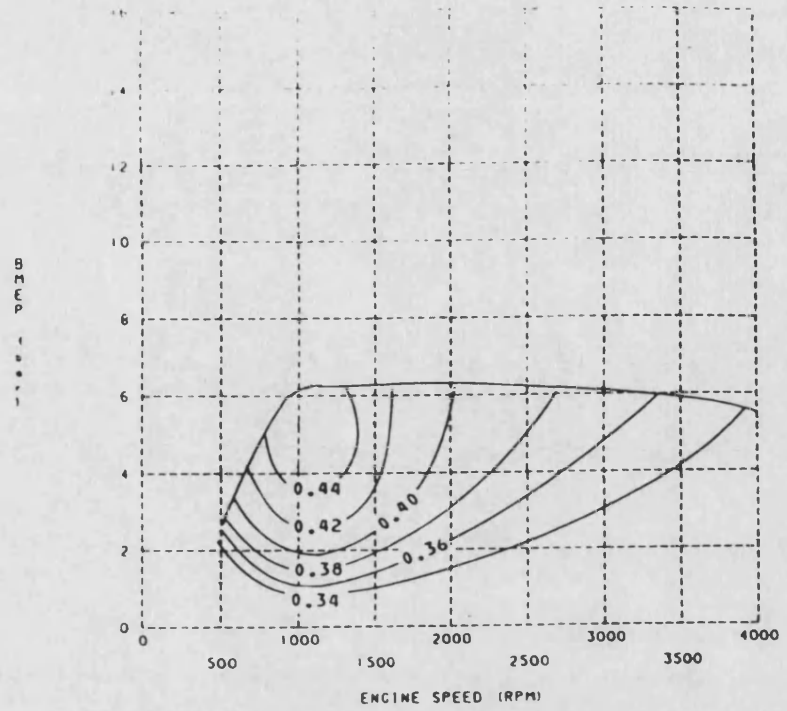

Fig. 9.29 Brake Thermal Efficiency Contours for Match 1

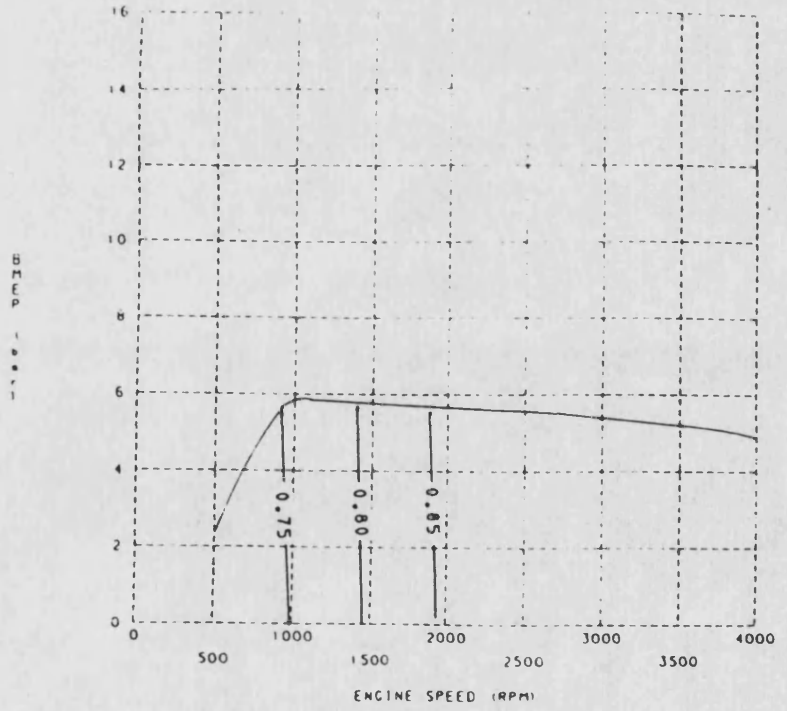

Fig. 9.30 Delivery Ratio Contours for Match 2

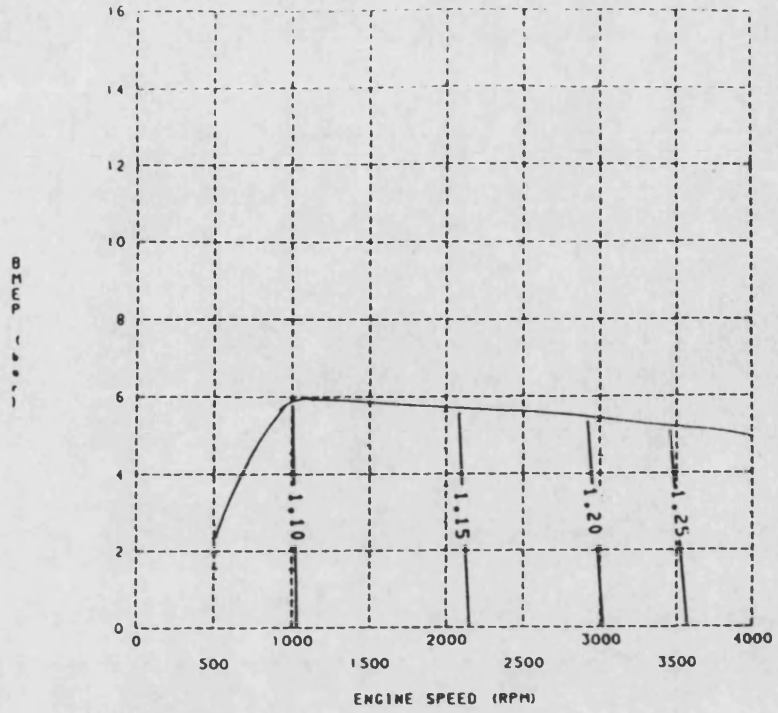

Fig. 9.31 Inlet Manifold Pressure Contours for Match 2

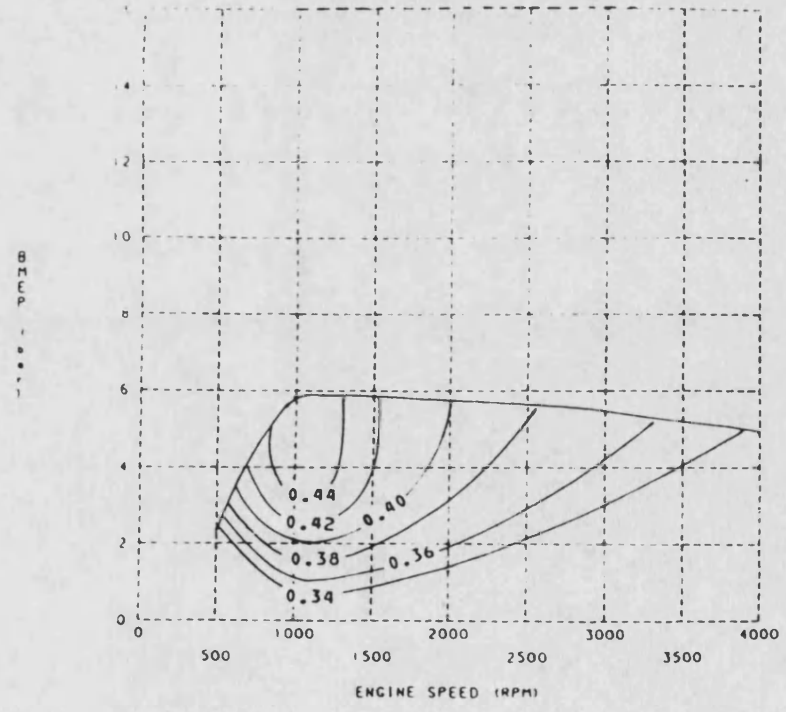

Fig. 9.32 Brake Thermal Efficiency Contours for Match 2

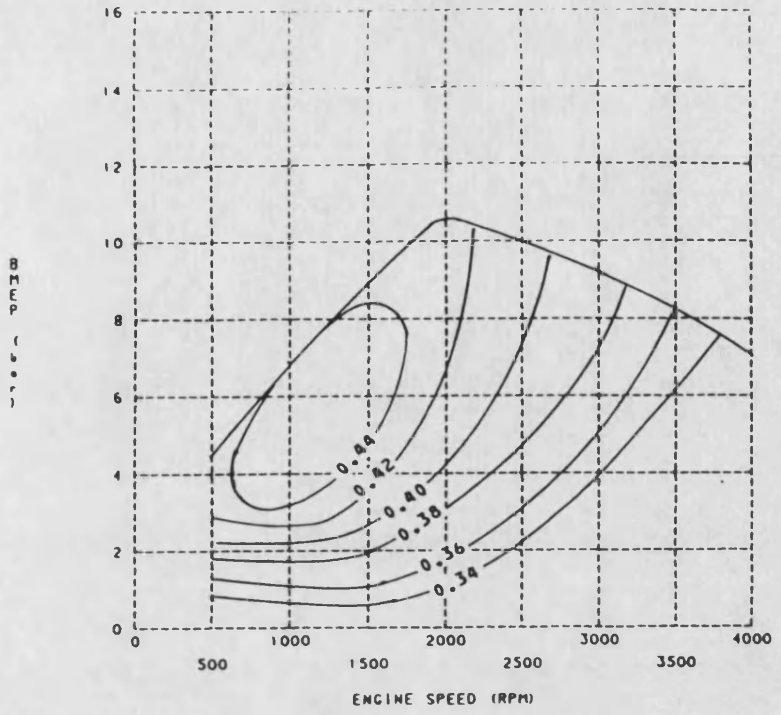

Fig. 9.33 Brake Thermal Efficiency Contours for Match 3

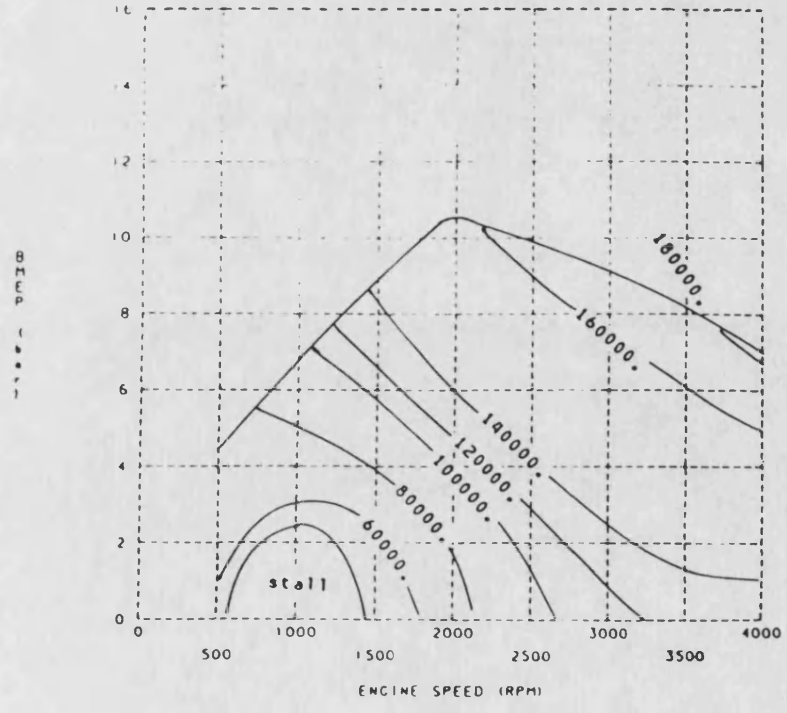

Fig. 9.34 Turbocharger Speed Contours for Match 3

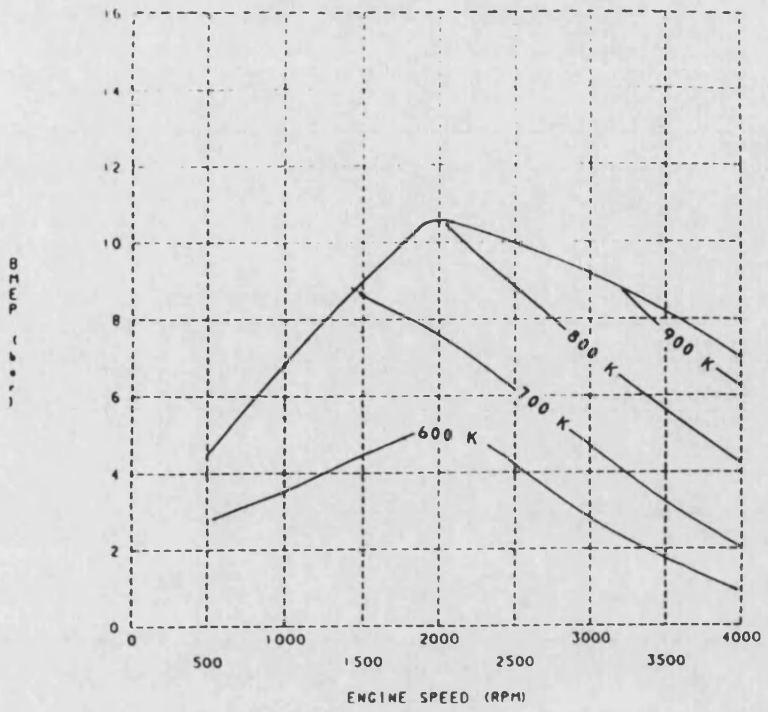

Fig. 9.35 Exhaust Temperature Contours for Match 3

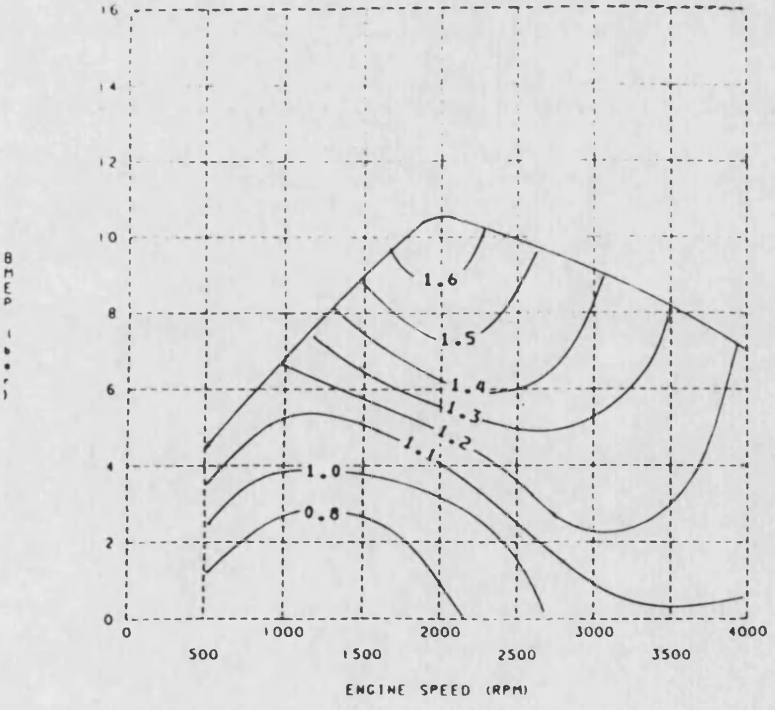

Fig. 9.36 Delivery Ratio Contours for Match 3

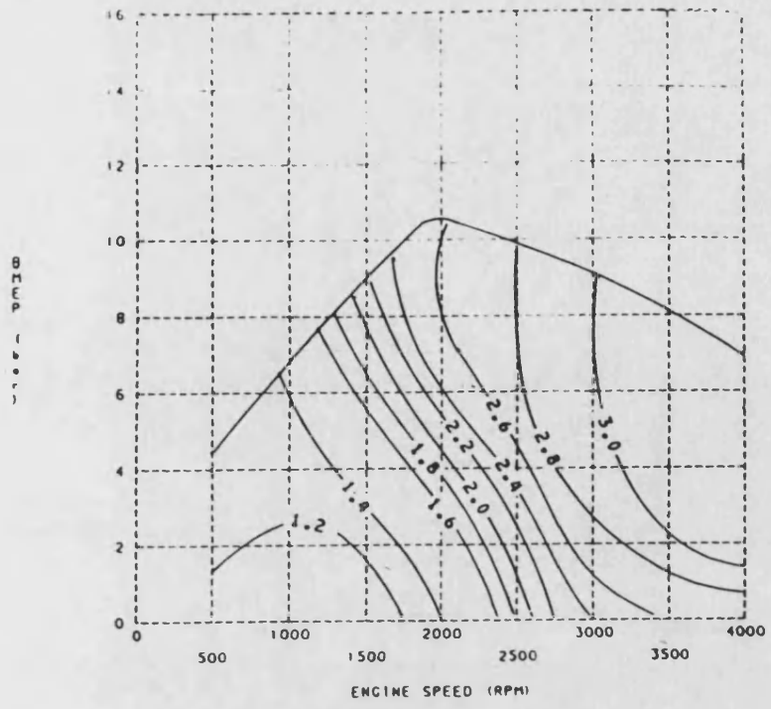

Fig. 9.37 Inlet Manifold Pressure Contours for Match 3

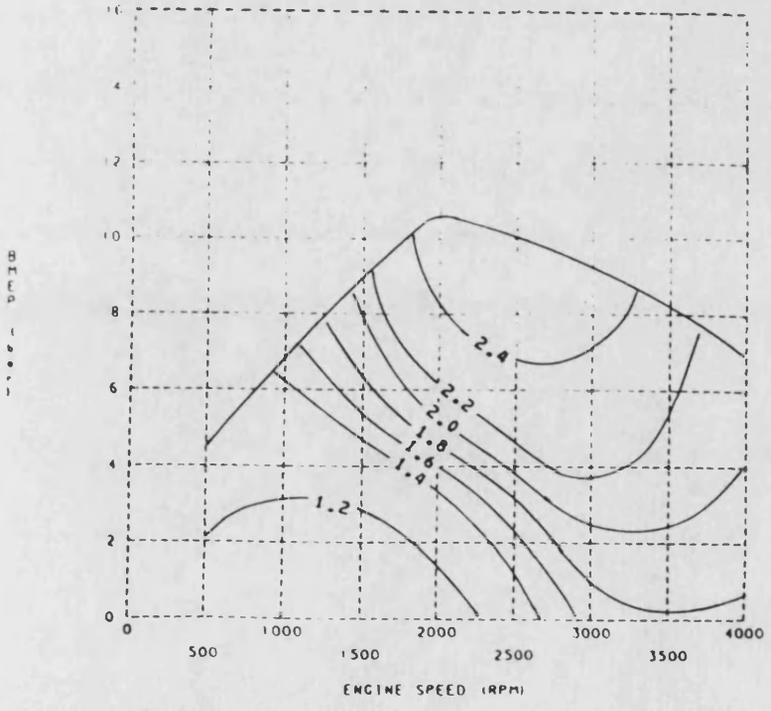

Fig. 9.38 Compressor Boost Ratio Contours for Match 3

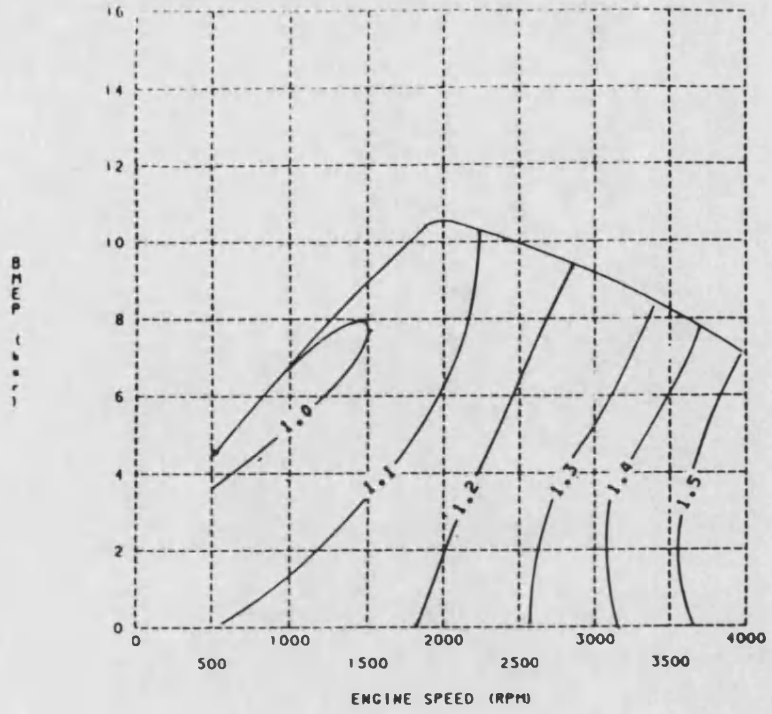

Fig. 9.39 Blower Boost Ratio Contours for Match 3

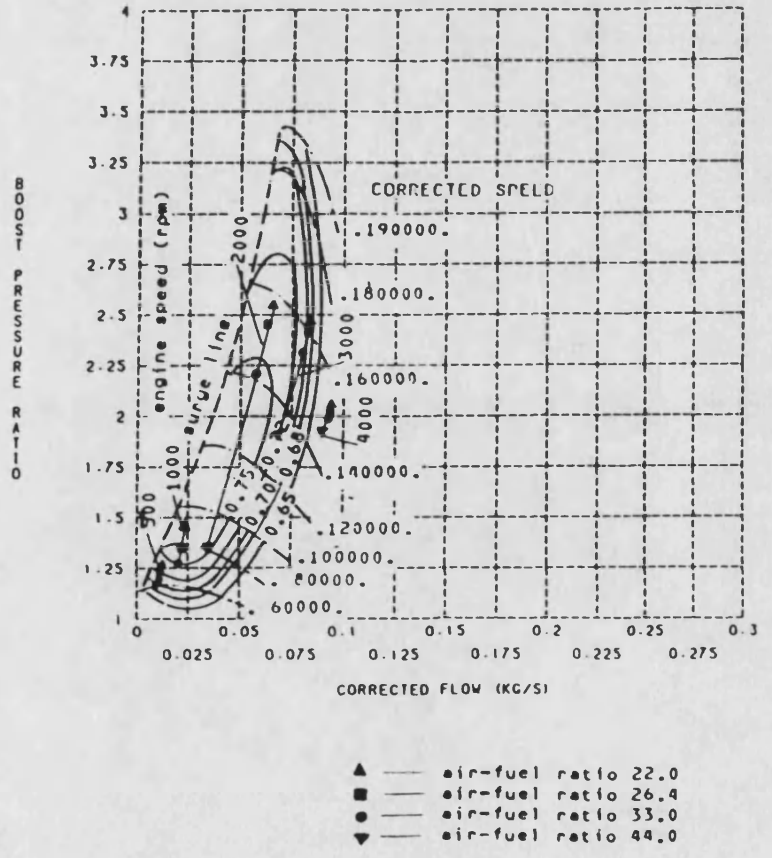

Fig. 9.40 Engine Operation Area Superimposed on Compressor Map for Match 3

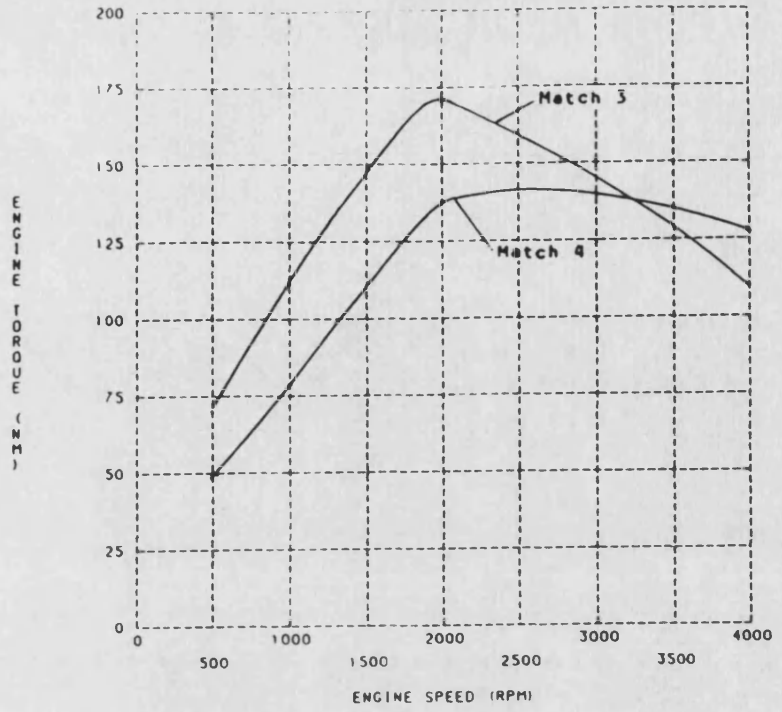

Fig. 9.41 Maximum Engine Torque Curves for Matches 3 and 4

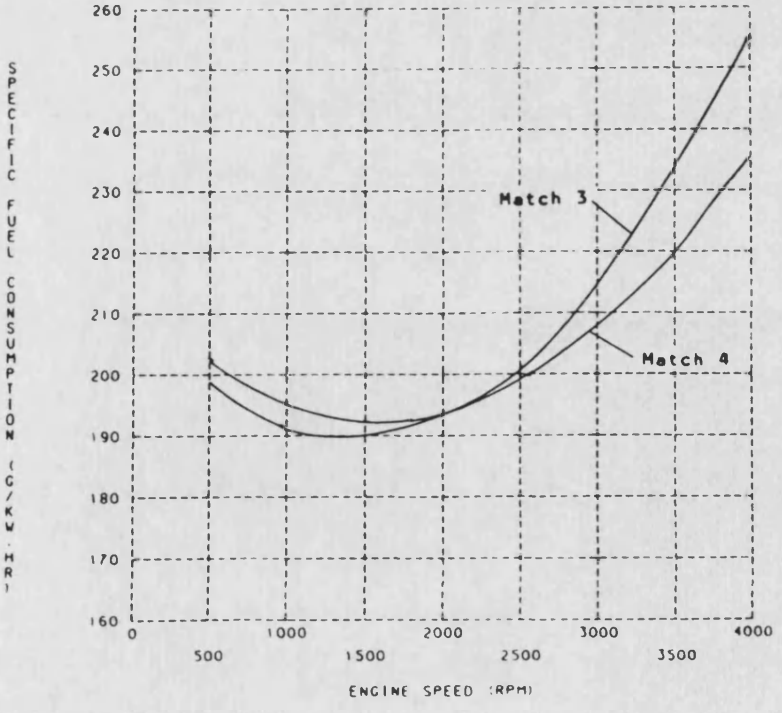

Fig. 9.42 Specific Fuel Consumptions at Full Load for Matches 3 and 4

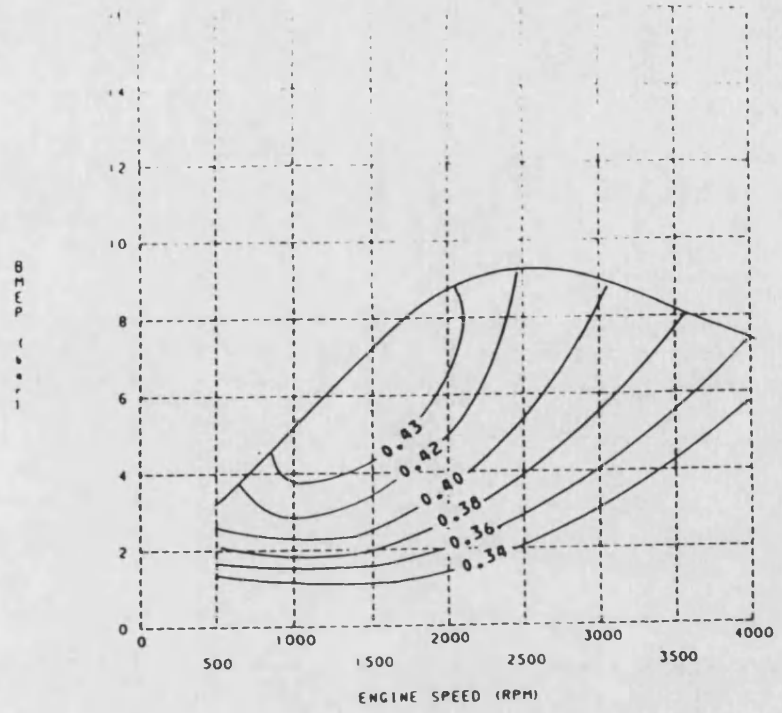

Fig. 9.43 Brake Thermal Efficiency Contours for Match 4

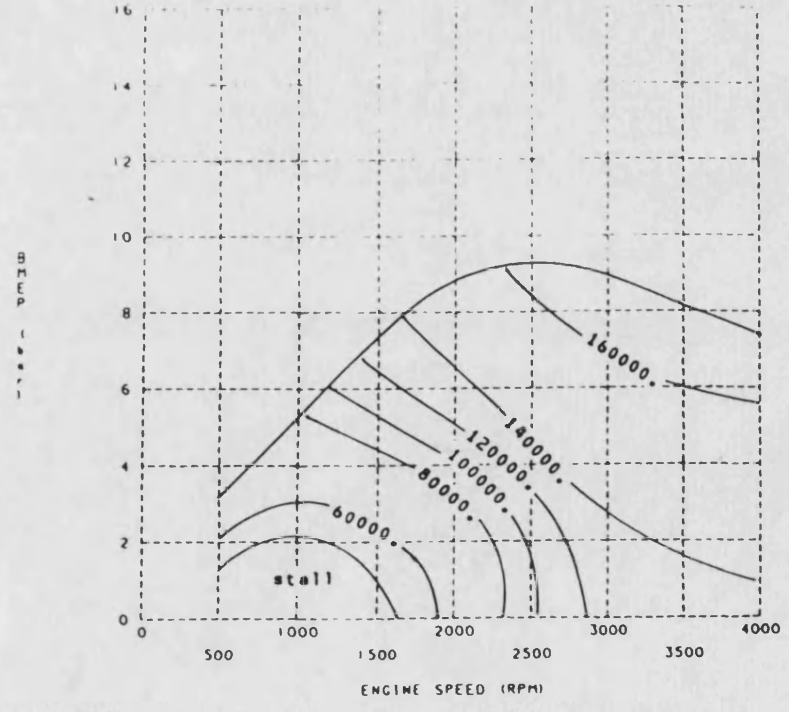

Fig. 9.44 Turbocharger Speed Contours for Match 4

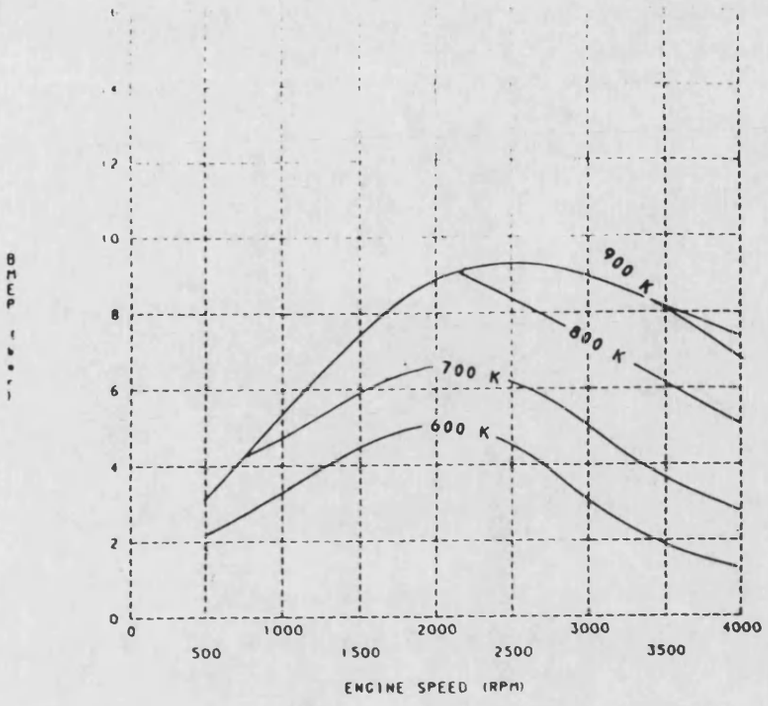

Fig. 9.45 Exhaust Temperature Contours for Match 4

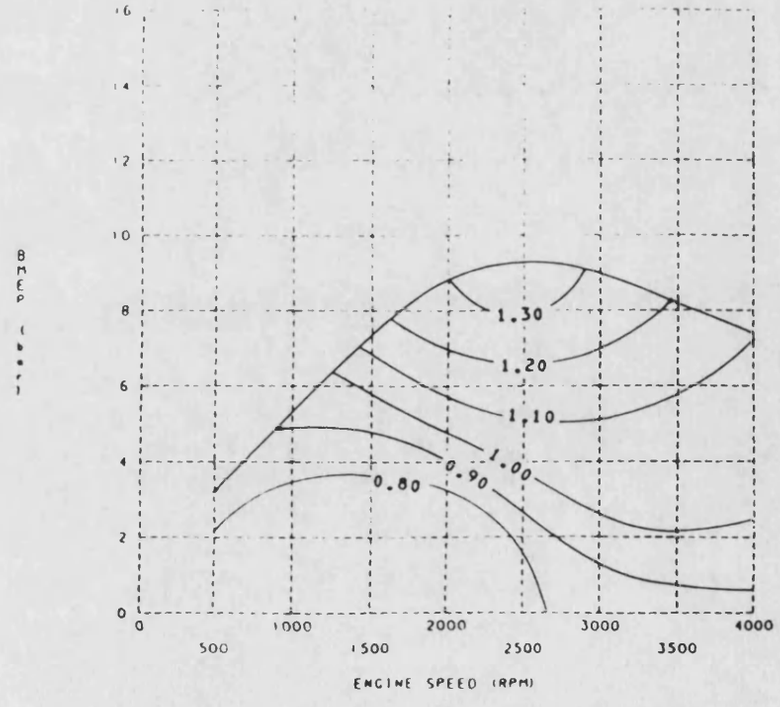

Fig. 9.46 Delivery Ratio Contours for Match 4

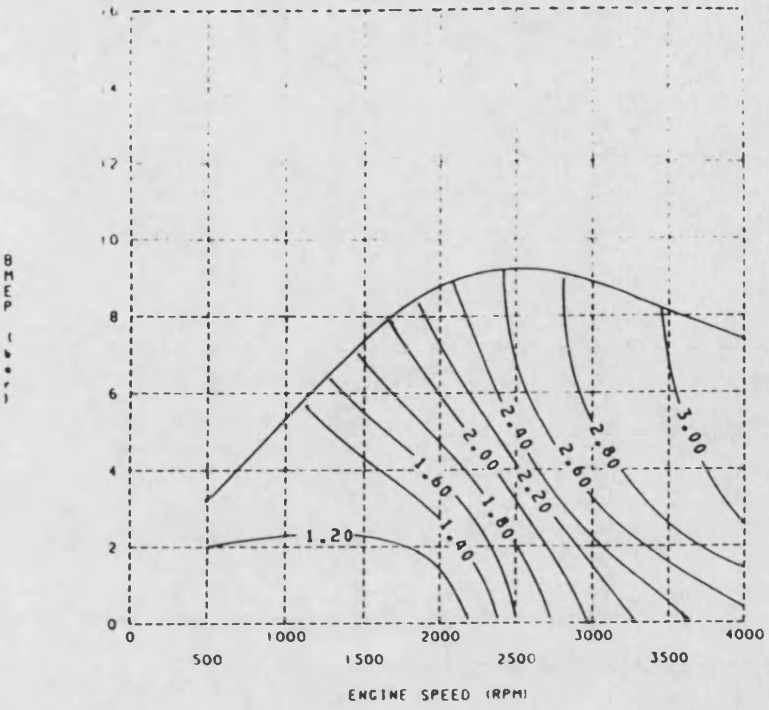

Fig. 9.47 Inlet Manifold Pressure Contours for Match 4

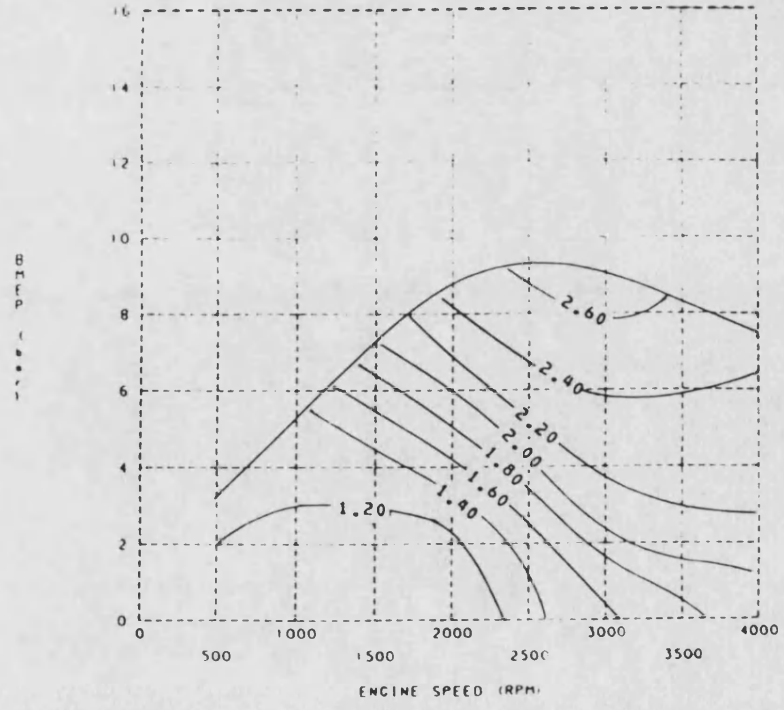

Fig. 9.48 Compressor Boost Ratio Contours for Match 4

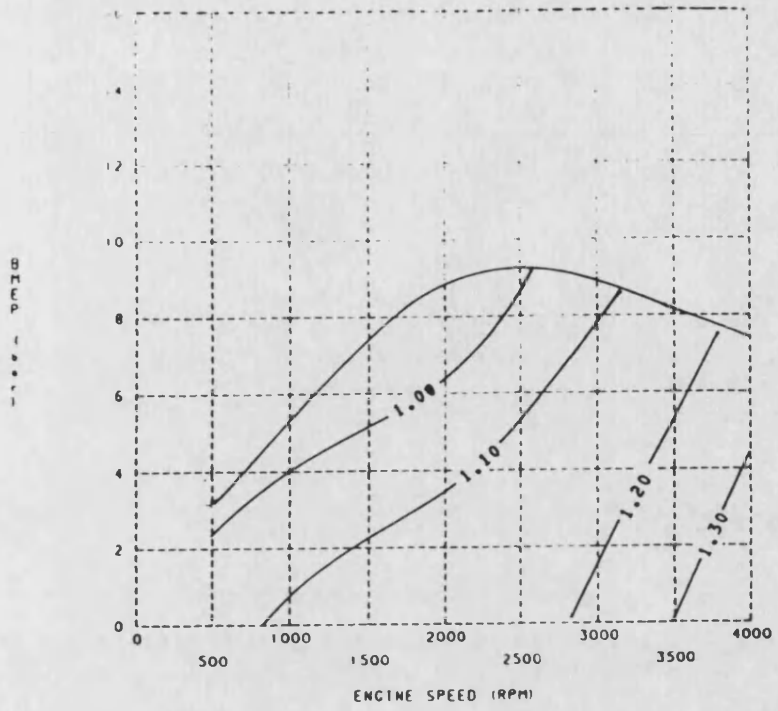

Fig. 9.49 Blower Boost Ratio Contours for Match 4

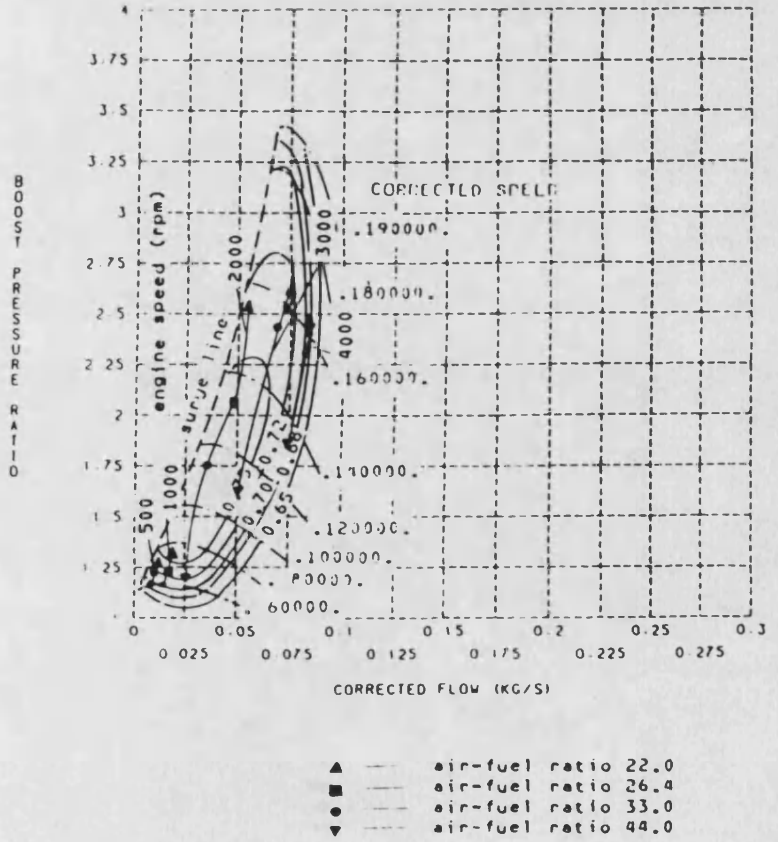

Fig. 9.50 Engine Operation Area Superimposed on Compressor Map for Match 4

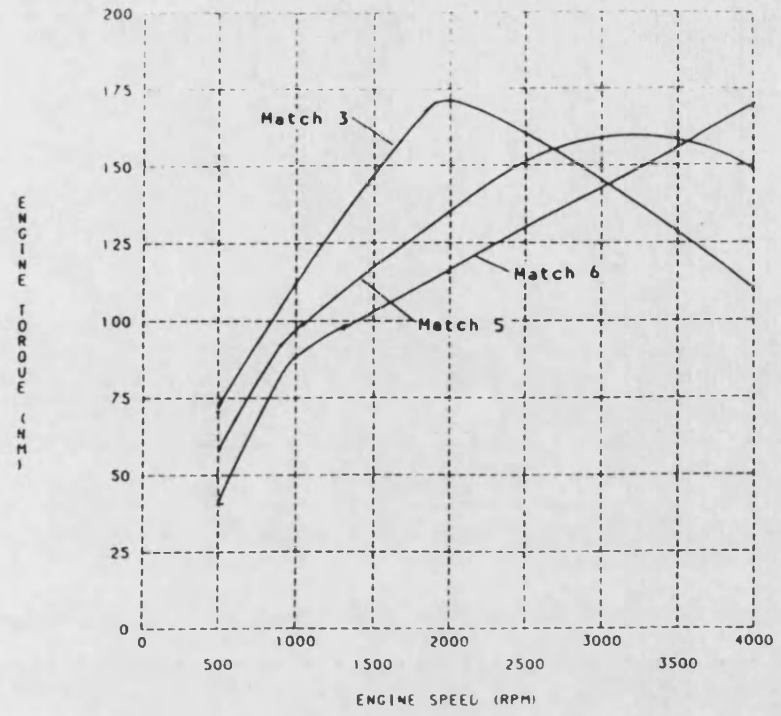

Fig. 9.51 Maximum Engine Torque Curves for Matches 3, 5 and 6

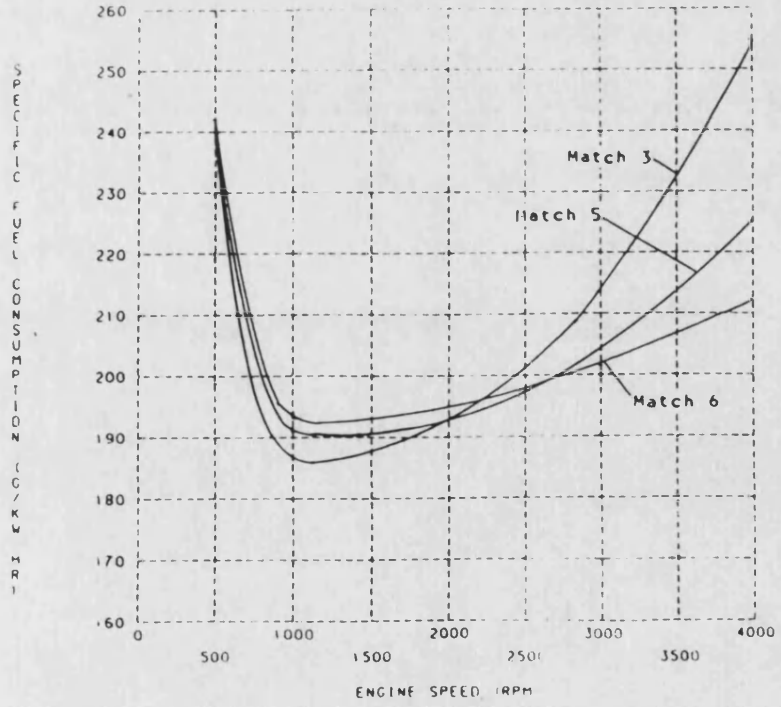

Fig. 9.52 Specific Fuel Consumptions at Full Load for Matches 3, 5 and 6

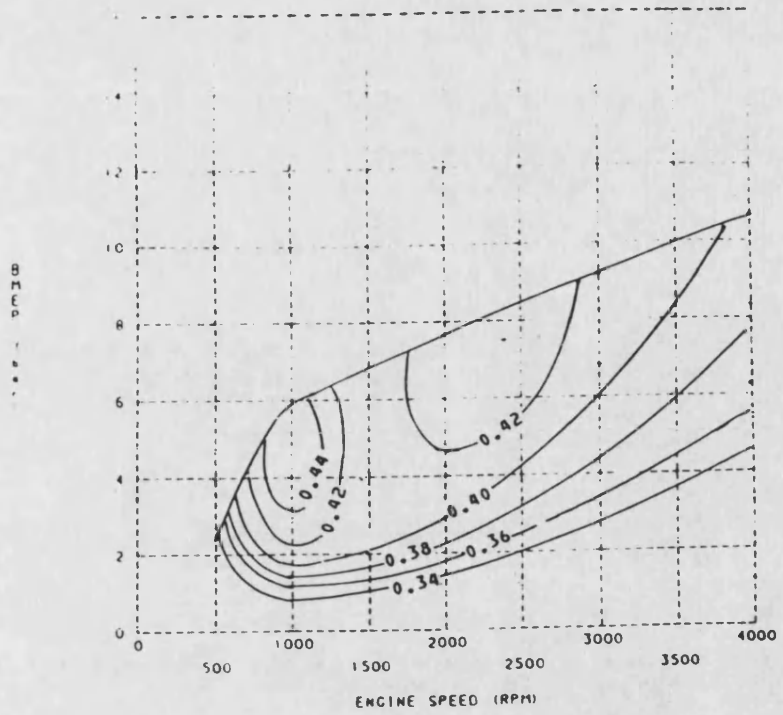

Fig. 9.53 Brake Thermal Efficiency Contours for Match 6

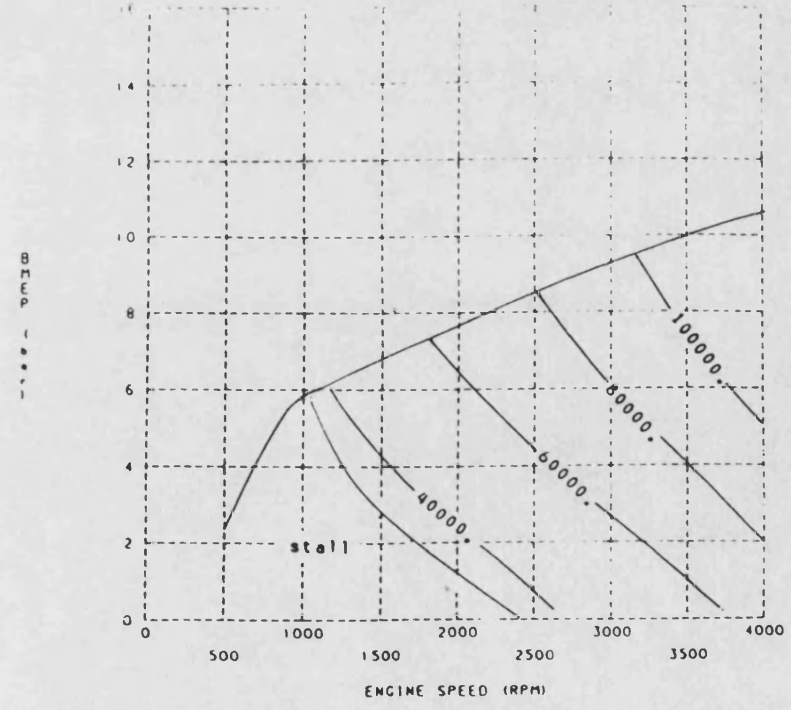

Fig. 9.54 Turbocharger Speed Contours for Match 6

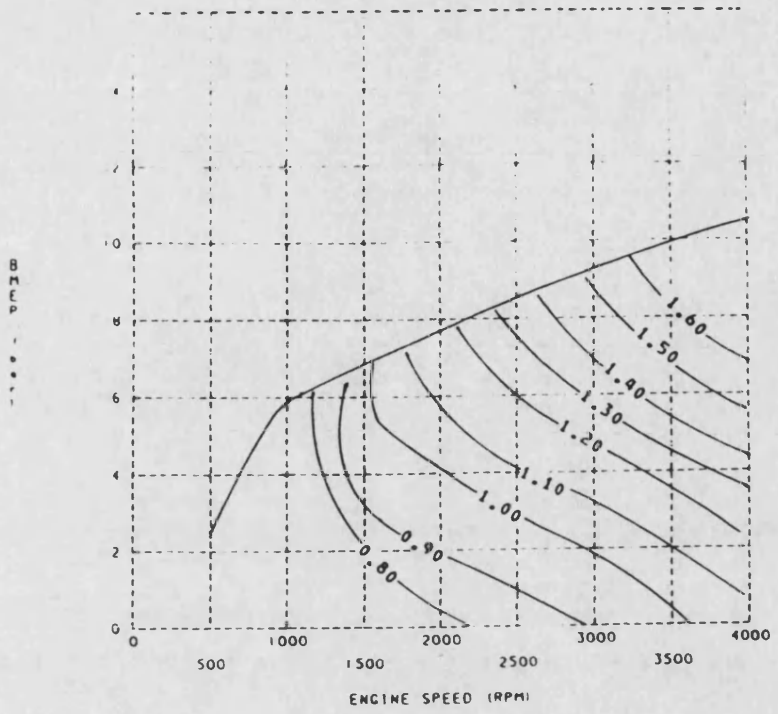

Fig. 9.55 Delivery Ratio Contours for Match 6

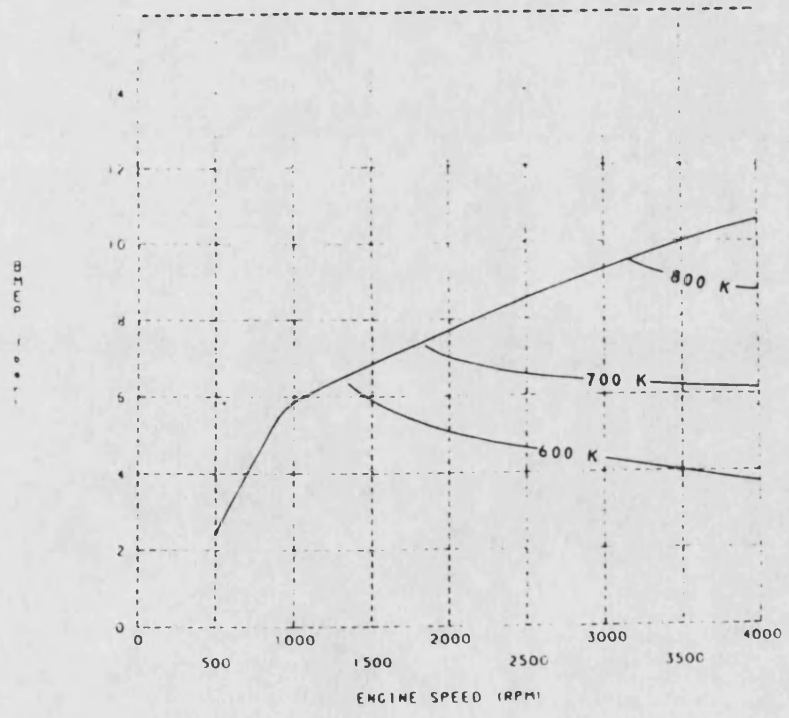

Fig. 9.56 Exhaust Temperature Contours for Match 6

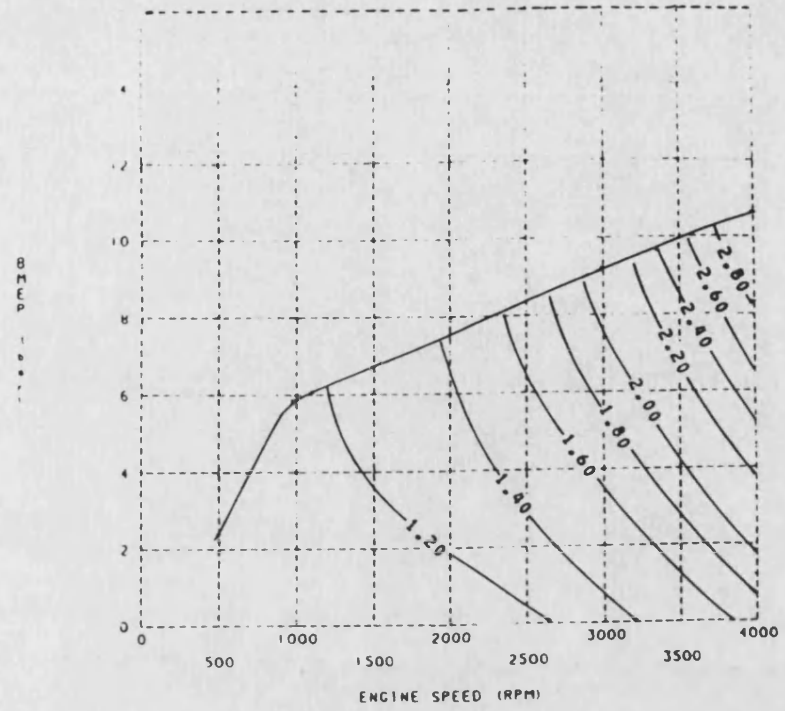

Fig. 9.57 Inlet Manifold Pressure Contours for Match 6

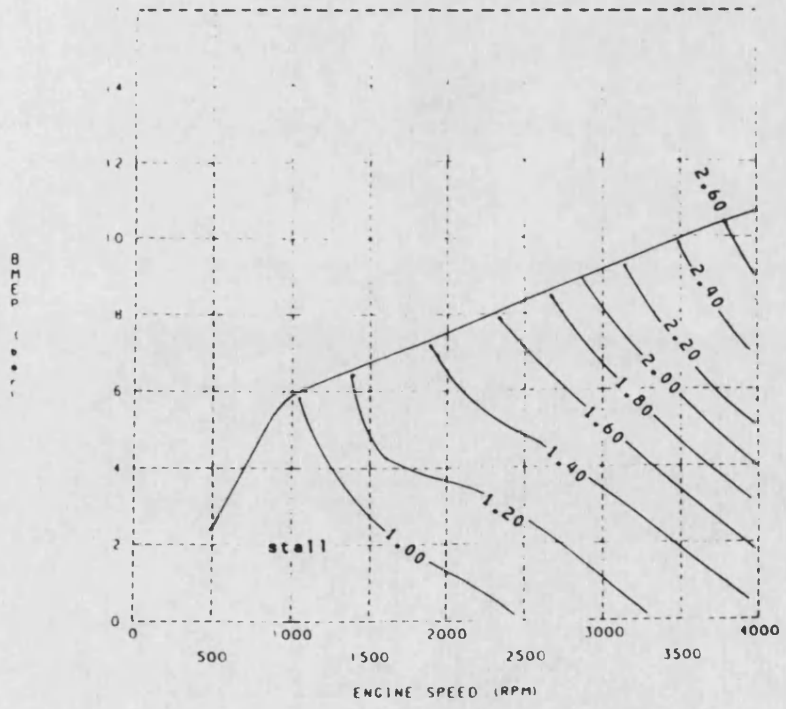

Fig. 9.58 Compressor Boost Ratio Contours for Match 6

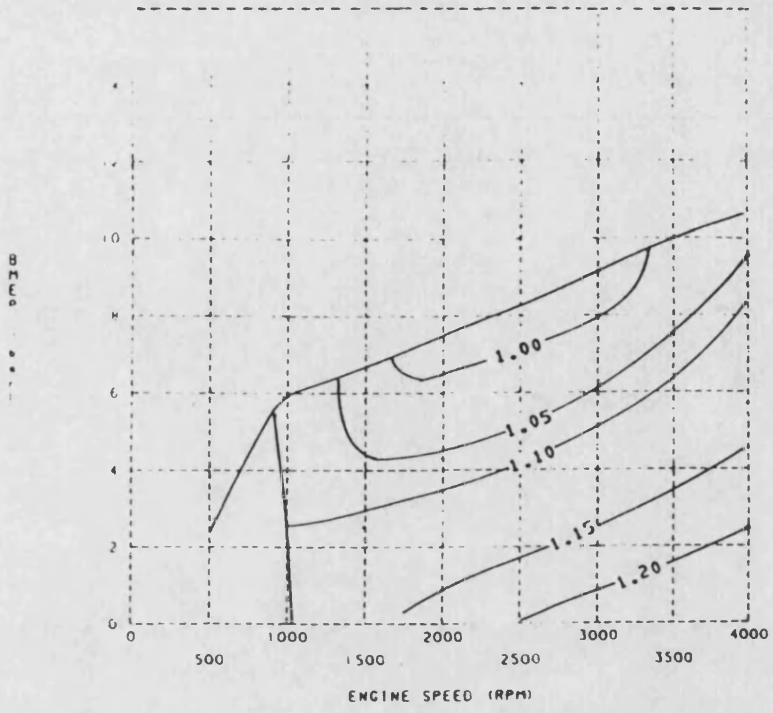

Fig. 9.59 Blower Boost Ratio Contours for Match 6

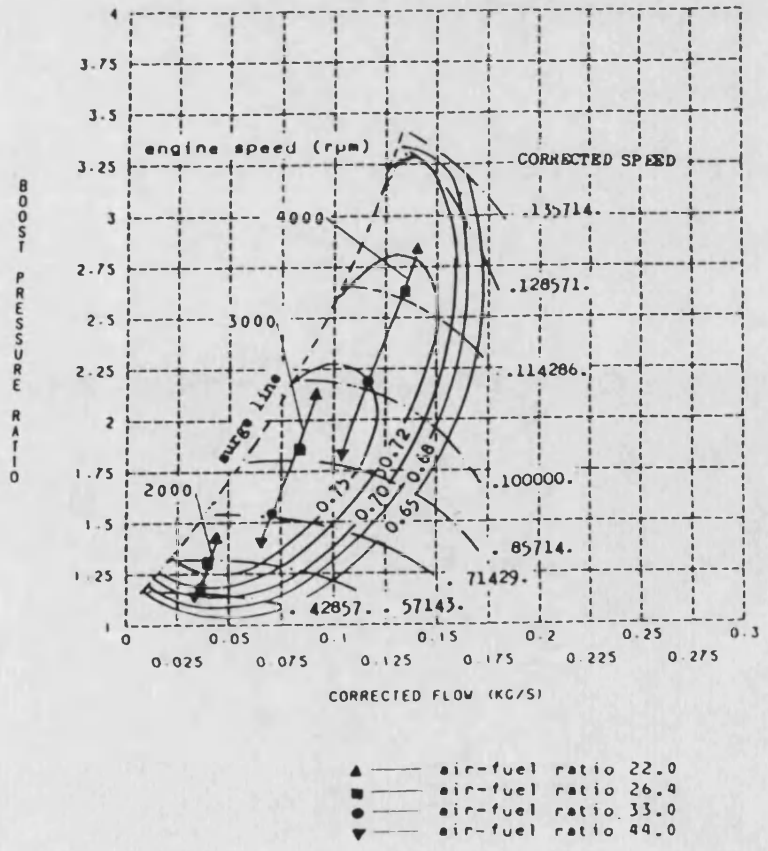

Fig. 9.60 Engine Operation Area Superimposed on Compressor Map for Match 6

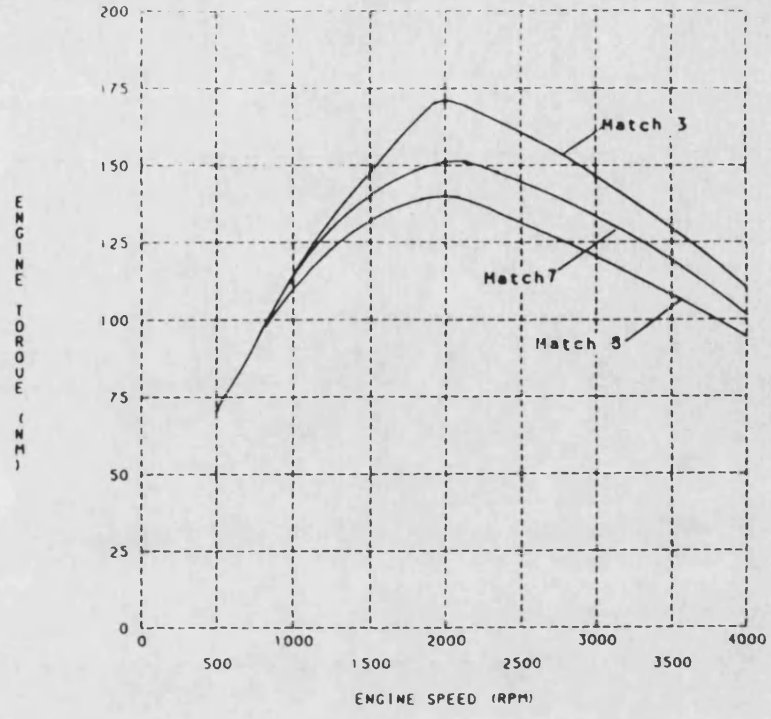

Fig. 9.61 Maximum Engine Torque Curves for Matches 3, 7 and 8

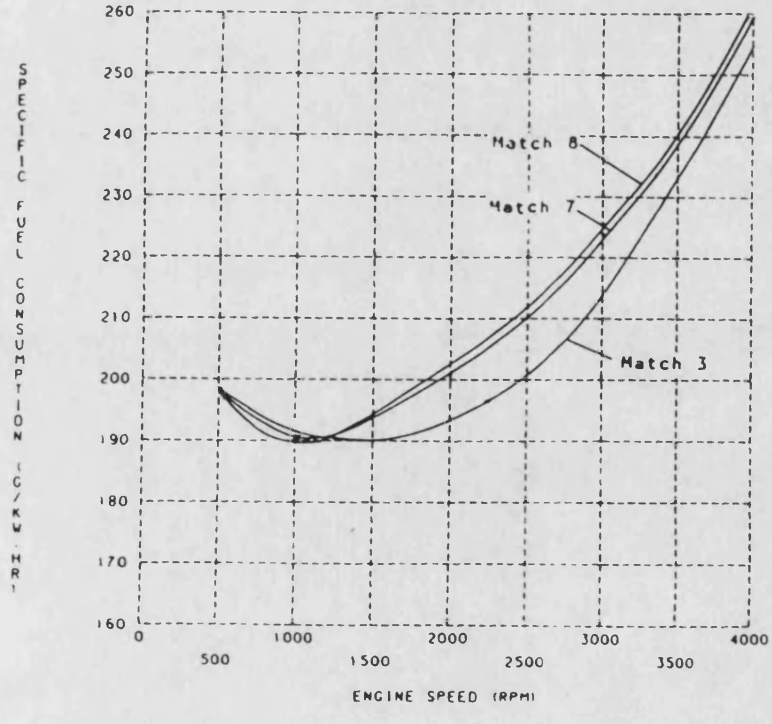

Fig. 9.62 Specific Fuel Consumptions at Full Load for Matches 3, 7 and 8

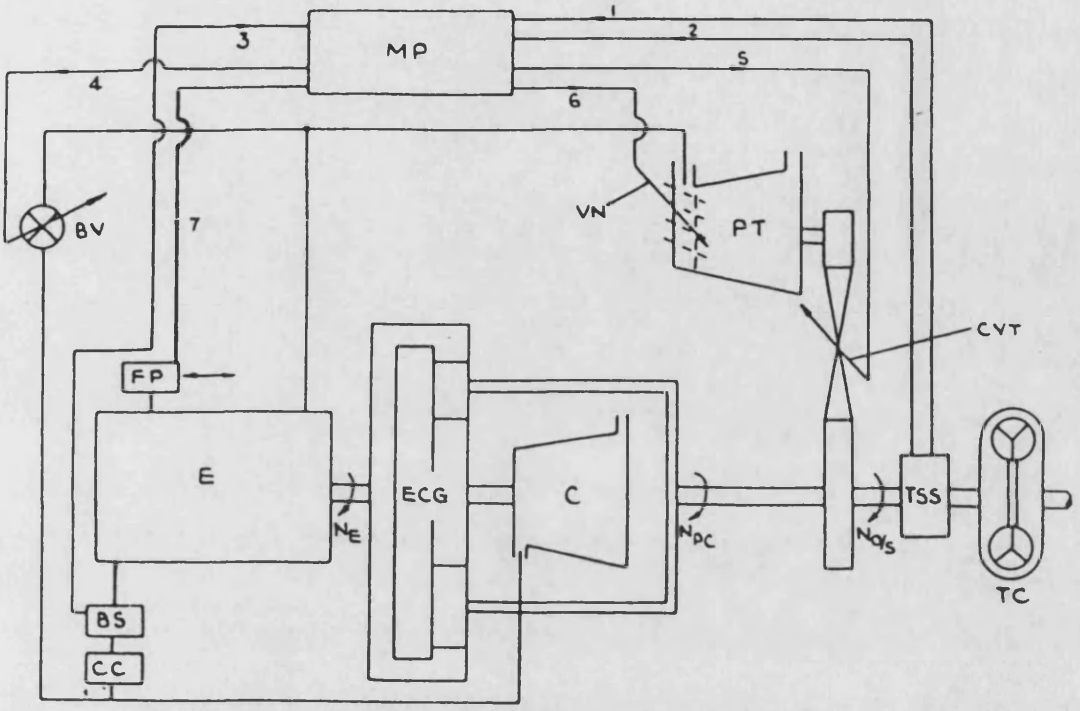

BV : bypass valve
BS : boost sensor
C : compressor
CC : charge cooler
E : engine
ECG: epicyclic gear train
FP : fuel pump
CVT: continuously variable transmission
TC : torque turbine
VN : variable turbine nozzles
TSS: output torque&speed sensor
Ne : engine speed
Nos: output shaft speed
Nps: planet carrier speed

INPUT SIGNALS:
1. torque transducer
2. speed transducer
3. pressure transducer

OUTPUT SIGNALS:
4. bypass valve control
5. CVT control
6. nozzle control
7. fuel pump control

Fig. 9.63 Layout of DCE

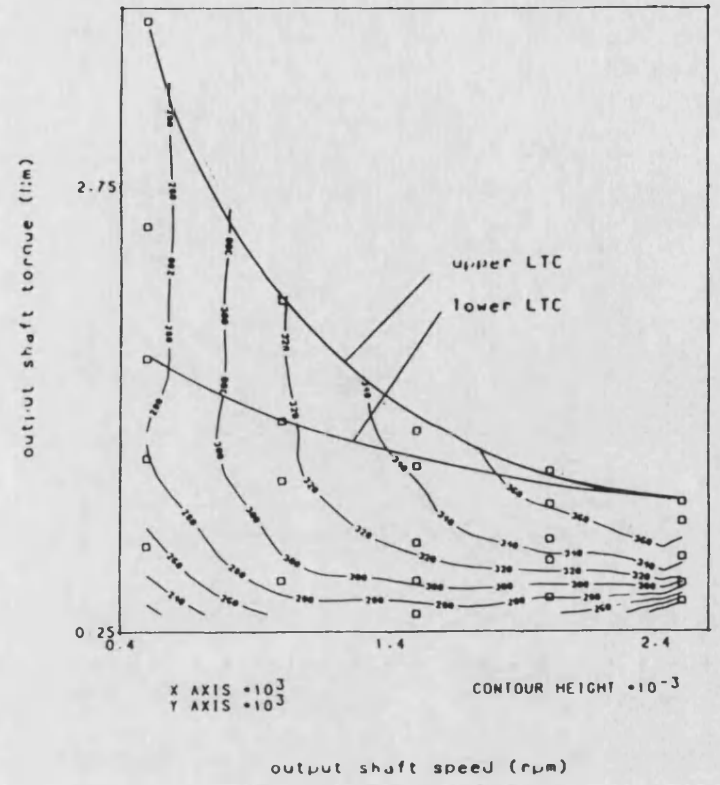

Fig. 9.64 Output Shaft Brake Thermal Efficiency of DCE without Bypass Valve

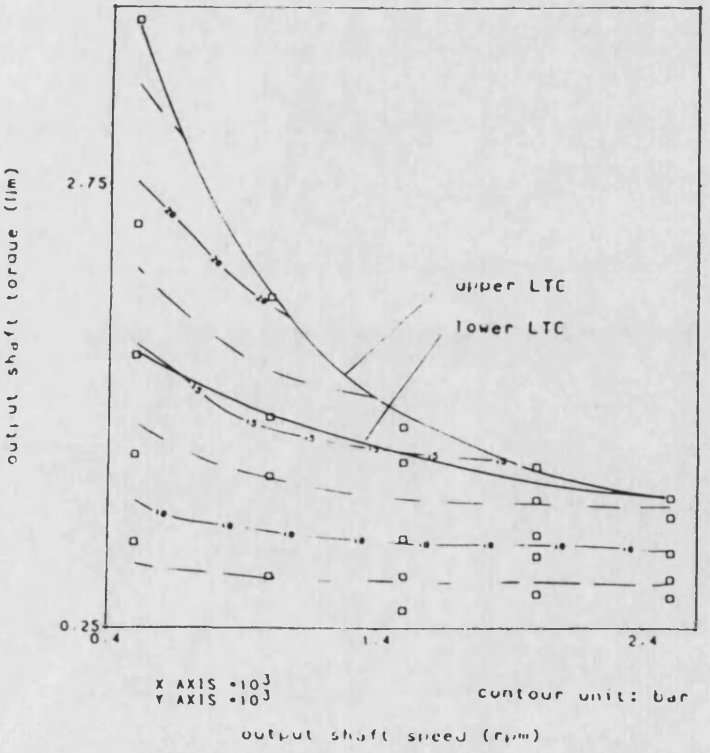

Fig. 9.65 Engine Brake Mean Effective Pressure of DCE without Bypass Valve

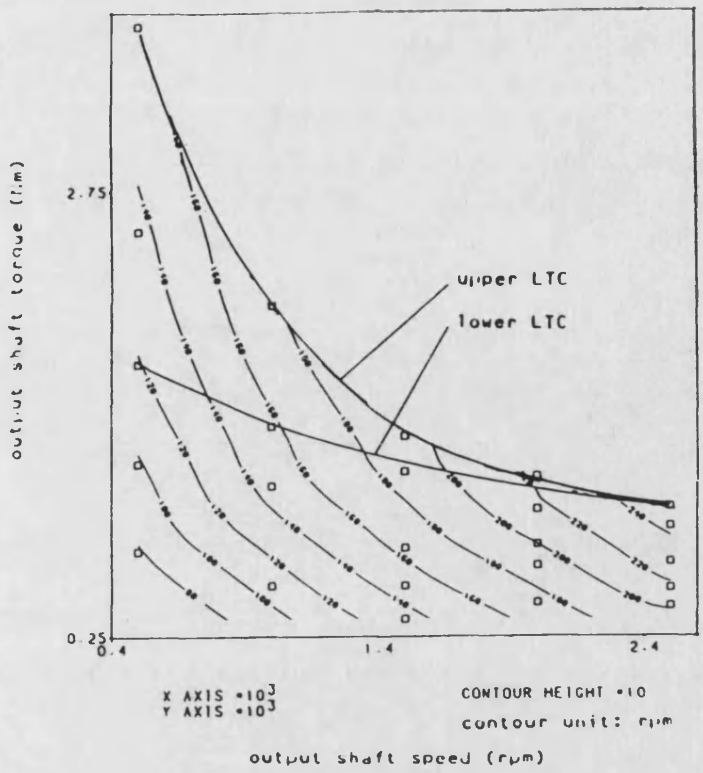

Fig. 9.66 Engine Speed of DCE without Bypass Valve

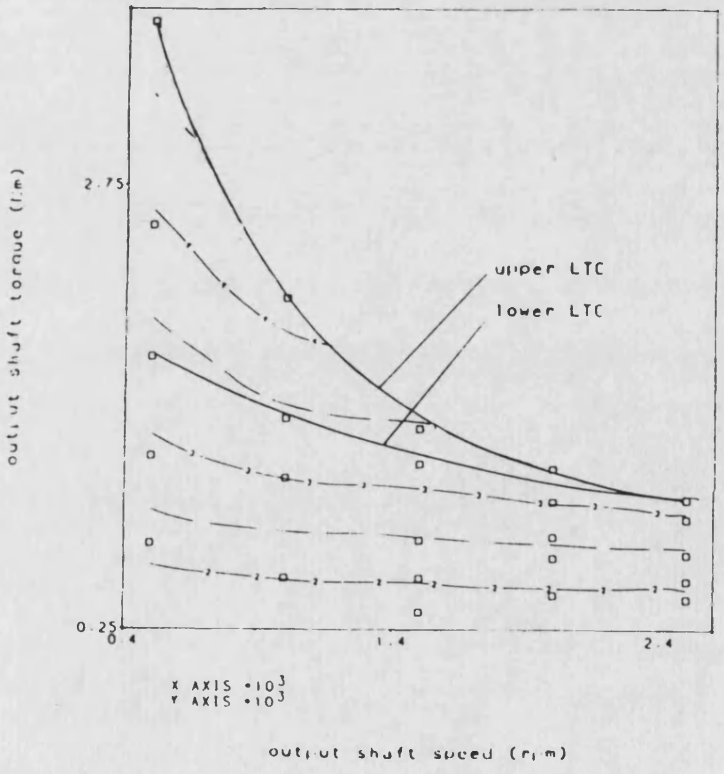

Fig. 9.67 Boost Pressure Ratio of DCE without Bypass Valve

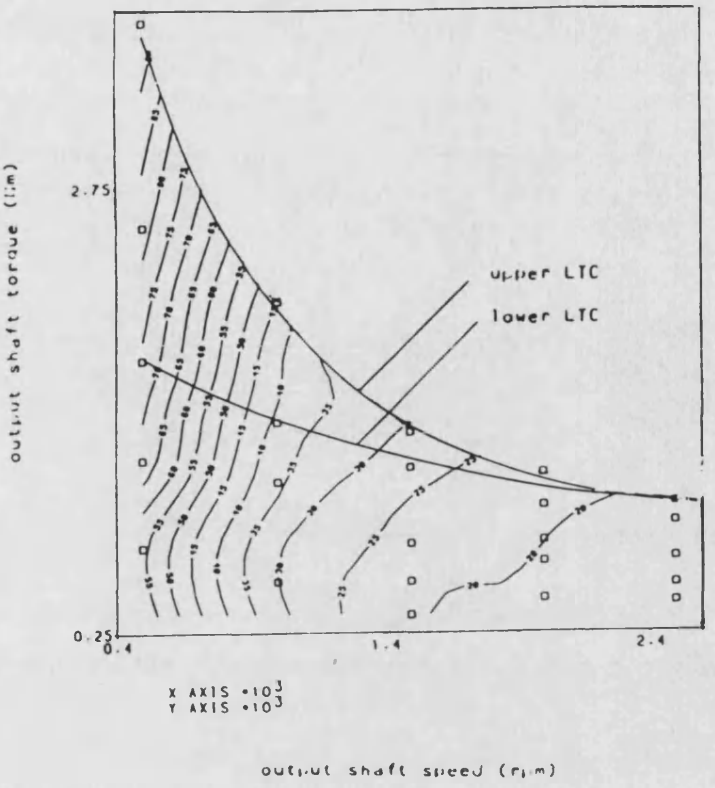

Fig. 9.68 Turbine Gear Ratio of DCE without Bypass Valve

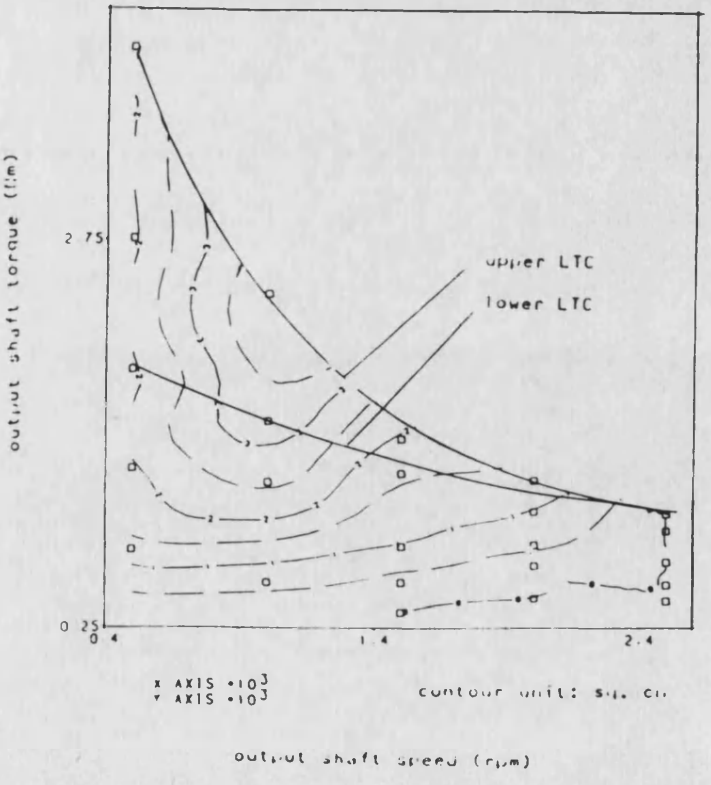

Fig. 9.69 Optimum Bypass Valve Opening of DCE

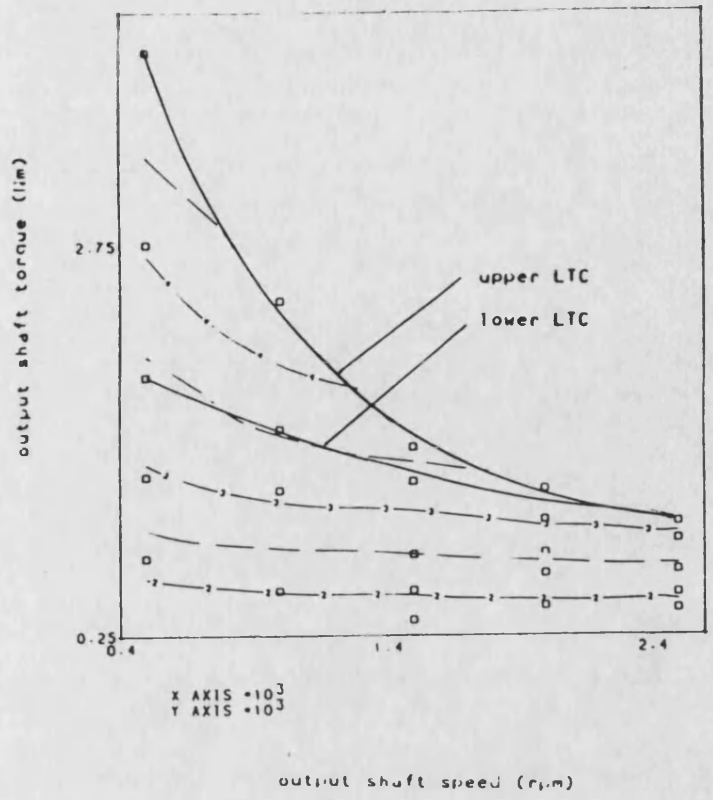

Fig. 9.70 Boost Pressure Ratio of DCE with Bypass Valve

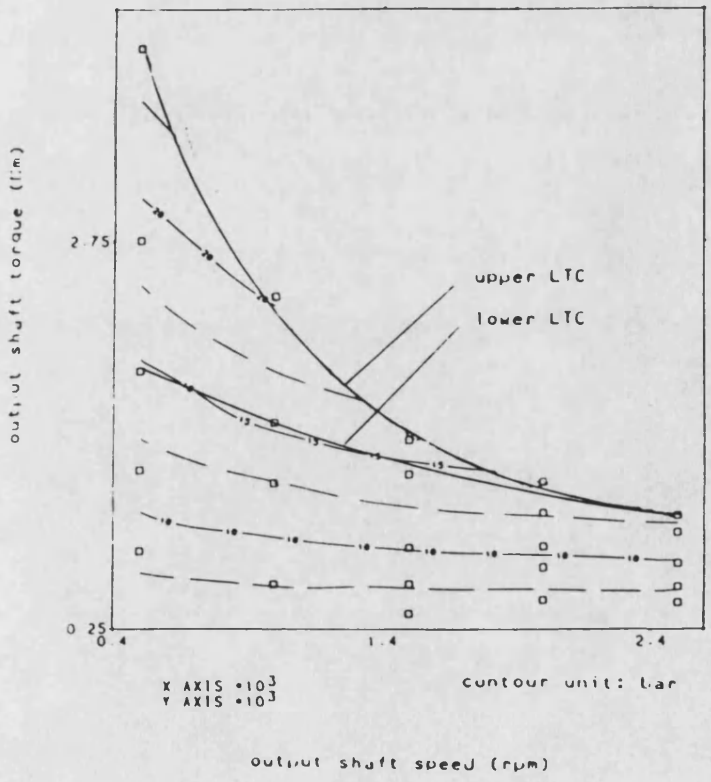

Fig. 9.71 Engine Brake Mean Effective Pressure of DCE with Bypass Valve

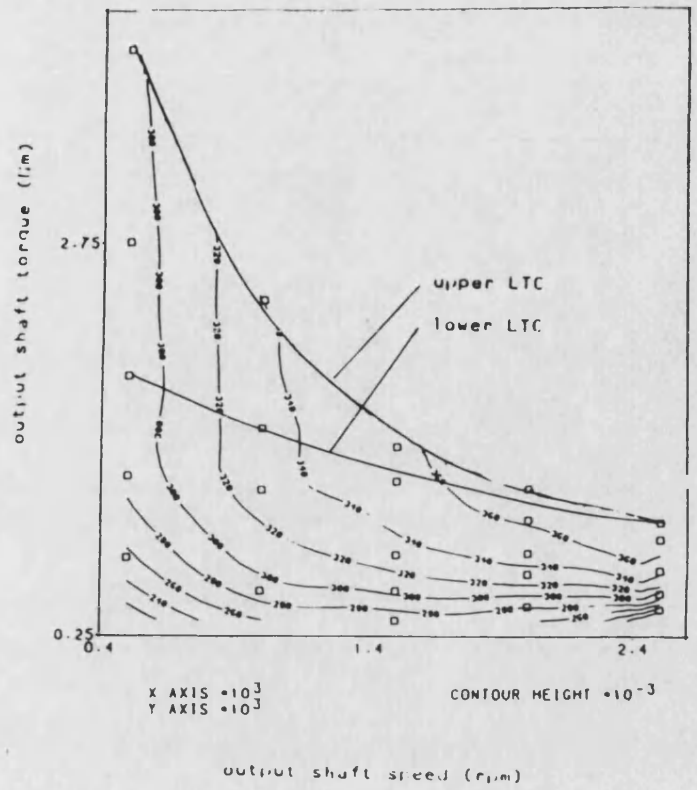

Fig. 9.72 Output Shaft Brake Thermal Efficiency of DCE with Bypass Valve

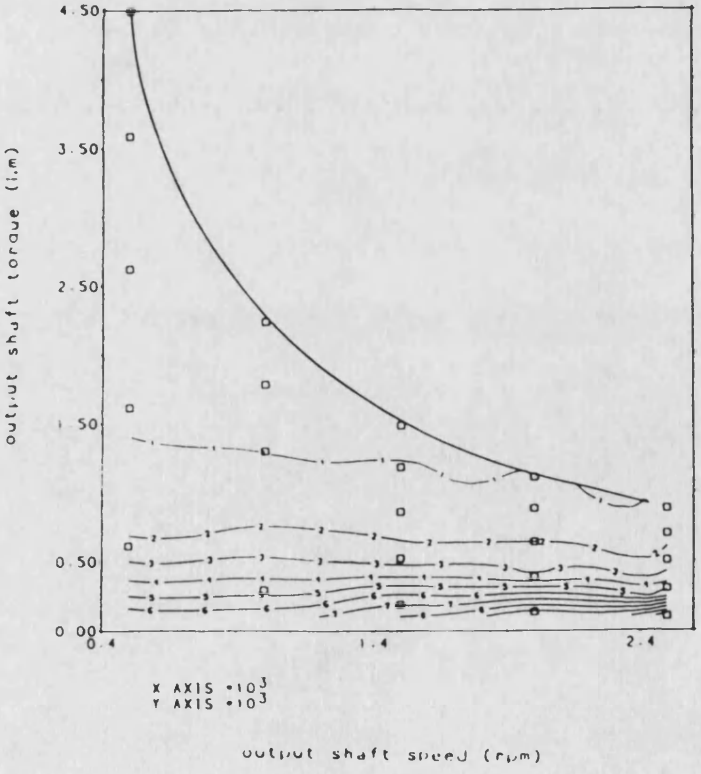

Fig. 9.73 Optimum Transmission Ratio of Output Shaft CVT of DCE

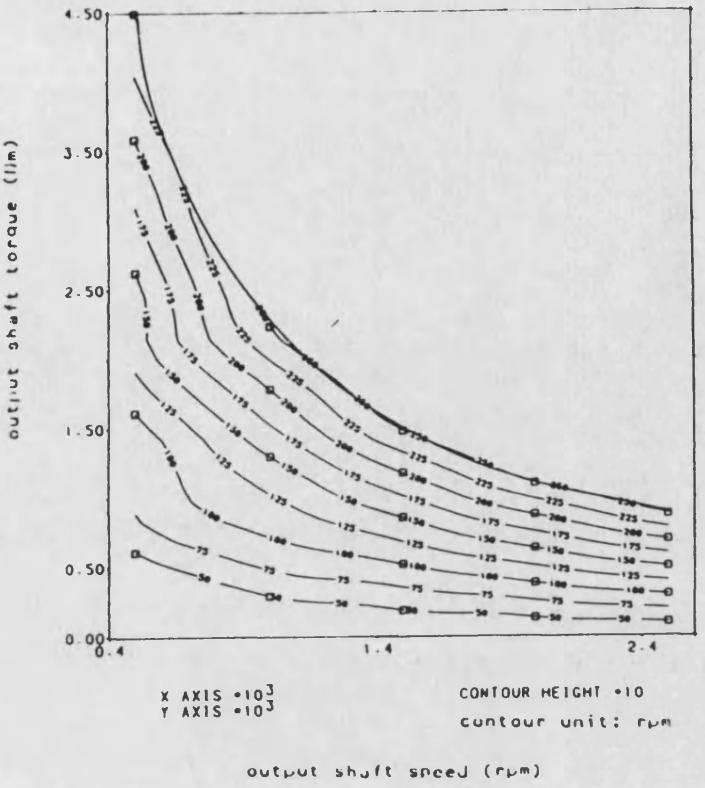

Fig. 9.74 Engine Speed of DCE with Output Shaft CVT

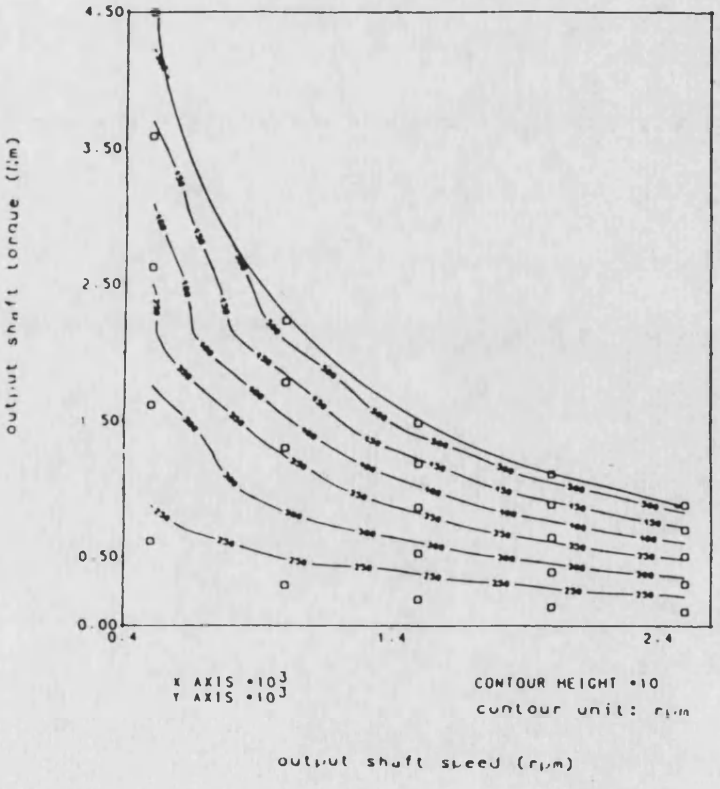

Fig. 9.75 Compressor Speed of DCE with Output Shaft CVT

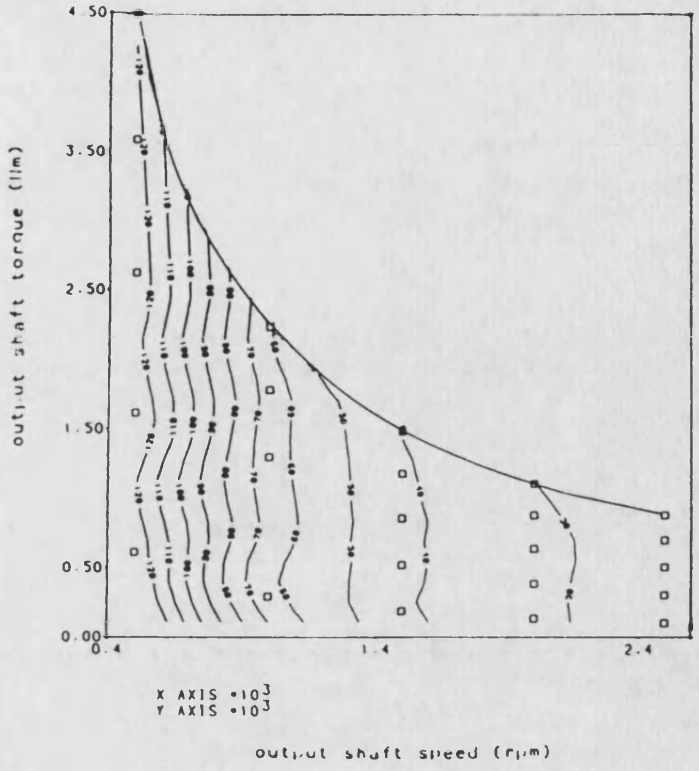

Fig. 9.76 Turbine Gear Ratio
of DCE with Output Shaft CVT

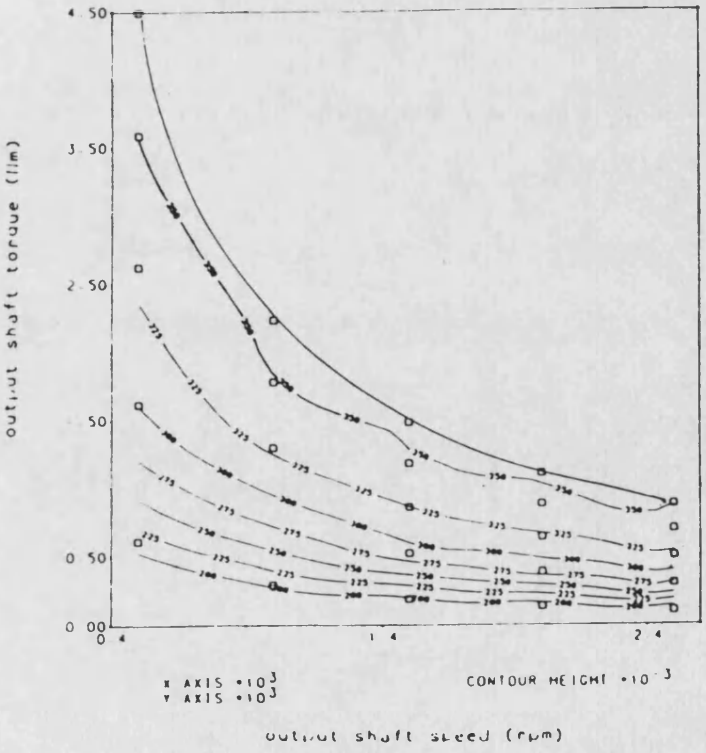

Fig. 9.77 Output Shaft Brake Thermal Efficiency
of DCE with Output Shaft CVT

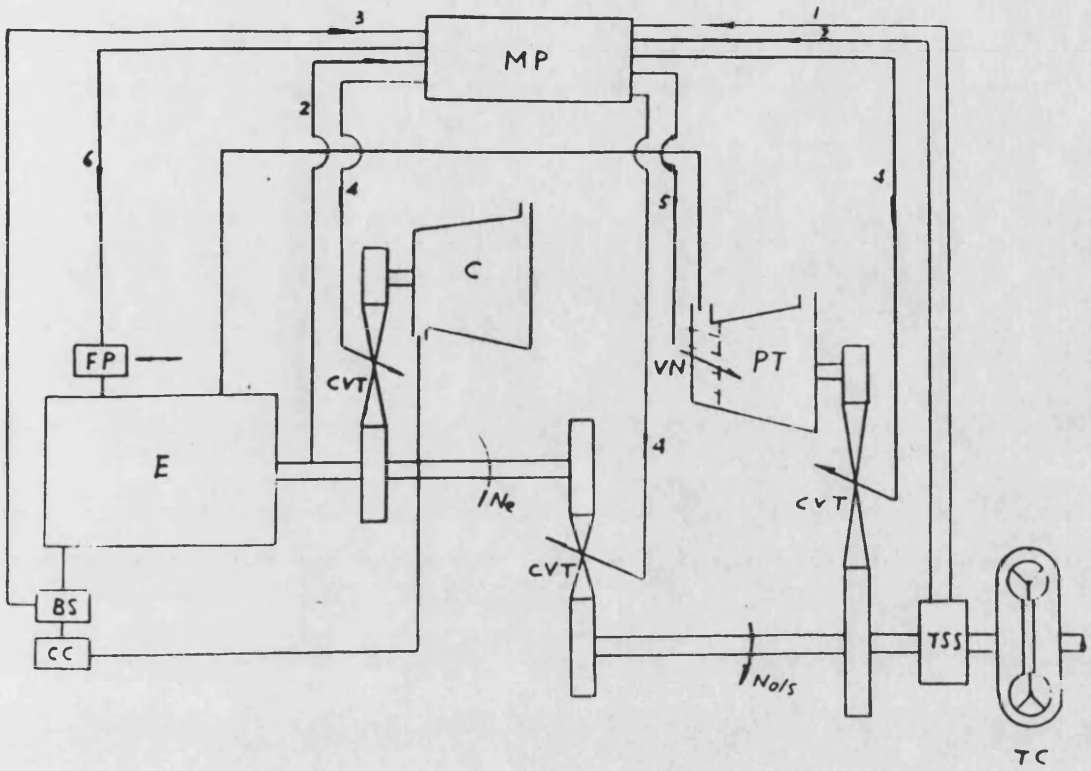

BS : boost sensor
C : compressor
CC : charge cooler
E : engine
FP : fuel pump

TC : torque turbine
VN : variable turbine nozzles
TSS: output torque&speed sensor
Ne : engine speed
Nos: output shaft speed

CVT: continuously variable transmission

INPUT SIGNALS:
1. torque transducer
2. speed transducer
3. pressure transducer

OUTPUT SIGNALS:
4. CVT control
5. nozzle control
6. fuel pump control

Fig. 9.78 Layout of CES with 3 CVTs

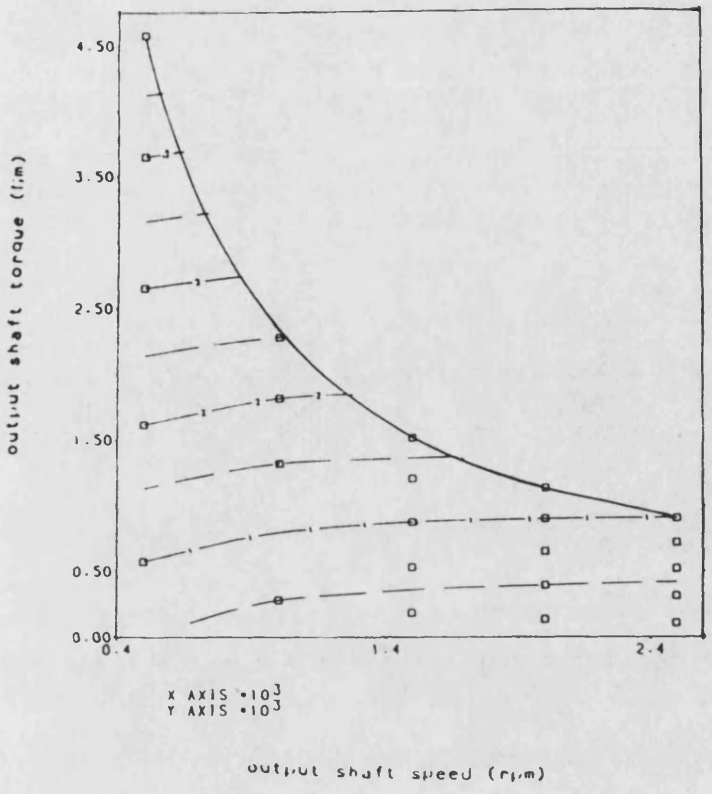

Fig. 9.79 Engine/Output Shaft Speed Ratio of CES with 3 CVTs

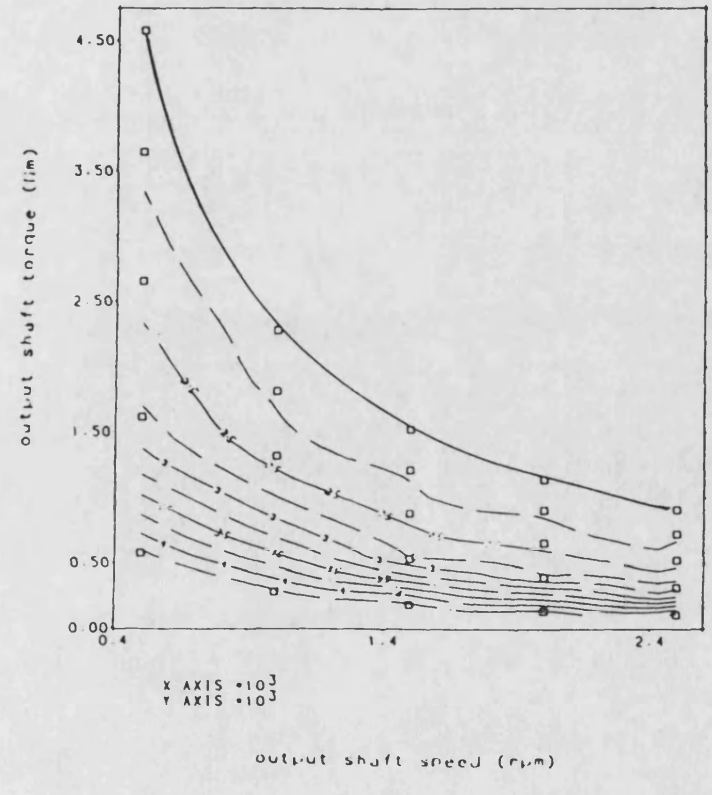

Fig. 9.80 Compressor/Engine Speed Ratio of CES with 3 CVTs

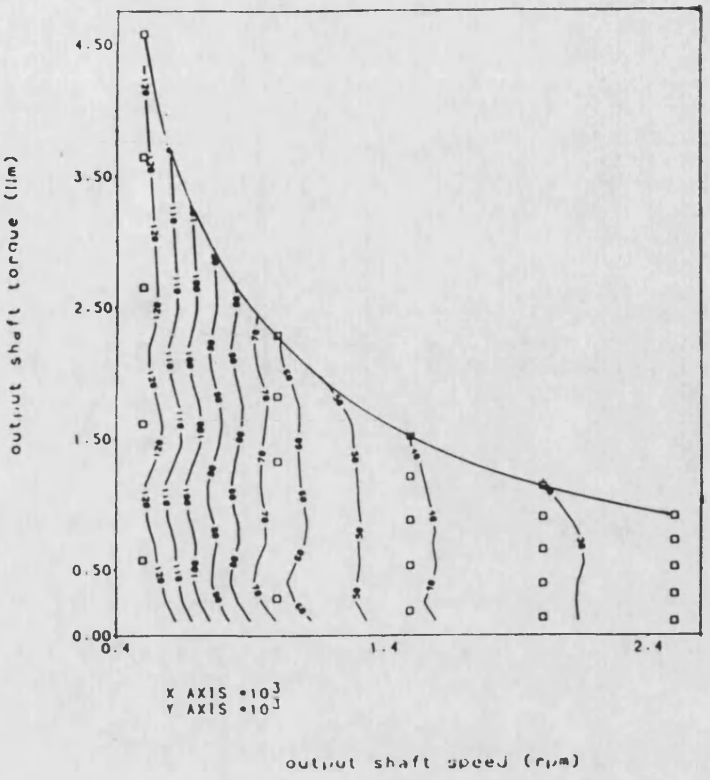

Fig. 9.81 Turbine/Output Shaft Speed ratio of CES with 3 CVTs

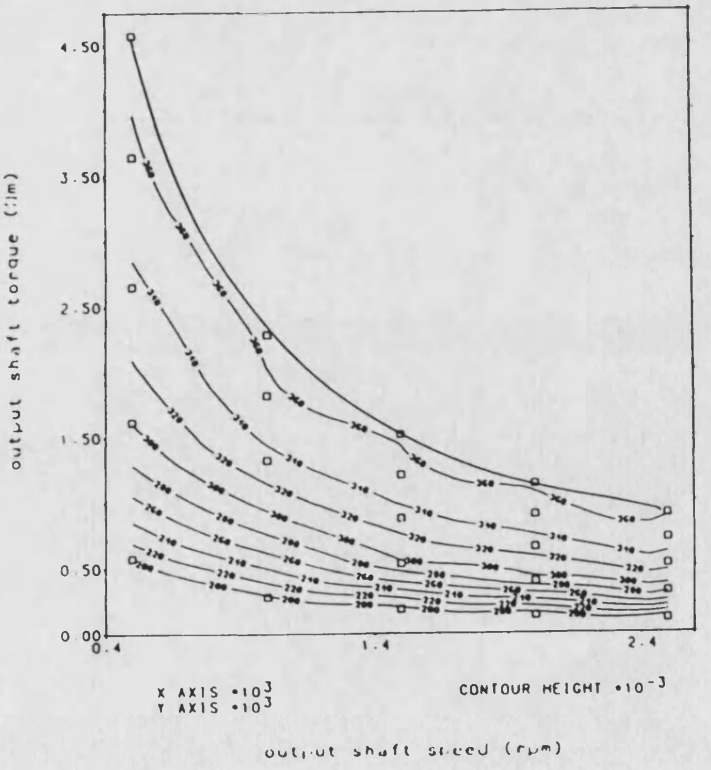

Fig. 9.82 Output Shaft Brake Thermal Efficiency of CES with 3 CVTs

Chapter 10 CONCLUSIONS

This thesis has investigated the three main aspects of two-stroke diesel engines: scavenging, supercharging and compounding.

(1). scavenging

As a non-predictive model of the scavenging process, the generalized thermodynamic model has been introduced. This model can give a thermodynamic description for any possible scavenging process. Having specified a history of the scavenging process, this model is suitable for all scavenging systems including cross, loop and uniflow scavenging schemes. As a step-by-step computer program, this model can give a detailed description of varying pressure and volume for the scavenging process, which is important for matching calculations of supercharging. For the simplified isobaric and isochoric model with respectively constant coefficients of intake and discharge proportions during different scavenging phases, analytical solutions for this model have been obtained. From these, all existing models with the isobaric and isochoric assumptions can be derived. Incorporated with experimental work and experiences, the analytical form of this model can provide an easy and quick performance estimation for the scavenging process.

As predictive models, the phenomenological fluid dynamic models: the steady jet model and the unsteady jet model, have been suggested. Based on jet mixing and propagation, these models can give an approximate description of velocity and concentration fields for the uniflow scavenging process, thus obviating the uncertainty of the thermodynamic models. In the steady jet model, it is assumed that during the scavenging process air and residual gas are imcompressible which impairs precision of this model. The unsteady jet model is soundly founded on the conservation laws of mass, momentum and energy for compressible flow. A comparison between the computational and experimental results of an opposed-piston two-stroke engine demonstrates good agreement.

A group of model laws for scale modelling the scavenging process has been established. The experimental work on a simple water rig has been done. It also validates that the unsteady jet model is satisfactory. This model can

be used to optimize port design.

(2). supercharging and compounding

Three engine models have been built into programs CSPS, CSP3Z and CSPMZ for modelling the two-stroke engine. The simple program CSPS uses the simple analytical formulae of the isobaric and isochoric thermodynamic model. This model is suitable for estimating the global performances over the complete range of speed and load because of its simplicity. In this model, the processes in the engine are treated as polytropic process with a variable exponent, which can combine a large computation step length with a relatively precise apparent rate of burnt fuel to improve the prediction for the combustion process. The intermediate program CSP3Z uses the generalized thermodynamic scavenging model. This model can provide a step-by-step description for any scavenging system which is beneficial for detailed and accurate matching calculation of an engine system. The complicated program CSPMZ uses the unsteady jet model with two optional versions of the entrainment laws by Ricou and Spalding [4.10] and by Scheitz [4.11]. This model is appropriate for optimizing port design of uniflow scavenged engines. In the heat transfer submodel of programs CSP3Z and CSPMZ, the piston is represented by a variable Delta resistance calculated based on the Bessel solution of Laplace's equation of steady-state heat conduction. Therefore, this submodel can estimate the temperatures of the combustion chamber of various engines including insulated engines. Programs CSPS, CSP3Z and CSPMZ can be used for modelling the differential compound engine. Based on engine model CSP3Z, program CSP3ZTC has been made for simulating the turbocharged engines.

Using program CSPMZ, the author has predicted the performance of the Ford ceramic two-stroke opposed-piston diesel engine, and optimized the port design of the Ford engine. The optimization procedure is suitable for any uniflow scavenged engine.

Using program CSP3ZTC, the author has predicted the performance for the turbocharged Ford caramic engine without and with blower.

Using program CSPS, the author has estimated the operating characteristics

for the differential compound two-stroke engine for a 30-48 ton truck. This performance analysis demonstrates that the DCE with the two-stroke engine combines improved power density and package size with its inherent advantages of high efficiency and high torque backup.

Furthermore, the author has suggested a new compound engine system with three continueously variable transmissions between the engine and compressor, the engine and output shaft, the power turbine and output shaft respectively. Its performance has been estimated based on program CSPSCVT. This new compound engine system enhances the improvements in the efficiency and the transient response under the normal mechanical and thermal loadings of the engine.

The author suggests that the following future research work is important:

(1). Based on the computational fluid dynamic method, to develop a comprehensive model for predicting the detailed velocity, temperature and concentration fields and scavenging effectiveness for all scavenging systems.
(2). Based on the generalized model law, to conduct the experimental work on an approximately "real" model for measuring the velocity, temperature and concentration fields and for validating the previous model.
(3). Based on the one-dimensional unsteady flow theory, to improve the author's present computer program in order to investigate wave effect in the intake and exhaust system and to optimize its design.
(4). To develop a computer program to predict the transient behavour of a compound two-stroke engine system.
(5). To investigate the feasibility of the new compound engine system with 3 CVTs in detail.

Appendix I KINEMATIC ANALYSIS OF HORIZONTAL OPPOSED PISTON ENGINES

Fig. AI.1 is the layout of the horizontal opposed piston engines concerned. The linkage is split into two parts. The lower part of the engine linkage, consisting of the crankshaft, the connecting rod and the lower portion of the rocker, is a four-bar chain. The upper portion, consisting of the piston, the piston rod and the upper portion of the rocker, is an engine mechanism with an off-set piston.

The position of the top dead center used in the analysis below as the reference condition from which crank angle is measured, is defined as the crank position giving the minimum volume in the combustion chamber between the two horizontally opposed pistons.

The analysis assumes rigid links, so that no allowance is made for the elasticity of the engine parts or for the bearing clearances.

In the kinematic analysis of two-stroke engine, there are two different tasks:

(1). to determine a piston displacement, that is, a crank angle is given, and the corresponding piston displacement needs to be found.
(2). to determine the timing of the inlet and exhaust ports, that is, a positions of the ports is given, and the corresponding crank angle needs to be determined.

The linkage can be analysed by the vector-loop method. [AI.1] With the notation in the Fig. AI.1, for the lower part of the linkage, the vector-loop equation, resolved into the horizontal and vertical components, is

$$rck\cos\alpha + cll\cos\beta + air\cos\epsilon - fvr = 0 \qquad (AI.1)$$

$$rck\sin\alpha + cll\sin\beta + air\sin\epsilon - fhr = 0 \qquad (AI.2)$$

The final aim is to find the relation between the crank angle, α, and the piston displacement, x. Above all, for the lower part of the linkage, the relation between the crank angle α and the lower rocker angle ϵ should be

obtained. Thus it is necessary to eliminate β. After rearrangement, the following equation can be achieved

$$K_1 - K_2\cos\epsilon - K_3\sin\epsilon - K_4\cos\alpha - K_5\cos\alpha + \cos\alpha\cos\epsilon + \sin\alpha\sin\epsilon = 0 \qquad \text{(A1.3)}$$

where $K_1 = (fvr^2 + fhr^2 + air^2 + rck^2 - cll^2)/(2\ rck\ air)$

$K_2 = fvr/rck$

$K_3 = fhr/rck$

$K_4 = fvr/air$

$K_5 = fhr/air$

The equation (A1.3) gives the relation between the crank angle, α, and the rocker angle, γ. For convenience, letting

$$w = \tan(\frac{\alpha}{2})$$

$$v = \tan(\frac{\epsilon}{2})$$

and substituting the following equations

$$\sin\alpha = \frac{2w}{(1+w^2)}$$

$$\cos\alpha = \frac{(1-w^2)}{(1+w^2)}$$

$$\sin\epsilon = \frac{2v}{(1+v^2)}$$

$$\cos\epsilon = \frac{(1-v^2)}{(1+v^2)}$$

into equation (A1.3), and rearranging yields the following equations

$$(C_1 w^2 - 2K_5 w + C_2)v^2 - 2(K_3 w^2 - 2w + K_3)v + (C_3 w^2 - 2K_5 w + C_4) = 0 \qquad \text{(A1.4)}$$

or

$$(C_1 v^2 - 2K_3 v + C_3)w^2 - 2(K_5 v^2 - 2v + K_5)w + (C_2 v^2 - 2K_3 v + C_4) = 0 \qquad \text{(A1.5)}$$

where $C_1 = K_1 + K_2 + K_4 + 1$

$C_2 = K_1 + K_2 - K_4 - 1$

$C_3 = K_1 - K_2 + K_4 - 1$

$C_4 = K_1 - K_2 - K_4 + 1$

The former equation (A1.4) is suitable to determine the lower rocker angle, ϵ, from the crank angle, α. And the latter equation (A1.5) is applicable to determine the crank angle, α, from the lower rocker angle, ϵ.

Similarly, for the upper part of the linkage, the vector-loop equation is

$$aur\cos\gamma - clu\cos\theta + x = 0 \qquad \text{(A1.6)}$$

$$aur\sin\gamma - clu\sin\theta - fpr = 0 \qquad \text{(A1.7)}$$

Because the aim is to find out the relationship between the upper rocker angle γ and the piston displacement x, the connecting rod angle must be elimineted. Following the previous procedure, the equation is

$$(x + aur\cos\gamma)^2 + (fpr - aur\sin\gamma)^2 = clu^2 \qquad \text{(A1.8)}$$

After rearrangement, the equation becomes

$$x = -aur\cdot\cos\gamma + \sqrt{clu^2 - (fpr - aur\cdot\sin\gamma)^2} \qquad \text{(A1.9)}$$

Similarly letting,

$$u = \tan(\frac{\gamma}{2})$$

and substituting the following relations

$$\sin\gamma = \frac{2u}{(1+u^2)}$$

$$\cos\gamma = \frac{(1-u^2)}{(1+u^2)}$$

into equation (A1.8) and rearranging obtain the following equation

$$(A+x)\ u^2 - 2\ fpr\ u + (A-x) = 0 \qquad \text{(A1.10)}$$

where

$$A = \frac{(x^2+fpr^2+aur^2-clu^2)}{2 \cdot aur}$$

The former equation (A1.9) can be used to calculate the piston displacement x from the upper rocker angle γ. The latter equation (A1.10) is suitable to find out the upper rocker angle γ from the displacement x.

From the relationship between the upper and lower rocker angles

$$\gamma = \epsilon + \zeta \qquad \text{(A1.11)}$$

where ζ is the angle contained by the upper and lower rockers.

the following equations are valid.

$$u = \frac{v+\tan(\epsilon/2)}{1-v \cdot \tan(\epsilon/2)} \qquad \text{(A1.12)}$$

$$v = \frac{u-\tan(\epsilon/2)}{1+u \cdot \tan(\epsilon/2)} \qquad \text{(A1.13)}$$

It is understandable that the incorporation of equation (AI.4) with equation (AI.9) will be able to determine the piston displacement from the crank angle, via equation (AI.12); and that the incorporation of equation (AI.10) with equation (AI.5) to determine the crank angle from the displcement, via equation (AI.13).

(1). Determination of the piston displacement from the crank angle

(a). calculate the tangent of the half lower rocker angle, v, from the tangent of the half crank angle, w, using equation (AI.4).
(b). calculate the tangent of the half upper rocker angle, u, from the tangent of the half lower rocker rocker angle, v, using equation (AI.12).
(c). calculate the sine and cosine of the rocker angle, γ.
(d). solve equation (AI.9) to obtain the piston displacement from the sine and cosine of the rocker angle.

(2). Determination of the crank angle from the piston displacement

(a). calculate the tangent of the half upper rocker angle, u, from the piston displacement, solving equation (AI.10).
(b). calculate the tangent of the half lower rocker angle, v, from the half upper rocker angle, u, using equation (AI.13).
(c). solve equation (AI.5) to get the tangent of the half crank angle, w, from the tangent of the half lower rocker angle, v.
(d). calculate the crank angle from the tangent of the half crank angle.

It is notable that the distance from the crank vertical centreline to the top of the piston, y, can be obtained from the following equation

$$y = fvr - dpc - x \qquad \text{(AI.14)}$$

Fig. A I.2 shows the definition of angles. It assumes that the right piston controls the inlet ports and the left piston controls the exhaust ports, and the crankshaft rotates clock-wise. For the crank linkage of the inlet piston, the relation is

$$\alpha = -\pi + \frac{\Delta}{2} - \varphi$$

where Δ is the phase angle between the inlet and exhaust crank arms.

φ is the crank angle from the top dead center.

However, for the crank linkage of the exhaust piston, the relation is

$$\alpha = \pi + \frac{\Delta}{2} + \varphi$$

because the exhaust crank linkage is symmetric to the inlet crank linkage.

REFERENCE

[Al. 1] S. Molian
"Mechanism Design"
Cambridge University Press, 1982

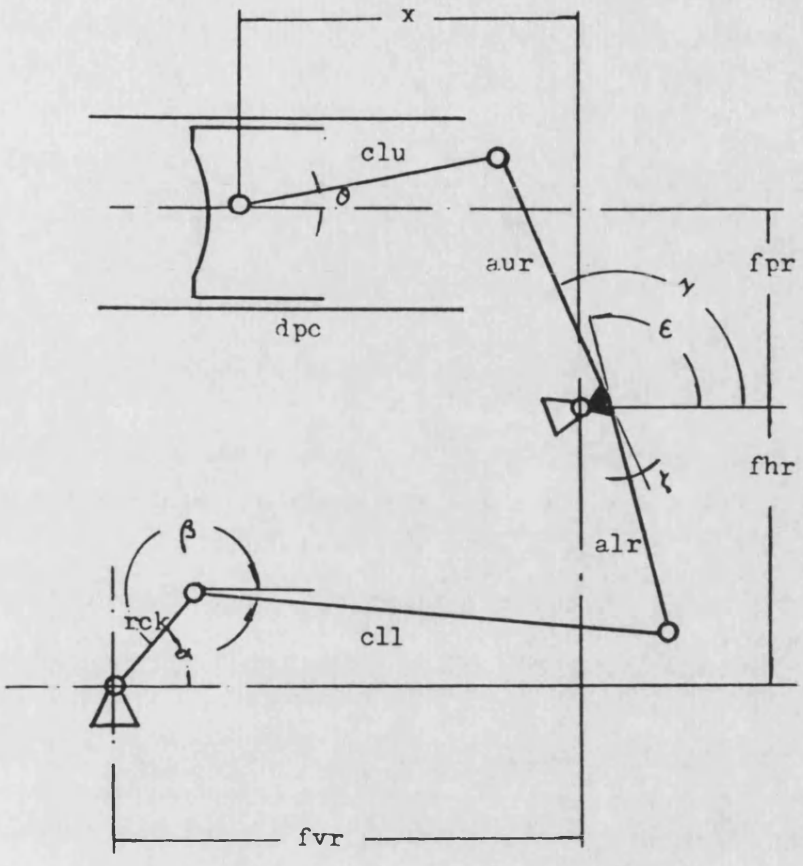

fvr--frame,crank vertical centre line to rocker pivot
fhr--frame,crank housing centre line to rocker pivots
fpr--frame,piston centre line to rocker pivots
cll--lower connecting rod
alr--lower rocker arm
aur--upper rocker arm
clu--upper connecting rod
dpc--piston compression distance
rck--crank radius

Fig. AI.1 Layout and Notation of Linkage

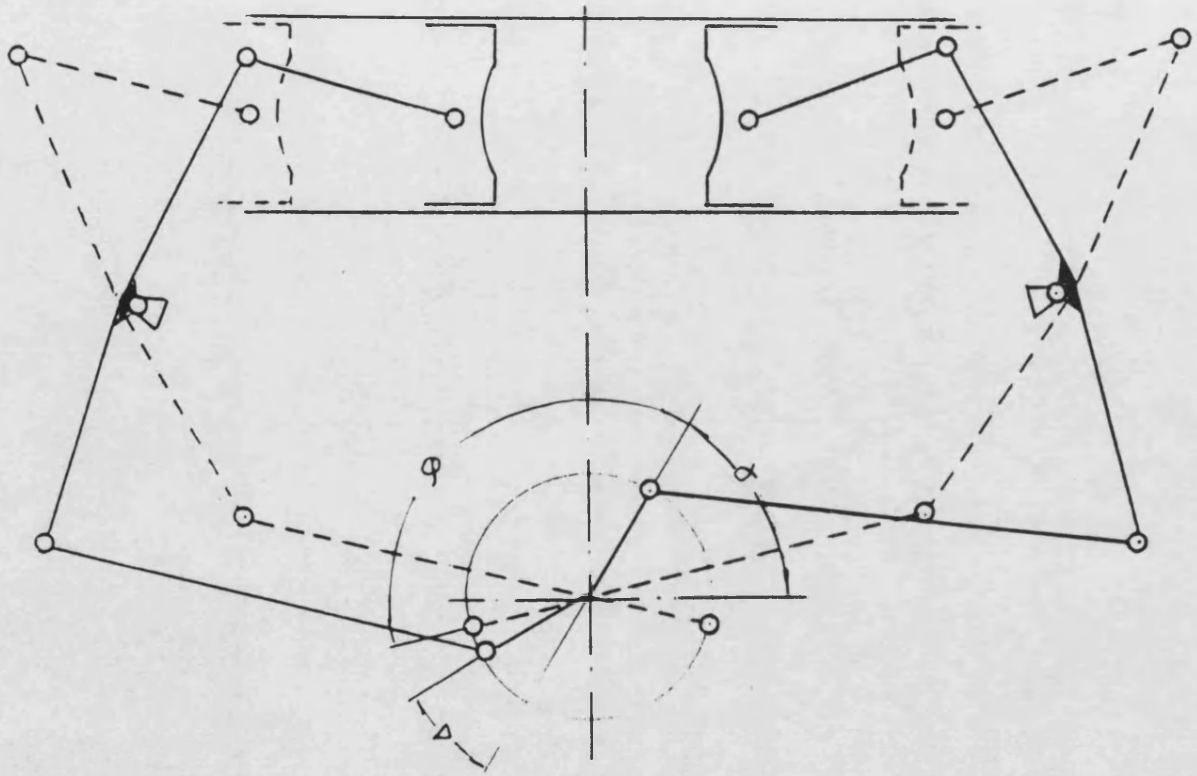

Fig. A1.2 Definition of Angles

Appendix II QUANTITATIVE ESTIMATION OF TRANSFER PHENOMENA

AII. 1 MOLECULAR MIXING AND TURBULENT MIXING

Two factors must be accounted for in analysing transfer processes in turbulent flows.

Molecular mixing: it has a vital role in the dissipation and transport occuring in the smaller scales of the turbulence and in the near-wall region.

Turbulent mixing: it actually is the convective transport accomplished by the time-mean motion of the fluid. and is dominant through most of the flow.

AII. 2 GENERALISED CONSERVATION EQUATIONS

For brevity. this appendix introduces the generalised form of the conservation equations. For a given control volume moving with a statistically steady turbulent flow. it is as follows.

$$\frac{\Delta}{\Delta t}\int_V \rho\varphi dV = \oint_A J dA + \int_V \varphi s dV \qquad \text{(AII. 1)}$$

i. e.

$$\frac{\Delta}{\Delta t}\int_V \varphi dm = \oint_A J dA + \int_m s dm \qquad \text{(AII. 2)}$$

change of the conservation amount in the control volume = flux of the conservation amount through the boundary surface of the control volume + source or sink of the conservation amount in the control volume

where V is the total control volume.

A is the surface area of the control volume.

φ is the specific property of the property amount Φ.

s is the specific source rate of the conservation amount.

J is the flux of the property Φ.

ρ is the fluid density.

The quantities φ, s and J for the mass, momentum and energy conservation are listed in Table AII.1.

For scavenging process, solely the source term among the conservation equations is the term involving heat transfer which is investigated fully. Only the problem left is to determine the fluxes of the properties.

AII.3 FLUX OF PROPERTY

A unit area element remaining stationary within the turbulent flow is considered. The fluctuating values of property and its flux are denoted by $\rho+\rho'$ and J+j'. The fluctuating component of velocity in the direction n nomal to the plane is denoted by U+u', as shown in Fig. AII.1. The fluid density is denoted by $\rho+\rho'$, and the molecular diffusivity of the property is denoted by K. In terms of these quantities, the instantaneous flux of the property is

$$J+j' = -(\rho+\rho')K\frac{\partial(\Phi+\varphi')}{\partial n} + (\rho+\rho')(\Phi+\varphi')(U+u') \qquad \text{(AII.3)}$$

This is the sum of the fluctuating convection and the simple gradient diffusion, like that in Fourier's and Fick's laws.

The time-mean value of the flux is then found to be

$$J = -\rho K\frac{\partial\Phi}{\partial n} + \rho\Phi U + \rho\overline{\varphi'u'} + \bar{\varphi}'\overline{\rho'u'} + \bar{u}'\overline{\rho'\varphi'} + \overline{\rho'\varphi'u'} \qquad \text{(AII.4)}$$

net flux = molecular diffusion + bulk convection + turbulent diffusion
+ interaction between desity and property variation
+ interaction between desity and velocity variation
+ triple correlation

According to the useful concept proposed by Morkovin [AII.1] that if the Mach number of the turbulent fluctuation is much less than unity, the effects of density fluctuations could be neglected, the terms of the contribution to the flux via an interaction between density and velocity variations, $\varphi'\rho'u'$ and $u'\rho'\varphi'$, and the term of the triple correlation $\rho'\varphi'u'$ can be neglected.

This last element may be formally converted to a diffussion term by introducing an eddy diffusity

$$\rho\overline{\varphi' u'} = -\rho \epsilon_{\varphi} \frac{\partial \Phi}{\partial n} \qquad \text{(All. 5)}$$

where ϵ_{φ} is the eddy diffusivity of the property Φ.

$\frac{\partial \Phi}{\partial n}$ is the normally directional derivative of the property Φ.

Alternatively, the effect of turbulent mixing can be represented by an eddy lateral convection velocity U_{φ} or an eddy mass flux or Reynolds flux G_{φ}

$$\rho\overline{\varphi' u'} = \rho U_{\varphi} \Phi \qquad \text{(All. 6)}$$

$$\rho\overline{\varphi' u'} = G_{\varphi} \Delta\Phi \qquad \text{(All. 7)}$$

where $\Delta\Phi$ is the change in Φ across some finite interval Δn. The former equation (All. 6) is suitable for the momentum transfer process because the absolute amount of momentum transported is concerned. However, the latter equation (All. 7) is suitable for the mass and energy transfer processes because only the relative amounts of mass and enthalpy transported need considering. Whether or not the transformations (All. 5) (All. 6) and (All. 7) prove useful depends on whether the hypothetical quantities ϵ_{φ}, U_{φ}, G_{φ} can be specified realistically.

From the above analysis, the flux equation becomes

$$J = -\rho(K+\epsilon_{\varphi}) \frac{\partial \Phi}{\partial n} + \rho \Phi U \qquad \text{(All. 8)}$$

or

$$J = -\rho K \frac{\partial \Phi}{\partial n} + \rho \Phi (U+U_{\varphi}) \qquad \text{(All. 9)}$$

or

$$J = -\rho K \frac{\partial \Phi}{\partial n} + \rho \Phi U + G_{\varphi} \Delta\Phi \qquad \text{(All. 10)}$$

It is noted that when the area element is tangential to the jet timelines the

term of bulk convection $\rho\Phi U$ disappears.

Based on equations (AII.5) and (AII.6), the eddy mass flux is

$$\rho U_\varphi = -\rho \epsilon_\varphi \frac{\partial \Phi / \partial n}{\Phi} \qquad \text{(AII.11)}$$

From equations (AII.5) and (AII.7), it is

$$G_\varphi = -\rho \epsilon_\varphi \frac{\partial \Phi / \partial n}{\partial \Phi} \qquad \text{(AII.12)}$$

Using relation (AII.11), the eddy mass flux in the momentum transfer process is

$$G_m = \rho U_m = -\rho \epsilon_m \frac{\partial U / \partial n}{U} \qquad \text{(AII.13)}$$

From relation (AII.12), the eddy mass flux in the mass and energy transfer process are

$$G_c = \rho C_c = -\rho \epsilon_c \frac{\partial C / \partial n}{C}$$

$$G_h = \rho H_h = -\rho \epsilon_h \frac{\partial H / \partial n}{H} \qquad \text{(AII.14)}$$

AII.4 REYNOLDS' ANALOGY

If the profiles of the time-mean properties U, C and H are similar, i.e.

$$\frac{1}{U}\frac{\partial U}{\partial n} = \frac{1}{\Delta C}\frac{\partial C}{\partial n} = \frac{1}{\Delta H}\frac{\partial H}{\partial n} \qquad \text{(AII.15)}$$

and the eddy diffusivities ϵ_m, ϵ_c and ϵ_h are equal, i.e.

$$Pr_t = \frac{\epsilon_m}{\epsilon_h} = 1$$

$$Sc_t = \frac{\epsilon_m}{\epsilon_c} = 1$$

$$Le_t = \frac{\epsilon_c}{\epsilon_h} = 1$$

where Sc_t is the turbulent Schmidt number,

Pr_t is the turbulent Prandtl number.

Le_t is the turbulent Lewis number.

then the eddy mass fluxes are the same for the three transfers.

$$G_m = G_c = G_h \qquad \text{(AII. 16)}$$

For the fully turbulent flow, the similarity of U, C and H is valid because the effect of turbulent mixing dominates over that of molecular mixing. However, for the flow influenced by molecular diffusion, the following additional relations must be satisfied to validate the similarity

$$Pr = \frac{\nu}{\kappa} = 1$$

$$Sc = \frac{\nu}{D} = 1$$

$$Le = \frac{D}{\kappa} = 1$$

where ν is the molecular viscosity,

κ is the thermal conductivity,

D is the diffusion coefficient.

This series of results is commonly referred to as Reynolds' analogy.

AII. 5 MASS ENTRAINMENT RATE

It is assumed that the phenomenological unsteady jet model in Chapter 4 obeys Reynolds' analogy and that the flow is fully turbulent. This indicates that the flux terms in the equations of momentum, mass and energy conservations are the same with the effective momentum flux, i.e. the mass entrainment rate

$$G_m = \frac{\Delta m}{\Delta t} = \rho U_m = -\rho \epsilon_m \frac{\partial U / \partial n}{U} \qquad \text{(AII. 17)}$$

This reflects the physical background that the momentum transfer dominates the mass and energy transfers.

It is evident that the entrainment rate can be dertermined either directly from the initial parameters of jet, e.g. by Ricou and Spalding, or indirectly from the eddy viscosity, e.g. by Scheitz and Lilley. The former approach is used in version 1 of the phenomenological unsteady jet model in Chapter 4 which

describes the "macroscopic" behaviour of jet. whereas the latter is used in version 2 which depicts the "microscopic" behaviour of jet.

REFERENCE

[All. 1] M.V. Morkovin
"The Mechanics of Turbulence"
Gordon and Breach. 1964

Table AII. 1 The Generalised Form of the Conservation Equations

conservation equation	specific property φ	specific source rate $\dot{s}$	flux J
mass	concentration c	0.	$\rho U_c c$
momentum	velocity u,v,w	0.	$\rho U_u u$
energy	total energy e	-q-Pv	$\rho U_h h$

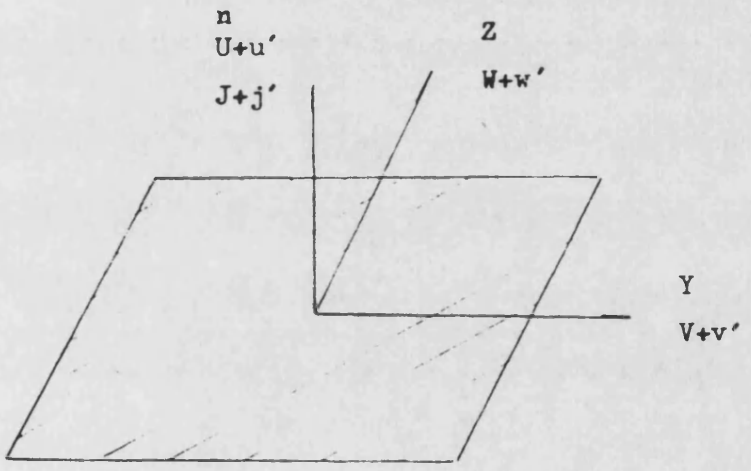

Fig. AII. 1 Plane Element of Area
In Analysing Transport Mechanisms

Appendix III SOLUTION OF HEAT CONDUCTION EQUATION

The general heat conduction equation in cylindrical coordinates is as follows

$$\frac{\partial^2 \theta}{\partial r^2} + \frac{1}{r}\frac{\partial \theta}{\partial r} + \frac{\partial^2 \theta}{\partial z^2} = 0 \qquad \text{(AIII. 1)}$$

In equation (AIII. 1) the temperature difference variable $\theta = T - T_c$ is introduced, where T_c is a constant reference temperature.

It is assumed that the piston is simplified as a cylinder. Thus the problem is as follows:

Find a solution giving the temperature distribution throughout the cylinder for the following boundary conditions, see Fig. AIII. 1.

At the oil side surface, i.e. z = 0

$$\theta = f_o(r) - T_c \qquad \text{(AIII. 2)}$$

At the gas side surface, i.e. z = L

$$\theta = f_g(r) - T_c \qquad \text{(AIII. 3)}$$

At the liner side surface, i.e. r = R

$$\theta = f_l(z) - T_c \qquad \text{(AIII. 4)}$$

According to the principle of superposition, the final solution is equal to the sum of the solutions of the corresponding three problems

$$\theta = \theta_g + \theta_o + \theta_l \qquad \text{(AIII. 5)}$$

Here, θ_g, θ_o and θ_l are the solutions of equation (AIII. 1) under the following conditions respectively

problem 1:

at $z = 0$, $\theta = 0$ (AIII. 6)

at $z = L$, $\theta = f_g(r) - T_c$ (AIII. 7)

at $r = R$, $\theta = 0$ (AIII. 8)

problem 2:

at $z = 0$, $\theta = f_o(r) - T_c$ (AIII. 9)

at $z = L$, $\theta = 0$ (AIII. 10)

at $r = R$, $\theta = 0$ (AIII. 11)

problem 3:

at $z = 0$, $\theta = 0$ (AIII. 12)

at $z = L$, $\theta = 0$ (AIII. 13)

at $r = R$, $\theta = f_l(z) - T_c$ (AIII. 14)

Thus, the problem of solving equation (AIII. 1) under the complex boundary conditions (AIII. 2) to (AIII. 4) is transformed into the summation of these three solutions of equation (AIII. 1) under the simple boundary conditions (AIII. 6) to (AIII. 8), (AIII. 9) to (AIII. 11), (AIII. 12) to (AIII. 14) respectively. By separating the variables, one seeks a solution of equation (AIII. 1) in the form

$$\theta = R(r)Z(z) \qquad \text{(AIII. 15)}$$

where $R(r)$ and $Z(z)$ are functions of only r or z respectively

After separation, the following two ordinary differential equations can be obtained from the original partial differential equation

$$\frac{d^2R}{dr^2} + \frac{1}{r}\frac{dR}{dr} + \lambda^2 R = 0 \qquad \text{(AIII. 16)}$$

$$\frac{d^2Z}{dz^2} - \lambda^2 Z = 0 \qquad \text{(AIII. 17)}$$

When λ's in equations (AIII. 16) and (AIII. 17) is taken as real number, equation (AIII. 16) is recognized as Bessel's equation of zero order, and

equation (AIII. 17) leads to the hyperbolic function. Thus, the solution of the differential equation (AIII. 1) may be expressed as

$$\theta = [B_1 J_0(\lambda r) + B_2 Y_0(\lambda r)] (B_3 \sinh\lambda z + B_4 \cosh\lambda z) \qquad \text{(AIII. 18)}$$

where $J_0(x)$ is Bessel's function of the first kind of zero order.
$Y_0(x)$ is Bessel's function of the second kind of zero order.

There exists one additional condition that the temperature must be finite at r=0. Because $Y_0(\lambda r) \to \infty$ as $r \to 0$, $B_2=0$ can be achieved.

The condition (AIII. 6) or (AIII. 10) makes B_4 vanish, hence the solution becomes

$$\theta = B \sin\lambda z \, J_0(\lambda r) \qquad \text{(AIII. 19)}$$

For problem 1, the application of condition (AIII. 8) demands that

$$J_0(\lambda R) = 0 \qquad \text{(AIII. 20)}$$

There are a countable infinite number of λ's satisfying the defining relation (AIII. 20)

$$J_0(\lambda_n R) = 0 \qquad \text{(AIII. 21)}$$

Firstly, the general solution is the sum of all the solutions corresponding to each of the λ_n's

$$\theta_g = \sum_{n=1}^{\infty} B_n^g \sinh\lambda_n z \, J_0(\lambda_n r) \qquad \text{(AIII. 22)}$$

Secondly, the application of condition (AIII. 7) determines the unknown B_n^g's

$$f_g(r) - T_c = \sum_{n=1}^{\infty} B_n^g \sinh\lambda_n L' \, J_0(\lambda_n r) \qquad \text{(AIII. 23)}$$

By the use of orthogonality of the Bessel functions, the constant coefficients

$(B_n^g \sinh\lambda_n L)$ are given by

$$B_n^g \sinh\lambda_n L = \frac{\int_o^R r[f_g(r)-T_c]J_0(\lambda_n r)\,dr}{\frac{R^2}{2}J_1^2(\lambda_n R)} \qquad \text{(AIII. 24)}$$

Finally, the solution of problem 1 is

$$\theta_g = \frac{2}{R^2}\sum_{n=1}^{\infty} \frac{\sinh\lambda_n z J_0(\lambda_n r)}{\sinh\lambda_n L J_1^2(\lambda_n R)} \int_o^R r[f_g(r)-T_c]J_0(\lambda_n r)\,dr \qquad \text{(AIII. 25)}$$

Similarly, for problem 2 the solution is

$$\theta_o = \frac{2}{R^2}\sum_{n=1}^{\infty} \frac{\sinh\lambda_n (L-z) J_0(\lambda_n r)}{\sinh\lambda_n L J_1^2(\lambda_n R)} \int_o^R r[f_o(r)-T_c]J_0(\lambda_n r)\,dr \qquad \text{(AIII. 26)}$$

When λ's in equation (AIII. 16) and (AIII. 17) are taken as imaginary number, i.e. $\lambda = i\mu$

equations (AIII. 16) and (AIII. 17) become

$$\frac{d^2R}{dr^2} + \frac{1}{r}\frac{dR}{dr} - \mu^2 R = 0 \qquad \text{(AIII. 27)}$$

$$\frac{d^2Z}{dz^2} + \mu^2 Z = 0 \qquad \text{(AIII. 28)}$$

Equation (AIII. 27) is a modified Bessel equation of zero order, whereas

equation (AIII.28) introduces the trigonometric function. Hence, the solution of the Laplace equation may possess the form

$$\theta = [B_1 I_0(\mu r) + B_2 K_0(\mu r)](B_3 \sin\mu z + B_4 \cos\mu z) \qquad \text{(AIII.29)}$$

where $I_0(x)$ is the modified Bessel function of the first kind of zero order, $K_0(x)$ is the modified Bessel function of the second kind of zero order.

From the boundness of the solution, $B_2 = 0$ can be obtained, because $K_0(\mu r) \to \infty$ as $\mu r \to 0$

The condition (AIII.12) makes B_4 vanish, so the solution is

$$\theta = B \sin\mu z \, I_0(\mu z) \qquad \text{(AIII.30)}$$

For problem 3, firstly, the application of condition (AIII.13) needs that

$$\mu = \frac{n\pi}{L} \qquad \text{(AIII.31)}$$

Hence, the general solution is the sum of all the solutions corresponding to each positive integer

$$\theta = \sum_{n=1}^{\infty} B_n' \sin\frac{n\pi z}{L} I_0\left(\frac{n\pi r}{L}\right) \qquad \text{(AIII.32)}$$

Secondly, the application of condition (AIII.14) determines the unknown B_n''s

$$f_1(z) - T_c = \sum_{n=1}^{\infty} [B_n' I_0\left(\frac{n\pi R}{L}\right)] \sin\frac{n\pi z}{L} \qquad \text{(AIII.33)}$$

Again using the orthogonality of the sine function, the coefficients can be obtained

$$B_n^I I_0\left(\frac{n\pi R}{L}\right) = \frac{2}{L}\int_0^L [f_1(z) - T_c]\sin\frac{n\pi z}{L}dz \qquad \text{(AIII. 34)}$$

Finally, the solution of problem 3 is

$$\theta_1 = \frac{2}{L}\sum_{n=1}^{\infty}\frac{I_0(n\pi r/L)\sin(n\pi z/L)}{I_0(n\pi R/L)}\int_0^L [f_1(z) - T_c]\sin\frac{n\pi z}{L}dz \qquad \text{(AIII. 35)}$$

Thus, the final solution giving the distribution of the piston temperature is

$$\theta = \theta_g + \theta_o + \theta_1 \qquad \text{(AIII. 36)}$$

where λ_n is the n-th root of equation (AIII. 20)

When all the surface temperatures are constant and uniform respectively, the solution is, further, simplified as

$$\theta = \frac{2(T_g - T_1)}{R}\sum_{n=1}^{\infty}\frac{\sinh\lambda_n z}{\lambda_n \sinh\lambda_n L}\frac{J_0(\lambda_n r)}{J_1(\lambda_n R)}$$

$$+ \frac{2(T_o - T_1)}{R}\sum_{n=1}^{\infty}\frac{\sinh\lambda_n (L-z)}{\lambda_n \sinh\lambda_n L}\frac{J_0(\lambda_n r)}{J_1(\lambda_n R)} \qquad \text{(AIII. 37)}$$

with the boundary conditions

at $z = L$, $\theta = T_g - T_1$ (AIII. 38)

at $z = 0$, $\theta = T_o - T_1$ (AIII. 39)

at $r = R$, $\theta = 0$ (AIII. 40)

It it evident that the corresponding heat flux is as follows

$$q = K \, \mathrm{grad}\theta \, dA \qquad \text{(AIII. 41)}$$

For the gas side of the piston, z = L, the heat flux is

$$Q_g = 2\pi K \int_o^R \left.\frac{\partial \theta}{\partial z}\right|_{z=L} r dr$$

$$= 4\pi K[(T_g - T_l) \sum_{n=1}^{\infty} \frac{\cosh\lambda_n L}{\lambda_n \sinh\lambda_n L} + (T_l - T_o) \sum_{n=1}^{\infty} \frac{1}{\lambda_n \sinh\lambda_n L}]$$

(AIII. 42)

Similarly, for the oil side surface, z= 0, the heat flux is

$$Q_o = -2\pi K \int_o^R \left.\frac{\partial \theta}{\partial z}\right|_{z=0} r dr$$

$$= 4\pi K \, [(T_l - T_g) \sum_{n=1}^{\infty} \frac{1}{\lambda_n \sinh\lambda_n L} + (T_o - T_l) \sum_{n=1}^{\infty} \frac{\cosh\lambda_n L}{\lambda_n \sinh\lambda_n L}]$$

(AIII. 43)

From the energy conservation, the heat flux through the liner side surface is

$$Q_l = Q_g + Q_o$$

$$= 4\pi K \, (2T_l - T_g - T_o) \sum_{n=1}^{\infty} \frac{\cosh\lambda_n L - 1}{\lambda_n \sinh\lambda_n L}$$

(AIII. 44)

The positive zeros λ_n of the Bessel function can be approximated as the following asymptotic representation

$$\lambda_n = \pi\left(\frac{4n-1}{4} + \frac{0.050661}{4n-1} - \frac{0.053041}{(4n-1)^3} + \frac{0.262051}{(4n-1)^5} - \cdots\right) \qquad \text{(AIII.45)}$$

And the hyperbolic functions cosechx and cothx can be approximated as

$$\text{cosechx} = 2(e^{-x} + e^{-3x} + e^{-5x} + e^{-7x} + \cdots) \qquad \text{(AIII.46)}$$

$$\text{cothx} = 1 + 2e^{-2x} + 2e^{-4x} + 2e^{-6x} + \cdots \qquad \text{(AIII.47)}$$

Thus, the heat fluxes of the piston can be determined.

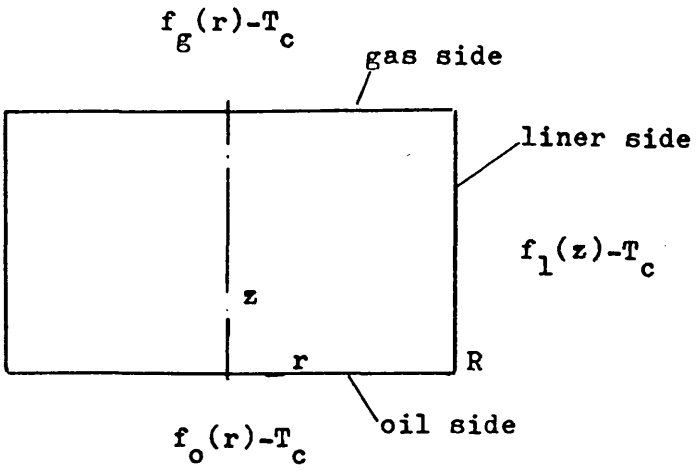

Fig. AIII. 1 Piston Temperature Distribution

Appendix IV ESSENTIALS OF PROGRAMS CSPS, CSP3Z, CSPMZ AND CSP3ZTC

```
      CONVENTIONAL OR OPPOSED PISTON ENGINE
      SIMPLE MODEL OF SCAVENGING
      ------------------------------------------

       Program:       cops

                      Subroutine associated:  afl
                                              arherb
                                              comlyb
                                              coolh
                                              cpgb
                                              enginb
                                              equr
                                              gb
                                              hb
                                              intxt1
                                              intxt2
                                              motpis
                                              orifh
                                              polyr
                                              scoeff
                                              simpit
                                              timex
                                              turbwb

                                    total:  18


    NAMELIST INPUT DATAFILE

  Line 1 : layout (30i1)
    layout=marker for engine layout
           if =2 for opposed  engine
              <>2 for conventional  engine
  Line 2 : cstrk  (10f10.4)
    cstrk=coefficient of engine operation
           if =2 for 2 stroke engine
           if =1 for 4 stroke engine
  Line 3-4 for conventional layout
  Line 3 : cyl,bore,strk,conlen,dvi,dve,cr,etmax (10f10.4)
      cyl=number of cylinders
     bore=cylinder bore (ft)
     strk=stroke (ft)
   conlen=connecting rod length (ft)
      dvi=inlet valve diameter (ft)
      dve=exhaust valve diameter (ft)
       cr=nominal compression ratio
    etmax=maximum engine torque (lbf-ft)
  Line 4 : xevc,xivc,xevo,xivo,xk,aorif,alf (10f10.4)
     xevc=angle of exhaust valve closing (deg)
     xivc=angle of inlet vavle closing (deg)
     xevo=angle of exhaust valve opening (deg)
     xivo=angle of inlet valve opening (deg)
       xk=emprical combustion rate factor - approximate value 0.1
    aorif=bypass orifice area (sq in)
      alf=emprical heat loss factor
  Line 5-7 for opposed piston 2 stroke engine
```

```
      bore=cylinder bore (ft)
        cr=nominal compression ratio
      etmax=maximum engine torque (lbf-ft)
        xk=empirical combustion rate factor
       alf=empirical heat loss factor
Line 6 : fvr,fhr,fpr,cll,alr,aur,clu,dpc,rck,zeta     (10f10.4)
      fvr=frame,crank vertical centre line to rocker pivot  (ft)
      fhr=frame,crank housing centre line to rocker pivots  (ft)
      fpr=frame,piston centre line to rocker pivots  (ft)
      cll=lower connecting rod  (ft)
      alr=lower rocker arm  (ft)
      aur=upper rocker arm  (ft)
      clu=upper connecting rod  (ft)
      dpc=piston compression distance  (ft)
      rck=crank radius  (ft)
     zeta=angle between lower and upper rocker arms (deg)
Line 7 : anhase,dip,dep,hip,hep,wip,wep  (10f10.4)
   anhase=phase angle between two crank arms  (degrees)
      dip=distance,crank vertical centre to inner edge of inlet port  (ft)
      dep=                                          exhaust port  (ft)
      hip=height of inlet port  (ft)
      hep=         exhaust port  (ft)
      wip=total width of inlet ports  (ft)
      wep=               exhaust ports  (ft)
Line 8 : cgr,tgr,ogr,cge,tge,oge,cafv,tjft,oaft (10f10.4)
      cgr=compressor gear ratio
      tgr=turbine gear ratio
      ogr=output shaft gear ratio
      cge=compressor gear efficiency
      tge=turbine gear efficiency
      oge=output shaft gear efficiency
     cafv=compressor bearing viscous friction factor
     tjft=turbine bearing friction torque (lbf-ft)
     oaft=output shaft bearing friction torque
Line 9 : eto,eta,cim,com (10f10.4)
      eto=ratio of the initial gas volume for mixing zone
          to the total cylinder volume
      eta=ratio of the final residual gas "dead space" volume
          to the total cylindel volume
      cim=coefficient of intake proportion into the mixing zone
      com=coefficient of discharge proportion from the mixing zone
Line 10:v0,ves (10f10.4)
      v0=initial engine speed, preferably 0.0
     ves= 5 values of engine speed
Line 11-15:ar1(i),(vdrs(i,j),j=1,5) (10f10.4)
       ar1= 5 values of exhaust to inlet pressure ratio
      vdrs= 25 values of delivery ratio based swep volume
Line 16-18:vfprev(i),(vxinj(i,j),j=1,5) (10f10.4)
     vfprev= 5 values of injection timing as a function of fprev
      vxinj
Line 19-21:vfprev(i),(vdinj(i,j),j=1,5) (10f10.4)
     vfprev= 5 values of injection duration as a function of fprev
      vdinj
Line 22: ved (10f10.4)
     ved= 5 values of diagram as a function of ves
Line 23: fo (10f10.4)
      fo= 5 values of fmep as a function of ves
Line 24: vesr (10f10.4)
```

```
    vbt= 5 values of ratio of output shaft torque to engine torque
Line 26: vet (10f10.4)
     vet= 5 values of engine torque
Line 27: vrc (10f10.4)
     vrc=   values of boost pressure ratio
Line 28: d1,d2t,d3o,d3i,a,b2,bp3,bt2  (10f10.4)
     d1=diameter at nozzle entry (ft)
     d2t=diameter at rotor tip (ft)
     d3o=diameter at exit shroud (ft)
     d3i=diameter at exit hub (ft)
      a=nozzle angle (deg)
     b2=blade angle at rotor entry (rad to tangential)
     bp3=screw pitch of rotor blades at exit (ft)
     bt2=blade thickness at rotor entry (ft)
Line 29: bb1,bb2s,bb2rr,psi,ff,tfric,bt3o,bt3i (10f10.4)
     bb1=passage width at exit from nozzle vanes (ft)
    bb2s=passage width just before rotor entry (ft)
   bb2rr=passage width just after rotor entry (ft)
     psi=cone angle at rotor entry (rad)
      ff=flow lossfactor, equals 1for no loss
   tfric=mechanical friction factor
    bt3o=blade thickness at rotor exit at tip (ft)
    bt3i=blade thickness at rotor exit at root (ft)
Line 30: r,calval,pa,ta,tw,e,tim,scfa (10f10.4)
       r=gas constant lbf.ft/lbm.deg r
  calval=caloric value of fuel
      pa=atmospheric pressure (psi)
      ta=atmospheric temperature (deg r)
      tw=engine water temperature (deg r)
       e=air cooler effectiveness
     tim=delay in injection timing
    scfa=compressor scale factor
Line 31: imark,jmark,metin,metout,iout,ioutpt,inject (9i1)
   imark=1 for error diagnostic output on first run
   jmark=1 for diagnostic information from engine subroutine
   metin=1 for metric (SI) input data
  metout=1 for metric (SI) output data
    iout=1 for array printout each run
  ioutpt=number of final printout copies
  inject=marker for injection timing input
         if =0 for mapping interpolation
         if =1 for data specification
Line 32:limit (i5)
   limit=limit on number of iterations for each loop
Line 33:io (i5)
      io=number of output file
Line 34:ihead (20a4)
   ihead=heading for printout over results
Line 35: os,ets,es,tgr1,tgr2,tim,rpd,aorif (10f10.4)
      os=output shaft speed (rpm)
     ets=engine torque specified (lbf-ft)
      es=engine speed (rpm)
   tgr1=bottom limit of turbine gear ratio (for optimization of tgr)
   tgr2=top limit of turbine gear ratio
    tim=delay in injection timing
    rpd=pressure difference of bypass valve actuation
  aorif=bypass orifice area (sq in)
        temperature units: ( °)
```

```
pressure units: lbf/in**2
  length units: ft
    mass units: lbm
```

```
        DATA FILE FOR CYCLE SIMULATION PROGRAM (CSP3Z)
        OPPOSED PISTON ENGINE
        MULTI ZONE MODEL OF SCAVENGING
        ------------------------------------------

         Program:       csp3z

                        Subroutine associated:  arhrl
                                                convtn
                                                comly
                                                crank
                                                elim
                                                eqnear
                                                eqnears
                                                heat
                                                gasprop
                                                init
                                                intxt1
                                                intxt2
                                                merge
                                                motpis
                                                nlsyst
                                                orifice
                                                out
                                                port
                                                qtpis
                                                resist1
                                                resph
                                                sum1
                                                timex
                                                turbw4

                                        total:  24

      NAMELIST OF INPUT DATAFILE

    Line 1 : title (20a4)
    Line 2 : firing order (i6)
    Line 3 : comment (i.e. Engine data,....) (20a4)
    Line 4 : ncyl (i2)
       ncyl=number of cylinders
    Line 5 : cr,sce   (3f10.4)
         cr=compression ratio
        sce=size    scaling factor for engine
    Line 6 : phase angle between cylinders (degrees)   (10f8.2)
    Line 7 : bore,fvr,fhr,fpr,cll,alr,aur,clu,dpc,rck,zeta     (11f10.6)
       bore=cylinder bore  (mm)
        fvr=frame,crank vertical centre line to rocker pivot  (mm)
        fhr=frame,crank housing centre line to rocker pivots  (mm)
        fpr=frame,piston centre line to rocker pivots  (mm)
        cll=lower connecting rod  (mm)
        alr=lower rocker arm  (mm)
        aur=upper rocker arm  (mm)
        clu=upper connecting rod  (mm)
        dpc=piston compression distance  (mm)
      zeta=angle between lower and upper rocker arms    (deg)
```

```
      hip=distance,crank vertical centre to inner edge of inlet port  (mm)
      hep=                                                exhaust port  (mm)
      hip=height of inlet port  (mm)
      hep=          exhaust port  (mm)
      wip=total width of inlet ports; if circular inlet port, default wip=0.  (mm)
      wep=                exhaust ports; if circular exhaust port, default wep=0.  (mm)
Line 10: nip,nep,alin,alex  (2i2,7f8.4)
      nip=number of inlet ports
      nep=          exhaust ports
     alin=angle of inlet port  (degrees)
     alex=          exhaust ports  (degrees)
Line 11: comment  (manifold data,.....) (20a4)
Line 12: nim, vim(i),i=1,nim  (i2, 7f10.4)  nim= no of inlet manifolds,vim=volume of inlet manifolds
Line 13: nem= no of exhaust manifolds, vem(i),i=1,nem = volume of exhaust manifold, aem(z)=1,nem = heat transfer area for manifolds
         (zero for inlet manifolds) (i2, 7f10.4)
Line 14: control volumes interconnection for the cylinders (10i2)
for example 3 cylinder engine with single inlet manifolds (c.v. 4) and
divided exhaust manifold (c.v. 5) and cooler (c. v. 6) has the following
arrangement
 1 4 5
 2 4 5
 3 4 5
Line 15: ach,apc,al,htc,swl  (8f10.4)
      ach= cylinder head heat transfer area (    ach=.01 for opposed piston engine)
      apc= piston crown
       al= liner (at tdc)
      htc=exhaust manifolds heat transfer coefficient (w/m2.k)
      swl= swirl ratio in woschni formula (8f10.4)
Line 16: friction scaling factor =1.0 , four values of scaling factors for heat release shape
Line 17: nbyp,ncool,byp,acool,vol(ncv)  (2i2,7f8.4)
     nbyp=number of bypas valves
    ncool=number of coolers
      byp=equivalent flow area of bypass valves
    acool=equivalent flow area of coolers
vol(nv)=volume of cooler
Line 18: vr0,vr1,cid(1),cid(2),cid(4),cid(5),cid(6) (8f10.4)
      vr0=ratio of the initial residual gas volume for mixing zone
          to the total cylinder volume
      vr1=ratio of the final residual gas "dead space" volume
          to the total cylinder volume
   cid(1)=coefficient of intake proportion into the air zone
   cid(2)=                                    mixing zone
   cid(4)=                discharge proportion from the air zone
   cid(5)=                                      mixing zone
   cid(6)=                                      gas zone
Line 19: comment (compressor map,.....) (20a4)
Line 20: compressor mode factor, 1 for compressor map 0 for compressor
subroutine. (i2)
Line 21: mass scaling factor,efficiency scaling factor for compressor (11f10.6)
Line 22: comment (turbine map,.....) (20a4)
Line 23: turbine mode factor (i2) same as for the compressor
Line 24: mass scaling factor,efficiency scaling factor for turbine (11f10.6)
Line 25: no of pressure points,no of non dimensional turbine speed points (i2)
Line 26:  pressure points vtp(i),i=1,np (10f8.6)
Line 27:  non dimensional turbine speed points. vts(j),j=1,nts (11f10.6)
Line 28: d1,d2t,d3o,d3i,a,h2,bp3,bt2  (11f10.6)
```

```
        a= nozzle angle (deg)
       b2= blade angle at rotor entry (rad to tangential)
      bp3= screw pitch of rotor blades at exit (mm)
      bt2= blade thickness at rotor entry (mm)
Line 29: bn1,bb2s,bb2rr,psi,ff,bt3o,bt3i (11f10.6)
      bb1= passage width at exit from nozzle vanes (mm)
    bb2s= passage width just before rotor entry (mm)
   bb2rr= passage width just after rotor entry (mm)
      psi= cone angle at rotor entry, (rad)
       ff=flow lossfactor, equals 1for no loss
     bt3o= blade thickness at rotor exit at tip (mm)
     bt3i= blade thickness at rotor exit at root (mm)
Line 30: comment (i.e. differential compound data)  (20a4)
Line 31: egr,cgr,tgr,ogr,ege,tge,oge,crge  (11f10.6)
      egr=epicyclic gear ratio
      cgr=overall compressor gear ratio
      tgr=turbine gear ratio
      ogr=output shaft gear ratio
      oge= output shaft gear efficiency
      tge=turbine*CVT   gear     "
    crge=carrier         "      "
      cge= compressor     "      "
Line 32: sge,age. (11f10.6) sge=sun gear efficiency, age=annulus gear efficienc,
Line 33: ja,je,jc,jcr,jp,js,jt,jo  (kgm2) (11f10.6)
       ja= annulus inertia
       je= engine inertia
       jc= compressor inertia
      jcr= carrier inertia
       jp= planet inertia
       js= sun inertia
       jt= turbine inertia
       jo=output shaft inertia
Line 34: oslt,oss (11f10.6)
     oslt=output shaft torque
      oss=output shaft speed
Line 35: comment (running condition) (20a4)
Line 36: es,ffrate,afr,calval (f10.2, 2f10.5, f10.0)
       es=engine speed (rev/min)
   ffrate=fuel flow rate (kg/sec)
      afr=air_fuel ratio
   calval=calorific value of the fuel (KJ/KG)
    notice:if ffrate wanted to be specified,then afr=<0.
           if afr wanted to be specified,then afr>0.,and to override an, ffrate
Line 37: ta,pa,tch,tp,tl,pb,pin,tin (10f8.2)
       ta=ambient temperature (degK)
       pa=ambient pressure (kN/m2)
      tch= temperature of cylinder head (degK)
       tp= temperature of piston crown (degK)
       tl= temperature of liner (max) (degK)
      pin= intak pressure (kN/m2)
       pb=back pressure (kN/m2)
      tin= intake temperature (degK)
Line 38: tcw,tco,hpis,csub,htcl,r2,r8,r9,r1x
      tcw= cooling water average temperature (degK)
      tco= cooling oil average temperature (degK)
     hpis= height of piston crown (um)
```

```
          if >0, the value is specified
     r2,r8,r9= heat transfer resistances
     rlx= relaxation factor for iteration
Line 39: static injection(degree),injection delay(degree) (10f8.2)
Line 40: crank increment (10f8.2)
Line 41: cfl,cfa,cfv,cfs (4f10.6)
Line 42: first estimate of temperature in each control volume temp(i),i=1,ncv (10f8.2)
Line 43: first estimate of pressure     "   "       "       "   pr(i),i=1,ncv (10f8.2)
Line 44: first estimate of equivalence ratio "   "       "       "   eq(i),i=1,ncv (10f8.2)
Line 45: ncyct (i2)
  ncyct= number of calculation cycles
Line 46: layout,istart,iecho,nl
 layout=0 for engine detached from compound unit
        =1 for compound unit
 istart is not used
  iecho=0 for no echoing
        =1 for echoing
     nl is not used
Line 47: two relaxation factors
Line 48: tolerances for the convergence (11f10.6)
Line 49: # of pressure iron(not used)
         cooler effectiveness
         charging cooler temperature
         temperature units: ( K)
            pressure units: KN/m**2
              length units: mm
                area units: cm**2
                mass units: grams

      NAMELIST OF MAJOR "FL" VARIABLES

      den=density of gas mixture
      effs=scavenging efficiency
      efftr=trapping efficiency
      etach=charging efficiency
      eta,=charge purity
      fuel=delivery ratio
      sair=mass of delivered air
      satot=total trapped air mass
      satr=mass of delivered air trapped

      1 dimensional array:
      dmex=increment of mass flowing from cylinder to exhaust manifold
      dmin=                          from inlet manifold to cylinder
      eqair=equivalence ratio of air within inlet manifold
      eqry=                    of residul gas within cylingder at the
           beginning of scavenging
      isca=indicator of scavenging
           if isca(icv)=0,then non-scavenging process
                       =1,then the beginning of scavenging process
                       =2,then scavenging process
                       =3,then the end of scavenging process
           if isca(icv+10)=1,pr(inlet manifold)>pr(cylinder)
                          =2,then both inlet and exhaust ports open

      2 dimensional array:
      ARRAY(i,j)=some quantity within zone(zone i,j-th cylinder)
```

```
                i=j          mixing zone
                i=j          gas zone

      aj=increment of air mass
      dmaj=sum [illegible] of mass
      dvvj=          of volume
      dmj=           of total mass
      dmhj=          of inflowing total enthalpy
      eqij=equivalence ratio at present step
      eqjo=                     at previous step
      hj=specific enthalpy at present step
      hjo=                  at previous step
      mj=total mass at present step
      mjo=          at previous step
      sj=mass of residual mass
      tj=temperature at present step
      tjo=          at previous step
      uj=specific internal energy at present step
      ujo=                        at previous step
      vj=volume at present step
      vjo=      at previous step
      xjo=              at previous step
      zjo=                 at previous step
```

MULTI ZONE MODEL OF SCAVENGING

Program: cspmz

Subroutine associated:
archr1
convtn
comlv
crank
elim
epgear
epgears
eqqr
heat
qaspropn
init
intxt1
intxt2
merge
motpis
nlsyst
order
orifice
out
port
qtpis
resist1
resph
sum1
timex
turbw4

total: 26

NAMELIST OF INPUT DATAFILE

Line 1 : title (20a4)
Line 2 : firing order (i6)
Line 3 : comment (i.e. Engine data,....) (20a4)
Line 4 : ncyl (i2)
ncyl=number of cylinders
Line 5 : cr,sce (8f10.4)
cr=compression ratio
sce=size scaling factor for engine
Line 6 : phase angle between cylinders (degrees) (10f8.2)
Line 7 : bore,fvr,fhr,fpr,cll,alr,aur,clu,dpc,rck,zeta (11f10.6)
bore=cylinder bore (mm)
fvr=frame,crank vertical centre line to rocker pivot (mm)
fhr=frame,crank housing centre line to rocker pivots (mm)
fpr=frame,piston centre line to rocker pivots (mm)
cll=lower connecting rod (mm)
alr=lower rocker arm (mm)
aur=upper rocker arm (mm)
clu=upper connecting rod (mm)
dpc=piston compression distance (mm)

```
      aphase=phase angle between two crank [illegible]
        dip=distance,crank vertical centre to inner edge of inlet port  (mm)
        dep=                                              exhaust port  (mm)
        hip=height of inlet port  (mm)
        hep=          exhaust port  (mm)
        wip=total width of inlet ports  (mm)
        wep=                exhaust ports  (mm)
    Line 10: nip,nep,alin,alex  (2i2,7f8.4)
        nip=number of inlet ports
        nep=          exhaust ports
       alin=angle of inlet port  (degrees)
       alex=         exhaust ports  (degrees)
    Line 11: comment  (manifold data,.....) (20a4)
    Line 12: nim, vim(i),i=1,nim  (i2, 7f10.4)  nim= no of inlet manifolds,vim=volume of inlet manifolds
    Line 13: nem= no of exhaust manifolds, vem(i),i=1,nem = volume of exhaust manifold, aem(z)=i,nem = heat transfer area for manifolds

             (zero for inlet manifolds) (i2, 7f10.4)
    Line 14: control volumes interconnection for the cylinders (10i2)
    for example 3 cylinder engine with single inlet manifolds (c.v. 4) and
    divided exhaust manifold (c.v. 5) and cooler (c. v. 6) has the following
    arrangement
     1 4 5
     2 4 5
     3 4 5
    Line 15: ach,apc,al,htc,swl  (9f10.4)
        ach= cylinder head heat transfer area (     ach=.01 for opposed piston engine)
        apc= piston crown
         al= liner (at tdc)
        htc=exhaust manifolds heat transfer coefficient (w/m2.k)
        swl= swirl ratio in woschni formula (8f10.4)
    Line 16: friction scaling factor =1.0 , four values of scaling factors for heat release shape
    Line 17: nbyp,ncool,byp,acool,vol(ncv)  (2i2,7f8.4)
       nbyp=number of bypas valves
      ncool=number of coolers
        byp=equivalent flow area of bypass valves
      acool=equivalent flow area of coolers
    vol(nv)=volume of cooler
    Line 18: njo,mkj,cj1,cj2,cj3 (2i2,7f8.4)
        njo=number of initial zones at beginning of scavenging
        mkj=number of strips into which cylinder is divided
        if mkj=2,then cj1=coeffient of entrainment rate
                      cj1,cj2 are not used
        if mkj>=3,then cj1=coefficient of momentun trasfer
                       cj2,cj3=coefficients of mixing length
    Line 19: comment (compressor map,.....) (20a4)
    Line 20: compressor mode factor, 1 for compressor map 0 for compressor
    subroutine. (i2)
    Line 21: mass scaling factor,efficiency scaling factor for compressor (11f10.6)
    Line 22: comment (turbine map,.....) (20a4)
    Line 23: turbine mode factor (i2) same as for the compressor
    Line 24: mass scaling factor,efficiency scaling factor for turbine (11f10.6)
    Line 25: no of pressure points,no of non dimensional turbine speed points (i2)
    Line 26:  pressure points vtp(i),i=1,np (10f8.6)
    Line 27:  non dimensional turbine speed points. vts(j),j=1,nts (11f10.6)
    Line 28: d1,d2t,d3o,d3i,a,b2,bp3,bt2  (11f10.6)
        d1= diameter at nozzle entry (mm)
```

```
        a= nozzle angle (deg)
       b2= blade angle at rotor entry (rad to tangential)
      np3= screw pitch of rotor blades at exit (mm)
      bt2= blade thickness at rotor entry (mm)
Line 29: bb1,bb2s,bb2rr,psi,ff,bt3o,bt3i (11f10.5)
      bb1= passage width at exit from nozzle vanes (mm)
    bb2s= passage width just before rotor entry (mm)
   bb2rr= passage width just after rotor entry (mm)
      psi= cone angle at rotor entry (rad)
       ff=flow lossfactor, equals 1for no loss
    bt3o= blade thickness at rotor exit at tip (mm)
    bt3i= blade thickness at rotor exit at root (mm)
Line 30: comment (i.e. differential compound data)  (20a4)
Line 31: egr,cgr,tgr,ogr,ege,tge,cge,oge  (11f10.6)
      egr=epicyclic gear ratio
      cgr=overall compressor gear ratio
      tgr=turbine gear ratio
      ogr=output shaft gear ratio
      oge= output shaft gear efficiency
      tge=turbine*CVT   gear      "
     cge=carrier         "       "
      cge= compressor     "       "
Line 32: sge,age. (11f10.6) sge=sun gear efficiency, age=annulus gear efficiency
Line 33: ja,je,jc,jcr,jp,js,jt,jo  (kgm2) (11f10.6)
       ja= annulus inertia
       je= engine inertia
       jc= compressor inertia
      jcr= carrier inertia
       jp= planet inertia
       js= sun inertia
       jt= turbine inertia
       jo=output shaft inertia
Line 34: oslt,oss (11f10.6)
    oslt=output shaft torque
     oss=output shaft speed
Line 35: comment (running condition) (20a4)
Line 36: es,ffrate,afr,calval (f10.2, 2f10.5, f10.0)
      es=engine speed (rev/min)
  ffrate=fuel flow rate (kg/sec)
     afr=air_fuel ratio
  calval=calorific value of the fuel (KJ/KG)
   notice:if ffrate wanted to be specified,then afr=<0.
          if afr wanted to be specified,then afr>0.,and to override any ffrate
Line 37: ta,pa,tch,tp,tl,pb,pin,tin (10f8.2)
      ta=ambient temperature (degK)
      pa=ambient pressure (kN/m2)
     tch= temperature of cylinder head (degK)
      tp= temperature of piston crown (degK)
      tl= temperature of liner (max) (degK)
     pin= intak pressure (kN/m2)
      pb=back pressure (kN/m2)
     tin= intake temperature (degK)
Line 38: tcw,tco,hpis,csub,htc1,r2,r8,r9,r1x (10f8.2)
     tcw= cooling water average temperature (degK)
     tco= cooling oil average temperature (degK)
    hpis= height of piston crown (mm)
    csub= heat conductivity of piston (kw/K)
```

```
      r2,r0,ry- heat transfer resistances
      rlx= relaxation factor for iteration
Line 39: static injection(degree),injection delay(degree) (10f8.2)
Line 40: crank increment (10f8.2)
Line 41: cfl,cfa,cfv,cfm (8f10.6)
Line 42: first estimate of temperature in each control volume temp(i),i=1,ncv (10f8.2)
Line 43: first estimate of pressure     "   "      "        "   pr(i),i=1,ncv (10f8.2)
Line 44: first estimate of equivalence ratio "   "      "        "   eq(i),i=1,ncv (10f8.2)
Line 45: ncyct (i2)
  ncyct= number of calculation cycles
Line 46: layout,istart,iecho,nl
  layout=0 for engine detached from compound unit
        =1 for compound unit
  istart is not used
  iecho=0 for no echoing
       =1 for echoing
      nl is not used
Line 47: two relaxation factors
Line 48: tolerances for the convergence (11f10.6)
Line 49: % of pressure drop(not used)
         cooler effectiveness
         charging cooler temperature
         temperature units: ( K)
            pressure units: KN/m**2
              length units: mm
                area units: cm**2
                mass units: grams

      NAMELIST OF MAJOR NEW VARIABLES

      alvb=critical intake angle of vortex breakdown
      denm=density of gas mixture
      effs=scavenging efficiency
      efftr=trapping efficiency
      etach=charging efficiency
      etap=charge purity
      ruel=delivery ratio
      sair=mass of delivered air
      satot=total trapped air mass
      satr=mass of delivered air trapped

      1 dimensional array:
      ajx=tangent of angle between adjecent zones within different strips
      dmex=increment of mass flowing from cylinder to exhaust manifold
      dmin=                          from inlet manifold to cylinder
      eqair=equivalence ratio of air within inlet manifold
      eqry=                      of residul gas within cylingder at the
           beginning of scavenging
      isca=indicator of scavenging
           if isca(icv)=0,then non-scavenging process
                        =1,then the beginning of scavenging process
                        =2,then scavenging process
                        =3,then the end of scavenging process
           if isca(icv+10)=1,pr(inlet manifold)>pr(cylinder)
                          =2,then both inlet and exhaust ports open
      mlj=maximum of zone within each strip
      maxlj=                     all strips
```

```
                =-1.0,then outer jet
sjx=distance of adjecent zones within different strips

3 dimensional array:
ARRAY(i,j,k)=some quantity within zone(i-th strip,j-zone,k-th cylinder)

aj=increment of air mass
dkej=        of total internal energy
dlmj=surplus of mass
dlvj=        of volume
dmj=           of total mass
dmhj=          of inflowing total enthalpy
dmwj=          of axial momentum
eqj=equivalence ratio at present step
eqjo=                 at previous step
fj=initial injected momentum flux at present step
fjo=                               at previous step
hj=specific enthalpy at present step
hjo=                 at previous step
mj=total mass at present step
mjo=          at previous step
rj=radius at present step
rjo=      at previous step
rjod=inner radius at previous step
sj=mass of residual gass
tj=temperature at present step
tjo=           at previous step
uj=specific internal energy at present step
ujo=                         at previous step
vj=volume at present step
vjo=      at previous step
wj=axial velocity at present step
wjo=                at previous step
zj=axial displacement at present step
zjo=                  at previous step
```

MATHEMATICAL MODEL OF TURBOCHARGED DIESEL ENGINE
WITH OR WITHOUT A BLOWER
DATA FILE FOR CYCLE SIMULATION PROGRAM (csp3ztc)
OPPOSED PISTON ENGINE
3 ZONE MODEL OF SCAVENGING

Program: csp3ztc

Subroutine associated: arhr1
comly
commap
convtn
cooler
crank
epgear
epgears
heat
gasprop
heading
init
intxt1
intxt2
merge
motpis
orifice
out
outcomp
outeny
outext
outheat
outhr
outturb
port
resist
simpit
sum1
timex
turbw4
turmap

total: 31

Subroutine library : GINO graphics

NAMELIST OF INPUT DATAFILE

Line 1 : title (20a4)
Line 2 : firing order (i6)
Line 3 : comment (i.e. Engine data,....) (20a4)
Line 4 : ncyl,ncomp,nturb,ncompl,nturbl,nbyp,icool,icooll (20i2)
ncyl= number of cylinders
ncomp= number of high pressure compressors
nturb= number of high pressure turbines
ncompl= number of low pressure compressors
nturbl= number of low pressure turbines
nbyp= number of bypass valves

```
    icool1= number of coolers after low pressure compressor
  Line 5 : cr,sce   (8f10.4)
       cr= compression ratio
      sce= size scaling factor for engine
  Line 6 : phase angle between cylinders (degrees)   (10f8.2)
  Line 7 : bore,fvr,fhr,fpr,cll,alr,aur,clu,dpc,rck,zeta     (11f10.6)
     bore= cylinder bore  (mm)
      fvr= frame,crank vertical centre line to rocker pivot  (mm)
      fhr= frame,crank housing centre line to rocker pivots  (mm)
      fpr= frame,piston centre line to rocker pivots  (mm)
      cll= lower connecting rod  (mm)
      alr= lower rocker arm  (mm)
      aur= upper rocker arm  (mm)
      clu= upper connecting rod  (mm)
      dpc= piston compression distance  (mm)
      rck= crank radius  (mm)
    zeta= angle between lower and upper rocker arms    (degree)
  Line 8 : comment (port data,...) (20a4)
  Line 9 : aphase,dip,dep,hip,hep,wip,wep  (10f10.6)
   aphase= phase angle between two crank arms  (degrees)
      dip= distance,crank vertical centre to inner edge of inlet port  (mm)
      dep=                                          exhaust port  (mm)
      hip= height of inlet port  (mm)
      hep=           exhaust port  (mm)
      wip= total width of inlet ports; if circular inlet port, defraud wip= 0.  (mm)
      wep=                exhaust ports; if circular exhaust port, defraud wep= 0.  (mm)
  Line 10: nip,nep,alin,alex  (2i2,7f8.4)
      nip= number of inlet ports
      nep=           exhaust ports
     alin= angle of inlet port  (degrees)
     alex=          exhaust ports  (degrees)
  Line 11: comment  (manifold data,......) (20a4)
  Line 12: nim,(vol(i),i= ncyl+1,ncyl+nim)  (i2,7f10.4)
      nim= no of inlet manifolds
   vol(i)= volume of inlet manifolds
  Line 13: nem,(vol(i),i= ncyl+nim+1,ncyl+nim+nem)  (i2,7f10.4)
      nem= no of exhaust manifolds
   vol(i)= volume of exhaust manifolds
  Line 14:(acv(i),i= ncyl+1,ncv)
   acv(i)= area of manifolds
  Line 15: control volumes interconnection for the cylinders (10i2)
  for example 3 cylinder engine with single inlet manifolds (c.v. 4) and
  divided exhaust manifold (c.v. 5) and cooler (c. v. 6) has the following
  arrangement
   1 4 5
   2 4 5
   3 4 5
  Line 16: ach,apc,al,htc,swl,htsf  (8f10.4)
      ach= cylinder head heat transfer area (    ach=.01 for opposed piston engine)
      apc= piston crown
       al= liner (at tdc)
      htc= exhaust manifolds heat transfer coefficient (w/m2.k)
      swl= swirl ratio in woschni formula
     htsf= heat transfer scaling factor
  Line 17: friction scaling factor =1.0 , four values of scaling factors for heat release shape
  Line 18: vr0,vr1,cid(1),cid(2),cid(4),cid(5),cid(6) (8f10.4)
      vr0= ratio of the initial residual gas volume for mixing zone
           to the total cylinder volume
```

```
                                                    mixing zone
    cic(4)=                 discharge partition from the air zone
    cic(5)=                                         mixing zone
    cic(6)=                                         gas zone
  Line 19: comment (high pressure compressor map,.....) (20a4)
  Line 20: ncm,ncs  (20i2)
      ncm= no of pressure points for high pressure compressor
      ncs= no of non dimensional turbine speed points
  Line 21: t0c,p0c,clsf,cmsf,cesf,tcs,tgr,jtc  (8f10.0)
      t0c= reference temperature for high pressure compressor
      p0c= reference pressure
     clsf= length scaling factor
     cmsf= mass flow rate scaling factor
     cesf= efficiency scaling factor
      tcs= turbocharger speed for high pressure turbocharger
      tgr= turbine gear ratio
      jtc= momentum of inertia
  Line 22: (vcs(i),i=1,ncs)  (8f10.0)
   vcs(i)= speed points for high pressure compressor
  Line 23: mass flow rate points (vcmf(i,j),i=1,ncm)  (8f10.0)
  Line 24: pressure points (vcp(i,j),i=1,ncm)  (8f10.0)
  Line 25: high pressure compressor efficiency (vce(i,j),i=1,ncm)  (8f10.0)
  Line 26: comment (low pressure compressor map,.....) (20a4)
  Line 27: ncml,ncsl  (20i2)
     ncml= no of pressure points for low pressure compressor
     ncsl= no of non dimensional turbine speed points
  Line 28: t0cl,p0cl,clsfl,cmsfl,cesfl,tcsl,tgrl,jtcl  (8f10.0)
     t0cl= reference temperature for low pressure compressor
     p0cl= reference pressure
    clsfl= length scaling factor
    cmsfl= mass flow rate scaling factor
    cesfl= efficiency scaling factor
     tcsl= turbocharger speed for low pressure turbocharger
     tgrl= turbine gear ratio
     jtcl= momentum of inertia
  Line 29: (vcsl(i),i=1,ncsl)
  vcsl(i)= speed points for low pressure compressor
  Line 30: mass flow rate points (vcmfl(i,j),i=1,ncml)  (8f10.0)
  Line 31: pressure points (vcpl(i,j),i=1,ncml)  (8f10.0)
  Line 32: low pressure compressor efficiency (vcel(i,j),i=1,ncml)  (8f10.0)
  Line 33: comment (low pressure turbine map,.....) (20a4)
  Line 34: ntsl,ntpl,iturbl  (20i2)
     ntsl= no of non dimensional turbine speed points for low pressure turbine
     ntpl= no of pressure points
   iturbl= no of low pressure turbine entry
  Line 35: tlsfl,tmsfl,tesfl,t0tl,p0tl,dtipl (8f10.0)
    tlsfl= length scaling factor for low pressure turbine
    tmsfl= mass flow rate scaling factor
    tesfl= turbine efficiency scaling factor
     t0tl= reference temperature
     p0tl= refenrence pressure
    dtipl= tip diameter (mm)
  Line 36: speed pointsl (vtsl(i),il=1,ntsl)
  Line 37: pressure point for low pressure turbine (vtpl(i),i=1,ntpl)  (8f10.0)
  Line 38: mass flow rate points (vtmfl(i,j),j=1,ntsl)  (8f10.0)
  Line 39: turbine efficiency pointsl (vtel(i,j),j=1,ntsl)  (8f10.0)
  Line 40: nwgl,awgl,pwgl,swgl  (8f10.0)
     nwgl= no of waste gate for low pressure turbine
```

```
      [illegible] spring stiffness of waste gate
Line 41: comment (running condition) (20a4)
Line 42: es,ffrate,afr,calval (f10.2, 2f10.5, f10.0)
      es= engine speed (rev/min)
   ffrate= fuel flow rate (kg/sec)
     afr= air_fuel ratio
  calval= calorific value of the fuel (KJ/KG)
  notice:if ffrate wanted to be specified,then afr= <0.
         if afr wanted to be specified,then afr>0.,and to override any ffrate
Line 43: ta,pa,tw,tch,tp,tl,pb,pin,tin (10f8.2)
      ta= ambient temperature (degK)
      pa= ambient pressure (kN/m2)
      tw= cooling water temperature (degK)
     tch= temperature of cylinder head (degK)
      tp= temperature of piston crown (degK)
      tl= temperature of liner (max) (degK)
     pin= intak pressure (kN/m2)
      pb= back pressure (kN/m2)
     tin= intake temperature (degK)
Line 44: tcw,tco,hpis,csub,htcl,r2,r8,r9,rlx (10f8.2)
     tcw= cooling water average temperature (degK)
     tco= cooling oil average temperature (degK)
    hpis= height of piston crown
    csub= heat conductivity of piston
    htcl= heat transfer coefficient of liner
    r2,r8,r9= heat transfer resistances
     rlx= relaxation factor for iteration
Line 45: static injection(degree),injection delay(degree) (10f8.2)
Line 46: crank increment (10f8.2)
Line 47: cfl,cfa,cfv,cfm (8f10.6)
Line 48: first estimate of temperature in each control volume temp(i),i=1,ncv (10f8.2)
Line 49: first estimate of pressure     "   "      "       "   pr(i),i=1,ncv (10f8.2)
Line 50: first estimate of equivalence ratio "   "      "       "   eq(i),i=1,ncv (10f8.2)
Line 51: ncyct (i2)
  ncyct= number of calculation cycles
Line 52: layout,istart,iecho,nl,iplot,icheck,ip,nitit
  layout= 0 for engine detached from compound unit
        = 1 for compound unit
  istart is not used
   iecho= 0 for no echoing
        = 1 for echoing
      nl is not used
   iplot= 0 for no plotting
        = 1 for plotting
  ichech= 0 for no checking
        = 1 for checking
      ip is not used
   ninit= no of calculation cycles for initiation
Line 53: two relaxation factors
Line 54: tolerances for the convergence (10f10.6)
         temperature units: ( K)
            pressure units: KN/m**2
              length units: mm
                area units: cm**2
                mass units: grams

      NAMELIST OF MAJOR NEW VARIABLES
```

```
denm=density of gas mixture
effs=scavenging efficiency
efftr=trapping efficiency
etach=charging efficiency
etap=charge purity
rdel=delivery ratio
sair=mass of delivered air
satot=total trapped air mass
satr=mass of delivered air trapped

1 dimensional array:
dmex=increment of mass flowing from cylinder to exhaust manifold
dmin=                            from inlet manifold to cylinder
eqair=equivalence ratio of air within inlet manifold
eqrg=                    of residul gas within cylinder at the
     beginning of scavenging
isca=indicator of scavenging
     if isca(icv)=0,then non-scavenging process
                 =1,then the beginning of scavenging process
                 =2,then scavenging process
                 =3,then the end of scavenging process
     if isca(icv+10)=1,pr(inlet manifold)>pr(cylinder)
                    =2,then both inlet and exhaust ports open

2 dimensional array:
ARRAY(i,j)=some quantity within zone(zone i,j-th cylinder)
          i=1 for the air zone
          i=2          mixing zone
          i=3          gas zone

aj=increment of air mass
dlmj=surplus of mass
dlvj=         of volume
dmj=            of total mass
dmhj=           of inflowing total enthalpy
eqj=equivalence ratio at present step
eqjo=                    at previous step
hj=specific enthalpy at present step
hjo=                  at previous step
mj=total mass at present step
mjo=           at previous step
sj=mass of residual gass
tj=temperature at present step
tjo=           at previous step
uj=specific internal energy at present step
ujo=                          at previous step
vj=volume at present step
vjo=       at previous step
wjo=                at previous step
zjo=                     at previous step
```